Unsymmetrical Aromatic Diamines in Siloxane Chemistry: Method Development and Mechanistic Studies on Diamino-Functionalized (Hydrido)siloxanes

Dissertation

zur Erlangung des

DOKTORGRADES DER NATURWISSENSCHAFTEN

(DR. RER. NAT)

an der Fakultät für Chemie und Pharmazie

der Universität Regensburg

vorgelegt von

Tobias Götz

aus Weiding

im Jahr 2023

Eidesstattliche Erklärung

Ich erkläre hiermit an Eides statt, dass ich die vorliegende Arbeit selbstständig verfasst und keine anderen als die angegebenen Quellen und Hilfsmittel benutzt habe. Die aus fremden Quellen direkt oder indirekt übernommenen Gedanken sind als solche gekennzeichnet. Die Arbeit wurde bisher in gleicher oder ähnlicher Form keiner anderen Prüfungsbehörde vorgelegt und auch nicht veröffentlicht.

_____ _____

Ort, Datum Unterschrift

Die vorliegende Arbeit entstand in der Zeit von November 2018 bis Dezember 2022 am Institut für Anorganische Chemie der naturwissenschaftlichen Fakultät IV für Chemie und Pharmazie der Universität Regensburg unter Anleitung von Herrn Dr. Jonathan O. Bauer.

Promotionsgesuch	Januar 2023
Promotion	März 2023
Prüfungsausschuss:	
Vorsitz:	Apl. Prof. Dr. R. Müller
Erster Gutachter:	Dr. J. O. Bauer
Zweiter Gutachter:	Prof. Dr. M. Scheer
Dritter Prüfer:	Prof. Dr. F. M. Matysik

Publikationsliste:

Chloropentaphenyldisiloxane – Model Study on Intermolecular Interactions in the Crystal Structure of a Monofunctionalized Disiloxane

J. O. Bauer, T. Götz

Chemistry **2021**, *3*, 444–453.

Functional Group Variation in *tert*-Butyldiphenylsilanes (TBDPS): Syntheses, Reactivities, and Effects on the Intermolecular Interaction Pattern in the Molecular Crystalline State

J. O. Bauer, N. A. Espinosa-Jalapa, N. Fontana, T. Götz, A. Falk

Eur. J. Inorg. Chem. **2021**, 2636–2642.

Molecular Scissors for Tailor-Made Modification of Siloxane Scaffolds

T. Götz, A. Falk, J. O. Bauer

Chem. Eur. J. **2022**, *28*, e202103531.

Preface

The herein presented results have already been published in part during the preparation of this thesis (see above). The corresponding citations are given at the beginning of the respective chapters.

Each chapter includes a list of authors and the individual contribution of each author is described.

Furthermore, all chapters have their own numeration of compounds. The molecular structures in the schemes and figures may differ slightly in style. In the beginning of this thesis, a general introduction and objectives of the work are presented together with a comprehensive conclusion at the end of this thesis.

Abbreviations

Ar	Aryl
coe	Cyclooctadiene
DFT	Density functional theory
Dipp	2,6-diisopropylaniline
DMAP	4-dimethylaminopyridine
DMF	Dimethylformamide
d.r.	Diastereomeric ratio
EI	Electron impact ionization
Et	Ethyl
FD	Field desorption ionization
h	Hour(s)
HR	High resolution
*i*Pr	*iso*-propyl
Me	Methyl
Mes	Mesityl = 2,3,6-trimethylbenzene
min	Minute(s)
mol	Moles
MS	Mass spectrometry
Napth	Naphtyl
*n*Bu	*n*-butyl
NMR	Nuclear magnetic resonance spectroscopy
Ph	Phenyl
*p*TsOH	*para*-toluene sulfonic acid
r.t.	Room temperature
*t*Bu	*tert*-butyl
Tf	Triflate
THF	Tetrahydrofurane

Table of Contents

1 Introduction

Silicon shapes our world – literally and figuratively. As the Earth's crust second most abundant element (26.3 w% Si) after oxygen (48.9 w% O), it can be primarily found as silicate minerals and various types of silicon dioxide known to most as rocks or sand.[1–5] Astonishingly, also living organisms like diatoms, sponges or radiolaria are able to produce silicon dioxide. They use the chemical and mechanical stability which is fundamental to the structural motif for building rigid exo- or endoskeletons.[3,4,6] These macromolecular properties have triggered human curiosity ever since and have found ubiquitous application in various technologies throughout the centuries. From production of glassware over concrete formulation to silicone plastics, the Si–O–Si moiety has always been an important chemical fragment. Since the end of the 20th century, some people refer to the era we live in as "Silicon Age" owing to the fact that elemental silicon is becoming more and more present in the digitalized world.[7] Its semiconducting properties combined with the relatively easy synthesis in different purities for different applications makes it an indispensable material for technologies like solar cells, microchips and modern computing in general. As a result of its versatility and applicability, research in silicon compounds both in materials science and molecular chemistry is expected to continue to grow. The latter one will be the main subject regarded in this work, focusing on silane- and especially siloxane chemistry as smallest building blocks for studying the chemical behavior of the structural motif of the most abundant Si–O–Si bond itself.

1.1 The siloxane bond motif and the controversy about its electronic description

Silicon can form bonds with various chemical elements resulting in a variety of different compound classes. The most abundant and therefore arguably most important bond is the Si–O bond. When two or more silicon atoms are linked to each other through oxygen atoms, we generally use the term 'siloxane' to classify the compound. Since silicon typically has four substituents, a deeper differentiation can be applied depending on the molecular structure. While naturally occurring silicates mostly have four oxygen atoms around Si, silsesquisiloxane cages usually have one different functional group and linear silicone polymers are designed to have two oxygen atoms and two organic substituents around the silicon atom (Figure 1.1).[1,4,5,8]

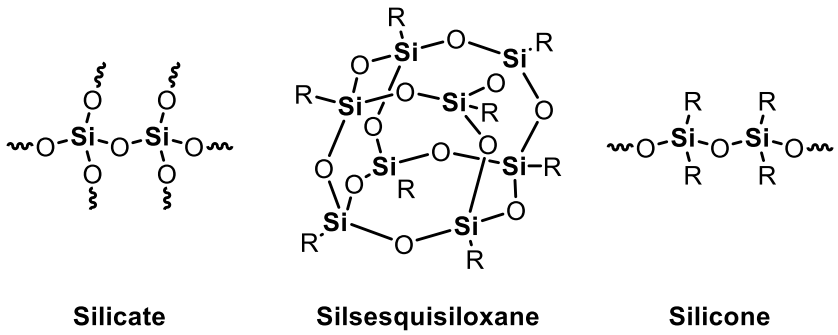

Figure 1.1. General structures of silicates, silicones and silsesquisiloxanes.

Most of the industrial and natural applications of these compound classes arise from to the chemical and mechanical robustness of the bond motif.[9] In order to understand the chemical and physical background of this robustness, the consideration of di- or oligosiloxane compounds is of great importance as they represent small and easily characterizable examples of the Si–O–Si functionality. Since silicon is located below carbon in the periodic table it is often compared to its lighter congener. Therefore, the siloxane bond can be well related to an ether C–O–C bond whereby the question of basicity of the free electron pair located at the oxygen atom arises. Due to the lower electronegativity of silicon (1.8 in the Pauling scale) compared to carbon (2.5 in the Pauling scale), one intuitively would assume an electron richer oxygen lone pair and thus higher basicity.[10] However, reality proves otherwise as siloxane compounds typically show extraordinary low basic properties[11,12] along with high bonding angles of 140° to 180°.[13] This phenomenon has been intensely studied since the 1950s and initially attributed to n(O)→d(Si) back-bonding. It has been argued that non-bonding 2p orbitals on the oxygen atom donate electron density into the 3d silicon orbitals, decreasing the HOMO energy and therefore also the proton affinity.[12,14] However, later studies have revealed a much smaller influence of the d-orbitals on the electronic behavior of the Si–O bond as the silicon d-orbitals are simply too high in energy.[15,16,17] This has been the starting point of long discussions about the true reasons for the high bond angle and low basicity of siloxanes whereby two seemingly opposing views have formed within the years. The one side attributes these unique properties to a high ionic character of the Si–O bond paired with steric repulsion[15,17,18] while the other side argues with n(O)→σ^*(SiR) hyperconjugative effects (Figure 2.2).[19,20]

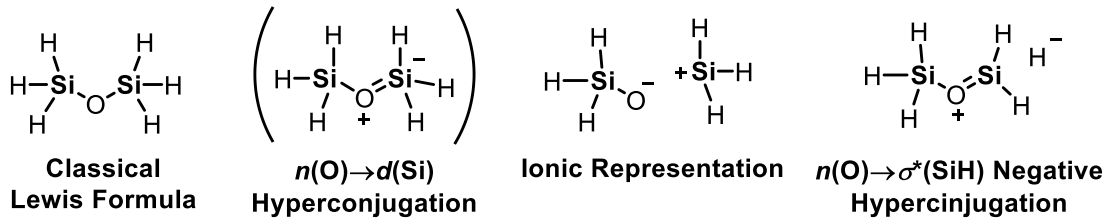

Figure 1.2. Lewis formula of disiloxane illustrating the respective electronic explanations for the low basicity and high bond angles.

Gillespie and Johnson,[15] and Grabowsky *et al*.[18] suggested the Si–O bond to be essentially ionic based on the calculations of Electron Localization Functions (ELF) of disiloxane. However, the

latter group found a far higher covalent aspect if the siloxane bond is forced towards smaller angles near the tetrahedral conformation by applying ring strain. They argue that by changing the bond angle it is possible to tune the basicity of the siloxane oxygen atom.[18] Nonetheless, it is stated that all arising questions as to the electronic nature of the bond motif can very well be explained by its ionicity.[15,18] In contrast to that, Weinhold and West have been using Natural Bond Orbital (NBO) calculations on disiloxane and hexamethyldisiloxane. They found the reason for the widening of the Si–O–Si bond angle compared with the respective carbon analogues in an increase of the $n(O)\rightarrow\sigma^*(SiR)$ negative hyperconjugation. Therefore, the low basicity fundamentally results from the competition between intramolecular hyperconjugation and intermolecular hydrogen bonding interactions of the type $n(O)\rightarrow\sigma^*(OH)$.[19,20] This behavior basically represents a fairly covalent nature of the bond and thus opposes the ionicity explanation. It was in 2018 when Grabowsky and co-workers published a very detailed theoretical study of the siloxane bond that was about to bring both concepts together. They were not solely looking into one theoretical method, but rather performing bonding analyses combining orbital-space, real-space and bond-index considerations on the disiloxane molecule ($H_3SiOSiH_3$) and cyclic siloxane systems $Si_2H_4O(CH_2)_{n-3}$ (with n=3,4,5).[21] Therein, Grabowsky and co-workers stated that looking at only one type of bonding analysis leads to an incomplete understanding of the bonds true nature. In NBO calculations, the negative hyperconjugation is increasing with the Si–O–Si bond angle, as the ionicity is simultaneously growing. In Quantum Theory of Atoms in Molecules (QTAIM), Natural Population Analysis (NPA) and Hirshfeld-I Charges calculations, a similar increase in both negative hyperconjugation and ionicity was confirmed. In terms of the Roby-Gould index, a parallel increase in covalent and ionic bond indices was found suggesting an equally important influence of both explanations. The authors argue that instead of an ongoing controversy, scientists should take this once labelled “elusive bond”[22] as indicator that single Lewis-formulary could never fully explain the real bonding situations in molecules, particularly when ion pairs and hyperconjugation effects play an important role.[21] Following, Apeloig[23] and Cypryk[24] have shown that adequate description of the siloxane bond is becoming even more difficult when more than one Si–O bond is located at the silicon centers like it is predominantly found in nature. Additional hyperconjugative interactions of the type $n(O)\rightarrow\sigma^*(SiO)$ are needed to complete the electronic description of the structural motif (Figure 3.3).

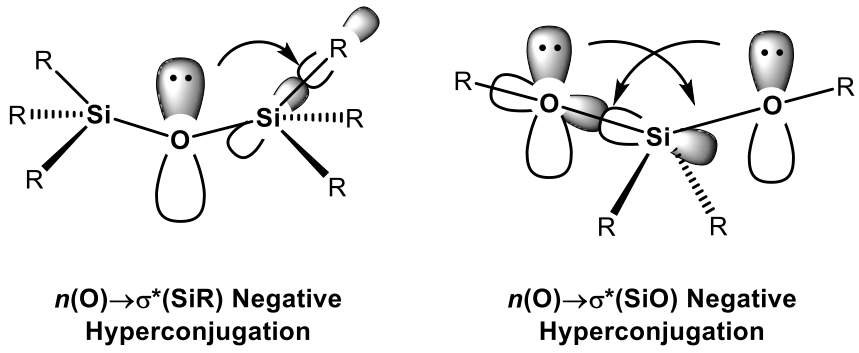

Figure 3.3. Structures highlighting the different orbital interactions in siloxane bonds.

These hyperconjugative interactions were found to play a significant role for the explanation of the low basicity and stereoelectronic arrangements of such compounds.[23,24] Even small anomeric effects can be deduced from that type of interaction, albeit much smaller than in analogous carbon-based compounds. Nonetheless, the authors suggest that these effects are strong enough to influence or even determine the structure of such silicon molecules.[23] It is evident that silicates and silicones, as omnipresent silicon materials in nature, industry, and our everyday life, can be electronically described by all the above discussed contributions. We need an ionic description of the Si–O bond *and* the hyperconjugative description of $n(O) \rightarrow \sigma^*(SiX)$ (X = H, C, O) in order to fully explain their physical and chemical stability.

1.2 Synthetic methodologies for siloxane preparation

Industrial synthesis of silicones has become more and more important since the introduction of the Müller-Rochow process in the 1940s in which the direct preparation of chlorosilanes from silicon and chloromethane is described together with the hydrolysis and follow-up polycondensation (Scheme 1.1, left).[25] Since then, the production of silicones has multiplied to an estimated amount of 8.1 million tons per year in 2020.[26] The type of produced polymer can easily be controlled by choice of chlorosilane stoichiometries. Higher $MeSiCl_3$ amounts therefore lead to a high degree of cross-linked fragments while higher quantities of Me_2SiCl_2 results in rather linear polymers. Additionally, Me_3SiCl acts as polymerization stopper and is therefore of great importance for controlling the average weight distribution of the produced silicones.

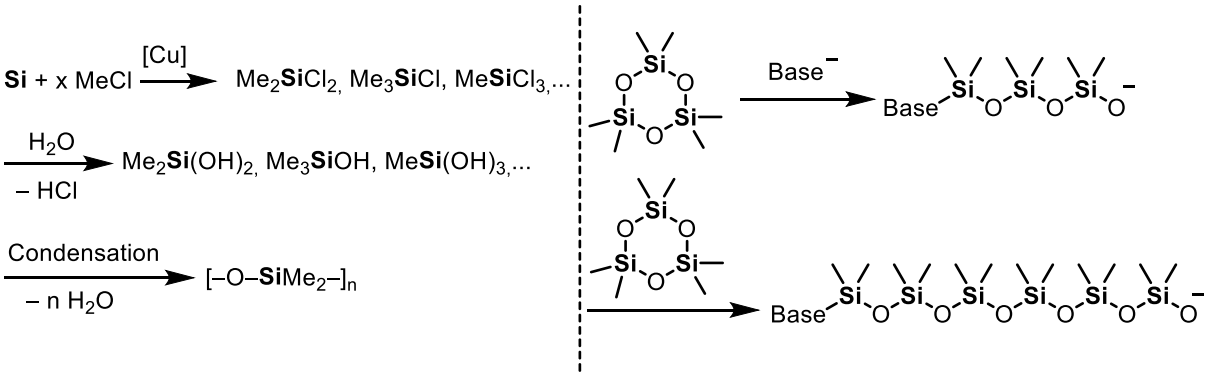

Scheme 1.1. Müller-Rochow process (left) and modern anionic ROP of cyclic oligosiloxanes (right). Only the chain initiation and growth for hexamethylcyclotrisiloxane (D_3) is shown.

However, the controllability of the polymerization degree of this “direct synthesis” method is far from perfect. Modern industry thus often relies on cyclic oligosiloxanes as precursors for ring-opening polymerization (ROP) in order to obtain narrower molecular weight distributions.[27] The most common procedure is the anionic ring-opening polymerization (Scheme 1.1, right) where a

variety of different polymerization initiators have been developed such as KOH,[28] ammonium salts, phosphonium salts, phosphazene bases[27,29] and more recently also nitrogen bases like N-heterocyclic carbenes (NHC's)[30] or bicyclic guanidines.[31] Nonetheless, by-products such as smaller or bigger cyclic siloxanes can never be fully prevented which is why research in controlled formation of specific siloxane compounds remains highly important.[27] Many research laboratories focus on the use of chlorosilanes and silanolates or silanols for a controlled build-up of specific siloxane compounds.[32–36] For the preparation of small and defined disiloxane compounds in laboratory scale, the silanols which should be reacted with a chlorosilane are metalated with alkaline metal reagents like *n*BuLi, NaOH or KOH beforehand. This method makes the silanol more reactive, resulting in higher yields and ease of workup as the only by-product is the metal chloride salt (Scheme 1.2, left).[32,33] The other method involves direct mixture of the chlorosilane and the silanol. An additional base – mostly triethylamine or pyridine – must be added to quench the formed hydrogen chloride with concomitant formation of the respective ammonium salt (Scheme 1.2, right).[34–36]

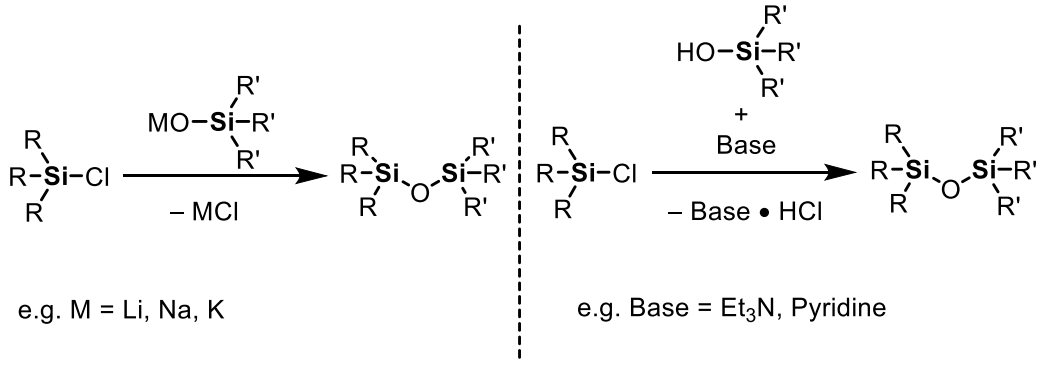

Scheme 1.2. General scheme for the transformation of a chlorosilane with a silanolate (left) and a silanol (right).

By application of these easy and straightforward synthetic methods, several oligosiloxanes have been prepared and studied as model compounds in materials science[35,37] and catalysis.[38] Their synthesis and reactivity[32,39,40–42] along with their structural analysis[40,43] has also been studied extensively. Due to the high chemoselectivity and the driving forces of salt and Si–O bond formation, this methodology often is the choice for small-scale synthesis of well-defined oligosiloxanes in laboratories. Our group has recently demonstrated that even asymmetrically functionalized disiloxanes can be easily prepared using a lithium silanolate and dichlorodiphenylsilane in a molar ratio of 1:1 to selectively substitute only one of the two Si–Cl units.[42]

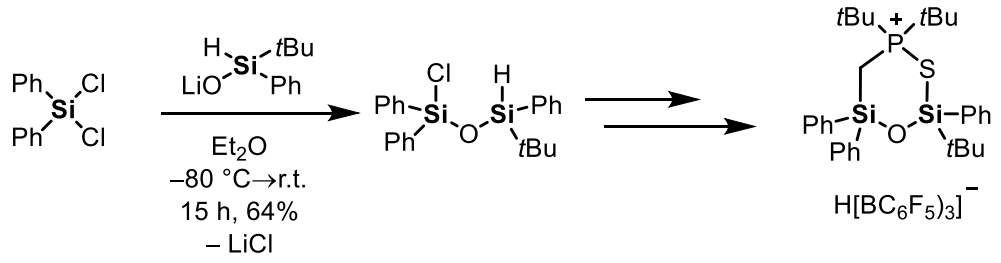

Scheme 1.3. Synthesis of an asymmetrically substituted disiloxane as precursor for a hidden silylium-type siloxane.[42]

Using this controlled mono-siloxylation of the dichlorosilane, it is possible to end up with a chlorosiloxane, which is easy to further functionalize. Thus, a phosphine group could be introduced which was then oxidized with sulfur. After addition of $B(C_6F_5)_3$ and subsequent abstraction of the silicon-bound hydride, a ring closure was observed to obtain a formal six-membered cyclic phosphonium ion which is capable of thermal fluoride abstraction from the perfluorated borate counterion upon heating to 120°C (Scheme 1.3).[42] This work not only demonstrates the still important use of the siloxane synthesis based on chlorosilanes and silanolates but also emphasizes the importance of structurally controllable Si–O–Si formations in general. As convenient as the formation of ammonium or alkaline metal halides might be due to their rather easy removal in laboratory scale, it displays a big hinderance for big scale applications in industry. The stoichiometric formation of salts and the additional need of acid scavengers or metalation agents makes production costly and non-profitable. Therefore, different approaches for siloxane formation are increasingly being pursued in academic research. Next to rather "exotic" approaches like the insertion of O_2 into disilenes $R_2Si{=}SiR_2$ followed by hydrolysis[44], more common methods using other leaving groups than halides have emerged. Aminosilanes represent easily accessible molecules which can be transformed into siloxane compounds by simple reaction with silanols without the need for further reagents.[32,45–47] Bauer and Strohmann developed the use of pyrrolidine-substituted silanes and showed that the aminosilane readily reacts with triphenylsilanol (Scheme 1.4).[46]

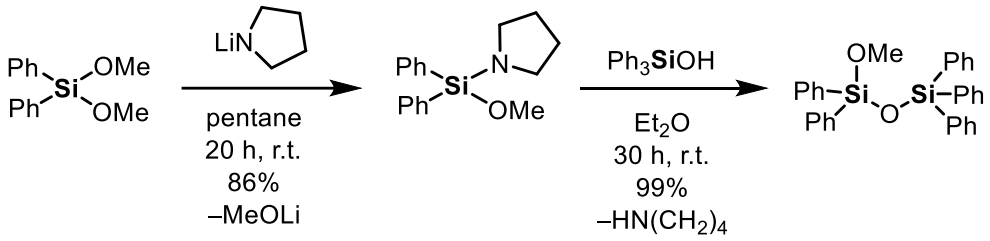

Scheme 1.4. Synthesis of an aminosilane and further reaction to a siloxane.[46]

They demonstrated the easy preparation of mixed *N,O*-functionalized organosilanes by selective substitution of a methoxide by a lithium amide. Albeit going from a thermodynamically more favored Si–O to a less preferred Si–N bond, they suggested an overall favorable thermodynamic reaction based on DFT calculations due to the salt formation of LiOMe and aggregation effects. The thereby synthesized mixed-functionalized silanes offer versatile possibilities for functionalization as it can selectively undergo stepwise substitutions by hydroxy groups or lithiated nucleophiles due to the different reactivity of the Si–NPyr and Si–OMe moieties. It can therefore give rise to siloxane compounds with methoxide substituents as precursor for even further functionalization.[46] The by-product formed in the amine substitution reactions is pyrrolidine which can be easily removed from the mixture by evaporation techniques making this strategy highly applicable not only for laboratory scale, but also for industrial purposes. However, production of such aminosilanes usually starts from chloro- or alkoxysilanes in which undesired solid by-products are formed.[47] In order to fully overcome this problematic need for stoichiometric

reagents and by-product removals, a range of catalytic siloxane formations has been developed to date. Many of those use transition metal salts or complexes of palladium,[48] rhodium,[49,50] ruthenium,[51] gold,[52] platinum,[53] molybdenum[54] cobalt[55] or iron[56] but also main group metal catalysts such as barium,[57] bismuth, [58–61], boron[62–65] or potassium[66,67] have been developed to bypass the need of expensive *d*-block metals. Already in 1980, Michalska has studied the couplings of hydrosilanes and silanols with a series of rhodium (I) complexes.[49] By using Wilkinson's catalyst [$(PPh_3)_3RhCl$], he reported quantitative coupling reactions of the starting materials at ambient pressures and temperatures already after minutes. Based on known reactivities of transition metals towards hydrosilanes in homogeneous catalysis, Michalska proposed a mechanism involving oxidative addition of the Si–H bond to the metal center followed by nucleophilic attack of the silanol onto the rhodium-bound silicon. Subsequent elimination of the newly formed siloxane affords an intermediate dihydride rhodium complex which produces the active catalyst species after reductive elimination of H_2 (Scheme 1.5, left).[49]

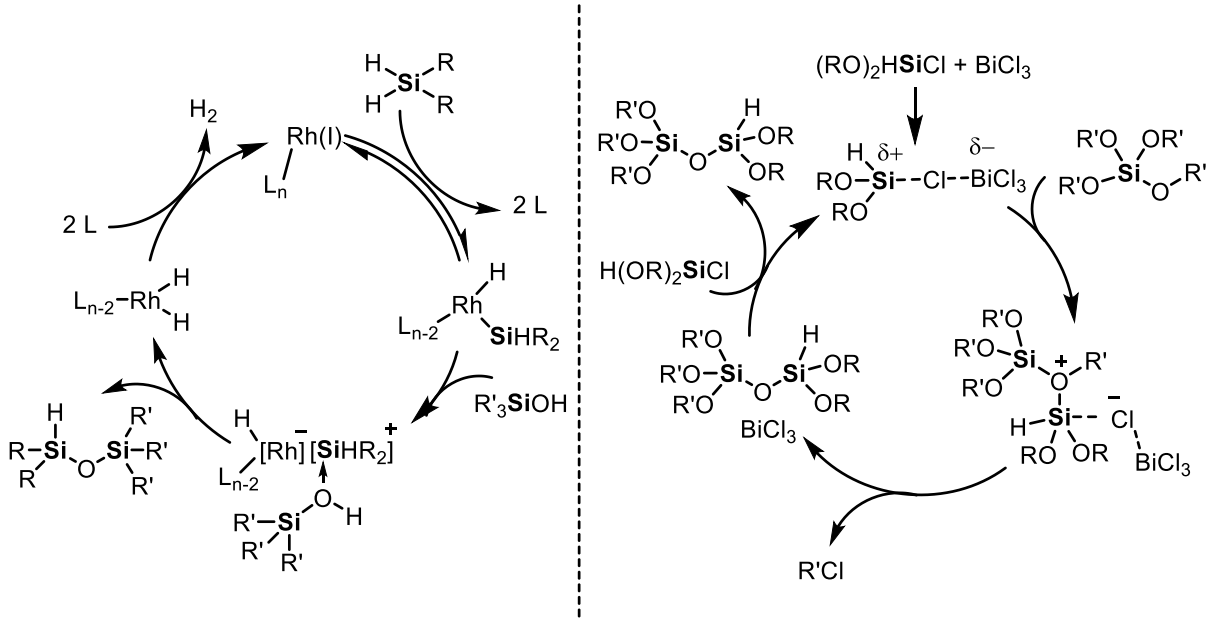

Scheme 1.5. Rhodium(I) (left) [49]) and $BiCl_3$ catalyzed (right)[58] siloxane formation. The mechanisms were proposed by the authors of the respective publications.

Main group metals on the other hand typically catalyze these reactions via their Lewis acidic character. $BiCl_3$ for example can coordinate to the chlorine atom in chlorosilanes and make them more reactive towards substitution by silanols or alkoxysilanes.[58,60,61] Wakabayashi *et al.* have impressively demonstrated the reactivity for the selective synthesis of some cross-linked oligosiloxanes with alkoxy substitution.[58] They reported the use of alkoxysilanes instead of silanols which extends the range of application by eliminating the limitation to stable silanols that are not prompt to self-condensation. The prepared siloxanes offer the possibility to be further altered in a precise way or in polymerization processes. Wakabayashi *et al.* additionally proposed a mechanism where the $BiCl_3$ catalyst first activates the Si–Cl bond and then a nucleophilic attack of the alkoxysilane onto the silicon atom occurs, leading to an intermediate oxonium cation. Following, alkyl chlorides are formed via rearrangement reactions and are removed from the

system leaving the desired siloxane compound (Scheme 1.5, right).[58] However, such main group metal catalysts like $BiCl_3$ typically do not work for hydrosilanes which are preferentially used over chlorosilanes in industry given their non-toxic and easy to handle properties. Another breakthrough in this regard was achieved when the groups of Piers and Rubinsztajn independently published conversions of hydrosilanes with a variety of nucleophiles catalyzed by the cheap and available borane $B(C_6F_5)$.[62–65,68,69] The discovery of these so called Piers-Rubinsztajn (PR) reactions have led to many applications in synthetic laboratories for the selective preparation of siloxane compounds.[70,71–75] Early examples of this reactivity used hydrosilanes together with silanols for creation of Si–O–Si bonds as direct replacement for transition metal complexes. In 2005, Zhou and Kawakami proved on a model system that chiral oligosiloxanes with well-defined structural patterns and optical activities can be produced by reaction of chiral dihydroxydisiloxanes with aryl-disilane linkers using $B(C_6F_5)_3$ as a catalyst (Scheme 1.6, top)[76]

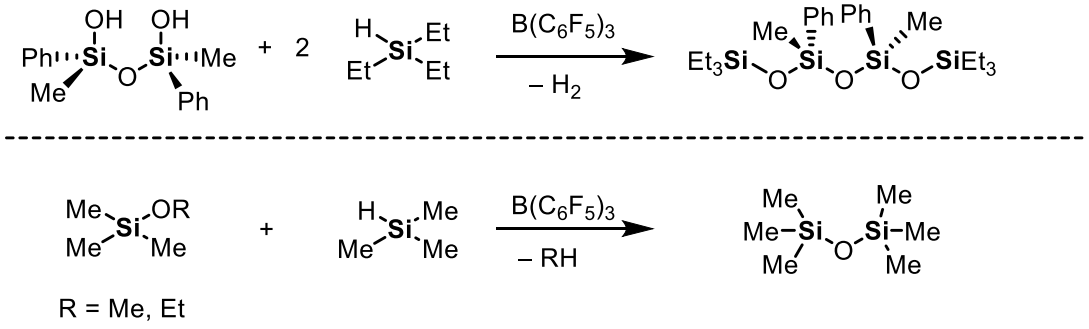

Scheme 1.6. Piers-Rubinsztajn reactions starting from hydrosilanes[76] with silanols (top) and alkoxysilanes[64] (bottom).

In this well-elaborated publication, the authors compared $B(C_6F_5)_3$ with a series of Pd- and Rh-based transition metal catalysts and demonstrated the dominance of the borane in terms of conversion, selectivity and stereochemical control.[58] The drawback, once again, for this procedure lays within the use of silanols or siloxanols which tend to self-condense and therefore limit the scope. However, Rubinsztajn himself has shown already in 2005 that hydrosilanes can also react with alkoxysilanes instead of silanols (Scheme 1.6, bottom).[64] Alkoxysilanes are easily producible and stable molecules which could therefore expand the possible scope of siloxane formations. Alkanes, mainly methane and ethane, are formed as sole by-products which can be removed from the reaction mixtures without difficulty.[64,77] This procedure has been applied in a variety of controlled syntheses of polysiloxanes to date.[72,74,75,78] From a mechanistic point of view, the borane activates the Si–H bond and reacts via an oxonium ion followed by hydride transfer step (Scheme 1.7).

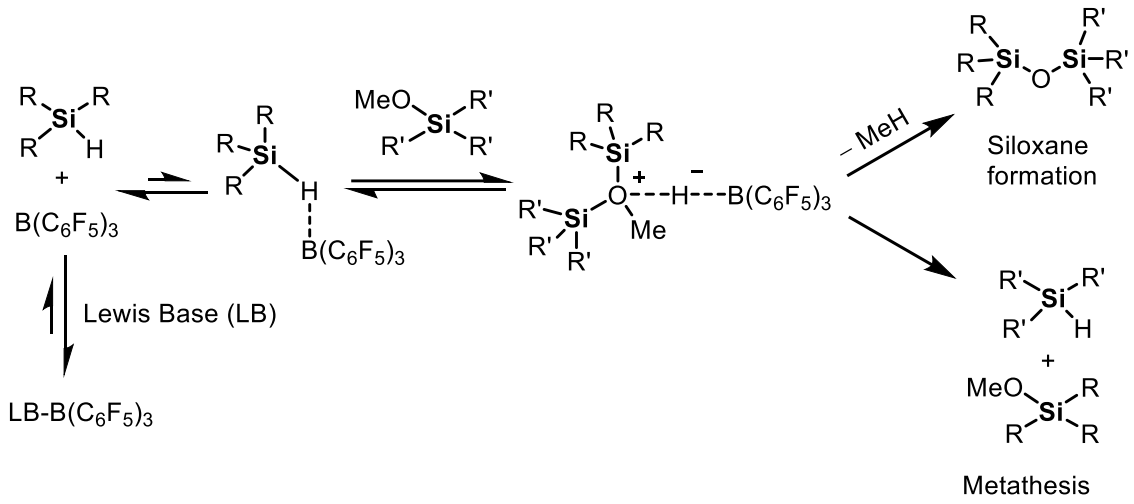

Scheme 1.7. Mechanism of the Piers-Rubinsztajn reaction of hydrosilanes with alkoxysilanes.[69,71]

A competition in the hydride transfer step occurs in which the hydride can go either to the alkoxy-carbon or the other silicon atom. Especially for secondary alkoxides, the latter metathesis reaction is facilitated leading to an exchange of hydride and alkoxide in the silane reagents followed by new siloxane formations to obtain undesired self-condensed siloxanes. To prevent this metathesis path, most examples use either methoxy- or ethoxysilanes and exploit the high driving force of alkane removal. Additional Lewis basic functions within the system like amines, thiols or epoxides will lead to side reactions or complete inhibition of the PR reaction due to Lewis Base/Acid interactions.[69,71] An elegant application of the PR reaction combined with iridium-catalyzed hydrosilylation was given by Matsumoto *et al.* in 2017.[79] Their strategy allows the preparation of oligosiloxanes without any by-product formation. They used a silyl ester and a hydrosilane to perform a hydrosilylation reaction which is catalyzed by $[Ir(coe)_2Cl]_2$ to obtain a disilyl acetal. A controlled rearrangement takes place that exploits the known side reaction of $B(C_6F_5)_3$ catalyzed siloxane formations. This sequence results in the formation of an alkoxysiloxane which can further react with hydrosilanes towards oligosiloxanes (Scheme 1.8).[79]

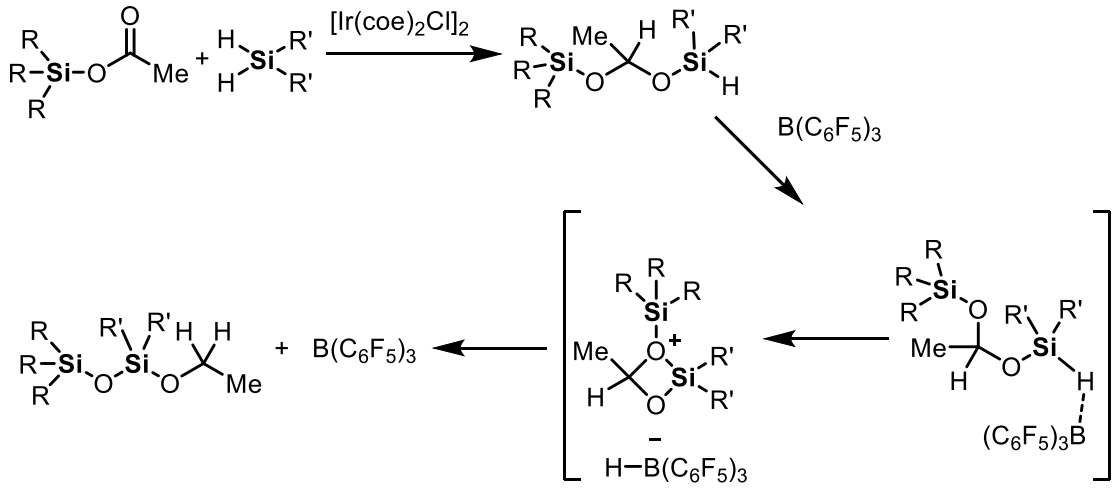

Scheme 1.8. General scheme for by-product-free oligosiloxane formations via combination of Ir(I) and $B(C_6F_5)$ catalysis (left).[79]

This procedure allows for the controlled build-up of unsymmetrical siloxane scaffolds without creating by-products that must be removed. However, it is limited to small oligosiloxanes and is therefore less interesting for polymer science. This problem has been tackled by Matsumoto and Sato only one year later in 2018 when they published a $B(C_6F_5)_3$-catalyzed iterative one-pot synthesis of siloxanes.[73] In this well-elaborated work, they described the utilization of *iso*-propyloxy-substituted silanes and their transformation with any dihydrosilane to form a hydrosiloxane following the PR procedure (Scheme 1.9).

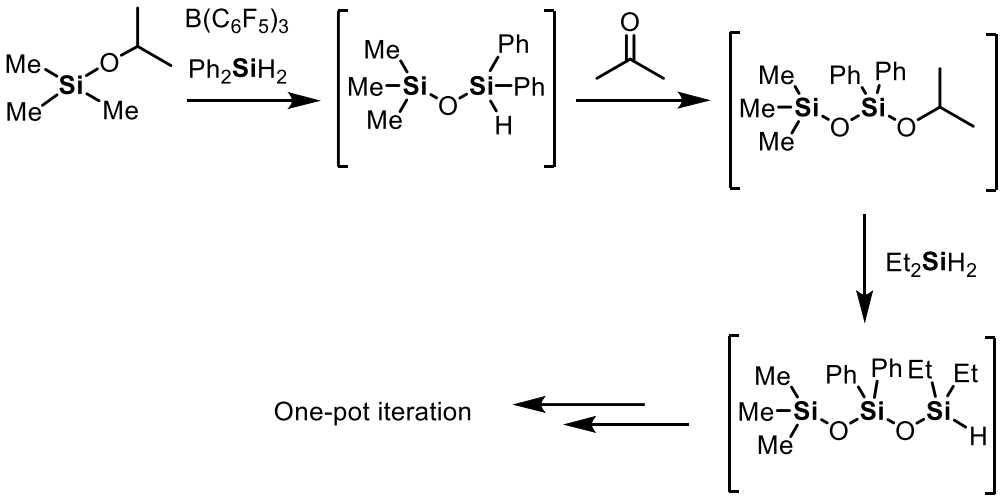

Scheme 1.9. General scheme for the sequence-controlled siloxane build-up (right).[73]

Iterative addition of equimolar amounts of acetone and a dihydrosilane resulted in the stepwise formation of alkoxysiloxanes and hydrosiloxanes which can selectively be further expanded. By choice of the added silane, Matsumoto and Sato controlled the substitution pattern of the formed oligo or polysiloxane. The chain length was easily regulated by the number of acetone/silane additions.[73,80] Despite all advantages of the PR reaction, it naturally also carries some drawbacks. This involves the aforementioned rearrangement reactions, inhibition of the reaction if two or more electronegative substituents are bound to the hydrosilane[64] and inhibition of the catalyst if thiols, amines or epoxides are present.[71] Its catalytic deterioration by the presence of moisture also displays a significant hinderance for industrial application.[62,81] For this reason, there is still an intensive search for new methods for the selective production of tailor-made siloxane compounds. Some recent examples involve the use of cheap potassium hexamethyldisilazane (KHMDS) for the catalytic synthesis of oligosiloxanes from hydrosilanes[67] or alkynylsilanes[66] with silanols or the catalyst-free reaction of silanols with disilazanes as silylation agents.[61] The latter one exploits the labile Si–N bond in disilazanes, which will be the subject in this work as well. Additionally, also transition metal catalysis remains prominent in recent literature, as impressively demonstrated by Zhu *et al.* They reported on the enantioselective dehydrogenative Si–O coupling to synthesize chiral siloxanes using $[Rh(cod)Cl]_2$ as pre-catalyst and Josiphos as an additional chiral ligand. Not only could they report high *ee* values of up to >99% for a library of different hydrosilane precursors and silanols, but also the potential application of such siloxane compounds in optoelectronic materials.[82] This example

from 2021 once more highlights the ongoing importance of controlled preparation of siloxanes and *Si*-stereogenic compounds in synthetic chemistry and materials science.

1.3 Concepts for decomposition of siloxane compounds

Regarding the facts that silicone polymers are produced in such high amounts and that they are chemically and mechanically very robust, it is evident that agglomeration in nature is becoming more and more problematic. To tackle this problem, research laboratories have taken a look at different approaches to cleave the strong Si–O–Si bond. Already back in the 1980s, some groups have investigated the influence of additives on the equilibrium between siloxanes and their cleavage products. It has been discovered by Pappas and co-workers that amines are able to completely dissolve cross-linked polysiloxanes based on their influence on the siloxane bond. Especially at crosslinking sites with the general formula $Si(OR)_4$ where the central silicon atom is the most electrophilic, aliphatic amines insert into the Si–O–Si bond to some extent creating a silanol function alongside a silylamine group (Scheme 1.10).[83,84]

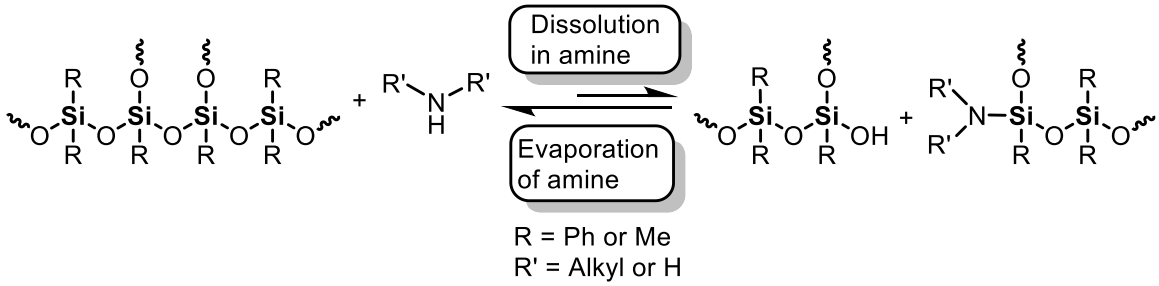

Scheme 1.10. General scheme for the influence of aliphatic amines on crosslinking sites of polysiloxanes.[83]

This aminolysis reaction was observed only when the amines were used in high excess after dissolving the polymers in them. The proposed equilibrium lies predominantly at the siloxane side owing to the significantly more stable Si–O bond compared to the Si–N bond. It is therefore forced to the siloxanol and aminosiloxane side by the high excess of amine. Removal of the amines *in vacuo* resulted in the re-formation of the siloxane motifs which supported the author's proposal of the species being in equilibrium. The same equilibrium has been confirmed also for linear silicone polymers, albeit even less pronounced than in the cross-linked congeners.[85] The addition of bases such as KOH or NaOEt to the amine resulted in a significantly enhanced cleavage ability.[85] Chang and Lin compared the efficiency of ethanolysis to aminolysis of silicone polymers and found that the latter one dominates the reaction kinetics and is therefore more suitable when it comes to the objective of silicone degradation.[86] Furthermore, the equilibrium between siloxane and silanol was found to be strongly influenced also by addition of Brønsted acids.[87] *Ab initio* calculations by Cypryk and Apeloig have shown the high impact of silyloxonium species in the ring opening polymerization of cyclic siloxanes which are created by addition of acids.[88,89] Hydrogen bonding strongly affects the kinetics of the polymerization/depolymerization process in

silicones, but also depends on the presence of water.[90] It has been demonstrated through a series of theoretical calculations that water is lowering the activation energy for the condensation/hydrolysis process by reducing angular strain.[89,91] All these contributions highlight the importance of equilibria in siloxane chemistry but also the difficulty in precise determination of reaction products. Therefore, also stoichiometric degradation reagents have been developed to ensure a more controllable decomposition of siloxanes. Dimethylcarbonate for example, has been described as a non-toxic and inexpensive reagent for the controlled decomposition of silica[92] or oligo- and polysiloxanes.[93] It allows for the selective production of tetramethoxysilane which can be further used in sol-gel processes to produce new polysiloxanes and therefore is of great importance for silicone recycling.[94] Other recycling strategies focus on the catalytic degradation of polymeric siloxanes. This has been demonstrated using acids and bases like triflic acid[95] and potassium hydroxide[85,95] but also reliably using fluoride agents like tetrabutylammonium fluoride ($Bu_4N^+F^-$) [95,96] or boron trifluoride etherate (BF_3•OEt_2).[97,98] The latter two exploit the formation of Si–F bonds which are amongst the strongest single bonds known with a bond strength of 582 kJ/mol. Rupasinghe and Furgal proposed for $Bu_4N^+F^-$, that the fluoride ion cleaves a Si–O bond and forms a smaller polysiloxane which can undergo fragment rearrangements resulting in cyclic oligosiloxanes after quenching the catalyst with $CaCl_2$.[96] Enthaler and co-workers on the other hand, demonstrated that BF_3•OEt_2 can be used to depolymerize linear, branched, and cross-linked end-of-life polymers into methylfluorosilanes $Me_{4-n}SiF_n$ and tetramethyldifluorodisiloxane (Scheme 1.11, left).[97,98]

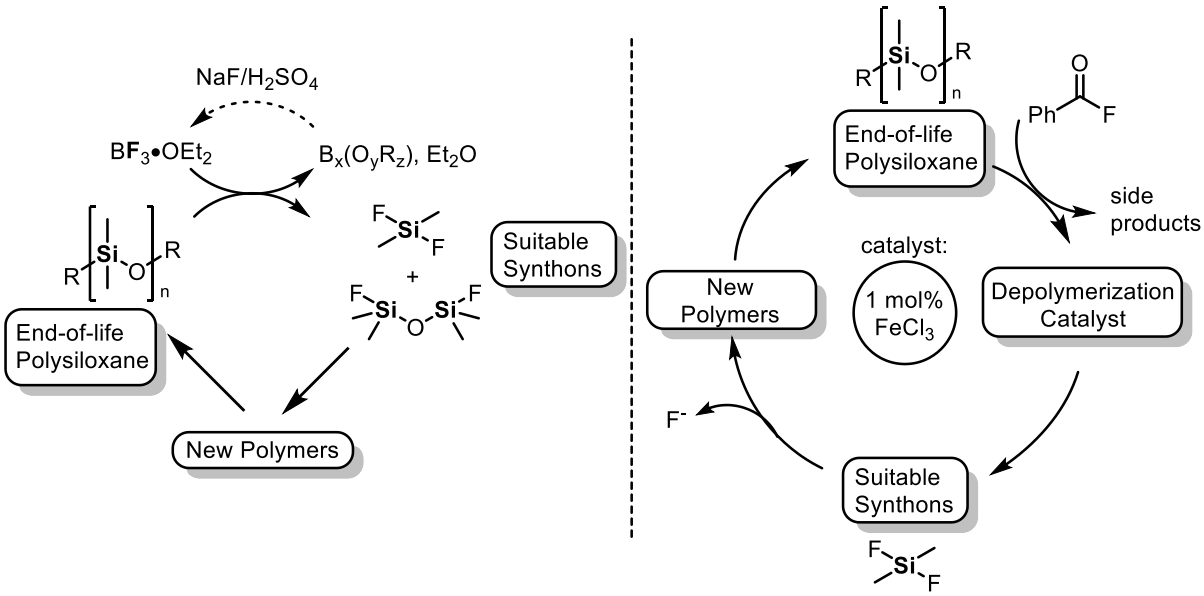

Scheme 1.11. General scheme for the depolymerization of end-of-life silicones with BF_3•OEt_2 (left)[98] and Fe(III) catalysis (right).[99]

In this sustainable catalysis, the depolymerization products Me_2SiF_2 and $Me_2FSiOSiFMe_2$ were additionally identified as well-suited precursors for the synthesis of new polymers only by reaction with water and bases like sodium hydroxide. Additionally, also the borane by-products $B_x(O_yR_z)$ can be easily converted back into BF_3 by addition of NaF and H_2SO_4.[98] Similar fluorination

reactions using benzoyl fluoride and inexpensive metal catalysts based on zinc and iron have also been established by Enthaler *et al.* (Scheme 1.11, right).[99,100] All the previously demonstrated methodologies focus on the degradation of polysiloxanes as direct recycling strategies to approach the pollution problem and ensure for a more sustainable preparation of silicone polymers. However, cleavage of Si–O–Si bonds can also give rise to very interesting new materials which are not necessarily associated with recycling backgrounds. Early cleavage attempts of oligosiloxanes using alkyllithium reagents were carried out already in the 1950s by Frye *et al.*[101] and Gilman *et al.*[33] who independently found that lithium siloxides are formed selectively. Sieburth and Mu expanded the understanding of these transformations by using different alkyl lithium reagents to produce silanolates and silanols.[102] Later on, alkyl aluminum reagents have been applied for cleavage of siloxanes in which the formed alumosiloxides were observed to exhibit interesting molecular structures.[103] In the following years, these so-called "metallasiloxides" have been prepared with transition[104] and main group metals[105] leading to a fascinating new chemistry. From water-stable complexes[41,106] over model compounds for ceramics[34,107,108] and hydrogen bonding[109] to transition metal catalysis,[110] metallasiloxides have found increasing popularity as structural motifs. An impressive example is given by Limberg and co-workers who synthesized a dinuclear Fe(II) complex from an oligosiloxane by simple treatment with sodium methoxide and iron(II) triflate (Scheme 1.12).[107]

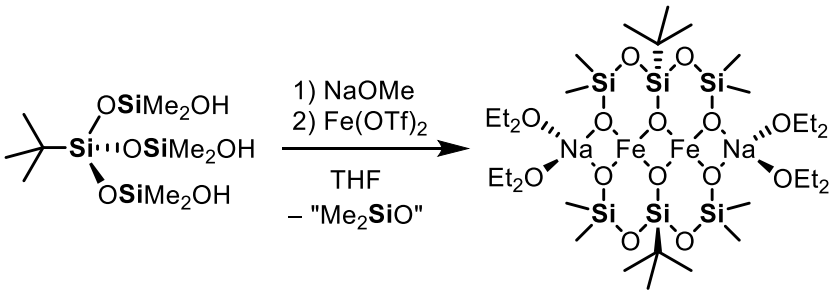

Scheme 1.12. Synthesis of a dinuclear Fe(II) siloxide complex.[107]

The obtained square planar complex is formed after deprotonation of the Si–OH groups and cleavage of one of the Si–O–Si bonds. Workup with Et_2O seemed to be crucial for the formation of the obtained product. The authors argued that the square planar FeO_4 motif is significantly more stable than the structure that would be given without any siloxane decomposition. Such pattern was not observed for its zinc analogue and is hoped to influence the research on new ceramic materials due to its resulting robustness.[107]

1.4 Aminosilanes as versatile reactive silicon-based compounds

When we think of different possibilities for the functionalization of amines with silyl substituents, we will find three different types. One is the threefold silylated nitrogen atom which is labelled as “trisilylamine” and the second is a nitrogen atom substituted with two silyl groups called “silazane”. Especially silazanes count as a very important class of compounds as they have found widespread use in polymer and materials science.[111] This thesis however, will primarily deal with the third type of Si–N containing species bearing only one silicon atom with one or more amine substituents called “aminosilanes” (sometimes also referred to as “silylamines”). Such aminosilanes can be easily prepared following standard functionalization procedures like the reaction of chloro- or alkoxysilanes with amines or their alkali metal salts (s chapter 1.2).[47,112] Another less common synthetic method involves the migration of silyl groups from a disilazane to a primary amine. The reaction is facilitated by the formation of ammonia, which is more volatile than the starting primary amine and therefore drives the reaction.[113] Additionally, lithium amides can be used to functionalize Si–H groups under formation of LiH as by-product (Scheme 1.13, left).[112] The reaction of hydrosilanes with amines can be likewise achieved without the formation of undesired solid by-products. Instead, the release of gaseous H_2 is anticipated. This so-called dehydroamination of silanes has been achieved catalytically using transition-,[114] main group-[115,116] and rare-earth[117] metal-based complexes.

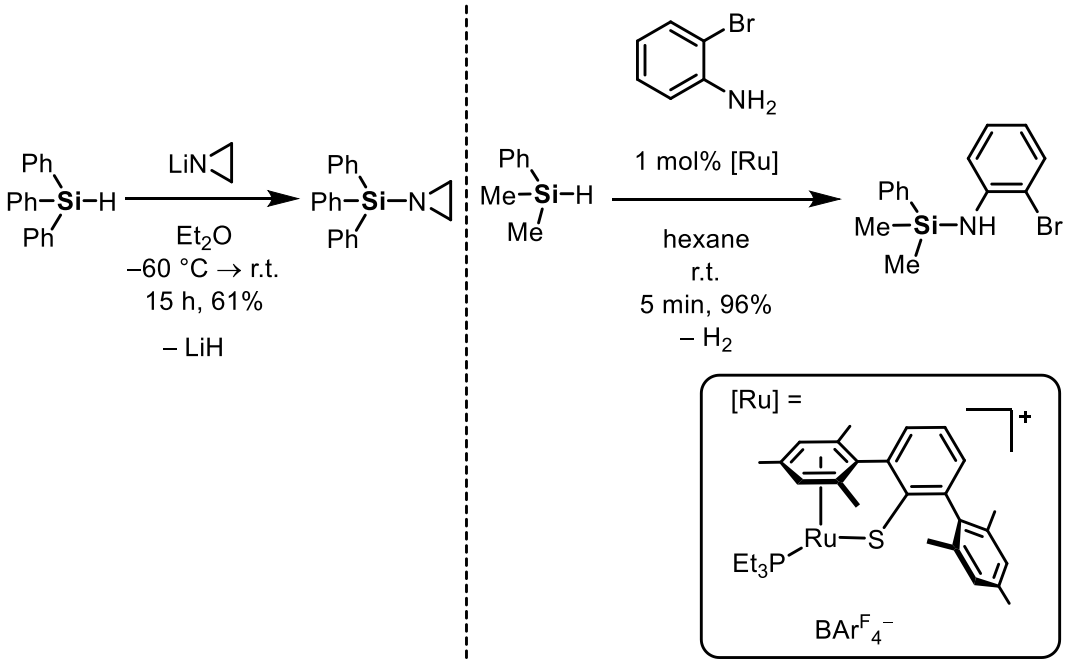

Scheme 1.13. Examples for stoichiometric (left)[112] and catalytic (right) preparation of aminosilanes.[116]

For instance, Oestreich and co-workers reported on the dehydrogenative Si–N coupling of hydrosilanes with heteroarenes or aryl-substituted amines with the use of a cationic ruthenium complex featuring a thiolate ligand. Their ruthenium catalyst proved highly active for the reaction

of dimethylphenylsilane with a series of aniline and indole derivatives. The best result was achieved in the reaction with *ortho*-bromoaniline in which a yield of 96% was obtained at ambient conditions already after five minutes (Scheme 1.13, right). The authors proposed a homogeneous mechanism in which a Ru–H complex and a sulfur-stabilized silylium ion take part after heterolytic cleavage of the labile Ru–S bond.[116] The research in the field of new aminosilane moiety preparation remains of high importance as the Si–N functionality enjoys high popularity in organic and medicinal chemistry in form of protecting group agents for alcohols, aldehydes and ketones.[118] Their advantage thereby lies in the easy hydrolysis of the silicon-nitrogen bond and consequently the straightforward removal of the protecting group. As stated also in chapter 1.2, this behavior also finds application in the mild-condition functionalization of silicon compounds. Aminosilanes can undergo self-condensation reactions,[119] hydrolysis or reaction with alcohols, thiols or silanols, for instance.[47] Diverse possibilities for the selective preparation of a manifold of functionalized silanes is feasible by the use of this compound class. Additionally, the introduction of Si–N functions can be useful in the field of insertion reactions. Specifically designed aminosilanes were found to react with unsaturated molecules like CO_2, CS_2 or other cumulenes.[120] Especially CO_2 insertion into the Si–N bond represents an important topic in current carbon capture research and has been widely studied in recent years. Groundbreaking results in that field were presented by Kroke[121] and Stephan.[122] While Kroke and co-workers introduced a high-pressure autoclave method for the insertion of CO_2 into silicon nitrogen bonds to produce isocyanides, Stephan and co-workers designed the method in a way that selectively delivers urea derivatives.

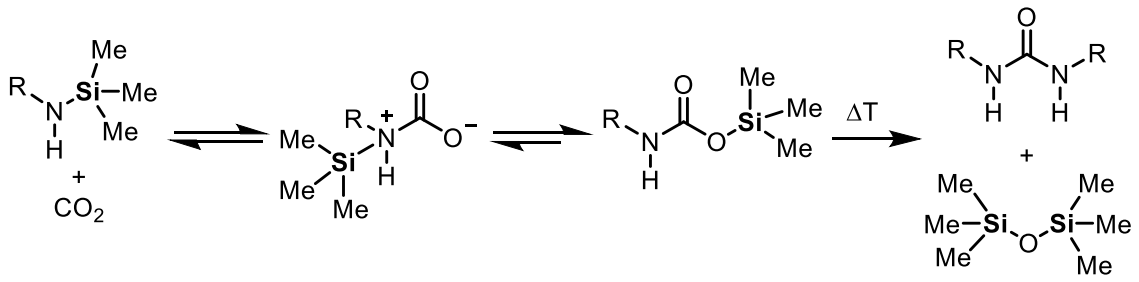

Scheme 1.14. General scheme for the CO_2 insertion into aminosilanes for the synthesis of urea derivatives. The pathway was proposed by the authors of the publication[122]

Stephan and co-workers proposed a reaction pathway in which the nitrogen atom attacks at the CO_2 molecule creating a zwitterionic intermediate which rearranges to a silylcarbamide (Scheme 1.14). The carbamides were stable and could be isolated. In screening reactions, the authors optimized the reaction conditions and suggested temperatures of 120°C, reaction time of 30 min and 5 atm of CO_2 pressure in pyridine for these reactions. Heating to 120–150 °C for additional time afforded the desired urea derivatives with hexamethyldisiloxane as a sole by-product. Their method therefore can be used for sustainable synthesis of urea derivatives from CO_2 as feedstock and the authors propose an application in the selective ^{13}C labelling of ureas. Another area of aminosilane research focuses on the introduction of chiral amines for the preparation of *Si*-stereogenic compounds. Enantiomerically or diasteriomerically enriched silanes

have found impressive applications in protecting group chemistry,[123] kinetic resolutions of chiral alcohols[124] or medicinal chemistry.[125]

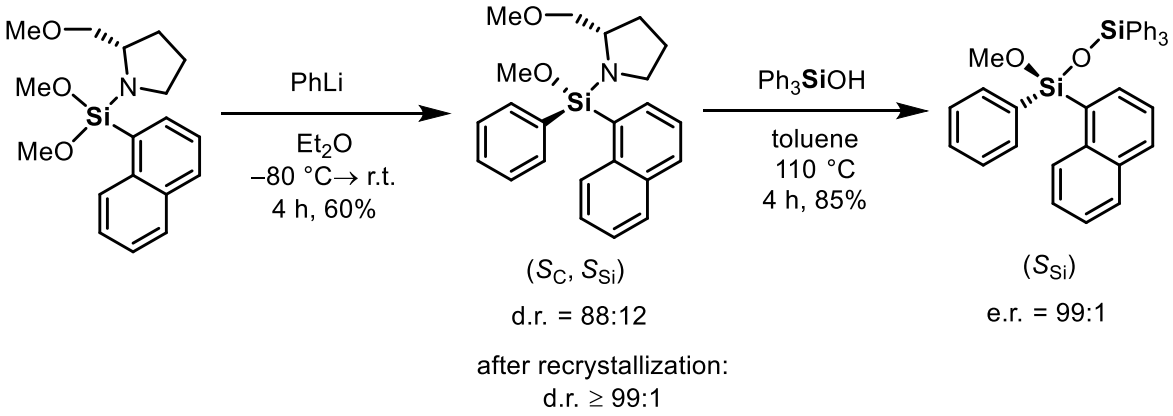

Scheme 1.15. Synthesis of chiral aminosilanes and application in chiral siloxane preparation.[45]

In a well-elaborated work by Bauer and Strohmann, an easy and straightforward synthesis of *Si*-chiral diastereomers was demonstrated by simple use of an α-chiral pyrrolidine substituent (Scheme 1.15). In this exemplary reaction, the formation of the *Si*-stereogenic silane was achieved after reaction of the prochiral dimethoxysilane with phenyllithium in which a stereoinduction with a diastereomeric ratio of 88:12 was observed. Simple recrystallization from pentane solution afforded the optically pure aminosilane and the absolute configuration of the silicon center could be assigned by single-crystal X-ray crystallographic analysis. Using the easy-to-cleave Si–N functionality combined with the known configuration of the chiral silane, they were able to study the stereochemical outcome after substitution of the chiral amine with nucleophiles like triphenylsilanol. By doing this, they discovered the substitution attack to perform under inversion of configuration at the silicon.[45] Examples like this highlight the importance of chiral amines to create *Si*-stereogenic compounds for the elucidation of mechanisms in silicon chemistry. Such investigations are fundamental to the understanding of silicon-based reactions and will also be touched in the premise of this thesis.

1.5 References

[1] T. W. Swaddle, J. Salerno, P. A. Tregloan, *Chem. Soc. Rev.* **1994**, *23*, 319–325.

[2] N. Wiberg, G. Fischer, A. F. Holleman, E. Wiberg, Lehrbuch der Anorganischen Chemie, De Gruyter, Berlin, Boston, **2008**.

[3] M. Sumper, E. Brunner, *Adv. Funct. Mat*. **2006**, *16*, 17–26.

[4] N. Kröger, R. Deutzmann, M. Sumper, *Science* **1999**, *286*, 1129–1132.

[5] F. Liebau, Structural Chemistry of Silicates. Structure, Bonding, and Classification, Springer Berlin Heidelberg, Berlin, Heidelberg, **1985**.

[6] a) W. E. G. Müller, A. Krasko, G. Le Pennec, H. C. Schröder, *Microsc. Res. Tech*. 2003, *62*, 368–377; b) H. E. Harper, A. H. Knoll, *Geology* **1975***, 3*, 175–177.

[7] M. Castells, *The information age*. *Economy, society and culture*, Wiley-Blackwell, Chichester, West Sussex, Malden, MA, **2010**.

[8] a) T. L. Simpson, B. E. Volcani, *Silicon and siliceous structures in biological systems*, Springer-Verlag, New York, NY, **2011**; b) R. Tacke, *Angew. Chem. Int. Ed.* **1999**, *38*, 3015–3018; *Angew. Chem.* **1999**, *111*, 3197–3200; c) G. V. Gibbs, A. F. Wallace, D. F. Cox, R. T. Downs, N. L. Ross, K. M. Rosso, *Am. Mineral.* **2009**, *94*, 1085–1102.

[9] a) W. Noll, *Angew. Chem.* **1954**, *66*, 41–55; b) M. A. Brook, *Silicon in Organic, Organometallic, and Polymer Chemistry*, Wiley, New York, **2000**; c) R. G. Jones, W. Ando, J. Chojnowski (Eds.) *Silicon-Containing Polymers*. *The Science and Technology of Their Synthesis and Applications*, Springer Netherlands, Dordrecht, **2000**; d) F. Ganachaud, S. Boileau, B. Boury, *Silicon Based Polymers*. *Advances in Synthesis and Supramolecular Organization*, Springer Netherlands, **2008**; e) U. Schubert, N. Hüsing, *Synthesis of inorganic materials*, Wiley-VCH, Weinheim, Germany, **2019**.

[10] L. Pauling, *J. Am. Chem. Soc.* **1932**, *54*, 3570–3582.

[11] a) *Hydrogen Bonding Studies. V. The Relative Basicities of Ethers, Alkoxysilanes and Siloxanes and the Nature of the Silicon-Oxygen Bond1,2*, **1961**; b) R. West, L. S. Wilson, D. L. Powell, *J. Organomet. Chem.* **1979**, *178*, 5–9.

[12] R. West, L. S. Whatley, K. J. Lake, *J. Am. Chem. Soc.* **1961**, *83*, 761–764.

[13] a) I. L. Karle, J. M. Karle, C. J. Nielsen, *Acta Crystallogr. C Cryst. Struct. Commun.* **1986**, *42*, 64–67; b) V. E. Shklover, H.-B. Bürgi, A. Raselli, T. Armbruster, W. Hummel, *Acta Crystallogr. B Struct. Sci.* **1991**, *47*, 544–548; c) J. A. Tossell, G. V. Gibbs, *Acta Crystallogr.* **1978**, *34*, 463–472.

[14] a) F. Stone, D. Seyferth, *J. Inorg. Nucl. Chem.* **1955**, *1*, 112–118; b) D. P. Craig, A. Maccoll, R. S. Nyholm, L. E. Orgel, L. E. Sutton, *J. Chem. Soc.* **1954**, 354.

[15] R. J. Gillespie, S. A. Johnson, *Inorg. Chem.* **1997**, *36*, 3031–3039.

[16] a) B. T. Luke, J. A. Pople, M. B. Krogh-Jespersen, Y. Apeloig, J. Chandrasekhar, P. v. R. Schleyer, *J. Am. Chem. Soc.* **1986**, *108*, 260–269; b) S. Shambayati, S. L. Schreiber, J. F. Blake, S. G. Wierschke, W. L. Jorgensen, *J. Am. Chem. Soc.* **1990**, *112*, 697–703; c) I.-T. Moraru, P. M. Petrar, G. Nemeş, *J. Phys. Chem. A* **2017**, *121*, 2515–2522.

[17] H. Oberhammer, J. E. Boggs, *J. Am. Chem. Soc.* **1980**, *102*, 7241–7244.

[18] S. Grabowsky, M. F. Hesse, C. Paulmann, P. Luger, J. Beckmann, *Inorg. Chem.* **2009**, *48*, 4384–4393.

[19] F. Weinhold, R. West, *Organometallics* **2011**, *30*, 5815–5824.

[20] F. Weinhold, R. West, *J. Am. Chem. Soc.* **2013**, *135*, 5762–5767.

[21] M. Fugel, M. F. Hesse, R. Pal, J. Beckmann, D. Jayatilaka, M. J. Turner, A. Karton, P. Bultinck, G. S. Chandler, S. Grabowsky, *Chem. Eur. J.* **2018**, *24*, 15275–15286.

[22] G. V. Gibbs, J. W. Downs, M. B. Boisen, *Rev. Mineral. Geochem.* **1994**, *29*, 331–368.

[23] Y. Apeloig, A. Stanger, *J. Organomet. Chem.* **1988**, *346*, 305–313.

[24] M. Cypryk, *Macromol. Theory Simul.* **2001**, *10*, 158–164.

[25] a) L. Rösch, P. John, R. Reitmeier in *Ullmann's encyclopedia of industrial chemistry* (Ed.: F. Ullmann), John Wiley & Sons, [Hoboken, N.J.], **2005**; b) M. P. Clarke, *J. Organomet. Chem.* **1989**, *376*, 165–222.

[26] "Silicone production per year", can be found under https://www.statista.com/statistics/573585/global-silicon-production/.

[27] P. Dubois, O. Coulembier, J.-M. Raquez, *Handbook of ring-opening polymerization*, Wiley-VCH, Weinheim, **2009**.

[28] T. Köhler, A. Gutacker, E. Mejía, *Org. Chem. Front.* **2020**, *7*, 4108–4120.

[29] a) J. Shi, N. Zhao, S. Xia, S. Liu, Z. Li, *Polym. Chem.* **2019**, *10*, 2126–2133; b) J. Shi, Z. Liu, N. Zhao, S. Liu, Z. Li, *Macromolecules* **2022**, *55*, 2844–2853.

[30] M. Rodriguez, S. Marrot, T. Kato, S. Stérin, E. Fleury, A. Baceiredo, *J. Organomet. Chem.* **2007**, *692*, 705–708.

[31] T. Ishikawa (Ed.) *Superbases for organic synthesis*. *Guanidines, amidines and phosphazenes and related organocatalysts*, John Wiley & Sons, Chichester, UK, **2009**.

[32] N. A. Espinosa-Jalapa, J. O. Bauer, *Z. Anorg. Allg. Chem.* **2020**, *646*, 828–834.

[33] H. Gilman, H. N. Benedict, H. Hartzfeld, *J. Org. Chem.* **1954**, *19*, 419–427.

[34] K. S. Lokare, N. Frank, B. Braun-Cula, I. Goikoetxea, J. Sauer, C. Limberg, *Angew. Chem. Int. Ed.* **2016**, *55*, 12325–12329; *Angew. Chem.* **2016**, *128*, 12513–12517.

[35] J. Suzuki, A. Shimojima, Y. Fujimoto, K. Kuroda, *Chem. Eur. J.* **2008**, *14*, 973–980.

[36] M. Unno, A. Suto, H. Matsumoto, *J. Am. Chem. Soc.* **2002**, *124*, 1574–1575.

[37] a) T. Sakaguchi, A. Takeda, T. Hashimoto, *Macromolecules* **2011**, *44*, 6810–6817; b) M. Dowds, D. Bank, J. Strueben, D. P. Soto, F. D. Sönnichsen, F. Renth, F. Temps, A. Staubitz, *J. Mater. Chem. C* **2020**, *8*, 1835–1845.

[38] a) K. M. Diemoz, S. O. Wilson, A. K. Franz, *Chem. Eur. J.* **2016**, *22*, 18349–18353; b) K. M. Diemoz, J. E. Hein, S. O. Wilson, J. C. Fettinger, A. K. Franz, *J. Org. Chem.* **2017**, *82*, 6738–6747.

[39] a) I. K. Goncharova, K. P. Silaeva, A. V. Arzumanyan, A. A. Anisimov, S. A. Milenin, R. A. Novikov, P. N. Solyev, Y. V. Tkachev, A. D. Volodin, A. A. Korlyukov et al., *J. Am. Chem. Soc.* **2019**, *141*, 2143–2151; b) I. K. Goncharova, A. V. Arzumanyan, S. A. Milenin, A. M. Muzafarov, *J. Organomet. Chem.* **2018**, *862*, 28–30; c) M. N. Missaghi, J. M.

Galloway, H. H. Kung, *Organometallics* **2010**, *29*, 3769–3779; d) G. W. Ritter, M. E. Kenney, *J. Organomet. Chem.* **1978**, *157*, 75–79.

[40] W. Malisch, M. Hofmann, M. Nieger, W. W. Schöller, A. Sundermann, *Eur. J. Inorg. Chem.* **2002**, *2002*, 3242–3252.

[41] C. Golz, P. Steffen, C. Strohmann, *Angew. Chem. Int. Ed.* **2017**, *56*, 8295–8298; *Angew. Chem.* **2017**, *129*, 8411–8414.

[42] N. Fontana, N. A. Espinosa-Jalapa, M. Seidl, J. O. Bauer, *Chem. Commun.* **2022**, *58*, 2144–2147.

[43] D. Čas, N. Hurkes, S. Spirk, F. Belaj, C. Bruhn, G. N. Rechberger, R. Pietschnig, *Dalton Trans.* **2015**, *44*, 12818–12823.

[44] a) P. Roesch, U. Warzok, M. Enke, R. Müller, C. Schattenberg, C. A. Schalley, M. Kaupp, T. Braun, P. Wittwer, *Chem. Eur. J.* **2017**, *23*, 13964–13972; b) M. J. Michalczyk, M. J. Fink, K. J. Haller, R. West, J. Michl, *Organometallics* **1986**, *5*, 531–538.

[45] J. O. Bauer, C. Strohmann, *Angew. Chem. Int. Ed.* **2014**, *53*, 720–724; *Angew. Chem.* **2014**, *126*, 738–742.

[46] J. O. Bauer, C. Strohmann, *Chem. Commun.* **2012**, *48*, 7212–7214.

[47] R. Fessenden, J. S. Fessenden, *Chem. Rev.* **1961**, *61*, 361–380.

[48] a) M. Igarashi, K. Kubo, T. Matsumoto, K. Sato, W. Ando, S. Shimada, *RSC Adv.* **2014**, *4*, 19099–19102; b) B. Genabeek, B. A. G. Lamers, C. J. Hawker, E. W. Meijer, W. R. Gutekunst, B. V. K. J. Schmidt, *J. Polym. Sci.* **2021**, *59*, 373–403; c) Y. Li, Y. Kawakami, *Macromolecules* **1999**, *32*, 8768–8773.

[49] Z. M. Michalska, *Transition Met. Chem.* **1980**, *5*, 125–129.

[50] R. Zhang, J. E. Mark, A. R. Pinhas, *Macromolecules* **2000**, *33*, 3508–3510.

[51] J. Kaźmierczak, K. Kuciński, D. Lewandowski, G. Hreczycho, *Inorg. Chem.* **2019**, *58*, 1201–1207.

[52] a) Y. Satoh, M. Igarashi, K. Sato, S. Shimada, *ACS Catal.* **2017**, *7*, 1836–1840; b) Y. Sawama, M. Masuda, N. Yasukawa, R. Nakatani, S. Nishimura, K. Shibata, T. Yamada, Y. Monguchi, H. Suzuka, Y. Takagi et al., *J. Org. Chem.* **2016**, *81*, 4190–4195; c) Y. Tsuchido, A. Kanda, K. Osakada, *Tetrahedron* **2020**, *76*, 131076.

[53] M. Foston, H. W. Beckham, *Polymer* **2010**, *51*, 2515–2519.

[54] H. K. Sharma, R. Arias-Ugarte, D. Tomlinson, R. Gappa, A. J. Metta-Magaña, H. Ito, K. H. Pannell, *Organometallics* **2013**, *32*, 3788–3794.

[55] S. Pattanaik, C. Gunanathan, *ACS Catal.* **2019**, *9*, 5552–5561.

[56] T. Takeshita, K. Sato, Y. Nakajima, *Dalton Trans.* **2018**, *47*, 17004–17010.

[57] E. Le Coz, S. Kahlal, J.-Y. Saillard, T. Roisnel, V. Dorcet, J.-F. Carpentier, Y. Sarazin, *Chem. Eur. J.* **2019**, *25*, 13509–13513.

[58] R. Wakabayashi, K. Kawahara, K. Kuroda, *Angew. Chem. Int. Ed.* **2010**, *49*, 5273–5277; *Angew. Chem.* **2010**, *122*, 5401–5405.

[59] M. Yoshikawa, Y. Tamura, R. Wakabayashi, M. Tamai, A. Shimojima, K. Kuroda, *Angew. Chem. Int. Ed.* **2017**, *56*, 13990–13994; *Angew. Chem.* **2017**, *129*, 14178–14182.

[60] R. Wakabayashi, Y. Sugiura, T. Shibue, K. Kuroda, *Angew. Chem. Int. Ed.* **2011**, *50*, 10708–10711; *Angew. Chem.* **2011**, *123*, 10896–10899.

[61] K. Kuciński, G. Hreczycho, *ChemSusChem* **2019**, *12*, 1043–1048.

[62] M. A. Brook, *Chem. Eur. J.* **2018**, *24*, 8458–8469.

[63] S. Rubinsztajn, M. Cypryk, J. Chojnowski, *J. Organomet. Chem.* **1989**, *367*, 27–37.

[64] S. Rubinsztajn, J. A. Cella, *Macromolecules* **2005**, *38*, 1061–1063.

[65] Parks, Blackwell, Piers, *J. Org. Chem.* **2000**, *65*, 3090–3098.

[66] K. Kuciński, H. Stachowiak, G. Hreczycho, *Eur. J. Org. Chem.* **2020**, *2020*, 4042–4049.

[67] K. Kuciński, H. Stachowiak, G. Hreczycho, *Inorg. Chem. Front.* **2020**, *7*, 4190–4196.

[68] S. Rubinsztajn, J. Cella, *Polym. Prep.* **2004**, 635–636.

[69] J. Chojnowski, S. Rubinsztajn, J. A. Cella, W. Fortuniak, M. Cypryk, J. Kurjata, K. Kaźmierski, *Organometallics* **2005**, *24*, 6077–6084.

[70] a) D. B. Thompson, M. A. Brook, *J. Am. Chem. Soc.* **2008**, *130*, 32–33; b) N. Drosos, B. Morandi, *Angew. Chem. Int. Ed.* **2015**, *54*, 8814–8818; *Angew. Chem.* **2015**, *127*, 8938–8942. c) Y. Kawakami, Y. Li, Y. Liu, M. Seino, C. Pakjamsai, M. Oishi, Y. H. Cho, I. Imae, *Macromol. Res.* **2004**, *12*, 156–171.

[71] J. B. Grande, D. B. Thompson, F. Gonzaga, M. A. Brook, *Chem. Commun.* **2010**, *46*, 4988–4990.

[72] J. Yu, Y. Liu, *Angew. Chem. Int. Ed.* **2017**, *56*, 8706–8710; *Angew. Chem.* **2017**, *129*, 8832–8836.

[73] K. Matsumoto, Y. Oba, Y. Nakajima, S. Shimada, K. Sato, *Angew. Chem. Int. Ed.* **2018**, *57*, 4637–4641; *Angew. Chem.* **2018**, *130*, 4727–4731.

[74] L. Ai, Y. Chen, L. He, Y. Luo, S. Li, C. Xu, *Chem. Commun.* **2019**, *55*, 14019–14022.

[75] H. Zhang, L. Xue, J. Li, Q. Ma, *Polymers* **2020**, *12*, 672–685.

[76] D. Zhou, Y. Kawakami, *Macromolecules* **2005**, *38*, 6902–6908.

[77] X. Chen, M. Yi, S. Wu, L. Tan, X. Ge, M. He, G. Yin, *Materials* **2019**, *12*, 304.

[78] a) A. F. Schneider, E. K. Lu, G. Lu, M. A. Brook, *J. Polym. Sci.* **2020**, *58*, 3095–3106; b) T. Chaiprasert, Y. Liu, N. Takeda, M. Unno, *Materials* **2021**, *14*, 2014; c) M. Melendez-Zamudio, K. E. C. Silverthorne, M. A. Brook, *Macromol. Rapid Commun.* **2022**, *43*, e2200022; d) M. Yoshikawa, H. Shiba, H. Wada, A. Shimojima, K. Kuroda, *Bull. Chem. Soc. Jpn.* **2018**, *91*, 747–753; e) M. Liao, Y. Chen, M. A. Brook, *Polymers* **2021**, *13*, 859.

[79] K. Matsumoto, K. V. Sajna, Y. Satoh, K. Sato, S. Shimada, *Angew. Chem. Int. Ed.* **2017**, *56*, 3168–3171; *Angew. Chem.* **2017**, *129*, 3216–3219.

[80] K. Matsumoto, S. Shimada, K. Sato, *Chem. Eur. J.* **2019**, *25*, 920–928.

[81] K. M. Rabanzo-Castillo, V. B. Kumar, T. Söhnel, E. M. Leitao, *Front. Chem.* **2020**, *8*, 477.

[82] J. Zhu, S. Chen, C. He, *J. Am. Chem. Soc.* **2021**, *143*, 5301–5307.

[83] Y.-C. Hsiao, L. W. Hill, S. P. Pappas, *J. Appl. Pol. Sc.* **1975**, *19*, 2817–2820.

[84] S. P. Pappas, R. L. Just, *J. Polym. Sci.* **1980**, *18*, 527–531.

[85] K.-H. Schimmel, E. Schröder, J. Schulz, T. Souvimonh, *Acta Polym.* **1988**, *39*, 310–314.

[86] C. L. Chang, Y. K. Lin, *Polym. Degrad. Stab.* **2005**, *87*, 207–211.

[87] L. Wilczek, J. Chojnowski, *Makromol. Chem.* **1983**, *184*, 77–90.

[88] M. Cypryk, Y. Apeloig, *Organometallics* **1997**, *16*, 5938–5949.

[89] M. Cypryk, Y. Apeloig, *Organometallics* **2002**, *21*, 2165–2175.

[90] a) L. Wilczek, J. Chojnowski, *Macromolecules* **1981**, *14*, 9–17; b) L. Wilczek, S. Rubinsztajn, J. Chojnowski, *Die Makrom. Chem.: Macromol. Chem. Phys.* **1986**, *187*, 39–51; c) P. Sigwalt, *Polym. J.* **1987**, *19*, 567–580.

[91] a) T. Kudo, M. S. Gordon, *J. Am. Chem. Soc.* **1998**, *120*, 11432–11438; b) S. Okumoto, N. Fujita, S. Yamabe, *J. Phys. Chem. A* **1998**, *102*, 3991–3998; c) T. Kudo, M. S. Gordon, *J. Phys. Chem. A* **2000**, *104*, 4058–4063; d) C. Hühn, A. Erlebach, D. Mey, L. Wondraczek, M. Sierka, *J. Comput. Chem.* **2017**, *38*, 2349–2353.

[92] E. Suzuki, M. Akiyama, Y. Ono, *J. Chem. Soc., Chem. Commun.* **1992**, 136–137.

[93] a) M. Okamoto, K. Miyazaki, A. Kado, E. Suzuki, *Chem. Commun.* **2001**, 1838–1839; b) I. Protsak, I. M. Henderson, V. Tertykh, W. Dong, Z.-C. Le, *Langmuir* **2018**, *34*, 9719–9730.

[94] U. Schubert, *The Sol-Gel handbook*. *Volume 1: Synthesis and Processing ; Volume 2: Characterization and Properties of Sol-Gel Materials ; Volume 3: Application of Sol-Gel Materials* (Eds.: D. Levy, M. Zayat), Wiley-VCH, Weinheim, **2015**, 1–28.

[95] M. A. Brook, S. Zhao, L. Liu, Y. Chen, *Can. J. Chem.* **2012**, *90*, 153–160.

[96] B. Rupasinghe, J. C. Furgal, *ACS Appl. Polym. Mater.* **2021**, *3*, 1828–1839.

[97] P. Döhlert, S. Enthaler, *J. Appl. Pol. Sc.* **2015**, *132*, 42814.

[98] P. Döhlert, J. Pfrommer, S. Enthaler, *ACS Sustainable Chem. Eng.* **2015**, *3*, 163–169.

[99] S. Enthaler, R. Kretschmer, *ChemSusChem* **2014**, *7*, 2030–2036.

[100] S. Enthaler, *Angew. Chem. Int. Ed.* **2014**, *53*, 2716–2721; *Angew. Chem.* **2014**, *126*, 2754–2759.

[101] C. L. Frye, R. M. Salinger, F. W. G. Fearon, J. M. Klosowski, T. DeYoung, *J. Org. Chem.* **1970**, *35*, 1308–1314.

[102] S. M. Sieburth, W. Mu, *J. Org. Chem.* **1993**, *58*, 7584–7586.

[103] C. N. McMahon, S. G. Bott, L. B. Alemany, H. W. Roesky, A. R. Barron, *Organometallics* **1999**, *18*, 5395–5408.

[104] a) F. J. Feher, T. A. Budzichowski, *Polyhedron* **1995**, *14*, 3239–3253; b) V. Lorenz, A. Fischer, S. Gießmann, J. W. Gilje, Y. Gun'ko, K. Jacob, F. T. Edelmann, *Coord. Chem. Rev.* **2000**, *206-207*, 321–368.

[105] a) J. Beckmann, K. Jurkschat, *Coord. Chem. Rev.* **2001**, *215*, 267–300; b) M. Schulte, M. Schürmann, K. Jurkschat, D. Dakternieks, *Chem. Commun.* **1999**, 1291–1292.

[106] a) C. Däschlein, J. O. Bauer, C. Strohmann, *Angew. Chem. Int. Ed.* **2009**, *48*, 8074–8077; *Angew. Chem.* **2009**, *121*, 8218–8221; b) J. O. Bauer, C. Strohmann, *Inorg. Chim. Acta* **2018**, *469*, 133–135.

[107] D. Pinkert, S. Demeshko, F. Schax, B. Braun, F. Meyer, C. Limberg, *Angew. Chem. Int. Ed.* **2013**, *52*, 5155–5158; *Angew. Chem.* **2013**, *125*, 5260–5263.

[108] K. S. Lokare, P. Wittwer, B. Braun-Cula, N. Frank, S. Hoof, T. Braun, C. Limberg, *Z. Anorg. Allg. Chem.* **2017**, *643*, 1581–1588.

[109] a) R. F. Weitkamp, B. Neumann, H.-G. Stammler, B. Hoge, *Angew. Chem. Int. Ed.* **2020**, *59*, 5494–5499; *Angew. Chem.* **2020**, *132*, 5536–5541; b) R. F. Weitkamp, B. Neumann, H.-G. Stammler, B. Hoge, *Chem. Eur. J.* **2021**, *27*, 915–920.

[110] C. Krempner, *Eur. J. Inorg. Chem.* **2011**, *2011*, 1689–1698.

[111] a) Hirayama, Caseri, Suter, *J. Colloid Interface Sci.* **1999**, *216*, 250–256; b) J. D. Hu, Z. M. Zheng, T. Ma, Z. J. Zhang, J. P. Ye, D. Y. Wang, Z. M. Xie, *J. Polym. Sci. A Polym. Chem.* **2004**, *42*, 2897–2903; c) I. Menapace, G. Mera, R. Riedel, E. Erdem, R.-A. Eichel, A. Pauletti, G. A. Appleby, *J. Mater. Sci.* **2008**, *43*, 5790–5796.

[112] G. Huber, A. Jockisch, H. Schmidbaur, *Eur. J. Inorg. Chem.* **1998**, *1998*, 107–112.

[113] S. H. Langer, S. Connell, I. Wender, *J. Org. Chem.* **1958**, *23*, 50–58.

[114] a) L. K. Allen, R. García-Rodríguez, D. S. Wright, *Dalton Trans.* **2015**, *44*, 12112–12118; b) S. Anga, Y. Sarazin, J.-F. Carpentier, T. K. Panda, *ChemCatChem* **2016**, *8*, 1373–1378; c) M. S. Hill, D. J. Liptrot, D. J. MacDougall, M. F. Mahon, T. P. Robinson, *Chem. Sci.* **2013**, *4*, 4212; d) L. J. Morris, G. R. Whittell, J.-C. Eloi, M. F. Mahon, F. Marken, I. Manners, M. S. Hill, *Organometallics* **2019**, *38*, 3629–3648; e) M. Rauch, R. C. Roberts, G. Parkin, *Inorg. Chim. Acta* **2019**, *494*, 271–279; f) M. B. Reuter, K. Hageman, R. Waterman, *Chem. Eur. J.* **2021**, *27*, 3251–3261; g) J. X. Wang, A. K. Dash, J. C. Berthet, M. Ephritikhine, M. S. Eisen, *J. Organomet. Chem.* **2000**, *610*, 49–57.

[115] a) W. D. Wang, R. Eisenberg, *Organometallics* **1991**, *10*, 2222–2227; b) S. Itagaki, K. Kamata, K. Yamaguchi, N. Mizuno, *Chem. Commun.* **2012**, *48*, 9269–9271; c) J. F. Dunne, S. R. Neal, J. Engelkemier, A. Ellern, A. D. Sadow, *J. Am. Chem. Soc.* **2011**, *133*, 16782–16785.

[116] C. D. F. Königs, M. F. Müller, N. Aiguabella, H. F. T. Klare, M. Oestreich, *Chem. Commun.* **2013**, *49*, 1506–1508.

[117] a) M. P. Cibuzar, R. Waterman, *Organometallics* **2018**, *37*, 4395–4401; b) A. E. Nako, W. Chen, A. J. P. White, M. R. Crimmin, *Organometallics* **2015**, *34*, 4369–4375; c) W. Xie, H. Hu, C. Cui, *Angew. Chem. Int. Ed.* **2012**, *51*, 11141–11144; *Angew. Chem.* **2012**, *124*, 11303–11306; d) X. Zhang, S. Zhou, X. Fang, L. Zhang, G. Tao, Y. Wei, X. Zhu, P. Cui, S. Wang, *Inorg. Chem.* **2020**, *59*, 9683–9692.

[118] a) Y. Tanabe, T. Misaki, M. Kurihara, A. Iida, Y. Nishii, *Chem. Commun.* **2002**, 1628–1629; b) Y. Tanabe, M. Murakami, K. Kitaichi, Y. Yoshida, *Tetrahedron Lett.* **1994**, *35*, 8409–8412.

[119] a) D. A. Armitage, R. J. P. Corriu, T. C. Kendrick, B. Parbhoo, T. D. Tilley, J. W. White, J. C. Young, S. Patai, Z. Rappoport (Eds.) *The chemistry of functional groups*, Wiley, Chichester, West Sussex, England, New York, **1991**; b) G. Huber, A. Schier, H. Schmidbaur, *Chem. Ber.* **1997**, *130*, 1167–1174.

[120] M. Herbig, U. Böhme, E. Kroke, *Inorg. Chim. Acta* **2018**, *473*, 20–28.

[121] a) F. Gründler, H. Scholz, M. Herbig, S. Schwarzer, J. Wagler, E. Kroke, *Eur. J. Inorg. Chem.* **2021**, *2021*, 2211–2224; b) K. Kraushaar, C. Wiltzsch, J. Wagler, U. Böhme, A. Schwarzer, G. Roewer, E. Kroke, *Organometallics* **2012**, *31*, 4779–4785.

[122] M. Xu, A. R. Jupp, M. S. E. Ong, K. I. Burton, S. S. Chitnis, D. W. Stephan, *Angew. Chem. Int. Ed.* **2019**, *58*, 5707–5711; *Angew. Chem.* **2019**, *131*, 5763–5767.

[123] a) Y. Zhao, J. Rodrigo, A. H. Hoveyda, M. L. Snapper, *Nature* **2006**, *443*, 67–70; b) Y. Zhao, A. W. Mitra, A. H. Hoveyda, M. L. Snapper, *Angew. Chem. Int. Ed.* **2007**, *46*, 8471–8474; *Angew. Chem.* **2007**, *119*, 8623–8626; c) S. Rendler, M. Oestreich, *Angew. Chem. Int. Ed.* **2008**, *47*, 248–250; *Angew. Chem.* **2008**, *120*, 6086–6089.

[124] a) S. Rendler, G. Auer, M. Oestreich, *Angew. Chem. Int. Ed.* **2005**, *44*, 7620–7624; *Angew. Chem.* **2005**, *117*, 1688–1691; b) H. F. T. Klare, M. Oestreich, *Angew. Chem. Int. Ed.* **2007**, *46*, 9335–9338; *Angew. Chem.* **2007**, *119*, 9496–9499.

[125] a) S. M. Sieburth, C.-A. Chen, *Eur. J. Org. Chem.* **2006**, *2006*, 311–322; b) M. Waelbroeck, J. Camus, M. Tastenoy, E. Mutschler, C. Strohmann, R. Tacke, G. Lambrecht, J. Christophe, *Eur. J. Pharmacol.* **1991**, *206*, 95–103.

2 Research objectives

The versatile potential of aminosilanes has been described in chapter 1.4. Such a functional group opens the possibility to synthesize siloxane compounds in a selective way without production of undesired solid by-products. Most of the known procedures make use of low-molecular-weight amine-substituents that can be removed *in vacuo* and therefore need to be taken out of the reaction system. The aim of this work is the expansion of such methodologies to cyclic diaminosilanes that offer the option to form siloxane bonds by selective cleavage of one Si–N bond while keeping the second one intact. The intramolecular free NH function will be further exploited for investigations on the cleavage of the siloxane motif bearing high synthetic potential in the selective formation of functionalized siloxanes. With this strategy, we will introduce model systems for the defined modification of oligosiloxanes at specific positions in the molecule. The fundamental results presented herein should enable the transfer of this methodology to more complex systems. Cyclic diaminosilanes have been prepared in the past, but their potential in further modification has never been fully explored. The new approach in this work relies on unsymmetrically substituted *ortho*-aminoanilines with the premise of a sufficient steric difference of the NH_2 compared to the RNH group. During these studies, we found an unexpected but highly interesting reactivity when a Si–H function is present at the silicon atom on which the diamine is bound. The reactivity of this compound towards silanols will be investigated and is believed to contribute significantly to the understanding of reaction mechanisms in silicon chemistry. The introduction of an enantiomerically pure *C*-chiral substituent on the diamine ligand will additionally be touched. It allows for the synthesis of diastereomerically pure *Si*-chiral compounds which are promising precursors for enantiomerically pure silanes. Moreover, they are well-suited for mechanistic investigations regarding inversion/retention of configuration at silicon centers. In combination of all these studies, we hope to increase the understanding of the true nature of the Si–O–Si bond with experimental insights into reactivities and mechanisms of both the formation and the cleavage of this ubiquitous chemical motif. The objectives of this work can therefore be summarized as follows:

- Preparation of new cyclic diaminosilanes with unsymmetrically substituted *ortho*-aminoanilines
- Investigation of their reactivity towards silanols for the synthesis of unsymmetrical N-functionalized oligosiloxanes
- Application of the diamine substituent in lithium-amide induced Si–O–Si cleavage
- Investigations on the influence of Si–H functions in the reaction of diaminosilanes with silanols
- Introduction of stereochemical information via the amine backbone for the chirality transfer from carbon to silicon to afford *Si*-stereogenic diaminosilanes

3 Molecular scissors for tailor-made modification of siloxane scaffolds

Preface

A synthetic version of the following chapter has already been published.
The article is reprinted with permission of Wiley-VCH. License-number: 5407660936837

“Molecular Scissors for Tailor-Made Modification of Siloxane Scaffolds”

Authors

T. Götz, A. Falk, J. O. Bauer, Chem. Eur. J. 2022, 28, e202103531.

Author contribution

All the reported syntheses and characteriations in this work were perfomed by T. Götz except for 1-pyrrolidino-1,1,3,3,3-pentaphenyldisiloxane which was synthezised and characterized by A. Falk. The original script and supporting information were prepared by T. Götz and revised by Dr. J. O. Bauer.

Acknowledgements

This work was jointly supported by the Elite Network of Bavaria (ENB), the Bavarian State Ministry of Science and the Arts (StMWK), and the University of Regensburg (N-LW-NW-2016-366). Further support was given by the Deutsche Forschungsgemeinschaft (DFG) through the Research Training Group “Ion Pair Effects in Molecular Reactivity” (RTG 2620, Project 426795949). The authors also thank Prof. Dr. Manfred Scheer for continuous support, Dr. Noel Angel Espinosa-Jalapa for helpful discussions, and Tuan Anh Nguyen for NMR measurements. Open Access funding enabled and organized by Projekt DEAL.

3.1 Abstract

The controlled design of functional oligosiloxanes is an important topic in current research. A consecutive Si–O–Si bond cleavage/formation using siloxanes that are substituted with 1,2-diaminobenzene derivatives acting as molecular scissors is presented. The method allows to cut at certain positions of a siloxane scaffold forming a cyclic diaminosilane or -siloxane intermediate and then to introduce new functional siloxy units. The procedure could be extended to a direct one-step cleavage of chlorooligosiloxanes. Both siloxane formation and cleavage proceed with good to excellent yields, high regioselectivity, and great variability of the siloxy units. Control of the selectivity is achieved by the choice of the amino substituent. Insight into the mechanism was provided by low temperature NMR studies and the isolation of a lithiated intermediate.

3.2 Introduction

The Si–O–Si bond is omnipresent in our nature[1] and forms an integral part in many technical products that are used in our everyday lives.[2] In the past few years, there have been impressive developments in the stepwise and tailor-made const-ruction of functional oligo- and polysiloxanes.[3,4] New methodologies for the formation of silicon–oxygen bonds are constantly stimulating progress in this research area.[5] Bulky, well-defined oligosiloxanols are important precursors for building molecular siloxide models to study structure and reactivity in alumino-silicates.[6] The extraordinary properties of the Si–O–Si bond[7] (high thermodynamic stability, low basicity, resistance towards heat, radiation, and chemicals) renders the targeted cleavage of the siloxane bond a particularly demanding undertaking.[8] The selective cleavage of an Si–O–Si linkage must therefore meet special requirements, such as the presence of amino side arms within the siloxane framework.[9] Acid-catalyzed[10] and alkyl-lithium-mediated[11] cleavage of siloxanes have been known for a long time. Examples of siloxane cleavage with lithium amides are limited to reactions with cyclic dimethylsilicones.[12] The search for sustainable and environmentally friendly processes for recycling end-of-life silicone materials has become a major concern in modern times.[13] Si–O–Si cleavage reactions have therefore mainly been investigated in the context of the depolymerization of polysiloxanes into valuable low-molecular-weight compounds as feedstocks for new polymers.[13,14] However, all these cleavage reactions on siloxane oligo- and polymers are rather unselective and often lead to a large number of different cleavage products, thus being unsuitable for targeted and regioselective bond break-ing for the precise equipment of siloxane frameworks with special functions. Kuroda et al. described the use of trimethylsilyl (TMS) units as protecting and leaving groups for the construction of alkoxy-siloxane oligomers (Scheme 3.1).[15] This is, to the best of our knowledge, so far the only example of an utilization of a controlled siloxane bond formation/cleavage for the step-by-step synthesis of functional siloxanes. However, a method in which Si–O–Si linkages can be selectively cleaved at certain positions and indivi-dual siloxy groups replaced by other units appears to be a novelty in the field of preparative siloxane chemistry. Herein, a convenient method that allows for a tailor-

made modification of siloxane scaffolds is reported (Scheme 3.1). Unsymmetrically substituted 1,2-diaminobenzene derivatives act as molecular scissors, which can be installed at specific positions and split off again at the end. The cyclic diaminosilane intermedi-ates readily react with functionalized silanols and siloxanols under ring opening. By incorporating molecular scissors into the siloxane backbone, controlled cutting at a certain position by cleaving the Si–O–Si bond, and replacing siloxy units by forming a new siloxane bond, new perspectives open up for the design of functional polymers and molecular siloxide models.

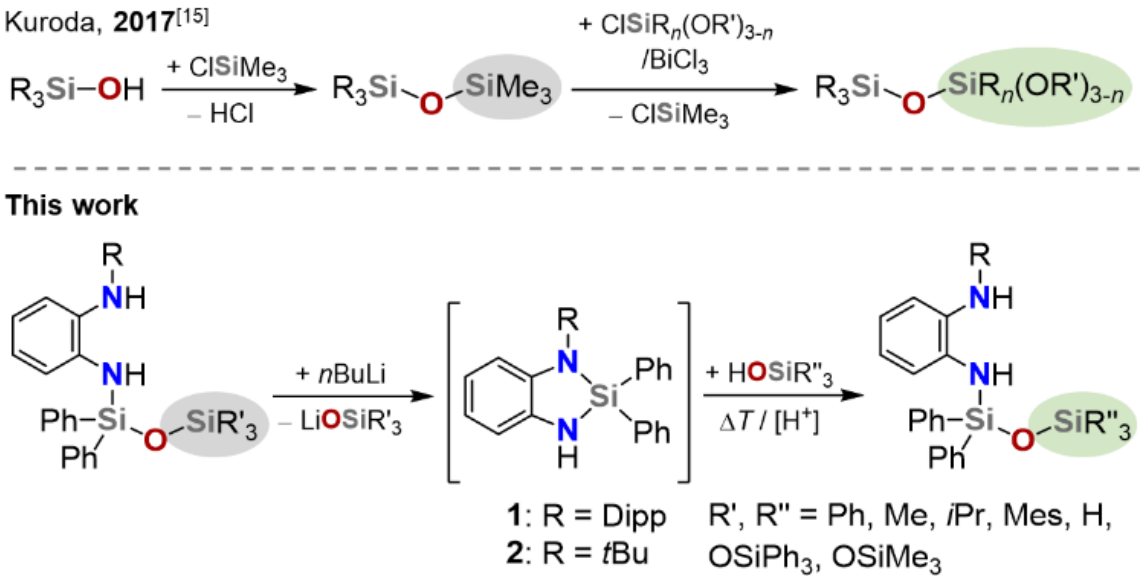

Scheme 3.1. Consecutive Si–O–Si bond cleavage/formation to easily exchange individual siloxy groups in oligosiloxanes (Dipp = 2,6-diisopropylphenyl).

The premise of the work was the development of a flexible molecular system that would easily allow the cleavage and introduction of a variety of siloxy groups for tailoring and equipping oligosiloxanes with functional units.

3.3 Results and discussion

3.3.1 Reaction of five-membered cyclic diaminosilanes with silanols

In order to provide a compound library that adequately reflects the diversity of the siloxane units, the diaminocyclosilanes **1** (R = Dipp) and **2** (R = *t*Bu) as suitable model systems were first prepared and reacted with a number of silanols (Table 3.1). Sterically demanding NH(R) units were chosen in order to achieve high selectivity for the ring-opening attack of the silanols at the heterocyclic silicon atom. The reactions with the silanols resulted in a regioselective opening of the Si–N(R) bond. Di- and trisiloxanes **3–11** were synthesized in excellent to moderate yields. In general, the reaction shows a high tolerance towards the steric hindrance of the silanol used.

Table 3.1. Introduction of different siloxy groups starting from diaminosilanes **1** and **2**,[a] and removal of the 1,2-diaminobenzene derivative with formation of a siloxanol.

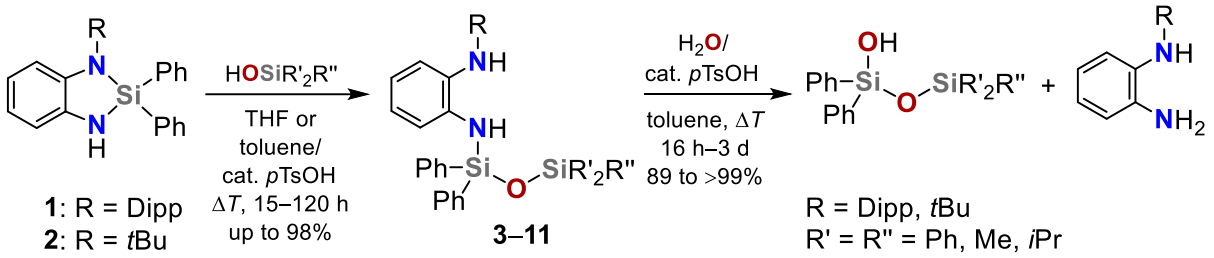

Entry	R	R'	R''	Product	Solvent	Additive	Reaction time [h]	Yield [%][b]
1	Dipp	Ph	Ph	**3**	THF	—	120	42 (68)
2	*t*Bu	Ph	Ph	**4**	THF	—	15	n.r.
3	*t*Bu	Ph	Ph	**4**	toluene	*p*TsOH	15	76
4[c]	Dipp	Me	Me	**5**	THF	—	15	98
5	*t*Bu	Me	Me	**6**	THF	—	120	27[d] (70)
6	Dipp	*i*Pr	*i*Pr	**7**	THF	—	15	98
7	*t*Bu	*i*Pr	*i*Pr	**8**	THF	—	120	30
8	Dipp	Mes	H	**9**	THF	—	120	(18)
9	Dipp	Mes	H	**9**	toluene	*p*TsOH	120	36[e] (78)
10	*t*Bu	Mes	H	**10**	toluene	*p*TsOH	15	70
11	*t*Bu	Ph	$OSiPh_3$	**11**	toluene	*p*TsOH	100	75

[a] Reaction conditions: Silane **1** or **2** (1.0 equiv.) and the respective silanol (1.0 equiv.) were dissolved in THF or toluene and, if indicated, catalytic amounts of *p*TsOH (1 mol%) were added. Unless otherwise stated, the solution was heated at reflux for the indicated time. [b] Yields of isolated products. Yields of products determined by ^{1}H NMR spectroscopy using hexamethylbenzene as internal standard are given in parentheses. [c] The reaction was carried out at room temperature. [d] The product was isolated by distillation. [e] Isolated single-crystalline product after recrystallization from pentane.

The best results were obtained when the more electrophilic compound **1** was reacted with Me_3SiOH (reaction at RT, entry 4) and iPr_3SiOH (entry 6), with both disiloxanes **5** and **7** being isolated in 98% yield. Some reactions with less nucleophilic arylsilanols[16] (entries 3 and 9–11) required catalytic amounts of *p*TsOH, which facilitated ring opening by protonation of the amine function. The described method even enables the introduction of synthetically highly valuable hydrosiloxy units[17] (entries 8–10), which are of particular interest for the cross-linking of oligosiloxanes[18] and the construction of complex siloxane architectures[19] by Piers-Rubinsztajn coupling of hydrosilanes with alkoxysilanes.[20] Entry 11 shows that also longer and sterically demanding siloxanols can easily be introduced with good isolated yields of 75%. Diaminocyclosilanes **1** and **2** as well as aminodisiloxanes **3**, **4**, and **9** were characterized by

single-crystal X-ray diffraction analysis (for details, see chapter 3.7). The molecular structures of cyclosilane **1** and hydrodisiloxane **9** are shown in Figure 3.1. The two Si–N bond lengths in **1** differ signifi-cantly with 1.7257(11) Å for Si–N(H) and 1.7460(10) Å for Si–N(Dipp), indicating the latter bond to be the weaker of the two. This structural finding nicely explains the regioselective ring open-ing in the reactions with silanols, which is also confirmed through X-ray crystallography of three ring-opened amino-substituted disiloxanes (Figure 3.1, right, and chapter 3.7).

3.3.2 Usage of the diamine -substitution as molecular scissors for cutting the siloxane bond

Although 1,2-diaminobenzene derivatives have been used in the stabilization of silylenes,[21] their synthetic potential to serve as molecular scissors is yet completely undiscovered. In the further course of the work, it was found that the open form of the diamino fragment in siloxanes **3–11** act as precise molecular scissors when adding *n*-butyllithium (Table 3.2). This leads to cleavage of the Si–O–Si bond with ring closure and formation of a lithium siloxide. Surprisingly, the Si–O–Si cleavage occurs intramolecu-larly by an in situ-formed lithium amide function and not by the alkyllithium reagent, which enables a high degree of control over the specific position of the cleavage in the siloxane structure. The NH(R) function rather than the Si–N(H) moiety is deprotonated, although the latter was actually expected to be more acidic. Probably the main factor behind the high thermodynamic driving force of these unusual reactions is the formation of stable aggregates of the cut off lithium siloxide.[22]

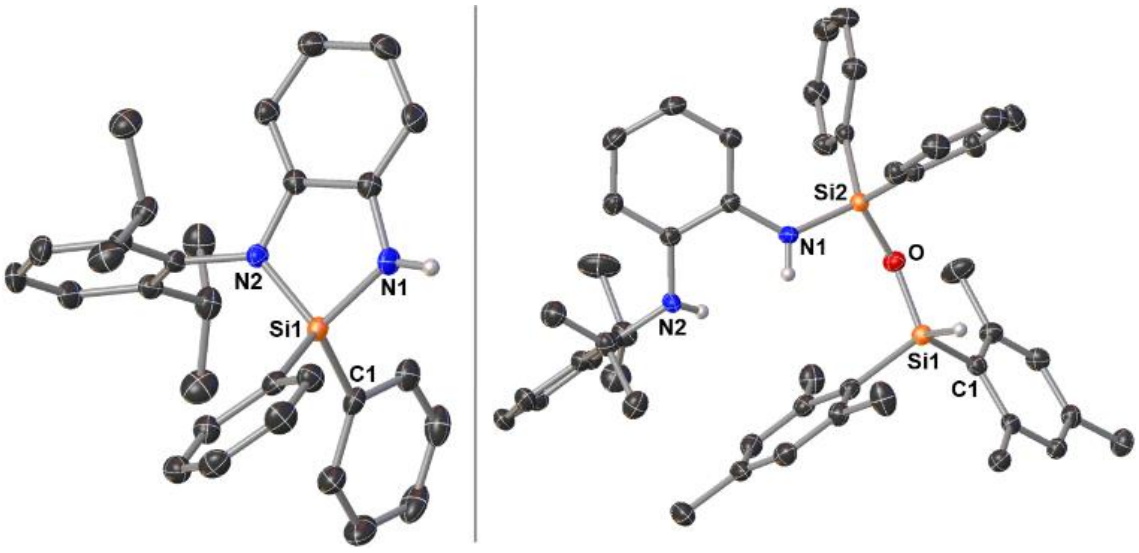

Figure 3.1. Molecular structures of **1** (left) and **9** (right) in the crystal (displace-ment ellipsoids are set at the 50 % probability level). Hydrogen atoms, except for the N–H and Si–H groups, are omitted for clarity. Only one molecule of the asymmetric unit of **1** is shown. Selected bond lengths [Å] and angles [°]: Compound **1**: Si1–N1 1.7257(11), Si1–N2 1.7460(10), N1–Si1–N2 91.50(5). Compound **9**: Si1–O 1.6406(10), Si2–O 1.6302(10), Si2–N1 1.7215(13), Si1–O–Si2 137.31(7).

Table 3.2. Si–O–Si bond cleavage in 1,2-diaminobenzyl-functionalized siloxanes **3-11** initiated by treatment with *n*BuLi.[a]

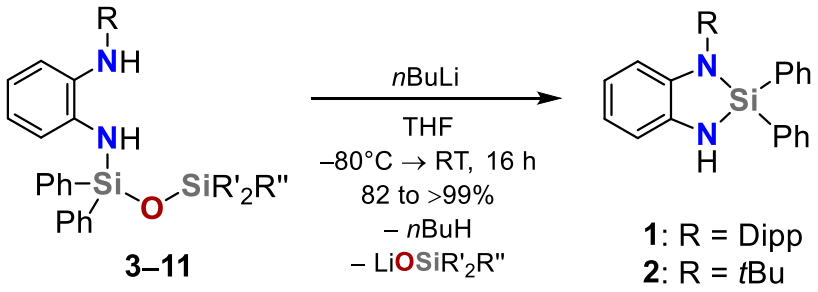

Entry	Substrate	R	R'	R''	Product	Yield [%][b]
1	**3**	Dipp	Ph	Ph	**1**	>99
2	**4**	*t*Bu	Ph	Ph	**2**	>99
3	**5**	Dipp	Me	Me	**1**	83
4	**6**	*t*Bu	Me	Me	**2**	83
5	**7**	Dipp	*i*Pr	*i*Pr	**1**	87
6	**8**	*t*Bu	*i*Pr	*i*Pr	**2**	82
7	**9**	Dipp	Mes	H	**1**	90
8	**10**	*t*Bu	Mes	H	**2**	>99
9	**11**	*t*Bu	Ph	$OSiPh_3$	**2**	90

[a] Reaction conditions: Siloxanes **3–11** (1.0 mmol) were each dissolved in 10 mL of THF and cooled to −80 °C. *n*BuLi (1.1 equiv.) was added dropwise, the solution slowly warmed to room temperature and stirred for 16 h. [b] Yields of products were determined by ^{1}H NMR spectroscopy using hexa-methylbenzene as internal standard.

The incorporated diamine scissors show excellent reactivity and selectivity towards cleavage of a wide range of siloxy units leading to yields from 82% (entry 6) up to >99% (entries 1, 2, and 8 in Table 3.2).[23] Due to the presence of two different silicon–nitrogen bonds in the heterocyclic intermediates **1** and **2**, new siloxy groups can now successively be inserted or the 1,2-diaminobenzene scissors completely split off through simple hydrolysis (Table 1; for details, see chapter 3.6.5). The formed siloxanols are precious building blocks not only for further Si–O–Si couplings[24] but also for the design of molecular models to mimic complex siloxide frameworks.[6]

3.3.3 One-step cleavage of chlorosiloxanes using the diamines

The next step was to find out whether the method can be extended to a one-step cleavage of chlorooligosiloxanes (Schemes 3.2 and 3.3). For this purpose, it was first investigated whether the diaminobenzenes **12** and **13** can be introduced selectively into the siloxane framework, the

location of the chlorine substituent determining the location of the cleavage. In line with previous studies by the authors,[25] the presence of a siloxy group required the use of the more nucleophilic lithium amides to substitute a Si–Cl bond. Therefore, chloropentaphenyldisiloxane (**14**)[26] was chosen as a simplified model compound and treated with both deprotonated **12** (Path A) and **13** (Path B), which were each obtained from the reaction of the respective diamine with one equivalent of *n*BuLi (Scheme 3.2). Interestingly, only in the case of diamine **13** (R = *t*Bu) the monosubstituted disiloxane **4** was the major product, which was formed in 63% yield together with 29% of the cyclic silane **2** (Scheme 3.2, Path B). When carrying out the reaction with the Dipp-substituted diamine **12**, the open form (compound **3**) was not obtained.

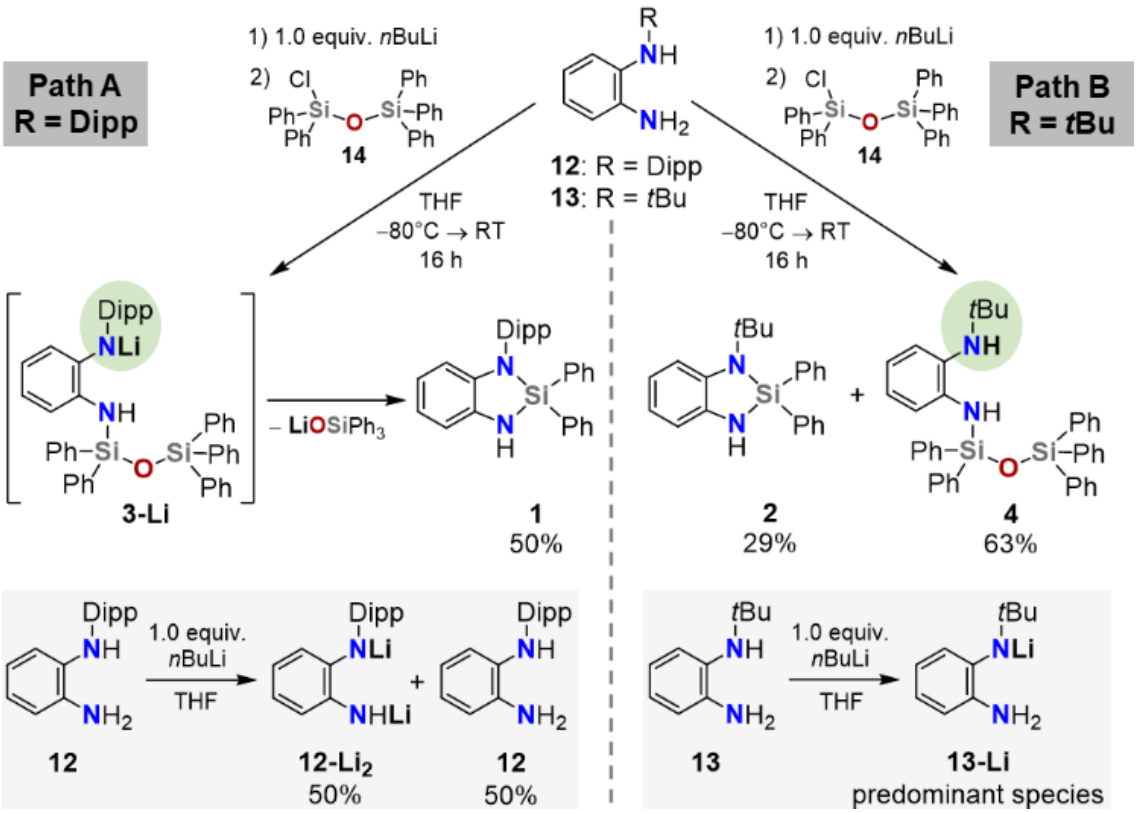

Scheme 3.2. Proposed mechanism for the direct Si–O–Si cleavage of chloro-disiloxanes using lithiated 1,2-diaminobenzene derivatives. Yields determined by ^{1}H NMR spectroscopy using hexamethylbenzene as internal standard.

Instead, cyclosilane **1** was formed as the only product in 50% yield (Path A). Apparently, there are fundamental differences in the stability of the lithiated intermediates depending on whether the amino function is equipped with an electron-withdrawing (Dipp) or an electron-donating group (*t*Bu). It appears that diamine **12** preferably forms a dilithiated rather than a monolithi-ated species. In the case of diamine **13**, the situation seems to be the opposite when one equivalent of *n*BuLi is used, with the monolithiated diamine being the predominant species (Scheme 3.2, bottom). The highly selective formation of compound **1** (with the maximum possible amount of 50%) can now be explained by the attack of the dilithium diamide **12-Li$_2$** at chlorodisiloxane **14** via the short-living intermediate **3-Li** (Scheme 3.2). Remarkably, from a mixture of diamine **12** and one equivalent of *n*BuLi in THF exclusively single-crystals of the double lithiated diamine suitable for X-ray diffraction analysis were obtained, which substantiated the assumption that the

dilithiated rather than the monolithiated structure was preferentially formed (Figure 3.2). **12-Li$_2$** crystallized in a previously unknown structure type for dilithiated 1,2-diaminobenzenes.[27] It forms the dimer **[12-Li$_2$·(THF)$_2$]$_2$**, which exhibits two sets of lithium atoms with different coordination spheres. Low temperature NMR spectroscopy of single-crystals of **[12-Li$_2$·(THF)$_2$]$_2$** in THF at –80°C showed only one set of signals in the ^{1}H NMR spectrum, but two signals in the ^{7}Li NMR spectrum at δ = 1.55 and 1.47 ppm, which corresponds to two inequivalent lithium centers.

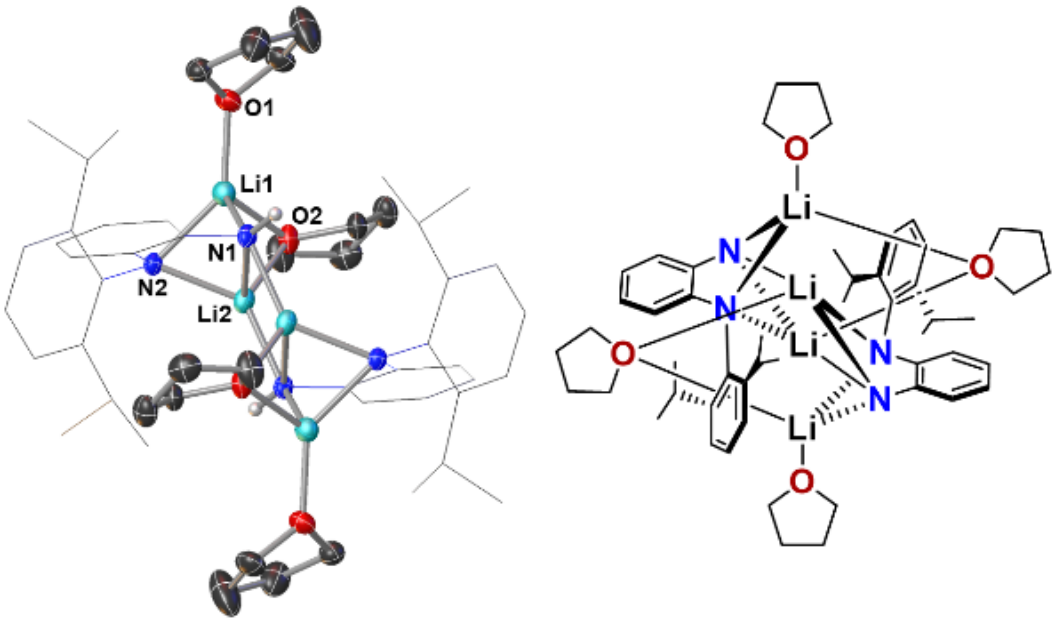

Figure 3.2. Molecular structure of double lithiated Dipp-substituted 1,2-diamino-benzene **[12-Li$_2$·(THF)$_2$]$_2$** in the crystal (displacement ellipsoids are set at the 50 % probability level). Hydrogen atoms, except for the N–H groups, are omitted for clarity.

This indicates that the struct ure of **12-Li$_2$** in solution correlates well with the molecular structure in the solid-state.[28] When one equivalent of *n*BuLi is added to diamine **12** in THF at –80°C, two sets of signals now appear in the ^{1}H NMR spectrum and only one signal in the ^{7}Li NMR spectrum (δ = 1.56 ppm). This suggests a simultaneous presence of the dilithiated species **12-Li$_2$** and diamine **12** in solution, presumably in the form of a coordination compound with equivalent coordination spheres around the lithium centers. This explains the outcome of the reactions in Scheme 3.2 very well. A quantitative, direct one-step cleavage of the Si–O–Si linkage of disiloxane **14** took place in all cases when using two equivalents of *n*BuLi, with compounds **1** and **2** being obtained in NMR yields of >99%. Not only Ph$_3$SiO but also Me$_3$SiO groups in chlorodisiloxanes can be cut off by the dilithiated diamines, as exemplified for disiloxane **15** (Scheme 3.3).

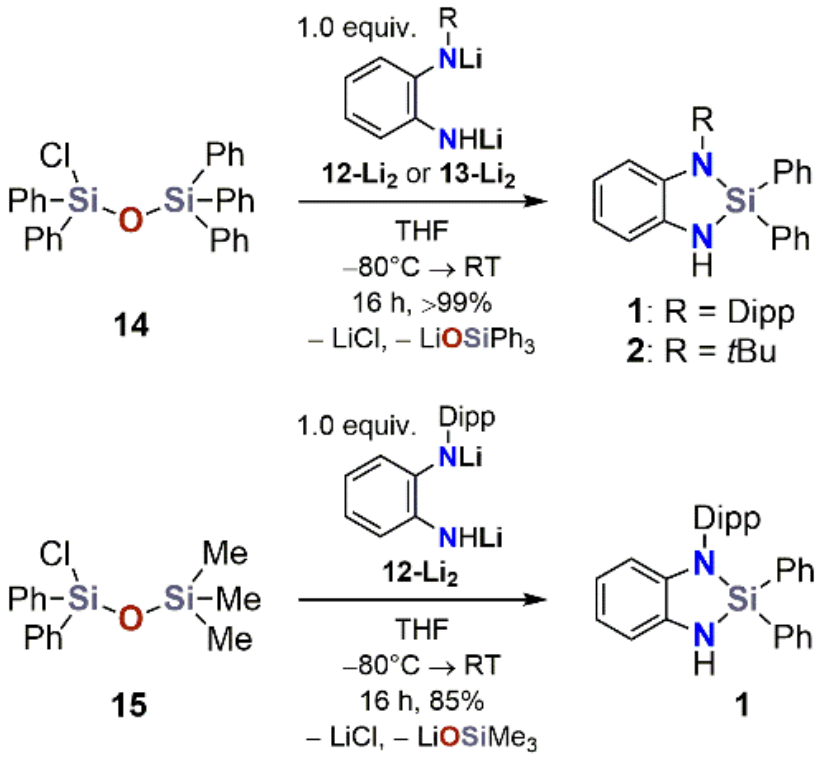

Scheme 3.3. Direct Si–O–Si cleavage of chlorodisiloxanes.

The method could easily be extended to other substitution patterns on the attacked silicon atom, as shown for the mesitylphenyl-substituted compound **16**[25a] (Scheme 3.4, top). Excellent regioselectivity of the Si–O–Si cleavage was observed when using an unsymmetric trisiloxane (**18**) (Scheme 3.4, bottom). Exclusively the bond to the triphenylsiloxy group is split off, most likely because of the better charge stabilization in the Ph_3SiOLi leaving group. It therefore appears that the steric hindrance of the NH(R) function has no discriminatory influence on the cleavage of the siloxy unit, but that the stability of the split off lithium siloxide rather controls the regioselectivity.

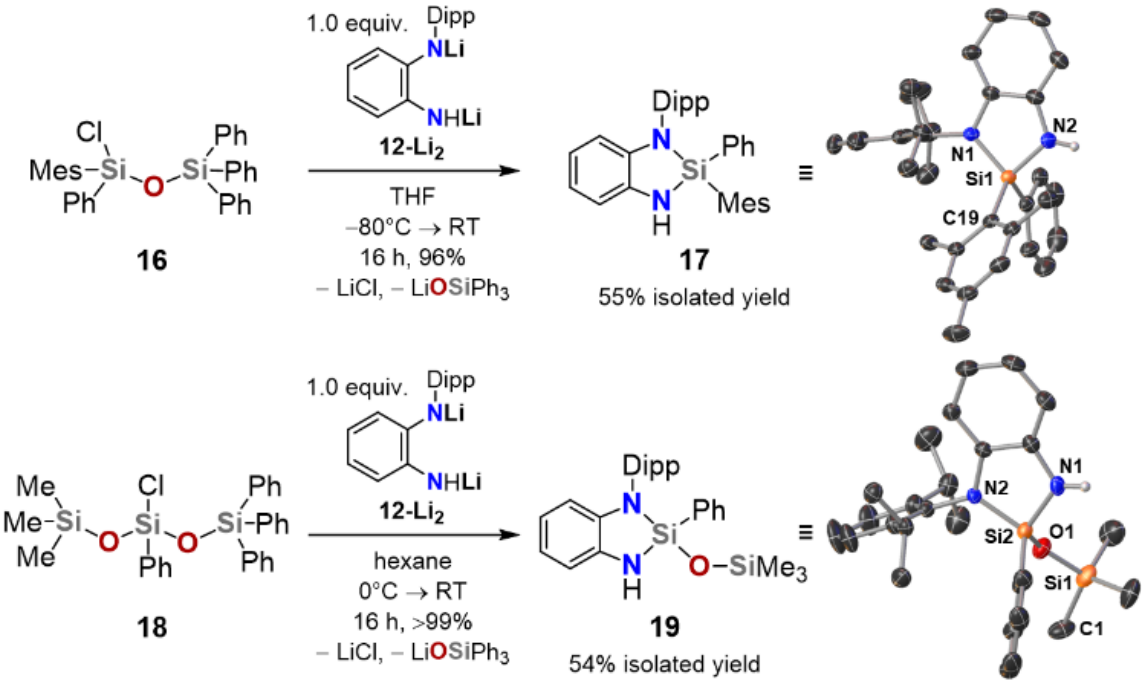

Scheme 3.4. Variation of the substituents on the attacked silicon atom (top). Regioselectivity of the Si–O–Si cleavage in an unsymmetrically substituted chlorotrisiloxane (bottom). Molecular structures of compounds **17** and **19** in the crystal (Mes = mesityl).

3.4 Conclusions

In conclusion, a powerful concept for the application-oriented design of siloxanes was provided. The method can have a direct impact on the development of new functional oligosiloxane scaffolds and the targeted construction of molecular siloxide models. The authors are currently working on testing this concept on silsequioxanes as the next step on the way to more complex Si–O–Si-based materials and elaborating an asymmetric version of this method for the desymmetrization of silanols.

3.5 References

[1] a) Silicon and Siliceous Structures in Biological Systems (Eds.: T. L. Simpson, B. E. V olcani), Springer, New York, **1981**; b) F. Liebau, Structural Chemistry of Silicates: Structure, Bonding, and Classification, Springer-Verlag, Berlin, Heidelberg, Germany, **1985**; c) T. W. Swaddle, J. Salerno, P. A. Tregloan, *Chem. Soc. Rev*. **1994**, *23*, 319-325; d) N. Kröger, R. Deutzmann, M. Sumper, *Science* **1999**, *286*, 1129-1132; e) R. Tacke, *Angew. Chem. Int. Ed*. **1999**, *38*, 3015-3018; *Angew. Chem*. **1999**, *111*, 3197-3200; f) G. V. Gibbs, A. F. Wallace, D. F. Cox, R. T. Downs, N. L. Ross, K. M. Rosso, *Am. Mineral*. **2009**, *94*, 1085-1102.

[2] a) W. Noll, *Angew. Chem.* **1954**, *66*, 41-55; b) M. A. Brook, *Silicon in Organic, Organometallic, and Polymer Chemistry*, John Wiley & Sons, New York, USA, **2000**; c) R. G. Jones, W. Ando, J. Chojnowski (Eds.), *Silicon-Containing Polymers: The Science and Technology of Their Synthesis and Applications*, Springer, Netherlands, **2000**; d) S. Ganachaud, S. Boileau, B. Boury (Eds.), *Silicon Based Polymers: Advances in Synthesis and Supramolecular Organization*, Springer, Netherlands, **2008**; e) U. Schubert, N. Hüsing, *Synthesis of Inorganic Materials* (4th Ed.), Wiley-VCH, Weinheim, Germany, **2019**.

[3] For reviews, see: a) M. Hong, J. Chen, E. Y.-X. Chen, *Chem. Rev.* **2018**, *118*, 10551-10616; b) K. Matsumoto, S. Shimada, K. Sato, *Chem. Eur. J.* **2019**, *25*, 920-928; c) F. Vidal, F. Jäkle, *Angew. Chem. Int. Ed.* **2019**, *58*, 5846-5870; *Angew. Chem.* **2019**, *131*, 5904-5929.

[4] a) R. Wakabayashi, K. Kawahara, K. Kuroda, *Angew. Chem. Int. Ed.* **2010**, *49*, 5273-5277; *Angew. Chem.* **2010**, *122*, 5401-5405; c) S. Saito, N. Yamasue, H. Wada, A. Shimojima, K. Kuroda, *Chem. Eur. J.* **2016**, *22*, 13857-13864; d) K. Matsumoto, K. V. Sajna, Y. Satoh, K. Sato, S. Shimada, *Angew. Chem. Int. Ed.* **2017**, *56*, 3168-3171; *Angew. Chem.* **2017**, *129*, 3216-3219; e) K. Matsumoto, Y. Oba, Y. Nakajima, S. Shimada, K. Sato, *Angew. Chem. Int. Ed.* **2018**, *57*, 4637-4641; *Angew. Chem.* **2018**, *130*, 4727-4731.

[5] a) J. O. Bauer, C. Strohmann, *Angew. Chem. Int. Ed*. **2014**, *53*, 720-724; *Angew. Chem*. **2014**, *126*, 738-742; b) Y. Satoh, M. Igarashi, K. Sato, S. Shimada, *ACS Catal*. **2017**, *7*, 1836-1840; c) K. Kuciński, G. Hreczycho, *ChemSusChem* **2019**, *12*, 1043-1048; d) S. Pattanaik, C. Gunanathan, *ACS Catal*. **2019**, *9*, 5552-5561; e) J. Zhu, S. Chen, C. He, *J. Am. Chem. Soc*. **2021**, *143*, 5301-5307.

[6] a) K. S. Lokare, N. Frank, B. Braun-Cula, I. Goikoetxea, J. Sauer, C. Limberg, *Angew. Chem. Int. Ed*. **2016**, *55*, 12325-12329; *Angew. Chem*. **2016**, *128*, 12513-12517; b) K. S. Lokare, P. Wittwer, B. Braun-Cula, N. Frank, S. Hoof, T. Braun, C. Limberg, Z. Anorg. *Allg. Chem*. **2017**, *643*, 1581-1588; c) K. S. Lokare, B. Braun-Cula, C. Limberg, M. Jorewitz, J. T. Kelly, K. R. Asmis, S. Leach, C. Baldauf, I. Goikoetxea, J. Sauer*, Angew. Chem. Int. Ed*. **2019**, *58*, 902-906; *Angew. Chem*. **2019**, *131*, 912-917.

[7] a) J. Sauer, *Z. Chem*. **1982**, *22*, 60-61; b) F. Weinhold, R. West, *Organometallics* **2011**, 30, 5815-5824; c) F. Weinhold, R. West, *J. Am. Chem. Soc*. **2013**, *135*, 5762-5767; d) M. Fugel, M. F. Hesse, R. Pal, J. Beckmann, D. Jayatilaka, M. J. Turner, A. Karton, P. Bultinck, G. S. Chandler, S. Grabowsky, *Chem. Eur. J*. **2018**, *24*, 15275-15286.

[8] W. Noll, Angew. *Chem. Int. Ed*. **1963**, *2*, 73-80; *Angew. Chem*. **1963**, *75*, 123-130.

[9] C. Däschlein, J. O. Bauer, C. Strohmann, *Angew. Chem. Int. Ed*. **2009**, *48*, 8074-8077; *Angew. Chem*. **2009**, *121*, 8218-8221.

[10] a) L. Wilczek, J. Chojnowski, *Macromolecules* **1981**, *14*, 9-17; b) J. Chojnowski, S. Rubinsztajn, L. Wilczek, *Macromolecules* **1987**, *20*, 2345-2355; c) W. Sarich, A. Surkus, D. Lange, E. Popowski, H. Kelling, *Z. Anorg. Allg. Chem*. **1990**, *581*, 199-208; d) S. Rubinsztajn, M. Cypryk, J. Chojnowski, *Macromolecules* **1993**, *26*, 5389-5395; e) M. Cypryk, Y. Apeloig, *Organometallics* **1997**, *16*, 5938-5949; f) M. Cypryk, Y. Apeloig, *Organometallics* **2002**, *21*, 2165-2175.

[11] a) D. Seyferth, D. L. Alleston, *Inorg. Chem*. **1963**, *2*, 418-420; b) I. Ruidisch, M. Schmidt, *Angew. Chem. Int. Ed*. **1963**, *2*, 328; *Angew. Chem*. **1963**, *75*, 575; c) C. L. Frye, R. M. Salinger, F. W. G. Fearon, J. M. Klosowski, T. DeYoung, *J. Org. Chem*. **1970**, *35*, 1308-1314; d) S. McN. Sieburth, W. Mu, *J. Org. Chem*. **1993**, *58*, 7584-7586.

[12] a) G. E. Herberich, T. P. Spaniol, A. Fischer, *Chem. Ber*. **1994**, *127*, 1619-1620; b) C. Jones, P. C. Junk, N. A. Smithies, *J. Organomet. Chem*. **2000**, *607*, 105-111.

[13] a) S. Enthaler, *Angew. Chem. Int. Ed*. **2014**, *53*, 2716-2721; *Angew. Chem*. **2014**, *126*, 2754-2759; b) R. F. Weitkamp, B. Neumann, H.-G. Stammler, B. Hoge, *Angew. Chem. Int. Ed*. **2020**, *59*, 5494-5499; *Angew. Chem*. **2020**, *132*, 5536-5541.

[14] a) S. Enthaler, R. Kretschmer, *ChemSusChem* **2014**, *7*, 2030-2036; b) P. Döhlert, J. Pfrommer, S. Enthaler, *ACS Sust. Chem. Eng*. **2015**, *3*, 163-169; c) M. Okamoto, K. Miyazaki, A. Kado, E. Suzuki, *Chem. Commun*. **2001**, 1838-1839; d) Y. Ikeda, W. Huang, A. Oku, *Green Chem*. **2003**, *5*, 508-511; e) B. Rupasinghe, J. C. Furgal, *ACS Appl. Polym*. *Mater*. **2021**, *3*, 1828-1839.

[15] M. Yoshikawa, Y. Tamura, R. Wakabayashi, M. Tamai, A. Shimojima, K. Kuroda, *Angew. Chem. Int. Ed*. **2017**, *56*, 13990-13994; *Angew. Chem*. **2017**, *129*, 14178-14182.

[16] For systematic studies on the stability of arylsilanols, see: a) N. Hurkes, S. Spirk, F. Belaj, R. Pietschnig, *Z. Anorg. Allg. Chem.* **2013**, *639*, 2631-2636; b) J.-F. Kannengießer, M. Briesenick, D. Meier, V. Huch, B. Morgenstern, G. Kickelbick, *Chem. Eur. J.* **2021**, DOI: 10.1002/chem.202102729.

[17] M. C. Lipke, A. L. Liberman-Martin, T. D. Tilley, *Angew. Chem. Int. Ed.* **2017**, *56*, 2260-2294; *Angew. Chem.* **2017**, *129*, 2298-2335.

[18] J. Yu, Y. Liu, *Angew. Chem. Int. Ed.* **2017**, *56*, 8706-8710; *Angew. Chem.* **2017**, *129*, 8832-8836.

[19] D. B. Thompson, M. A. Brook, *J. Am. Chem. Soc.* **2008**, *130*, 32-33.

[20] a) S. Rubinsztajn, J. A. Cella, *Macromolecules* **2005**, *38*, 1061-1063; b) J. Chojnowski, S. Rubinsztajn, J. A. Cella, W. Fortuniak, M. Cypryk, J. Kurjata, K. Kaźmierski, *Organometallics* **2005**, *24*, 6077-6084.

[21] a) B. Gehrhus, M. F. Lappert, J. Heinicke, R. Boese, D. Bläser, *J. Chem. Soc., Chem. Commun.* **1995**, 1931-1932; b) W. M. Boesveld, B. Gehrhus, P. B. Hitchcock, M. F. Lappert, P. v. R. Schleyer, *Chem. Commun.* **1999**, 755-756; c) J. C. Slootweg, F. J. J. de Kanter, M. Schakel, A. W. Ehlers, B. Gehrhus, M. Lutz, A. M. Mills, A. L. Spek, K. Lammertsma, *Angew. Chem. Int. Ed.* **2004**, *43*, 3474-3477; *Angew. Chem.* **2004**, *116*, 3556-3559; d) B. Gehrhus, P. B. Hitchcock, M. Parruci, *Dalton Trans.* **2005**, 2720-2725.

[22] a) J. O. Bauer, C. Strohmann, *Chem. Commun.* **2012**, *48*, 7212-7214; b) M. Achternbosch, L. Zibula, J.-L. Kirchhoff, J. O. Bauer, C. Strohmann, *Inorg. Chem.* **2021**, *60*, 11562-11568.

[23] A control experiment showed that intermolecular cleavage of disiloxanes does not happen (for details, see chapter 3.6.7).

[24] a) S. Spirk, M. Nieger, F. Belaj, R. Pietschnig, *Dalton Trans.* **2009**, 163-167; b) N. Hurkes, C. Bruhn, F. Belaj, R. Pietschnig, *Organometallics* **2014**, *33*, 7299-7306; c) N. Oguri, Y. Egawa, N. Takeda, M. Unno, *Angew. Chem. Int. Ed.* **2016**, *55*, 9336-9339; *Angew. Chem.* **2016**, *128*, 9482-9485.

[25] a) N. A. Espinosa-Jalapa, J. O. Bauer, *Z. Anorg. Allg. Chem.* **2020**, *646*, 828-834; b) J. O. Bauer, N. A. Espinosa-Jalapa, N. Fontana, T. Götz, A. Falk, *Eur. J. Inorg. Chem.* **2021**, 2636-2642.

[26] J. O. Bauer, T. Götz, *Chemistry* **2021**, *3*, 444-453.

[27] a) S. Danièle, C. Drost, B. Gehrhus, S. M. Hawkins, P. B. Hitchcock, M. F. Lappert, P. G. Merle, S. G. Bott, *J. Chem. Soc., Dalton Trans.* **2001**, 3179-3188; b) P. B. Hitchcock, M. F. Lappert, X.-H. Wei, *Dalton Trans.* **2006**, 1181-1187; c) T. James, J. M. Rawson, D. Song, *Dalton Trans.* **2013**, *42*, 10640-10648; d) S. Robinson, E. S. Davies, W. Lewis, A. J. Blake, S. T. Liddle, *Dalton Trans.* **2014**, *43*, 4351-4360; e) T. Janes, M. Xu, D. Song, *Dalton Trans.* **2016**, *45*, 10672-10680; f) K. Yu. Monakhov, J. van Leusen, P. Kögerle, E.-L. Zins, M. E. Alikhani, M. Tromp, A. A. Danopoulos, P. Braunstein, *Chem. Eur. J.* **2017**, *23*, 6504-6508.

[28] N. A. Espinosa-Jalapa, N. Berg, M. Seidl, I. G. Shenderovich, R. M. Gschwind, J. O. Bauer, *Chem. Commun*. **2020**, *56*, 13335-13338.

3.6 Syntheses and characterizations

3.6.1 General remarks

All experiments were performed in an inert atmosphere of purified nitrogen by using standard Schlenk techniques or an MBraun Unilab 1200/780 glovebox. Glassware was heated at 600 °C prior to use. Diethyl ether (Et_2O), dichloromethane (DCM), hexane, pentane, tetrahydrofuran (THF), and toluene were dried and degassed with an MBraun SP800 solvent purification system. *n*-Butyllithium (2.5 M or 1.6 M solution in hexane, Merck KGaA), trichlorophenylsilane (97%, Alfa Aesar), dichlorodiphenylsilane (98%, Merck KGaA), triphenylsilanol (98%, Merck KGaA), trimethylsilanol (≥ 97.5%, Merck KGaA), tri-*iso*-propylsilanol (98%, Merck KGaA), hexamethylbenzene (HMB, 99%, Merck KGaA), di-*iso*-propylamine (≥ 99.0%, Merck KGaA), pyrrolidine (for synthesis, Merck KGaA), lithium trimethylsiloxide (95%, Merck KGaA), bromomesitylene (98%, Merck KGaA), 1-fluoro-2-nitrobenzene (99%, Fluorochem Ltd), 2,6-di-*iso*-propylaniline (90%, Merck KGaA), *tert*-butylamine (98%, Merck KGaA), *N*,*N*-dimethylformamide DMF (99.5%, Acros) and trichlorosilane (99%, Merck KGaA) were used as received without any further purification. Triethylamine (≥99%, Merck KGaA) was heated at reflux over CaH_2 and distilled prior to use. 1-Chloro-1,1,3,3,3-pentaphenyldisiloxane (**14**)[1] and 1-Chloro-1-mesityl-1,3,3,3-tetraphenyldisiloxane (**16**)[2] were synthesized according to previously published procedures. C_6D_6 used for NMR spectroscopy was dried over 3 Å molecular sieves and degassed by a standard freeze-pump-thaw procedure. NMR spectra were either recorded using a Bruker Avance 300 (300.13 MHz), a Bruker Avance 400 (400.13 MHz) or a Bruker Avance III HD 400 (400.13 MHz) at 25 °C. Chemical shifts (δ) are reported in parts per million (ppm). ^{1}H and $^{13}C\{^{1}H\}$ NMR spectra are referenced to tetramethylsilane ($SiMe_4$, δ = 0.0 ppm) as external standard, with the deuterium signal of the solvent serving as internal lock and the residual solvent signal as an additional reference. $^{29}Si\{^{1}H\}$ NMR spectra are referenced to $SiMe_4$. $^{7}Li\{^{1}H\}$ spectra are not referenced. For the assignment of the multiplicities, the following abbreviations are used: s = singlet, d = doublet, t = triplet, sept = septet, m = multiplet. For simplicity, multiplets of order higher than one are described approximating them to the closest first-order type. High-resolution mass spectrometry was carried out on a Jeol AccuTOF GCX and an Agilent Q-TOF 6540 UHD spectrometer. Elemental analyses were performed on a Vario MICRO cube apparatus.

3.6.2 Synthesis of precursors

4.1.1.1 (DippNH)Ph(NO_2)

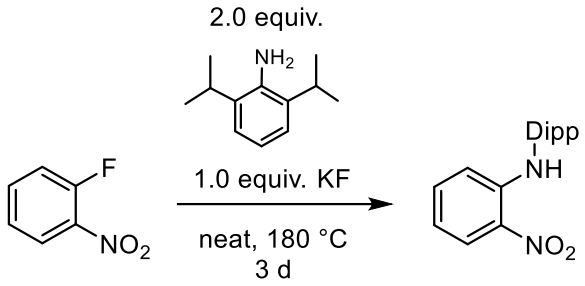

According to a modified literature procedure,[3] 1-fluoro-2-nitrobenzene (21.0 mL, 200.0 mmol, 1.0 equiv.), 2,6-di-*iso*-propylaniline (60.0 mL, 400.0 mmol, 2.0 equiv.), and potassium fluoride (11.60 g, 200.0 mmol, 1.0 equiv.) were mixed and heated in neat conditions to 180 °C while stirring for 3 days. The orange mixture was treated with ethyl acetate (ca. 200 mL) and water (ca. 200 mL) and extracted using a separation funnel. The aqueous phase was again extracted with ethyl acetate (3 × 100 mL). The combined organic phases were extracted with brine (ca. 200 mL) and then dried over $MgSO_4$. After removal of the solids via filtration, all volatiles were removed via rotatory evaporation. The remaining orange oil was recrystallized from hot ethanol and afforded an orange crystalline solid of (DippNH)Ar(NO_2), which was isolated by filtration and washed with ethanol (31.50 g, 106 mmol, 53%).

^{1}H NMR (400 MHz, $CDCl_3$, 298 K): δ[ppm] = 1.09 [d, $^3J_{H\text{-}H}$ = 6.87 Hz, 6H, CH(CH_3)$_2$], 1.15 [d, $^3J_{H\text{-}H}$ = 6.87 Hz, 6H, CH(CH_3)$_2$], 3.02 [sept, $^3J_{H\text{-}H}$ = 6.84 Hz, 2H, CH(CH$_3$)$_2$], 6.36 [dd, $^3J_{H\text{-}H}$ = 8.70, $^4J_{H\text{-}H}$ = 1.23 Hz, 1H, H_{Ph}], 6.63–6.69 [m, 1H, H_{Ph}], 7.21–7.28 [m, 3H, H_{Ph}], 7.33–7.49 [m, 1H, H_{Ph}], 8.21 [dd, $^3J_{H\text{-}H}$ = 8.70, $^4J_{H\text{-}H}$ = 1.54 Hz, 1H, H_{Ph}], 9.19 [s, 1H, NH].

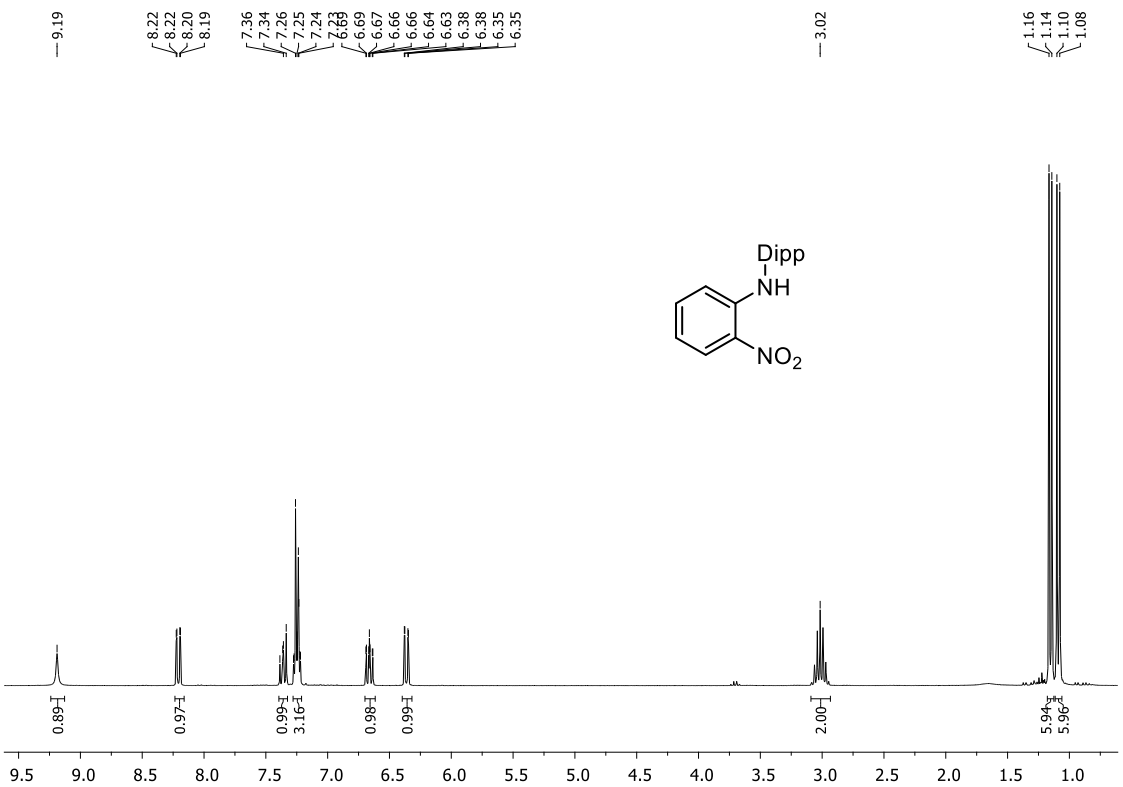

Figure S3.1. ^{1}H NMR spectrum ($CDCl_3$, 298 K) of (DippNH)Ph(NO_2).

4.1.1.2 (DippNH)Ph(NH_2) (12)

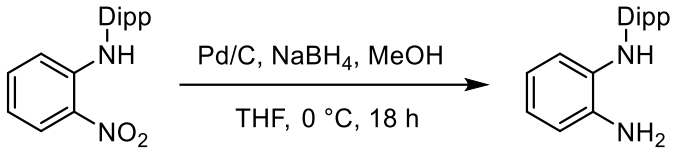

12

According to modified literature procedures,[4,5] (DippNH)Ph(NO_2) (27.60 g, 92.0 mmol, 1.0 equiv.), Pd/C (1.00 g, 0.8 mmol, 0.9 mol%), and sodium borohydride (8.70 g, 230.0 mmol, 2.5 equiv.) were dissolved in 200 mL of THF and cooled to 0 °C. Methanol (ca. 100 mL) was added dropwise under gas formation. After the addition had been completed, the dark purple reaction mixture was stirred for further 18 h. The solids were filtered off and the filtrate was extracted with ethyl acetate (3 × 100 mL) and brine (100 mL) using a separation funnel. The combined organic phases were dried over $MgSO_4$ and the solids removed by filtration. All volatiles were removed via rotatory evaporation to afford a purple oil which was recrystallized from hot ethanol. Storing the solution at −20 °C resulted in the precipitation of a purple crystalline solid of (DippNH)Ph(NH_2) (**12**), which was isolated by filtration and washed with ethanol (18.09 g, 67.0 mmol, 73%).

^{1}H NMR (400 MHz, C_6D_6, 298 K): δ[ppm] = 1.09 [br, 12H, CH(CH_3)$_2$], 2.80 [s, 2H, NH_2], 3.13 [sept, $^{3}J_{H\text{-}H}$ = 6.80 Hz, 2H, CH(CH$_3$)$_2$], 4.86 [s, 1H, NH], 6.35 [dd, $^{3}J_{H\text{-}H}$ = 7.81 Hz, $^{4}J_{H\text{-}H}$ = 1.44 Hz, 1H,

H_{Ph}], 6.48 [dd, $^{3}J_{H\text{-}H}$ = 7.51 Hz, $^{4}J_{H\text{-}H}$ = 1.58 Hz, 1H, H_{Ph}], 6.62–6.78 [m, 2H, H_{Ph}], 7.17–7.27 [m, 3H, H_{Ph}].

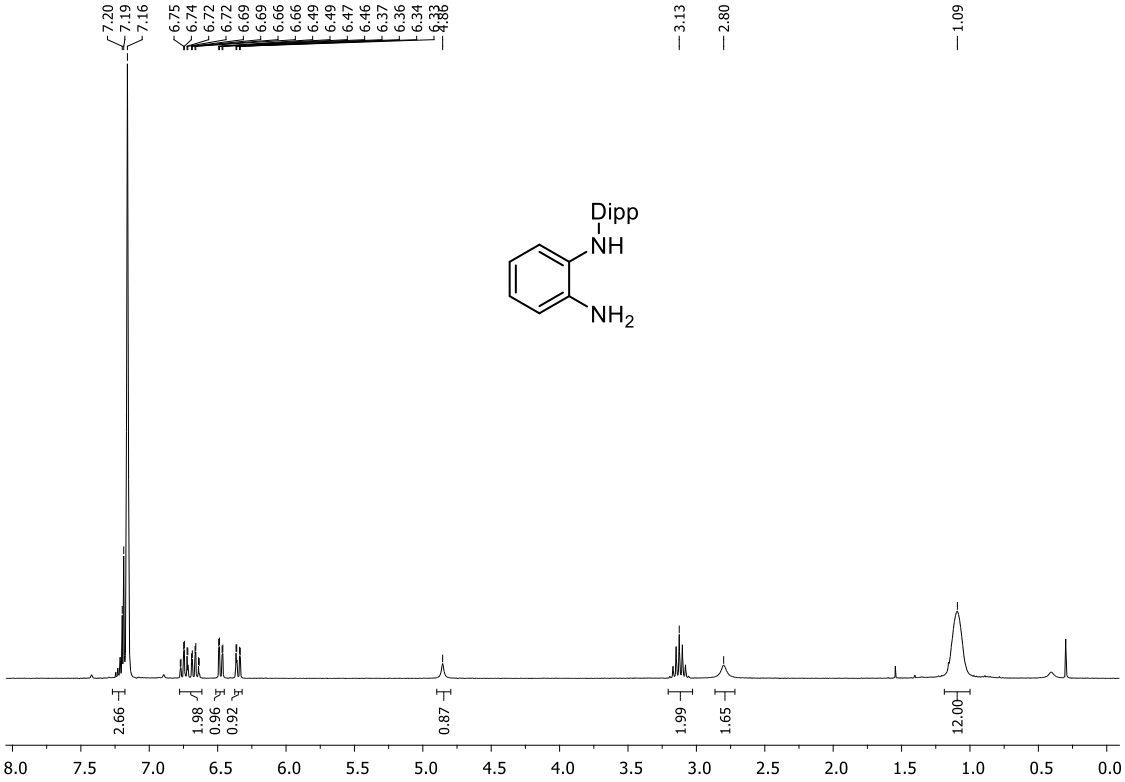

Figure S3.2. ^{1}H NMR spectrum (C_6D_6, 298 K) of (DippNH)Ph(NH_2) (**12**).

4.1.1.3 (*t*BuNH)Ph(NO_2)

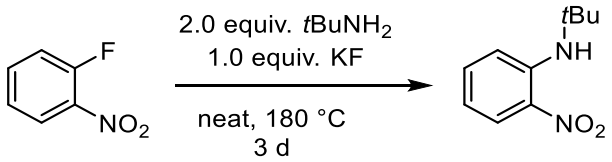

According to a modified literature procedure,[5] 1-fluoro-2-nitrobenzene (21.0 mL, 200.0 mmol, 1.0 equiv.), *tert*-butylamine (104.0 mL, 400.0 mmol, 2.0 equiv.), and potassium fluoride (6.50 g, 200.0 mmol, 1.0 equiv.) were dissolved in 300 mL of *N*,*N*-dimethylformamide (DMF) and stirred at 100 °C for 3 days. The solids were filtered off and the light orange solution was transferred into a separation funnel. 100 mL of water were added and the orgaic phase extracted with ethyl acetate (3 × 100 mL). The combined organic fractions were extracted one time with brine solution and then dried over $MgSO_4$. Removal of the solids by filtration resulted in a light orange solution, which was dried via rotatory evaporation followed by drying five hours *in vacuo*. (*t*BuNH)Ph(NO_2) was obtained as an intense orange liquid (38.50 g, 198.0 mmol, 99%).

^{1}H NMR (300 MHz, $CDCl_3$, 298 K): δ[ppm] = 1.51 [s, 9H, C(CH_3)$_3$], 6.65–6.71 [m, 1H, H_{Ph}], 7.16–7.21 [m, 1H, H_{Ph}], 7.38–7.44 [m, 1H, H_{Ph}], 8.17–8.21 [m, 1H, H_{Ph}].

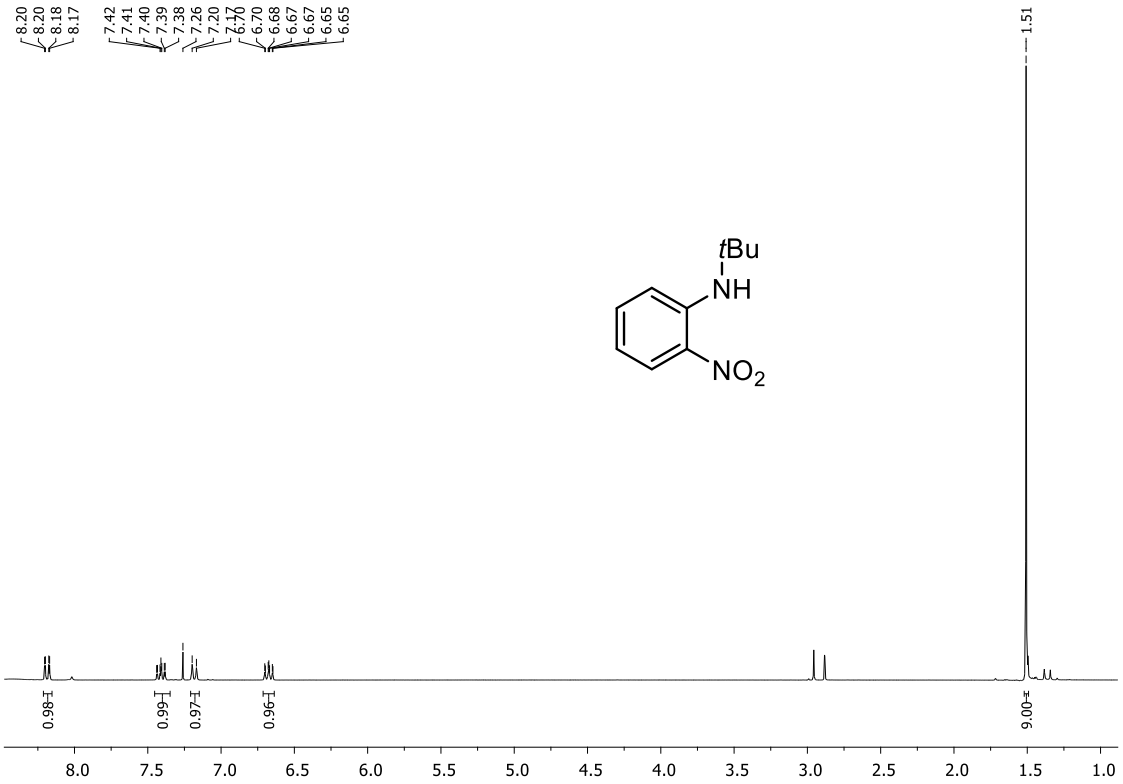

Figure S3.3. ^{1}H NMR spectrum ($CDCl_3$, 298 K) of (*t*BuNH)Ph(NO_2).

4.1.1.4 (*t*BuNH)Ph(NH_2) (13)

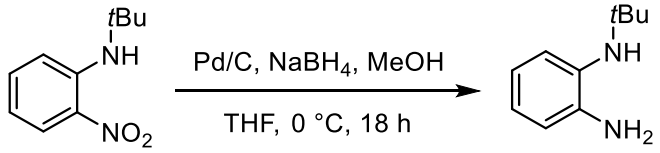

13

According to modified literature procedures,[5,6] (*t*BuNH)Ph(NO_2) (38.80 g, 200.0 mmol, 1.0 equiv.), Pd/C (4.20 g, 4.0 mmol, 2.0 mol%), and sodium borohydride (16.65 g, 440.0 mmol, 2.2 equiv.) were dissolved in 200 mL of THF and cooled to 0 °C. Methanol (ca. 100 mL) was added dropwise under gas formation. After the addition had been completed, the dark brown reaction mixture was stirred for further 18 h. The solids were filtered off and the filtrate was extracted with ethyl acetate (3 × 100 mL) and brine (100 mL) using a separation funnel. The combined organic phases were dried over $MgSO_4$ and the solids removed by filtration. All volatiles were removed via rotatory evaporation to afford a brown oil, which was distilled *in vacuo* (60 °C, 4.1 × 10^{-1} mbar). (*t*BuNH)Ph(NH_2) (**13**) was obtained as a yellow liquid (21.40 g, 130.0 mmol, 65%).

^{1}H NMR (300 MHz, C_6D_6, 298 K): δ[ppm] = 1.19 [s, 9H, C(C*H*$_3$)$_3$], 3.27 [br, 2H, N*H*$_2$], 6.60–6.64 [m, 1H, *H*$_{Ph}$], 6.85–7.03 [m, 3H, *H*$_{Ph}$].

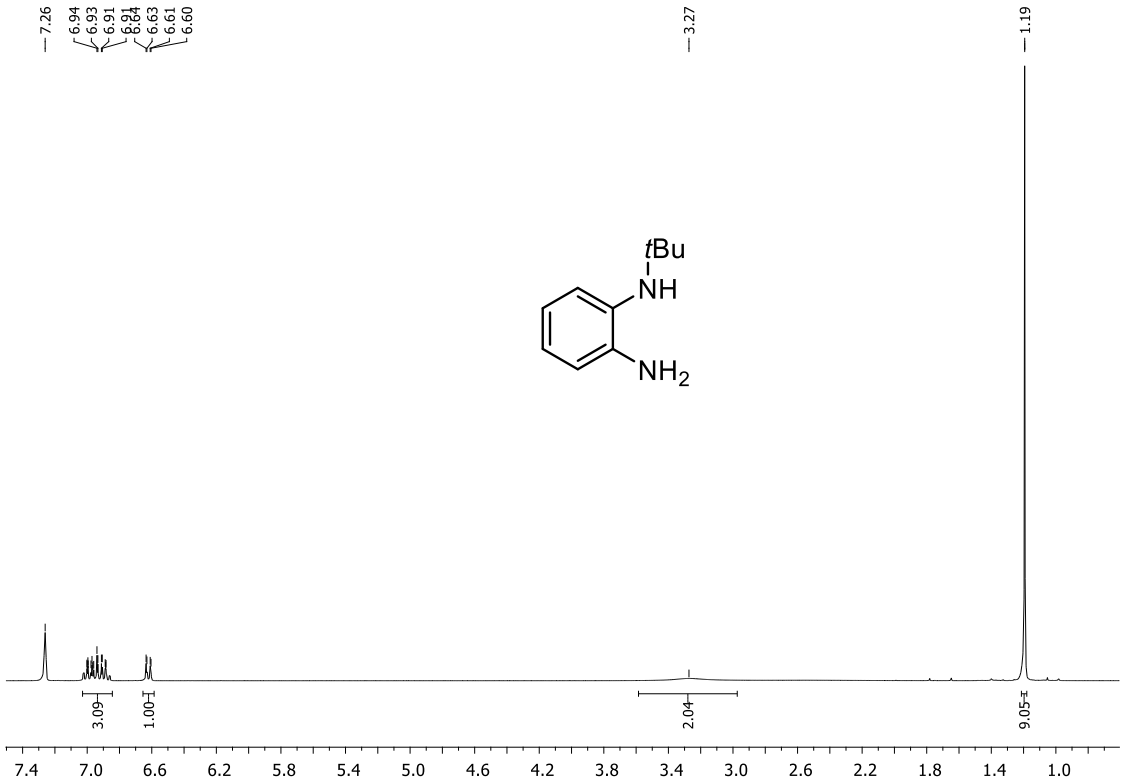

Figure S3.4. ^{1}H NMR spectrum (C_6D_6, 298 K) of (*t*BuNH)Ph(NH_2) (**13**).

4.1.1.5 Low temperature NMR study of 12-Li_2

Reaction 1: 2 equiv. *n*BuLi

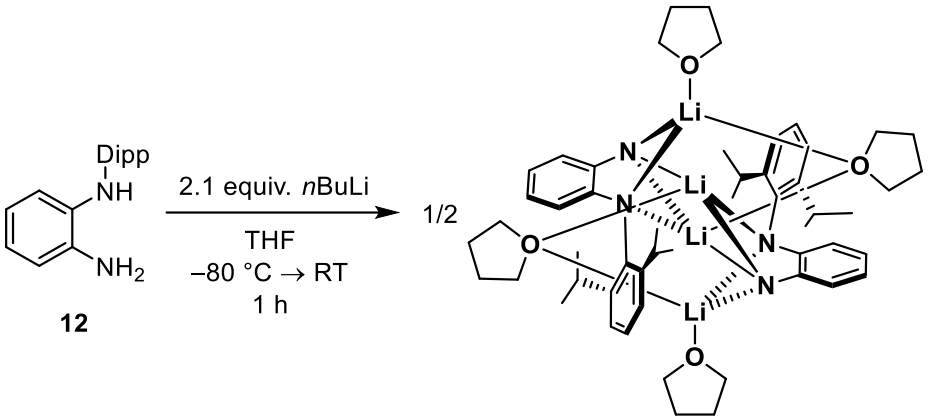

[12-Li_2·$(THF)_2$]$_2$

n-Butyllithium (0.84 mL of a 2.5 M solution in hexane, 2.1 mmol, 2.1 equiv.) was added dropwise to a solution of **12** (268 mg, 1.0 mmol, 1.0 equiv.) in 10 mL of THF at −80 °C. The resulting beige suspension was allowed to slowly warm up to room temperature and kept stirring for 2 h. Then, all volatiles were removed *in vacuo*, the residue washed with pentane (3 × 10 mL), and filtered via cannula filtration. The residue was dried *in vacuo* to afford **12-Li_2** as an off-white solid (389 mg, 0.92 mmol, 92%). Recrystallization from a toluene solution layered with pentane afforded yellow crystals suitable for single-crystal X-ray diffraction analysis (for details, see chapter 3.8). **12-Li_2** crystallized as the dimer **[12-Li_2·$(THF)_2$]$_2$** with two bridging and two terminally coordinating THF molecules. The compound was high sensitivity towards moisture. Single-crystals of **[12-Li_2·$(THF)_2$]$_2$** were subjected to NMR analysis.

The molecular structure in the crystalline state shows a dimer with two sets of inequivalent lithium atoms. The ^{1}H NMR spectrum at 193 K shows one set of signals, the ^{7}Li{^{1}H} spectrum two signals in accordance with the structure obtained from single-crystal X-ray diffraction analysis. It is likely that the solid-state structure of **12-Li_2** corresponds to the solution structure.

^{1}H NMR (400 MHz, THF-d_8, 193 K): *δ*[ppm] = 1.05 [d, $^{3}J_{H\text{-}H}$ = 6.49 Hz, 12H, CH(C*H*$_3$)$_2$], 3.34–3.42 [m, 2H, C*H*(CH$_3$)$_2$], 3.74 [s, 1H, N*H*], 5.46 [dd, $^{3}J_{H\text{-}H}$ = 8.07 Hz, $^{4}J_{H\text{-}H}$ = 1.02 Hz, 1H, *H*$_{Ph}$], 5.62 [td, $^{3}J_{H\text{-}H}$ = 7.05 Hz, $^{4}J_{H\text{-}H}$ = 1.10 Hz, 1H, *H*$_{Ph}$], 6.26 [td, $^{3}J_{H\text{-}H}$ = 7.46 Hz, $^{4}J_{H\text{-}H}$ = 1.49 Hz, 1H, *H*$_{Ph}$], 6.48 [dd, $^{3}J_{H\text{-}H}$ = 7.17 Hz, $^{4}J_{H\text{-}H}$ = 1.11 Hz, 1H, *H*$_{Ph}$], 6.93 [t, $^{3}J_{H\text{-}H}$ = 7.40 H, 3H, *H*$_{Ph}$]. **^{7}Li{^{1}H} NMR** (156 MHz, THF-d_8, 193 K): *δ*[ppm] = 1.47 [s], 1.55 [s].

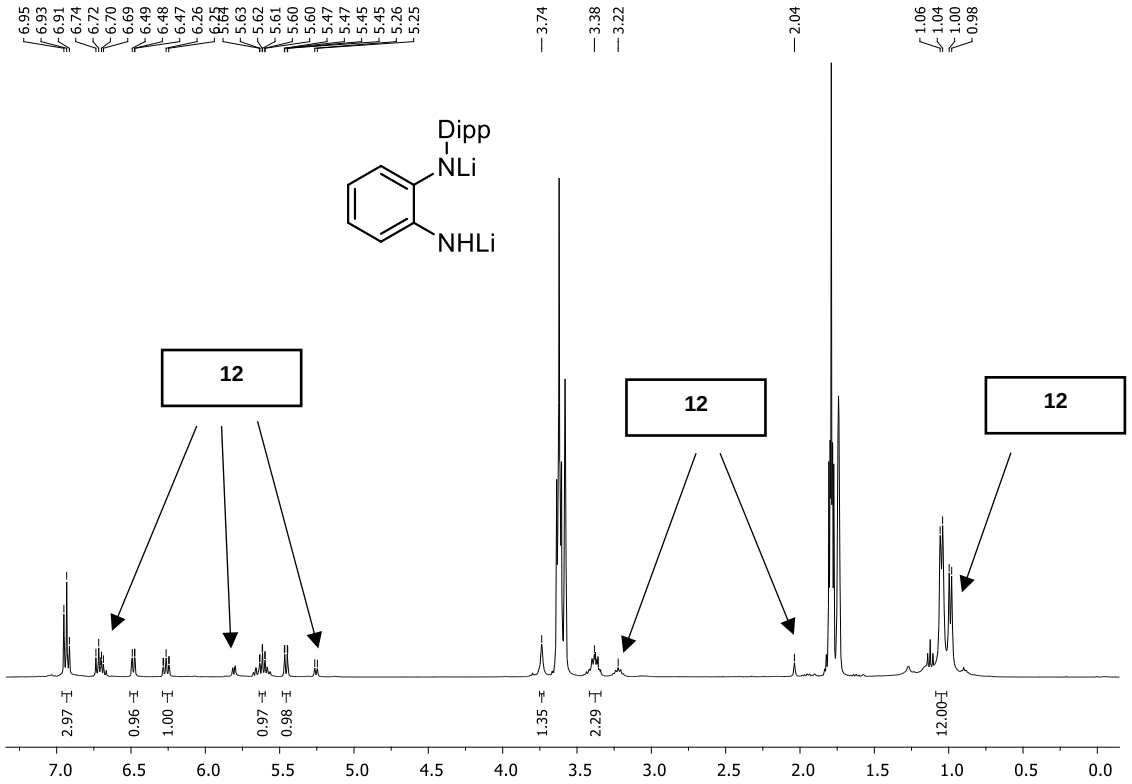

Figure S3.5. ^{1}H NMR spectrum (THF-d_8, 193 K) of **[12-Li$_2$·(THF)$_2$]$_2$**.

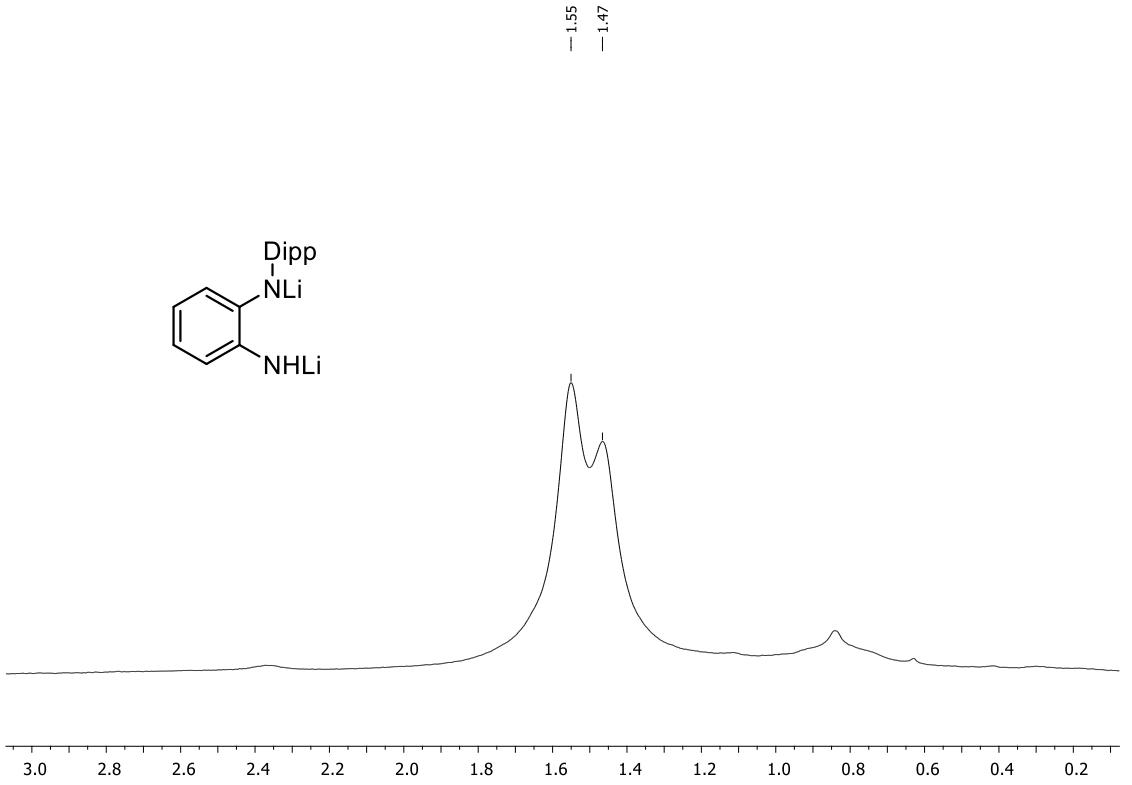

Figure S3.6. ^{7}Li{^{1}H} NMR spectrum (THF-d_8, 193 K) of **[12-Li2·(THF)2]$_2$**.

Reaction 2: 1 equiv. *n*BuLi

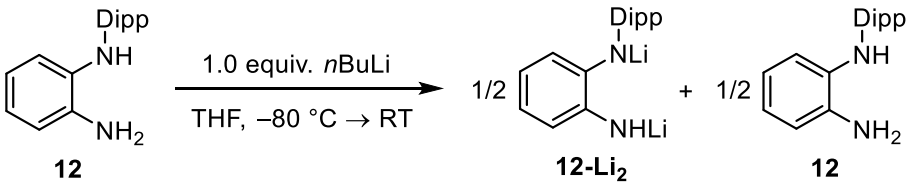

12 **12-Li$_2$** **12**

Compound **12** (268 mg, 1.0 mmol, 1.0 equiv.) was dissolved in 20 mL of THF and cooled down to −80 °C. *n*-Butyllithium (0.40 mL of a 2.5 M solution in hexane, 1.0 mmol, 1.0 equiv.) was added dropwise and the reaction mixture stirred for 16 h. An aliquot was taken from the dark brown solution and transferred into an NMR tube. All volatiles were removed *in vacuo*, the remaining brown residue dissolved in 0.6 mL THF-d$_8$, and the sample analyzed by NMR spectroscopy.
In the ^{1}H NMR spectrum at 193 K, unreacted **12** can be observed while the ^{7}Li{^{1}H} spectrum shows only one lithium species. Formation of a symmetric adduct with equivalent lithium centers consisting of the dilithiated compound **12-Li$_2$** and coordinating diamine **12** can be assumed. From reactions with one equiv. *n*BuLi were exclusively single-crystals of **[12-Li$_2$·(THF)$_2$]$_2$** obtained.

^{1}H NMR (400 MHz, THF-d$_8$, 193 K): *δ*[ppm] = 0.99 [d, $^3J_{H\text{-}H}$ = 6.76 Hz, 6H, CH(C*H*$_3$)], 1.05 [d, $^3J_{H\text{-}H}$ = 7.33 Hz, 6H, CH(C*H*$_3$)], 3.38 [m, 2H, CH(CH$_3$)$_2$], 3.74 [s, 1H, N*H*], 5.46 [d, $^3J_{H\text{-}H}$ = 7.80 Hz, 1H, *H*$_{Ph}$], 5.62 [t, $^3J_{H\text{-}H}$ = 7.10 Hz, 1H, *H*$_{Ph}$], 6.27 [t, $^3J_{H\text{-}H}$ = 7.70 Hz, 1H, *H*$_{Ph}$], 6.47–6.50 [m, 1H, *H*$_{Ph}$], 6.72 [t, $^3J_{H\text{-}H}$ = 7.50 Hz, 1H, *H*$_{Ph}$], 6.94 [d, , $^3J_{H\text{-}H}$ = 7.50 Hz, 2H, *H*$_{Ph}$].]. **^{7}Li{^{1}H} NMR** (156 MHz, THF-d$_8$, 193 K): *δ*[ppm] = 1.56 [s].

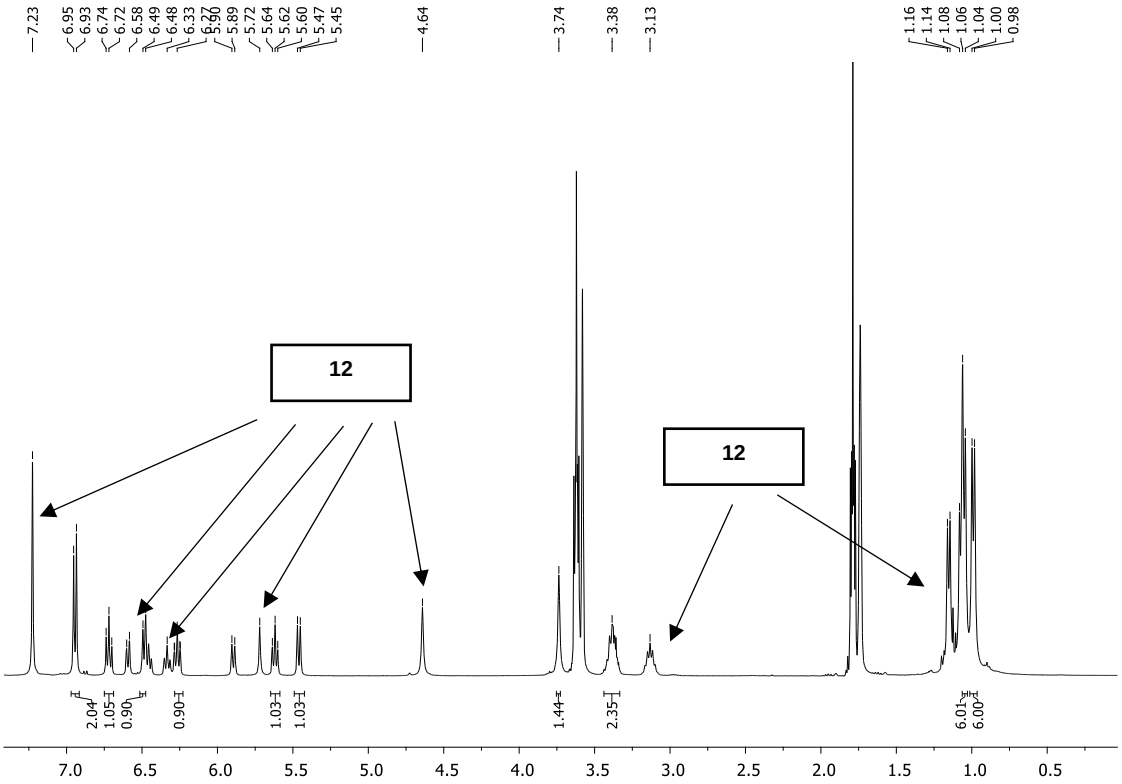

Figure S3.7. ^{1}H NMR spectrum (THF-d_8, 193 K) of the reaction of **12** with 1.0 equiv. *n*BuLi.

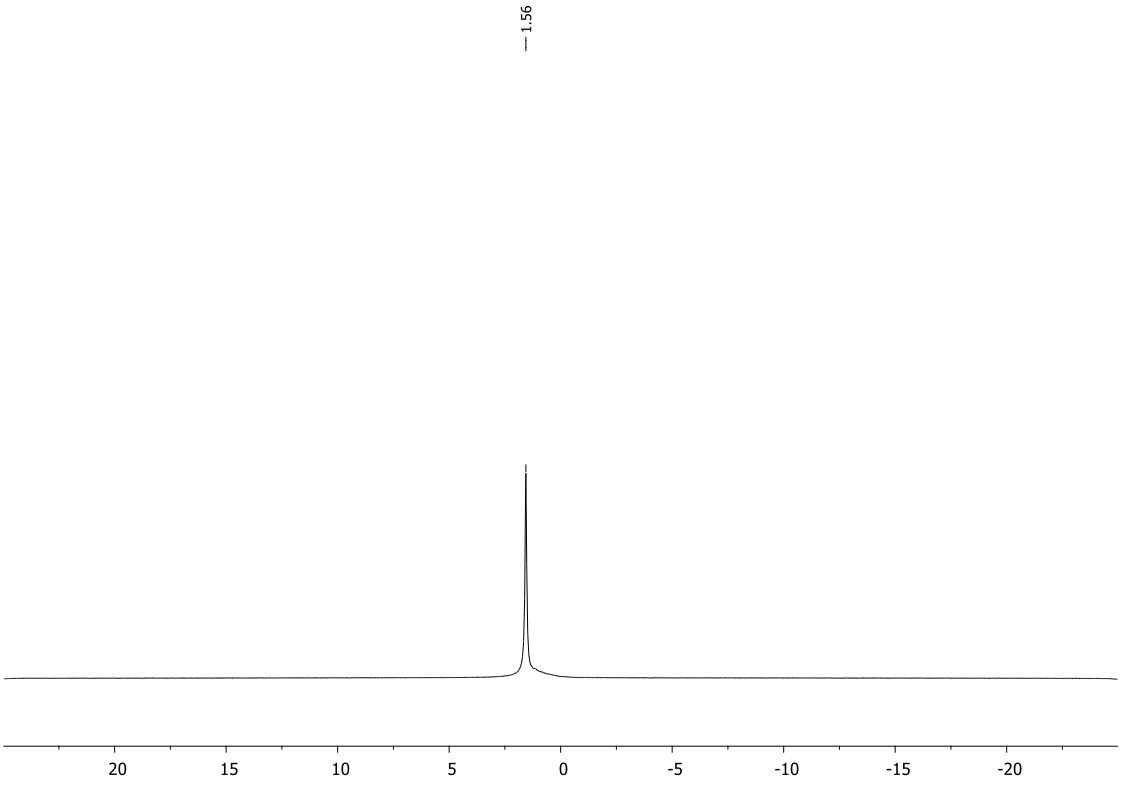

Figure S3.8. ^{7}Li{^{1}H} NMR spectrum (THF-d_8, 193 K) of the reaction of **12** with 1.0 equiv. *n*BuLi.

4.1.1.6 Compound 13-Li_2

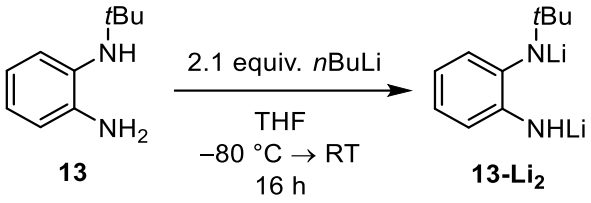

n-Butyllithium (0.88 mL of a 2.5 M solution in hexane, 2.1 mmol, 2.1 equiv.) was added dropwise to a solution of **13** (164 mg, 1.0 mmol, 1.0 equiv.) in 20 mL of THF at −80 °C. The resulting brown solution was allowed to slowly warm up to room temperature and kept stirring for 16 h. Then, all volatiles were removed *in vacuo*, the remaining brown residue washed with pentane (3 × 5 mL), and filtered via cannula filtration. The residue was dried *in vacuo* to afford **13-Li_2** as an off-white solid (152 mg). Even after repeated attempts, no crystalline material suitable for X-ray crystallography was achieved.

Both the ^{1}H NMR and ^{7}Li{^{1}H} spectrum at 193 K indicates the existence of one species with equivalent lithium centers.

^{1}H NMR (400 MHz, THF-d_8, 193 K): δ[ppm] = 1.26 [s, 9H, C(C*H*)$_3$], 1.82 [s, 1H, N*H*], 5.51 [t, $^{3}J_{H\text{-}H}$ = 6.99 Hz, 1H, H_{Ph}], 5.62–5.81 [m, 3H, H_{Ph}]. **^{7}Li{^{1}H} NMR** (156 MHz, THF-d_8, 193 K): δ[ppm] = 1.32 [s].

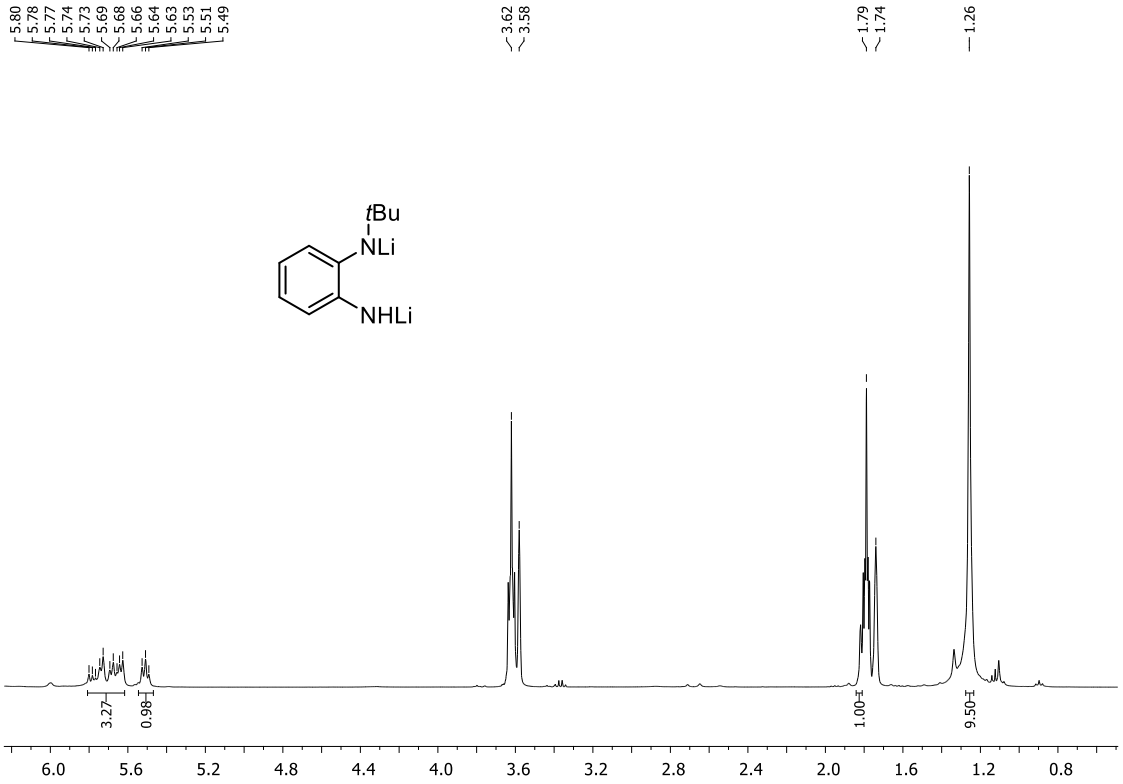

Figure S3.9. ^{1}H NMR spectrum (THF-d_8, 193 K) of **13-Li_2**.

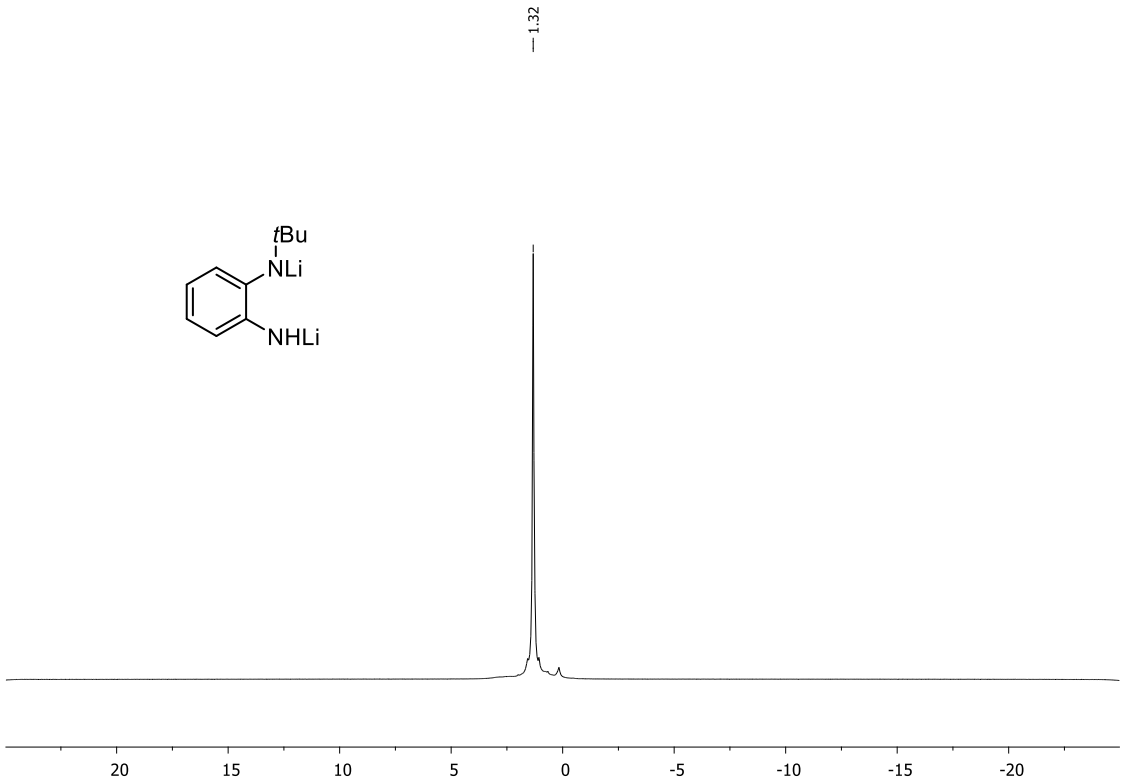

Figure S3.10. $^{7}Li\{^{1}H\}$ NMR spectrum (THF-d_8, 193 K) of **13-Li$_2$**.

4.1.1.7 Compound 1

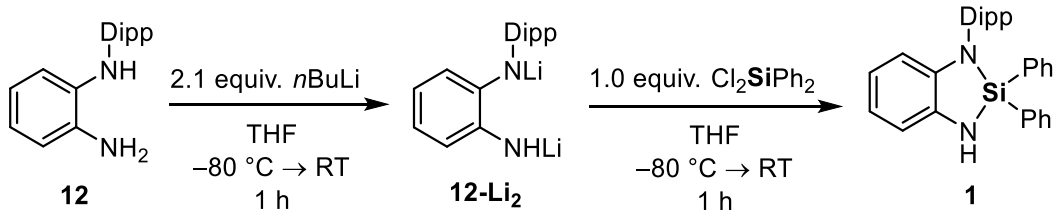

Compound **12** (6.10 g, 23.0 mmol, 1.0 equiv.) was dissolved in 180 mL of THF and the solution cooled down to −80 °C. *n*-Butyllithium (30.0 mL of a 2.5 M solution in hexane, 48.0 mmol, 2.1 equiv.) was added dropwise and the mixture was stirred for 2 h while warming up to room temperature. The formed brown suspension was again cooled down to −80 °C and dichlorodiphenylsilane (4.8 mL, 23.0 mmol, 1.0 equiv.) was added via syringe. The mixture was stirred for 16 h. Then, all volatiles were removed *in vacuo*. The crude residue was extracted with DCM (3 × 10 mL) and the remaining solids were removed via cannula filtration. The clear filtrates were collected and all volatiles removed *in vacuo* yielding a thick oily dark red residue. The residue was recrystallized from hot pentane affording **1** as a colorless crystalline solid (5.45 g, 12.0 mmol, 52%) suitable for single-crystal X-ray diffraction analysis (for details, see chapter 3.8).

^{1}H NMR (400 MHz, C_6D_6, 298 K): δ[ppm] = 0.42 [d, $^{3}J_{H\text{-}H}$ = 6.80 Hz, 6H, CH(CH_3)$_2$], 0.96 [d, $^{3}J_{H\text{-}H}$ = 6.80 Hz, 6H, CH(*C*H_3)$_2$], 3.01 [sept, $^{3}J_{H\text{-}H}$ = 6.80 Hz, 2H, C*H*(CH$_3$)$_2$], 3.44 [s, 1H, N*H*], 6.65–6.71

[m, 2H, H_{Ph}], 6.81–6.85 [m, 1H, H_{Ph}], 6.98–7.20 [m, 10H, H_{Ph}], 7.46–7.50 [m, 4H, H_{Ph}]. **$^{13}C\{^1H\}$ NMR** (101 MHz, C_6D_6, 298 K): δ[ppm] = 23.1 [s, $CH(CH_3)_2$], 26.8 [s, $CH(CH_3)_2$], 28.6 [s, $CH(CH_3)_2$], 111.3 [s, C_{Ph}], 111.6 [s, C_{Ph}], 118.5 [s, C_{Ph}], 118.7 [s, C_{Ph}], 124.7 [s, C_{Ph}], 130.6 [s, C_{Ph}], 133.7 [s, C_{Ph}], 135.2 [s, C_{Ph}], 135.5 [s, C_{Ph}], 138.6 [s, C_{Ph}], 141.7 [s, C_{Ph}], 149.1 [s, C_{Ph}]. **$^{29}Si\{^1H\}$ NMR** (79 MHz, C_6D_6, 298 K): δ[ppm] = -14.4 [s]. **CHN Analysis** $C_{30}H_{32}N_2Si$: calculated: C 80.31, H 7.19, N 6.24, Si 6.26; found: C 80.35, H 6.97, N 6.25. **HR-MS(EI+)**, calculated m/z for $C_{30}H_{32}N_2Si$ [M+H$^+$]: 448.23293; found: 448.23406.

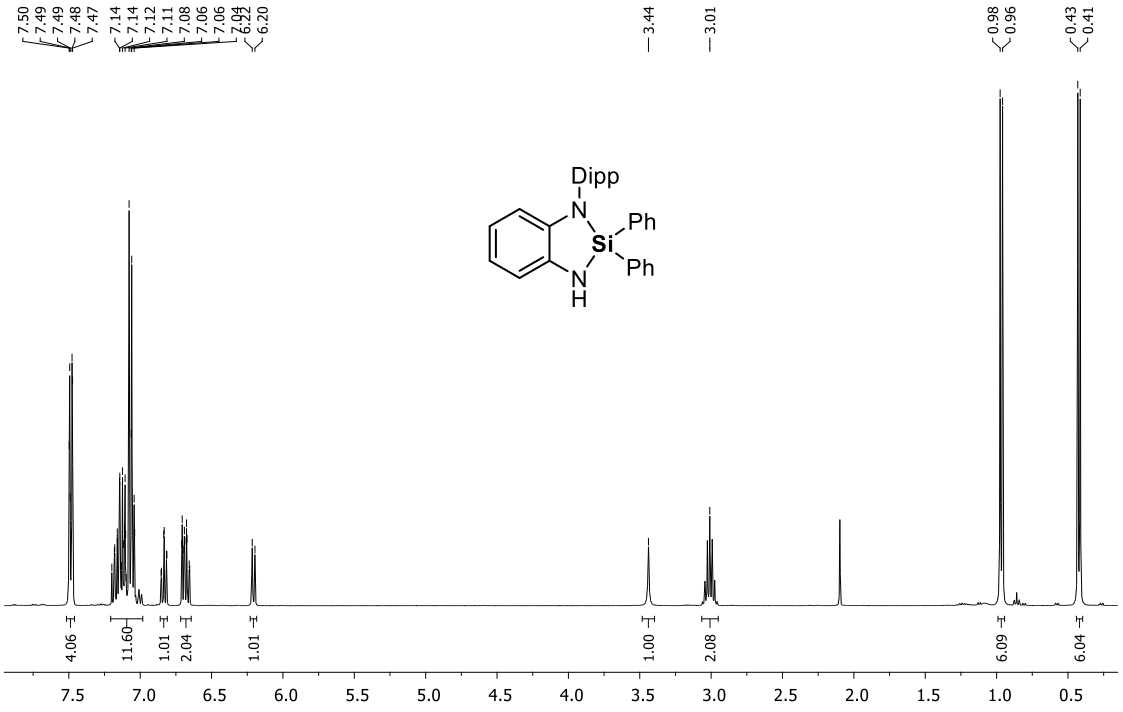

Figure S3.11. ^{1}H NMR spectrum (C_6D_6, 298 K) of **1**.

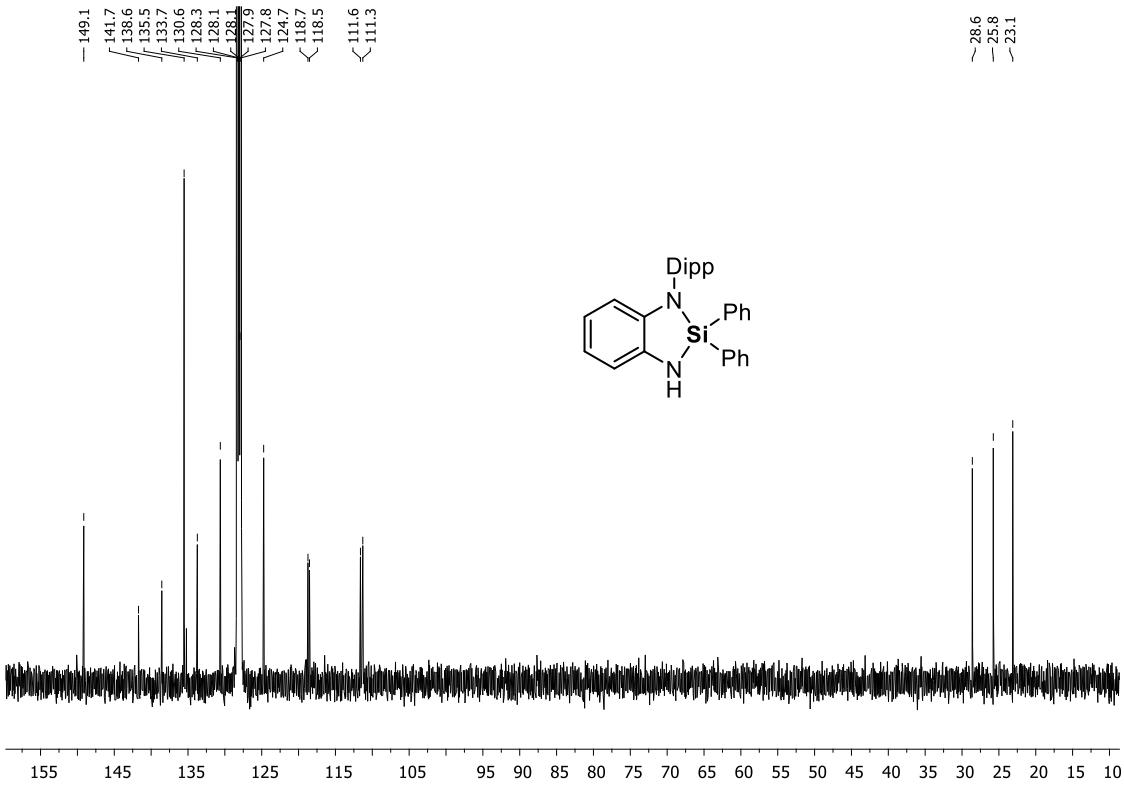

Figure S3.12. $^{13}C\{^{1}H\}$ NMR spectrum (C_6D_6, 298 K) of **1**.

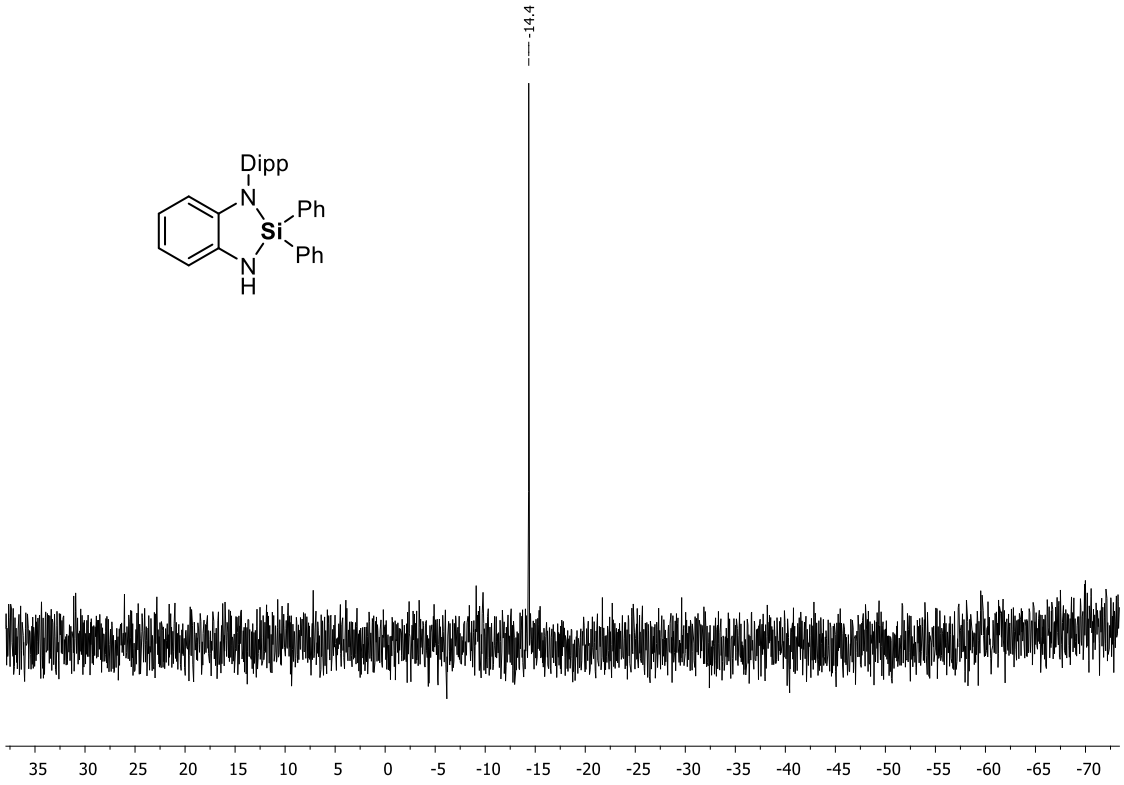

Figure S3.13. $^{29}Si\{^{1}H\}$ NMR spectrum (C_6D_6, 298 K) of **1**.

4.1.1.8 Compound 2

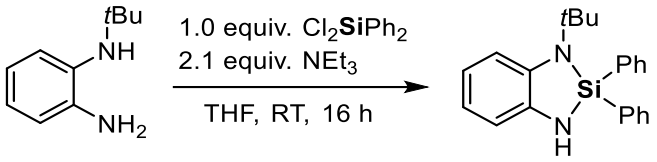

13 **2**

Compound **13** (4.93 g, 30.0 mmol, 1.0 equiv.) and triethylamine (8.8 mL, 63.0 mmol, 2.1 equiv.) were dissolved in 200 mL of THF. Dichlorodiphenylsilane (6.3 mL, 30.0 mmol, 1.0 equiv.) was added dropwise via syringe. The clear colorless solution turned cloudy immediately and was stirred for further 16 h. The formed precipitate was filtered off by cannula filtration and the filtrate was dried *in vacuo*. The afforded white solid was washed with Et_2O (3 × 10 mL) affording compound **2** as a colorless solid (6.00 g, 17.4 mmol, 58%). Crystals suitable for single-crystal X-ray diffraction analysis were obtained after dissolving a pure sample of **2** in the minimum amount of hot pentane and storing at 0 °C (for details, see chapter 3.8).

^{1}H NMR (400 MHz, C_6D_6, 298 K): δ[ppm] = 1.37 [s, 9H, C(CH_3)$_3$], 3.17 [s, 1H, N*H*], 6.51–6.57 [m, 1H, H_{Ph}], 6.83–6.94 [m, 2H, H_{Ph}], 7.02–7.08 [s, 1H, H_{Ph}], 7.18–7.23 [m, 6H, H_{Ph}], 7.71–7.79 [m, 4H, H_{Ph}]. **^{13}C{^{1}H} NMR** (101 MHz, C_6D_6, 298 K): δ[ppm] = 30.0 [s, C(CH$_3$)$_3$], 52.8 [s, C(CH$_3$)$_3$], 111.2 [s, C_{Ph}], 113.5 [s, C_{Ph}], 117.7 [s, C_{Ph}], 117.8 [s, C_{Ph}], 128.1 [s, C_{Ph}], 130.4 [s, C_{Ph}], 136.0 [s, C_{Ph}], 136.2 [s, C_{Ph}], 138.3 [s, C_{Ph}], 140.4 [s, C_{Ph}]. **^{29}Si{^{1}H}** NMR (79 MHz, C_6D_6, 298 K): δ[ppm] = −14.5 [s]. **CHN Analysis** $C_{22}H_{24}N_2Si$ calculated: C 76.70, H 7.02, N 8.13, Si 8.15; found: C 76.11, H 7.00, N 8.01. **MS(EI+)**, calculated m/z for $C_{22}H_{24}N_2Si$ [M+H$^+$]: 344.17; found: 344.17.

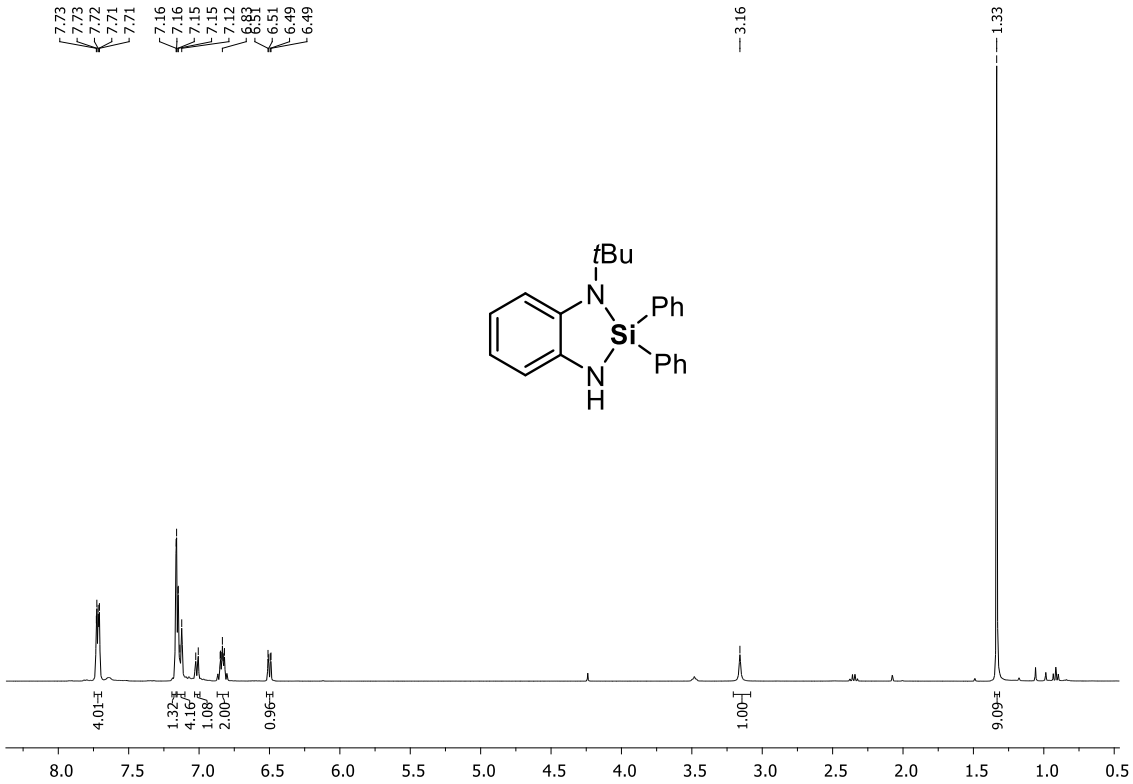

Figure S3.14. ^{1}H NMR spectrum (C_6D_6, 298 K) of **2**.

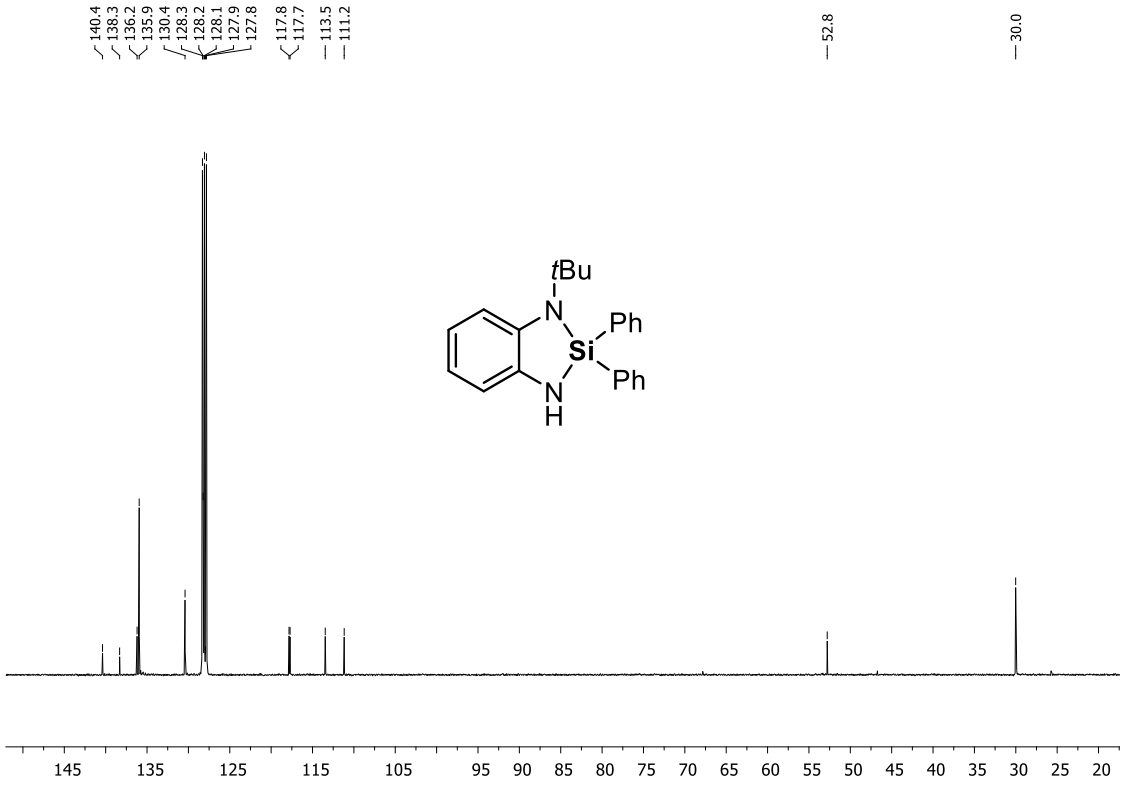

Figure S3.15 $^{13}C\{^{1}H\}$ NMR spectrum (C_6D_6, 298 K) of **2**.

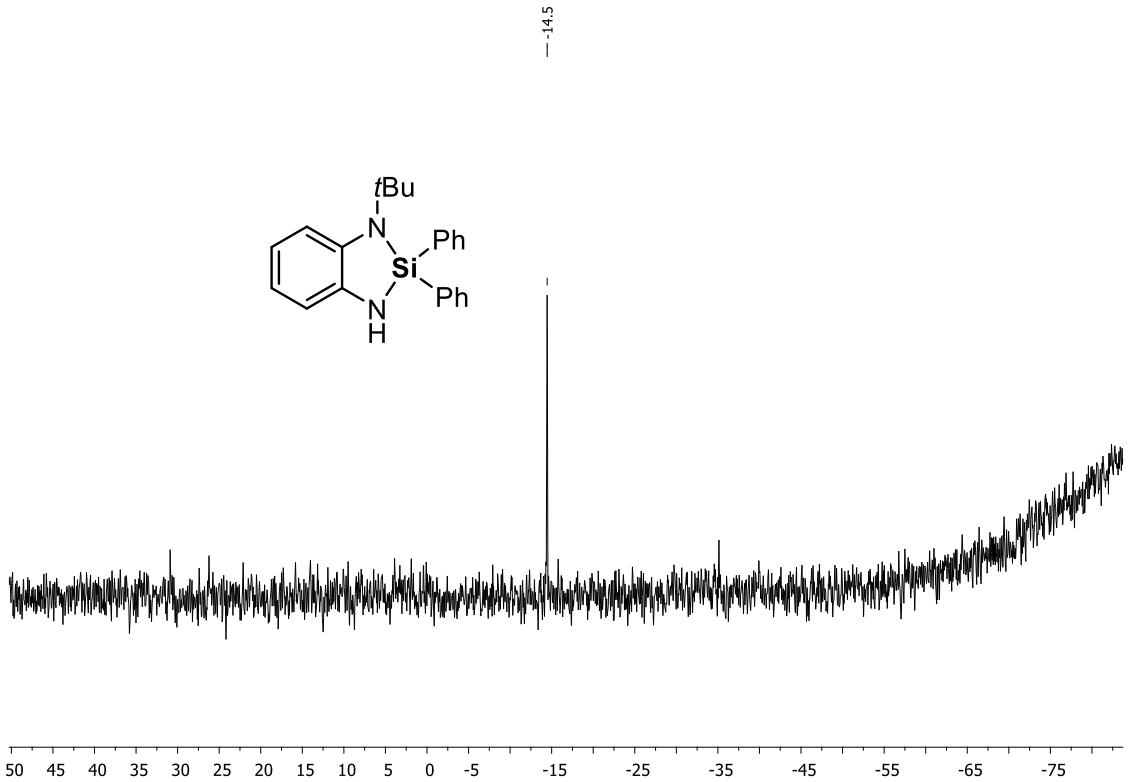

Figure S3.16. $^{29}Si\{^{1}H\}$ NMR spectrum (C_6D_6, 298 K) of **2**.

4.1.1.9 Dimesitylsilanol

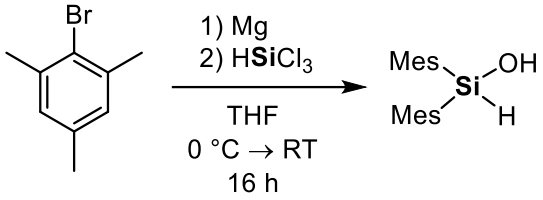

According to a modified literature procedure,[7] magnesium turnings (1.34 g, 55.0 mmol, 2.2 equiv.) were dispersed in 150 mL of THF and bromomesitylene (7.65 mL, 50.0 mmol, 2.0 equiv.) was added. After stirring for 10 min., the clear colorless solution turned black indicating the formation of the mesityl-Grignard reagent. The reaction mixture was cooled down to 0 °C and further stirred for 1 hour. Trichlorosilane (2.53 mL, 25.0 mmol, 1.0 equiv.) was added dropwise via syringe, the dark solution warmed up to room temperature, and stirred at for 16 h. The formed white solid was filtered off and the solution quenched with an aqueous $NaHCO_3$ solution until slightly basic pH was reached. The mixture was extracted with hexane (3 × 50 mL) using a separation funnel. The combined organic phases were extracted one time with brine solution and then dried over $MgSO_4$. The solids were removed by filtration and the colorless solution was dried *in vacuo* to afford dimesitylsilanol as a white solid (4.51 g, 16.0 mmol, 64%).

^{1}H NMR (400 MHz, C_6D_6, 298 K): *δ*[ppm] = 1.32 [s, 1H, O*H*], 2.10 [s, 6H, *para*-CH_3], 2.42 [s, 12H, *ortho*-CH_3], 6.12 [s, 1H, Si*H*], 6.71 [s, 4H, H_{Ph}].

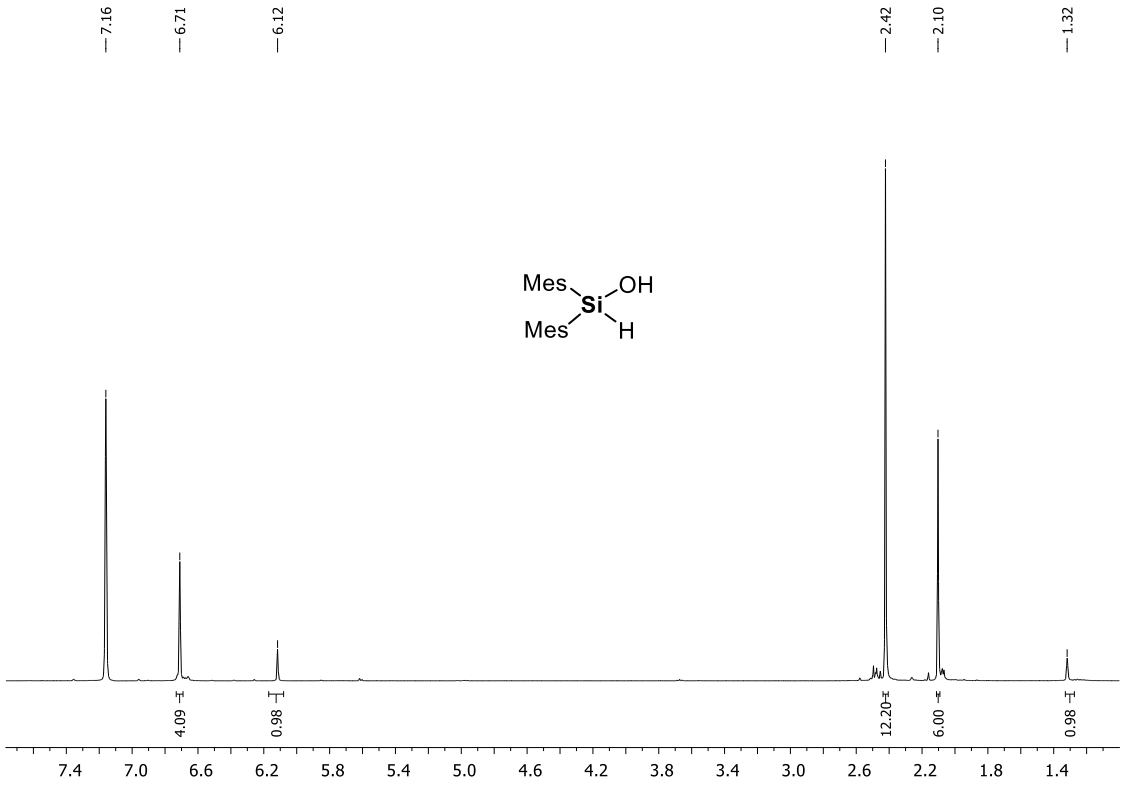

Figure S3.17. ^{1}H NMR spectrum (C_6D_6, 298 K) of dimesitylsilanol.

4.1.1.10 1-Hydroxy-1,1,3,3,3-pentaphenyldisiloxane

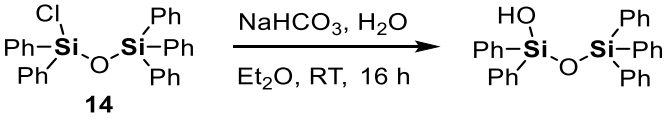

According to a modified literature procedure,[8] compound **14** (5.69 g, 11.5 mmol, 1.0 equiv.) and $NaHCO_3$ (1.16 g, 13.8 mmol, 1.2 equiv.) were dissolved in 30 mL of Et_2O. H_2O (3 mL, 54.0 mmol, 4.8 equiv.) was added dropwise and the white suspension stirred at room temperature for 16 h. Dry $MgSO_4$ was added directly to the mixture and vigorously stirred for 1 h. The solids were filtered off by cannula filtration and the clear filtrates collected. The colorless solution was dried *in vacuo*. The obtained residue was extracted with 5 mL of toluene and filtered. Then, all volatiles were removed *in vacuo* to obtain the disiloxanol as a white solid (4.80 g, 10.1 mmol, 88%).

^{1}H NMR (400 MHz, C_6D_6, 298 K): *δ*[ppm] = 2.27 [s, 1H, O*H*], 7.04–7.15 [m, 12H, H_{Ph}], 7.16–7.21 [m, 3H, H_{Ph}], 7.69–7.78 [m, 12H, H_{Ph}]. **^{13}C{^{1}H} NMR** (101 MHz, C_6D_6, 298 K): *δ*[ppm] = 128.1 [s, C_{Ph}], 128.2 [s, C_{Ph}], 130.3 [s, C_{Ph}], 130.4 [s, C_{Ph}], 134.9 [s, C_{Ph}], 135.5 [s, C_{Ph}], 135.6 [s, C_{Ph}], 136.0 [s, C_{Ph}]. **^{29}Si{^{1}H} NMR** (77 MHz, C_6D_6, 298 K): *δ*[ppm] = −18.0 [s]. **CHN Analysis** $C_{30}H_{26}O_2Si_2$ calculated: C 75.91, H 5.52, O 6.74, Si 11.83; found: C 75.85, H 5.52. **MS(FD)**, calculated m/z for $C_{30}H_{26}O_2Si_2$ [M+H$^+$]: 474.15; found: 474.04.

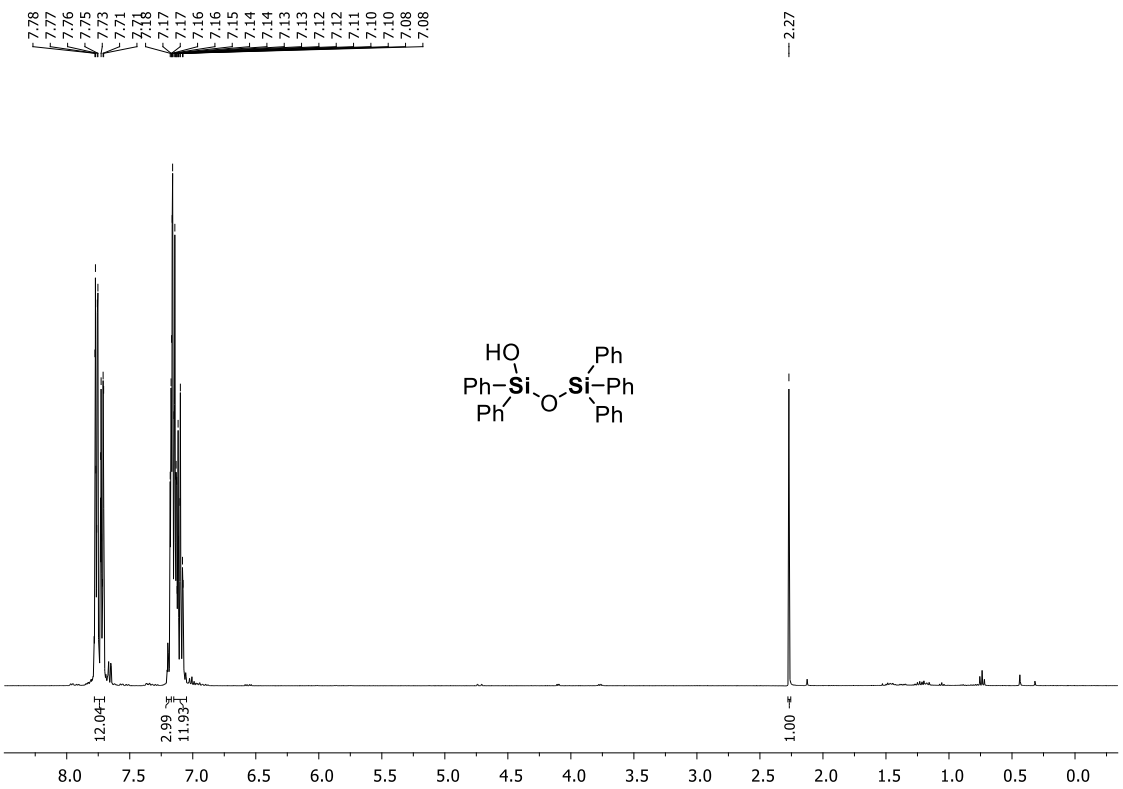

Figure S3.18. ^{1}H NMR spectrum (C_6D_6, 298 K) of 1-hydroxy-1,1,3,3,3-pentaphenyldisiloxane.

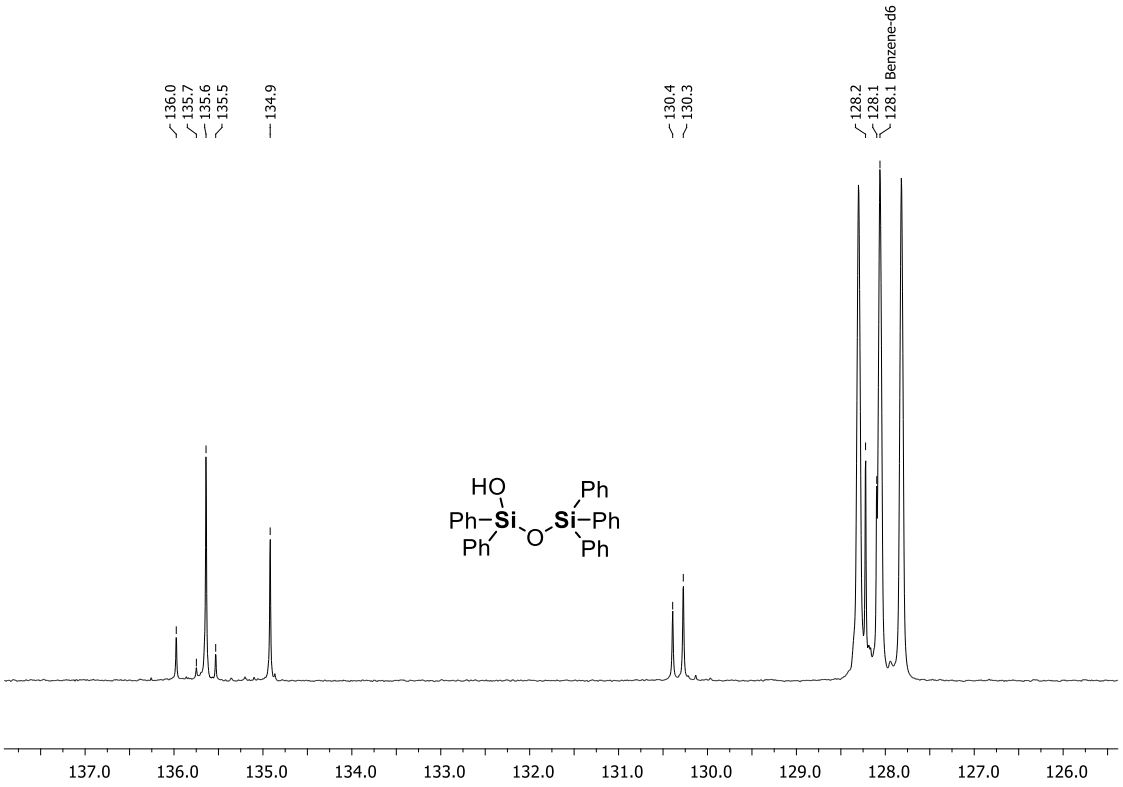

Figure S3.19. $^{13}C\{^{1}H\}$ NMR spectrum (C_6D_6, 298 K) of 1-hydroxy-1,1,3,3,3-pentaphenyldisiloxane.

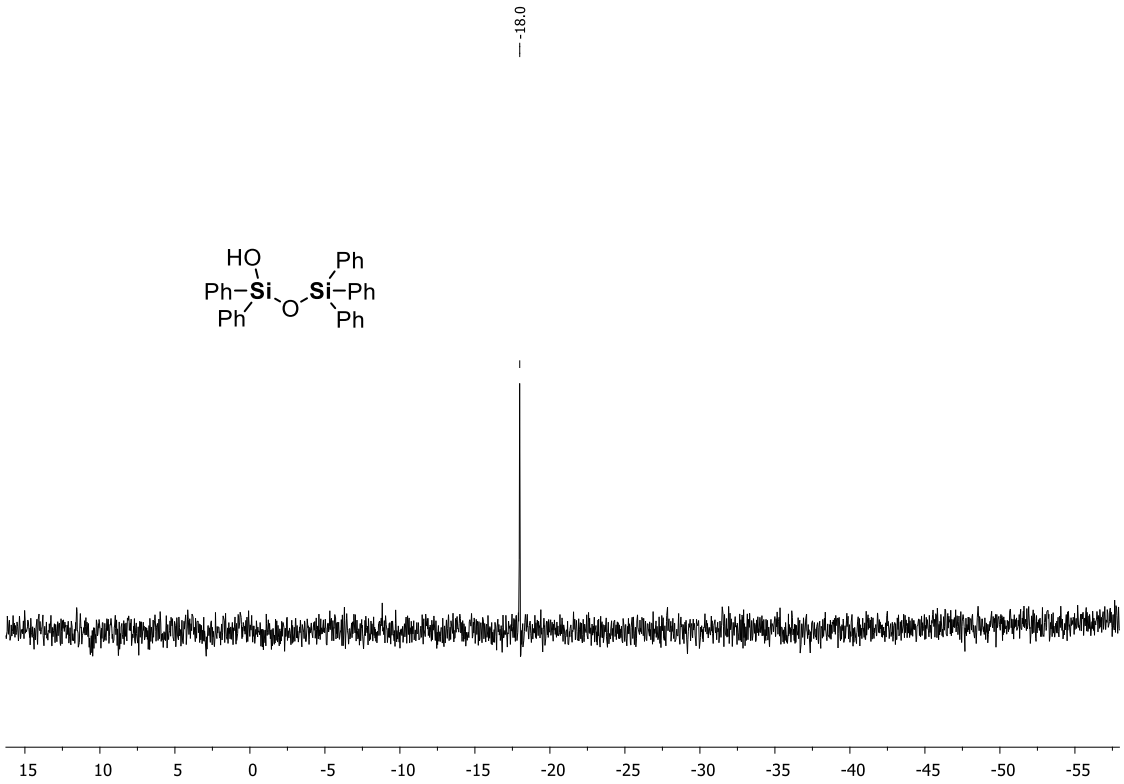

Figure S3.20. $^{29}Si\{^{1}H\}$ NMR spectrum (C_6D_6, 298 K) of 1-hydroxy-1,1,3,3,3-pentaphenyldisiloxane.

4.1.1.11 1-Hydroxy-1,1-diphenyl-3,3,3-trimethyldisiloxane

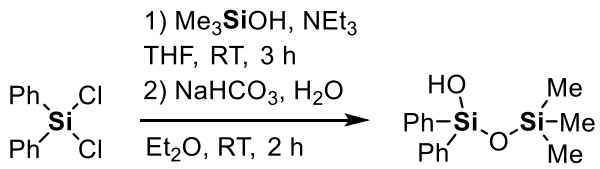

Dichlorodiphenylsilane (0.47 mL, 5.0 mmol, 1.0 equiv.), trimethylsilanol (1.05 mL, 5.0 mmol, 1.0 equiv.), and triethylamine (1.05 mL, 7.5 mmol, 1.5 equiv.) were dissolved in 20 mL of THF and stirred at room temperature for 3 h. Then, all volatiles were removed *in vacuo* and the resulting white residue was treated with 20 mL of Et_2O. The solids were filtered off by cannula filtration to obtain a colorless solution. $NaHCO_3$ (840 mg, 10.0 mmol, 2.0 equiv.) was added and the suspension was placed in a water bath. Water (1.0 mL, 18.0 mmol, 3.6 equiv.) was slowly added via syringe and the reaction mixture stirred at room temperature for 2 h. $MgSO_4$ was added and the suspension vigorously stirred for 10 min. The solids were removed via cannula filtration and the colorless filtrate was dried *in vacuo* to afford 1-hydroxy-1,1-diphenyl-3,3,3-trimethyldisiloxane as a colorless solid (1.25 g, 4.3 mmol, 86%).

^{1}H NMR (400 MHz, C_6D_6, 298 K): δ[ppm] = 0.15 [s, 9H, Si(CH_3)$_3$], 2.48 [s, 1H, O*H*], 7.17–7.21 [m, 6H, H_{Ph}], 7.72–7.76 [m, 4H, H_{Ph}]. **^{13}C{^{1}H} NMR** (101 MHz, C_6D_6, 298 K): δ[ppm] = 2.00 [s, Si(*C*H$_3$)$_3$], 128.1 [s, C_{Ph}], 130.3 [s, C_{Ph}], 134.8 [s, C_{Ph}], 136.3 [s, C_{Ph}]. **^{29}Si{^{1}H} NMR** (77 MHz, C_6D_6, 298 K): δ[ppm] = −37.5 [s, *Si*(CH$_3$)$_3$], 10.8 [s, *Si*OH]. **CHN Analysis** $C_{15}H_{20}O_2Si_2$ calculated: C 62.45, H 6.99, O 11.09, Si 19.47; found: C 62.51, H 6.47. **HR-MS(EI+)**, calculated m/z for $C_{15}H_{20}O_2Si_2$ [M+H$^+$]: 288.09963; found: 288.09920.

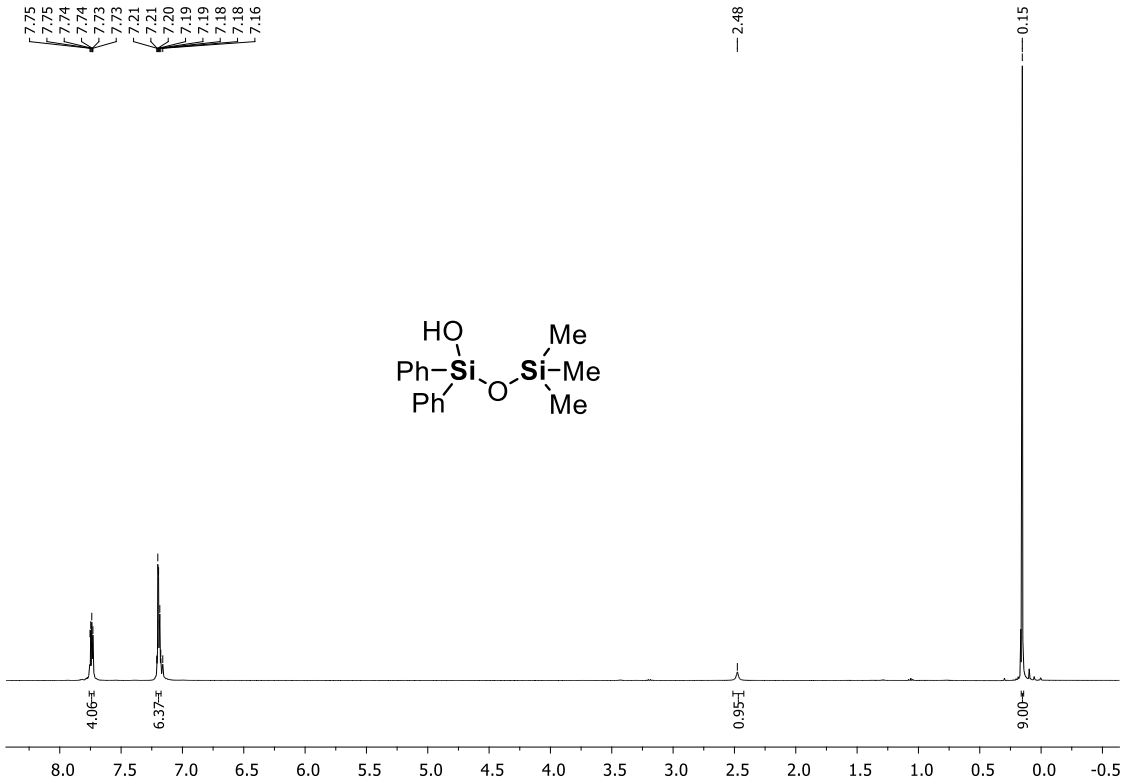

Figure S3.21. ^{1}H NMR spectrum (C_6D_6, 298 K) of 1-hydroxy-1,1-diphenyl-3,3,3-trimethyldisiloxane.

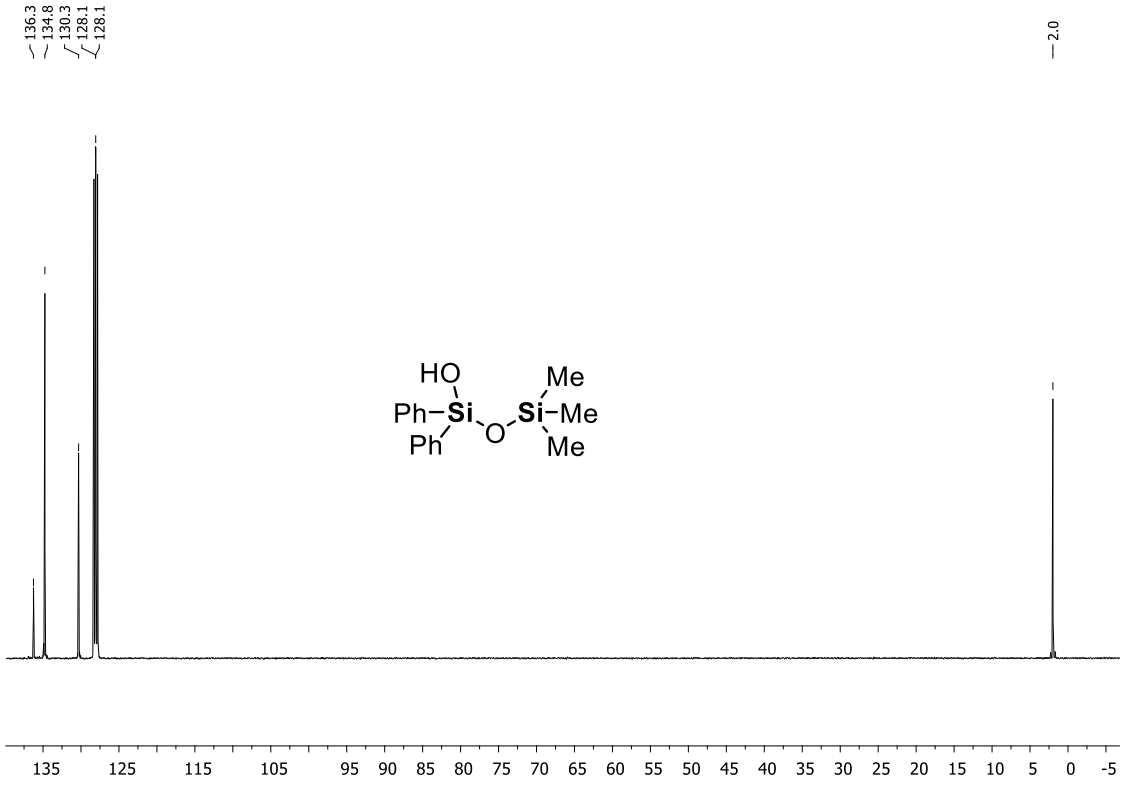

Figure S3.22. $^{13}C\{^{1}H\}$ NMR spectrum (C_6D_6, 298 K) of 1-hydroxy-1,1-diphenyl-3,3,3-trimethyldisiloxane.

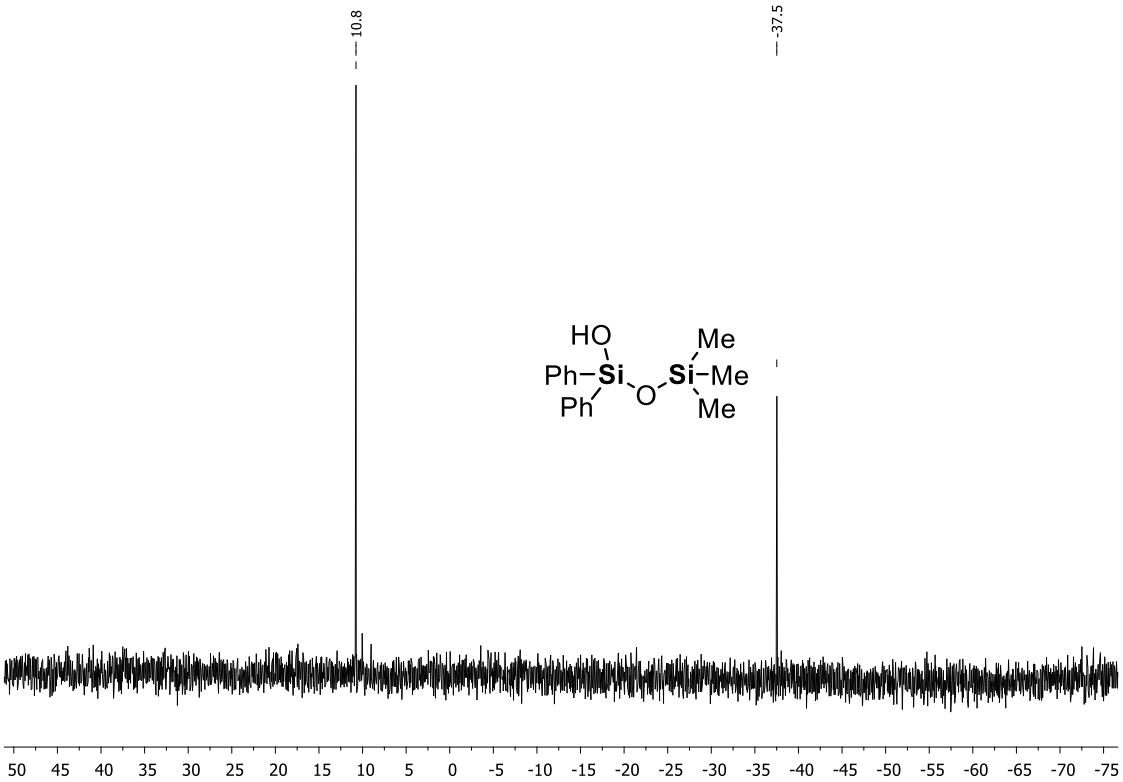

Figure S3.23. $^{29}Si\{^{1}H\}$ NMR spectrum (C_6D_6, 298 K) of 1-hydroxy-1,1-diphenyl-3,3,3-trimethyldisiloxane.

4.1.1.12 1-Chloro-3,3,3-trimethyl-1,1-diphenyldisiloxane (15)

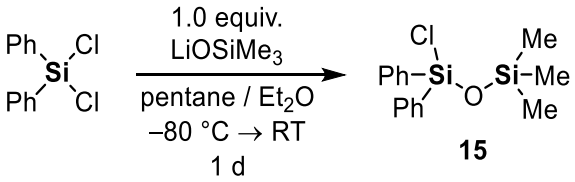

According to a modified literature procedure,[9] lithium trimethylsiloxide (1.06 g, 11.0 mmol, 1.0 equiv.) was dissolved in a mixture of 15 mL pentane and 10 mL Et_2O and cooled down to −80 °C. Dichlorodiphenylsilane (2.5 mL, 12.0 mmol, 1.1 equiv.) was added via syringe and the colorless solution stirred for 1 d. The formed white precipitate was filtered off by cannula filtration and the colorless filtrate dried *in vacuo*. The remaining colorless liquid was purified via Kugelrohr distillation (80 °C oven temperature, 1.3×10^{-1} mbar) to yield chlorodisiloxane **15** as a colorless liquid (1.40 g, 5.0 mmol, 41%).

^{1}H NMR (300 MHz, C_6D_6, 298 K): δ[ppm] = 0.16 [s, 9H, Si(CH_3)$_3$], 7.11–7.15 [m, 5H, H_{Ph}], 7.75–7.80 [m, 5H, H_{Ph}].

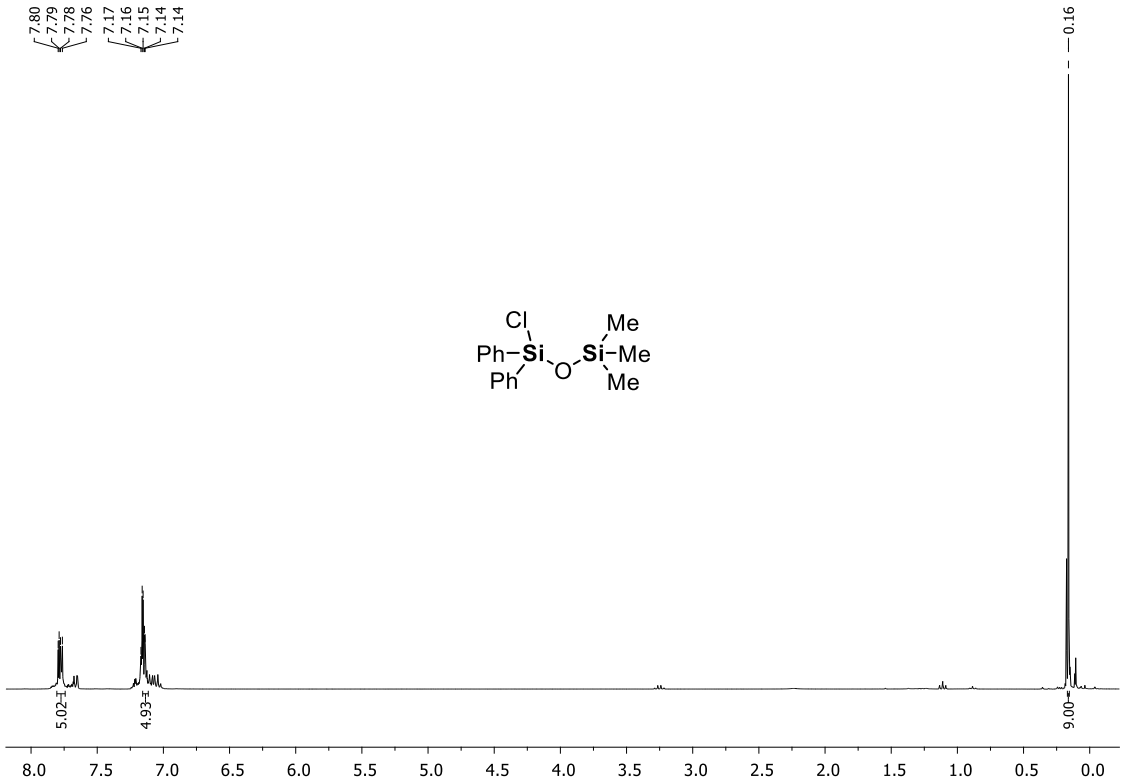

Figure S3.24. ^{1}H NMR spectrum (C_6D_6, 298 K) of **15**.

4.1.1.13 3-Chloro-1,1,1-trimethyl-3,5,5,5-tetraphenyltrisiloxane (18)

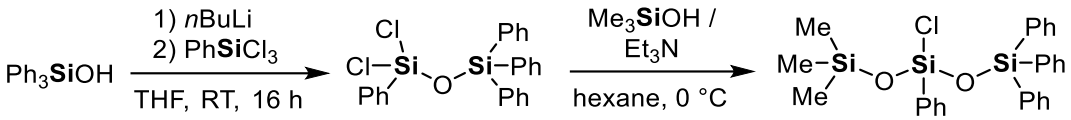

18

n-Butyllithium (12.0 mL of a 2.5 M solution in hexane, 30.0 mmol, 1.0 equiv.) was added dropwise to a solution of triphenylsilanol (8.29 g, 30.0 mmol, 1.0 equiv.) in 200 mL of THF at room temperature. The mixture was stirred for 30 min. Then, trichlorophenylsilane (4.8 mL, 30.0 mmol, 1.0 equiv.) was added in one portion. The mixture was stirred at room temperature for 16 h followed by removal of all volatiles *in vacuo*. The colorless remaining liquid was dissolved in 100 mL of hexane and triethylamine (6.3 mL, 45.0 mmol, 1.5 equiv.) was added. The mixture was cooled down to 0 °C and trimethylsilanol (2.8 mL, 30.0 mmol, 1.0 equiv.) was added dropwise. The mixture was stirred for 16 h during which a white precipitate was formed. The solids were filtered off and the residue was washed with hexane (3 × 10 mL). The clear colorless filtrates were collected and all volatiles removed *in vacuo*. The crude mixture was purified via Kugelrohr distillation (220 °C oven temperature, 1.0×10^{-2} mbar, all distilled fractions were discarded, pure chlorotrisiloxane **18** was recovered from the undistilled tail fraction) to obtain **18** as a colorless liquid (8.19 g, 16.0 mmol, 53%).

^{1}H NMR (400 MHz, C_6D_6, 298 K): δ[ppm] = 0.08 [s, 9H, Si(CH_3)$_3$], 7.03–7.15 [m, 10H, H_{Ph}], 7.17–7.21 [m, 2H, H_{Ph}], 7.76–7.80 [m, 8H, H_{Ph}]. **^{13}C{^{1}H}** NMR (101 MHz, C_6D_6, 298 K): δ[ppm] = 1.5 [s, Si(CH_3)], 128.3 [s, C_{Ph}], 128.3 [s, C_{Ph}], 130.5 [s, C_{Ph}], 131.1 [s, C_{Ph}], 134.0 [s, C_{Ph}], 135.1 [s, C_{Ph}], 135.6 [s, C_{Ph}]. **^{29}Si{^{1}H}** NMR (79 MHz, C_6D_6, 298 K): δ[ppm] = −56.5 [s, *Si*Cl], −16.8 [s, *Si*(Ph)$_3$], 13.7 [s, *Si*(CH_3)$_3$]. **HR-MS(EI+)**, calculated m/z for $C_{27}H_{29}ClO_2Si_3$ [M+H$^+$]: 504.11584; found: 504.11485.

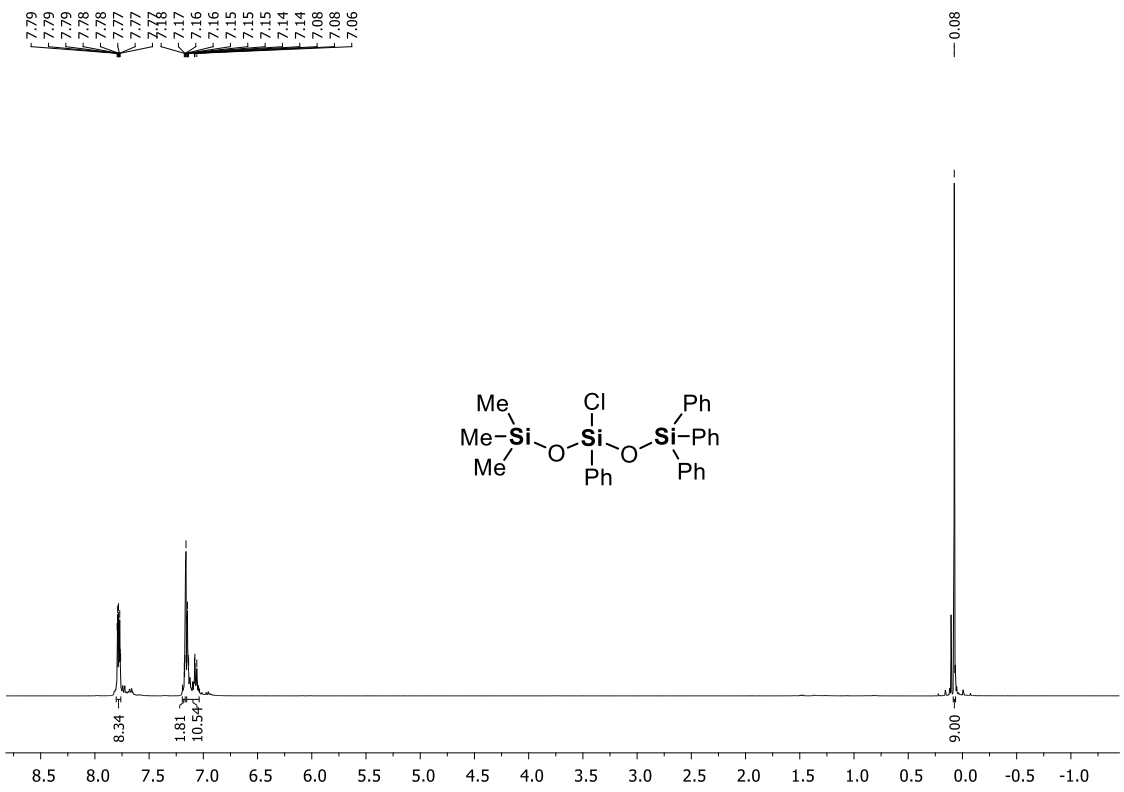

Figure S3.25. ^{1}H NMR spectrum (C_6D_6, 298 K) of **18**.

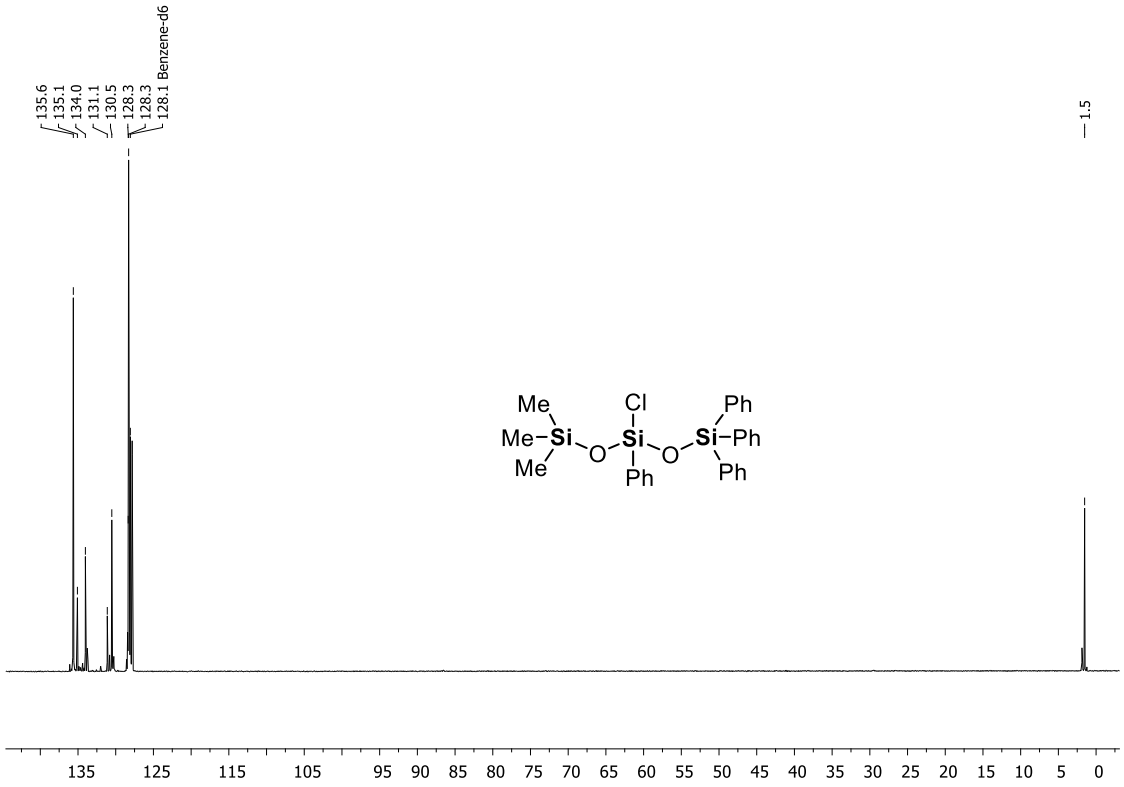

Figure S3.26. $^{13}C\{^{1}H\}$ NMR spectrum (C_6D_6, 298 K) of **18**.

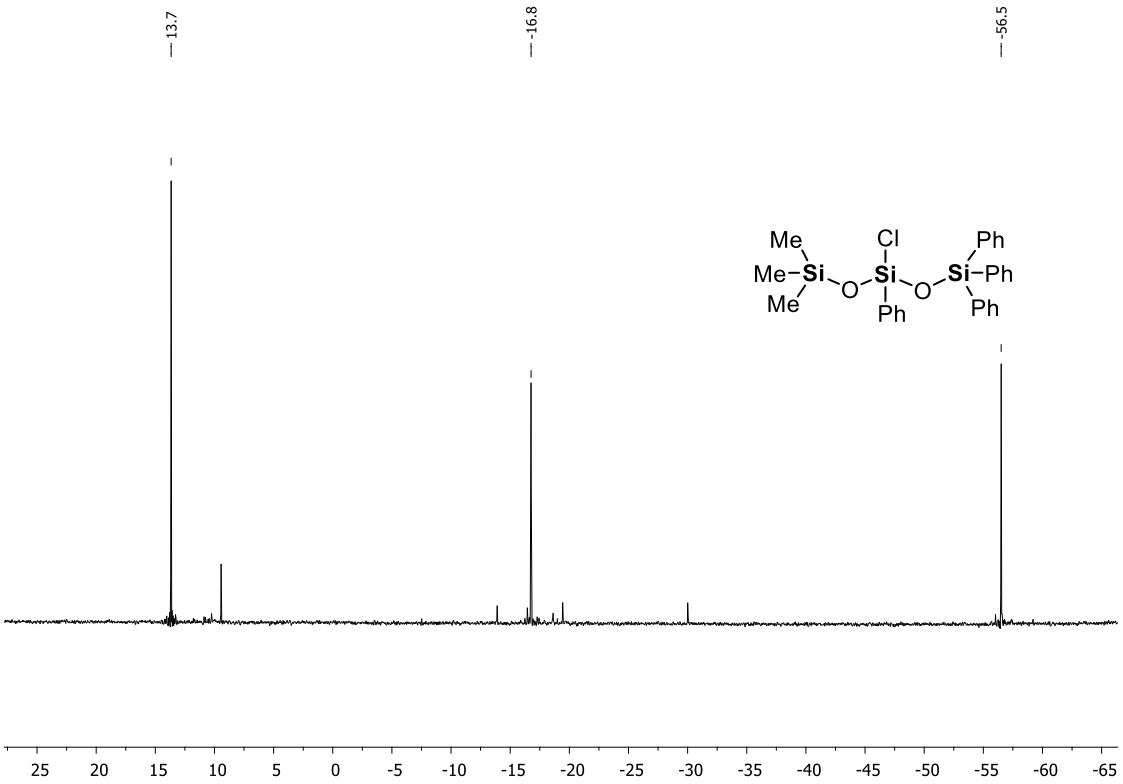

Figure S3.27. $^{29}Si\{^{1}H\}$ NMR spectrum (C_6D_6, 298 K) of **18**.

3.6.3 Synthesis of compounds 3–11

4.1.1.14 Compound 3

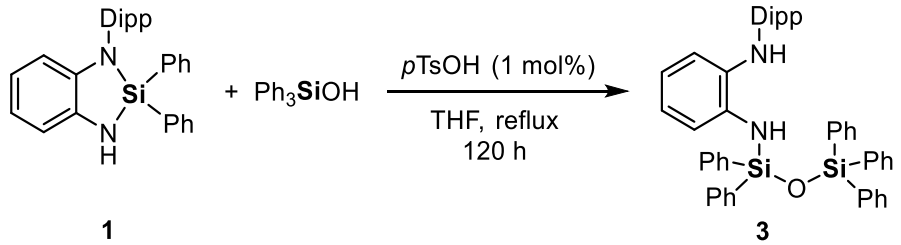

1 **3**

Compound **1** (4.49 g, 10.0 mmol, 1.0 equiv.), triphenylsilanol (2.76 g, 10.0 mmol, 1.0 equiv.), and *para*- toluenesulfonic acid (17 mg, 0.1 mmol, 1 mol%) were dissolved in 100 mL of THF and heated at reflux for 120 h. then, all volatiles were removed from the slightly yellow solution to obtain a brown waxy residue, which was washed with pentane (3 × 20 mL). After the solids had been removed by cannula filtration, the pentane solution was repeatedly precipitated by cooling down to 8 °C. After drying the combined solids *in vacuo*, **3** was obtained as a colorless solid (3.01 g, 4.2 mmol, 42%). Crystals suitable for single-crystal X-ray diffraction analysis were obtained by recrystallization from hot pentane (for details, see chapter 3.8).

For the determination of the NMR yield, an individual experiment was performed. For this purpose, compound **1** (449 mg, 1.0 mmol, 1.0 equiv.), triphenylsilanol (276 mg, 1.0 mmol, 1.0 equiv.), and hexamethylbenzene (81 mg, 0.5 mmol, 0.5 equiv.) as internal standard were dissolved in 10 mL of THF. The reaction mixture was heated at reflux for 120 h and then an aliquot of ca. 0.5 mL was transferred into an NMR tube. All volatiles were removed *in vacuo* and 0.5 mL of C_6D_6 was added. An NMR yield of 68% was determined by integration in the ^{1}H NMR spectrum (Figure S3.31).

^{1}H NMR (400 MHz, C_6D_6, 298 K): *δ*[ppm] = 1.07 [d, $^3J_{H–H}$ = 6.86 Hz, 12H, CH(C*H*$_3$)$_2$], 3.08 [sept, $^3J_{H–H}$ = 6.86 Hz, 2H, C*H*(CH$_3$)$_2$], 4.62 [s, 1H, N*H*], 4.81 [s, 1H, N*H*], 6.40–6.49 [m, 2H, *H*$_{Ph}$], 6.51–6.57 [m, 1H, *H*$_{Ph}$], 7.05–7.22 [m, 19H, *H*$_{Ph}$], 7.73–7.79 [m, 6H, *H*$_{Ph}$], 7.81–7.87 [m, 4H, *H*$_{Ph}$]. **^{13}C{^{1}H} NMR** (101 MHz, C_6D_6, 298 K): *δ*[ppm] = 23.5 (s, CH(*C*H$_3$)$_2$], 24.6 [s, CH(*C*H$_3$)$_2$], 28.4 [s, *C*H(CH$_3$)$_2$], 117.4 [s, *C*$_{Ph}$], 120.0 [s, *C*$_{Ph}$], 121.2 [s, *C*$_{Ph}$], 121.6 [s, *C*$_{Ph}$], 124.3 [s, *C*$_{Ph}$], 126.2 [s, *C*$_{Ph}$], 128.2 [s, *C*$_{Ph}$], 128.4 [s, *C*$_{Ph}$], 130.3 [s, *C*$_{Ph}$], 130.6 [s, *C*$_{Ph}$], 135.2 [s, *C*$_{Ph}$], 135.3 [s, *C*$_{Ph}$], 135.4 [s, *C*$_{Ph}$], 135.7 [s, *C*$_{Ph}$], 135.8 [s, *C*$_{Ph}$], 138.1 [s, *C*$_{Ph}$], 138.3 [s, *C*$_{Ph}$], 144.8 [s, *C*$_{Ph}$]. **^{29}Si{^{1}H} NMR** (79 MHz, C_6D_6, 298 K): *δ*[ppm] = −33.2 [s, *Si*N], −17.8 [s, O*Si*Ph$_3$]. **CHN Analysis** $C_{48}H_{48}N_2OSi_2$ calculated: C 79.51, H 6.67, N 3.86, O 2.21, Si 7.75; found: C 79.49, H 6.76, N 3.66. **HR-MS (ESI+)**, calculated m/z for $C_{48}H_{48}N_2OSi_2$ [M+H$^+$]: 725.3378; found: 725.3375.

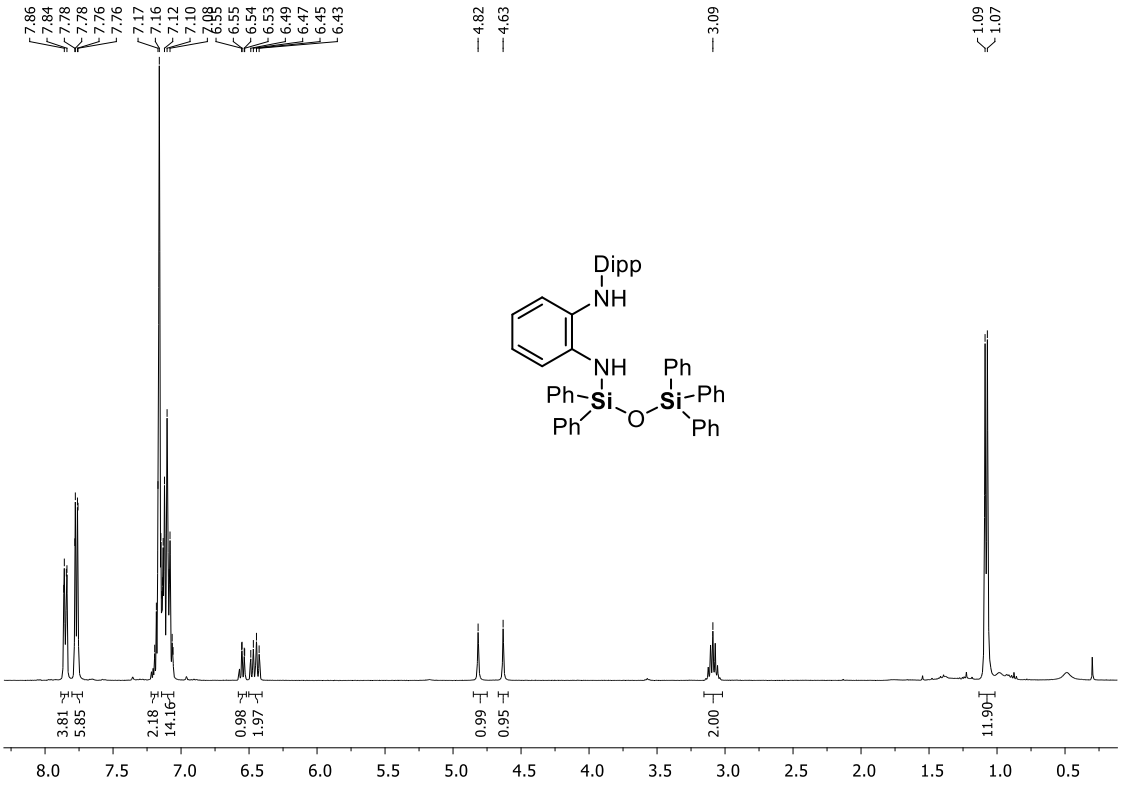

Figure S3.28. ^{1}H NMR spectrum (C_6D_6, 298 K) of **3**.

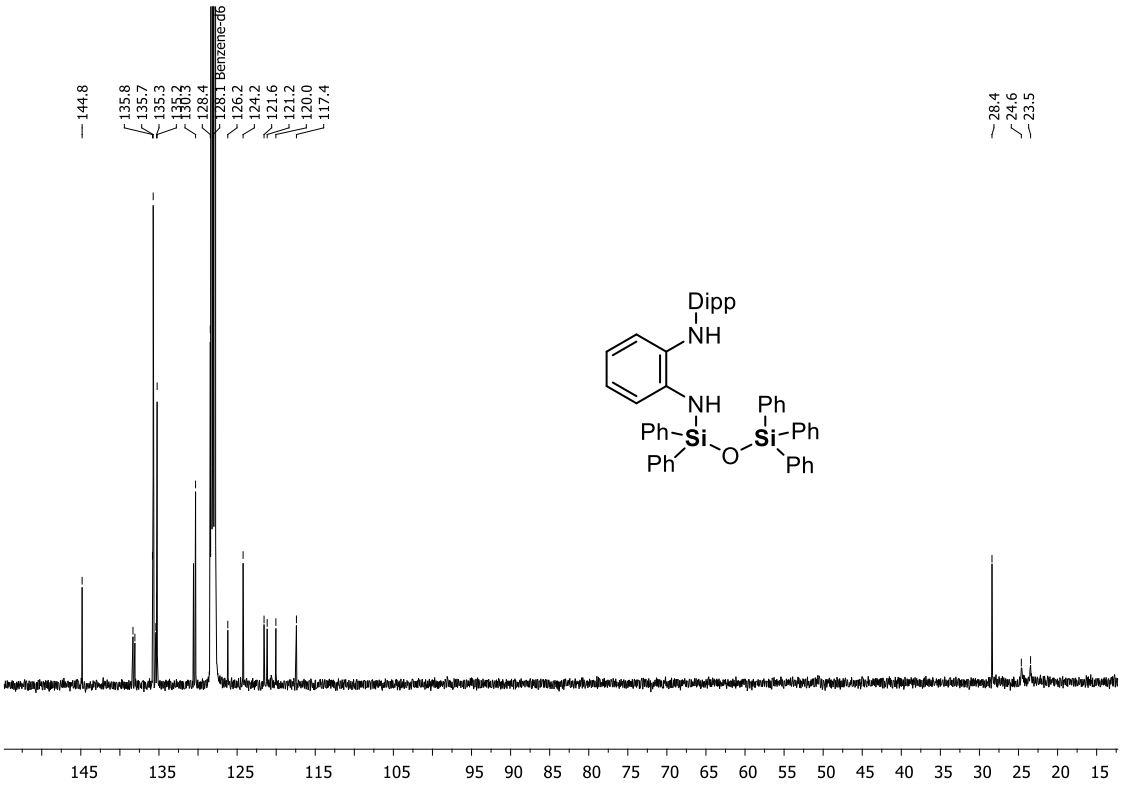

Figure S3.29. $^{13}C\{^{1}H\}$ NMR spectrum (C_6D_6, 298 K) of **3**.

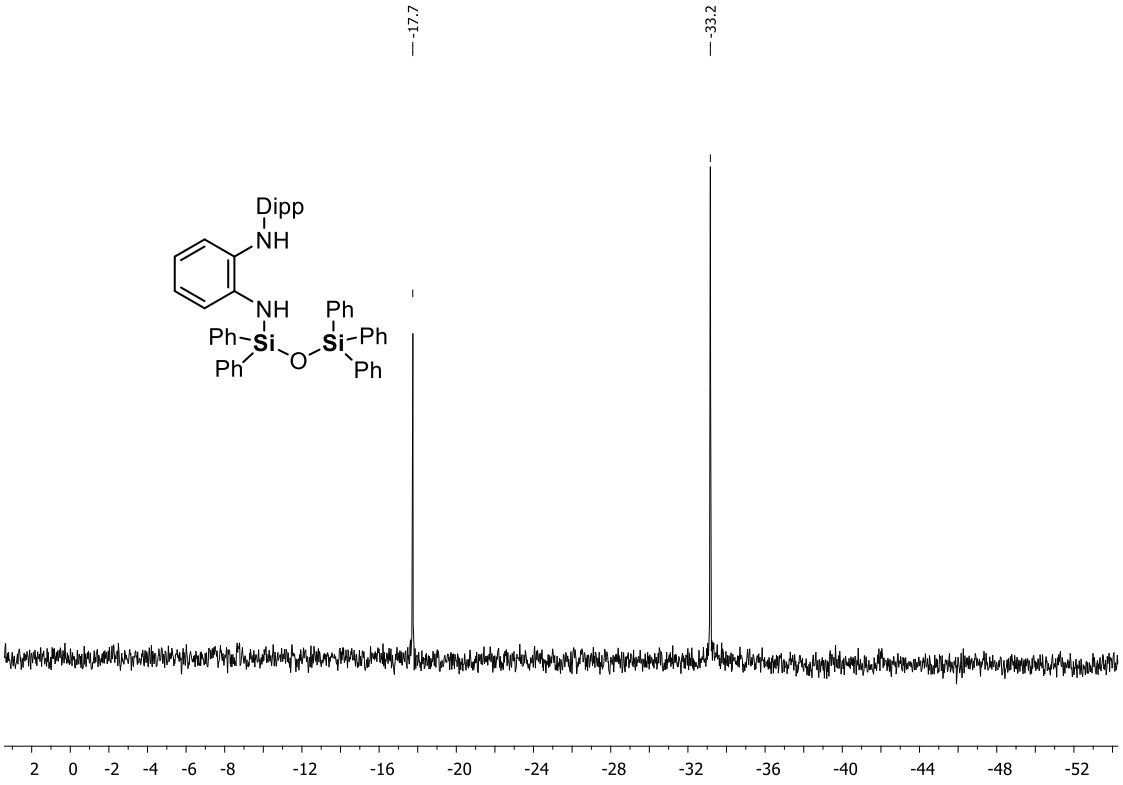

Figure S3.30. $^{29}Si\{^{1}H\}$ NMR spectrum (C_6D_6, 298 K) of **3**.

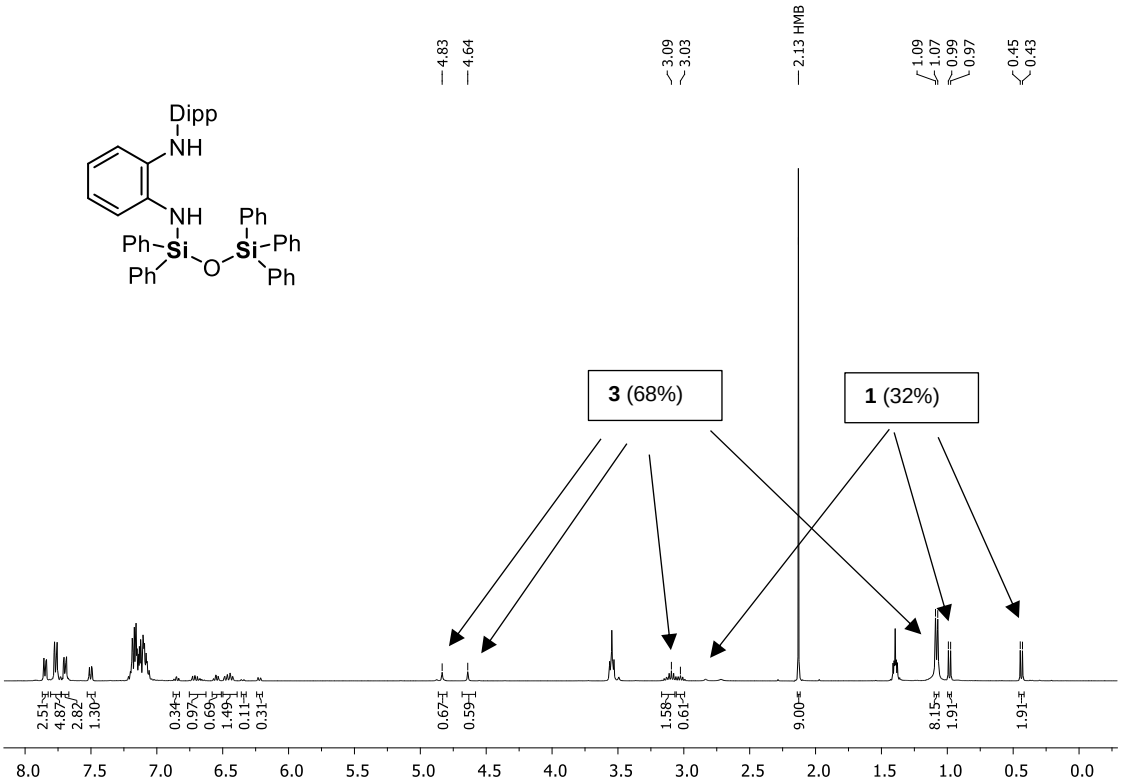

Figure S3.31. ^{1}H NMR spectrum (C_6D_6, 298 K) with 0.5 equiv. HMB as internal standard for determination of the NMR yield of **3**.

4.1.1.15 Compound 4

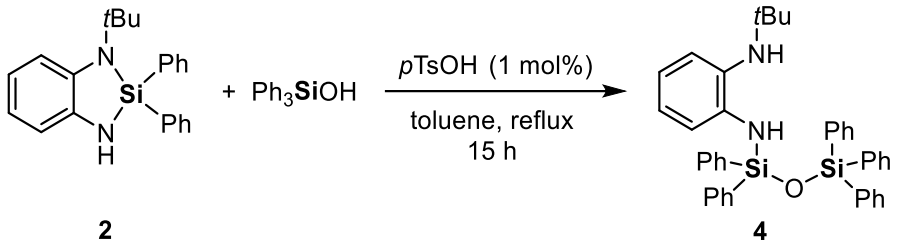

2 **4**

Compound **2** (1.72 g, 5.0 mmol, 1.0 equiv.), triphenylsilanol (1.52 g, 5.0 mmol, 1.0 equiv.), and *para*- toluenesulfonic acid (9 mg, 0.05 mmol, 1 mol%) were dissolved in 100 mL of toluene and heated at reflux for 15 h. All volatiles were removed *in vacuo* from the slightly yellow solution to obtain an off-white solid, which was washed with pentane (3 × 5 mL). After drying *in vacuo*, **4** was obtained as a colorless solid (2.36 g, 3.8 mmol, 76%). Crystals suitable for single-crystal X-ray diffraction analysis were obtained by recrystallization from hot pentane (for details, see chapter 3.8).

^{1}H NMR (400 MHz, C_6D_6, 298 K): δ[ppm] = 1.02 [s, 9H, C(C*H*$_3$)$_3$], 2.04 [s, 1H, N*H*], 6.15 [s, 1H, N*H*], 6.57–6.70 [m, 2H, *H*$_{Ph}$], 6.85–6.79 [m, 1H, *H*$_{Ph}$], 7.03–7.19 [m, 16H, *H*$_{Ph}$], 7.72–7.78 [m, 6H, *H*$_{Ph}$], 7.82–7.88 [m, 4H, *H*$_{Ph}$]. **^{13}C{^{1}H} NMR** (101 MHz, C_6D_6, 298 K): δ[ppm] = 29.9 [s, C(*C*H$_3$)$_3$]. 53.5 [s, *C*(CH$_3$)$_3$], 117.5 [s, *C*$_{Ph}$], 118.4 [s, *C*$_{Ph}$], 125.9 [s, *C*$_{Ph}$], 130.2 [s, *C*$_{Ph}$], 130.4 [s, *C*$_{Ph}$], 132.8

[s, C_{Ph}], 135.2 [s, C_{Ph}], 135.5 [s, C_{Ph}], 135.8 [s, C_{Ph}], 136.0 [s, C_{Ph}], 144.8 [s, C_{Ph}]. **^{29}Si{^{1}H} NMR** (79 MHz, C_6D_6, 298 K): δ[ppm] = −34.5 [s, *Si*N], −18.1 [s, O*Si*Ph_3]. **CHN Analysis** $C_{40}H_{40}N_2OSi_2$ calculated: C 77.37, H 6.49, N 4.51, O 2.58, Si 9.05; found: C 77.31, H 6.58, N 4.26. **MS (FD+)**, calculated m/z for $C_{40}H_{40}N_2OSi_2$ [$M+H^+$]: 620.27; found: 620.27.

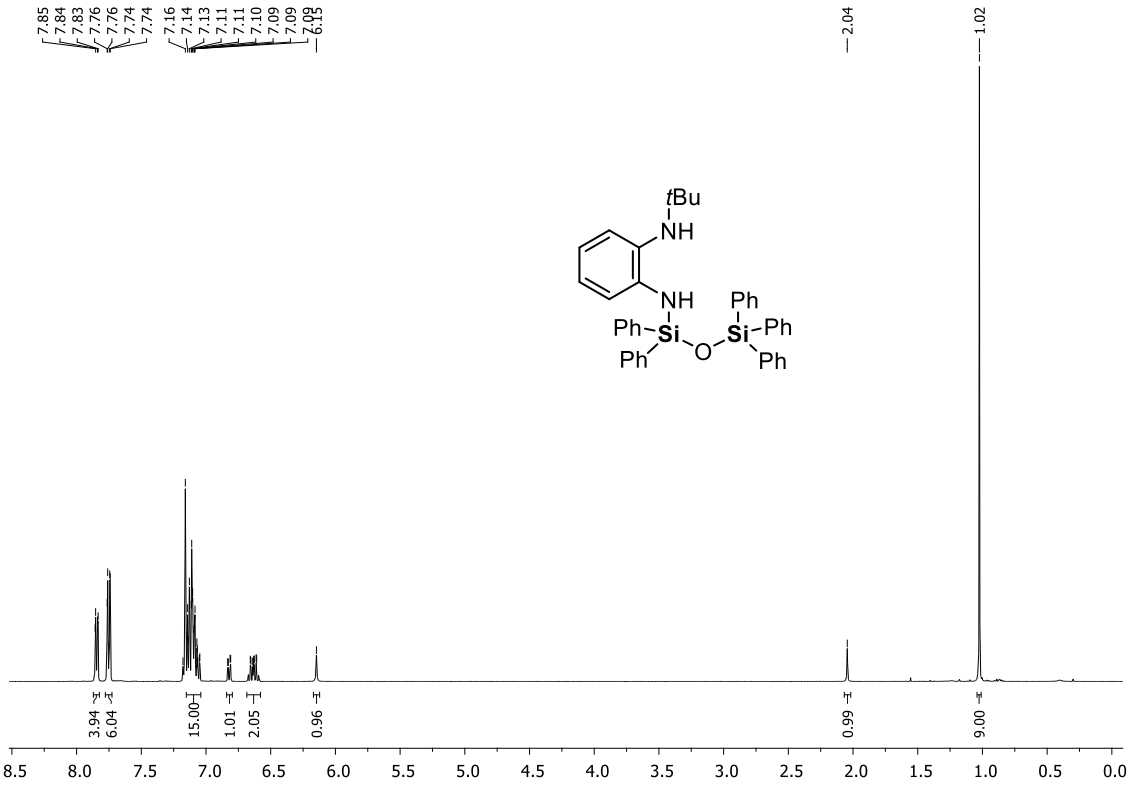

Figure S3.32. ^{1}H NMR spectrum (C_6D_6, 298 K) of **4**.

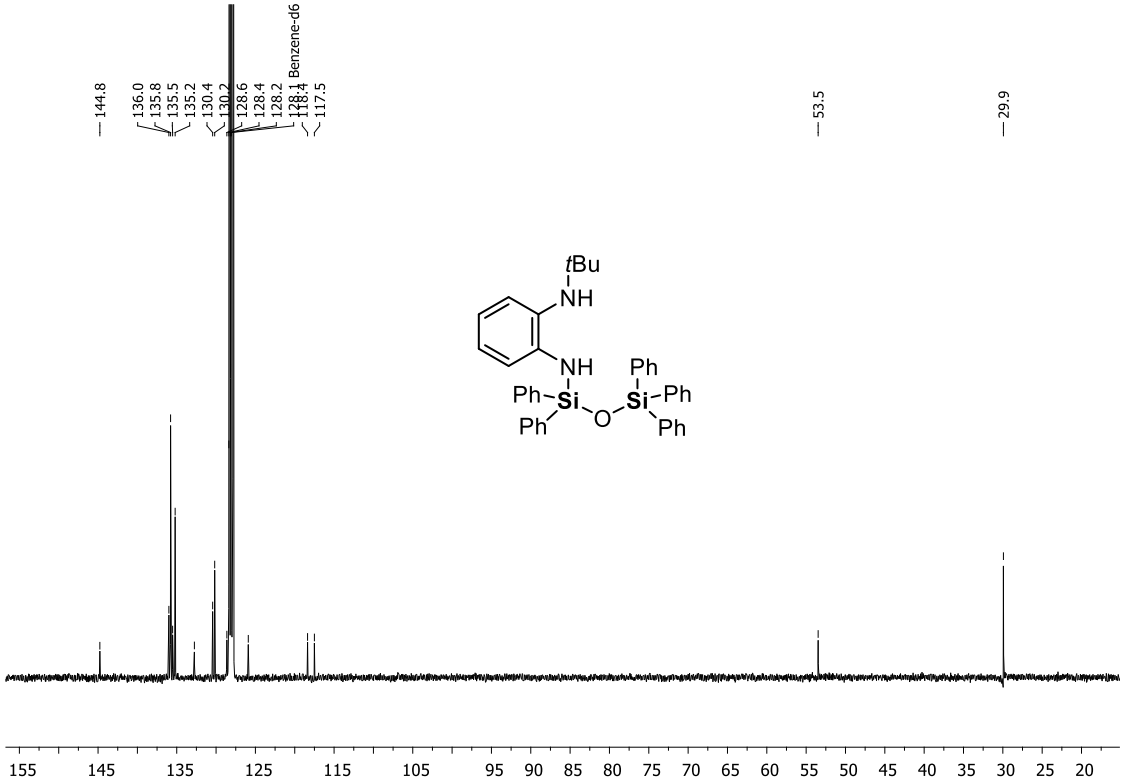

Figure S3.33. $^{13}C\{^{1}H\}$ NMR spectrum (C_6D_6, 298 K) of **4**.

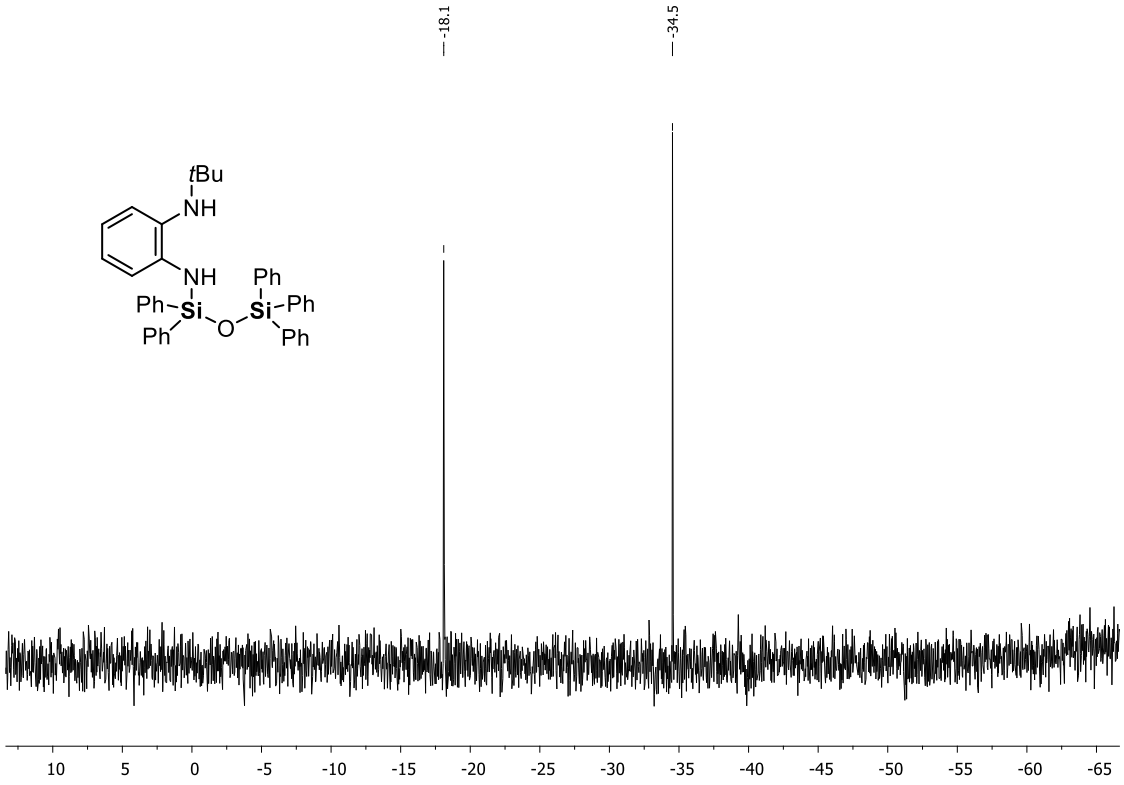

Figure S3.34. $^{29}Si\{^{1}H\}$ NMR spectrum (C_6D_6, 298 K) of **4**.

4.1.1.16 Compound 5

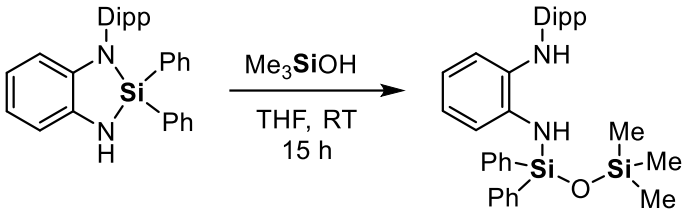

1 **5**

Compound **1** (2.24 g, 5.0 mmol, 1.0 equiv.) and Me_3SiOH (0.52 mL, 5.5 mmol, 1.1 equiv.) were dissolved in 25 mL of THF. The slightly violet mixture was stirred for 15 h at room temperature. All volatiles were removed *in vacuo* and the violet waxy residue was dissolved in pentane. After drying *in vacuo*, **5** was obtained as a red wax (2.63 g, 4.9 mmol, 98%).

^{1}H NMR (400 MHz, C_6D_6, 298 K): δ[ppm] = 0.19 [s, 9H, Si(CH_3)$_3$], 1.09 [br, 12H, CH(CH_3)$_2$], 3.11 [sept, $^3J_{H–H}$ = 6.71 Hz, 2H, CH(CH$_2$)$_2$], 4.73 [s, 1H, NH], 4.84 [s, 1H, NH], 6,47 [dd, $^3J_{H–H}$ = 7.91 Hz, $^3J_{H–H}$ = 1.51 Hz, 1H, H_{Ph}], 6.56 [td, $^3J_{H–H}$ = 7.72 Hz, $^4J_{H–H}$ = 1.52 Hz, 1H, H_{Ph}], 6.64 [td, $^3J_{H–H}$ = 7.68 Hz, $^4J_{H–H}$ = 1.51Hz, 1H H_{Ph}], 7.02–7.22 [m, 10H, H_{Ph}], 7.85–7.90 [m, 4H, H_{Ph}]. **^{13}C{^{1}H} NMR** (101 MHz, C_6D_6, 298 K): δ[ppm] = 2.0 [s, Si(CH$_3$)$_3$], 23.5 [s, CH(CH$_3$)$_2$], 24.7 [CH(CH$_3$)$_2$], 25.7 [s, CH(CH$_3$)$_2$], 28.4 [s, CH(CH$_3$)$_2$], 118.1 [s, C_{Ph}], 119.2 [s, C_{Ph}], 120.9 [s, C_{Ph}], 121.8 [s, C_{Ph}], 124.3 [s, C_{Ph}], 126.1 [s, C_{Ph}], 128.5 [s, C_{Ph}], 130.5 [s, C_{Ph}], 134.9 [s, C_{Ph}], 136.0 [s, C_{Ph}], 136.2 [s, C_{Ph}], 138.0 [s, C_{Ph}], 138.3 [s, C_{Ph}], 144.6 [s, C_{Ph}]. **^{29}Si{^{1}H} NMR** (79 MHz, C_6D_6, 298 K): δ[ppm] = –35.57 [s, SiN], 10.70 [s, OSi(CH$_3$)$_3$]. **HR-MS (FD+)**, calculated m/z for $C_{33}H_{42}N_2OSi_2$: [M+H$^+$]: 538.28302; found: 538.28309.

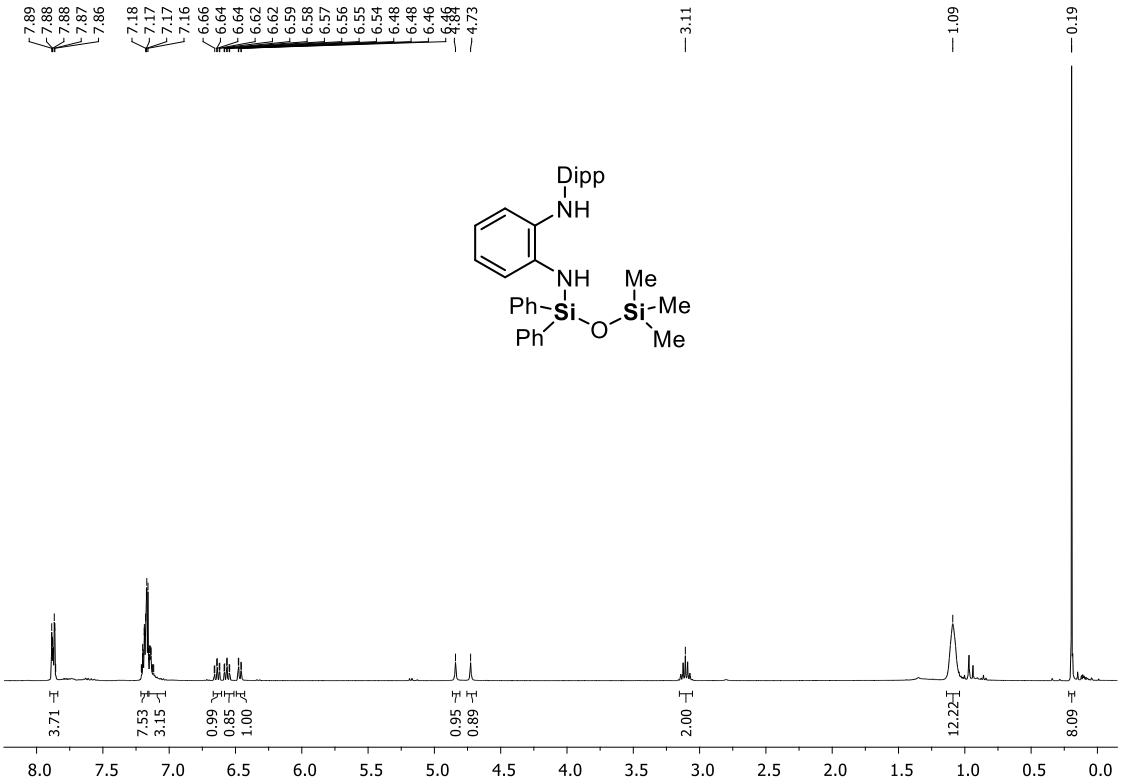

Figure S3.35. ^{1}H NMR spectrum (C_6D_6, 298 K) of **5**.

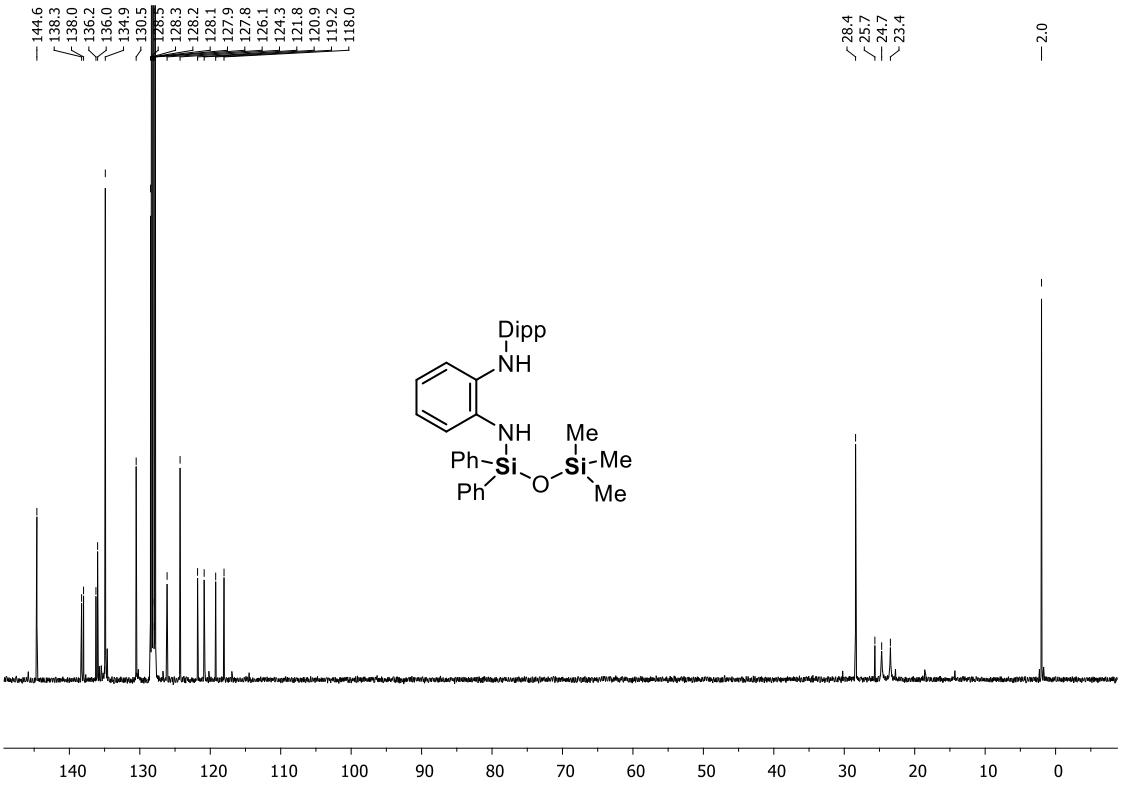

Figure S3.36. $^{13}C\{^{1}H\}$ NMR spectrum (C_6D_6, 298 K) of **5**.

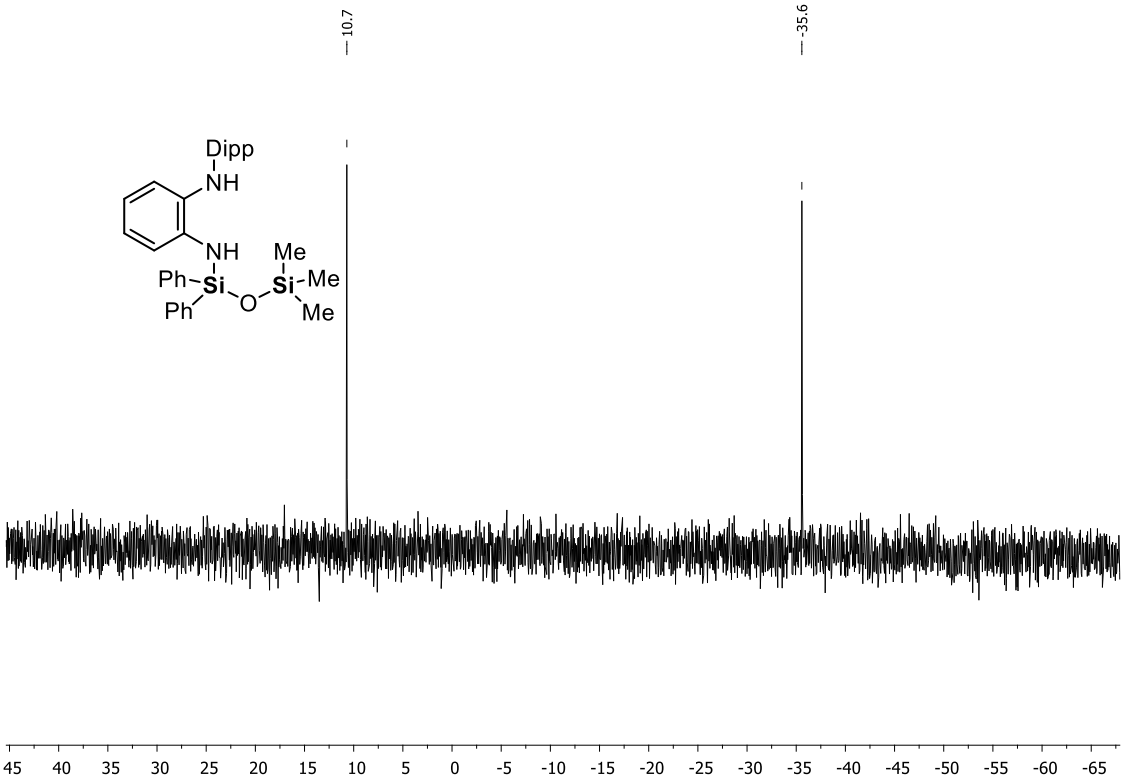

Figure S3.37. $^{29}Si\{^{1}H\}$ NMR spectrum (C_6D_6, 298 K) of **5**.

4.1.1.17 Compound 6

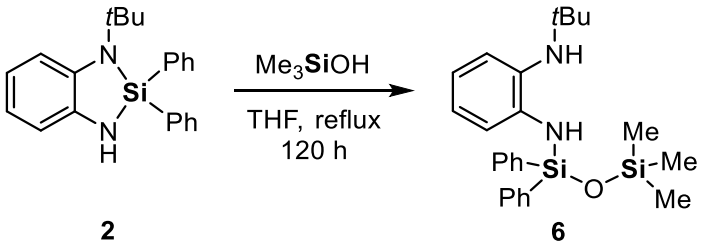

2 **6**

Compound **2** (345 mg, 1.0 mmol, 1.0 equiv.) and Me_3SiOH (0.10 mL, 1.1 mmol, 1.1 equiv.) were dissolved in 10 mL of THF. The yellowish mixture was heated at reflux for 120 h. All volatiles were removed *in vacuo* and the oily residue was purified via Kugelrohr distillation (110 °C oven temperature, 2.0×10^{-2} mbar) to obtain **9** as a colorless oil (117 mg, 0.2 mmol, 27%).

For the determination of the NMR yield, an individual experiment was performed. For this purpose, compound **2** (345 mg, 1.0 mmol, 1.0 equiv.), trimethylsilanol (0.14 mL, 1.5 mmol, 1.5 equiv.), and hexamethylbenzene (81 mg, 0.5 mmol, 0.5 equiv.) as internal standard were dissolved in 10 mL of THF. The reaction mixture was heated at reflux for 120 h and then an aliquot of ca. 0.5 mL was transferred into an NMR tube. All volatiles were removed *in vacuo* and 0.5 mL of C_6D_6 was added. An NMR yield of 70% was determined by integration in the ^{1}H NMR spectrum (Figure S3.41).

^{1}H NMR (300 MHz, C_6D_6, 298 K): *δ*[ppm] = 0.20 [s, 9H, Si(*C*H$_3$)$_3$], 1.06 [s, 9H, C(*C*H$_3$)$_3$], 2.03 [s, 1H, N*H*], 6.19 [s, 1H, N*H*], 6.62–6.68 [m, 1H, *H*$_{Ph}$], 6.80–6.87 [m, 2H, *H*$_{Ph}$], 7.07–7.13 [m, 1H, *H*$_{Ph}$], 7.18–7.25 [m, 6H, *H*$_{Ph}$], 7.77–7.94 [m, 4H, *H*$_{Ph}$]. **^{13}C{^{1}H} NMR** (101 MHz, C_6D_6, 298 K): *δ*[ppm] = 2.0 [s, Si(*C*H$_3$)$_3$], 29.9 [s, C(*C*H$_3$)$_3$], 53.6 [s, *C*(CH$_3$)$_3$], 117.1 [s, *C*$_{Ph}$], 118.2 [s, *C*$_{Ph}$], 126.0 [s, *C*$_{Ph}$], 128.4 [s, *C*$_{Ph}$], 129.0 [s, *C*$_{Ph}$], 130.3 [s, *C*$_{Ph}$], 132.7 [s, *C*$_{Ph}$], 134.9 [s, *C*$_{Ph}$], 136.3 [s, *C*$_{Ph}$], 145.4[s, *C*$_{Ph}$]. **^{29}Si{^{1}H} NMR** (79 MHz, C_6D_6, 298 K): *δ*[ppm] = −36.7 [s, *Si*N], 10.3 [s, *Si*(CH$_3$)$_3$]. **HR-MS (FD+)**, calculated m/z for $C_{25}H_{24}N_2OSi_2$: [M+H$^+$]: 434.22042; found: 434.2200.

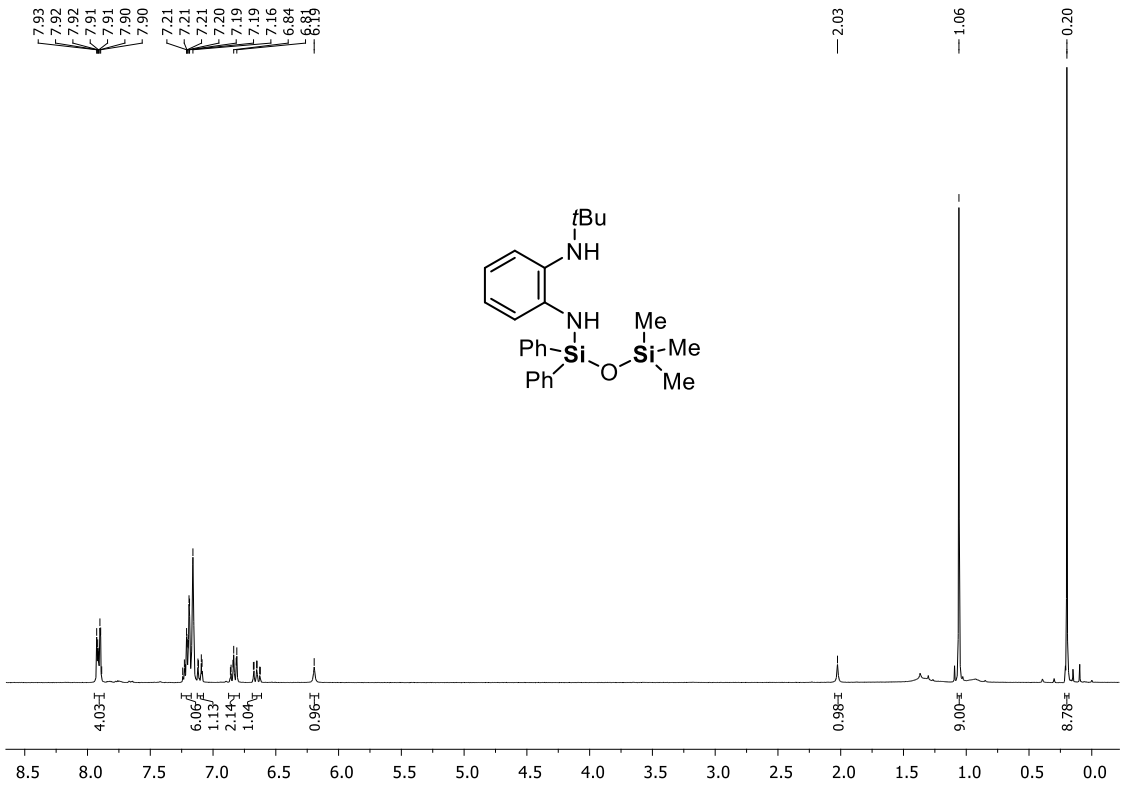

Figure S3.38. ^{1}H NMR spectrum (C_6D_6, 298 K) of **6**.

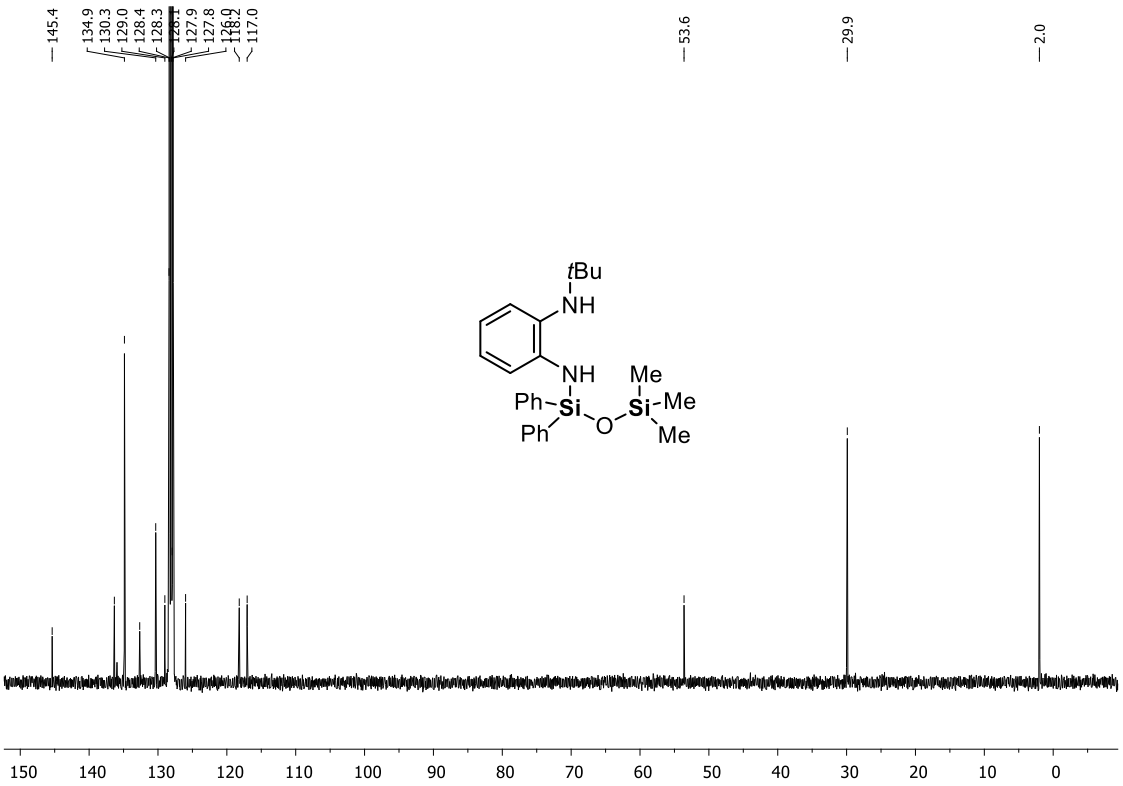

Figure S3.39. $^{13}C\{^{1}H\}$ NMR spectrum (C_6D_6, 298 K) of **6**.

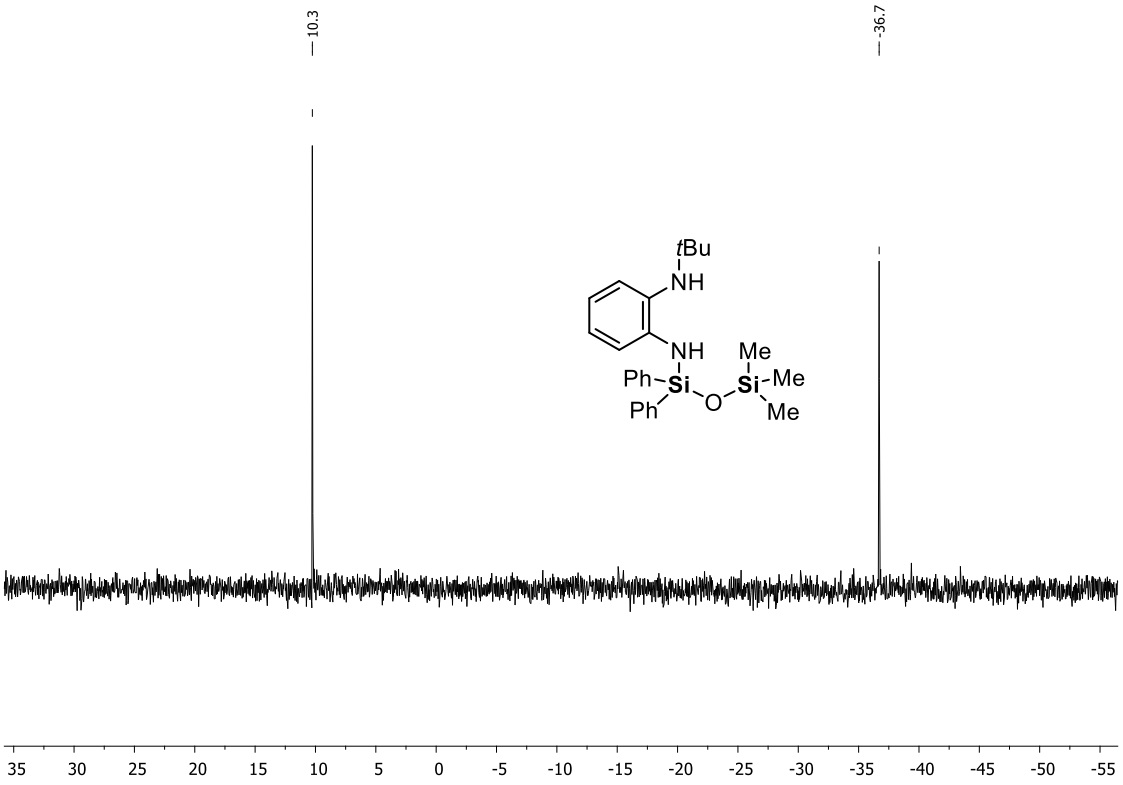

Figure S3.40. $^{29}Si\{^{1}H\}$ NMR spectrum (C_6D_6, 298 K) of **6**.

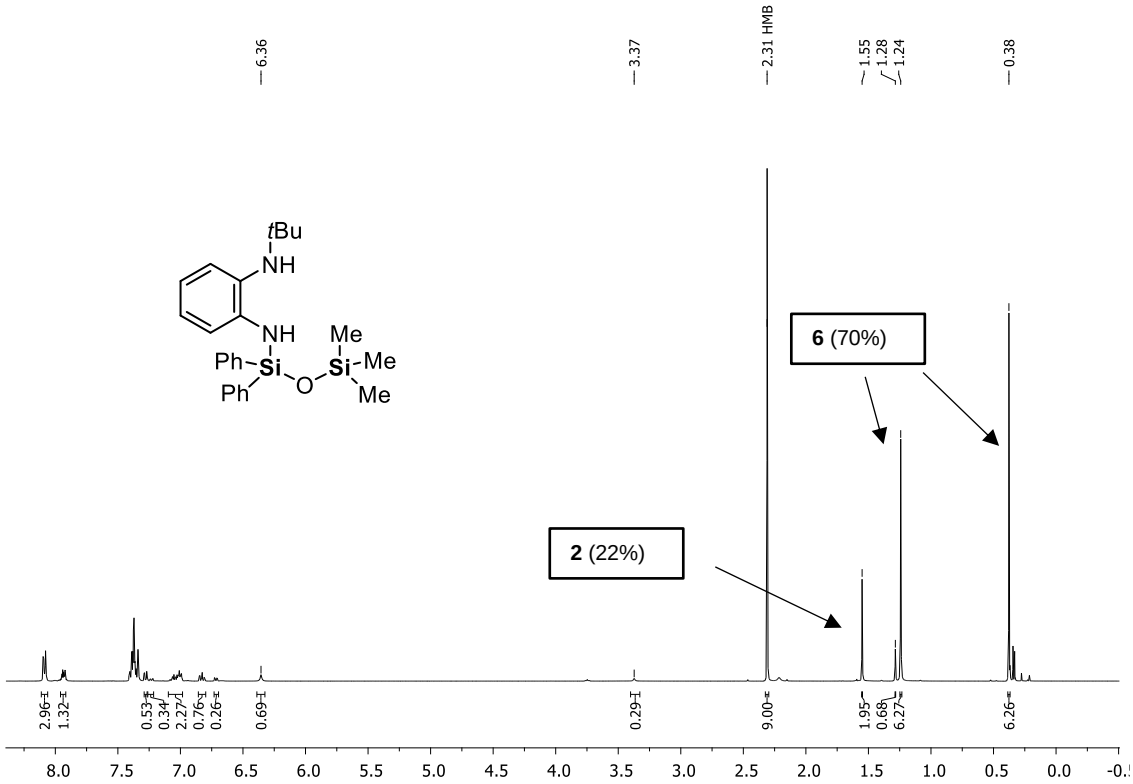

Figure S3.41. ^{1}H NMR spectrum (C_6D_6, 298 K) with 0.5 equiv. HMB as internal standard for determination of the NMR yield of **6**.

4.1.1.18 Compound 7

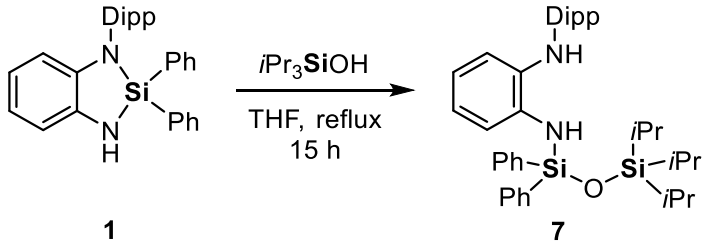

Compound **1** (2.24 g, 5.0 mmol, 1.0 equiv.) and *i*Pr$_3$SiOH (0.99 mL, 5.0 mmol, 1.0 equiv.) were dissolved in 25 mL of THF. The slightly violet solution was heated at reflux for 15 h. All volatiles were removed *in vacuo* and the violet residue was dissolved in 5 mL hexane, After removing all volatiles *in vacuo*, **7** was obtained as a red wax (3.05 g, 4.90 mmol, 98%).

^{1}H NMR (400 MHz, C_6D_6, 298 K): *δ*[ppm] = 1.03–1.20 [m, 33H, CH(C*H*$_3$)$_2$], 3.12 [sept, $^{3}J_{H–H}$ = 6.78 Hz, 2H, CH(C*H*$_3$)$_2$], 4.83 [s, 1H, N*H*], 4.89 [s, 1H, N*H*], 6.53 [td, $^{3}J_{H–H}$ = 7.83 Hz, $^{4}J_{H–H}$ = 1.38 Hz, 1H, *H*$_{Ph}$], 6.63 [td, $^{3}J_{H–H}$ = 7.51 Hz, $^{4}J_{H–H}$ = 1.54 Hz, 1H, *H*$_{Ph}$], 7.02–7.21 [m, 10H, *H*$_{Ph}$], 7.87–7.95 [m, 4H, *H*$_{Ph}$]. **^{13}C{^{1}H} NMR** (101 MHz, C_6D_6, 298 K): *δ*[ppm] = 13.4 [s, CH(*C*H$_3$)$_2$], 18.2 [s, CH(*C*H$_3$)$_2$], 23.3 [s, *C*H(CH$_3$)$_2$], 24.8 [s, *C*H(CH$_3$)$_2$], 28.4 [s, *C*H(CH$_3$)$_2$], 118.2 [s, *C*$_{Ph}$], 118.8 [s, *C*$_{Ph}$], 120.5 [s, *C*$_{Ph}$], 122.0 [s, *C*$_{Ph}$], 124.3 [s, *C*$_{Ph}$], 126.1 [s, *C*$_{Ph}$], 128.4 [s, *C*$_{Ph}$], 130.6 [s, *C*$_{Ph}$], 135.2 [s, *C*$_{Ph}$], 136.0 [s, *C*$_{Ph}$], 136.6 [s, *C*$_{Ph}$], 137.5 [s, *C*$_{Ph}$], 138.2 [s, *C*$_{Ph}$], 144.5 [s, *C*$_{Ph}$].

^{29}Si{^{1}H} NMR (79 MHz, C_6D_6, 298 K): *δ*[ppm] = −35.7 [s, O*Si*(CH(CH$_3$)$_2$)$_3$], 10.2 [s, *Si*N]. **HR-MS (FD+)**, calculated m/z for $C_{39}H_{54}N_2OSi_2$: [M+H$^+$]: 622.37692; found: 622.3759.

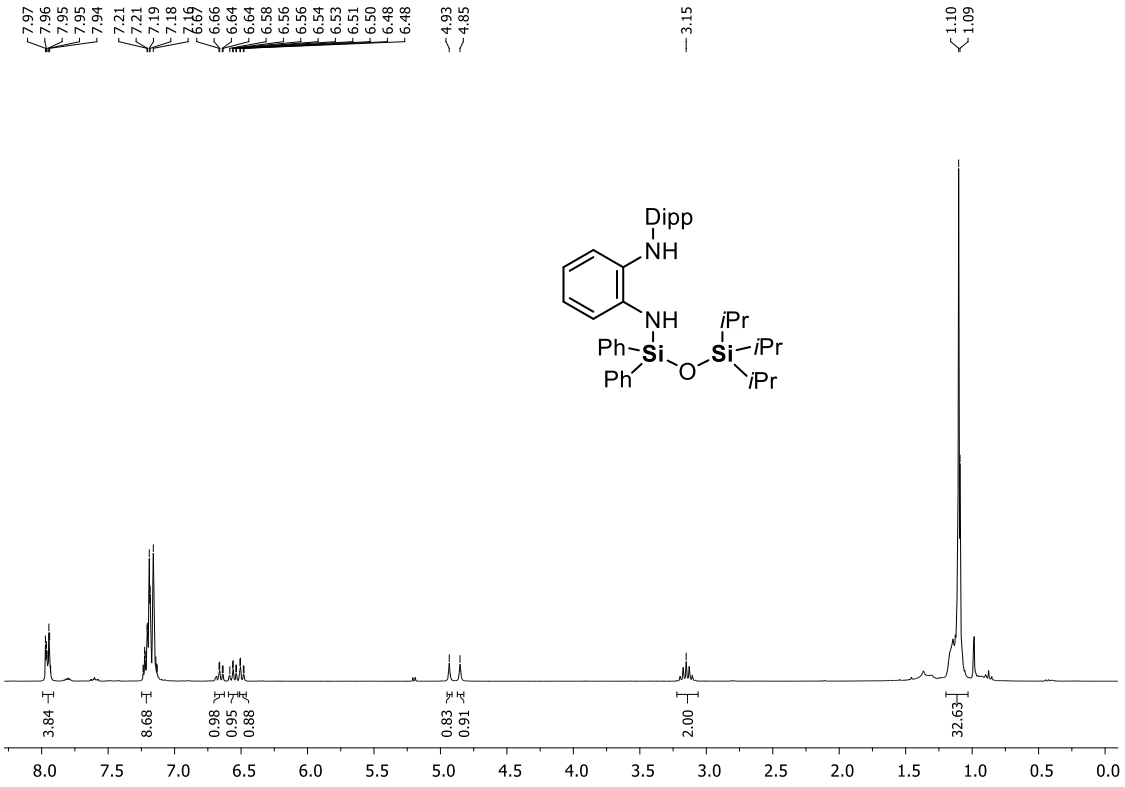

Figure S3.42. ^{1}H NMR spectrum (C_6D_6, 298 K) of **7**.

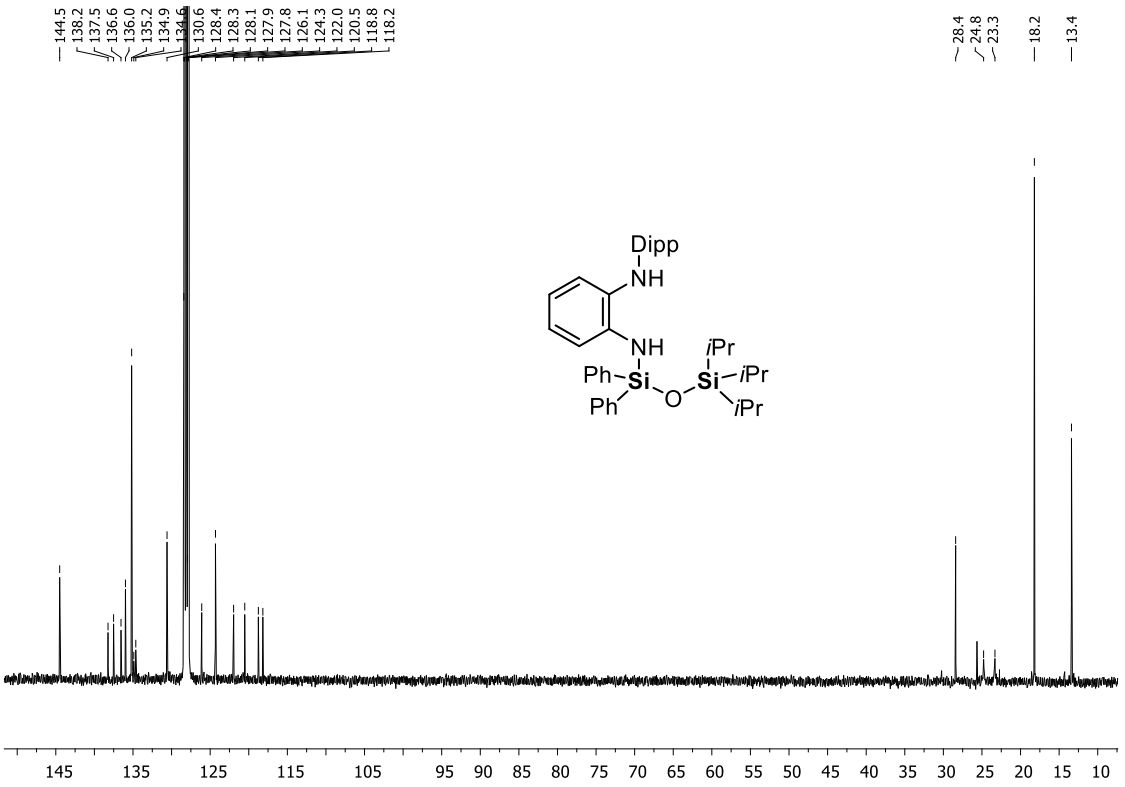

Figure S3.43. ^{13}C{^{1}H} NMR spectrum (C_6D_6, 298 K) of **7**.

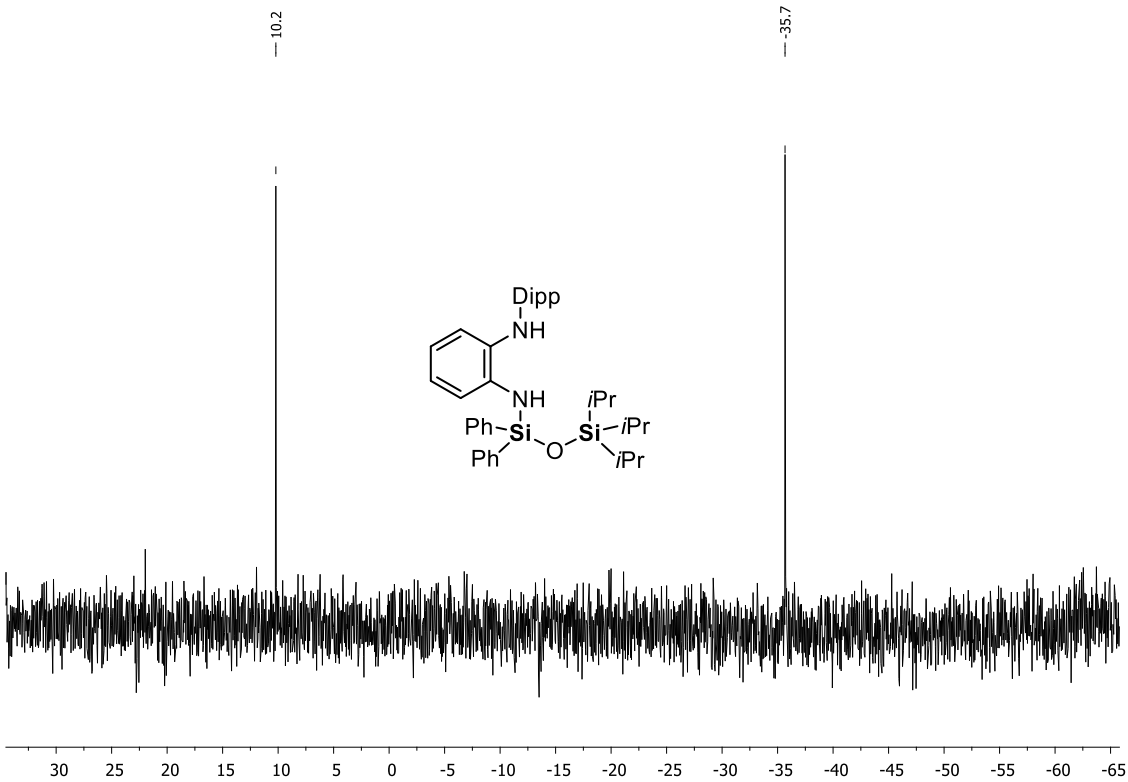

Figure S3.44. $^{29}Si\{^{1}H\}$ NMR spectrum (C_6D_6, 298 K) of **7**.

4.1.1.19 Compound 8

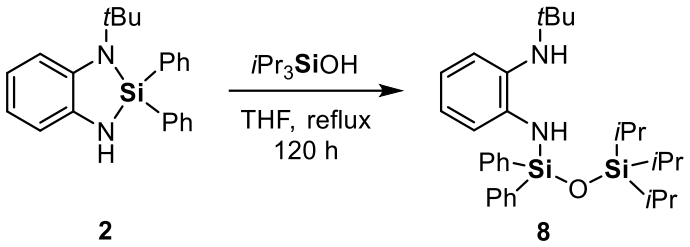

2 **8**

Compound **2** (345 mg, 1.0 mmol, 1.0 equiv.) and *i*Pr$_3$SiOH (0.2 mL, 1.0 mmol, 1.0 equiv.) were dissolved in 10 mL of THF. The colorless solution was heated at reflux for 120 h. All volatiles were removed *in vacuo* and the residue was purified via Kugelrohr distillation (130 °C oven temperature, 9.4 × 10^{-3} mbar). **8** was obtained as a yellow wax (155 mg, 0.30 mmol, 30%).

^{1}H NMR (400 MHz, C_6D_6, 298 K): *δ*[ppm] = 1.07–1.12 [m, 28H, C(C*H*$_3$)$_3$+CH(C*H*$_3$)$_2$], 2.07 [s, 1H, N*H*], 6.28 [s, 1H, N*H*], 6.61–6.66 [td, $^{3}J_{H–H}$ = 7.48 Hz, $^{4}J_{H–H}$ = 1.50 Hz, 1H, *H*$_{Ph}$], 6.81–6.87 [m, 2H, *H*$_{Ph}$], 7.09–7.12 [m, 1H, *H*$_{Ph}$], 7.17–7.25 [m, 6H, *H*$_{Ph}$], 7.93–7.97 [m, 4H, *H*$_{Ph}$]. **^{13}C{^{1}H} NMR** (101 MHz, C_6D_6, 298 K): *δ*[ppm] = 13.4 [s, CH(*C*H$_3$)$_2$], 18.2 [s, *C*H(CH$_3$)$_2$], 29.9 [s C(*C*H$_3$)$_3$], 53.6 [s, *C*(CH$_3$)$_3$], 117.1 [s, *C*$_{Ph}$], 118.1 [s, *C*$_{Ph}$], 128.1 [s, *C*$_{Ph}$], 128.3 [s, *C*$_{Ph}$], 128.96 [s, *H*$_{Ph}$], 130.4 [s, *H*$_{Ph}$], 132.5 [s, *H*$_{Ph}$], 135.2 [s, *H*$_{Ph}$], 136.2 [s, *H*$_{Ph}$], 145.4 [s, *H*$_{Ph}$]. **^{29}Si{^{1}H} NMR** (79 MHz, C_6D_6, 298 K): *δ*[ppm] = −37.1 [s, *Si*N], 9.5 [s, O*Si*(CH(CH$_3$)$_2$]. **HR-MS (FD+)**, calculated m/z for $C_{39}H_{54}N_2OSi_2$: [M+H$^+$]: 518.3143; found: 518.3144.

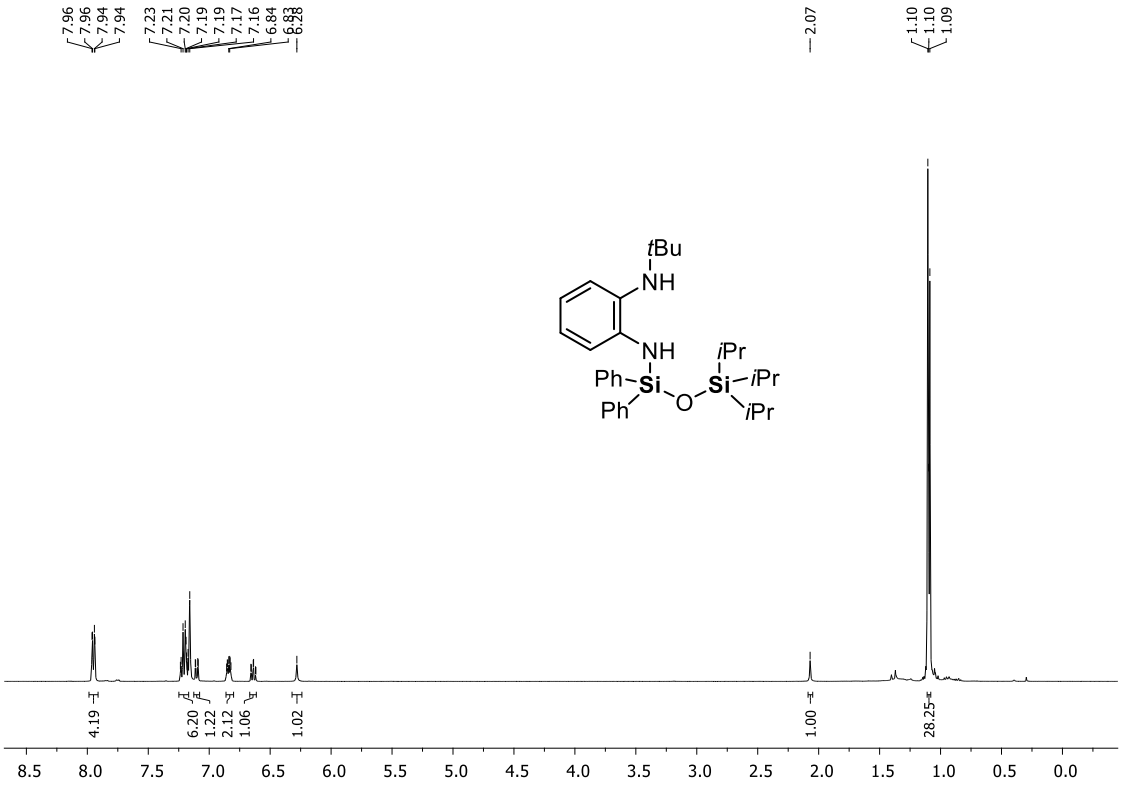

Figure S3.45. ^{1}H NMR spectrum (C_6D_6, 298 K) of **8**.

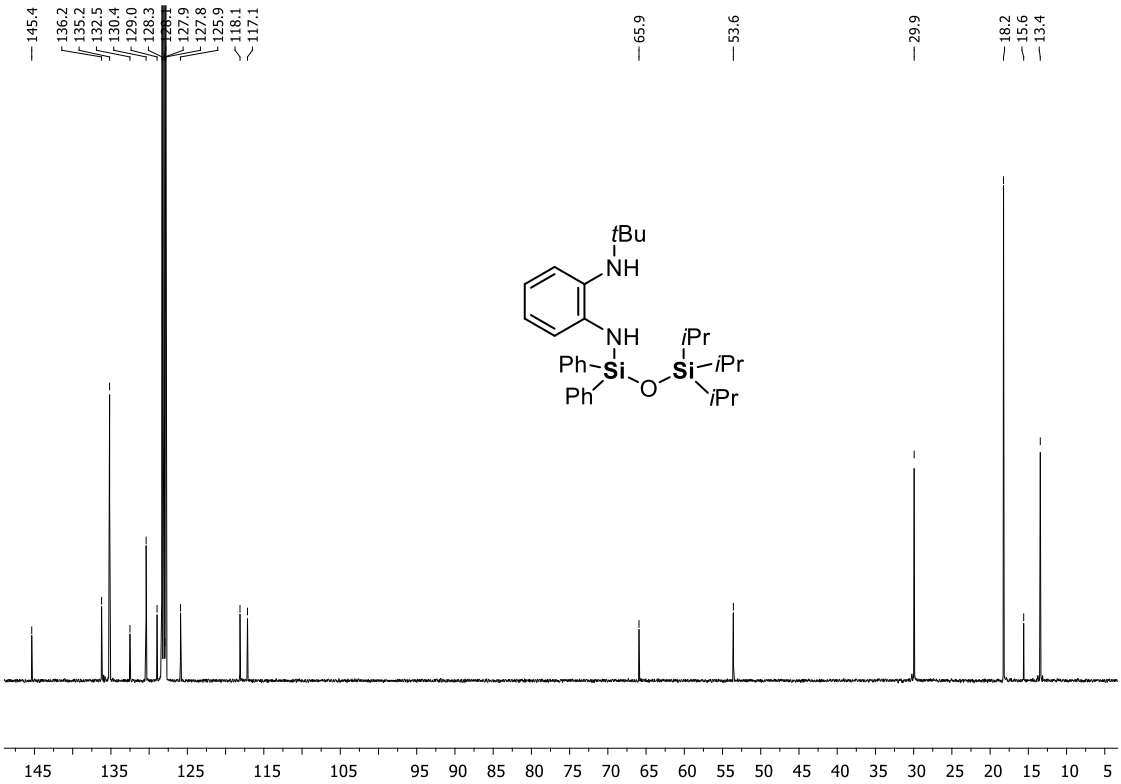

Figure S3.46. $^{13}C\{^{1}H\}$ NMR spectrum (C_6D_6, 298 K) of **8**.

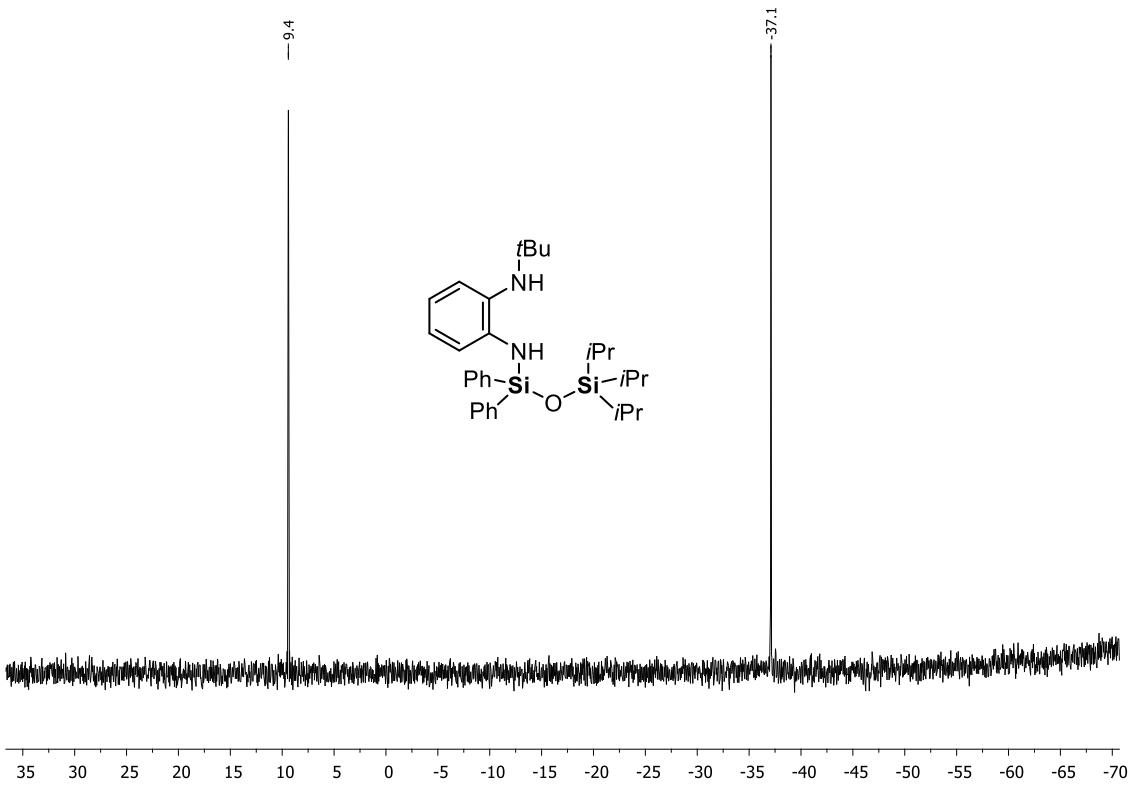

Figure S3.47. $^{29}Si\{^{1}H\}$ NMR spectrum (C_6D_6, 298 K) of **8**.

4.1.1.20 Compound 9

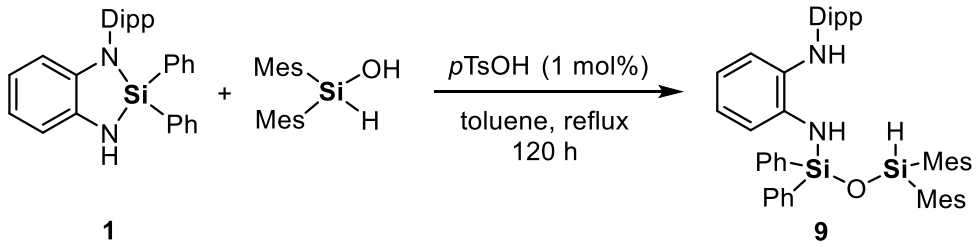

1 **9**

Compound **1** (2.38 g, 5.3 mmol, 1.0 equiv.), dimesitylsilanol (1.52 g, 5.3 mmol, 1.0 equiv.), and *para*-toluenesulfonic acid (85 mg, 0.05 mmol, 1 mol%) were dissolved in 50 mL of toluene and heated at reflux for 120 h. All volatiles were removed *in vacuo* and the crude residue was suspended in hot pentane followed by immediate filtration. After removing all volatiles, an off-white solid was obtained. Recrystallization from hot pentane gave single-crystals of compound **9** (1.41 g, 1.9 mmol, 36%) suitable for single-crystal X-ray diffraction analysis (for details, see chapter 3.8).

For the determination of the NMR yield, an individual experiment was performed. For this purpose, compound **1** (449 mg, 1.0 mmol, 1.0 equiv.), dimesitylsilanol (285 mg, 1.0 mmol, 1.0 equiv.), *para*-toluenesulfonic acid (17 mg, 0.1 mmol, 1 mol%), and hexamethylbenzene (81 mg, 0.5 mmol, 0.5 equiv.) as internal standard were dissolved in 10 mL of toluene. The reaction mixture was heated at reflux for 15 h and then an aliquot of ca. 0.5 mL was transferred into an

NMR tube. All volatiles were removed *in vacuo* and 0.5 mL of C_6D_6 was added. An NMR yield of 78% was determined by integration in the ^{1}H NMR spectrum (Figure S3.52).

^{1}H NMR (400 MHz, C_6D_6, 298 K): *δ*[ppm] = 1.20–1.05 [m, 12H, CH(C*H*$_3$)$_3$], 2.06 [s, 6H, Mes-*para*-C*H*$_3$], 2.47 [s, 12H, Mes-*ortho*-C*H*$_3$], 3.14 [sept, $^3J_{H-H}$ = 6.80 Hz, 2H, C*H*(CH$_3$)$_2$], 4.68 [s, 1H, N*H*], 4.80 [s, 1H, N*H*], 6.47–6.43 [m, 1H, *H*$_{Ph}$], 6.59–6.51 [m, 3H, *H*$_{Ph}$], 6.69 [s, 4H, *H*$_{Ph}$], 7.10–7.16 [m, 3H, *H*$_{Ph}$], 7.15–7.24 [m, 7H, *H*$_{Ph}$], 7.85-7.90 [m, 4H, *H*$_{Ph}$]. **^{13}C{^{1}H} NMR** (101 MHz, C_6D_6, 298 K): *δ*[ppm] = 21.1 [s, Mes-*para*-*C*H$_3$], 22.9 [s, Mes-*ortho*-*C*H$_3$], 23.5 [s, CH(*C*H$_3$)$_2$], 24.6 [s, CH(*C*H$_3$)$_2$], 28.4 [s, *C*H(CH$_3$)$_2$], 117.4 [s, *C*$_{Ph}$], 119.5 [s, *C*$_{Ph}$], 120.9 [s, *C*$_{Ph}$], 121.58 [s, *C*$_{Ph}$], 124.3 [s, *C*$_{Ph}$], 126.2 [s, *C*$_{Ph}$], 128.4 [s, *C*$_{Ph}$], 129.6 [s, *C*$_{Ph}$], 130.6 [s, *C*$_{Ph}$], 130.9 [s, *C*$_{Ph}$], 135.0 [s, *C*$_{Ph}$], 135.2 [s, *C*$_{Ph}$], 135.6 [s, *C*$_{Ph}$], 138.1 [s, *C*$_{Ph}$], 138.2 [s, *C*$_{Ph}$], 139.9 [s, *C*$_{Ph}$], 144.5[s, *C*$_{Ph}$], 144.82 [s, *C*$_{Ph}$]. **^{29}Si{^{1}H}** NMR (79 MHz, C_6D_6, 298 K): *δ*[ppm] = −31.5 [s, *Si*N], −29.2 [s, *Si*H]. **^{29}Si NMR** (79 MHz, C_6D_6, 298 K): *δ*[ppm] = −31.5 [m, SiN], −29.2 [d, $^1J_{Si-H}$ = 214.54 Hz, *Si*H). **CHN Analysis** $C_{48}H_{56}N_2OSi_2$ calculated: C 78.64, H 7.70, N 3.82, O 2.18, Si 7.66; found: C 78.83, H 7.83, N 3.83. **MS (FD+)**, calculated m/z for $C_{48}H_{56}N_2OSi_2$ [M+H$^+$]: 732.39; found: 732.40.

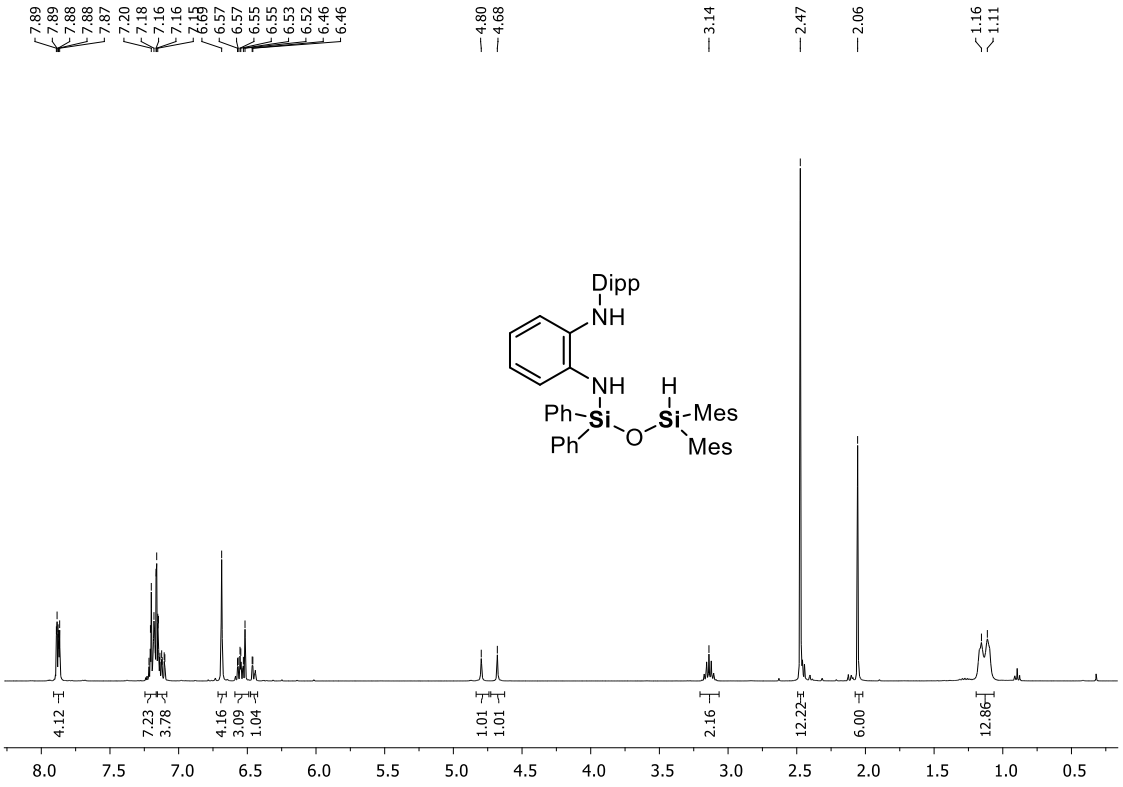

Figure S3.48. ^{1}H NMR spectrum (C_6D_6, 298 K) of **9**.

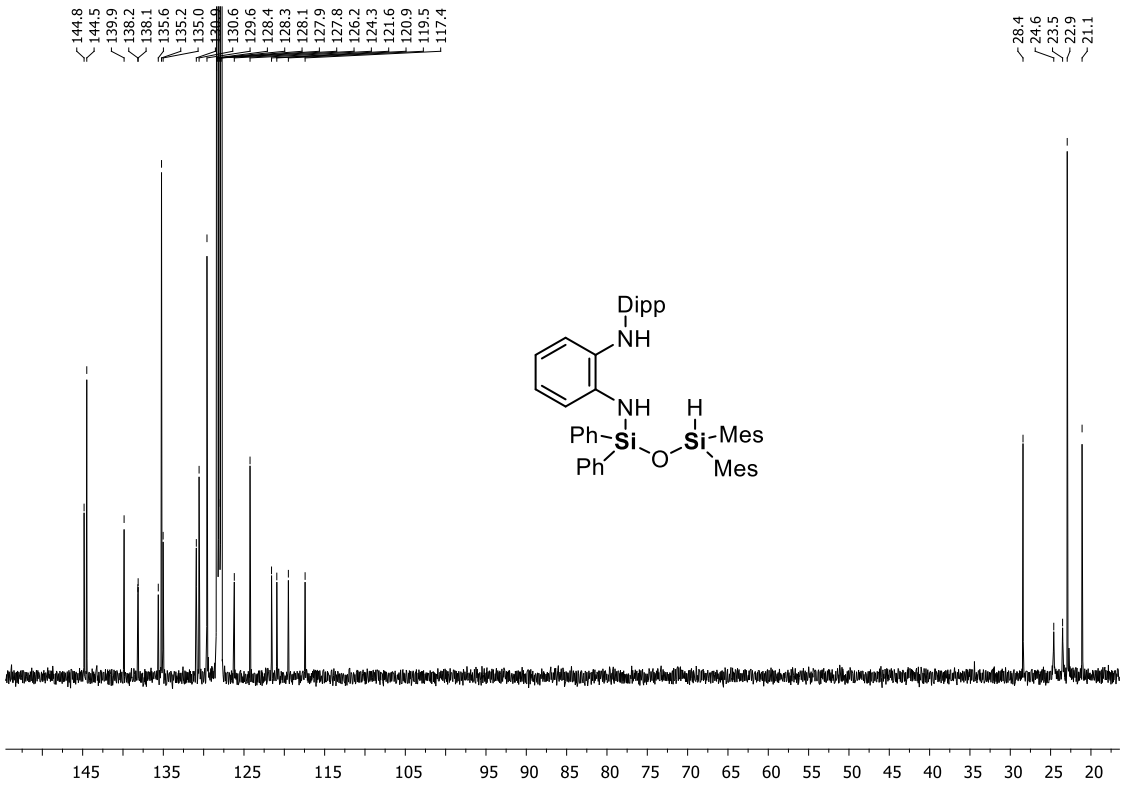

Figure S3.49. $^{13}C\{^{1}H\}$ NMR spectrum (C_6D_6, 298 K) of **9**.

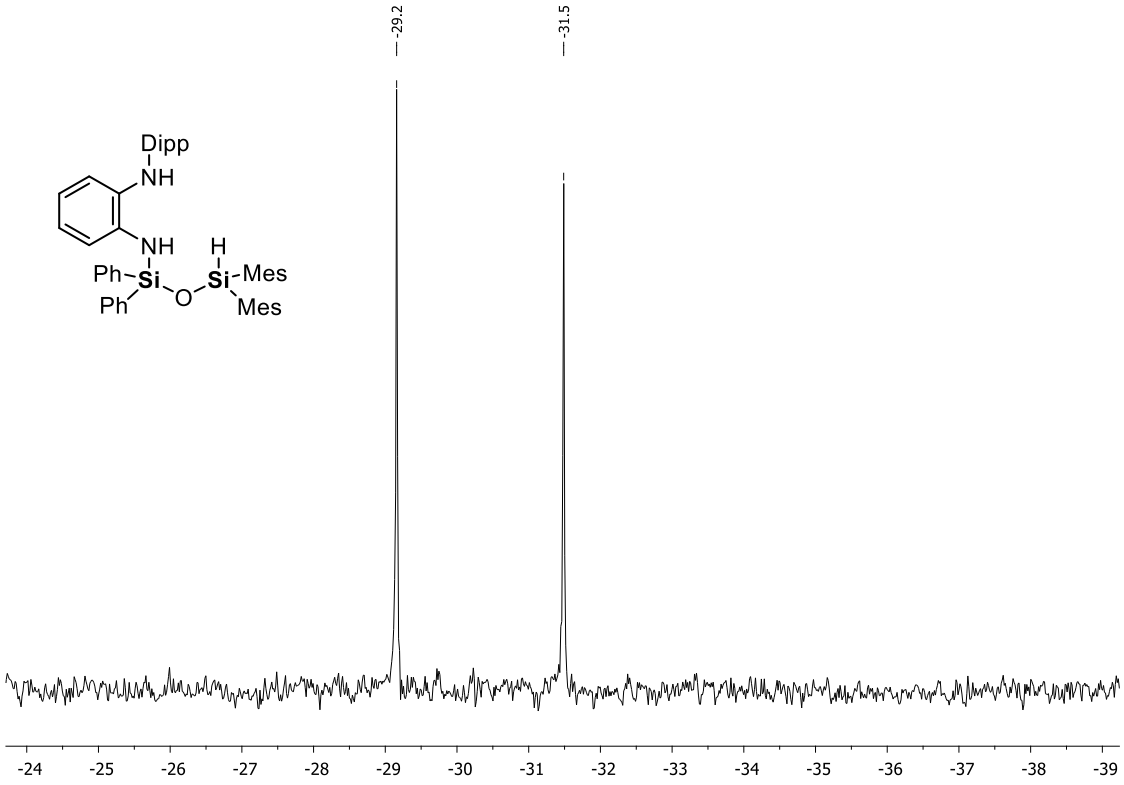

Figure S3.50. $^{29}Si\{^{1}H\}$ NMR spectrum (C_6D_6, 298 K) of **9**.

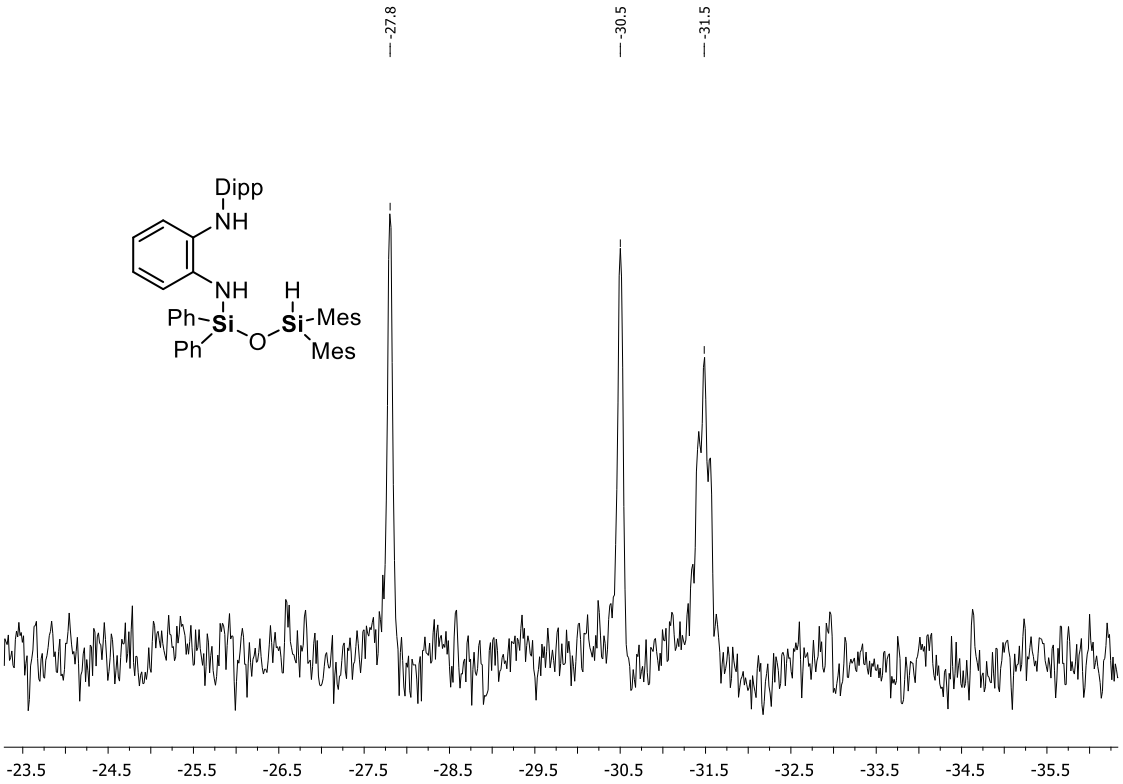

Figure S3.51. ^{29}Si NMR spectrum (C_6D_6, 298 K) of **9**.

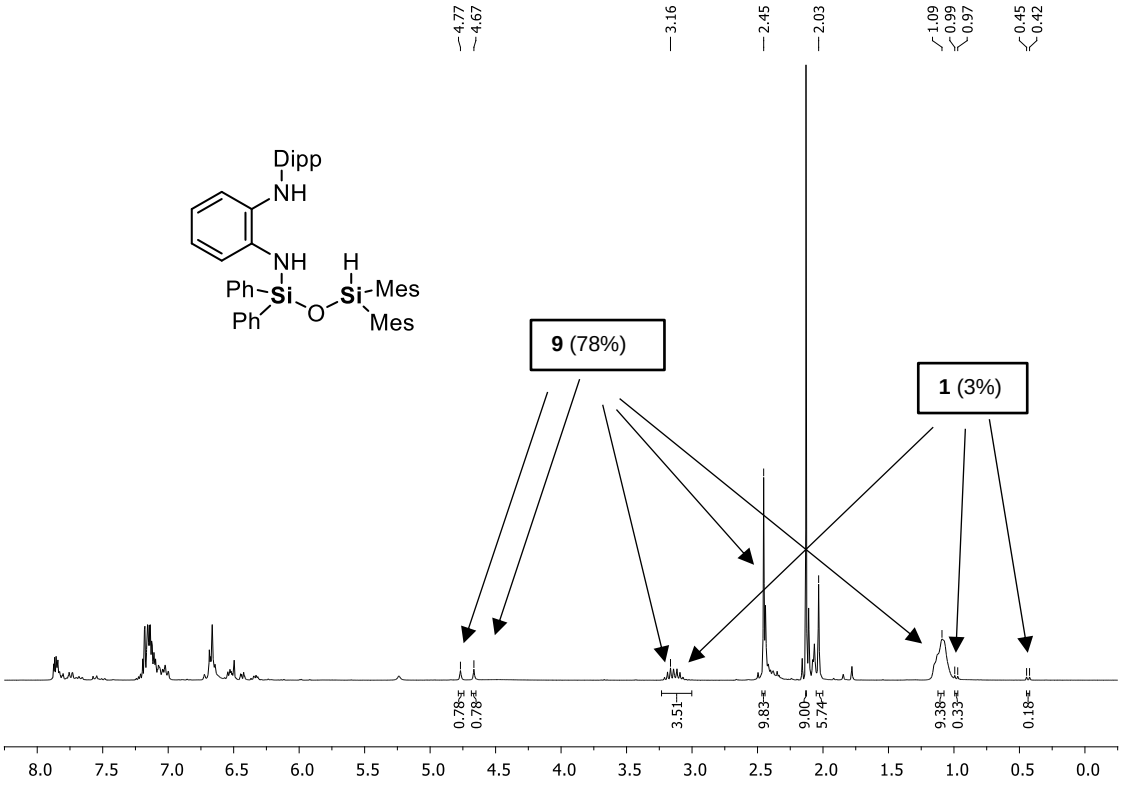

Figure S3.52. ^{1}H NMR spectrum (C_6D_6, 298 K) with 0.5 equiv. HMB as internal standard for determination of the NMR yield of **9**.

4.1.1.21 Compound 10

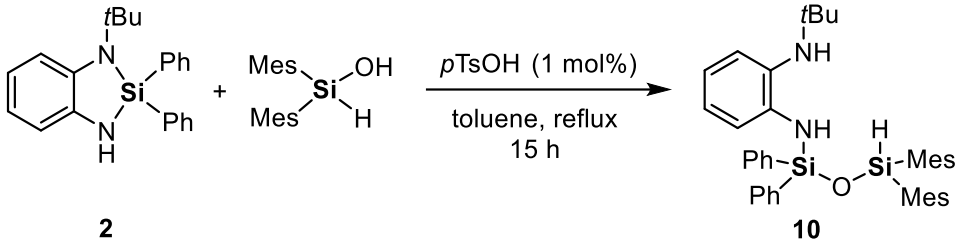

2 **10**

Compound **2** (1.03 g, 3.0 mmol, 1.0 equiv.), dimesitylsilanol (1.02 g, 3.6 mmol, 1.2 equiv.), and *para*-toluenesulfonic acid (51 mg, 0.03 mmol, 1 mol%) were dissolved in 40 mL of toluene and heated at reflux for 15 h. All volatiles were removed *in vacuo* and the residue purified via Kugelrohr distillation (150 °C oven temperature, 4.1×10^{-2} mbar) Compound **10** was recovered from the undistilled tail fraction by extraction with 5 mL pentane. The solids were removed via cannula filtration and the organic phase was dried *in vacuo* to obtain **10** as an off-white solid (1.32 g, 2.1 mmol, 70%).

^{1}H NMR (400 MHz, C_6D_6, 298 K): δ[ppm] = 1.05 [s, 9H, C(C*H*$_3$)$_3$], 2.03 [s, 1H, N*H*], 2.08 [s, 6H, Mes-*para*-C*H*$_3$], 2.44 [s, 12H, Mes-*ortho*-C*H*$_3$], 6.24 [s, 1H, N*H*], 6.49 [s, 1H, Si*H*], 6.62 [td, $^{3}J_{H–H}$ = 7.56 Hz, $^{4}J_{H–H}$ = 1.58 Hz, 1H, *H*$_{Ph}$], 6.66 [s, 4H, *H*$_{Ph}$], 6.71 [td, $^{3}J_{H–H}$ = 7.54 Hz, $^{4}J_{H–H}$ = 1.65 Hz, 1H, *H*$_{Ph}$], 6.82 [dd, $^{3}J_{H–H}$ = 7.66 Hz, $^{4}J_{H–H}$ = 1.56 Hz, 1H, *H*$_{Ph}$], 7.01 [dd, $^{3}J_{H–H}$ = 7.91 Hz, $^{4}J_{H–H}$ = 1.50 Hz, 1H, *H*$_{Ph}$], 7.11–7.15 [m, 6H, *H*$_{Ph}$], 7.82–7.86 [m, 4H, *H*$_{Ph}$]. **^{13}C{^{1}H} NMR** (101 MHz, C_6D_6, 298 K): δ[ppm] = 21.2 [s, Mes-*para*-*C*H$_3$], 22.9 [s, Mes-*ortho*-*C*H$_3$], 29.9 [s, C(*C*H$_3$)$_3$], 53.5 [s, C(CH$_3$)$_3$], 117.2 [s, *C*$_{Ph}$], 118.2 [s, *C*$_{Ph}$], 126.0 [s, *C*$_{Ph}$], 128.3 [s, *C*$_{Ph}$], 128.8 [s, *C*$_{Ph}$], 129.5 [s, *C*$_{Ph}$], 130.4 [s, *C*$_{Ph}$], 131.1 [s, *C*$_{Ph}$], 132.6 [s, *C*$_{Ph}$], 135.2 [s, *C*$_{Ph}$], 135.2 [s, *C*$_{Ph}$], 139.6 [s, *C*$_{Ph}$], 144.6 [s, *C*$_{Ph}$], 145.1 [s, *C*$_{Ph}$]. **^{29}Si{^{1}H} NMR** (79 MHz, C_6D_6, 298 K): δ[ppm] = −33.3 [s, *Si*N], −29.2 [s, *Si*H]. **^{29}Si NMR (**101 MHz, C_6D_6, 298 K): δ[ppm] = –33.2 [m, *Si*N], –29.2 (d, $^{1}J_{Si-H}$ = 2.71 Hz, *Si*H]. **CHN Analysis** $C_{40}H_{48}N_2OSi_2$ calculated: C 76.38, H 7.69, N 4.45, O 2.54, Si 8.93; found: C 76.12, H 7.39, N 4.25. **HR-MS (FD+)**, calculated m/z for $C_{40}H_{48}N_2OSi_2$ [M+H$^+$]: 628.32997; found: 628.3285.

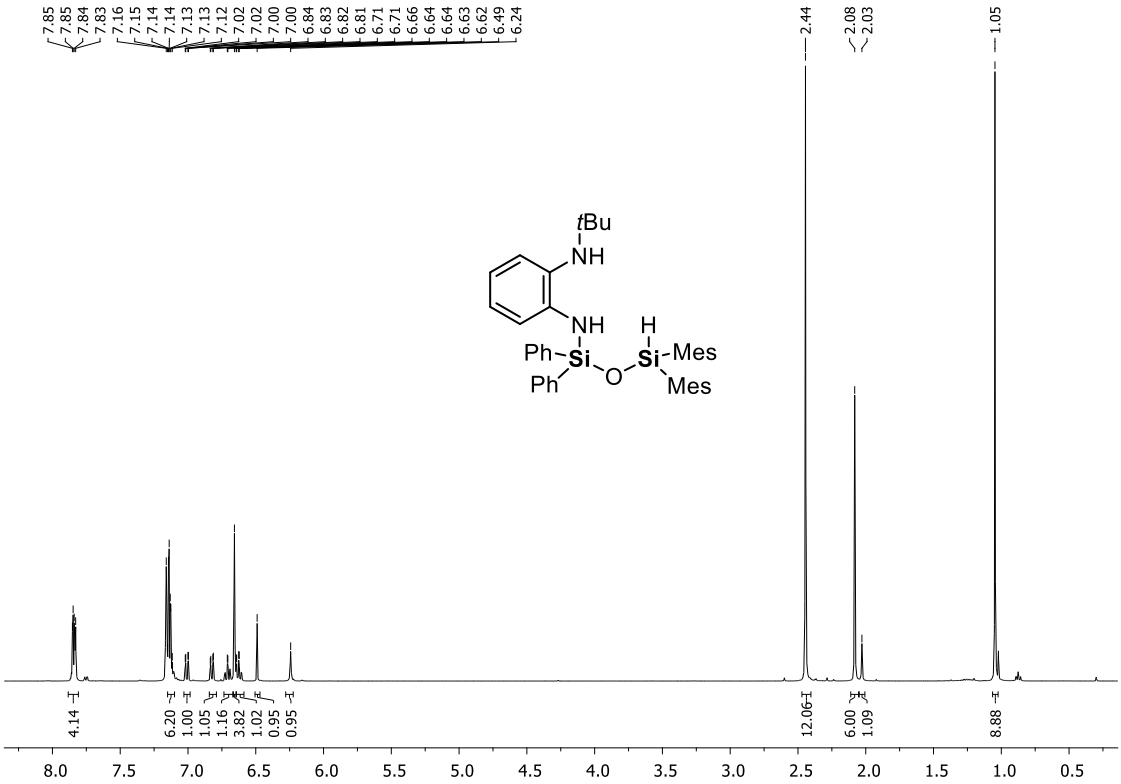

Figure S3.53. ^{1}H NMR spectrum (C_6D_6, 298 K) of **10**.

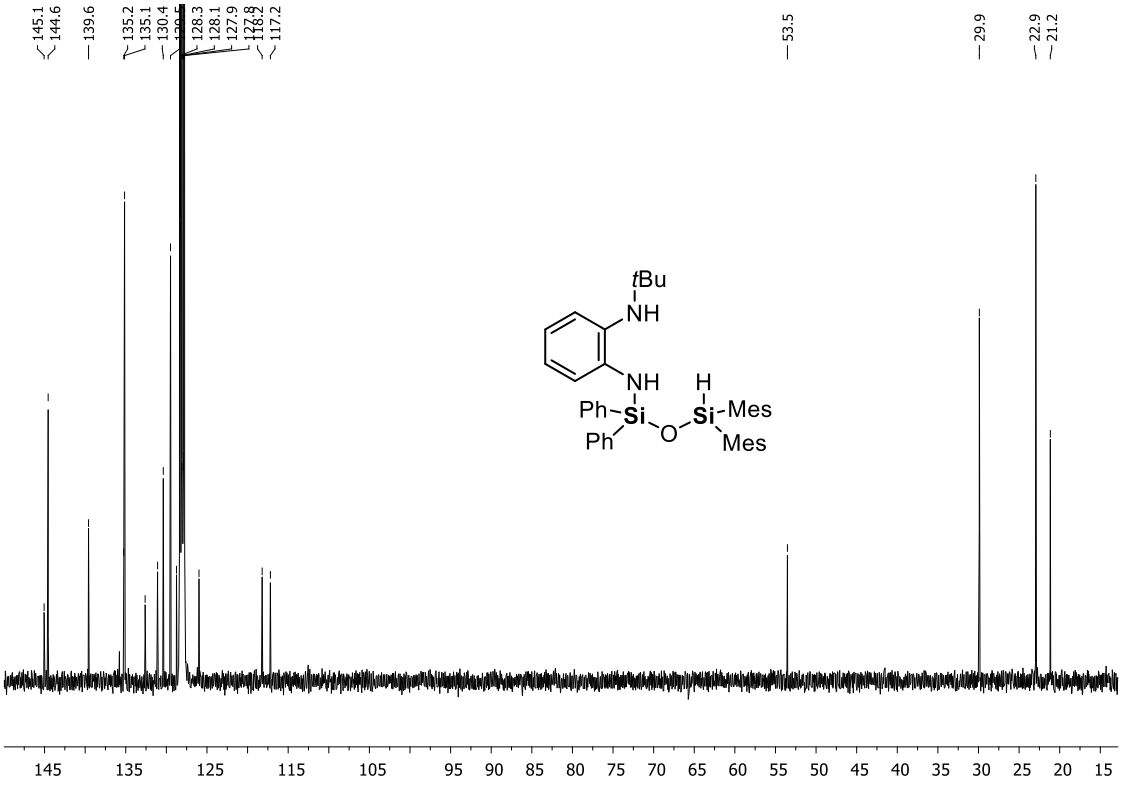

Figure S3.54. ^{13}C{^{1}H} NMR spectrum (C_6D_6, 298 K) of **10**.

15

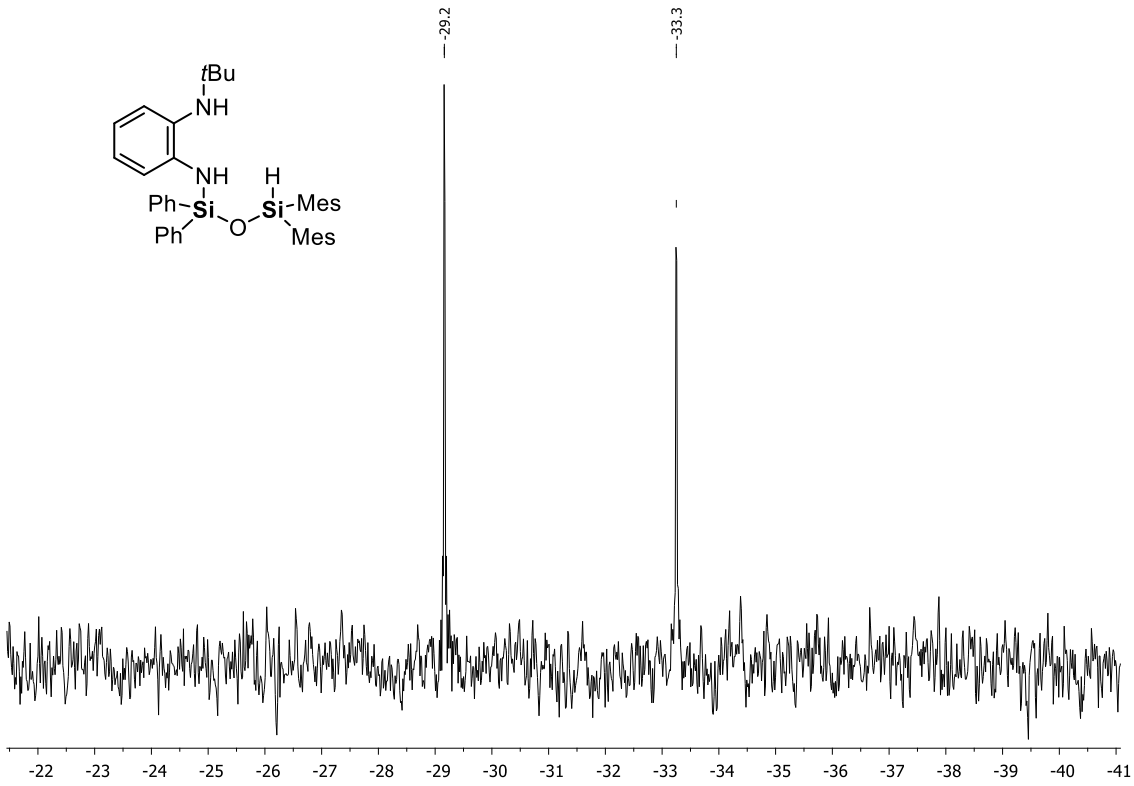

Figure S3.55. $^{29}Si\{^{1}H\}$ NMR spectrum (C_6D_6, 298 K) of **10**.

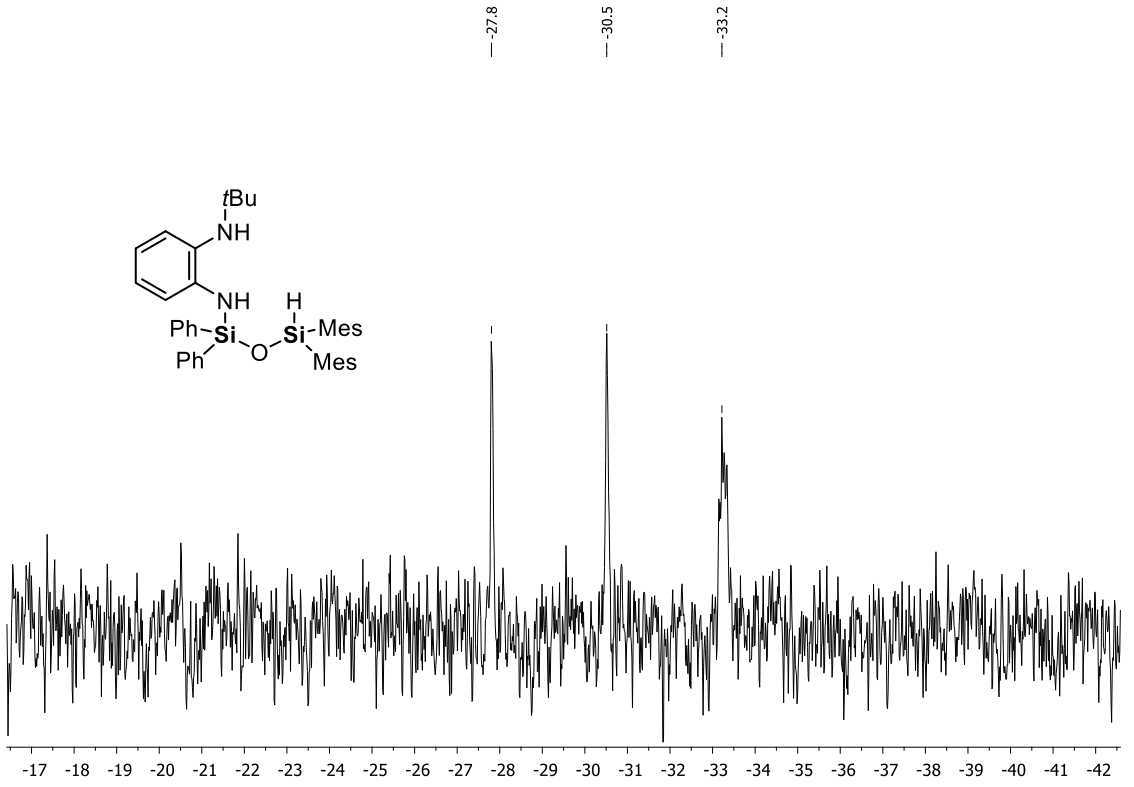

Figure S3.56. ^{29}Si NMR spectrum (C_6D_6, 298 K) of **10**.

4.1.1.22 Compound 11

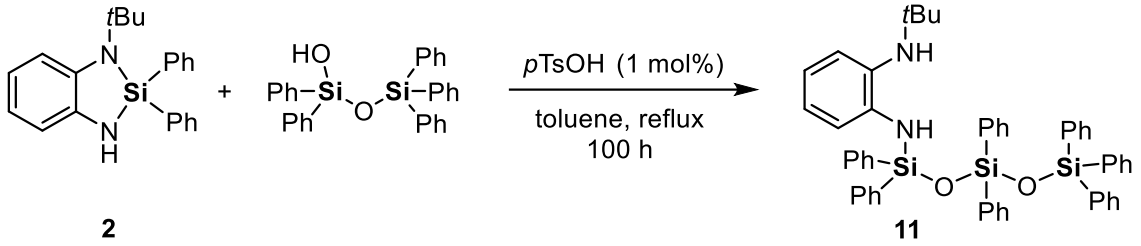

Compound **2** (1.14 g, 3.3 mmol, 1.0 equiv.), 1-hydroxy-1,1,3,3,3-pentaphenyldisiloxane (1.57 g, 3.3 mmol, 1.0 equiv.), and *para*-toluenesulfonic acid (52 mg, 0.03 mmol, 1 mol%) were dissolved in 40 mL of toluene and heated at reflux for 100 h. All volatiles were removed *in vacuo* and the product was extracted with hexane (2 × 10 mL). After the solids had been filtered off by cannula filtration, the filtrate was cooled down to −80 °C during which a solid precipitated out. The solids were filtered off by cannula filtration and washed with cold hexane (2 × 5 mL). After drying *in vacuo*, **11** was obtained as an off-white waxy solid (2.02 g, 2.47 mmol, 75%).

^{1}H NMR (400 MHz, C_6D_6, 298 K): *δ*[ppm] = 1.01 [s, 9H, C(C*H*$_3$)$_3$], 2.01 (s, 1H, N*H*], 6.13 [s, 1H, N*H*], 6.59–6.65 [m, 1H, *H*$_{Ph}$], 6.81–6.84 [m, 1H, *H*$_{Ph}$], 6.99–7.11 [m, 18H, *H*$_{Ph}$], 7.64–7.82 [m, 18H, *H*$_{Ph}$]. **^{13}C{^{1}H} NMR** (101 MHz, C_6D_6, 298 K): *δ*[ppm] = 29.9 [s, C(*C*H$_3$)$_3$], 53.5 [s, *C*(CH$_3$)$_3$], 117.6 [s, *C*$_{Ph}$], 118.3 [s, *C*$_{Ph}$], 126.0 [s, *C*$_{Ph}$], 128.0 [s, *C*$_{Ph}$], 128.2 [s, *C*$_{Ph}$], 128.2 [s, *C*$_{Ph}$], 130.1 [s, *C*$_{Ph}$], 130.3 [s, *C*$_{Ph}$], 130.3 [s, *C*$_{Ph}$], 130.4 [s, *C*$_{Ph}$], 132.7 [s, *C*$_{Ph}$], 134.9 [s, *C*$_{Ph}$], 135.2 [s, *C*$_{Ph}$], 135.2 [s, *C*$_{Ph}$], 135.3 [s, *C*$_{Ph}$], 135.5 [s, *C*$_{Ph}$], 135.6 [s, *C*$_{Ph}$], 135.8 [s, *C*$_{Ph}$], 135.9 [s, *C*$_{Ph}$], 144.8 [s, *C*$_{Ph}$]. **^{29}Si{^{1}H} NMR** (79 MHz, C_6D_6, 298 K): *δ*[ppm] = −44.8 [s, *Si*O$_2$], −35.5 [s, *Si*N], -18.4 [s, *Si*(Ph)$_3$]. **HR-MS (FD+)**, calculated m/z for $C_{52}H_{50}N_2O_2S_3$ [M+H$^+$]: 818.31746; found: 818.31802.

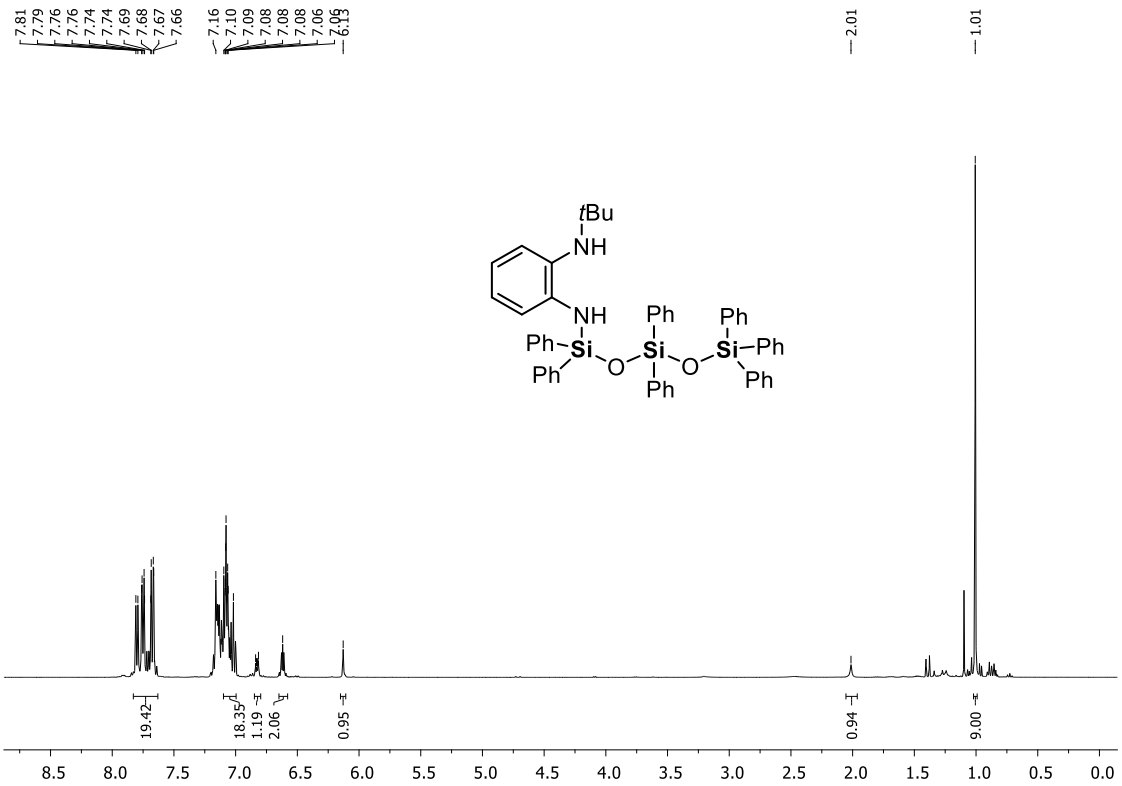

Figure S3.57. ^{1}H NMR spectrum (C_6D_6, 298 K) of **11**.

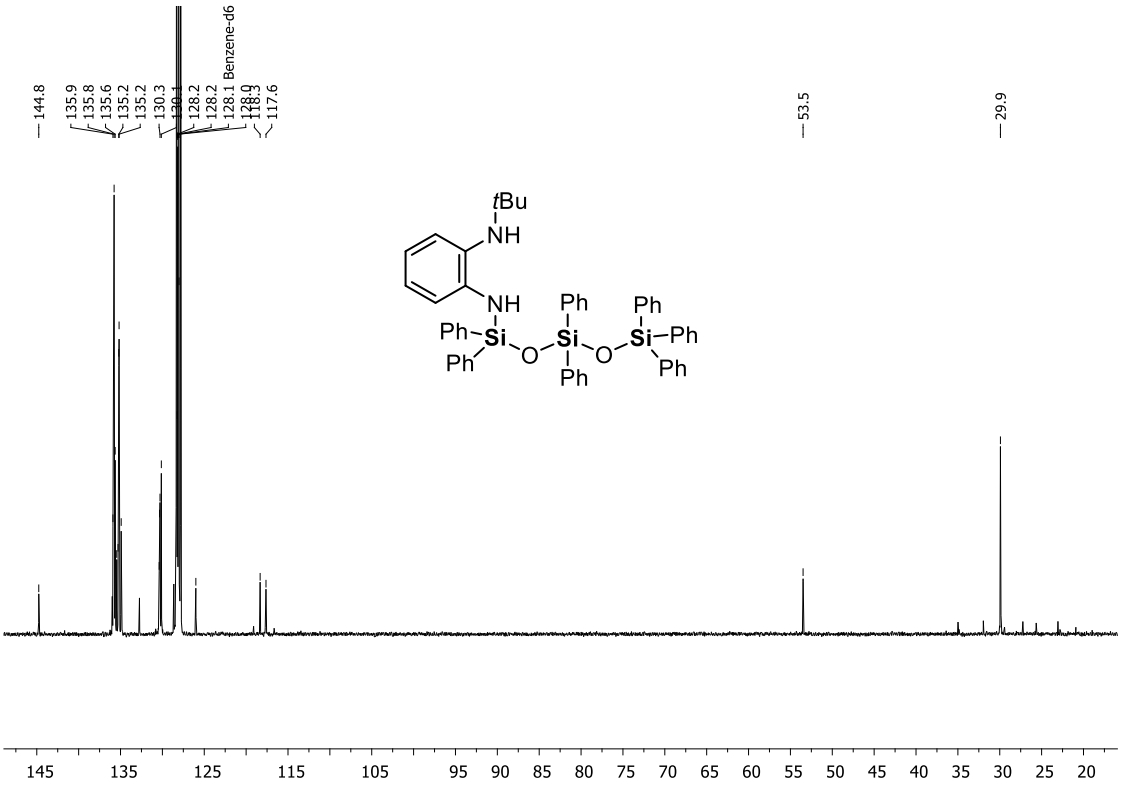

Figure S3.58. ^{13}C {^{1}H} NMR spectrum (C_6D_6, 298 K) of **11**.

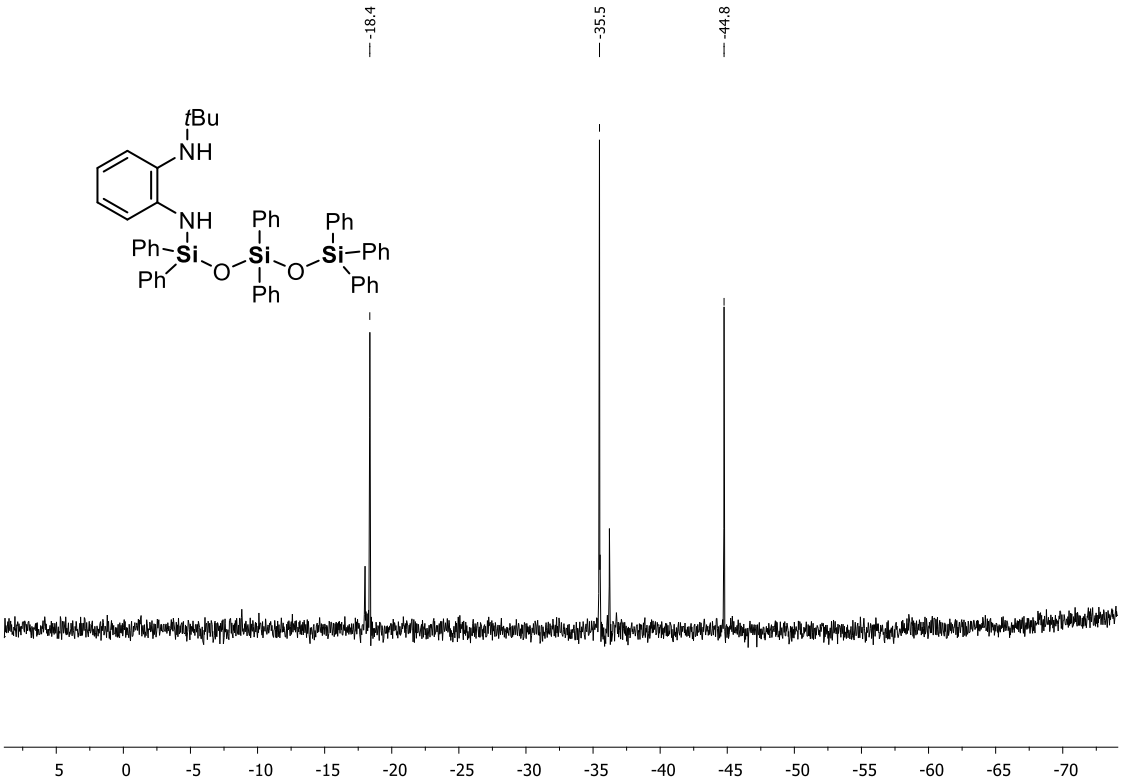

Figure S3.59. $^{19}Si\{^{1}H\}$ NMR spectrum (C_6D_6, 298 K) of **11**.

3.6.4 Si–O–Si bond cleavage reactions

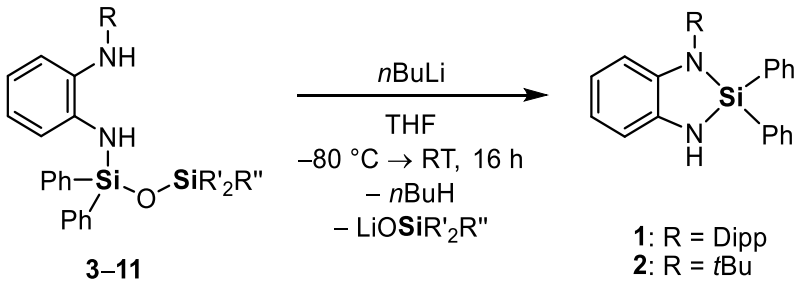

4.1.1.23 General procedure for the cleavage of siloxanes 3–11

Siloxanes **3–11** (1.0 mmol) and hexamethylbenzene (81 mg, 0.5 mmol, 0.5 equiv.) as internal standard were dissolved in 10 mL of THF. The solution was cooled to −80 °C and *n*BuLi (0.44 mL of a 2.5 M solution in hexanes, 1.1 mmol, 1.1 equiv.) was added dropwise. The reaction mixture was slowly warmed to room temperature and stirred for 16 h. Then, an aliquot of 1.0 mL was transferred into an NMR tube. All volatiles were removed *in vacuo* and the residue was dissolved in 0.5 mL of C_6D_6. NMR yields were determined by integration in the ^{1}H NMR spectrum (Figures S3.60–S3.68).

4.1.1.24 Determination of NMR yields

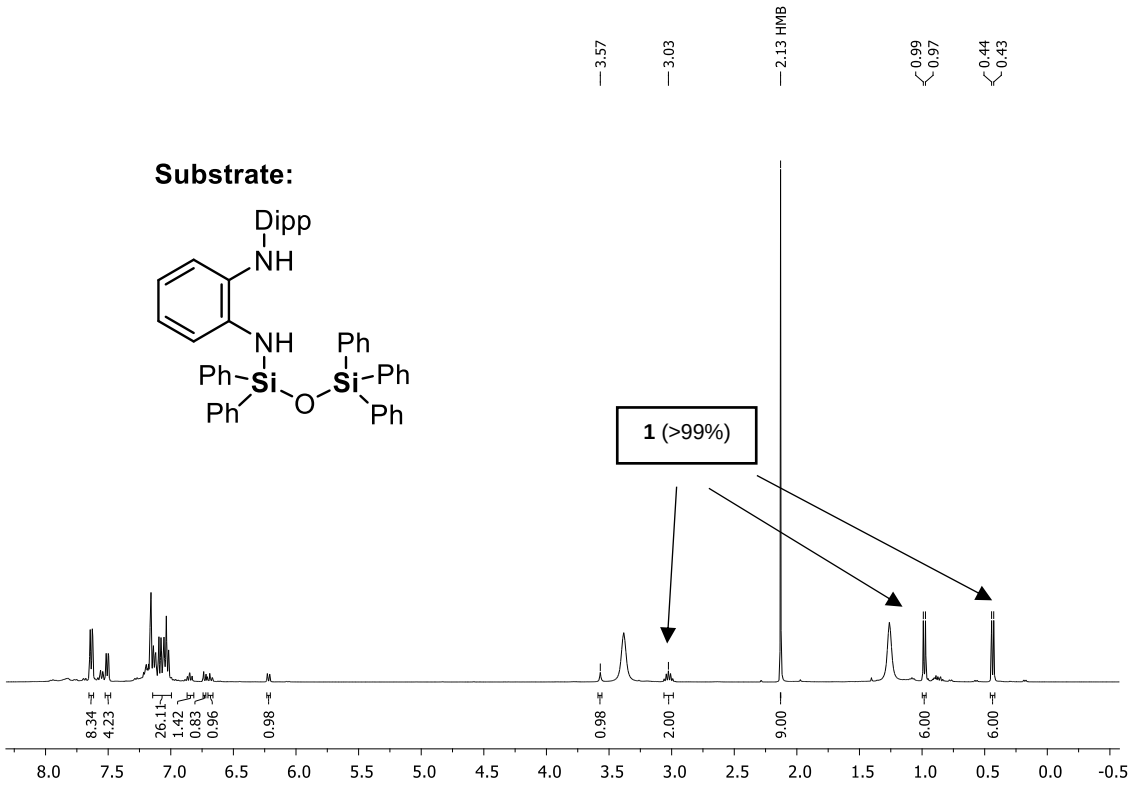

Figure S3.60. Cleavage of **3**: ^{1}H NMR spectrum (C_6D_6, 298 K) with 0.5 equiv. HMB as internal standard for determination of the NMR yield.

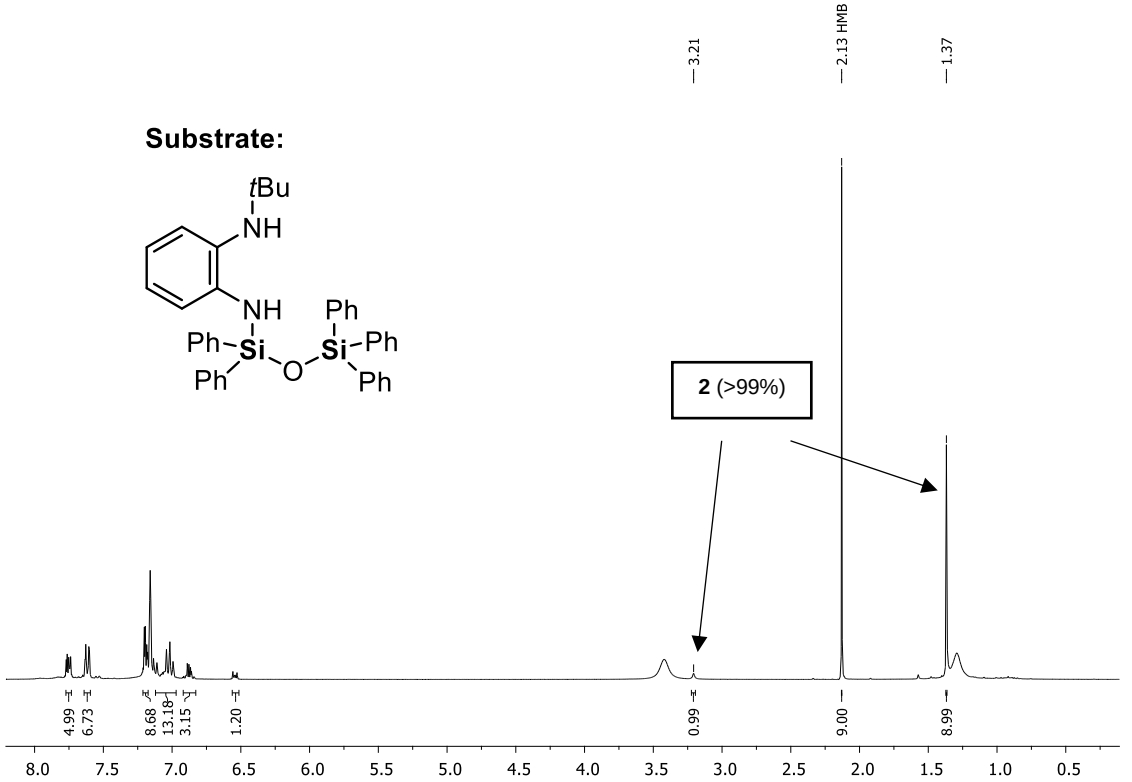

Figure S3.61. Cleavage of **4**: ^{1}H NMR spectrum (C_6D_6, 298 K) with 0.5 equiv. HMB as internal standard for determination of the NMR yield.

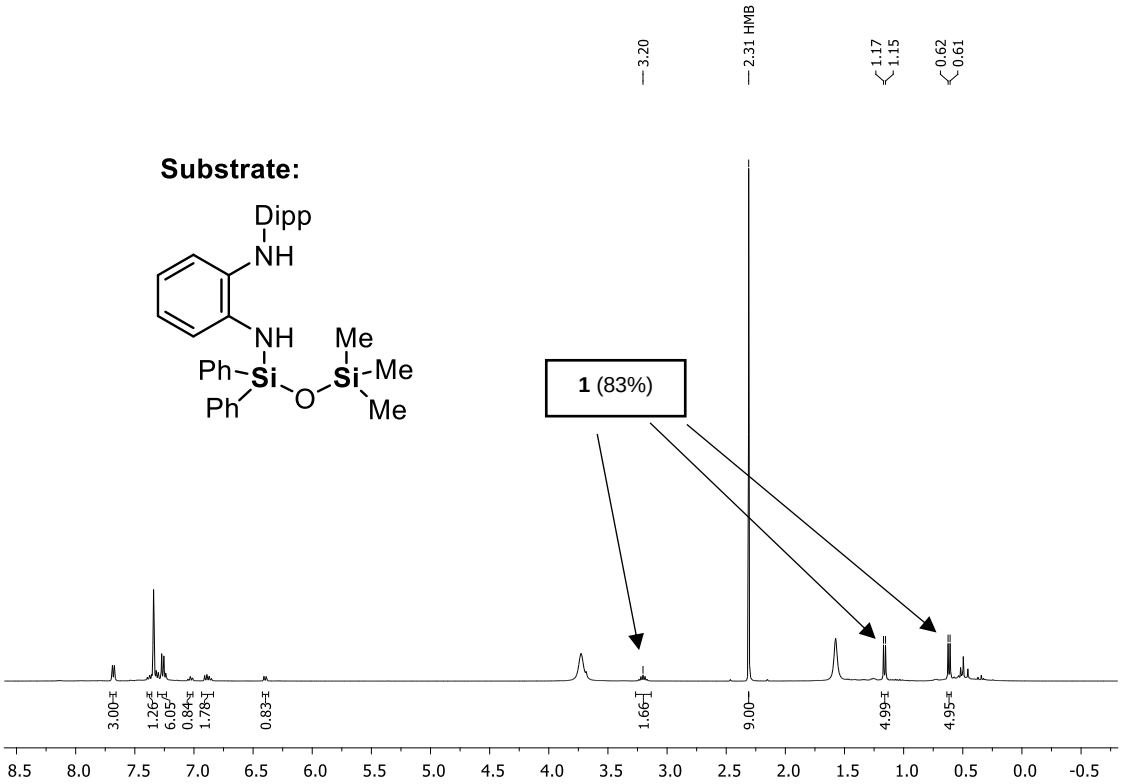

Figure S3.62. Cleavage of **5**: ^{1}H NMR spectrum (C_6D_6, 298 K) with 0.5 equiv. HMB as internal standard for determination of the NMR yield.

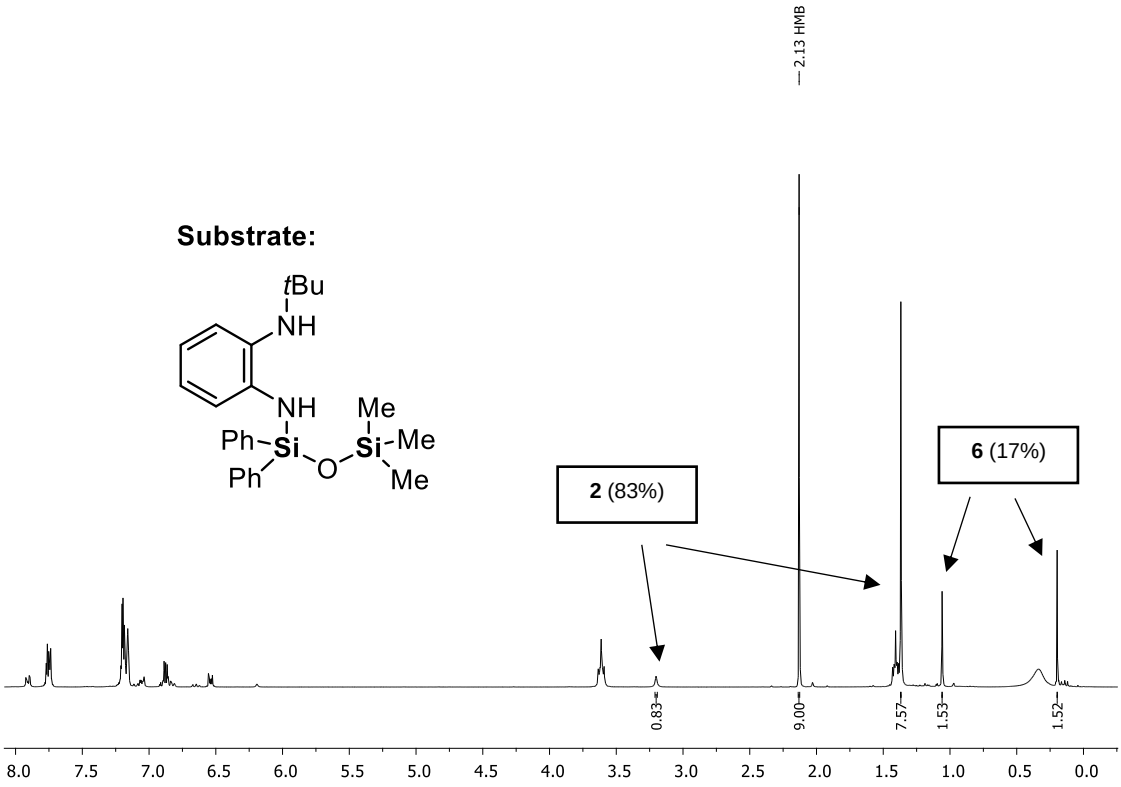

Figure S3.63. Cleavage of **6**: ^{1}H NMR spectrum (C_6D_6, 298 K) with 0.5 equiv. HMB as internal standard for determination of the NMR yield.

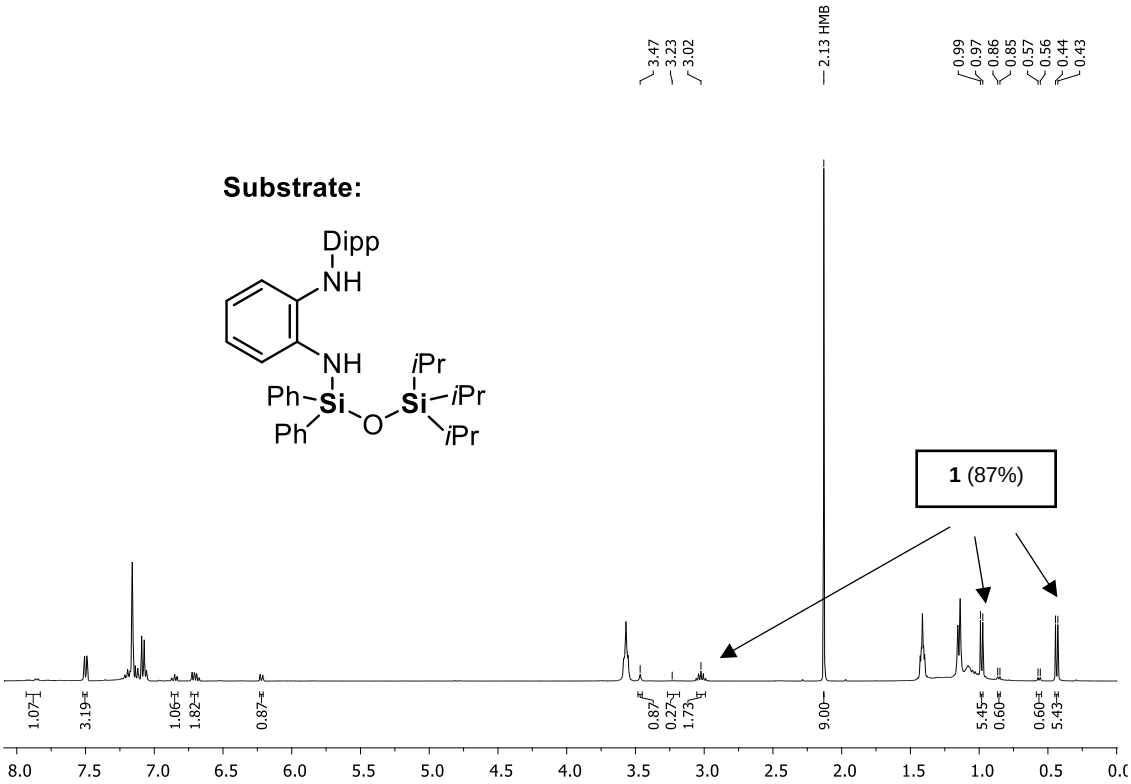

Figure S3.64. Cleavage of **7**: ^{1}H NMR spectrum (C_6D_6, 298 K) with 0.5 equiv. HMB as internal standard for determination of the NMR yield.

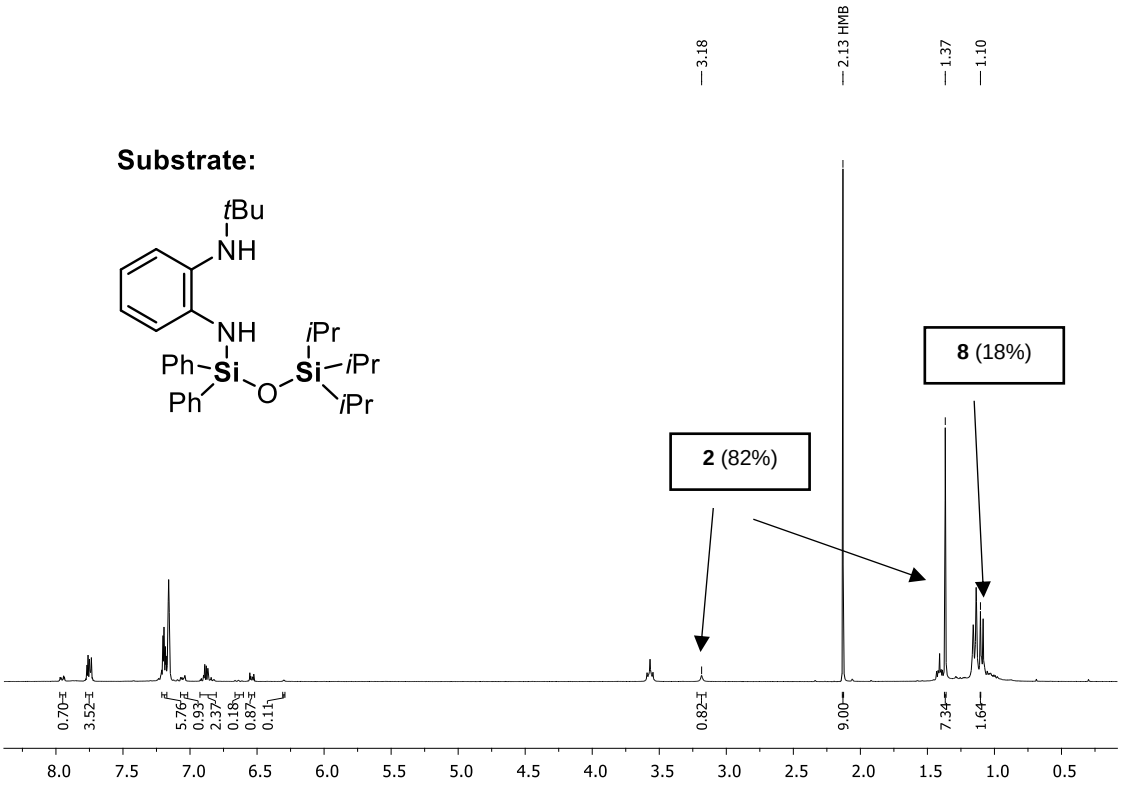

Figure S3.65. Cleavage of **8**: ^{1}H NMR spectrum (C_6D_6, 298 K) with 0.5 equiv. HMB as internal standard for determination of the NMR yield.

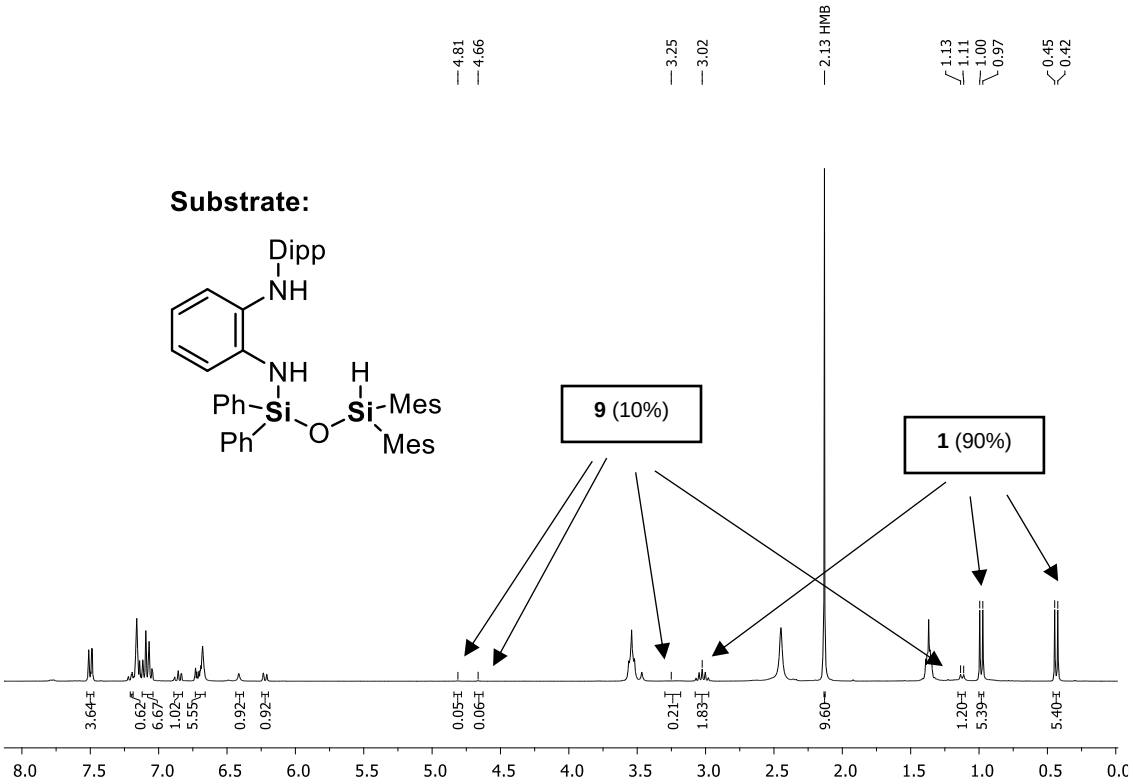

Figure S3.66. Cleavage of **9**: ^{1}H NMR spectrum (C_6D_6, 298 K) with 0.5 equiv. HMB as internal standard for determination of the NMR yield.

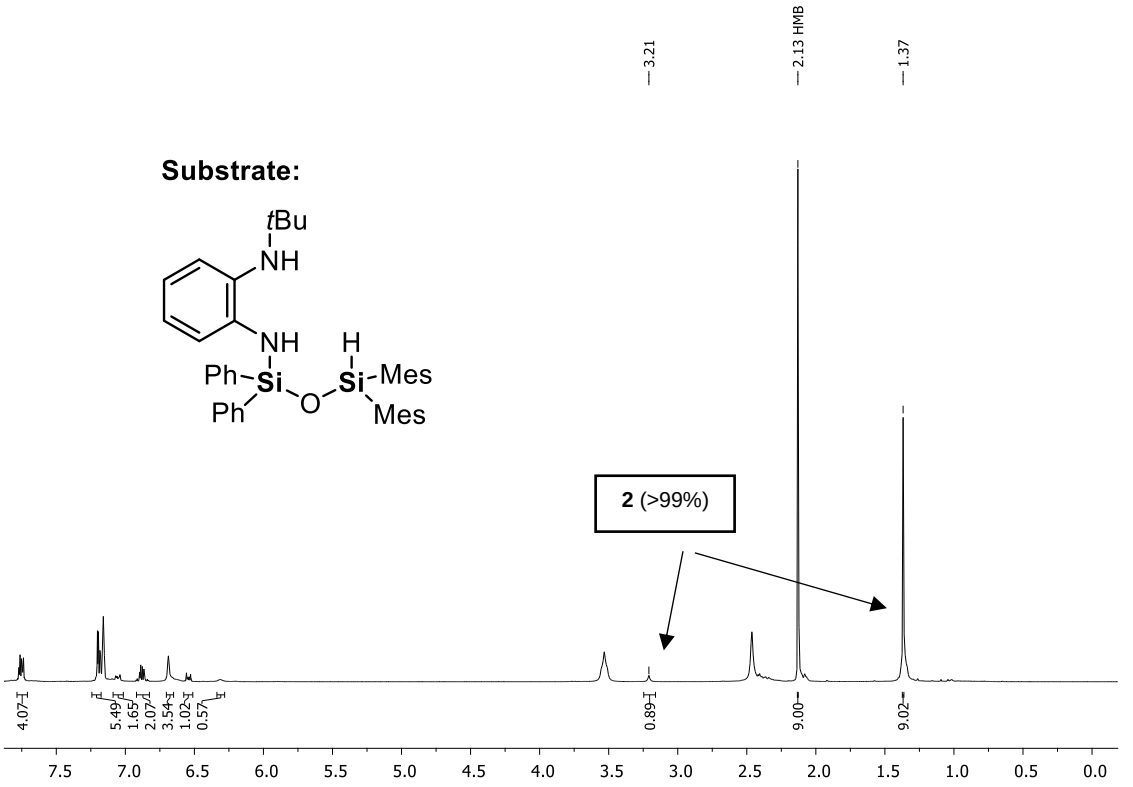

Figure S3.67. Cleavage of **10**: ^{1}H NMR spectrum (C_6D_6, 298 K) with 0.5 equiv. HMB as internal standard for determination of the NMR yield.

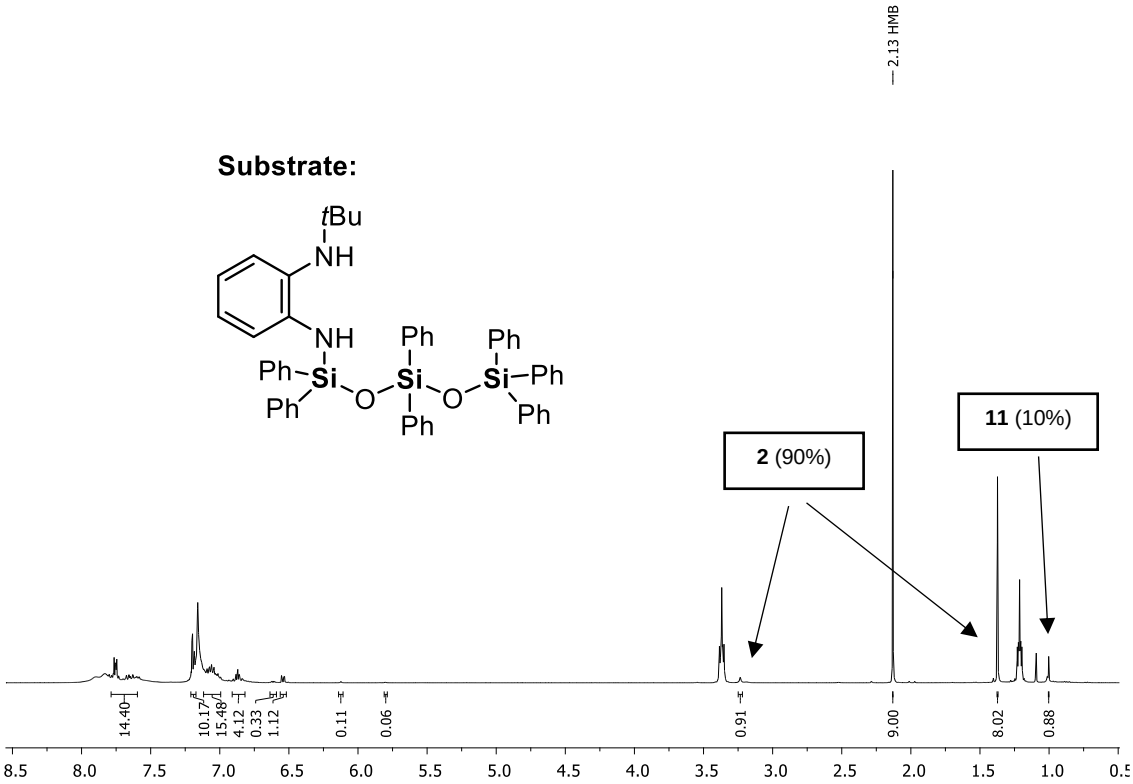

Figure S3.68. Cleavage of **11**: ^{1}H NMR spectrum (C_6D_6, 298 K) with 0.5 equiv. HMB as internal standard for determination of the NMR yield.

3.6.5 Removal of the 1,2-diaminobenzene derivative from the siloxane framework

4.1.1.25 General procedure for the hydrolysis

Diaminosiloxanes **3**, **5**, and **7** (1.0 mmol, 1.0 equiv.), *para*-toluenesulfonic acid (17 mg, 0.01 mmol, 1 mol%), water (0.2 mL), and hexamethylbenzene (81 mg, 0.5 mmol, 0.5 equiv.) as internal standard were dissolved in 15 mL of toluene. The solution was heated at reflux for the time indicated in the respective reaction schemes. Then, an aliquot of 0.6 mL was transferred into an NMR tube. All volatiles were removed *in vacuo* and the residue was dissolved in 0.6 mL of C_6D_6. NMR yields were determined by integration in the ^{1}H NMR spectrum.

4.1.1.26 Hydrolysis of compound 3

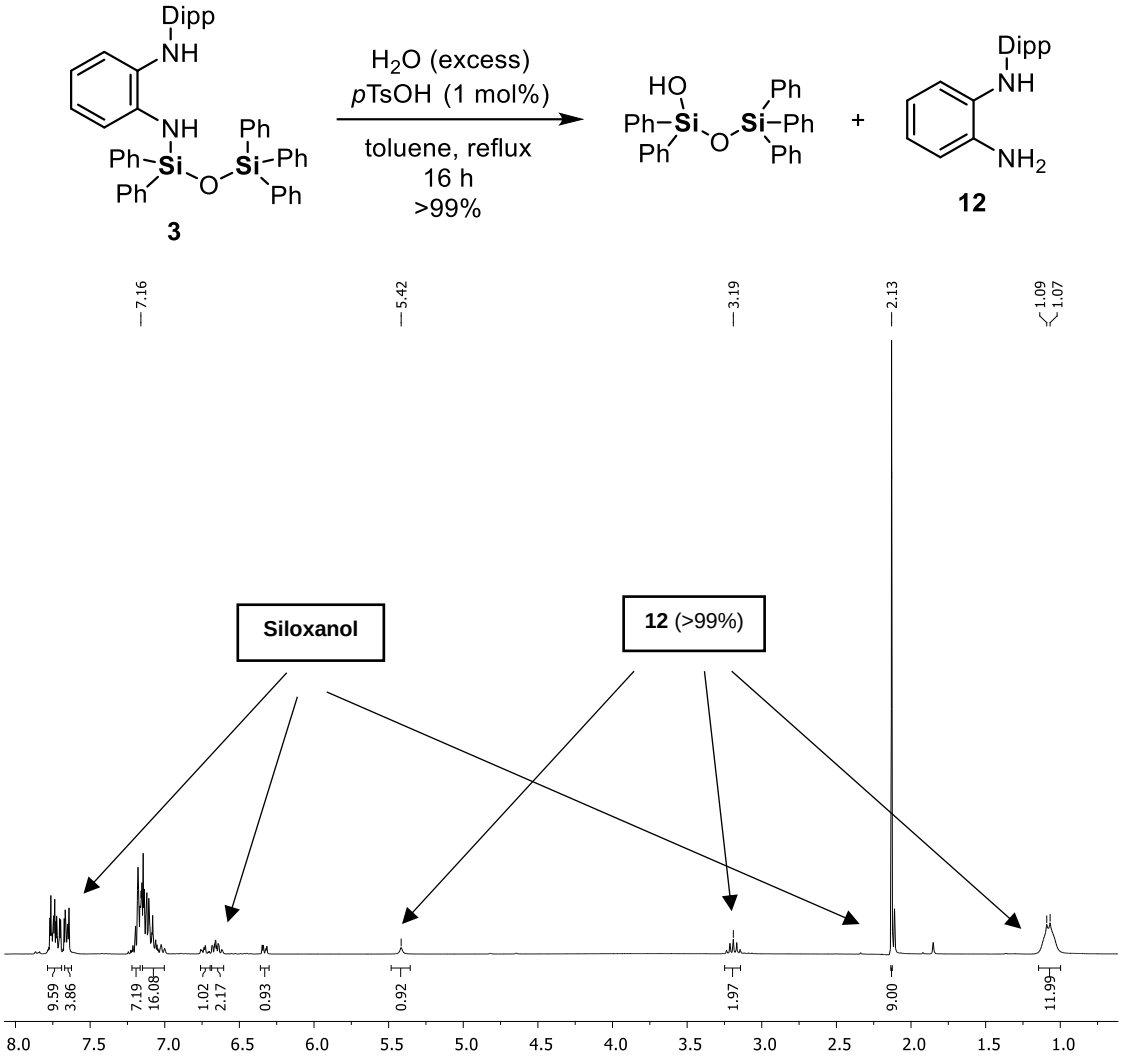

Figure S3.69. Hydrolysis of **3**: ^{1}H NMR spectrum (C_6D_6, 298 K) with 0.5 equiv. HMB as internal standard for determination of the NMR yield.

4.1.1.27 Hydrolysis of compound 5

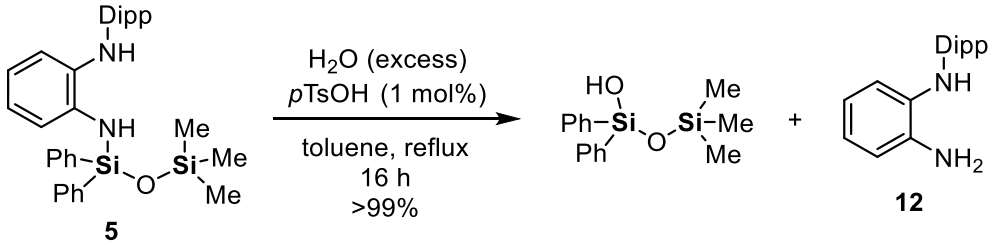

For the isolation of 1-hydroxy-1,1-diphenyl-3,3,3-trimethyldisiloxane, the reaction mixture was dried *in vacuo* and the resulting purple residue purified by flash column chromatography over alumina (hexane/DCM 3:1) to obtain 1-hydroxy-1,1-diphenyl-3,3,3-trimethyldisiloxane as a colorless wax (172 mg, 0.60 mmol, 60%). For an alternative synthesis and full characterization of the disiloxanol, see chapter 3.6.2.

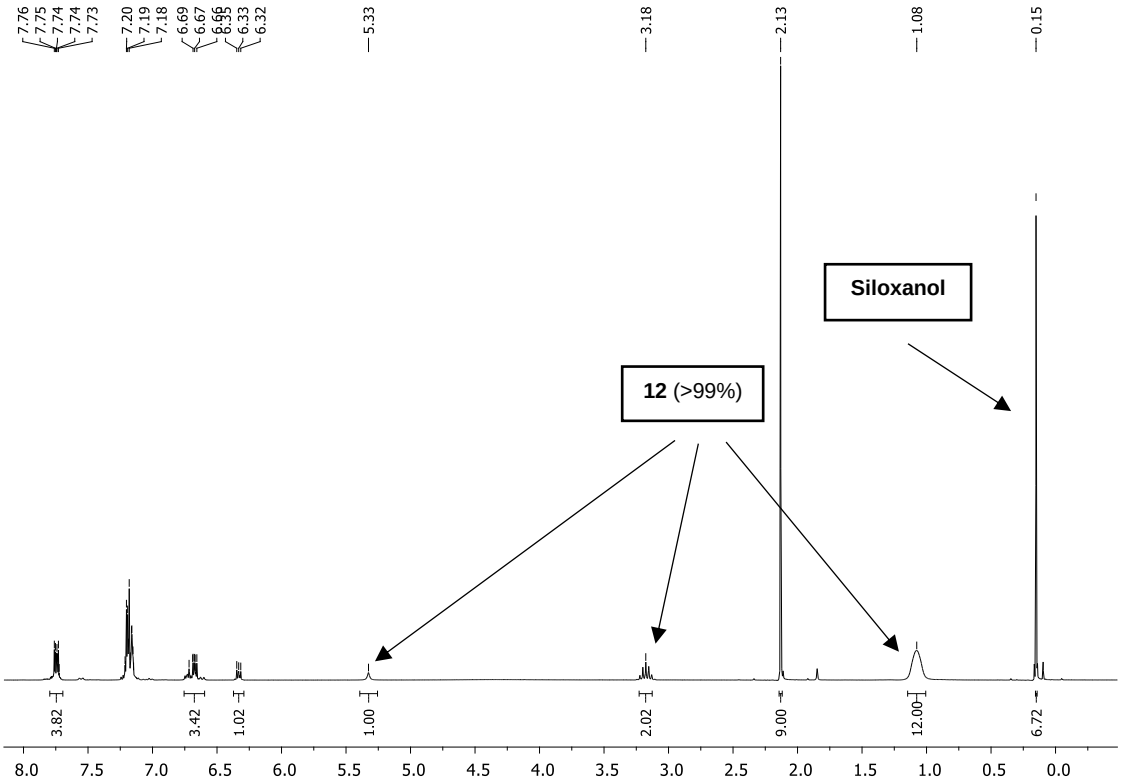

Figure S3.70. Hydrolysis of **5**: ^{1}H NMR spectrum (C_6D_6, 298 K) with 0.5 equiv. HMB as internal standard for determination of the NMR yield.

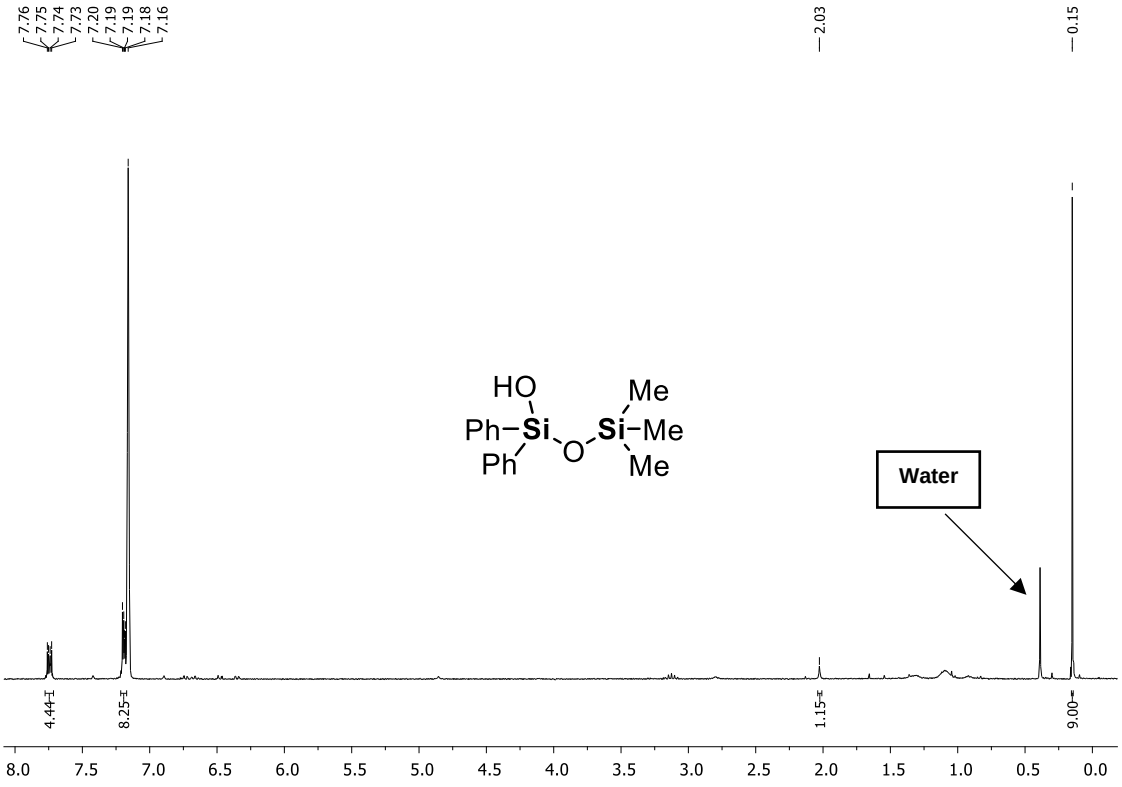

Figure S3.71. ^{1}H NMR spectrum (C_6D_6, 298 K) of 1-hydroxy-1,1-diphenyl-3,3,3-trimethyldisiloxane.

4.1.1.28 Hydrolysis of compound 7

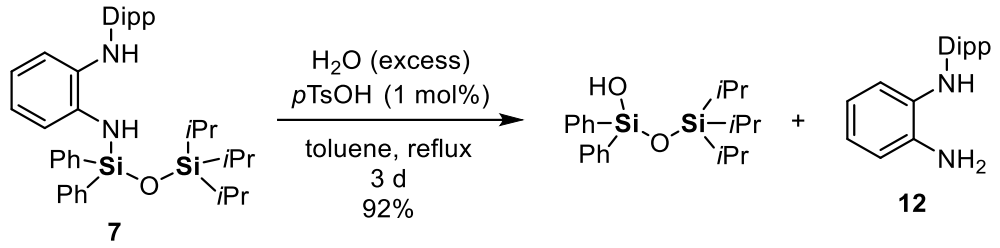

For the isolation of 1-hydroxy-1,1-diphenyl-3,3,3-tri-*iso*-propyldisiloxane, the reaction mixture was dried *in vacuo* and the resulting red residue purified by flash column chromatography over alumina (hexane/DCM 3:1) to obtain 1-hydroxy-1,1-diphenyl-3,3,3-tri-*iso*-propyldisiloxane as a colorless wax (234 mg, 0.63 mmol, 63%).

^{1}H NMR (400 MHz, C_6D_6, 298 K): δ[ppm] = 1.06–1.09 [m, 21H, C*H*(C*H*$_3$)$_2$], 2.12 [s, 1H, O*H*], 7.18–7.22 [m, 6H, *H*$_{Ph}$], 7.76–7.81 [m, 4H, *H*$_{Ph}$]. **^{13}C{^{1}H} NMR** (101 MHz, C_6D_6, 298 K): δ[ppm] = 13.2 [s, *C*H(CH$_3$)$_2$], 18.1 [s, CH(*C*H$_3$)$_2$], 128.1 [s, *C*$_{Ph}$], 130.3 [s, *C*$_{Ph}$], 134.8 [s, *C*$_{Ph}$], 136.4 [s, *C*$_{Ph}$]. **^{29}Si{^{1}H} NMR** (77 MHz, C_6D_6, 298 K): δ[ppm] = −39.0 [s, *Si*(CH(CH$_3$)$_2$], 10.3 [s, *Si*OH]. **HR-MS(ESI−)**, calculated m/z for $C_{21}H_{31}O_2Si_2$ [M−H$^+$]: 371.1868; found: 371.187.

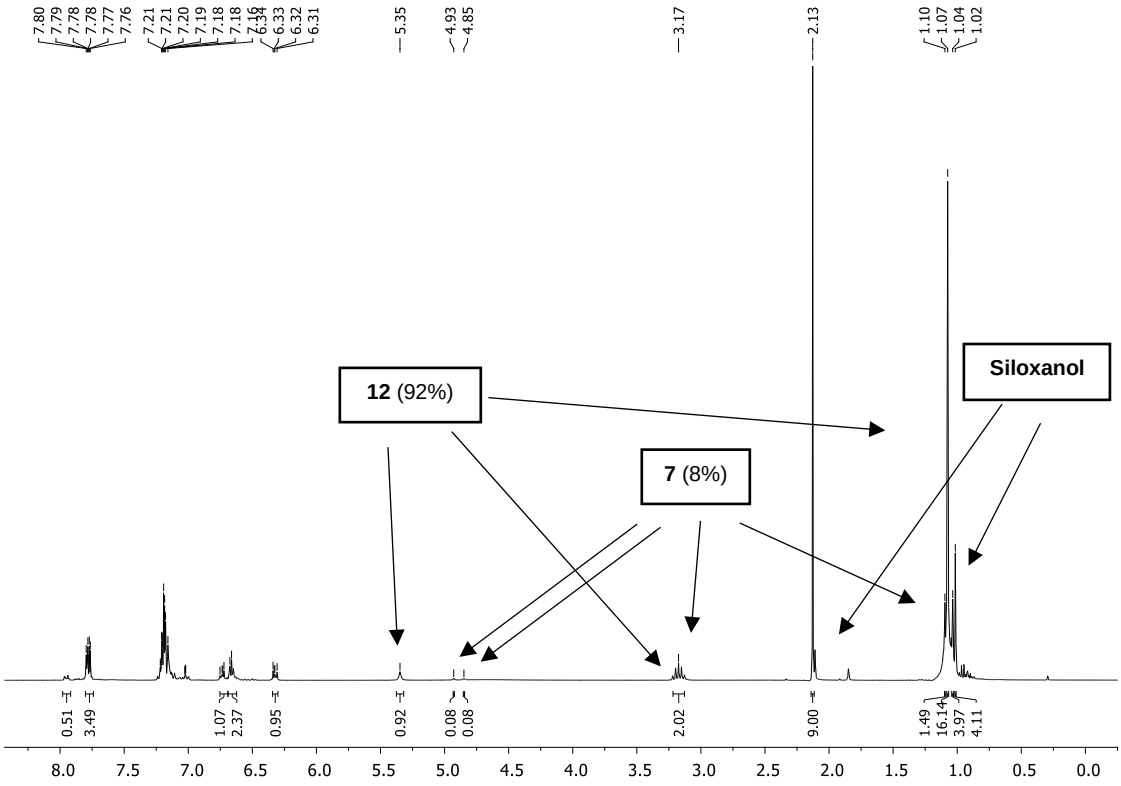

Figure S3.72. Hydrolysis of **7**: ^{1}H NMR spectrum (C_6D_6, 298 K) with 0.5 equiv. HMB as internal standard for determination of the NMR yield.

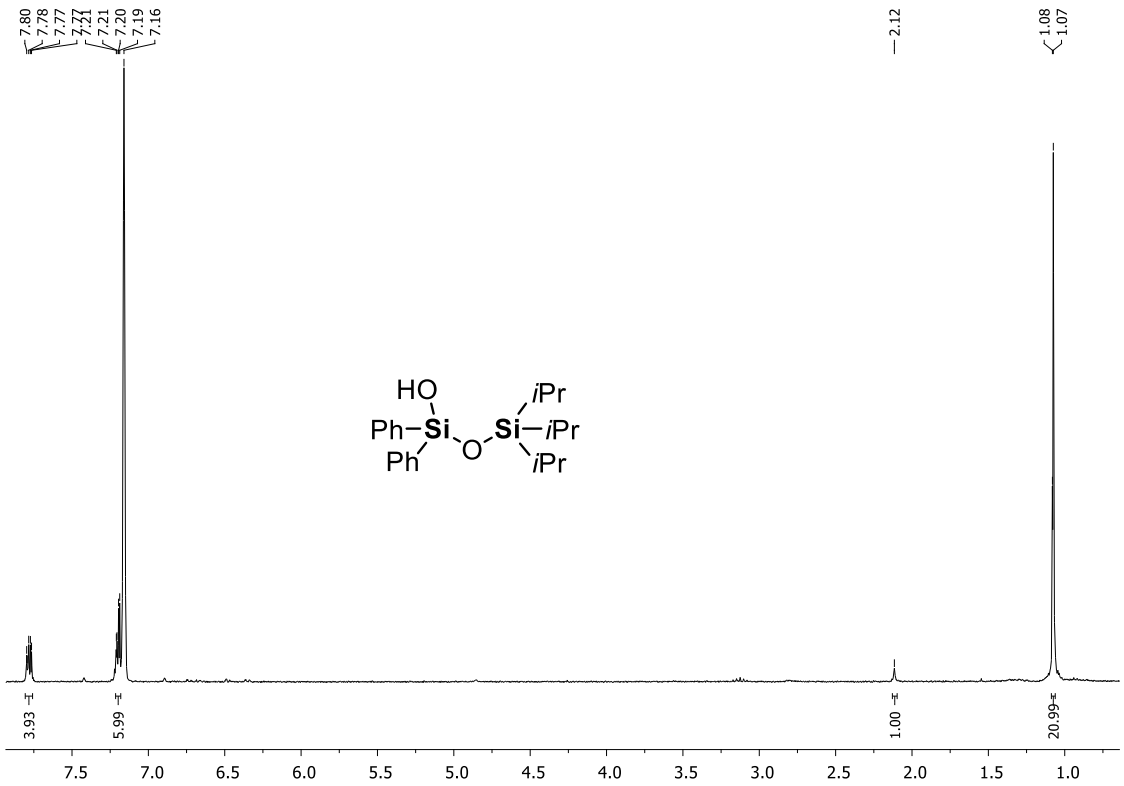

Figure S3.73. ^{1}H NMR spectrum (C_6D_6, 298 K) of 1-hydroxy-1,1-diphenyl-3,3,3-tri-*iso*-propyldisiloxane.

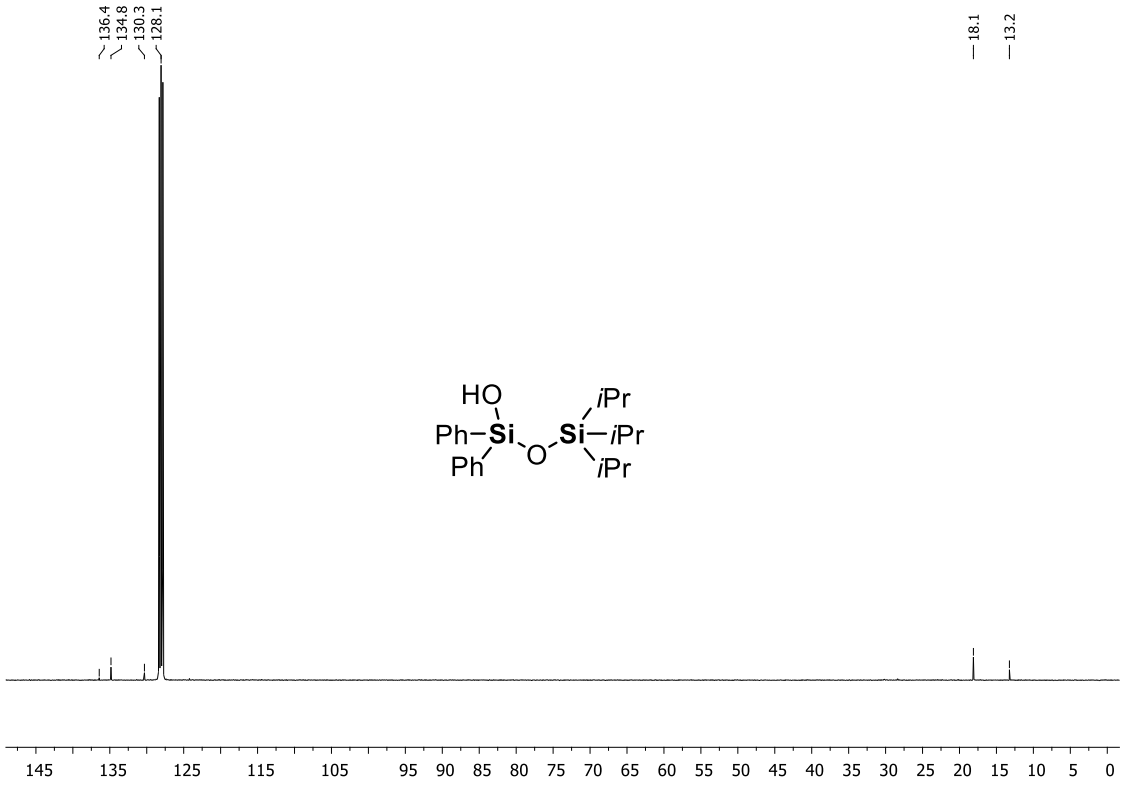

Figure S3.74. ^{13}C{^{1}H} NMR spectrum (C_6D_6, 298 K) of 1-hydroxy-1,1-diphenyl-3,3,3-tri-*iso*-propyldisiloxane.

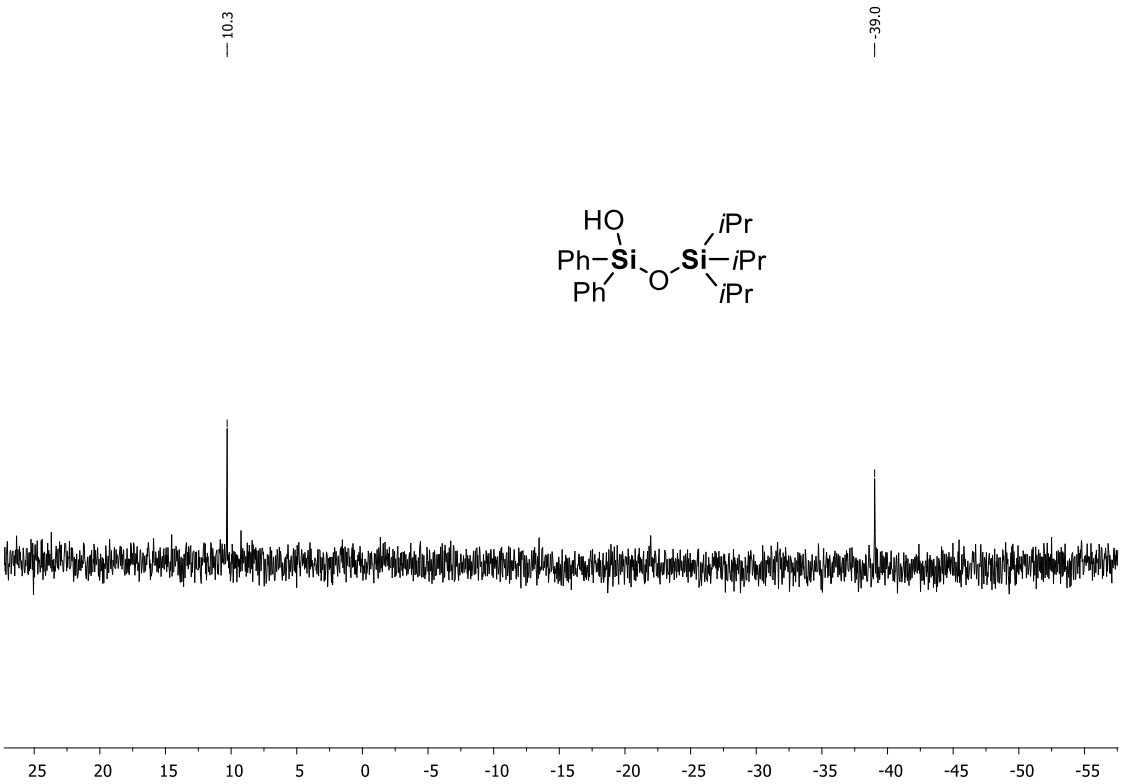

Figure S3.75. $^{29}Si\{^{1}H\}$ NMR spectrum (C_6D_6, 298 K) of 1-hydroxy-1,1-diphenyl-3,3,3-tri-*iso*-propyldisiloxane.

3.6.6 Si–O–Si bond cleavage in chlorosiloxanes

4.1.1.29 Cleavage of 1-chloro-1,1,3,3,3-pentaphenyldisiloxane (14) using diamine 12

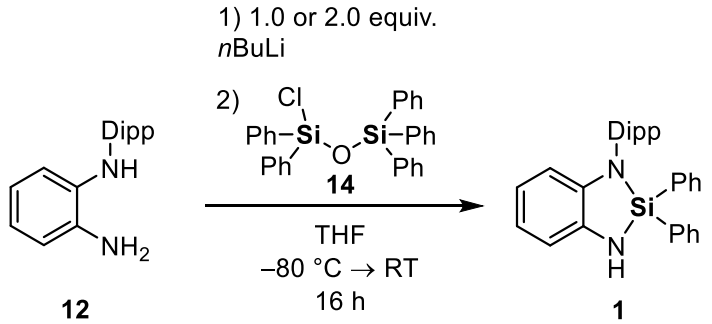

Compound **12** (268 mg, 1.0 mmol, 1.0 equiv.) and hexamethylbenzene (81 mg, 0.5 mmol, 0.5 equiv.) as internal standard were dissolved in 10 mL of THF. The solution was cooled down to −80 °C and *n*-butyllithium (either 1.0 equiv. or 2.0 equiv.) was added dropwise via syringe. The mixture was stirred for 1 h while slowly warming up to room temperature. Then, the reaction mixture was again cooled down to −80 °C and a solution of compound **14** in 5 mL of THF was added in one portion. The mixture was stirred for 16 h while slowly warming up to room temperature. An aliquot of ca. 0.6 mL was transferred into an NMR tube, dried *in vacuo*, dissolved in 0.6 mL of C_6D_6, and analyzed by ^{1}H NMR spectroscopy.

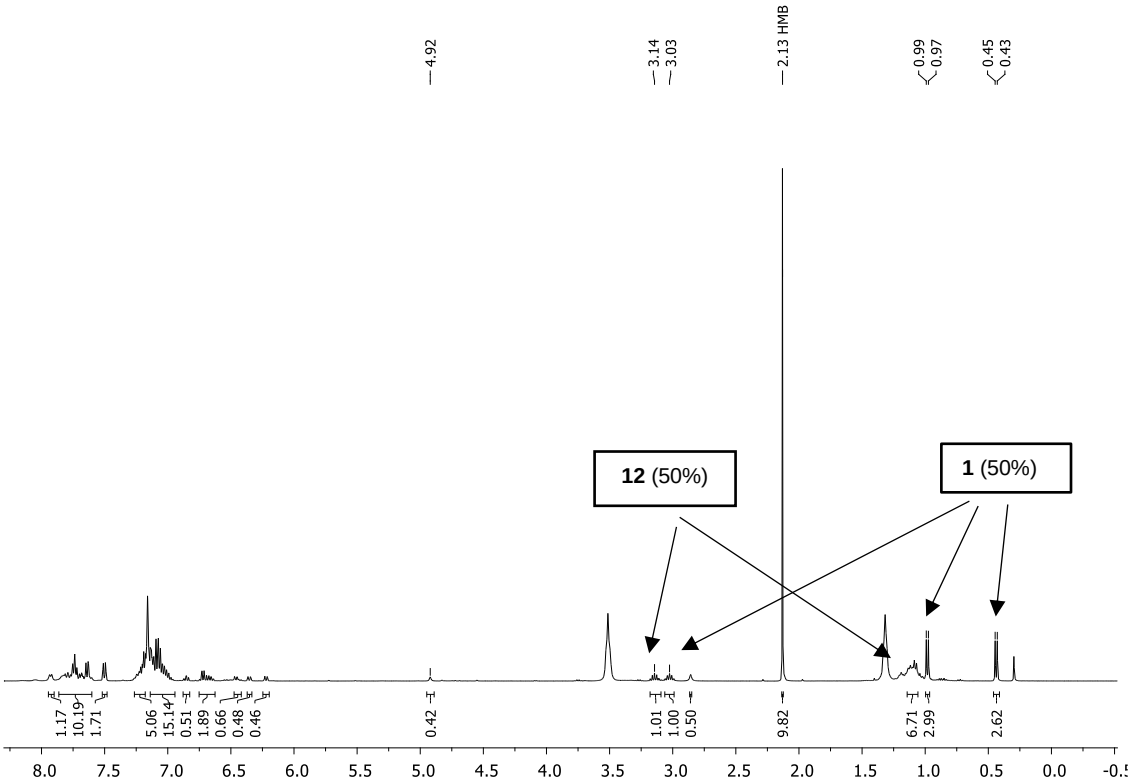

Figure S3.77. ^{1}H NMR spectrum (C_6D_6, 298 K) of the reaction of chloropentaphenyldisiloxane (**14**) with diamine **12** when using 1.0 equiv. of *n*BuLi. HMB (0.5 equiv.) as internal standard for determination of the NMR yield.

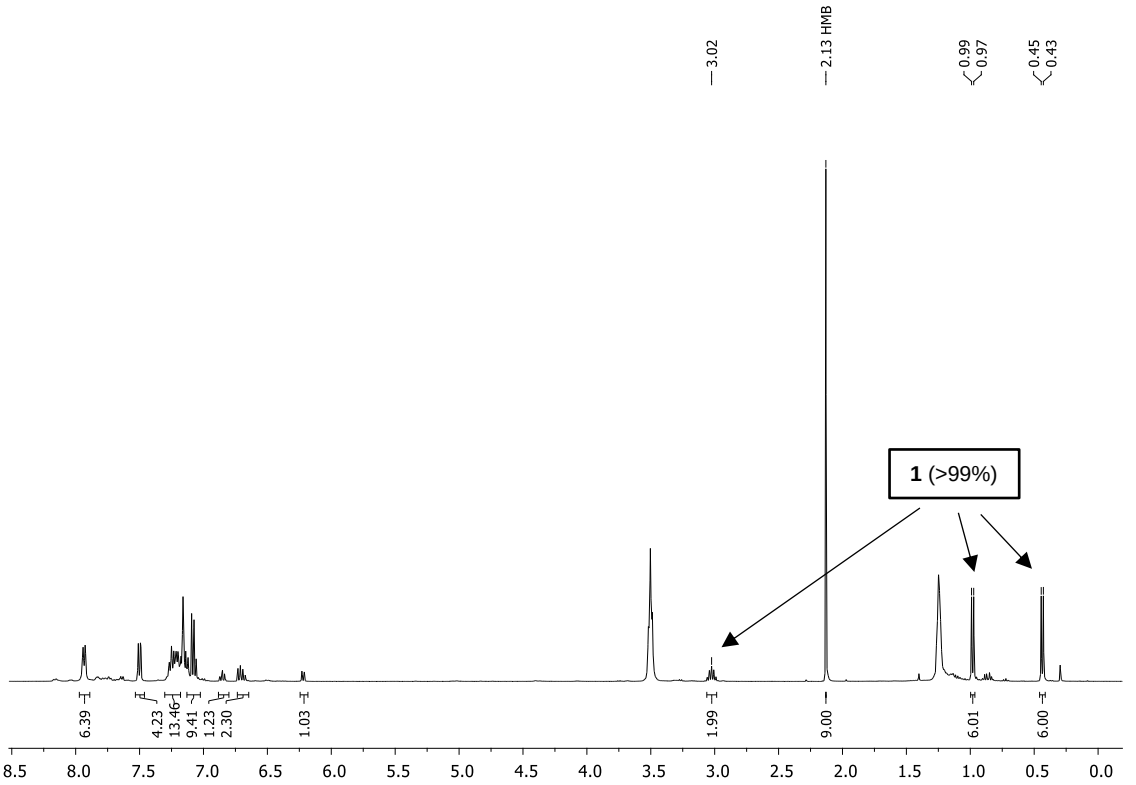

Figure S3.78. ^{1}H NMR spectrum (C_6D_6, 298 K) of the reaction of chloropentaphenyldisiloxane (**14**) with diamine **12** when using 2.0 equiv. of *n*BuLi. HMB (0.5 equiv.) as internal standard for determination of the NMR yield.

4.1.1.30 Cleavage of 1-chloro-1,1,3,3,3-pentaphenyldisiloxane (14) using diamine 13

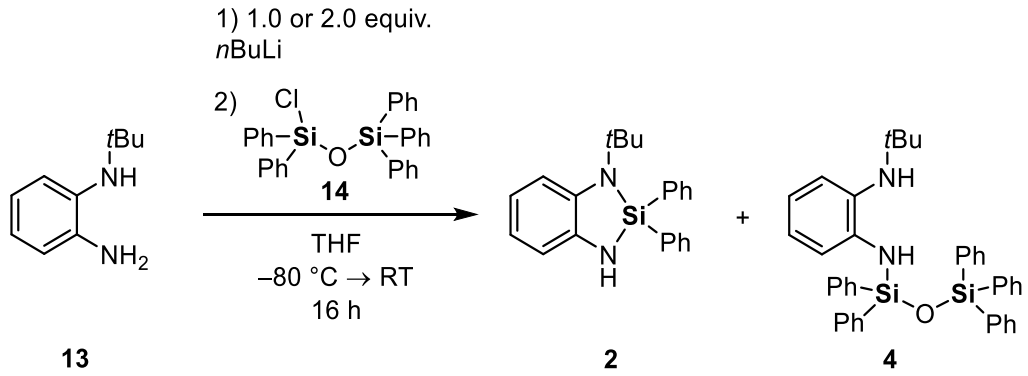

Compound **13** (164 mg, 1.0 mmol, 1.0 equiv.) and hexamethylbenzene (81 mg, 0.5 mmol, 0.5 equiv.) as internal standard were dissolved in 10 mL of THF. The solution was cooled down to −80 °C and *n*-butyllithium (either 1.0 equiv. or 2.0 equiv.) was added dropwise via syringe. The mixture was stirred for 1 h while slowly warming up to room temperature. Then, the reaction mixture was again cooled down to −80 °C and a solution of compound **14** in 5 mL of THF was added in one portion. The mixture was stirred for 16 h while slowly warming up to room temperature. An aliquot of ca. 0.6 mL was transferred into an NMR tube, dried *in vacuo*, dissolved in 0.6 mL of C_6D_6, and analyzed by ^{1}H NMR spectroscopy.

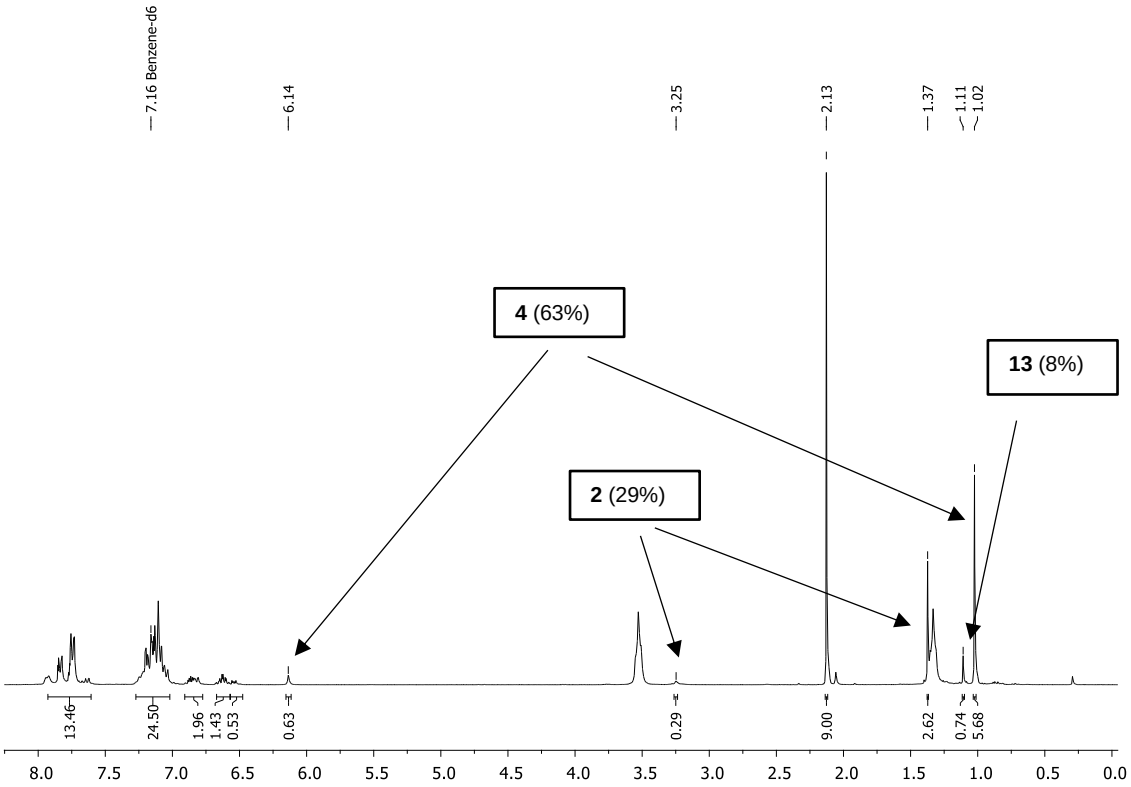

Figure S3.79. ^{1}H NMR spectrum (C_6D_6, 298 K) of the reaction of chloropentaphenyldisiloxane (**14**) with diamine **13** when using 1.0 equiv. of *n*BuLi. HMB (0.5 equiv.) as internal standard for determination of the NMR yield.

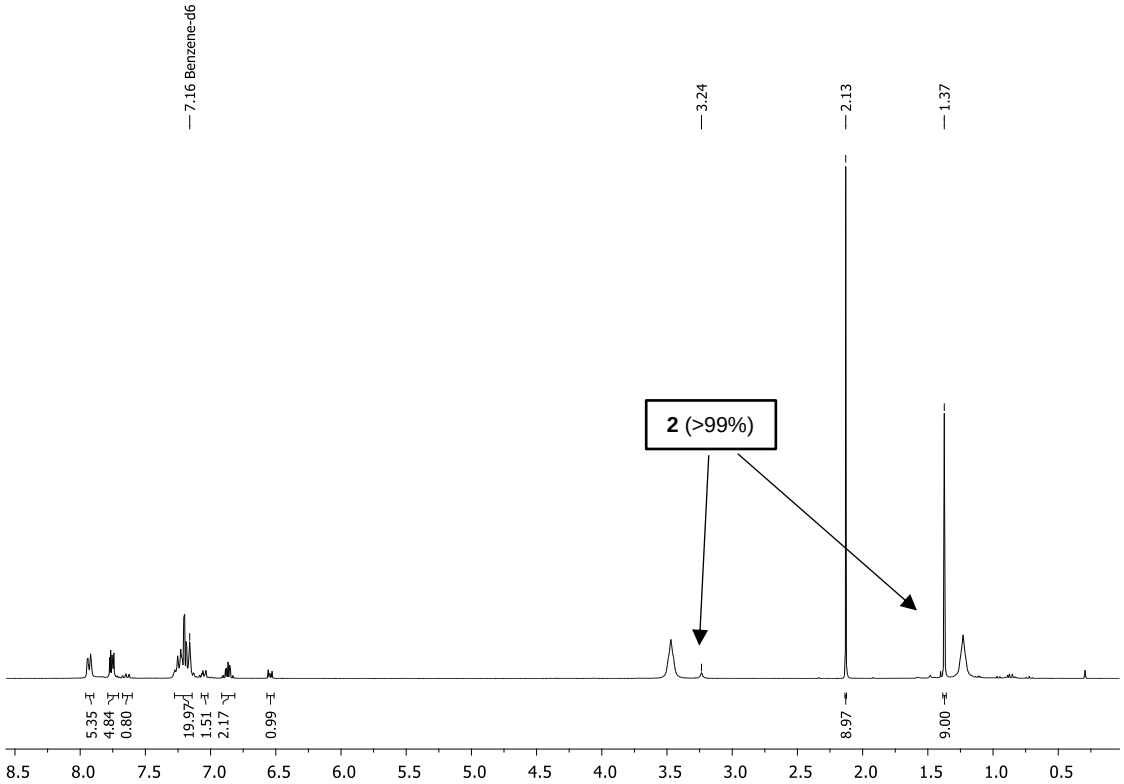

Figure S3.80. ^{1}H NMR spectrum (C_6D_6, 298 K) of the reaction of chloropentaphenyldisiloxane (**14**) with diamine **13** when using 2.0 equiv. of *n*BuLi. HMB (0.5 equiv.) as internal standard for determination of the NMR yield.

4.1.1.31 Cleavage of 1-chloro-3,3,3-trimethyl-1,1-diphenyldisiloxane (15) using diamine 12

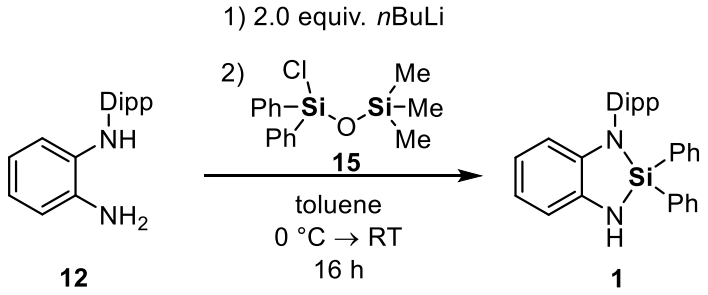

Compound **12** (268 mg, 1.0 mmol, 1.0 equiv.) and hexamethylbenzene (81 mg, 0.5 mmol, 0.5 equiv.) as internal standard were dissolved in 5 mL of toluene. The solution was cooled down to 0 °C and *n*-butyllithium (0.88 mL of a 2.5 M solution in hexane, 2.1 mmol, 2.0 equiv.) was added dropwise via syringe. The mixture was stirred for 30 min while slowly warming up to room temperature. Then, the reaction mixture was again cooled down to 0 °C and a solution of compound **15** in 5 mL of toluene was added in one portion. The mixture was stirred for 16 h while slowly warming up to room temperature. An aliquot of ca. 0.6 mL was transferred into an NMR tube, dried *in vacuo*, dissolved in 0.6 mL of C_6D_6, and analyzed by ^{1}H NMR spectroscopy.

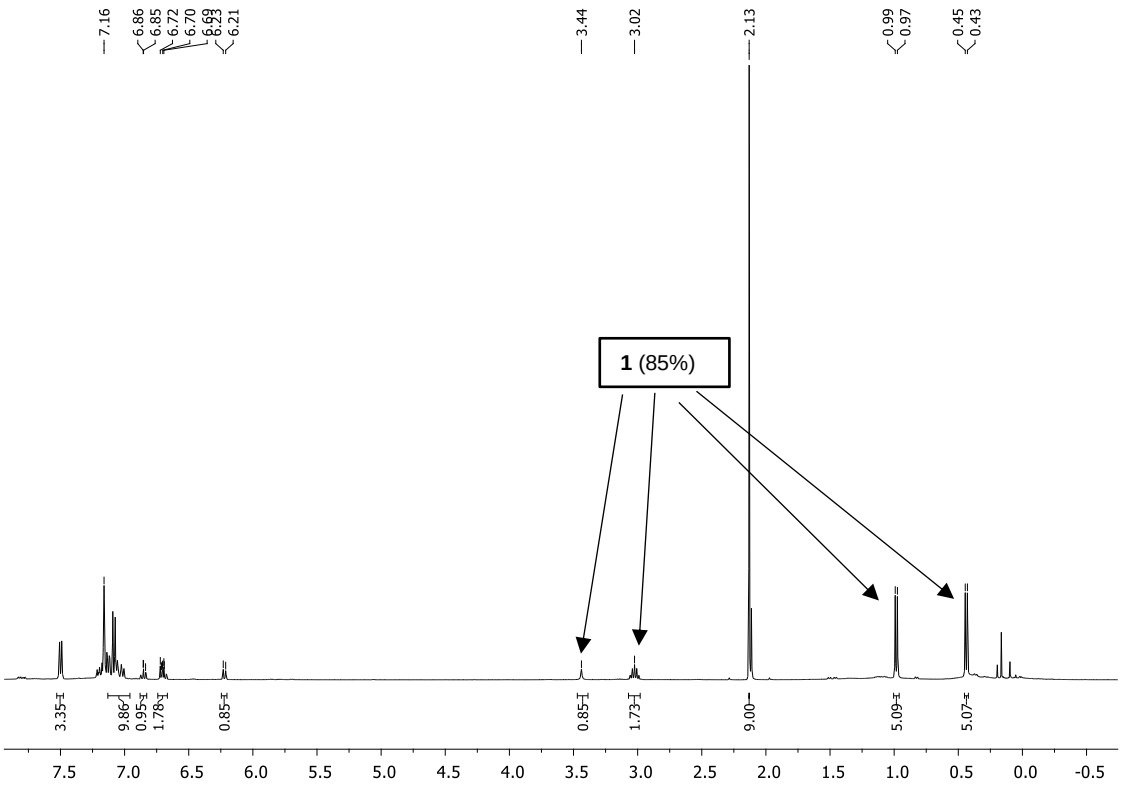

Figure S3.81. ^{1}H NMR spectrum (C_6D_6, 298 K) of the reaction of 1-chloro-3,3,3-trimethyl-1,1-diphenyldisiloxane (**15**) with diamine **12** when using 2.0 equiv. of *n*BuLi. HMB (0.5 equiv.) as internal standard for determination of the NMR yield.

4.1.1.32 Cleavage of 1-chloro-1-mesityl-1,3,3,3-tetraphenyldisiloxane (16) using diamine 12

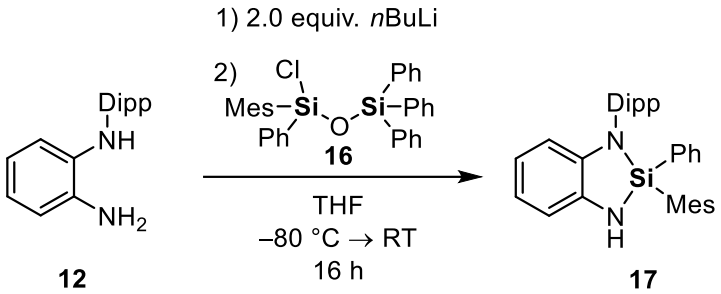

Compound **12** (268 mg, 1.0 mmol, 1.0 equiv.) was dissolved in 10 mL of THF and cooled down to −80 °C. *n*-Butyllithium (0.88 mL of a 2.5 M solution in hexane, 2.1 mmol, 2.0 equiv.) was added dropwise and the solution was stirred while slowly warming up to room temperature. Then, the reaction mixture was again cooled down to −80 °C and a solution of compound **16** (535 mg, 1.0 mmol, 1.0 equiv.) in 10 mL THF was added. The mixture was further stirred for 16 h while slowly warming up to room temperature. All volatiles of the dark green solution were removed *in vacuo* and the crude product was treated with 10 mL of pentane. After the solids were filtered off by cannula filtration, the filtrate was stored at −20 °C. The white precipitate formed was isolated by means of cannula filtration and washed three times with 5 mL of pentane to obtain compound

17 as a white solid (270 mg, 0.55 mmol, 55%). Crystals suitable for single-crystal X-ray diffraction analysis were obtained by recrystallization from hot pentane (for details, see chapter 3.7).

For the determination of the NMR yield, an individual experiment was performed. For this purpose, compound **12** (264 mg, 1.0 mmol, 1.0 equiv.) and hexamethylbenzene (81 mg, 0.5 mmol, 0.5 equiv.) as internal standard were dissolved in 10 mL of THF. The reaction mixture was cooled down to −80 °C and *n*-butyllithium (0.88 mL of a 2.5 M solution in hexane, 2.1 mmol, 2.1 equiv.) was added dropwise via syringe. The mixture was stirred for 1 h while slowly warming up to room temperature. Then, the reaction mixture was again cooled down to −80 °C and a solution of compound **16** (535 mg, 1.0 mmol, 1.0 equiv.) in 10 mL of THF was added in one portion. The mixture was stirred for 16 h while slowly warming up to room temperature. An aliquot of ca. 0.6 mL was transferred into an NMR tube, dried *in vacuo*, dissolved in 0.6 mL of C_6D_6, and analyzed by ^{1}H NMR spectroscopy (Figure S3.85).

^{1}H NMR (400 MHz, C_6D_6, 298 K): δ[ppm] = 0.36 [d, $^3J_{H\text{-}H}$ = 6.77 Hz, 3H, CH(C*H*)$_3$], 0.78 [d, $^3J_{H\text{-}H}$ = 6.83 Hz, 3H, CH(C*H*)$_3$], 0.86 [d, $^3J_{H\text{-}H}$ = 6.77 Hz, 3H, CH(C*H*)$_3$], 1.28 [d, $^3J_{H\text{-}H}$ = 6.88 Hz, 3H, CH(C*H*)$_3$], 1.64 [br, 3H, *ortho*-C*H*$_3$], 2.07 [s, 3H, *para*-C*H*$_3$], 2.52 [br, 3H, *ortho*-C*H*$_3$], 2.85 [sept, $^3J_{H\text{-}H}$ = 6.78 Hz, 3H, C*H*(CH)$_3$], 3.41 [s, 1H, N*H*], 3.73 [sept, $^3J_{H\text{-}H}$ = 6.85 Hz, 3H, CH(C*H*)$_3$], 6.28 [d, $^3J_{H\text{-}H}$ = 7.45 Hz, 1H *H*$_{Ph}$], 6.53 [br, 1H, *H*$_{Ph}$], 6.63–6.72 [m, 2H, *H*$_{Ph}$], 6.80 [br, 1H, *H*$_{Ph}$], 6.85 [td, $^3J_{H\text{-}H}$ = 7.48 Hz, $^4J_{H\text{-}H}$ = 1.22 Hz, 1H, *H*$_{Ph}$], 7.00 [dd, $^3J_{H\text{-}H}$ = 7.51 Hz, $^4J_{H\text{-}H}$ = 1.70 Hz, 1H, *H*$_{Ph}$], 7.04–7.09 [m, 2H, *H*$_{Ph}$], 7.11–7.14 [m, 2H, *H*$_{Ph}$], 7.17–7.21 [m, 1H, *H*$_{Ph}$], 7.56–7.60 [m, 2H, *H*$_{Ph}$]. **^{13}C{^{1}H} NMR** (101 MHz, C_6D_6, 298 K): δ[ppm] = 21.1 [s, CH(*C*H$_3$)], 22.3 [s, CH(*C*H$_3$)], 23.7 [s, CH(*C*H$_3$)], 24.8 [s, [s, *C*H(CH$_3$)], 26.0 [s, *ortho*-*C*H$_3$], 26.2 [s, CH(*C*H$_3$)], 28.4 [s, *para*-*C*H$_3$], 28.9 [s, *ortho*-*C*H$_3$], 30.1 [s, *C*H(CH$_3$)], 110.6 [s, *C*$_{Ph}$], 111.8 [s, *C*$_{Ph}$], 118.0 [s, *C*$_{Ph}$], 118.9 [s, *C*$_{Ph}$], 124.3 [s, *C*$_{Ph}$], 124.9 [s, *C*$_{Ph}$], 126.4 [s, *C*$_{Ph}$], 127.8 [s, *C*$_{Ph}$], 128.0 [s, *C*$_{Ph}$], 130.5 [s, *C*$_{Ph}$], 135.3 [s, *C*$_{Ph}$], 137.6 [s, *C*$_{Ph}$],138.2 [s, *C*$_{Ph}$], 139.2 [s, *C*$_{Ph}$],140.2 [s, *C*$_{Ph}$], 141.8 [s, *C*$_{Ph}$], 148.9[s, *C*$_{Ph}$], 149.3 [s, *C*$_{Ph}$]. **^{29}Si{^{1}H}** NMR (79 MHz, C_6D_6, 298 K): δ[ppm] = −11.8 [s]. **CHN Analysis** $C_{33}H_{38}N_2Si$ calculated: C 80.76, H 7.80, N 5.71, Si 5.72; found: C 80.73, H 8.01, N 5.63. **HR-MS (FD+)**, calculated m/z for $C_{33}H_{38}N_2Si$ [M+H$^+$]: 490.27988; found: 490.28098.

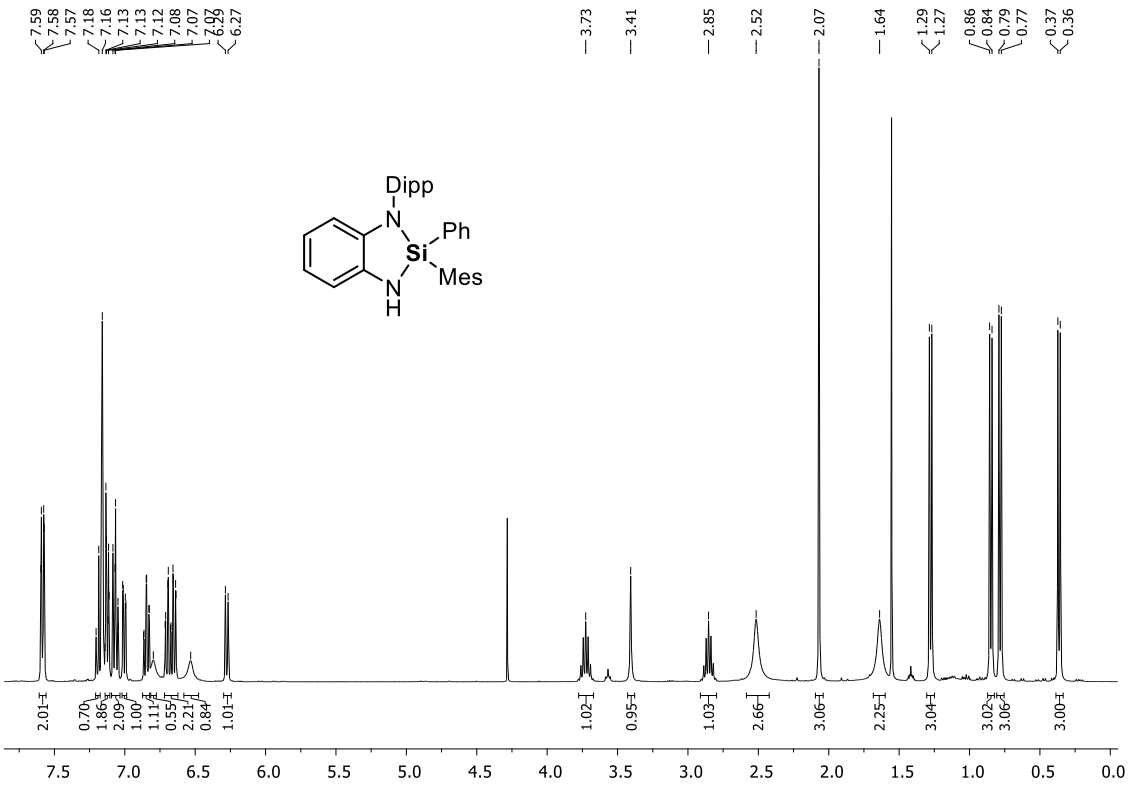

Figure S3.82. ^{1}H NMR spectrum (C_6D_6, 298 K) of **17**.

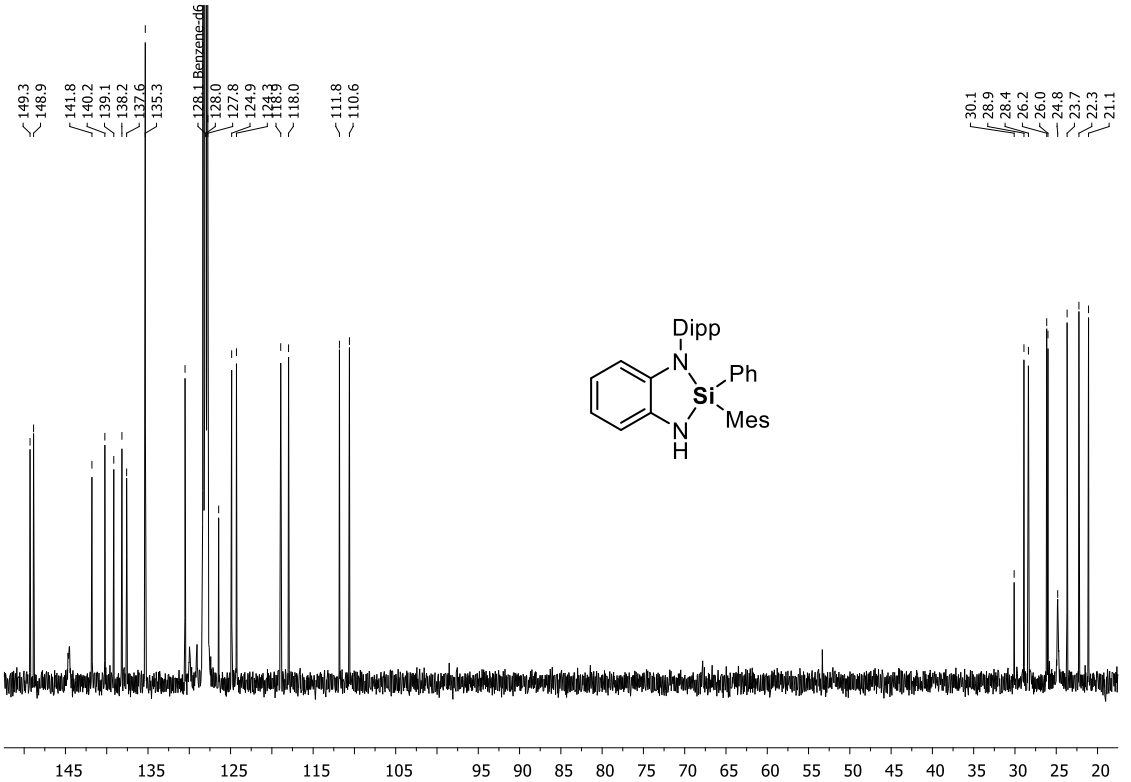

Figure S3.83. $^{13}C\{^{1}H\}$ NMR spectrum (C_6D_6, 298 K) of **17**.

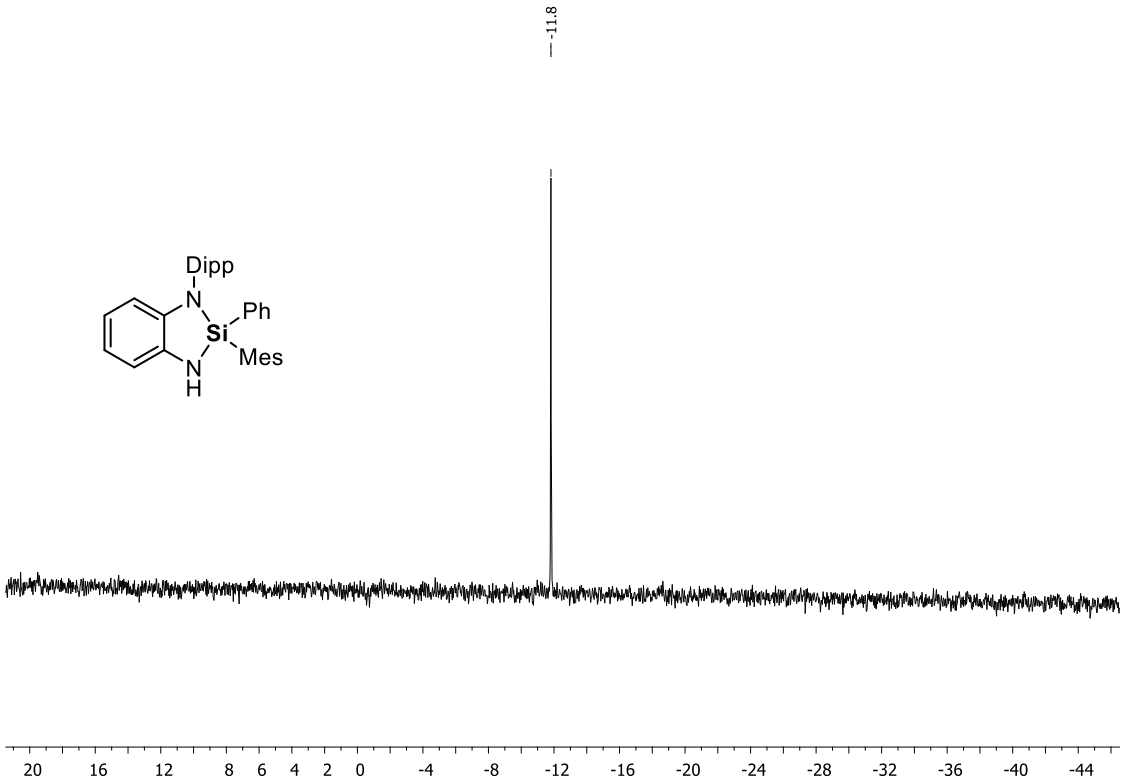

Figure S3.84. $^{29}Si\{^{1}H\}$ NMR spectrum (C_6D_6, 298 K) of **17**.

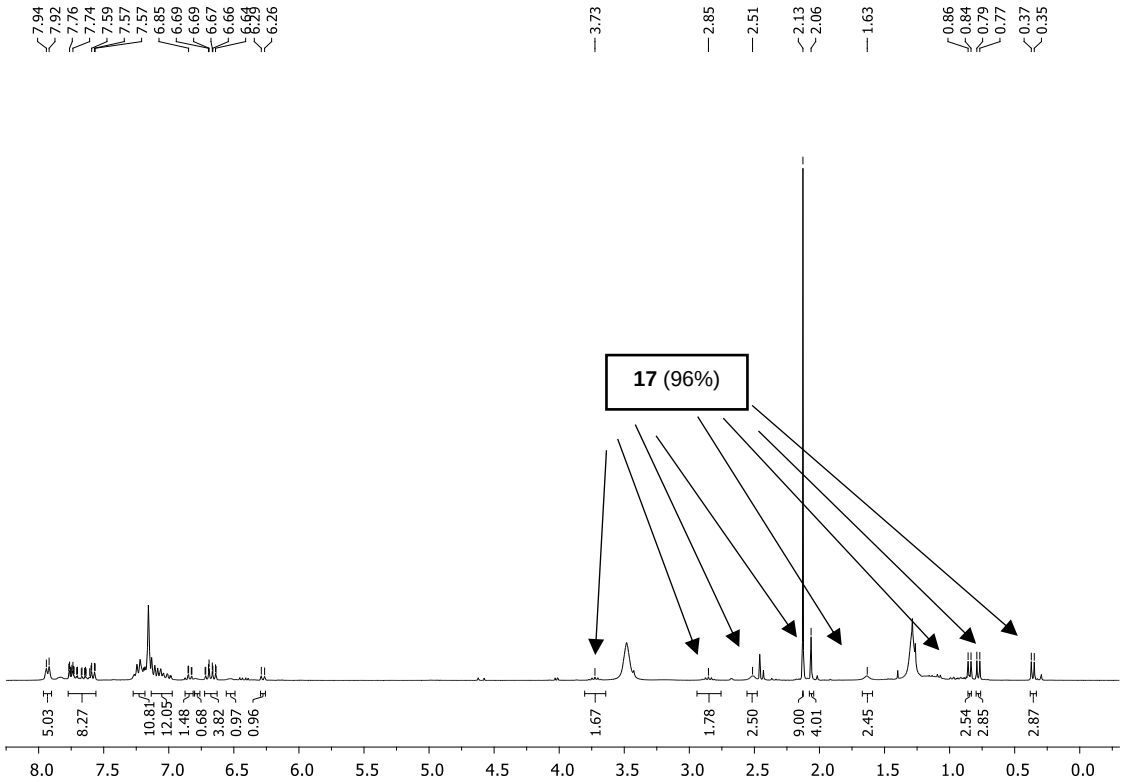

Figure S3.85. ^{1}H NMR spectrum (C_6D_6, 298 K) of the reaction of 1-chloro-1-mesityl-1,3,3,3-tetraphenyldisiloxane (**16**) with diamine **12** when using 2.0 equiv. of *n*BuLi. HMB (0.5 equiv.) as internal standard for determination of the NMR yield.

4.1.1.33 Cleavage of 3-chloro-1,1,1-trimethyl-3,5,5,5-tetraphenyltrisiloxane (18) using diamine 12

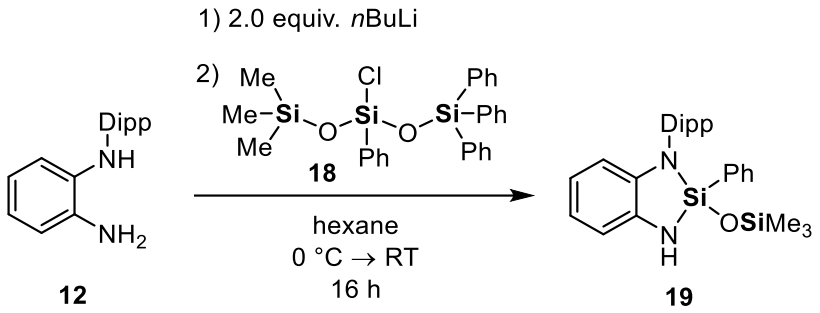

Compound **12** (376 mg, 1.4 mmol, 1.0 equiv.) was dissolved in 30 mL of hexane and cooled down to 0 °C. *n*-Butyllithium (1.12 mL of a 2.5 M solution in hexane, 2.8 mmol, 2.0 equiv.) was added dropwise and the solution was stirred while slowly warming up to room temperature. Then, the reaction mixture was again cooled down to 0 °C and a solution of compound **18** (836 mg, 1.4 mmol, 1.0 equiv.) in 10 mL hexane was added. The mixture was further stirred for 16 h while slowly warming up to room temperature. All volatiles of the brown suspension were removed *in vacuo* and the crude product was purified via Kugelrohr distillation (170 °C oven temperature, 1.8×10^{-2} mbar). The distilled waxy compound was recrystallized from hexane to obtain siloxane **19** as a colorless crystalline solid (554 mg, 0.75 mmol, 54 %) suitable for single-crystal X-ray diffraction analysis (for details, see chapter 3.7).

^{1}H NMR (400 MHz, C_6D_6, 298 K): δ[ppm] = 0.06 [s, 9H, Si(CH_3)$_3$], 0.31 [d, $^{3}J_{H\text{-}H}$ = 6.8 Hz, 3H, CH(CH_3)$_2$] , 0.92 [d, $^{3}J_{H\text{-}H}$ = 6.8 Hz, 3H, CH(CH_3)$_2$], 1.16 [d, $^{3}J_{H\text{-}H}$ = 6.9 Hz, 3H, CH(CH_3)$_2$], 1.42 [d, $^{3}J_{H\text{-}H}$ = 6.9 Hz, 3H, CH(CH_3)$_2$], 2.76 [sept, $^{3}J_{H\text{-}H}$ = 6.7 Hz, 1H, CH(CH$_3$)$_2$] , 3.71[sept, $^{3}J_{H\text{-}H}$ = 6.9 Hz, 1H, CH(CH$_3$)$_2$], 3.87 [s, 1H, NH], 6.16 (d, $^{3}J_{H\text{-}H}$ = 7.7 H, 1H, H_{Ph}], 6.65–6.72 [m, 1H, H_{Ph}] , 6.81–6.86 [m, 1H, H_{Ph}], 7.00–7.13 [m, 4H, H_{Ph}], 7.17–7.25 [m, 2H, H_{Ph}], 7.49–7.53 [m, 2H, H_{Ph}]. **^{13}C{^{1}H} NMR** (101 MHz, C_6D_6, 298 K): δ[ppm] = 2.0 [s, Si(CH_3)$_3$], 23.2 [s, CH(CH_3)$_2$], 25.4 [s, CH(CH_3)$_2$], 25.7 [s, CH(CH_3)$_2$], 25.7 [s, CH(CH_3)$_2$], 28.2 [s, CH(CH$_3$)$_2$], 28.3 [s, CH(CH$_3$)$_2$], 110.8 [s, C_{Ph}], 111.2 [s, C_{Ph}], 118.6 [s, C_{Ph}], 118.7 [s, C_{Ph}], 124.5 [s, C_{Ph}], 124.9 [s, C_{Ph}], 127.9 [s, C_{Ph}], 130.8 [s, C_{Ph}], 133.0 [s, C_{Ph}], 134.4 [s, C_{Ph}], 135.8 [s, C_{Ph}], 136.5 [s, C_{Ph}], 140.2 [s, C_{Ph}], 148.7 [s, C_{Ph}], 149.2[s, C_{Ph}]. **^{29}Si{^{1}H} NMR** (79 MHz, C_6D_6, 298 K): δ[ppm] = −40.2 [s, SiN], 11.3 [s, Si(CH$_3$)$_3$]. **CHN Analysis** calculated: C 70.38, H 7.88, N 6.08, O 3.47, 12.19; found: C 70.47, H 7.39, N 5.75. **HR-MS (FD+)**, calculated m/z for $C_{27}H_{36}N_2OSi_2$ [M+H$^+$]: 460.23607; found: 460.23721.

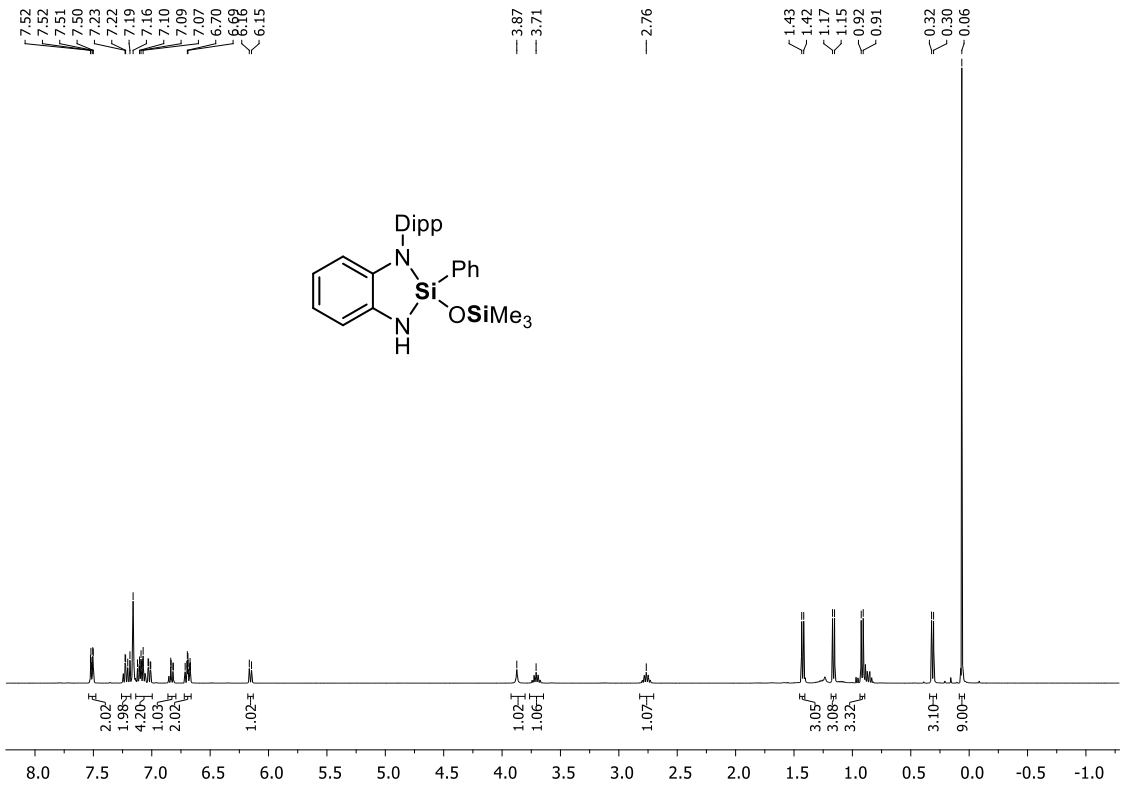

Figure S3.86. ^{1}H NMR spectrum (C_6D_6, 298 K) of **19**.

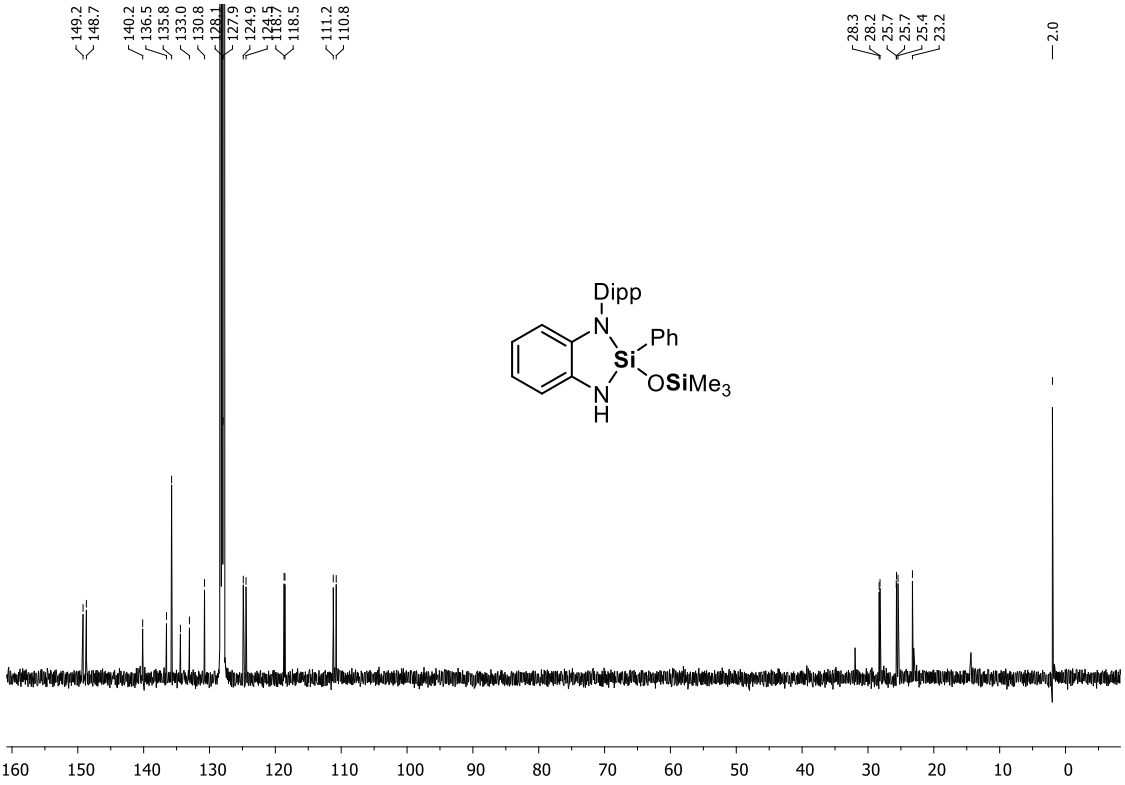

Figure S3.87. $^{13}C\{^{1}H\}$ spectrum (C_6D_6, 298 K) of **19**.

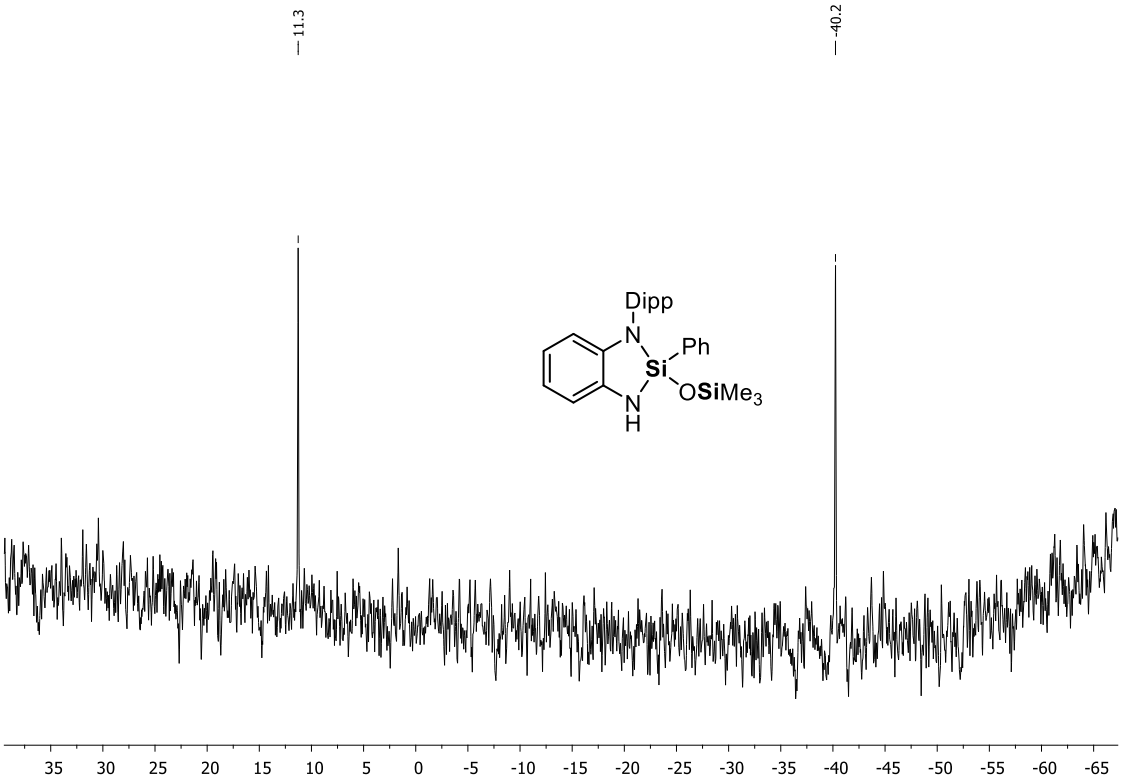

Figure S3.88. $^{29}Si\{^{1}H\}$ NMR spectrum (C_6D_6, 298 K) of **19**.

3.6.7 Intermolecular cleavage attempt

4.1.1.34 Synthesis of a suitable model system

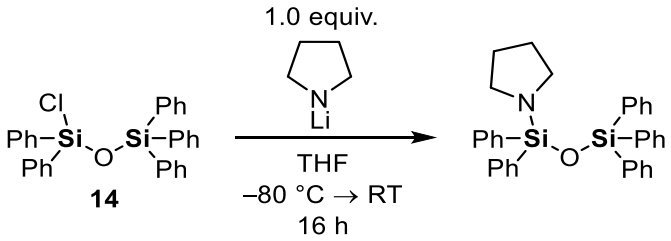

According to a modified literature procedure,[2] compound **14** (8.00 g, 16.2 mmol, 1.0 equiv.) was dissolved in 100 mL of THF and cooled down to −80 °C. A solution of *N*-pyrrolidinyllithium (1.25 g, 16.22 mmol, 1.0 equiv.) in 5 mL THF was added and the suspension stirred for 16 h while slowly warming up to room temperature. All volatiles were removed *in vacuo* and the residue was extracted with 30 mL of DCM. The solids were filtered off by cannula filtration, the clear filtrates collected. and dried *in vacuo*. The residue was purified via Kugelrohr distillation (230 °C oven temperature, 2.4×10^{-3} mbar) and then precipited from DCM at −80 °C to obtain 1-pyrrolidino-1,1,3,3,3-pentaphenyldisiloxane as a colorless solid (7.65 g, 14.5 mmol, 90%).

^{1}H NMR (400 MHz, C_6D_6, 298 K): *δ*[ppm] = 1.42 (m, 4H, C*H*$_2$C*H*$_2$], 2.97 [m, 4H, NC*H*$_2$], 7.12–7.20 [m, 10H, *H*$_{Ph}$], 7.80–7.85 [m, 10H, *H*$_{Ph}$]. **^{13}C{^{1}H} NMR** (101 MHz, C_6D_6, 298 K): *δ*[ppm] = 27.0 [s, *C*H$_2$*C*H$_2$], 47.7 [s, N*C*H$_2$], 128.2 [s, *C*$_{Ph}$], 130.0 [s, *C*$_{Ph}$], 130.2 [s, *C*$_{Ph}$], 135.5 [s, *C*$_{Ph}$], 135.7 [s, *C*$_{Ph}$], 136.4 [s, *C*$_{Ph}$], 136.6 [s, *C*$_{Ph}$]. **^{29}Si{^{1}H} NMR (**77 MHz, C_6D_6, 298 K) = *δ*[ppm] = −32.3 [s, *Si*N], −19.3 [s, *Si*Ph$_3$]. **CHN Analysis** $C_{34}H_{33}NOSi_2$ calculated: C 77.37, H 6.30, N 2.65, O 2.02, Si 10.64; found: C 77.46, H 6.33, N 2.56. **MS (FD+)**, calculated m/z for $C_{34}H_{33}N_1OSi_2$ [M+H$^+$]: 527.21; found: 527.20.

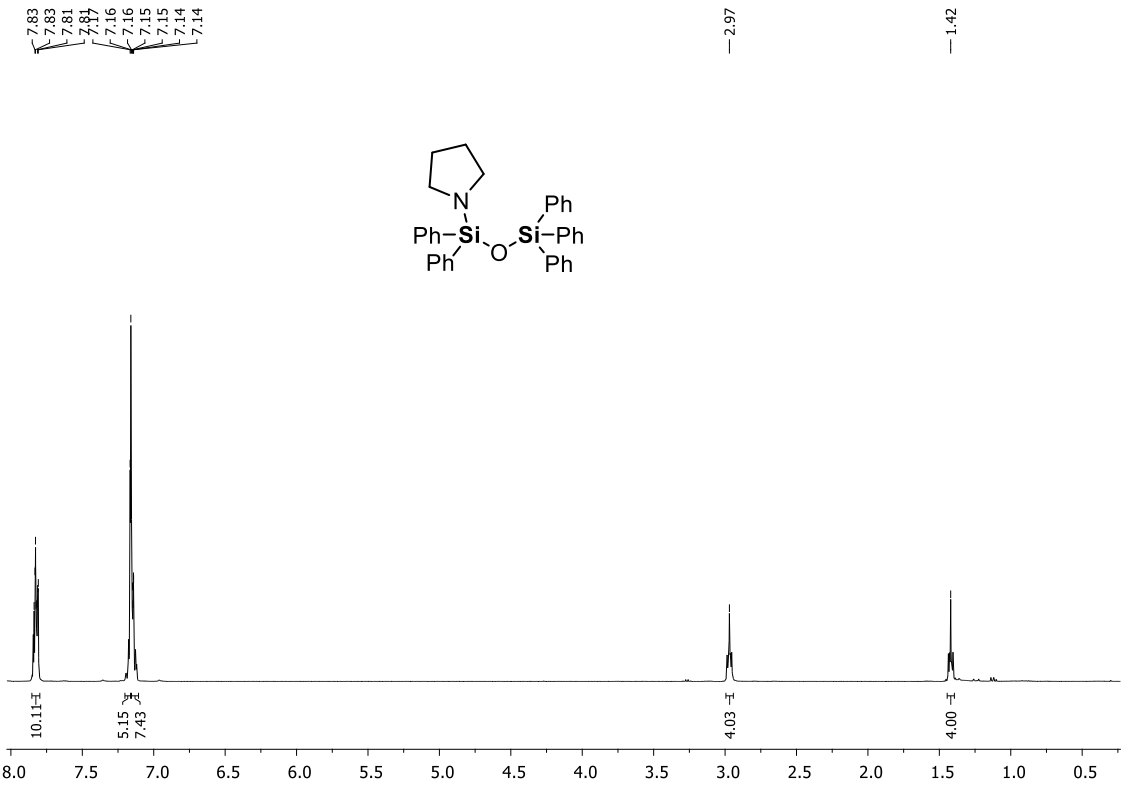

Figure S3.89. ^{1}H NMR spectrum (C_6D_6, 298 K) of 1-pyrrolidino-1,1,3,3,3-pentaphenyldisiloxane.

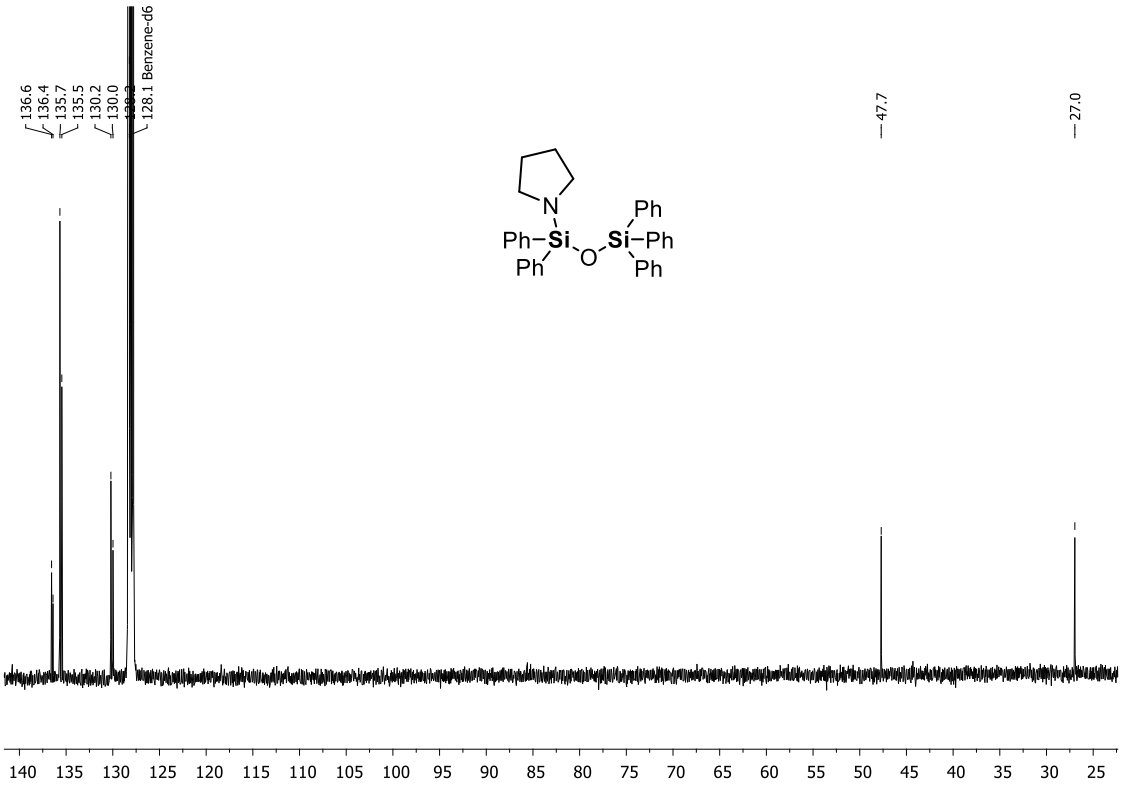

Figure S3.90. $^{13}C\{^{1}H\}$ NMR (C_6D_6, 298 K) of 1-pyrrolidino-1,1,3,3,3-pentaphenyldisiloxane.

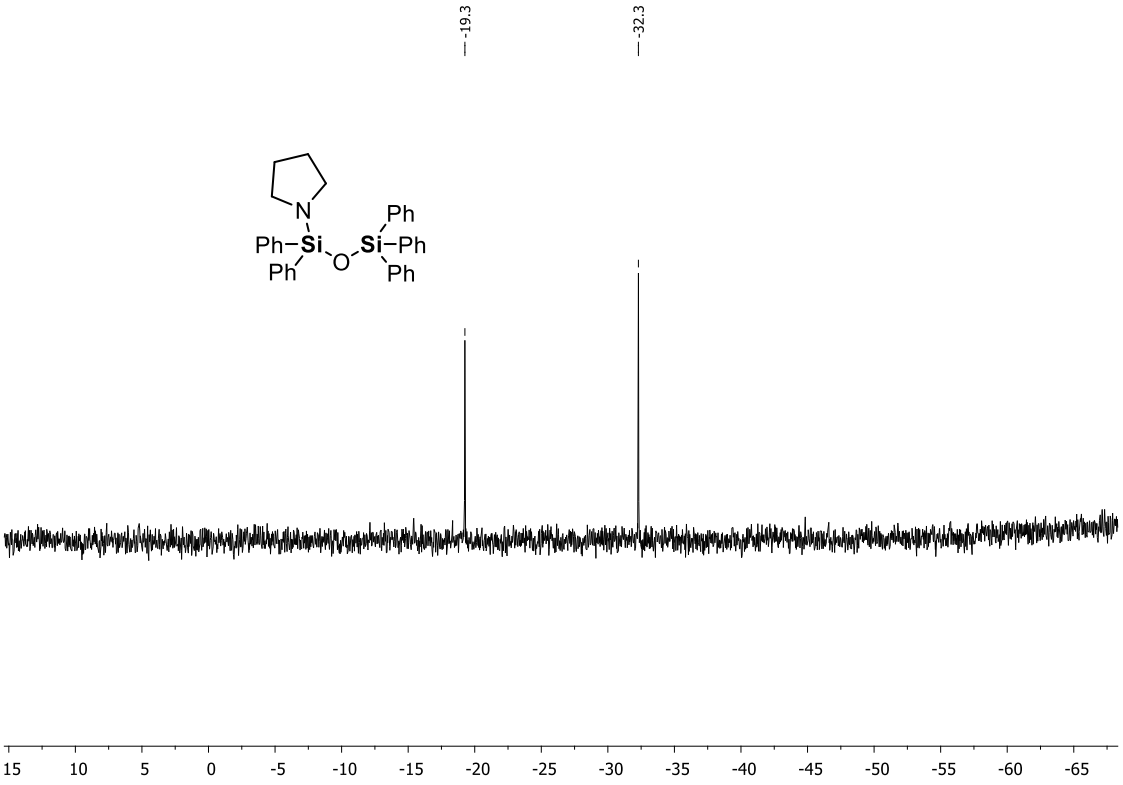

Figure S3.91. $^{29}Si\{^{1}H\}$ NMR (C_6D_6, 298 K) of 1-pyrrolidino-1,1,3,3,3-pentaphenyldisiloxane.

4.1.1.35 Attempt to cleave 1-pyrrolidino-1,1,3,3,3-pentaphenyldisiloxane

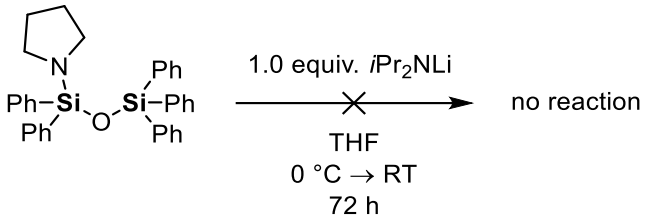

Di-*iso*-propylamine (0.21 mL, 1.5 mmol, 1.0 equiv.) was dissolved in 20 mL of THF and cooled down to 0 °C. Then, *n*-butyllithium (0.66 mL of a 2.5 M solution in hexane, 1.7 mL, 1.1 equiv.) was added and the solution stirred for 1 h while warming up to room temperature. The mixture was again cooled down to 0 °C and a solution of pyrrolidinopentaphenyldisiloxane (800 mg, 1.5 mmol, 1.0 equiv.) was added. After warming up to room temperature, the mixture was stirred for 72 h. An aliquot was transferred into an NMR tube, dried *in vacuo*, dissolved in 0.6 mL C_6D_6, and analyzed by ^{1}H NMR spectroscopy. Only starting material was detected, which proves that no intermolecular Si–O–Si cleavage occurred.

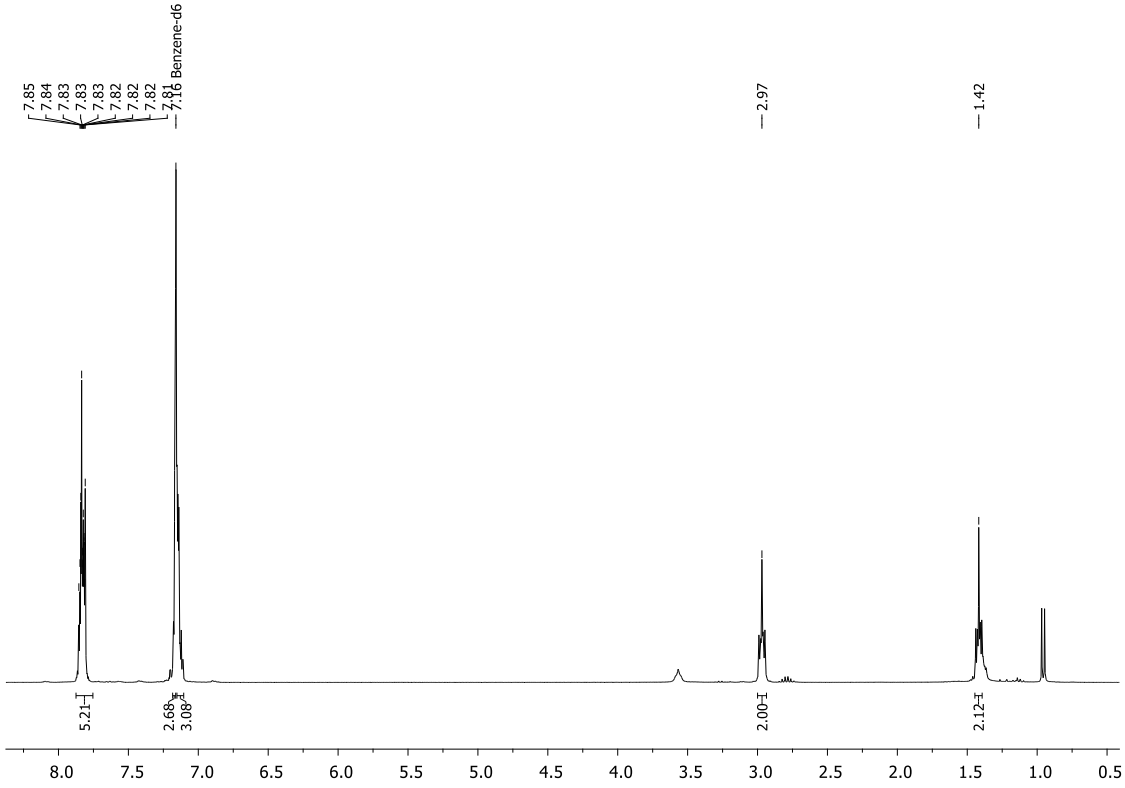

Figure S3.92. ^{1}H NMR spectrum (C_6D_6, 298 K) of the test reaction, which shows only unconverted starting material (compare with Figure S3.66).

3.7 X-ray crystallographic details

The crystals were selected and measured either on a GV50 diffractometer equipped with a TitanS2 detector (**1**, **2**, **3**, and **[12-Li$_2$·(THF)$_2$]$_2$**), a Gemini Ultra diffractometer equipped with an Atlas S2 CCD detector (**4**), a SuperNova Dualflex diffractometer equipped with a TitanS2 detector (**9**), a XtaLAB Synergy R, DW system, equipped with a HyPix-Arc 150 detector (**17**) or on a Superova diffractometer equipped with an Atlas detector (**19**). Data collection and reduction were performed with **CrysAlisPro** [Version 1.171.41.54a or 1.17.41.76a].[10] A numerical absorption correction using spherical harmonics as implemented in SCALE3 ABSPACK was applied. Using **Olex2**,[11] the structures were solved with **ShelXT**[12] and a least-square refinement on F^2 was carried out with **ShelXL**[13]. All non-hydrogen atoms were refined anisotropically. Hydrogen atoms at the carbon atoms were located in idealized positions and refined isotropically according to the riding model. The hydrogen atoms on the nitrogen atoms were located from the difference Fourier map and refined without restraints. Figures were created with **Olex2**[11].

Compound 1: The asymmetric unit contains two molecules.
Compound 2: The asymmetric unit contains one molecule.
Compound 3: The asymmetric unit contains one molecule. The Dipp moiety is disordered over three positions and split into three parts with occupancies of 40:39:21. SIMU and SADI restraints were applied to model this disorder.
Compound 4: The asymmetric unit contains one molecule.
Compound 9: The asymmetric unit contains one molecule. The hydrogen atom on the silicon atom was located from the difference Fourier map and refined without restraints.
Compound 17: The asymmetric unit contains two molecules.
Compound 19: The asymmetric unit contains two molecules of **19** and half a molecule of hexamethylbenzene. The Me_3Si fragments in both molecules of **19** are disordered over two positions and split into two parts with occupancies of 55:45.
[12-Li$_2$·(THF)$_2$]$_2$: The asymmetric unit contains one half of the dimer **[12-Li$_2$·(THF)$_2$]$_2$**. Both THF molecules are partially disordered over two positions and split into two parts with occupancies of 84:16.

CCDC-2110741 (**1**), CCDC-2110739 (**2**), CCDC-2110743 (**3**), CCDC-2110742 (**4**), CCDC-2110745 (**9**), CCDC-2116391 (**17**), CCDC-2110744 (**19**), and CCDC-2110740 (**[12-Li$_2$·(THF)$_2$]$_2$**) contain the supplementary crystallographic data for this paper. These data can be obtained free of charge at www.ccdc.cam.ac.uk/conts/retrieving.html (or from the Cambridge Crystallographic Data Centre, 12 Union Road, Cambridge CB2 1EZ, UK; Fax: + 44-1223-336-033; E-mail: deposit@ccdc.cam.ac.uk).

Table S3.1. Crystallographic data for compounds **1**, **2**, and **3**.

Compound	**1**	**2**	**3**
Data set (internal naming)	TG189	TG077	TG307_mP_abs_gaus
Formula	$C_{30}H_{32}N_2Si$	$C_{22}H_{24}N_2Si$	$C_{48}H_{48}N_2OSi_2$
$\rho_{calc.}$ / g·cm^{-3}	1.183	1.245	1.182
μ/mm^{-1}	0.958	1.156	1.074
Formula Weight	448.66	344.52	725.06
Color	clear colorless	clear colorless	clear colorless
Shape	block	block	plate
Size/mm^3	0.278×0.186×0.132	0.13× 0.08×0.05	0.288×0.154×0.033
T/K	293(2)	122.97(10)	122.97(13)
Crystal System	monoclinic	triclinic	monoclinic
Space Group	$P2_1/c$	$P\bar{1}$	$P2_1/c$
a/Å	10.85140(10)	9.5368(7)	25.3635(6)
b/Å	25.7319(2)	10.3860(4)	8.9468(2)
c/Å	18.0365(2)	10.3860(4)	19.1067(5)
α/°	90	81.372(5)	90
β/°	90.2650(10)	75.669(5)	110.000(3)
γ/°	90	70.753(7)	90
V/Å^3	5036.23(8)	918.88(11)	4074.26(19)
Z	8	2	4
Z'	2	1	1
Wavelength/Å	1.54184	1.54184	1.54184
Radiation type	Cu K_α	Cu K_α	Cu K_α
Θ_{min}/°	3.435	4.406	3.709
Θ_{max}/°	72.929	73.596	74.120
Measured Refl.	21303	15884	23542
Independent Refl.	9709	3622	7962
R_{int}	0.0191	0.0405	0.0214
Parameters	611	233	714
Restraints	0	0	159
Largest Peak	0.33	0.32	0.35
Deepest Hole	−0.27	−0.29	−0.35
GooF	1.021	1.036	1.082
wR_2 (all data)	0.0899	0.0897	0.1176
wR_2	0.0855	0.0867	0.1138
R_1 (all data)	0.0422	0.0382	0.0486
R_1	0.0343	0.0344	0.0438

Table S3.2. Crystallographic data for compounds **4**, **9**, and **17**.

Compound	**4**	**9**	**17**
Data set (internal naming)	TG268	TG541	TG586
Formula	$C_{40}H_{40}N_2OSi_2$	$C_{48}H_{56}N_2OSi_2$	$C_{30}H_{38}N_2Si$
$\rho_{calc.}$ / g·cm^{-3}	1.198	1.189	1.133
μ/mm^{-1}	1.186	1.069	0.877
Formula Weight	620.92	733.12	490.74
Color	clear colorless	clear colorless	clear colorless
Shape	plate	block	block
Size/mm^3	0.359 × 0.206 × 0.143	0.21 × 0.17 × 0.1	0.16 × 0.11 × 0.08
T/K	293(2)	122.96(16)	123.01(10)
Crystal System	monoclinic	triclinic	monoclinic
Space Group	$P2_1/n$	$P\bar{1}$	$P2_1/c$
a/Å	12.68740(10)	10.7294(2)	17.6813(2)
b/Å	19.01590(10)	12.1269(2)	19.26710(10)
c/Å	14.96520(10)	17.9904(3)	18.8643(2)
α/°	90	99.1100(10)	90
β/°	107.4760(10)	101.7280(10)	116.4360(10)
γ/°	90	112.326(2)	90
V/Å^3	3433.87(4)	2047.18(7)	5754.45(10)
Z	4	2	8
Z'	1	1	2
Wavelength/Å	1.54184	1.54184	1.54184
Radiation type	Cu K_α	Cu K_α	Cu K_α
Θ_{min}/°	3.872	4.081	5.582
Θ_{max}/°	71.906	66.833	147.962
Measured Refl.	41086	63310	93032
Independent Refl.	6718	7253	11388
R_{int}	0.0238	0.0534	0.0237
Parameters	413	500	671
Restraints	0	0	0
Largest Peak	0.39	0.47	0.27
Deepest Hole	−0.22	−0.41	−0.28
GooF	1.038	1.044	1.020
wR_2 (all data)	0.0866	0.1063	0.0903
wR_2	0.0842	0.1046	0.0883
R_1 (all data)	0.0339	0.0418	0.0366
R_1	0.0311	0.0400	0.0337

Table S3.3. Crystallographic data for compounds **19** and **[12-Li_2·$(THF)_2$]$_2$**

Compound	**19**	**[12-Li_2·$(THF)_2$]$_2$**
Data set (internal naming)	TG341	TG139
Formula	$C_{60}H_{81}N_4O_2Si_4$	$C_{52}H_{76}Li_4N_4O_4$
$\rho_{calc.}$ / g·cm^{-3}	1.126	1.145
μ/mm^{-1}	1.260	0.541
Formula Weight	1002.64	848.92
Color	clear colorless	light yellow
Shape	block	block
Size/mm^3	0.193 × 0.152 × 0.098	0.125 × 0.09 × 0.039
T/K	123.00(10)	122.97(10)
Crystal System	triclinic	monoclinic
Space Group	$P\bar{1}$	$P2_1/n$
a/Å	9.9224(2)	11.9723(4)
b/Å	16.4456(4)	15.9044(4)
c/Å	19.7403(5)	13.7478(4)
α/°	112.275(2)	90
β/°	95.831(2)	109.860(3)
γ/°	91.739(2)	90
V/Å^3	2957.10(13)	2462.06(13)
Z	2	2
Z'	2	0.5
Wavelength/Å	1.54184	1.54184
Radiation type	Cu K_α	Cu K_α
$2\Theta_{min}$/°	4.461	4.241
$2\Theta_{max}$/°	72.697	73.351
Measured Refl.	61543	8438
Independent Refl.	11595	4732
R_{int}	0.0458	0.0339
Parameters	706	358
Restraints	6	12
Largest Peak	0.51	0.30
Deepest Hole	−0.65	−0.21
GooF	1.033	1.020
wR_2 (all data)	0.1295	0.1226
wR_2	0.1213	0.1097
R_1 (all data)	0.0553	0.0636
R_1	0.0442	0.0445

Compound 1

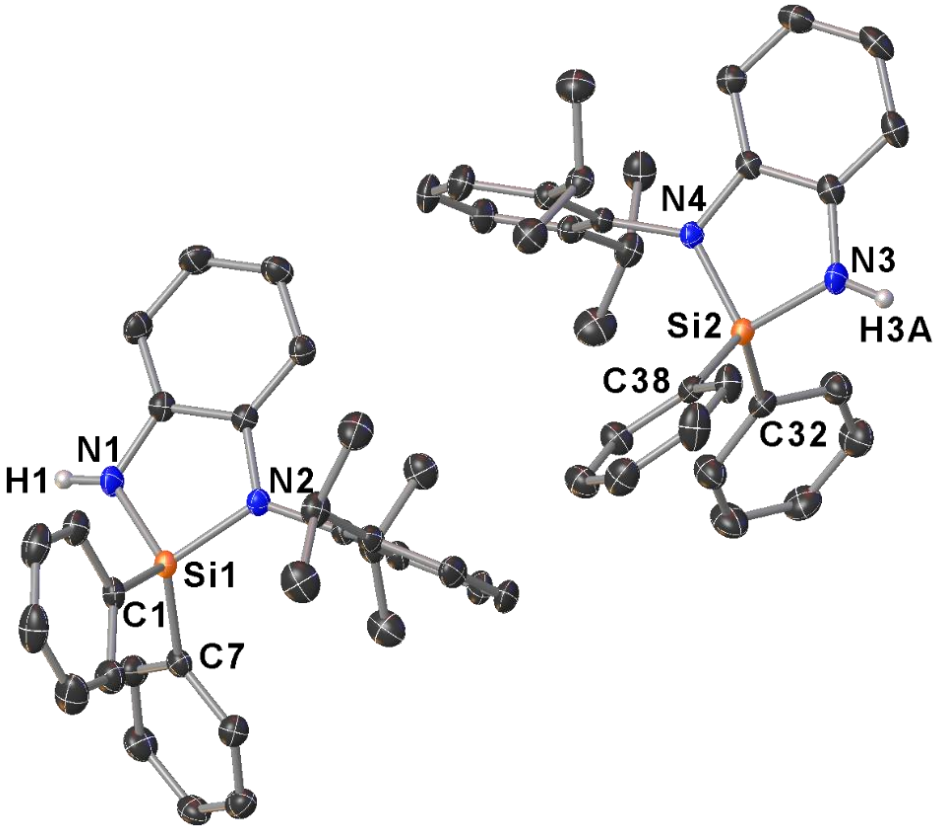

Selected Bond Lengths in Å		Selected Bond Angles in °	
Si1–N1	1.7257(11)	**N1–Si1–N2**	91.50(5)
Si1–N2	1.7460(10)	**N3–Si2–N4**	91.58(5)
Si2–N3	1.7291(11)	**N1–Si1–C1**	111.52(6)
Si2–N4	1.7466(11)	**N1–Si1–C7**	115.25(6)
Si1–C1	1.8684(13)	**N2–Si1–C1**	114.41(5)
Si1–C7	1.8627(13)	**N2–Si1–C7**	114.43(5)
Si2–C32	1.8698(13)	**N3–Si2–C32**	110.13(6)
Si2–C38	1.8673(13)	**N3–Si2–C38**	113.58(6)
N2–C20	1.4347(15)	**N4–Si2–C32**	114.78(5)
N4–C50	1.4359(15)	**N4–Si2–C38**	113.29(5)

Compound 2

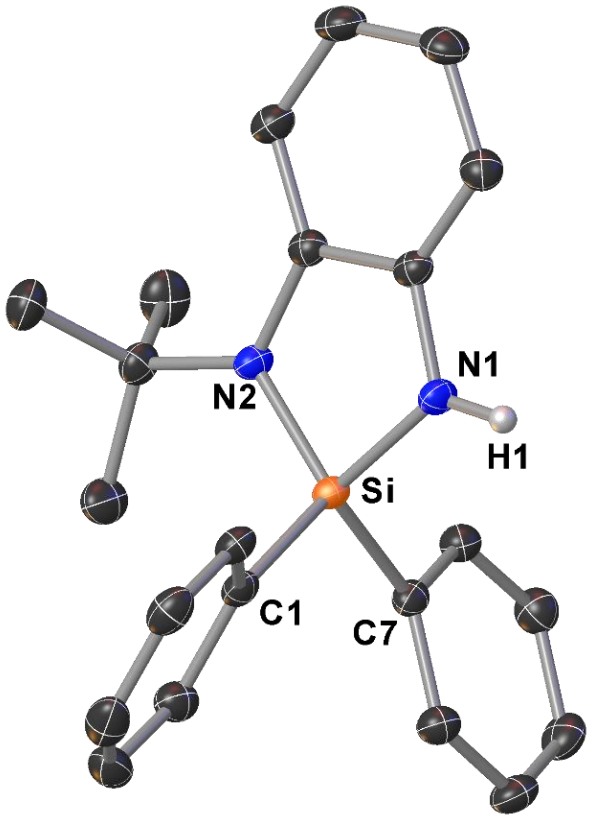

Selected Bond Lengths in Å		Selected Bond Angles in °	
Si–N1	1.7222(12)	**N1–Si1–N2**	91.70(5)
Si–N2	1.7500(11)	**N1–Si–C1**	109.85(6)
Si–C1	1.8770(14)	**N1–Si–C7**	111.82(6)
Si–C7	1.8701(13)	**N2–Si–C1**	116.75(6)
N2–C19	1.4148(17)	**N2–Si–C7**	114.86(6)

Compound 3

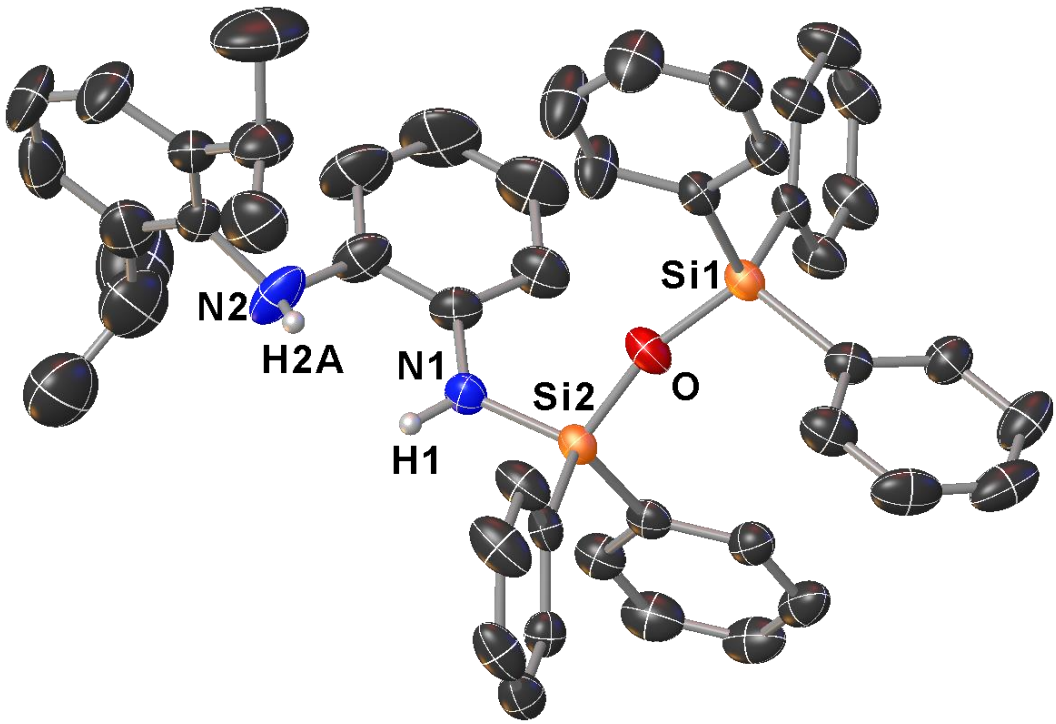

Selected Bond Lengths in Å		Selected Bond Angles in °	
Si1–O	1.6222(11)	**Si1–O–Si2**	163.89(9)
Si2–O	1.6154(11)	**N1–Si2–O**	107.82(7)
Si2–N1	1.7149(15)		

Compound 4

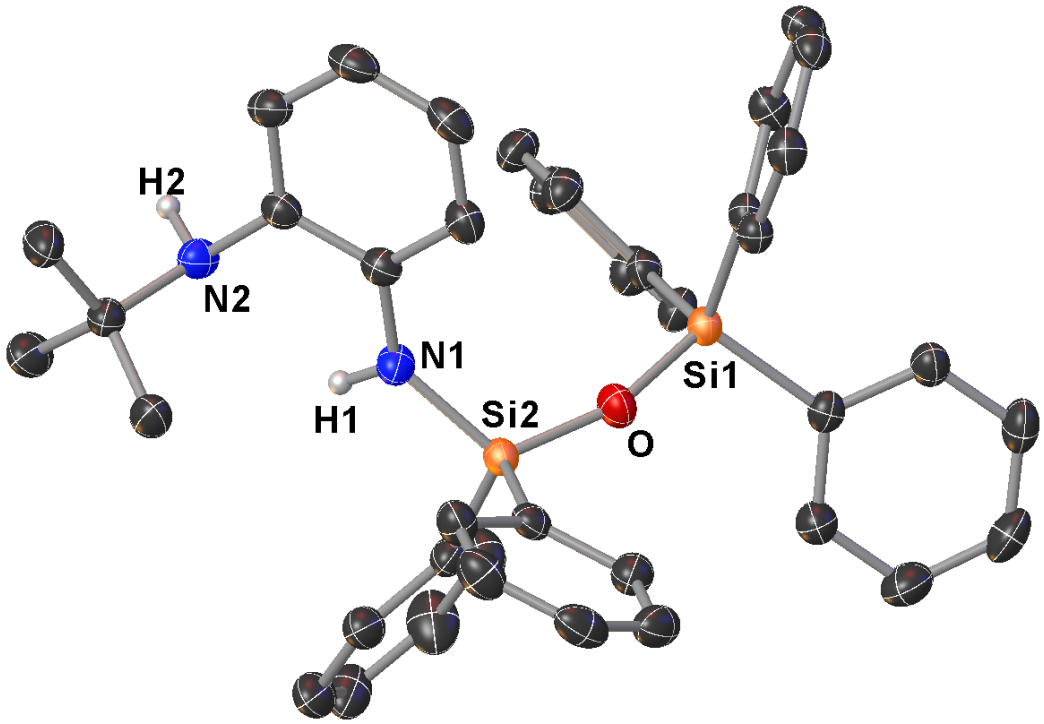

Selected Bond Lengths in Å		Selected Bond Angles in °	
Si1–O	1.6284(9)	**Si1–O–Si2**	160.50(6)
Si2–O	1.6205(9)	**N1–Si2–O**	114.68(5)
Si2–N1	1.71430(10)		

Compound 9

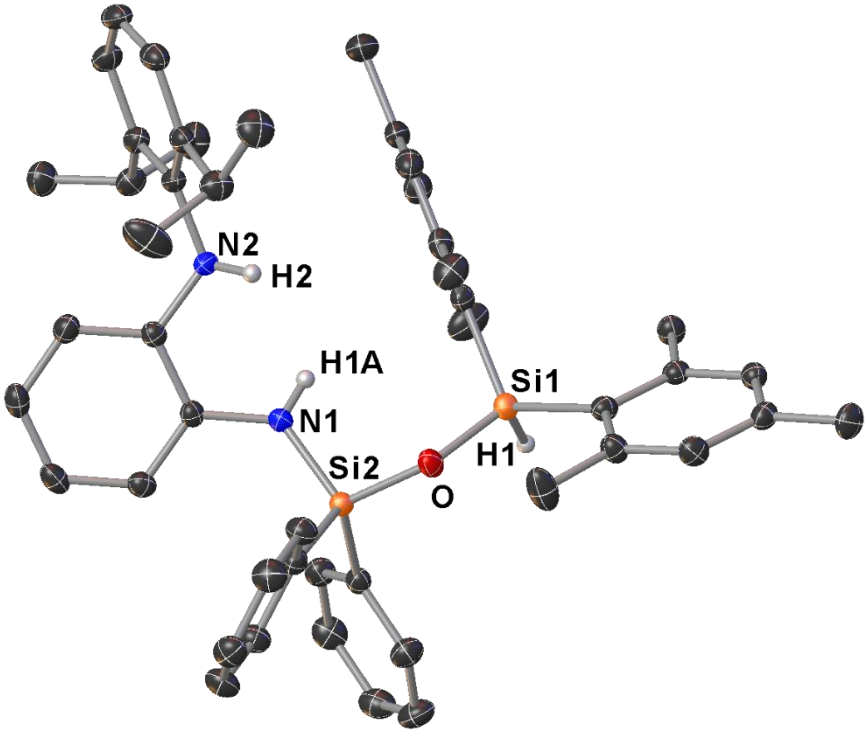

Selected Bond Lengths in Å		Selected Bond Angles in °	
Si1–O	1.6406(10)	**Si1–O–Si2**	137.31(7)
Si2–O	1.6302(10)	**N1–Si2–O**	105.40(6)
Si2–N1	1.7215(13)		
Si1–H1	1.379(15)		

Compound 17

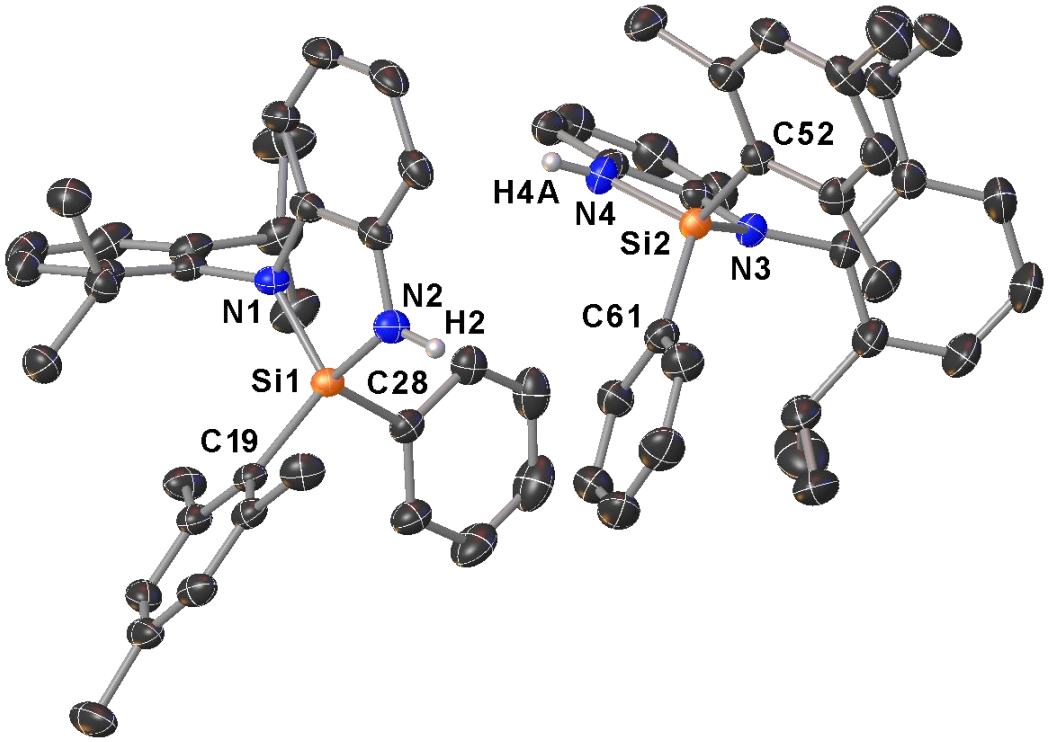

Selected Bond Lengths in Å		Selected Bond Angles in °	
Si1–N1	1.7562(9)	**N1–Si1–N2**	90.22(5)
Si1–N2	1.7339(10)	**N3–Si2–N4**	90.50(5)
Si2–N3	1.7562(10)	**N1–Si1–C19**	114.73(5)
Si2–N4	1.7273(10)	**N1–Si1–C28**	115.40(5)
Si1–C19	1.8793(11)	**N2–Si1–C19**	119.32(5)
Si1–C28	1.8696(11)	**N2–Si1–C28**	108.04(5)
Si2–C52	1.8805(12)	**N3–Si2–C52**	114.69(5)
Si2–C61	1.8783(12)	**N3–Si2–C61**	115.50(5)
		N4–Si2–C52	118.80(5)
		N4–Si2–C61	109.36(5)

Compound 19

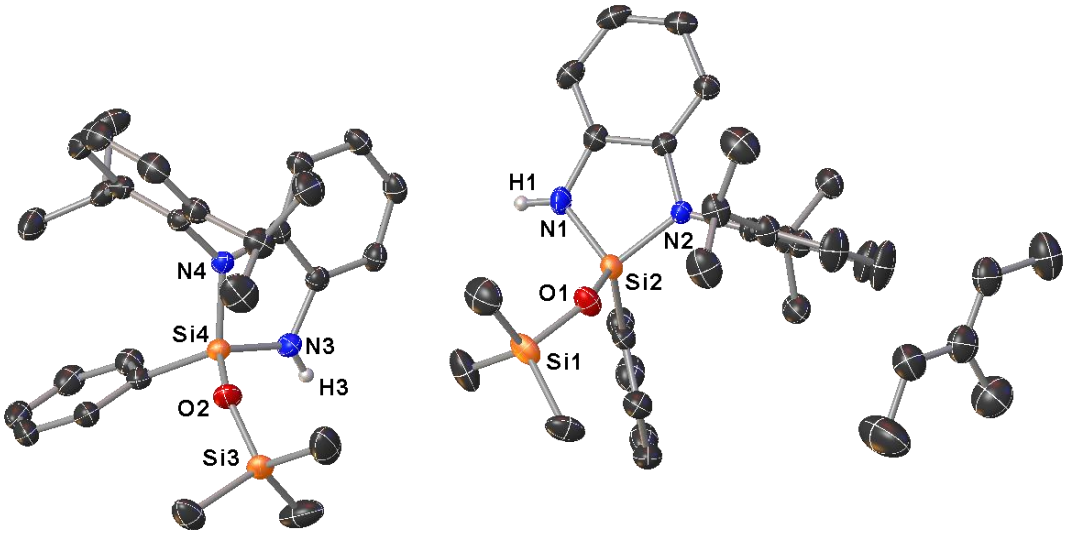

Selected Bond Lengths in Å		Selected Bond Angles in °	
Si1–O1	1.630(2)	**Si1–O1–Si2**	139.38(12)
Si2–O1	1.6145(13)	**N1–Si2–N2**	91.68(7)
Si2–N1	1.7161(15)	**O1–Si2–N1**	115.97(7)
Si2–N2	1.7313(14)	**O1–Si2–N2**	112.87(7)

[12-Li_2·$(THF)_2$]$_2$

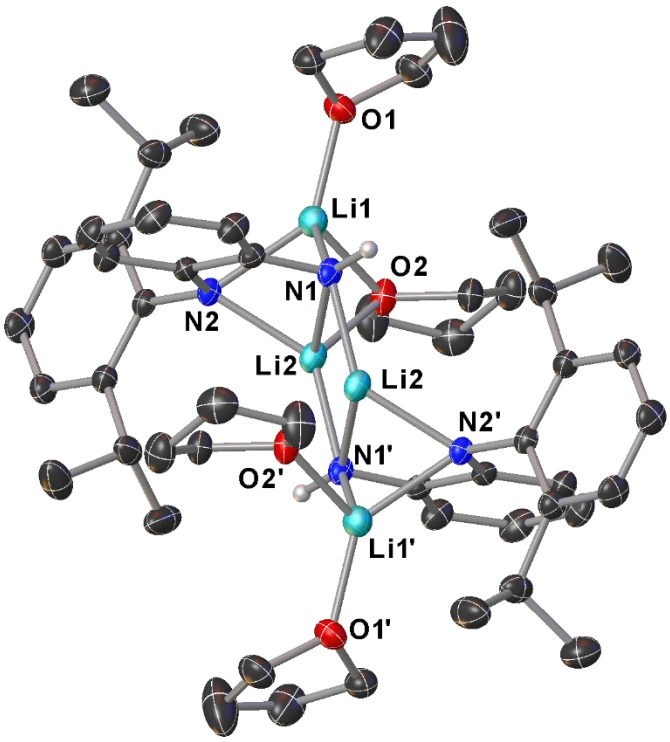

Selected Bond Lengths in Å		Selected Bond Angles in °	
N1–Li1	2.046(3)	**N1–Li1–N2**	80.10(11)
N1–Li2	2.075(3)	**N1–Li2–N2**	80.31(10)
N2–Li1	2.073(3)	**Li1–N1–Li2**	66.70(11)
N2–Li2	2.035(3)	**Li1–N2–Li2**	66.95(11)
Li1–O1	1.930(4)	**O1–Li1–O2**	113.93(17)
Li1–O2	1.997(3)	**O2–Li2–N1**	94.73(12)
Li2–N1'	2.061(3)	**Li2–N1–Li2'**	71.28(11)
		N1'–Li2–N1	108.72(11)

3.8 Supplementary references

[1] J. O. Bauer, T. Götz, *Chemistry* **2021**, *3*, 444–453. (Ref. [25] in the article)

[2] N. A. Espinosa-Jalapa, J. O. Bauer, *Z. Anorg. Allg. Chem.* **2020**, *646*, 828–834. (Ref. [24a] in the article)

[3] S. P. Heins, W. D. Morris, P. T. Wolczanski, E. B. Lobkovsky, T. R. Cundari, *Angew. Chem. Int. Ed.* **2015**, *54*, 14407–14411; *Angew. Chem.* **2015**, *27*, 14615–14619.

[4] S. Khumsubdee, Y. Fan, K. Burgess, *J. Org. Chem.* **2013**, *78*, 9969–9974.

[5] P. Zhang, E. A. Terefenko, J. Bray, D. Deecher, A. Fensome, J. Harrison, C. Kim, E. Koury, L. Mark, C. C. McComas, C. A. Mugford, E. J. Trybulski, A. T. Vu, G. T. Whiteside, P. E. Mahaney, *J. Med. Chem.* **2009**, *52*, 5703–5711.

[6] H. Quast, K.-H. Ross, G. Philipp, M. Hagedorn, H. Hahn, K. Banert, *Eur. J. Org. Chem.* **2009**, 3940–3952.

[7] K. Tanino, N. Yoshitani, F. Moriyama, I. Kuwajima, *J. Org. Chem.* **1997**, *62*, 4206–4207.

[8] a) A. C. Coelho, T. R. Amarante, J. Klinowski, I. S. Gonçalves, F. A. Almeida Paz, *Acta Crystallogr.* **2008**, *E64*, o237–o238; b) T. R. Amarante, A. C. Coelho, J. Klinowski, I. S. Gonçalves, F. A. Almeida Paz, *Acta Crystallogr.* **2008**, *E64*, o239.

[9] J. Harloff, E. Popowski, H. Reinke, *J. Organomet. Chem.* **2007**, *692*, 1421–1441.

[10] CrysAlisPro Software System, Rigaku Oxford Diffraction, **2020**.

[11] O. V. Dolomanov, L. J. Bourhis, R. J. Gildea, J. A. K. Howard, H. Puschmann, *J. Appl. Crystallogr.* **2009**, *42*, 339–341.

[12] G. M. Sheldrick, *Acta Crystallogr*. **2015**, *A71*, 3–8.

[13] G. M. Sheldrick, *Acta Crystallogr.* **2015**, *C71*, 3–8.

4 Pentacoordinated silane intermediates and subsequent H_2 formation in the reaction of a tetravalent hydrosilane with silanols

Preface

The following chapter and supporting information are based on a manuscript in preparation about the synthesis of cyclic diaminohydrosilanes and mechanistic investigations regarding their reactivity towards Ph_3SiOH.

Authors

T. Götz, F. Westermair, and J. O. Bauer

Author contribution

All the reported syntheses and characterizations in this work were performed by T. Götz. The VT-NMR studies were performed by F. Westermair in the group of Prof. Dr. Ruth Gschwind. Quantum chemical calculations were performed by Dr. J. O. Bauer. The manuscript draft was prepared by T. Götz.

Acknoledgements

This work was jointly supported by the Elite Network of Bavaria (ENB), the Bavarian State Ministry of Science and the Arts (StMWK), and the University of Regensburg (N-LW-NW-2016-366).

4.1 Abstract

A new tetravalent hydrosilane equipped with a Dipp-substituted *ortho*-phenylenediamine is presented which shows unprecedented high reactivity towards dehydrogenative coupling with silanols. Variable temperature ^{1}H NMR and ^{29}Si NMR studies revealed an equilibrium between two pentacoordinated reaction intermediates. Quantum chemical calculations suggested that the H_2 formation occurs from only one of the two intermediates based on a significant difference in transition state energies. Changing the substituent from Dipp to *t*Bu resulted in a different reactivity where the Si–H remains untouched highlighting the importance of the type of organic substituents on the amine.

4.2 Introduction

Hydrogen storage displays a prominent topic in sustainable energy economics and in current research. While H_2 can be physically stored via adsorption or absorption processes, also chemical approaches introducing hydrogen–heteroatom bonds are highly sought after.[1] Silicon-based molecular chemistry provides versatile possibilities for hydrogen activation by using silylenes,[2] silylium ions[3] and recently also neutral Si(IV) compounds.[4,5] However, the release of H_2 after binding covalently to these species renders a highly difficult undertaking that makes most of the examples unsuited for hydrogen storage purposes. The use of hydrosilanes as hydride donor has been established in form of hydrosilylation reactions for reduction of various types of unsaturated molecules like carbonyl compounds[6] or imines.[7] The direct formation of H_2 from hydrosilanes typically requires protic nucleophiles like alcohols,[8] amines[9,10] or silanols[11] and addition of transition metal[9,12] or main-group metal[13] catalysts which are often toxic and lose their catalytic activity after time. Some elegant examples for catalyst-free dehydrogenative silylation reactions involve hypervalent silicon compounds as silicon can exceed the coordination sphere of four.[14–19] This behaviour strongly enhances the reactivity towards nucleophilic attacks on the silicon atom and has been an important discovery in silicon chemistry which enables hydrodefluorination[20], reduction of carbonyl compounds[21] or dehydrogenative coupling reactions.[22] Most known examples of catalyst-free hydrosilane substitution reactions feature either neutral highercoordinated silanes with tertiary amine sidearms as flexible coordinating moiety[15–19] or anionic hydrosilicates as reactive hydride donor molecules.[20,23–25] In an elegant recent study, also an air-stable single electron donor silicate has been developed.[26] The preparation and investigation of pentacoordinated silanes remains a highly attractive undertaking in recent research e.g. in form of hypervalent *Si*-chiral compounds which have only been synthesized in limited amounts so far.[27,28–33] Such pentacoordinated silanes have been important for the fundamental understanding of nucleophilic attacks on silicon atoms[34,35] and it is well-established, that typical nucleophilic substitutions proceed through pentacoordinated trigonal-bipyramidal intermediates. Depending on the apicophilicity of the leaving group and the hardness of the nucleophile, either retention or inversion on the silicon center takes place. Good leaving

groups such as chloride or triflate tend to be in the apical position and hard nucleophiles on the second apical position favouring a fast reaction with inversion of configuration. Weaker leaving groups like hydride, on the other hand, tend to go into the equatorial position in the trigonal plane and allow for a more stable pentacoordinated intermediate which can undergo pseudo-rotations leading to a retention of configuration.[35,36] In studies about such pseudo-rotations on pentacoordinated silanes bearing a coordinating tertiary amine sidearm, it was found that also Si–N dissociative processes play a significant role especially for chelating substituents where double-equatorial position is unfavourable.[35,37–42] Such dynamic studies on pentacoordinated silanes are restricted to stable compounds with intramolecular coordination motifs or spirocyclic silicates.[28–33] A similar study for neutral pentacoordinated intermediates after reaction of a tetravalent silane with a nucleophile remains elusive. The formation of hypervalent species starting from regular tetravalent silanes are predominantly restricted to strongly nucleophilic organolithium reagents or alkaline-metal salts that form anionic silicates.[23–25,43–45] However, a handful of examples are reported by Tacke[46] and others[5] in which tetravalent hydrosilanes are functionalized with heteroatoms like thiols, alcohols or amines without the addition of a catalyst. Despite creating pentacoodinated zwitterionic silicates, they did not shed light on the fundamental reason behind the high reactivity of their amine-substituted silanes or the involved mechanism. A detailed understanding of the Si–H availability and dynamic processes in highercoordinated silicon chemistry is still ilimited in the literature[47] and can provide an important milestone in the development of silicon-based hydrogen storage materials.

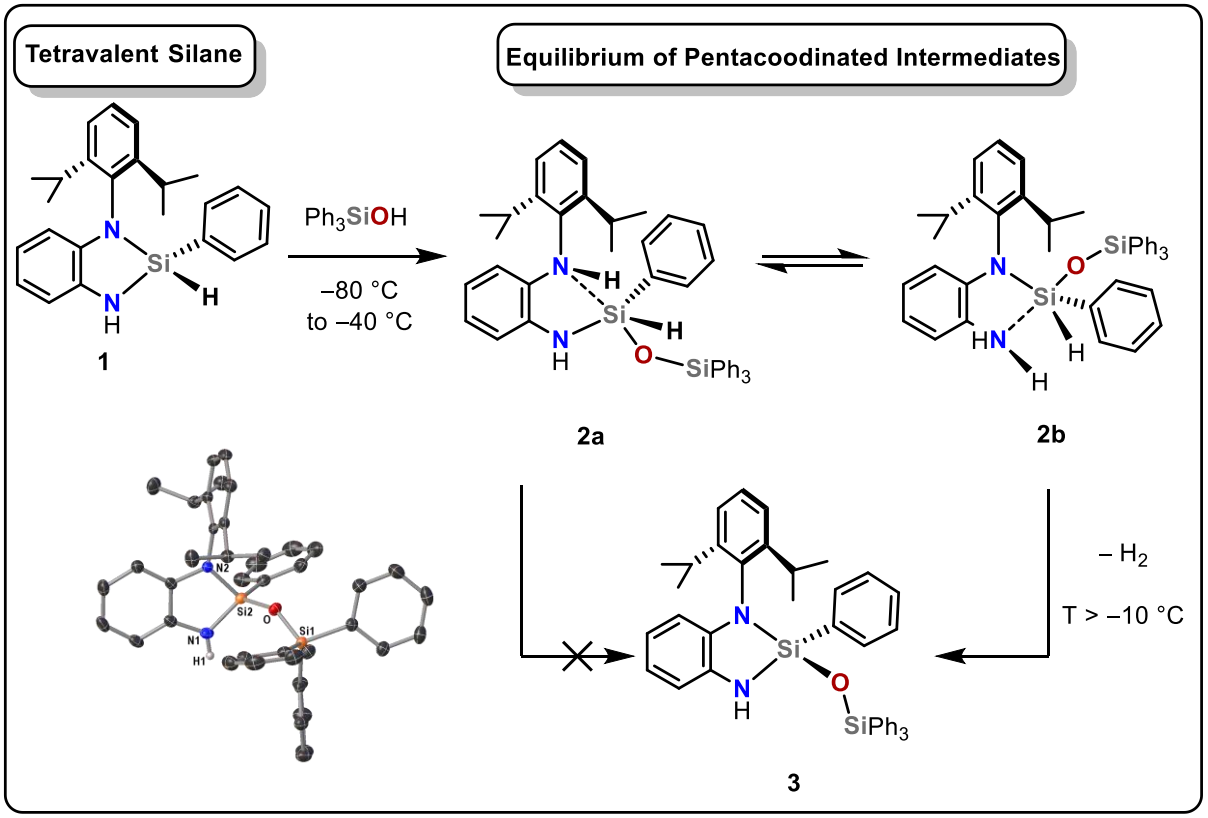

Scheme 4.1. Overall reactivity of the tetravalent silane **1** with Ph_3SiOH and the proposed equilibrium of the pentacoodinated intermediates.

4.3 Results and discussion

We present herein a tetravalent cyclic hydrosilane **1** with a Dipp (2,6-diisoproypaniline)-substituted *ortho*-phenylenediamine ligand capable of dehydrogenative siloxane formation upon reaction with silanols like Ph_3SiOH. A comprehensive mechanistic investigation using variable temperature ^{1}H and ^{29}Si NMR is given and suggests the formation of two neutral pentacoordinated siloxane intermediates **2a** and **2b** in equilibrium after reaction of a tetravalent silane with a silanol (Scheme 4.1). Quantum chemical calculations suggest that the H_2 formation takes place only from intermediate **2b** based on the lower activation barrier. The feasible capture of the intermediates at temperatures below that point makes it possible to further improve the molecular design with the goal to create a compound that can bind and lose H_2 reversibly. Our example extends the reactant scope for the preparation of highercoordinated silane intermediates from strong organolithium bases to OH- acidic nucleophiles like silanols based on an opening/closing mechanism of the diaminosilane. The dehydrogenative siloxane bond formation from **1** to **3** is quantitative and occurs at room temperature in THF. A rearrangement equilibrium of two pentacoordinated intermediates is suggested showing a reversible Si–N bond formation/dissociation of the two amine units. Literature examples of such dissociative behavior are limited to dative Si←N[37–39,42] and Si←O[41] bonding of electron donating moieties. Our investigations can provide a better understanding of the mechanisms in the context of highercoordinated main group element-based compounds and can help to tune the reactivities of hydrosilanes.

4.3.1 Variable temperature ^{1}H NMR experiments of the reaction between compound 1 and Ph_3SiOH

Our studies began with the measurements of variable temperature ^{1}H NMR spectra starting from temperatures as low as −80 °C and warming up to room temperature. Figure 4.1 displays the relevant regions for the Dipp isopropyl groups (green), the NH groups (gray) and the SiH groups (blue). The Dipp signals are diastereotopic when the DippN atom is bound to the stereogenic Si atom and therefore shows four distinct dublets. At −80 °C, one could clearly observe two different species with a ratio of 1:1.8, which we assigned to the intermediate species **2a** and **2b** based on the observation of both Si–H and NH functions. The two species can be seen as constitutional isomers as the result of Si–N bond dissociation/association processes. Warming the solution to −10 °C led to a precise spectrum of seemingly one species with one Si–H and a one NH_2 signal. In multiple cooling and thawing experiments between these temperatures, we observed essentially the same spectra for each of the respective temperatures. Given this reversibility of the system between −80 °C and −10 °C, we concluded the two intermediates to coalesce at slightly elevated temperatures showing only one averaged set of broadened signals. Similar

coalescence phenomena of enantiotopic and diastereotopic groups have been observed before for pentacoodinated silanes.[31,32,38–40,43,48,49]

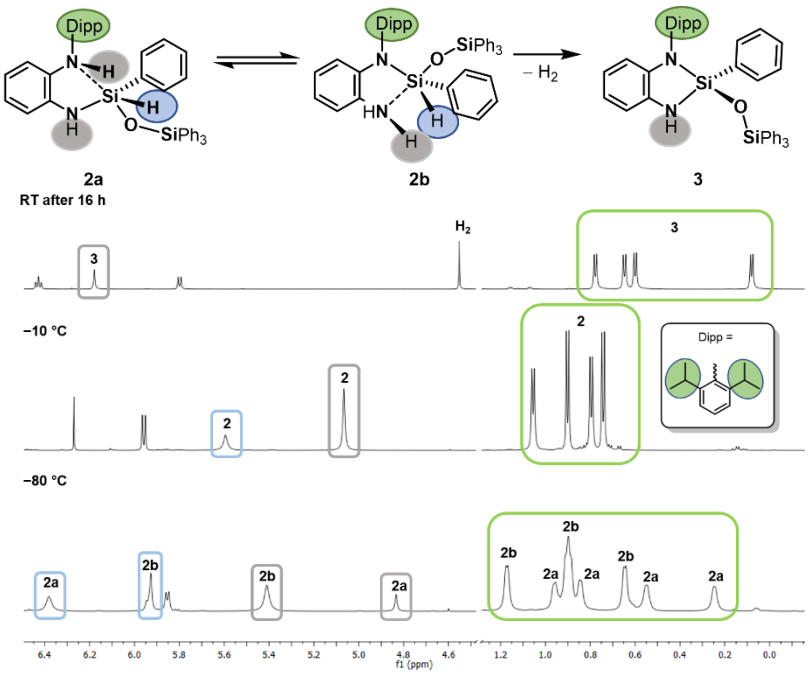

Figure 4.1. ^{1}H NMR spectra at −80 °C (bottom), −10 °C (center) and at room temperature after 16 (top). Only the relevant regions of chemical shift are shown for clarity.

Upon increasing the temperature even higher, we observed a slow decrease of the intermediates with simultaneous formation of product **3**. The full conversion to **3** is reached after keeping the reaction at room temperature overnight and is also characterized by the appearance of the characteristic H_2 signal at δ = 4.46 ppm.

4.3.2 Variable temperature ^{29}Si NMR experiments of the reaction between compound 1 and Ph_3SiOH

In order to determine the nature of the intermediates, we conducted ^{29}Si NMR measurements at the respective temperatures to obtain more information on the nature of the intermediates. Figure 4.2 shows the highfield-shifted region of interest (for the full spectra, see chapter 4.6).

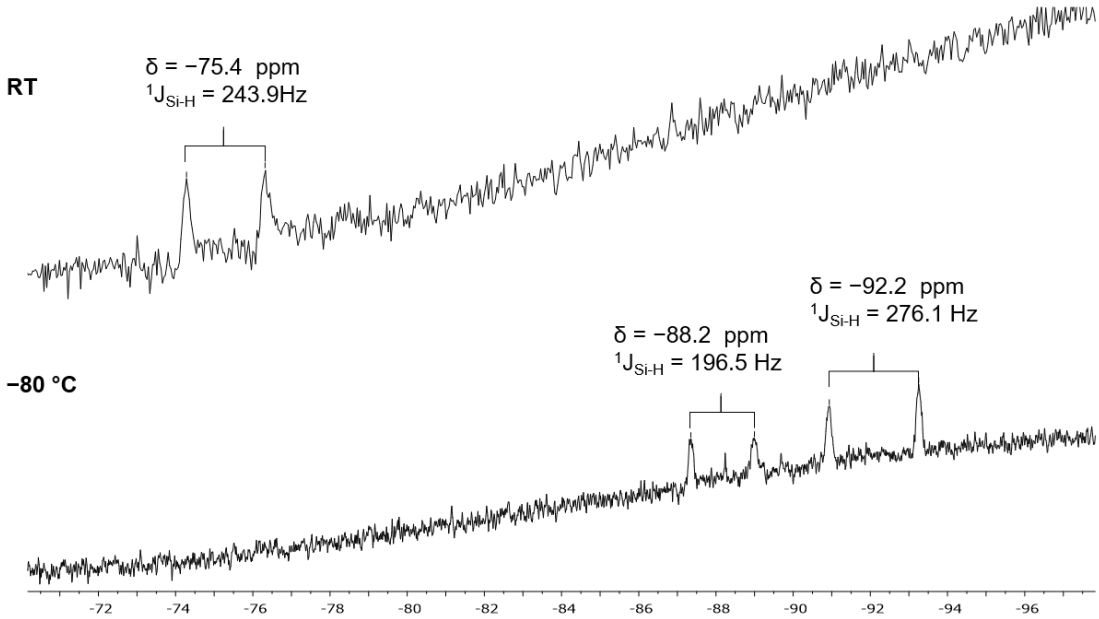

Figure 4.2. ^{29}Si NMR spectra at room temperature (top) and at −80 °C (bottom). Only the highfield region from –72 ppm to –96 ppm is displayed for clarity.

At very low temperatures of −80 °C, two sets of doublets can be observed at δ = −88.2 ppm and δ = −92.2 ppm, while only one doublet at δ = −74.4 ppm is present at room temperature. Such highfield shifted signals in ^{29}Si NMR are very characteristic for pentacoordinated silanes.[24,25,49,50] The shifts are also influenced by temperature which is why the doublet is significantly shifted towards lower field at room temperature.[39,51] The coupling constant of $^{1}J_{Si-H}$ = 243.9 Hz at room temperature lies in-between the ones for both isomers at −80 °C ($^{1}J_{Si-H}$ = 196.5 Hz and $^{1}J_{Si-H}$ = 276.1 Hz) which supports our suggestion for coalescence of the signals. Such strong difference in coupling constant can be explained by the orientation of the hydride atom in the trigonal bipyramidal arrangement in the intermediate. For **2a**, the hydride is shifted towards the axial position resulting in an elongation of the Si–H bond and therefore in a smaller coupling constant of $^{1}J_{Si-H}$ = 196.5 Hz. In **2b**, the hydride is suggested to be in the equatorial position, leading to a higher *s*-character of the bond and consequently an increase of coupling constant to $^{1}J_{Si-H}$ = 276.1 Hz.[45] The observation of two species with doublet splitting patterns at −80 °C at chemical shifts around δ = −90 ppm strongly suggests the presence of two isomeric highercoordinated silanes which coalesce into one set of signals at higher temperatures. We had significant difficulties in capturing selectively only the intermediate species of **2** in our NMR studies as either starting material **1** or product **3** were additionally present in most of our attempts. A reaction monitoring was performed also by ^{1}H NMR analysis suggesting a slow formation of **2** accompanied by even slower formation of **3** over the period of three days when the probe was kept at −20 °C (for details, see chapter 4.6).

4.3.3 Quantum chemical calculations in the reaction between compound 3 and Ph_3SiOH

In order to examine the H_2 evolution from the two intermediates **2a** and **2b** in more detail, we performed quantum chemical calculations on the M062X/6-311+G(d,p) level of theory to investigate mechanistic paths for the H_2 liberation (Scheme 4.2). For the purpose of easier calculation, the Ph_3Si group was replaced by a Me_3Si group.

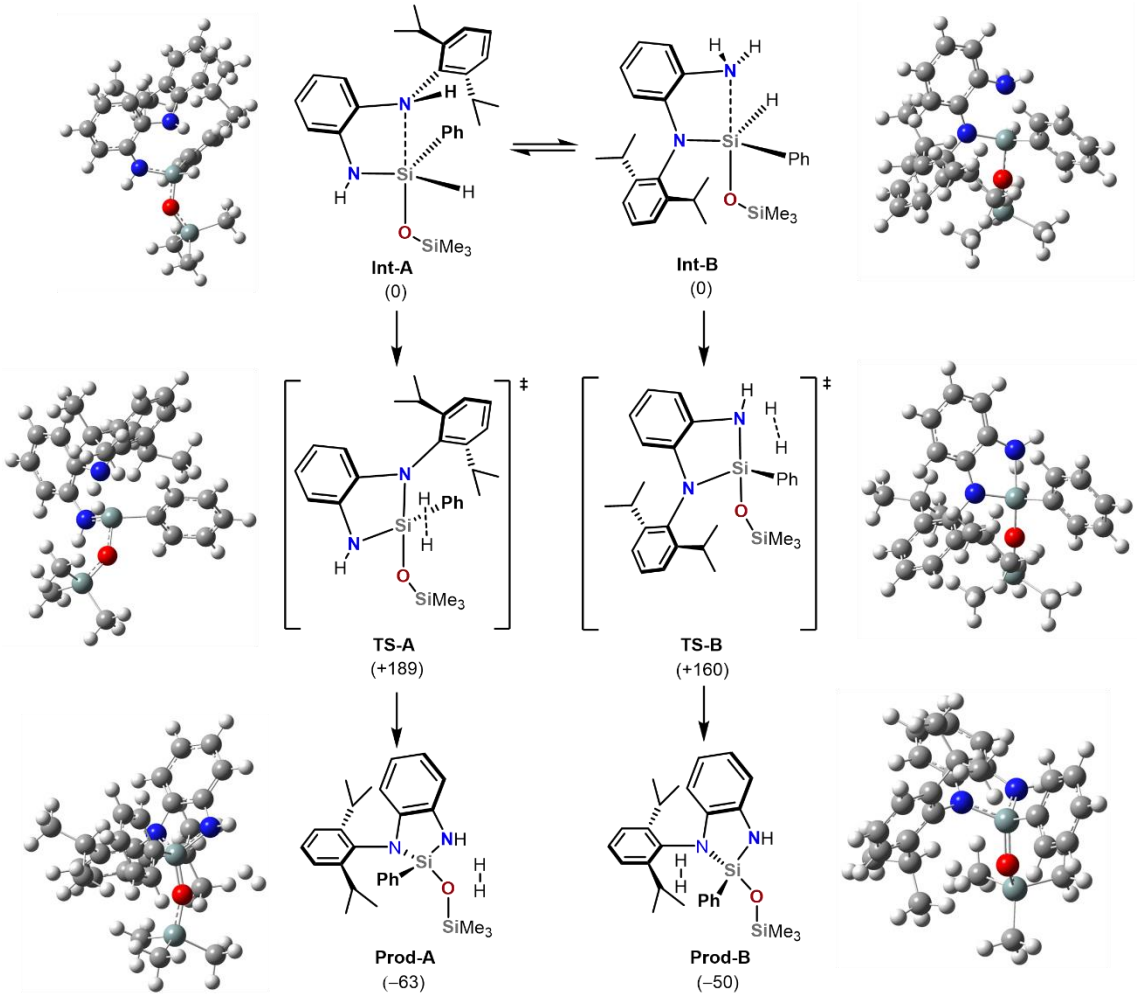

Scheme 4.2. Gibbs energies (*ΔG*) [kJ mol^{-1}] calculated on the M062X/6-311+G(d,p) level of theory for the H_2 evolution from the two intermediates.[52] For the sake of easier calculation, a simpler Me_3Si group was modelled instead of the Ph_3Si group.

Starting from the intermediates **Int-A** and **Int-B**, the hydrogen evolution occurs via spatial approach of the respective nitrogen-bound hydrogen atom and the silicon-bound hydride. The transition states **TS-A** (+189 kJ mol^{-1}) and **TS-B** (+160 kJ mol^{-1}) differ significantly in energy where **TS-B** is favored by 29 kJ mol^{-1}. After complete reaction, the products **Prod-A** (−63 kJ mol^{-1}) and **Prod-B** (−50 kJ mol^{-1}) are formed in which the H_2 molecule is still oriented closely next to the silane compound. The Gibbs energies were calculated without solvent influences. It should be noted, that the activation barriers are still much too high in their energies

given that the reaction already slowly occurs at -10 °C. However, solvent stabilization of these zwitterionic transition state structures may also play an important role and is therefore expected to further decrease the relatively high activation barriers. A modified mechanistic model also considering solvent effects is therefore currently being applied in ongoing investigations in the group of Dr. Bauer. Nonetheless, a clear trend for the preference of transition state **TS-B** in a first theoretical approach suggests that the formation of product **3** in the reaction of compound **1** with Ph_3SiOH occurs out of intermediate **2b** by dihydrogen elimination from the NH_2 and Si–H groups. Due to the equilibrium between the intermediates **2a** and **2b**, the full consumption of the starting material **1** is assured.

4.3.4 Reaction of compound 4 and Ph_3SiOH

Changing the substituent on the nitrogen atom from the aromatic Dipp group in compound **1** to a bulky aliphatic *t*Bu group in compound **4** resulted in a single or even double Si–N bond substitution by Ph_3SiOH, depending on whether triethylamine is added or not (Scheme 4.3). Formation of H_2 is not observed even at reflux conditions in both cases.

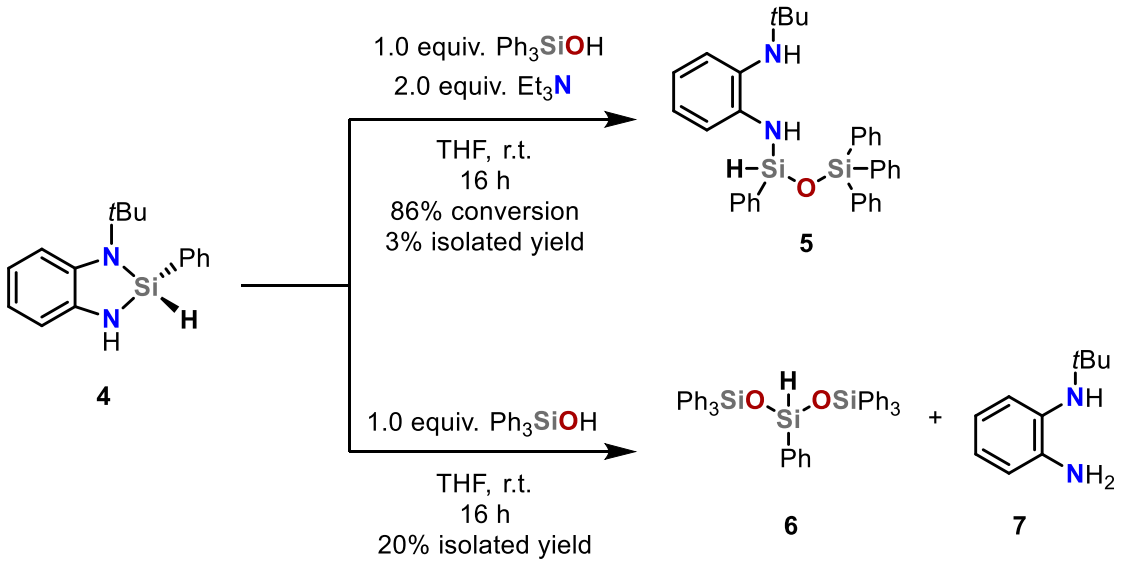

Scheme 4.3. The reaction between compound **4** and Ph_3OH with and without addition of Et_3N.

The reaction of compound **4** with one equivalent of Ph_3SiOH and additional two equivalents of triethylamine to ensure for a basic pH resulted in the isolation of compound **5**. Crude ^1H NMR showed a conversion of ca. 86% towards **5**. However, the difficult separation of compound **5** from the reaction mixture resulted in the very low isolated yield of 3%. In this case, no pentacoordinated compound is formed and thus no hydrogen elimination could occur. When no triethylamine was added to the reaction of compound **4** with one equivalent of Ph_3SiOH, we repeatedly obtained compound **6** as white crystalline solids. It is the result of a two-fold substitution of both Si–N bonds and comes along with the formation of the free diamine **7**. This particular reactivity is presubambly faciliated by the slightly acidic pH value resulting from the silanol reagent. Both of these observations underline the importance of the Dipp group for creating pentacoodinated

intermediate species to facilitate the H_2 release and additionally seem to help preventing the full removal of the diamine ligand. However, the cyclic diaminosiloxane with *t*Bu substitution was accessible by an alternative, more classical approach using a chlorosilane and $LiOSiPh_3$ (Chapter 4.6.2). We are currently working on enantiomerically pure diamine ligands for the preparation of *Si*-stereogenic analogues of **1** as mechanistic probes to get more information about the process of the here described dehydrogenative substitution reaction. Additionally, a new molecular design of similar cyclic diaminohydrosilanes is targeted in which the stability of the pentacoodinated intermediates is further improved. We seek to find a design in which the HOMO and LUMO orbitals of the intermediate and product are close in order to facilitate reversible H_2 activation.

4.4 Conclusions

In conclusion, we prepared a highly reactive cyclic diaminohydrosilane **1** by simple synthetic methods and observed an interesting reactivity with Ph_3SiOH. Siloxane bond formation takes place with loss of H_2 which was previously observed in the context of highercoordinated silicon species. Deeper mechanistic investigations based on variable temperature ^{1}H NMR and ^{29}Si NMR and quantum chemical calculations shed new light on the mechanism of this uncommon reactivity and suggested an unprecedented equilibrium of two neutral pentacoordinated intermediates one of which reacts in a dehydrogenative Si–N bond formation. The observed dissociative behavior of the Si–N bonds matches the behavior of Si←N dative bond dissociation which is discussed in the literature. The intermediates can be NMR spectroscopically distinguished at temperatures below −10 °C. Our studies provide new and important insights into mechanistic aspects regarding substitution reactions at silicon atoms and focuses on diamines as versatile substituents for controlling the reactivity of hydrosilanes. We demonstated the importance of highercoordinated species in silicon chemistry which could be of high significance for the design of reversible H_2 storage materials.

4.5 References

[1] U. Eberle, M. Felderhoff, F. Schüth, *Angew. Chem. Int. Ed.* **2009**, *48*, 6608–6630; *Angew. Chem.* **2009**, *121*, 6732–6757.

[2] a) M. Driess, *Nat. Chem.* **2012**, *4*, 525–526; b) A. V. Protchenko, K. H. Birjkumar, D. Dange, A. D. Schwarz, D. Vidovic, C. Jones, N. Kaltsoyannis, P. Mountford, S. Aldridge, *J. Am. Chem. Soc.* **2012**, *134*, 6500–6503; c) C. Shan, S. Yao, M. Driess, *Chem. Soc. Rev.* **2020**, *49*, 6733–6754.

[3] a) A. Schäfer, M. Reissmann, A. Schäfer, W. Saak, D. Haase, T. Müller, *Angew. Chem. Int. Ed.* **2011**, *50*, 12636–12638; 12636–12638; *Angew. Chem.* **2011**, *123*, 12845–12848; b) M. Reißmann, A. Schäfer, S. Jung, T. Müller, *Organometallics* **2013**, *32*, 6736–6744; c) T. J. Herrington, B. J. Ward, L. R. Doyle, J. McDermott, A. J. P. White, P. A. Hunt, A. E. Ashley, *Chem. Commun.* **2014**, *50*, 12753–12756.

[4] T. Thorwart, D. Hartmann, L. Greb, *Chem. Eur. J.* **2022**, e202202273.

[5] N. von Wolff, G. Lefèvre, J.-C. Berthet, P. Thuéry, T. Cantat, *ACS Catal.* **2016**, *6*, 4526–4535.

[6] a) R. Becker, H. Brunner, S. Mahboobi, W. Wiegrebe, *Angew. Chem. Int. Ed.* **1985**, *24*, 995–996; *Angew. Chem.* **1985**, *97*, 969–970; b) D. J. Parks, W. E. Piers, *J. Am. Chem. Soc.* **1996**, *118*, 9440–9441; c) J. Yang, T. D. Tilley, *Angew. Chem. Int. Ed.* **2010**, *49*, 10186–10188; *Angew. Chem.* **2010**, *122*, 10384–10363; d) F. Ritter, D. Mukherjee, T. P. Spaniol, A. Hoffmann, J. Okuda, *Angew. Chem. Int. Ed.* **2019**, *58*, 1818–1822; *Angew. Chem.* **2019**, *131*.1832–1836.

[7] a) Blackwell, Sonmor, Scoccitti, Piers, *Org. Lett.* **2000**, *2*, 3921–3923; b) B. H. Lipshutz, H. Shimizu, *Angew. Chem. Int. Ed.* **2004**, *43*, 2228–2230; *Angew. Chem.* **2004**, *116*, 2278–2280; c) A. K. Roy, *Adv. Organomet. Chem.* **2007**, *55*, 1–59.

[8] L.-W. Xu, Y. Chen, Y. Lu, *Angew. Chem. Int. Ed.* **2015**, *54*, 9456–9466; *Angew. Chem.* **2015**, *127*, 9590–9601.

[9] J. F. Dunne, S. R. Neal, J. Engelkemier, A. Ellern, A. D. Sadow, *J. Am. Chem. Soc.* **2011**, *133*, 16782–16785.

[10] a) S. Anga, Y. Sarazin, J.-F. Carpentier, T. K. Panda, *ChemCatChem* **2016**, *8*, 1373–1378; b) K. Kuciński, G. Hreczycho, *ChemCatChem* **2017**, *9*, 1868–1885; c) M. B. Reuter, K. Hageman, R. Waterman, *Chem. Eur. J.* **2021**, *27*, 3251–3261.

[11] a) Z. M. Michalska, *Transition Met. Chem.* **1980**, *5*, 125–129; b) D. Zhou, Y. Kawakami, *Macromolecules* **2005**, *38*, 6902–6908; c) Y. Satoh, M. Igarashi, K. Sato, S. Shimada, *ACS Catal.* **2017**, *7*, 1836–1840; d) T. Takeshita, K. Sato, Y. Nakajima, *Dalton Trans.* **2018**, *47*, 17004–17010; e) J. Kaźmierczak, K. Kuciński, D. Lewandowski, G. Hreczycho, *Inorg. Chem.* **2019**, *58*, 1201–1207; f) S. Pattanaik, C. Gunanathan, *ACS Catal.* **2019**, *9*, 5552–5561.

[12] a) H. Ito, K. Takagi, T. Miyahara, M. Sawamura, *Org. Lett.* **2005**, *7*, 3001–3004; b) T. Stahl, H. F. T. Klare, M. Oestreich, *J. Am. Chem. Soc.* **2013**, *135*, 1248–1251; c) J. M.

Cardoso, R. Lopes, B. Royo, *J. Organomet. Chem.* **2015**, *775*, 173–177; d) T. Mitsudome, T. Urayama, Z. Maeno, T. Mizugaki, K. Jitsukawa, K. Kaneda, *Chem. Eur. J.* **2015**, *21*, 3202–3205; e) S. Pramanik, A. Fernandes, V. Liautard, M. Pucheault, F. Robert, Y. Landais, *Chem. Eur J.* **2019**, *25*, 728–732; f) H. Zhang, D. Zhao, *ACS Catal.* **2021**, *11*, 10748–10753; g) J. Gao, P.-L. Mai, Y. Ge, W. Yuan, Y. Li, C. He, *ACS Catal.* **2022**, *12*, 8476–8483.

[13] a) M. A. Brook, *Chem. Eur. J.* **2018**, *24*, 8458–8469; b) N. Li, B.-T. Guan, *Eur. J. Inorg. Chem.* **2019**, *2019*, 2231–2235; c) K. Kuciński, H. Stachowiak, G. Hreczycho, *Eur. J. Org. Chem.* **2020**, *2020*, 4042–4049; d) K. Kuciński, H. Stachowiak, G. Hreczycho, *Inorg. Chem. Front.* **2020**, *7*, 4190–4196.

[14] M. Weinmann, O. Walter, G. Huttner, H. Lang, *J. Organomet. Chem.* **1998**, *561*, 131–141.

[15] Y. Domoto, A. Fukushima, Y. Kasuga, S. Sase, K. Goto, T. Kawashima, *Org. Lett.* **2010**, *12*, 2586–2589.

[16] Y. Domoto, K. Saruhashi, A. Fukushima, S. Sase, K. Goto, T. Kawashima, *Phosphorus Sulfur Silicon Relat. Elem.* **2010**, *185*, 1221–1229.

[17] Y. Domoto, S. Sase, K. Goto, *Chem. Eur. J.* **2014**, *20*, 15998–16005.

[18] J. Boyer, C. Breliere, R. Corriu, A. Kpoton, M. Poirier, G. Royo, *J. Organomet. Chem.* **1986**, *311*, C39-C43.

[19] A. Yoshida, K. Goto, T. Kawashima, *Bull. Chem. Soc. Jpn.* **2006**, *79*, 793–795.

[20] K. Kikushima, M. Grellier, M. Ohashi, S. Ogoshi, *Angew. Chem. Int. Ed.* **2017**, *56*, 16191–16196; *Angew. Chem.* **2017**, *129*, 16409–16414.

[21] a) A. Hosomi, H. Hayashida, S. Kohra, Y. Tominaga, *J. Chem. Soc., Chem. Commun.* **1986**, 1411; b) S. Kobayashi, M. Yasuda, I. Hachiya, *Chem. Lett.* **1996**, *25*, 407–408; c) R. Schiffers, H. Kagan, *Synlett* **1997**, *1997*, 1175–1178.

[22] a) A. A. Toutov, W.-B. Liu, K. N. Betz, A. Fedorov, B. M. Stoltz, R. H. Grubbs, *Nature* **2015**, *518*, 80–84; b) A. A. Toutov, K. N. Betz, D. P. Schuman, W.-B. Liu, A. Fedorov, B. M. Stoltz, R. H. Grubbs, *J. Am. Chem. Soc.* **2017**, *139*, 1668–1674; c) T. Yoshida, L. Ilies, E. Nakamura, *Org. Lett.* **2018**, *20*, 2844–2847.

[23] M. J. Bearpark, G. S. McGrady, P. D. Prince, J. W. Steed, *J. Am. Chem. Soc.* **2001**, *123*, 7736–7737.

[24] P. D. Prince, M. J. Bearpark, G. S. McGrady, J. W. Steed, *Dalton Trans.* **2008**, 271–282.

[25] R. Corriu, C. Guérin, B. Henner, Q. Wang, *Inorg. Chim. Acta* **1992**, *198-200*, 705–713.

[26] F. Ebner, L. Greb, *J. Am. Chem. Soc.* **2018**, *140*, 17409–17412.

[27] a) E. F. Perozzi, J. C. Martin, *J. Am. Chem. Soc.* **1979**, *101*, 1591–1593; b) E. F. Perozzi, R. S. Michalak, G. D. Figuly, W. H. Stevenson, D. Dess, M. R. Ross, J. C. Martin, *J. Org. Chem.* **1981**, *46*, 1049–1053; c) W. H. Stevenson, S. Wilson, J. C. Martin, W. B. Farnham, *J. Am. Chem. Soc.* **1985**, *107*, 6340–6352; d) T. Deis, J. Maury, F. Medici, M. Jean, J. Forte, N. Vanthuyne, L. Fensterbank, G. Lemière, *Angew. Chem. Int. Ed.* **2022**, *61*, e202113836; *Angew. Chem.* **2022**, *134*, e202113836.

[28] L. J. P. van der Boon, L. van Gelderen, T. R. de Groot, M. Lutz, J. C. Slootweg, A. W. Ehlers, K. Lammertsma, *Inorg. Chem.* **2018**, *57*, 12697–12708.

[29] E. P. A. Couzijn, D. W. F. van den Engel, J. C. Slootweg, F. J. J. de Kanter, A. W. Ehlers, M. Schakel, K. Lammertsma, *J. Am. Chem. Soc.* **2009**, *131*, 3741–3751.

[30] E. P. A. Couzijn, M. Schakel, F. J. J. de Kanter, A. W. Ehlers, M. Lutz, A. L. Spek, K. Lammertsma, *Angew. Chem. Int. Ed.* **2004**, *43*, 3440–3442; *Angew. Chem.* **2004**, *116*, 3522–3524.

[31] R. Tacke, B. Pfrommer, M. Pülm, R. Bertermann, *Chem. Ber.* **1999**, *1999*, 807–816.

[32] R. Tacke, R. Bertermann, A. Biller, O. Dannappel, M. Pülm, R. Willeke, *Chem. Ber.* **1999**, *1999*, 795–805.

[33] R. Tacke, R. Bertermann, C. Burschka, S. Dragota, M. Penka, I. Richter, *J. Am. Chem. Soc.* **2004**, *126*, 14493–14505.

[34] J. O. Bauer, C. Strohmann, *J. Am. Chem. Soc.* **2015**, *137*, 4304–4307.

[35] A. R. Bassindale, S. J. Glynn, P. G. Taylor in *An Interscience publication* (Eds.: S. Patai, Z. Rappoport, Y. Apeloig), Wiley, Chichester, **1998**, 495–511.

[36] a) R. J. Corriu, C. Guerin, *J. Organomet. Chem.* **1980**, *198*, 231–320; b) R. Corriu, C. Guerin in *Advances in Organometallic Chemistry* (Eds.: F. G. A. Stone, R. West), Academic Press, New York, **1982**, 265–312.

[37] R. J. Corriu, A. Kpoton, M. Poirier, G. Royo, J. Y. Corey, *J. Organomet. Chem.* **1984**, *277*, C25-C30.

[38] F. H. Carre, R. J. P. Corriu, G. F. Lanneau, Z. Yu, *Organometallics* **1991**, *10*, 1236–1243.

[39] I. Kalikhman, S. Krivonos, A. Ellern, D. Kost, *Organometallics* **1996**, *15*, 5073–5076.

[40] A. R. Bassindale, D. J. Parker, P. G. Taylor, R. Turtle, *Z. Anorg. Allg. Chem.* **2009**, *635*, 1288–1294.

[41] O. V. Kuznetsova, A. N. Egorochkin, V. V. Negrebetsky, N. M. Khamaletdinova, L. G. Domratcheva-Lvova, *J. Phys. Org. Chem.* **2012**, *25*, 658–666.

[42] S. Schlecht, M. Finze, R. Bertermann, W. Frank, A. Domann, M. Braun, *Chem. Ber.* **2013**, *2013*, 1488–1492.

[43] L. J. P. van der Boon, J. H. Hendriks, D. Roolvink, S. J. O'Kennedy, M. Lutz, J. C. Slootweg, A. W. Ehlers, K. Lammertsma, *Chem. Ber.* **2019**, *2019*, 3318–3328.

[44] T. Ikeuchi, K. Hirano, M. Uchiyama, *J. Am. Chem. Soc.* **2021**, *143*, 4879–4885.

[45] N. Rot, T. Nijbacker, R. Kroon, F. J. J. de Kanter, F. Bickelhaupt, M. Lutz, A. L. Spek, *Organometallics* **2000**, *19*, 1319–1324.

[46] a) R. Tacke, M. Mallak, R. Willeke, *Angew. Chem. Int. Ed.* **2001**, *40*, 2339–2341; *Angew. Chem.* **2001**, *113*, 2401–2403; b) R. Bertermann, A. Biller, M. Kaupp, M. Penka, O. Seiler, R. Tacke, *Organometallics* **2003**, *22*, 4104–4110; c) D. Troegel, C. Burschka, S. Riedel, M. Kaupp, R. Tacke, *Angew. Chem. Int. Ed.* **2007**, *46*, 7001–7005; *Angew. Chem.* **2007**, *119*, 7131–7135; d) G. González-García, J. A. Gutiérrez, S. Cota, S. Metz, R. Bertermann, C. Burschka, R. Tacke, *Z. Anorg. Allg. Chem.* **2008**, *634*, 1281–1286.

[47] a) E. P. A. Couzijn, A. W. Ehlers, M. Schakel, K. Lammertsma, *J. Am. Chem. Soc.* **2006**, *128*, 13634–13639; b) E. P. A. Couzijn, J. C. Slootweg, A. W. Ehlers, K. Lammertsma, *Z. Anorg. Allg. Chem.* **2009**, *635*, 1273–1278.

[48] V. V. Negrebetsky, P. G. Taylor, E. P. Kramarova, S. Y. Bylikin, I. Y. Belavin, A. G. Shipov, A. R. Bassindale, Y. I. Baukov, *J. Organomet. Chem.* **2006**, *691*, 3976–3988.

[49] D. Kost, I. Kalikhman in *An Interscience publication* (Eds.: S. Patai, Z. Rappoport, Y. Apeloig), Wiley, Chichester, **1998**, pp. 1339–1445.

[50] A. I. Albanov, L. I. Gubanova, M. F. Larin, V. A. Pestunovich, M. G. Voronkov, *J. Organomet. Chem.* **1983**, *244*, 5–16.

[51] B. M. Kraft, W. W. Brennessel, *Organometallics* **2014**, *33*, 158–171.

[52] Frisch, M. J.; Trucks, G. W.; Schlegel, H. B.; Scuseria, G. E.; Robb, M. A.; Cheeseman, J. R.; Scalmani, G.; Barone, V.; Mennucci, B.; Petersson, G. A.; Nakatsuji, H.; Caricato, M.; Li, X.; Hratchian, H. P.; Izmaylov, A. F.; Bloino, J.; Zheng, G.; Sonnenberg, J. L.; Hada, M.; Ehara, M.; Toyota, K.; Fukuda, R.; Hasegawa, J.; Ishida, M.; Nakajima, T.; Honda, Y.; Kitao, O.; Nakai, H.; Vreven, T.; Montgomery, J. A., Jr.; Peralta, J. E.; Ogliaro, F.; Bearpark, M.; Heyd, J. J.; Brothers, E.; Kudin, K. N.; Staroverov, V. N.; Kobayashi, R.; Normand, J.; Raghavachari, K.; Rendell, A.; Burant, J. C.; Iyengar, S. S.; Tomasi, J.; Cossi, M.; Rega, N.; Millam, J. M.; Klene, M.; Knox, J. E.; Cross, J. B.; Bakken, V.; Adamo, C.; Jaramillo, J.; Gomperts, R.; Stratmann, R. E.; Yazyev, O.; Austin, A. J.; Cammi, R.; Pomelli, C.; Ochterski, J. W.; Martin, R. L.; Morokuma, K.; Zakrzewski, V. G.; Voth, G. A.; Salvador, P.; Dannenberg, J. J.; Dapprich, S.; Daniels, A. D.; Farkas, O.; Foresman, J. B.; Ortiz, J. V.; Cioslowski, J.; Fox, D. J. *Gaussian 09*, revision E.01; Gaussian, Inc.: Wallingford, CT, **2009**.

4.6 Syntheses and characterizations

4.6.1 General remarks

All experiments were performed in an inert atmosphere of purified nitrogen by using standard Schlenk techniques or an MBraun Unilab 1200/780 glovebox. Glassware was heated at 600 °C prior to use. Diethyl ether (Et_2O), dichloromethane (DCM), hexane, pentane and tetrahydrofuran (THF) were dried and degassed with an MBraun SP800 solvent purification system. *n*-Butyllithium (2.5 M or 1.6 M solution in hexane, Merck KGaA), trichlorophenylsilane (97%, Alfa Aesar), triphenylsilanol (98%, Merck KGaA) and dichlorophenylsilane (96%, abcr GmbH) were used as received without any further purification. Triethylamine (≥99%, Merck KGaA) was heated at reflux over CaH_2 and distilled prior to use. Compounds **S1** and **S2** were synthesized according to a previously published procedure.[1] C_6D_6 and THF-d_8 used for NMR spectroscopy were dried over 3 Å molecular sieves and degassed by a standard freeze-pump-thaw procedure. NMR spectra were either recorded using a Bruker Avance 400 (400.13 MHz), a Bruker Avance III HD 400 (400.13 MHz) or a Bruker Avance III HD 600 (600.13 MHz). Chemical shifts (δ) are reported in parts per million (ppm). ^1H and $^{13}C\{^1H\}$ NMR spectra are referenced to tetramethylsilane ($SiMe_4$, δ = 0.0 ppm) as external standard, with the deuterium signal of the solvent serving as internal lock and the residual solvent signal as an additional reference. ^{29}Si NMR spectra are referenced to $SiMe_4$. For the assignment of the multiplicities, the following abbreviations are used: s = singlet, d = doublet, t = triplet, sept = septet, m = multiplet. For simplicity, multiplets of order higher than one are described approximating them to the closest first-order type. High-resolution mass spectrometry was carried out on a Jeol AccuTOF GCX and an Agilent Q-TOF 6540 UHD spectrometer. Elemental analyses were performed on a Vario MICRO cube apparatus.

4.6.2 Synthesis of compounds

4.6.2.1 Compound 1

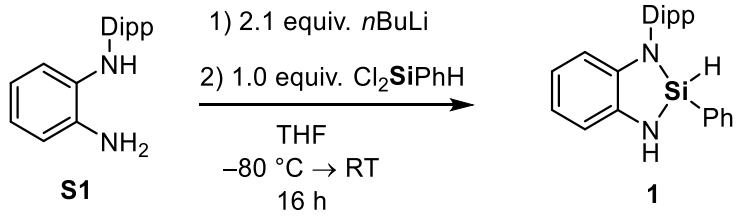

Compound **S1** (2.68 g, 10.0 mmol, 1.0 equiv.) was dissolved in 50 mL of THF and the solution cooled down to −80 °C. *n*-Butyllithium (8.0 mL of a 2.5 M solution in hexane, 20.0 mmol, 2.0 equiv.) was added dropwise and the mixture was stirred for 10 min while warming up to room temperature. The formed brown suspension was again cooled down to −80 °C and dichlorophenylsilane (1.46 mL, 10.0 mmol, 1.0 equiv.) was added via syringe. The mixture was

stirred for 16 h. Then, all volatiles were removed *in vacuo*. The crude residue was extracted with pentane (3 × 5 mL) and the remaining solids were removed via cannula filtration. The clear brown filtrates were collected and stored at −20 °C overnight after which colourless crystals were obtained. The crystals were isolated via cannula filtration and washed with pentane to afford compound 1 as a white crystalline solid (535 mg, 1.4 mmol, 14%) suitable for single-crystal X-ray diffraction analysis.

^{1}H NMR (400 MHz, C_6D_6, 298 K): *δ*[ppm] = 0.37 [d, $^{3}J_{H\text{-}H}$ = 6.7 Hz, 3H, CH(C*H*$_3$)$_2$], 1.03 [d, $^{3}J_{H\text{-}H}$ = 6.8 Hz, 6H, CH(C*H*$_3$)$_2$], 1.31 [d, $^{3}J_{H\text{-}H}$ = 6.8 Hz, 3H, CH(C*H*$_3$)$_2$], 3.02 [sept, $^{3}J_{H\text{-}H}$ = 6.8 Hz, 1H, C*H*(CH$_3$)$_2$], 3.16 [s, 1H, N*H*], 3.32 [sept, $^{3}J_{H\text{-}H}$ = 6.8 Hz, 1H, C*H*(CH$_3$)$_2$], 6.14 [s, 1H, Si*H*], 6.13–6.17 [m, 1H, *H*$_{Ar}$], 6.59–6.62 [m, 1H, *H*$_{Ar}$], 6.63–6.69 [m, 1H, *H*$_{Ar}$], 6.76–6.82 [m, 1H, *H*$_{Ar}$], 7.00–7.09 [m, 3H, *H*$_{Ar}$], 7.12–7.18 [m, 2H, *H*$_{Ar}$], 7.36–7.41 [m, 2H, *H*$_{Ar}$]. **^{13}C{^{1}H} NMR** (101 MHz, C_6D_6, 298 K): *δ*[ppm] = 23.6 [s, CH*C*H$_3$], 24.8 [s, CH*C*H$_3$], 25.0 [s, CH*C*H$_3$], 25.5 [s, CH*C*H$_3$], 28.2 [s, *C*HCH$_3$], 28.5 [s, *C*HCH$_3$], 110.3 [s, *C*H$_{Ar}$], 11.3 [s, *C*H$_{Ar}$], 118.5 [s, *C*H$_{Ar}$], 118.7 [s, *C*H$_{Ar}$], 124.6 [s, *C*H$_{Ar}$], 124.9 [s, *C*H$_{Ar}$], 128.1 [s, *C*H$_{Ar}$], 128.3 [s, *C*H$_{Ar}$], 131.6 [s, *C*H$_{Ar}$], 134.1 [s, *C*$_{Ar}$], 134.4 [s, *C*$_{Ar}$], 135.1 [s, *C*H$_{Ar}$], 138.3 [s, *C*$_{Ar}$], 141.3 [s, *C*$_{Ar}$], 148.6 [s, *C*$_{Ar}$], 149.3 [s, *C*$_{Ar}$]. **^{29}Si{^{1}H} NMR** (79 MHz, C_6D_6, 298 K): *δ*[ppm] = −13.8 [s, *Si*]. **^{29}Si NMR** (79 MHz, C_6D_6, 298 K): *δ*[ppm] = −13.8 [dm, $^{1}J_{Si\text{-}H}$ = 233.2 Hz, *Si*]. **CHN Analysis** $C_{24}H_{28}N_2Si$: calculated: C 77.37, H 7.58, N 7.52, Si 7.54; found: C 77.38, H 7.17, N 7.30. **HR-MS(FD+)**, calculated m/z for $C_{24}H_{28}N_2Si$ [M+H$^+$]: 372.20239; found: 372.20163.

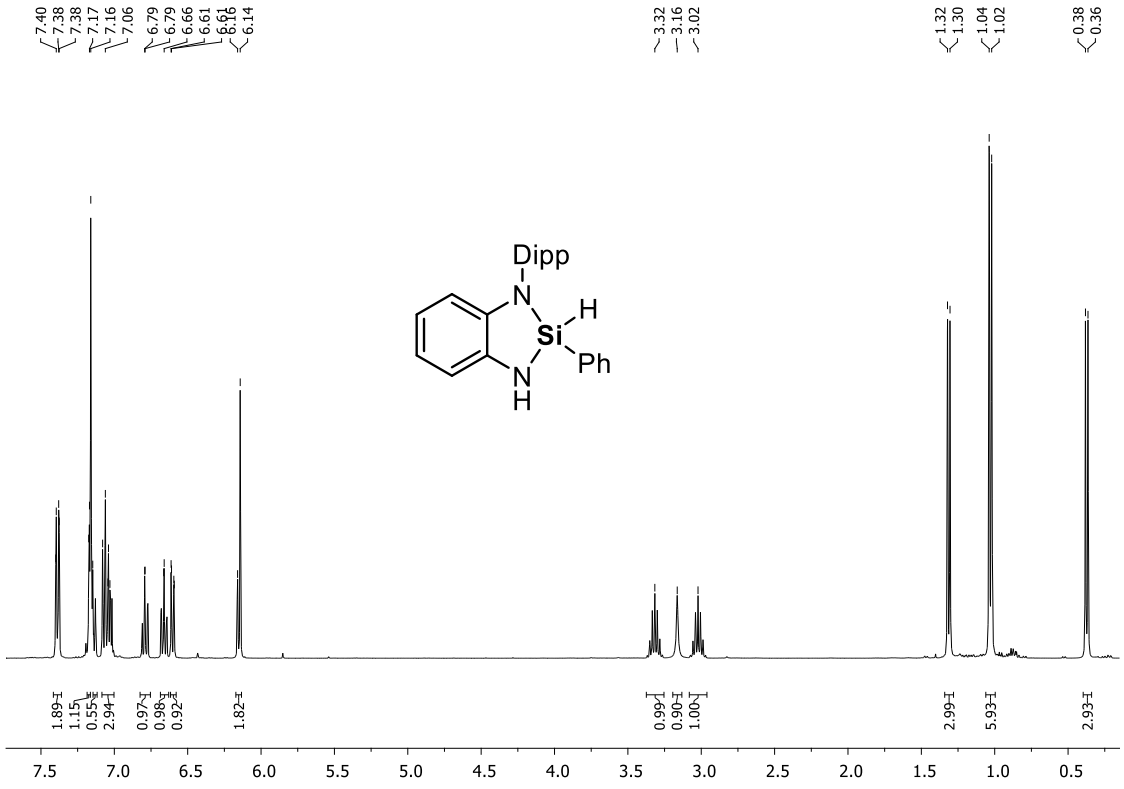

Figure S4.1. ^{1}H NMR spectrum (C_6D_6, 298 K) of **1**.

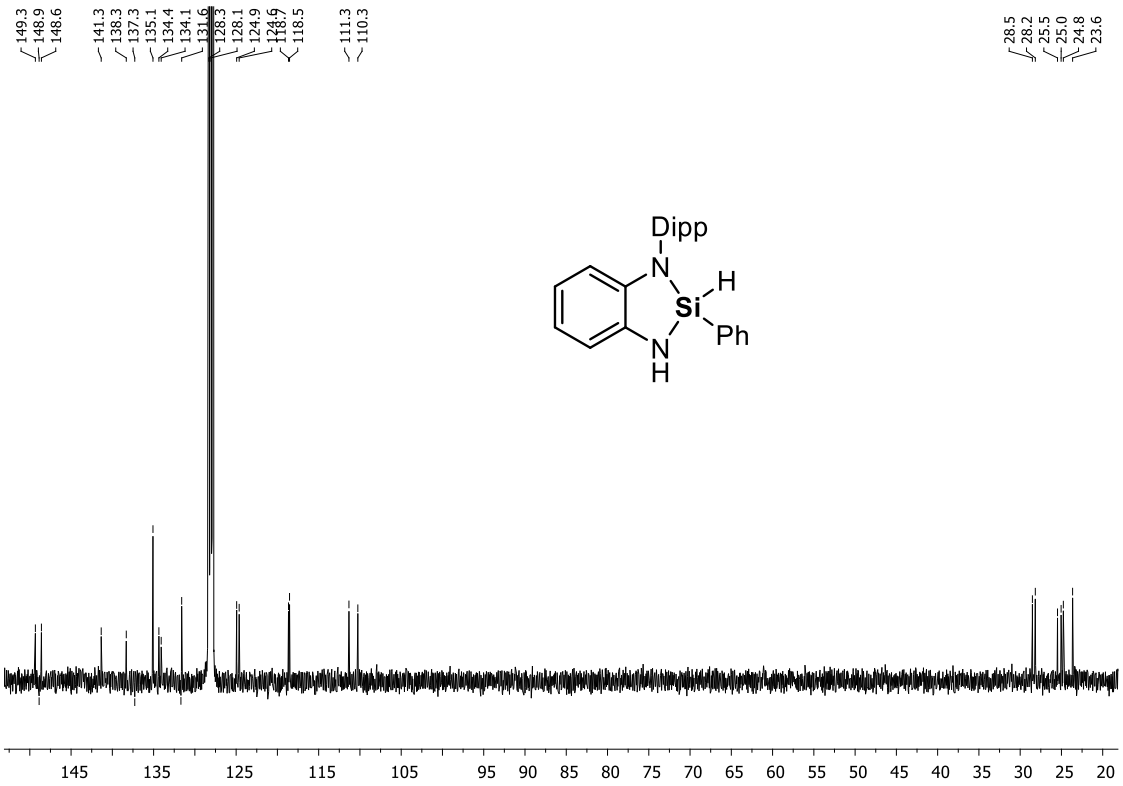

Figure S4.2. $^{13}C\{^{1}H\}$ NMR spectrum (C_6D_6, 298 K) of **1**.

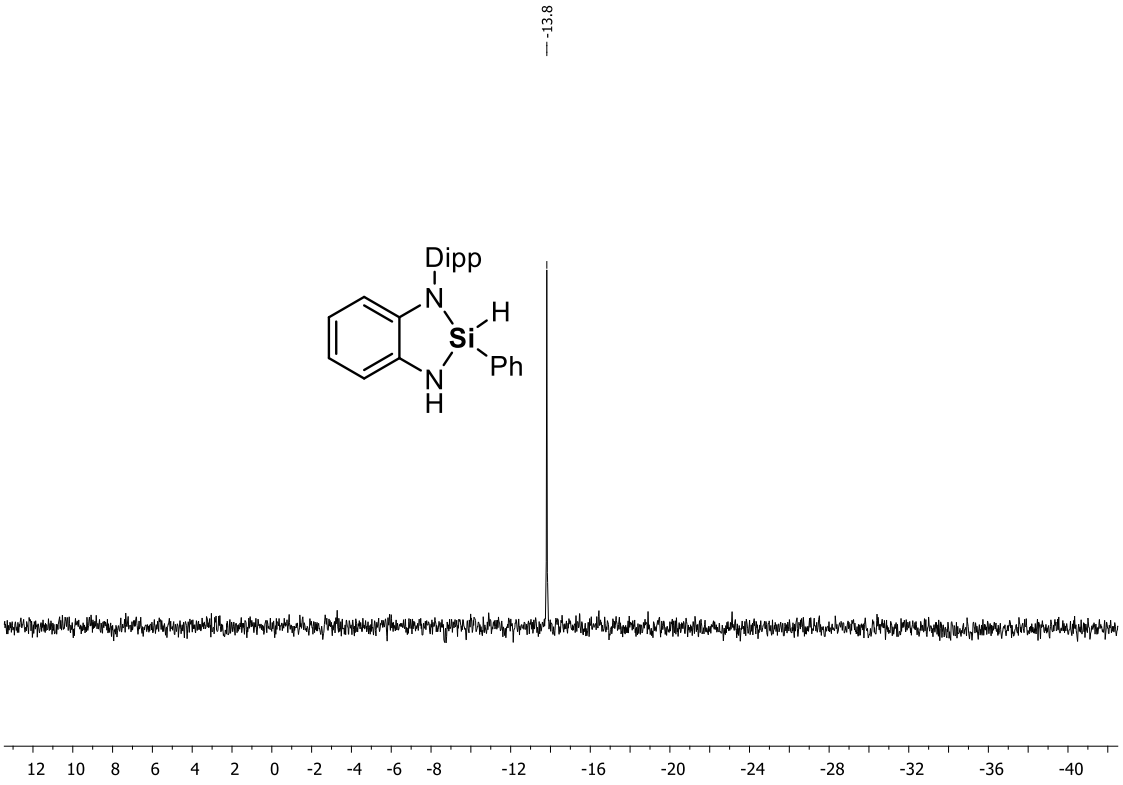

Figure S4.3. $^{29}Si\{^{1}H\}$ NMR spectrum (C_6D_6, 298 K) of **1**.

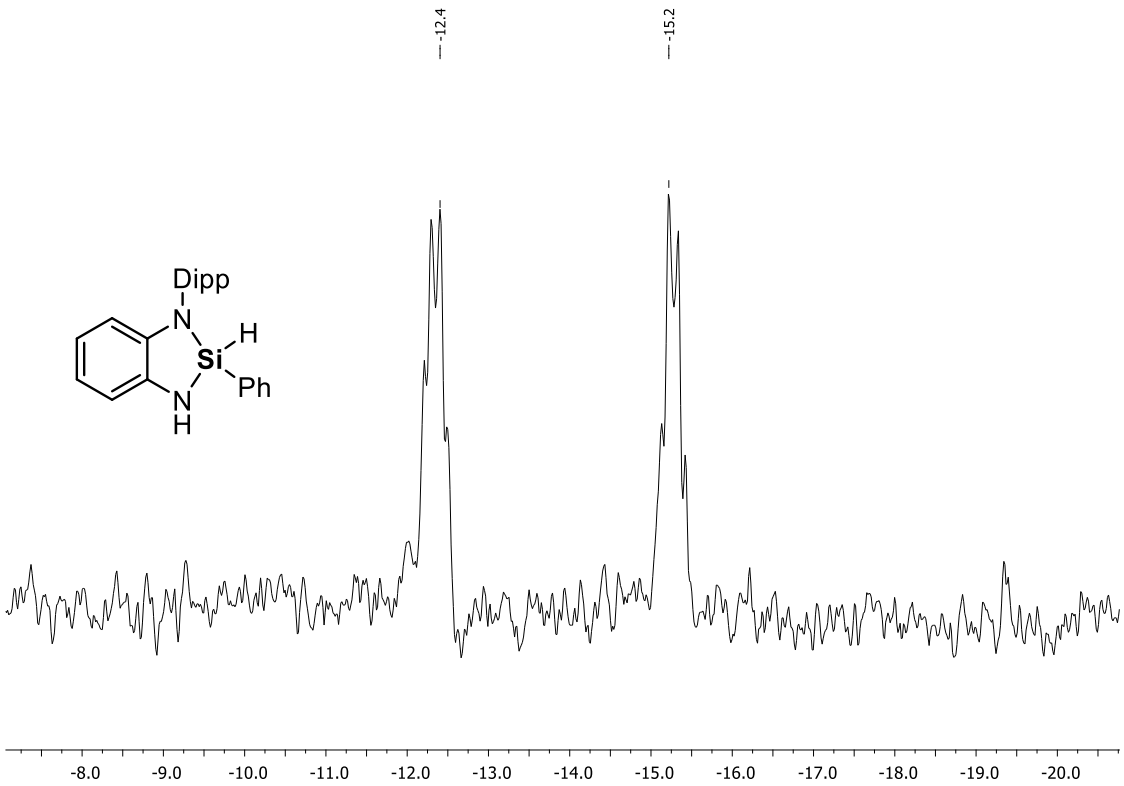

Figure S4.4. ^{29}Si NMR spectrum (C_6D_6, 298 K) of **1**.

4.6.2.2 Compound 4

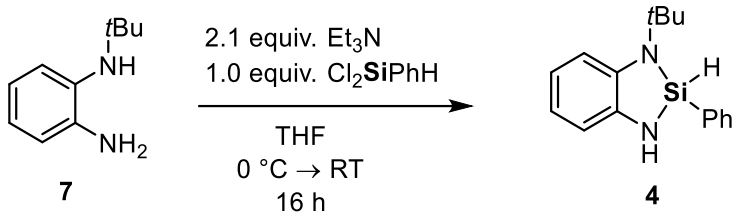

Compound **7** (1.64 g, 10.0 mmol, 1.0 equiv.) and triethylamine (2.90 mL, 21.0 mmol, 2.1 equiv.) were dissolved in 100 mL of THF and the solution cooled down to 0 °C. Dichlorophenylsilane (1.46 mL, 10.0 mmol, 1.0 equiv.) was added via syringe. The mixture was stirred for 16 h. Then, the solids were filtered off via cannula filtration and he filtrate was dried *in vacuo*. The crude residue was extracted with hexane (4 × 10 mL) and the remaining solids were removed via cannula filtration. The clear brown filtrates were collected and dried *in vacuo* to obtain **4** as a brown wax (1.16 g, 4.4 mmol, 44%).

^{1}H NMR (400 MHz, C_6D_6, 298 K): *δ*[ppm] = 1.30 [s, 9H, CHC*H*$_3$], 3.00 [s, 1H, N*H*], 6.14 [s, 1H, Si*H*], 6.46–6.49 [m, 1H, *H*$_{Ar}$], 6.73–6.87 [m, 3H, *H*$_{Ar}$], 6.92–6.96 [m, 1H, *H*$_{Ar}$], 7.10–7.15 [m, 1H, *H*$_{Ar}$], 7.16–7.19 [m, 1H, *H*$_{Ar}$], 7.46–7.51[m, 2H, *H*$_{Ar}$]. **^{13}C{^{1}H} NMR** (101 MHz, C_6D_6, 298 K): *δ*[ppm] = 29.6 [s, C(*C*H$_3$)$_3$], 52.5 [s, *C*(CH$_3$)$_3$], 11.3 [s, *C*H$_{Ar}$], 112.9 [s, *C*H$_{Ar}$], 117.7 [s, *C*H$_{Ar}$], 117.8 [s, *C*H$_{Ar}$], 128.5 [s, *C*H$_{Ar}$], 131.1 [s, *C*H$_{Ar}$], 134.0 [s, *C*H$_{Ar}$], 138.1 [s, *C*$_{Ar}$], 138.4 [s, *C*$_{Ar}$], 140.7 [s, *C*$_{Ar}$]. **^{29}Si{^{1}H} NMR** (79 MHz, C_6D_6, 298 K): *δ*[ppm] = −18.0 [s, *Si*]. **^{29}Si NMR** (79 MHz, C_6D_6, 298 K): *δ*[ppm] = [dm, $^{1}J_{Si\text{-}H}$ = −18.0 [dm, $^{1}J_{SiH}$ = 233.6 Hz, *Si*]. **CHN Analysis** $C_{16}H_{20}N_2Si$ • 0.1 DCM: calculated: C 69.83, H 7.35, N 10.12; found: C 69.87, H 7.52, N 10.05. **HR-MS(EI+)**, calculated m/z for $C_{16}H_{20}N_2Si$ [M+H$^+$]: 268.13903; found: 268.13984.

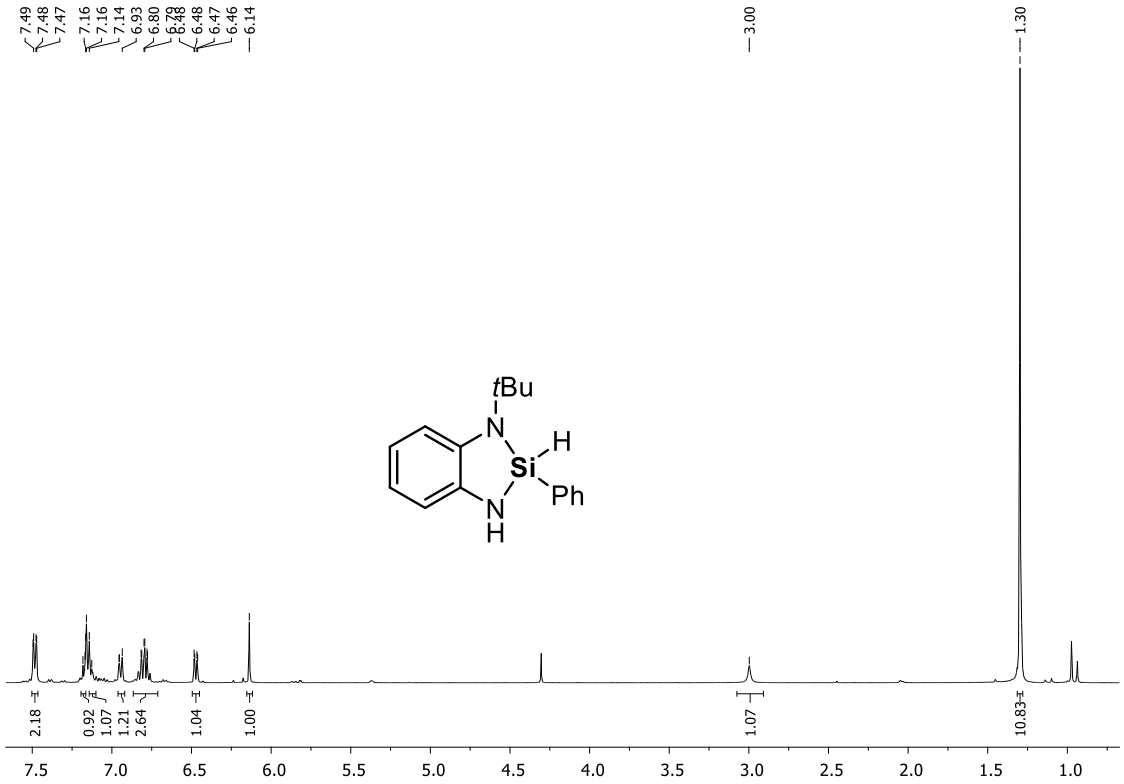

Figure S4.5. ^{1}H NMR spectrum (C_6D_6, 298 K) of **4**.

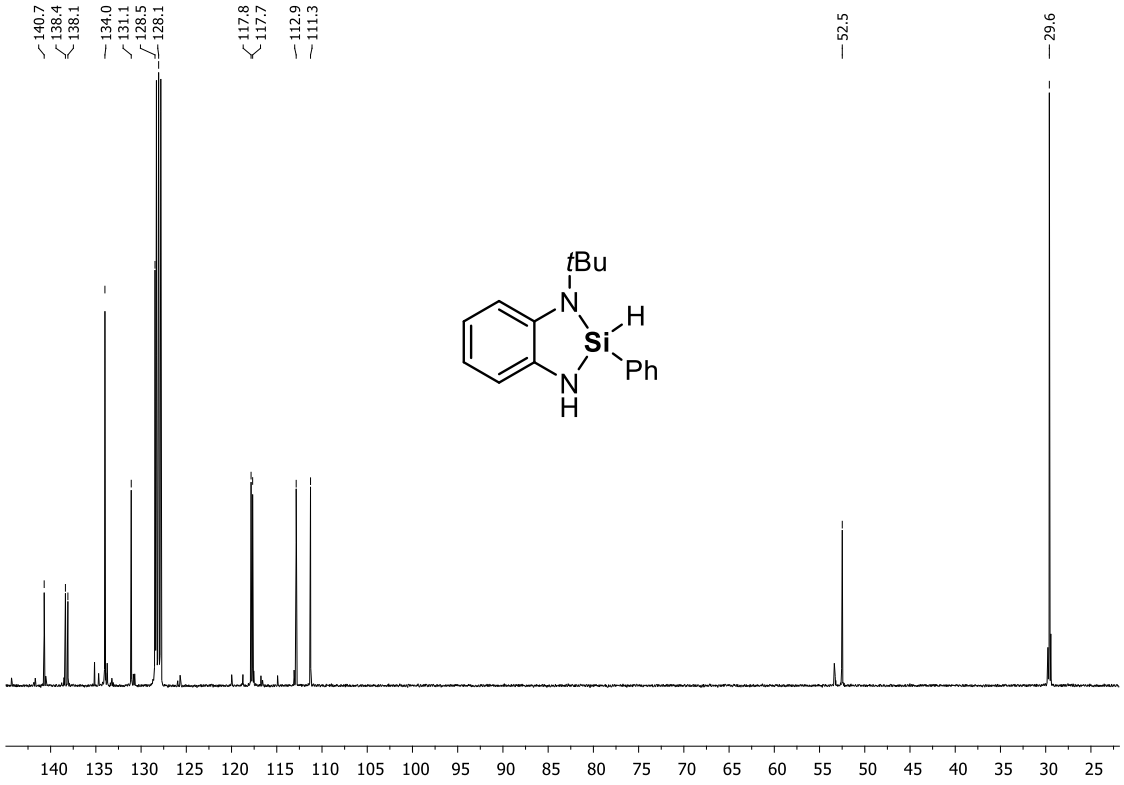

Figure S4.6. $^{13}C\{^{1}H\}$ NMR spectrum (C_6D_6, 298 K) of **4**.

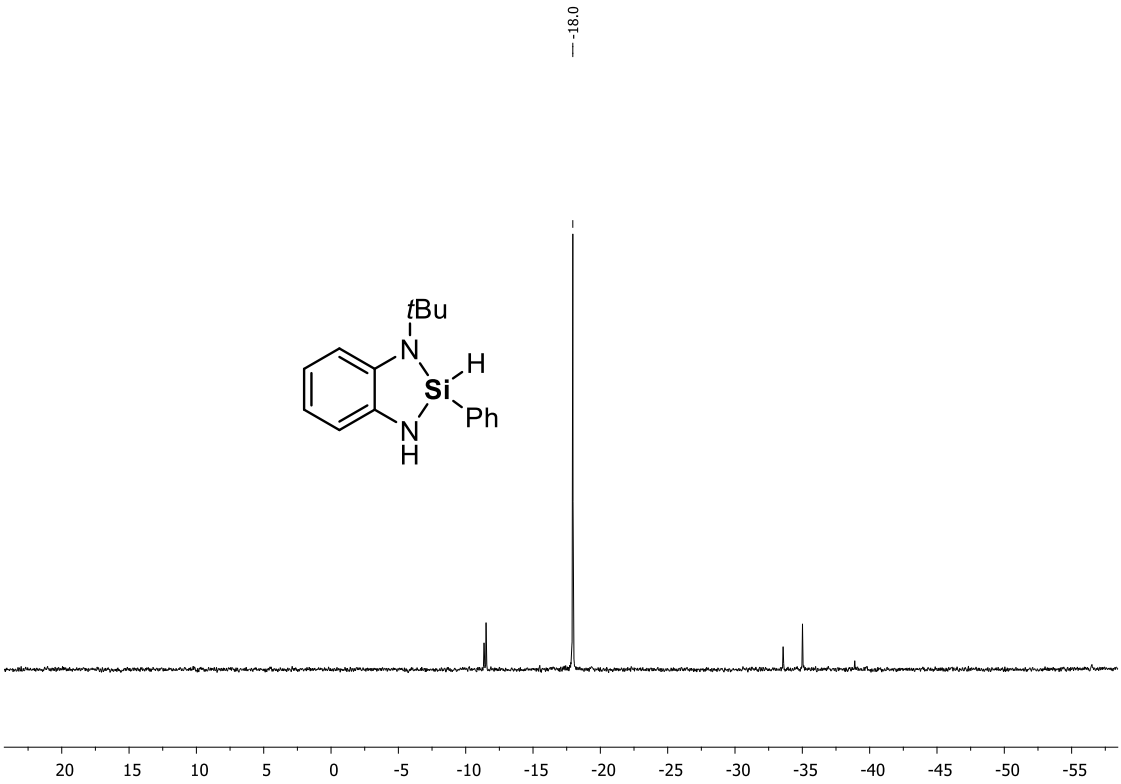

Figure S4.7. $^{29}Si\{^{1}H\}$ NMR spectrum (C_6D_6, 298 K) of **4**.

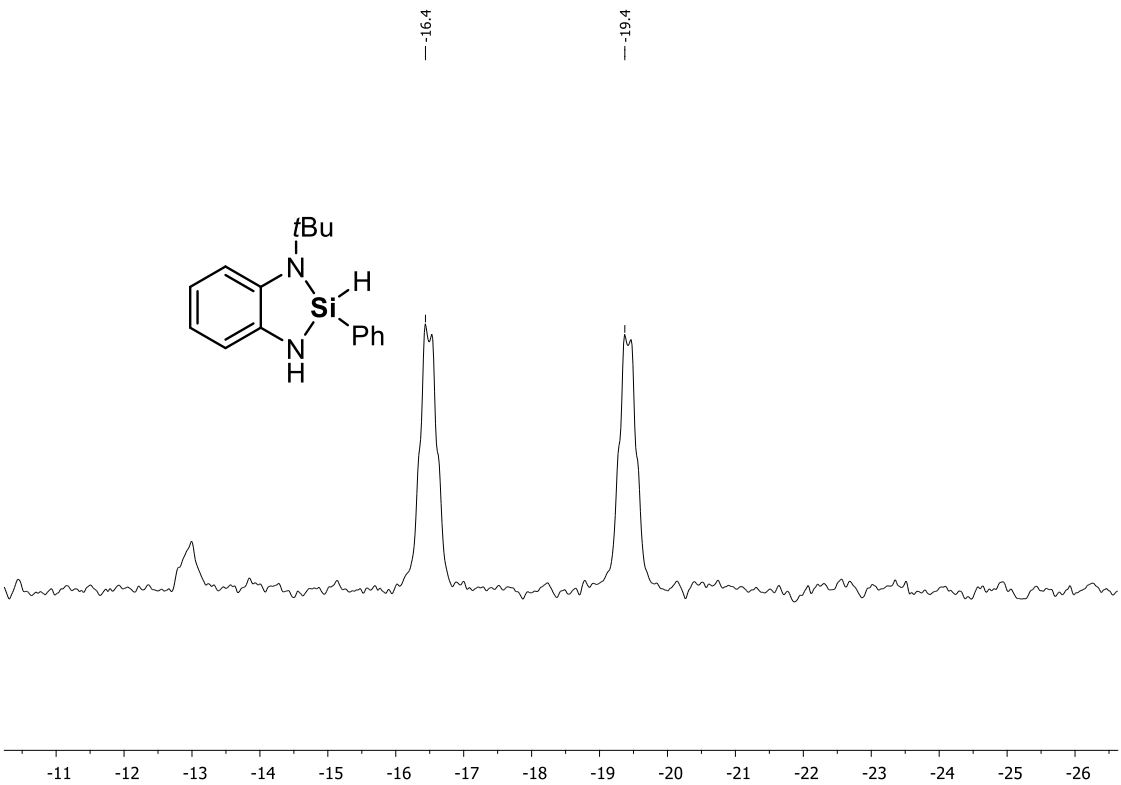

Figure S4.8. ^{29}Si NMR spectrum (C_6D_6, 298 K) of **4**.

4.6.2.3 Compound 3

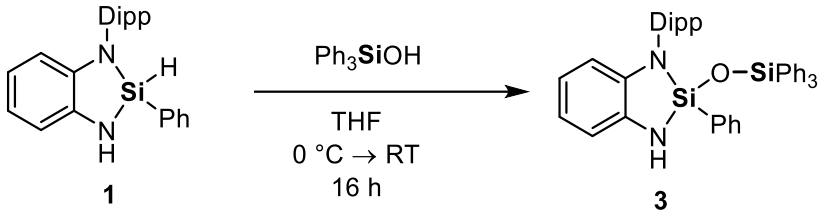

Compound **1** (373 mg, 1.0 mmol, 1.0 equiv.) and triphenylsilanol (276 mg, 1.0 mmol, 1.0 equiv.) were dissolved in 20 mL of THF and stirred at room temperature for 16 h. All volatiles were removed *in vacuo* and the resulting white solid was washed with pentane to afford compound **3** (471 mg, 0.73 mmol, 73%). Crystals suitable for X-ray diffraction were obtaine by recrystallization from pentane.

^{1}H NMR (400 MHz, C_6D_6, 298 K): *δ*[ppm] = 0.32 [d, 3H, $^{3}J_{CH}$ = 6.8 Hz, CH(C*H*)$_3$], 0.91 [d, 3H, $^{3}J_{CH}$ = 6.8 Hz, CH(C*H*)$_3$], 0.93 [d, 3H, $^{3}J_{CH}$ = 6.8 Hz, CH(C*H*)$_3$], 0.99 [d, 3H, $^{3}J_{CH}$ = 6.8 Hz, CH(C*H*)$_3$], 2.83 [sept, 1H, $^{3}J_{CH}$ = 6.8 Hz, C*H*(CH)$_3$], 3.62 [sept, 1H, $^{3}J_{CH}$ = 6.8 Hz, C*H*(CH)$_3$], 3.84 [s, 1H, N*H*], 6.15 [d, 1H, $^{3}J_{CH}$ = 7.6 Hz, C*H*$_{Ar}$], 6.47 [dd, $^{3}J_{CH}$ = 7.5 Hz, $^{4}J_{CH}$ = 1.1 Hz, C*H*$_{Ar}$], 6.68 [td, $^{3}J_{CH}$ = 7.6 Hz, $^{4}J_{CH}$ = 1.3 Hz, C*H*$_{Ar}$], 6.80 [td, $^{3}J_{CH}$ = 7.5 Hz, $^{4}J_{CH}$ = 1.2 Hz, C*H*$_{Ar}$], 7.00–7.13 [m, 14H, C*H*$_{Ar}$], 7.17–7.21 [m, 2H, C*H*$_{Ar}$], 7.61–7.65 [m, 6H, C*H*$_{Ar}$], 7.69–7.72 [m, 2H, C*H*$_{Ar}$]. **^{13}C{^{1}H} NMR** (101 MHz, C_6D_6, 298 K): *δ*[ppm] = 23.4 [s, CH(*C*H$_3$)$_2$], 24.7 [s, CH(*C*H$_3$)$_2$], 25.5 [s, CH(*C*H$_3$)$_2$], 25.7 [s, CH(*C*H$_3$)$_2$], 28.3 [s, *C*H(CH$_3$)$_2$], 28.4 [s, *C*H(CH$_3$)$_2$], 111.0 [s, *C*H$_{Ar}$], 111.2 [s, *C*H$_{Ar}$], 118.7 [s, *C*H$_{Ar}$], 118.8 [s, *C*H$_{Ar}$], 124.5 [s, *C*H$_{Ar}$], 124.9 [s, *C*H$_{Ar}$], 127.9 [s, *C*H$_{Ar}$], 130.4 [s, *C*H$_{Ar}$], 130.9 [s, *C*H$_{Ar}$], 132.7 [s, *C*$_{Ar}$],, 134.4 [s, *C*$_{Ar}$], 135.5 [s, *C*$_{Ar}$], 135.6 [s, *C*H$_{Ar}$], 135.9 [s, *C*H$_{Ar}$], 136.3 [s, *C*$_{Ar}$], 140.1 [s, *C*$_{Ar}$], 148.7 [s, *C*$_{Ar}$], 149.5 [s, *C*$_{Ar}$]. **^{29}Si{^{1}H} NMR** (79 MHz, C_6D_6, 298 K): *δ*[ppm] = −38.7 [s, *Si*N], −16.6 [s, *Si*Ph$_3$]. **CHN Analysis** $C_{42}H_{42}N_2OSi$: calculated: C 77.97, H 6.54, N 4.33, O 2.47, Si 8.68; found: C 78.25, H 6.65, N 4.19. **HR-MS(FD+)**, calculated m/z for $C_{42}H_{42}N_2OSi$ [M+H$^+$]: 646.28302; found: 646.28402.

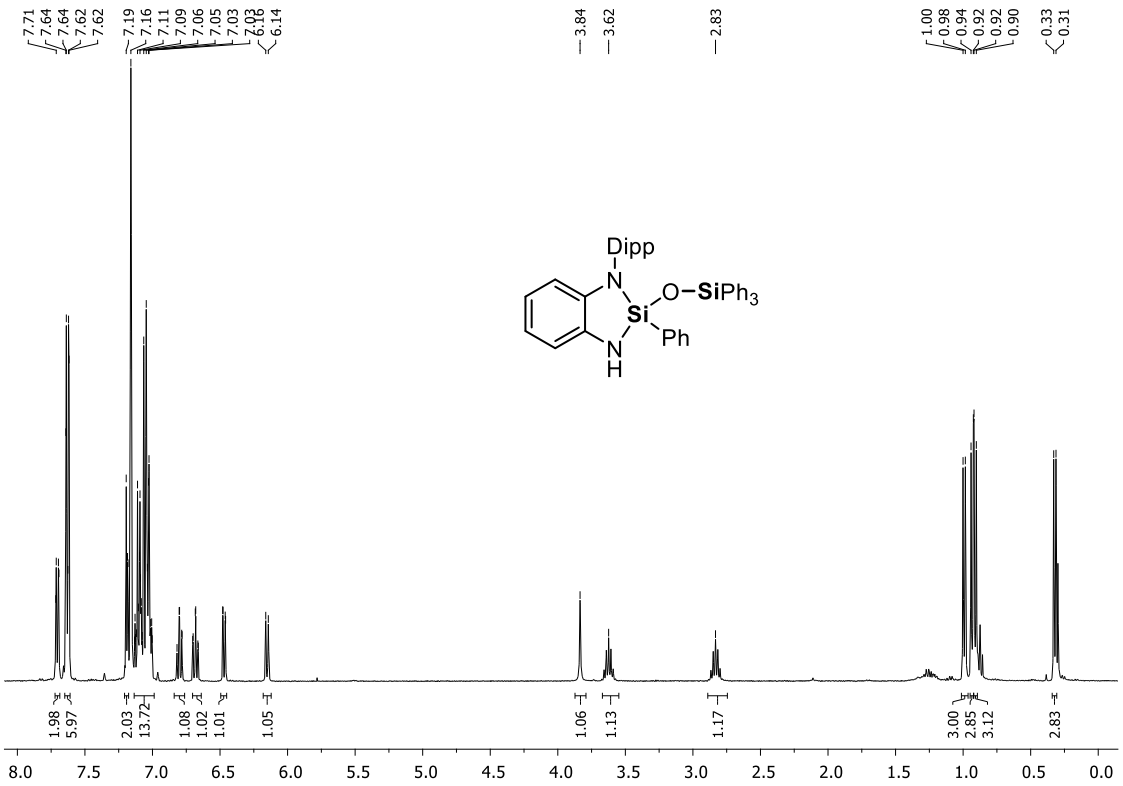

Figure S4.9. ^{1}H NMR spectrum (C_6D_6, 298 K) of **3**.

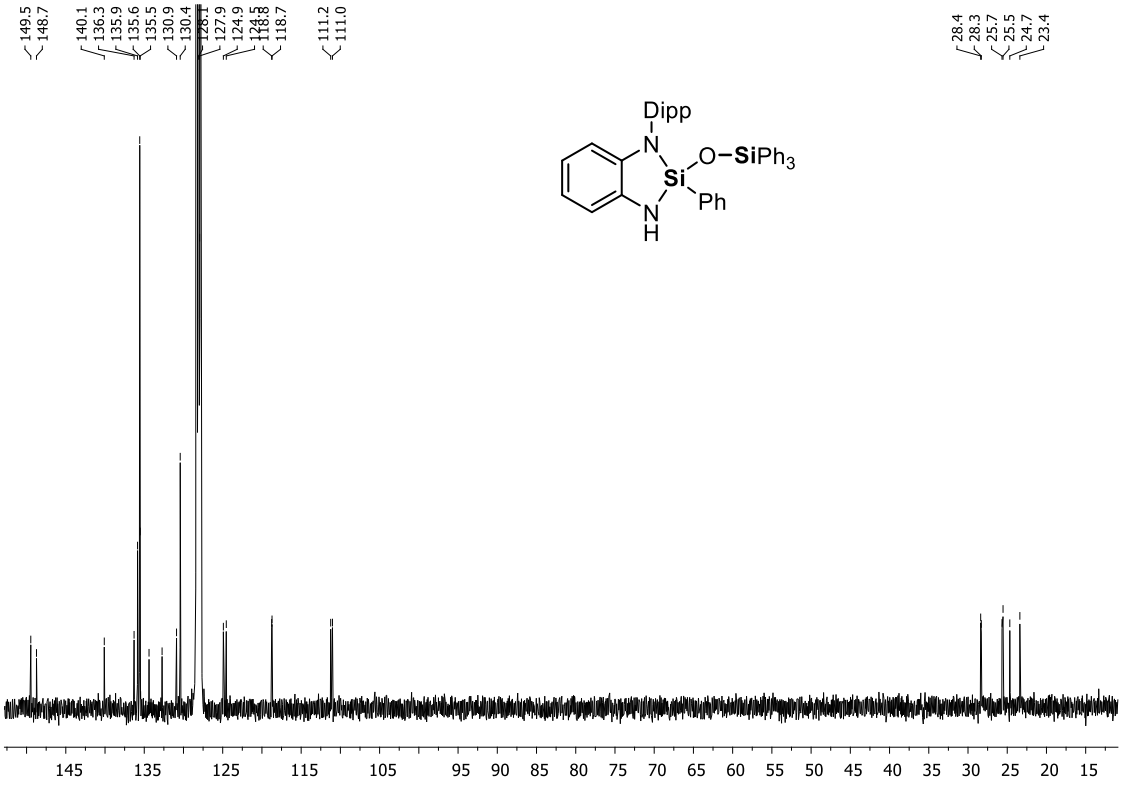

Figure S4.10. $^{13}C\{^{1}H\}$ NMR spectrum (C_6D_6, 298 K) of **3**.

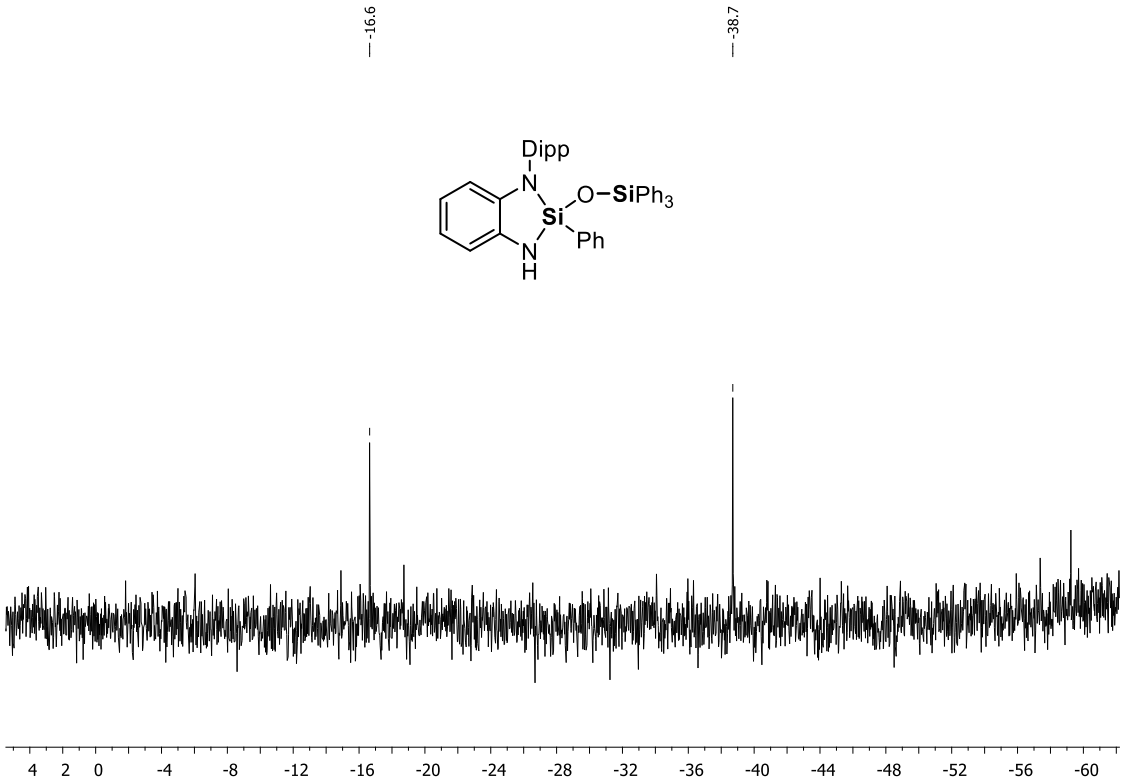

Figure S4.11. $^{29}Si\{^{1}H\}$ NMR spectrum (C_6D_6, 298 K) of **3**.

4.6.2.4 Compound 5

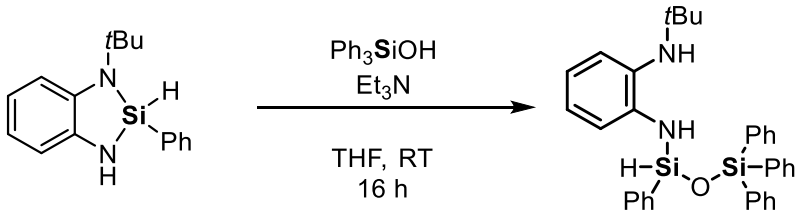

4 **5**

Compound **4** (130 mg, 0.48 mmol, 1.0 equiv.) was dissolved in 10 mL of THF and triethylamine (0.13 mL, 0.96 mmol, 2.0 equiv.) was added followed by addition of triphenylsilanol (133 mg, 0.48 mmol, 1.0 equiv.). The clear colourless solution was stirred at room temperature for 16 h. All volatiles were removed *in vacuo* and the brown residue was dissolved in 2 mL of pentane. The solution was cooled to −80 °C upon which a solid precipitated which was isolated via cold cannula filtration. Upon warming up to room temperature, the white solid turned into a brown wax. 1 mL of pentane was layered on top of the wax and the flask was transferred to a 8 °C cold fridge. Crystals suitable for single crystal X-ray analysis were obtained after two weeks and isolated by cannula filtration to obtain compound **5** as white crystalline solid (8 mg, 0.01 mmol, 3%).

^{1}H NMR (400 MHz, C_6D_6, 298 K): δ[ppm] = 0.98 [s, 9H, C(C*H*$_3$)$_3$], 2.03 8 [s, 1H, *t*Bu-N*H*], 5.71 [d, 1H, $^{3}J_{HH}$ = 3.0 Hz, Si-N*H*], 5.81 [d, 1H, $^{3}J_{HH}$ = 3.1 Hz, Si*H*], 6.67–6.72 [m, 1H, H_{Ar}], 6.77–6.83 [m,

2H, H_{Ar}], 7.05–7-16 [m, 8H, H_{Ar}], 7.16–7.21 [m, 3H, H_{Ar}], 7.73–7.78 [m, 8H, H_{Ar}]. **$^{13}C\{^1H\}$ NMR** (101 MHz, C_6D_6, 298 K): δ[ppm] = 29.8 [s, C(CH_3)$_3$], 53.4 [s, C(CH_3)$_3$], 117.0 [s, CH_{Ar}], 118.9 [s, CH_{Ar}], 125.7 [s, CH_{Ar}], 128.2 [s, CH_{Ar}], 128.2 [s, CH_{Ar}], 128.4 [s, CH_{Ar}], 130.3 [s, CH_{Ar}], 130.7 [s, CH_{Ar}], 133.1 [s, C_{Ar}], 134.3 [s, CH_{Ar}], 135.3 [s, C_{Ar}], 135.7 [s, CH_{Ar}], 135.8 [s, C_{Ar}], 144.2 [s, C_{Ar}]. **$^{29}Si\{^1H\}$ NMR** (79 MHz, C_6D_6, 298 K): δ[ppm] = −38.7 [s, SiH], −17.6 [s, $SiPh_3$]. **^{29}Si NMR** (79 MHz, C_6D_6, 298 K): δ[ppm] = −38.7 [d, $^1J_{SiH}$ = 240.6 Hz, SiH], −17.6 [s, $SiPh_3$]. **CHN Analysis** $C_{34}H_{36}N_2OSi_2$: calculated: C 74.95, H 6.66, N 5.14, O 2.94, Si 10.31; found: C 75.00, H 6.53, N 5.10. **HR-MS(FD+)**, calculated m/z for $C_{34}H_{36}N_2OSi_2$ [M+H$^+$]: 544.23607; found: 544.23416.

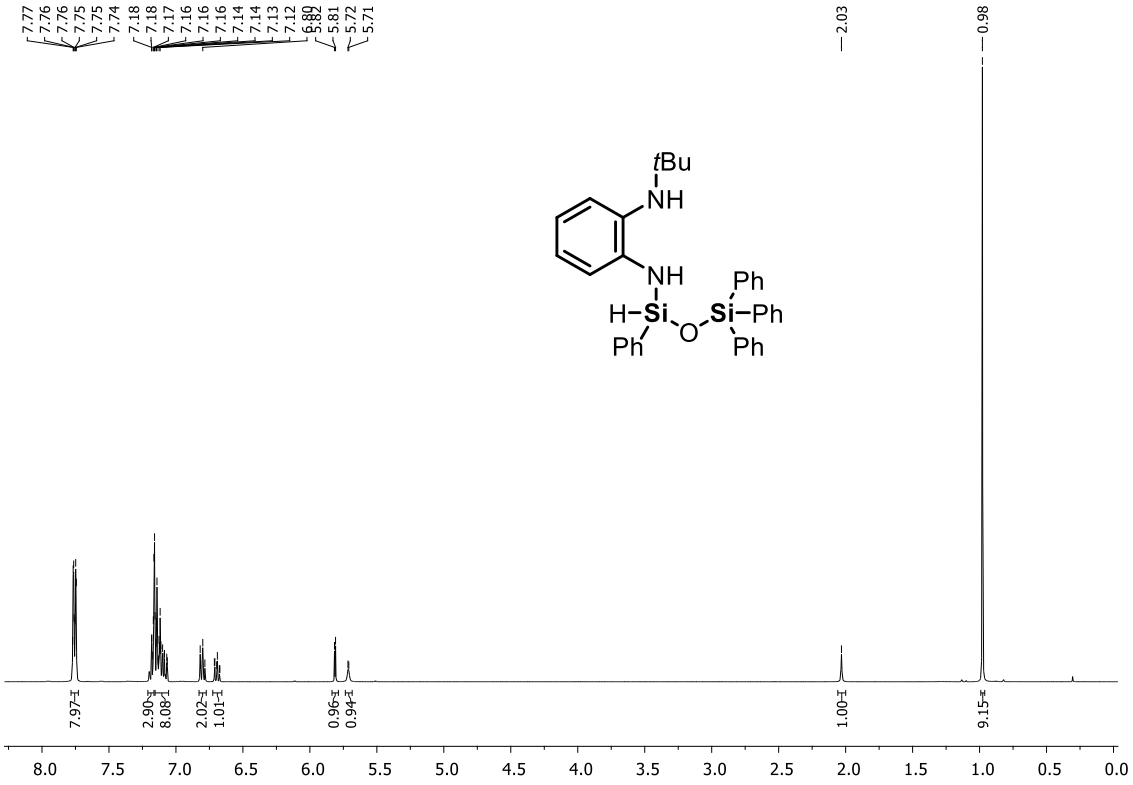

Figure S4.12. ^{1}H NMR spectrum (C_6D_6, 298 K) of **5**.

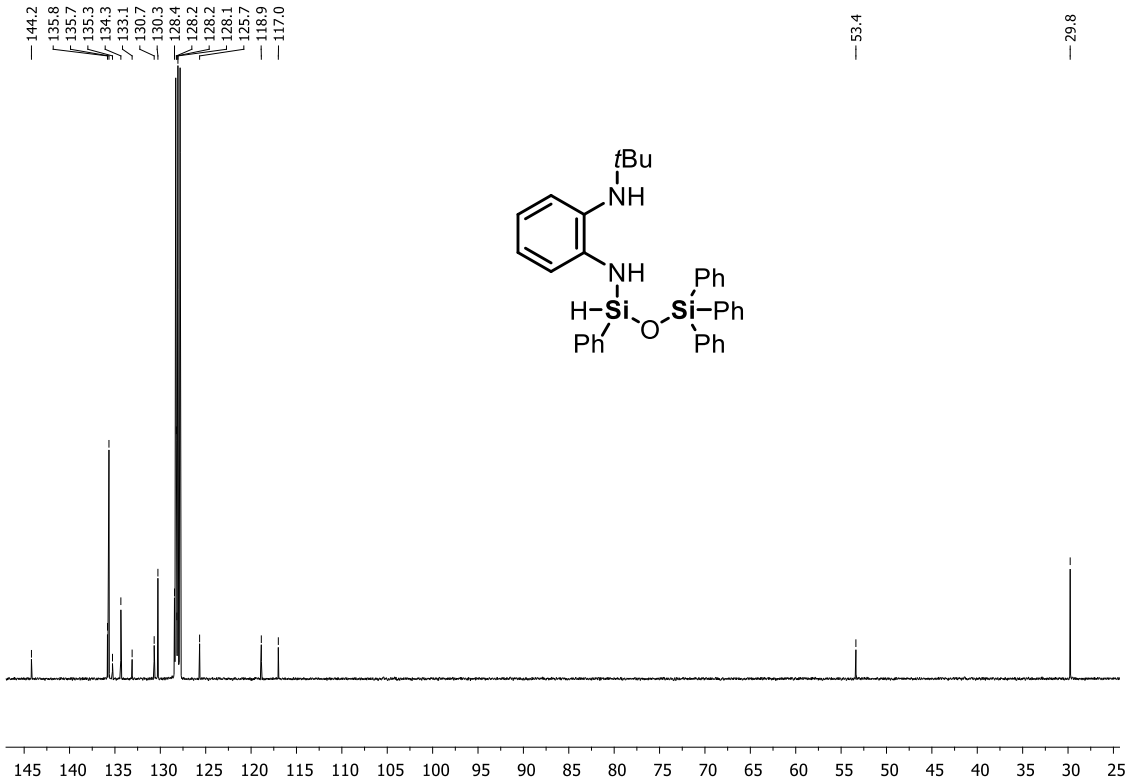

Figure S4.13. $^{13}C\{^{1}H\}$ NMR spectrum (C_6D_6, 298 K) of **5**.

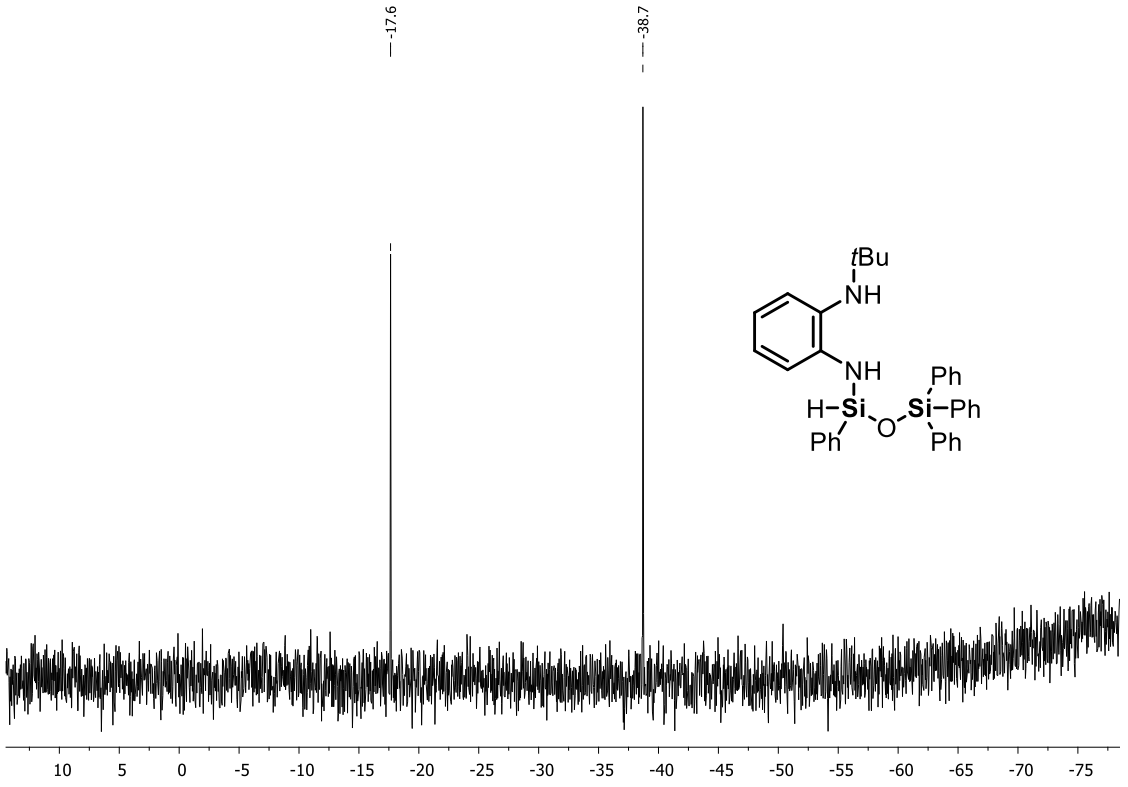

Figure S4.14. $^{29}Si\{^{1}H\}$ NMR spectrum (C_6D_6, 298 K) of **5**.

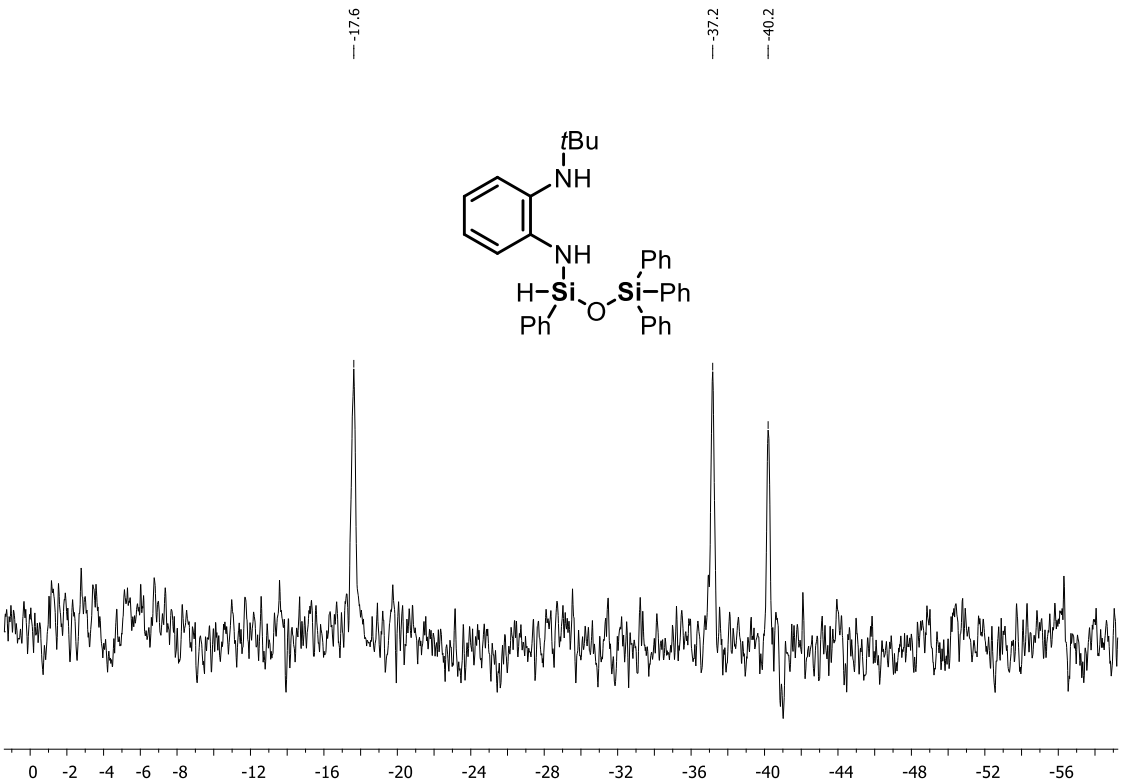

Figure S4.15. ^{29}Si NMR spectrum (C_6D_6, 298 K) of **5**.

4.6.2.5 Compound 6

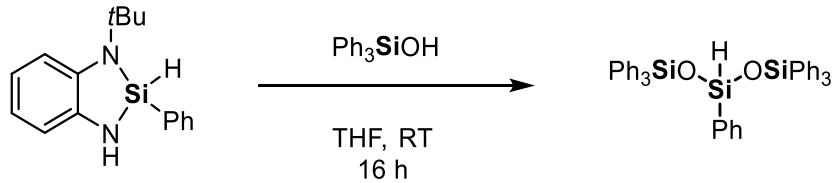

4 **6**

Compound **4** (1.34 g, 5.0 mmol, 1.0 equiv.) was dissolved in 50 mL of THF and triphenylsilanol (1.38 g, 5.0 mmol, 1.0 equiv.) and the red solution was stirred at room temperature for 16 h. All volatiles were removed *in vacuo* and the residue was taken up in 50 mL pentane. The solids were removed via cannula filtration and the red filtrate was stored at 8 °C for one day. Crystals suitable for X-ray crystallographic analysis formed which were isolated via cannula filtration and washed with pentane to obtain compound **6** as an off-white crystalline solid (680 mg, 1.0 mmol, 20%).

^{1}H NMR (400 MHz, C_6D_6, 298 K): *δ*[ppm] = 5.80 [s, 1H, Si*H*], 6.97–7.15 [m, 20H, H_{Ar}], 7.17–7.19 [m, 1H, H_{Ar}], 7.57–7.61 [m, 2H, H_{Ar}], 7.63–7.68 [m, 12H, H_{Ar}]. **^{13}C{^{1}H} NMR** (101 MHz, C_6D_6, 298 K): *δ*[ppm] = 138.2 [s, CH_{Ar}], 130.2 [s, CH_{Ar}],130.7 [s, CH_{Ar}], 138.8 [s, CH_{Ar}], 156.6 [s, CH_{Ar}], 135.9 [s, C_{Ar}]. **^{29}Si{^{1}H} NMR** (79 MHz, C_6D_6, 298 K): *δ*[ppm] = −46.6 [s, *Si*H], −17.9 [s, *Si*Ph$_3$]. **^{29}Si NMR** (79 MHz, C_6D_6, 298 K): *δ*[ppm] = −46.2 [dm, $^1J_{SiH}$ = 250.5 Hz, *Si*H], −17.4 [m, *Si*Ph$_3$]. **CHN Analysis** $C_{42}H_{36}O_2Si_3$: calculated: C 76.78, H 5.52, O 4.87, Si 12.82; found: C 76.68, H 5.43. **HR-MS(FD+)**, calculated m/z for $C_{42}H_{36}O_2Si_3$ [M+H$^+$]: 656.20176; found: 656.20401.

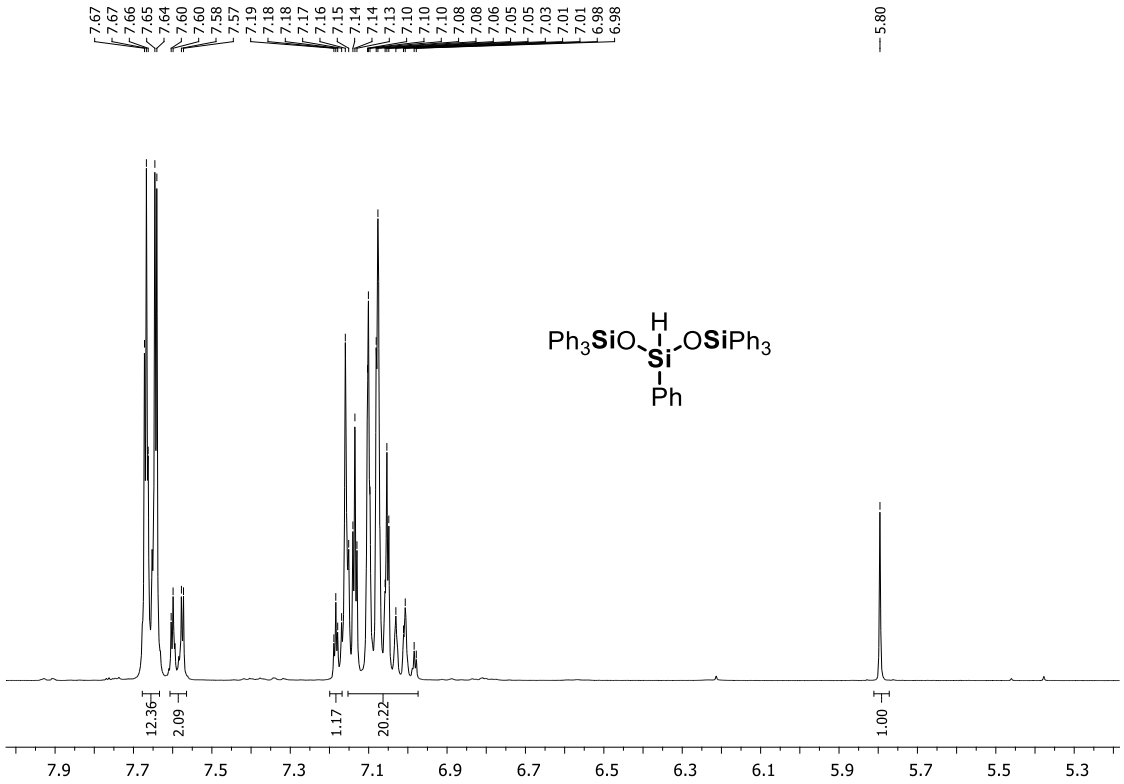

Figure S4.16. ^{1}H NMR spectrum (C_6D_6, 298 K) of **6**.

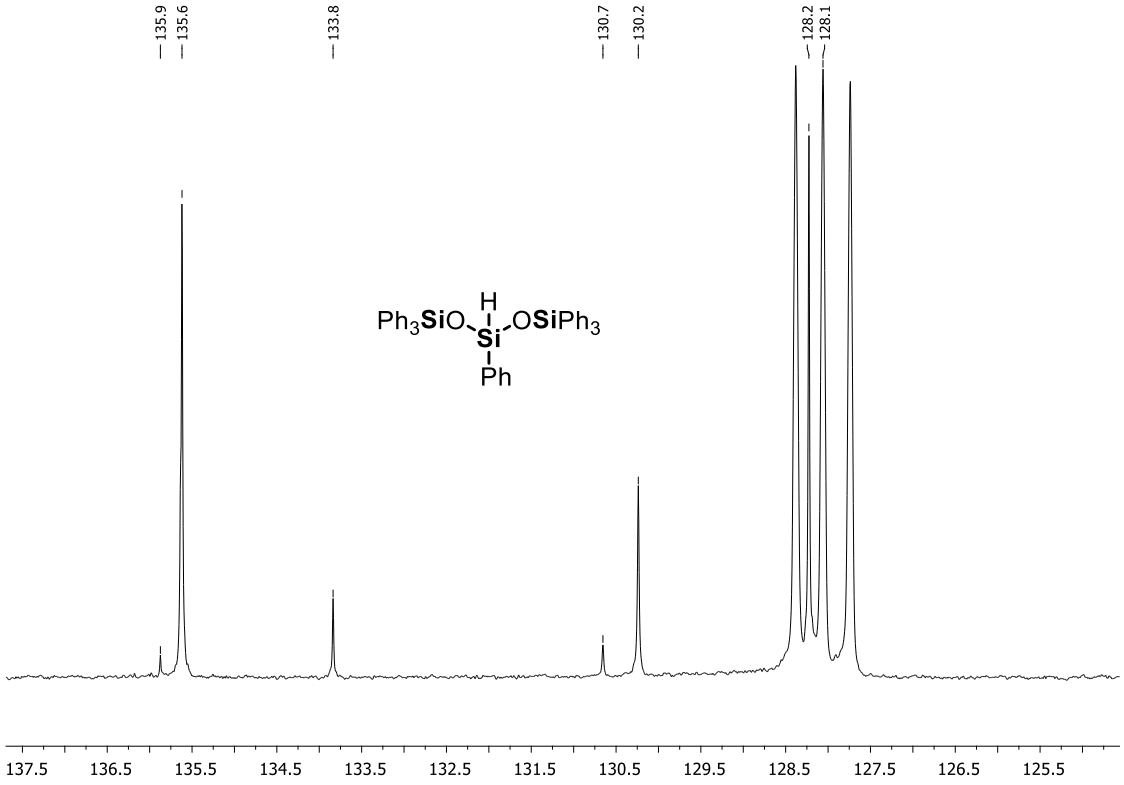

Figure S4.17. $^{13}C\{^{1}H\}$ NMR spectrum (C_6D_6, 298 K) of **6**.

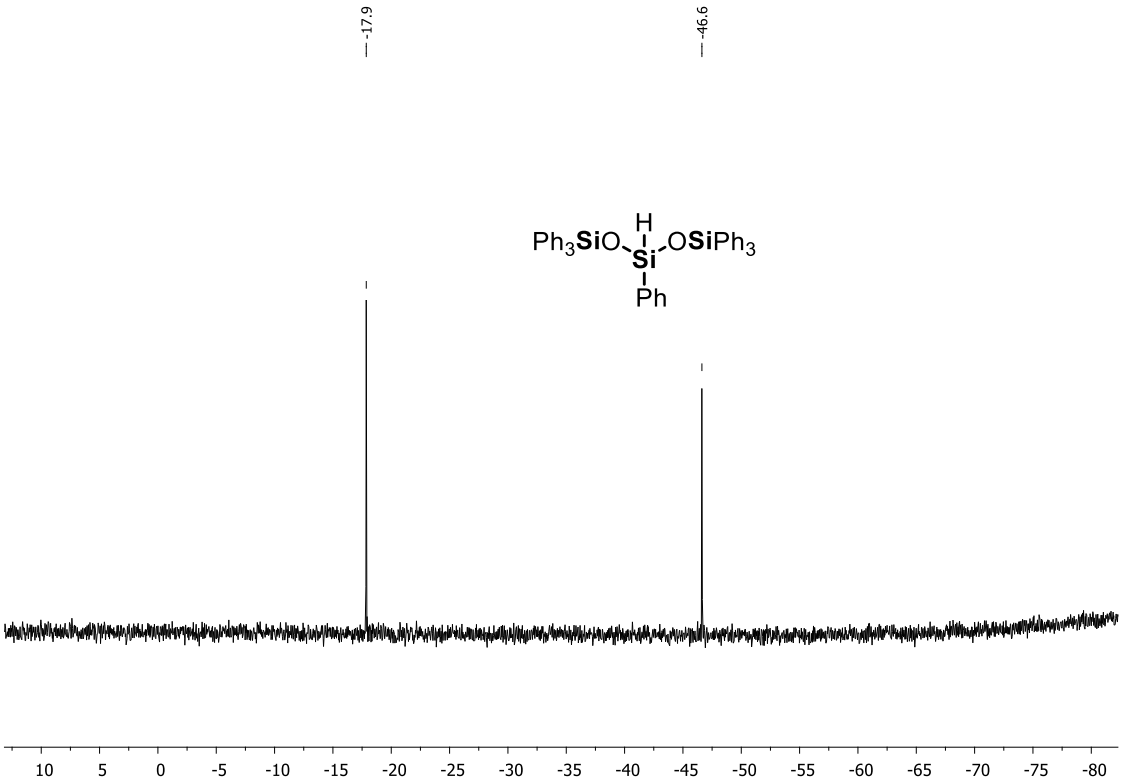

Figure S4.18. $^{29}Si\{^{1}H\}$ NMR spectrum (C_6D_6, 298 K) of **6**.

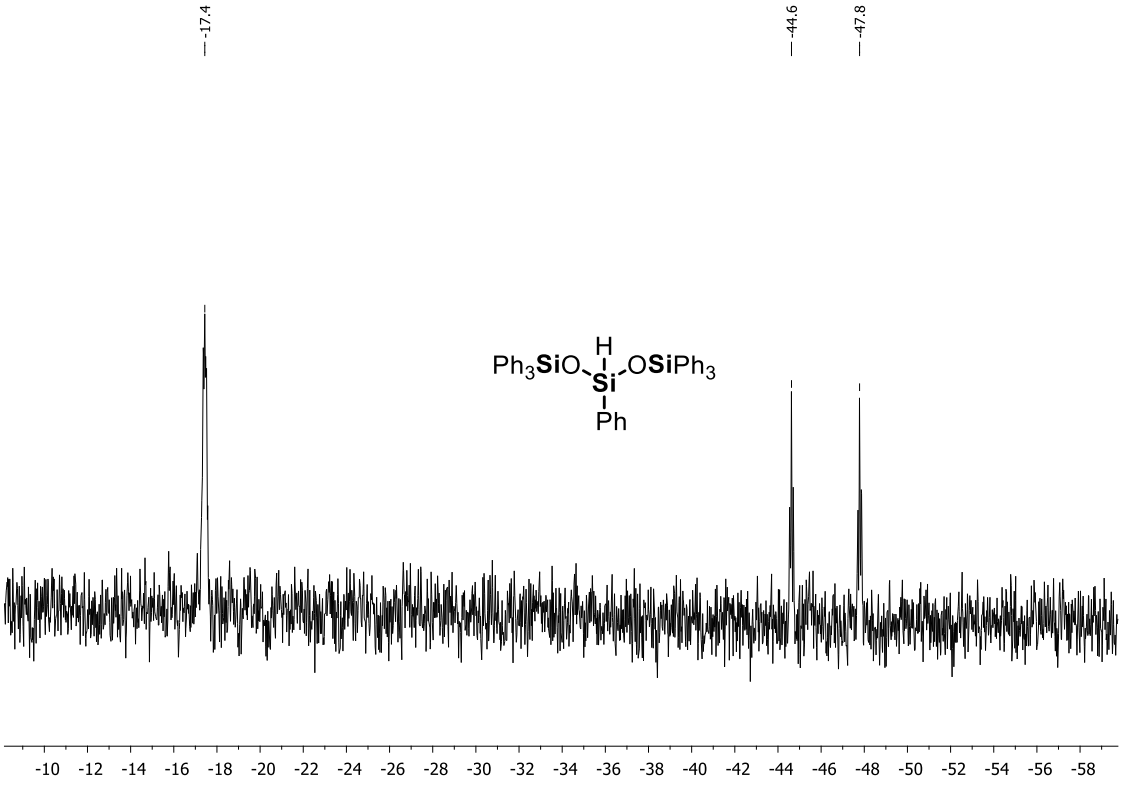

Figure S4.19. ^{29}Si NMR spectrum (C_6D_6, 298 K) of **6**.

4.6.2.6 Compound S2

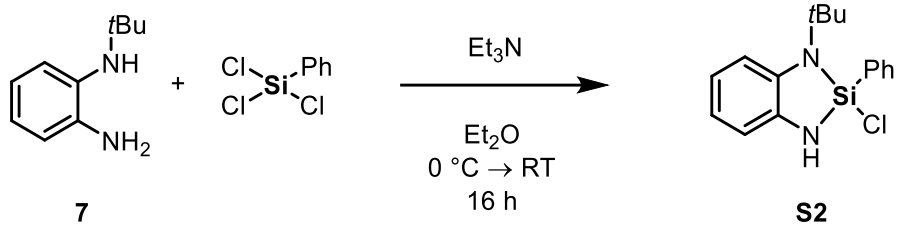

7 **S2**

Compound **7** (1.64 g, 10.0 mmol, 1.0 equiv.) was dissolved in 30 mL of Et_2O and triethylamine (5.58 mL, 40.0 mmol, 4.0 equiv.) was added. The mixture was cooled down to 0 °C and trichlorophenylsilane (1.60 mL, 10.0 mmol, 1.0 equiv) was added while stirring. The brown solution was stirred for 16 h while slowly warming to room temperature. The formed precipitate was removed by cannula filtration and the brown filtrate was dried *in vacuo* to afford compound **S2** as a brown wax (3.13 g, 10.0 mmol, >99%).

^{1}H NMR (400 MHz, C_6D_6, 298 K): *δ*[ppm] = 1.35 [s, 9H, C(C*H*$_3$)$_3$], 3.45 [s, 1H, N*H*], 6.47–6.50 [m, 1H, *H*$_{Ar}$], 6.80–6.88 [m, 2H, *H*$_{Ar}$], 7.00–7.04 [m, 1H, *H*$_{Ar}$], 7.09–7.15 [m, 3H, *H*$_{Ar}$], 7.72–7.75 [m, 2H, *H*$_{Ar}$]. **^{13}C{^{1}H} NMR** (101 MHz, C_6D_6, 298 K): *δ*[ppm] = 29.7 [s, C(*C*H$_3$)$_3$], 53.2 [s, *C*(CH$_3$)$_3$], 111.9 [s, *C*H$_{Ar}$], 114.0 [s, *C*H$_{Ar}$], 118.5 [s, *C*H$_{Ar}$], 118.5 [s, *C*H$_{Ar}$], 128.4 [s, *C*H$_{Ar}$], 131.4 [s, *C*H$_{Ar}$], 134.9 [s, *C*$_{Ar}$], 135.4 [s, *C*H$_{Ar}$], 136.4 [s, *C*$_{Ar}$], 137.7 [s, *C*$_{Ar}$]. **^{29}Si{^{1}H} NMR** (79 MHz, C_6D_6, 298 K): *δ*[ppm] = −18.4 [s, *Si*]. **CHN Analysis** $C_{16}H_{19}ClN_2Si$: calculated: C 63.45, H 6.32, Cl 11.70, N 9.25, Si 9.27; found: C 63.07, H 6.56, N 9.25. **HR-MS(EI+)**, calculated m/z for $C_{16}H_{19}ClN_2Si$ [M+H$^+$]: 302.10005; found: 302.09939.

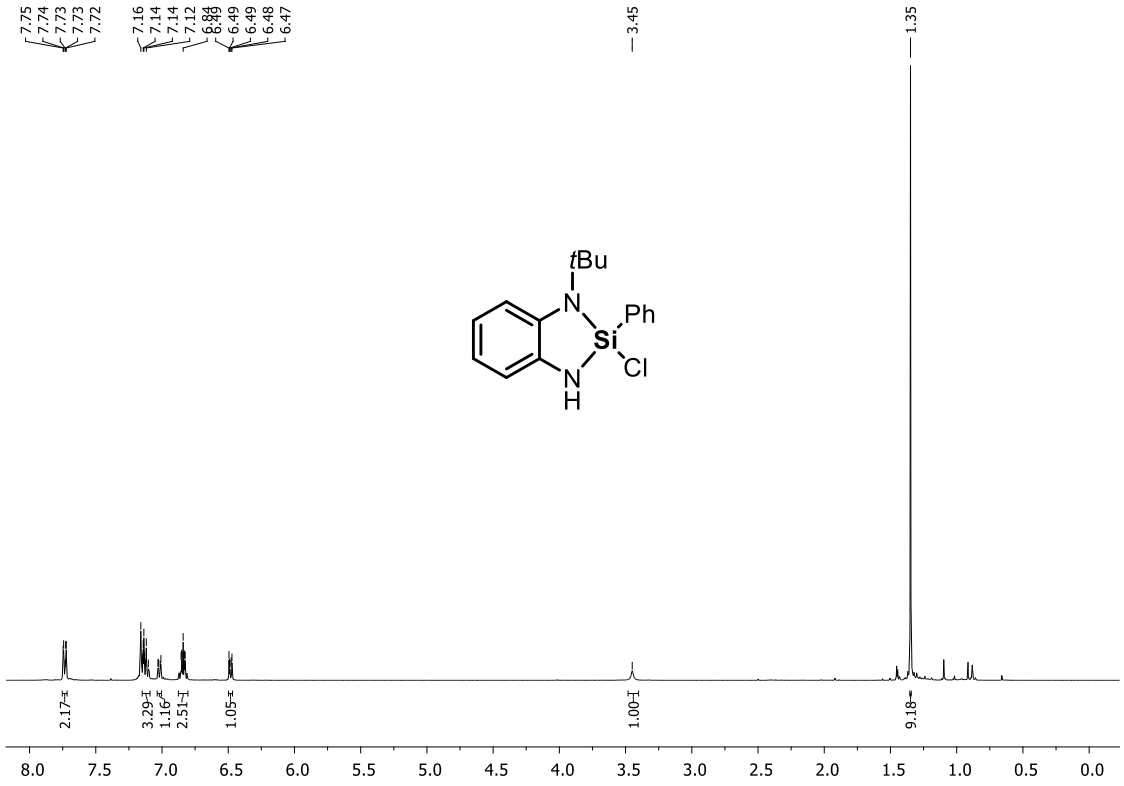

Figure S4.20. ^{1}H NMR spectrum (C_6D_6, 298 K) of **S2**.

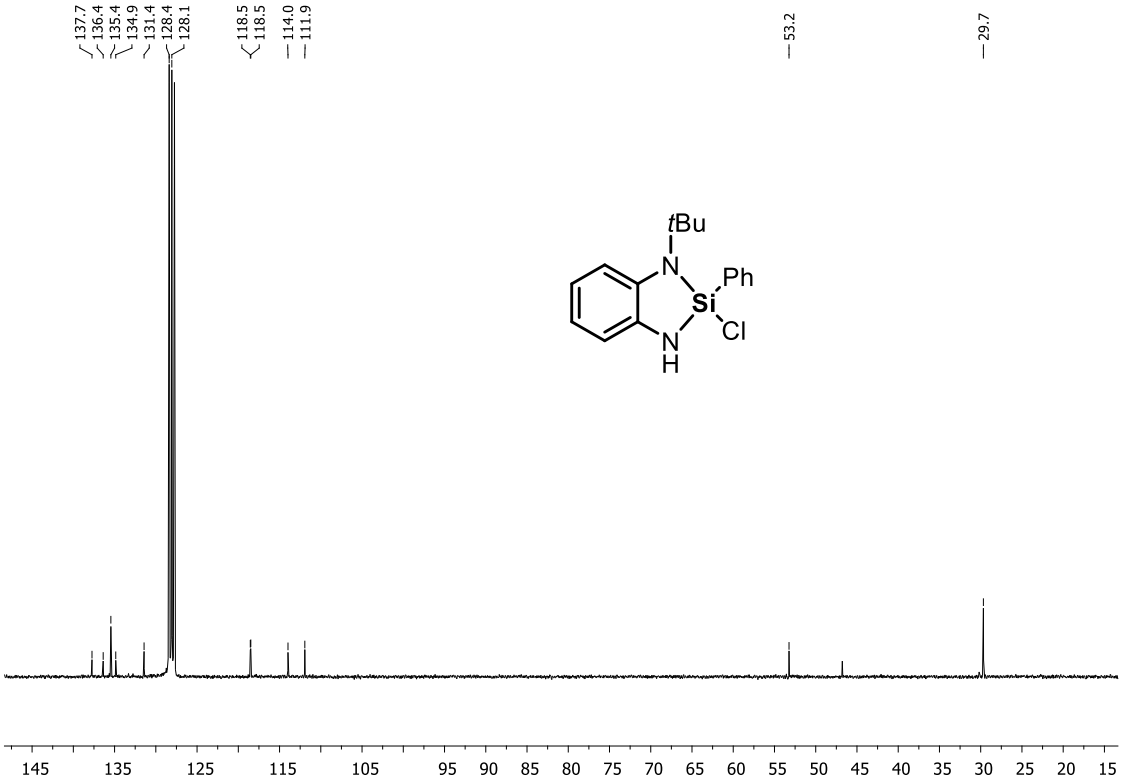

Figure S4.21. $^{13}C\{^{1}H\}$ NMR spectrum (C_6D_6, 298 K) of **S2**.

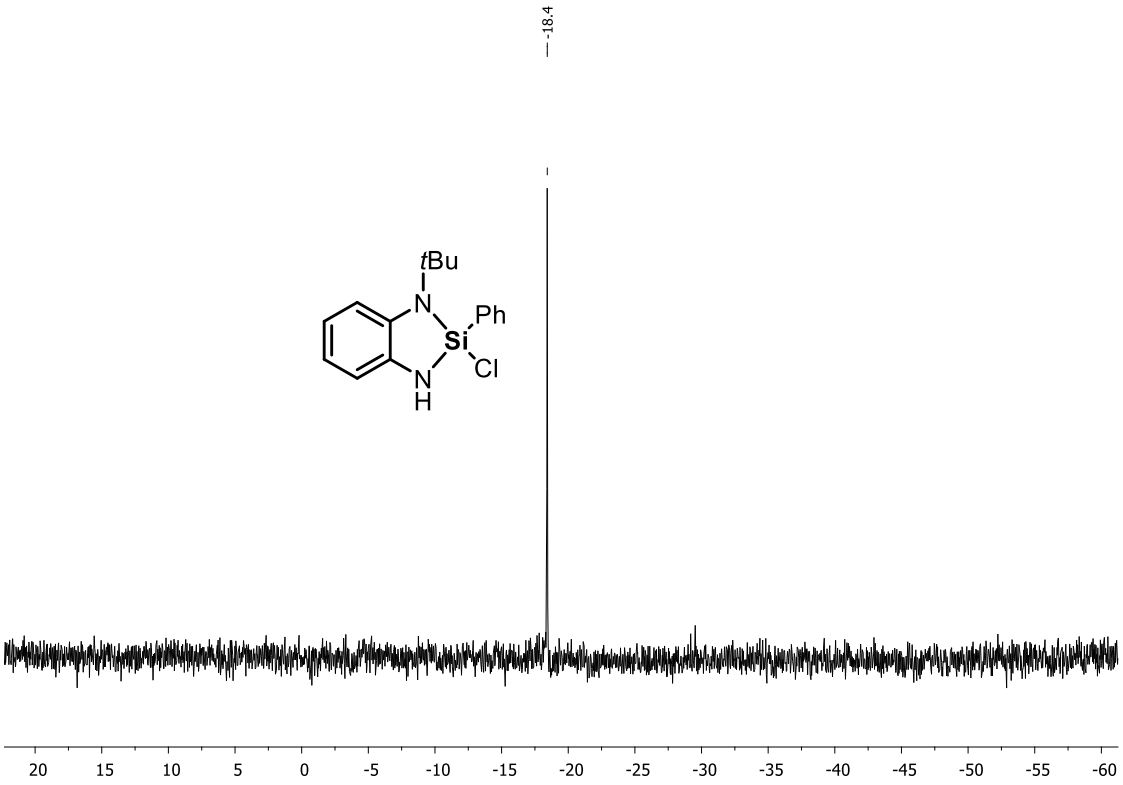

Figure S4.22. $^{29}Si\{^{1}H\}$ NMR spectrum (C_6D_6, 298 K) of **S2**.

4.6.2.7 Compound S2

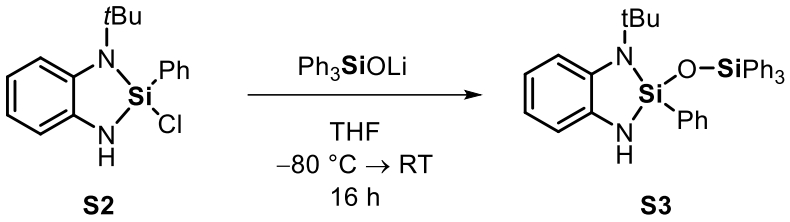

S2 **S3**

Triphenylsilanol (2.76 g, 10.0 mmol, 1.0 equiv.) was dissolved in 30 mL of THF and *n*BuLi (4.40 mL, 11.0 mmol, 1.1 equiv. of a 2.5 M solution in hexanes) was added dropwise while stirring. Afters strirring at room temperature for 10 min, the solution was cooled down to −80 °C and a solution of compound **S2** in 20 mL of THF was added via cannula. The resulting brown solution was stirred for 16 h while slowly warming up to room temperature. Afterwads, all volatiles were removed *in vacuo* and remaining brown cake was washed 3 times with pentane (ca. 20 mL). The remaining crude product was taken up in 20 mL of DCM and the solids were removed via cannula filtration. The brown filtrate was dried *in vacuo* resulting in a brownish solid which was recrystallized in pentane to afford compound **S3** as an off white crystalline solid suitable for X-ray single crystal analysis (2.36 g, 4.3 mmol, 43%).

^{1}H NMR (400 MHz, C_6D_6, 298 K): δ[ppm] = 1.27 [s, 9H, C(CH_3)$_3$], 3.47 [s, 1H, N*H*], 6.31 [dd, $^{3}J_{H\text{-}H}$ = 7.4 Hz, $^{4}J_{H\text{-}H}$ = 1.4 Hz, 1H, H_{Ar}], 6.81 [td, $^{3}J_{H\text{-}H}$ = 7.5 Hz, $^{4}J_{H\text{-}H}$ = 1.0 Hz, 1H, H_{Ar}], 6.88 [td, $^{3}J_{H\text{-}H}$ = 7.6 Hz, $^{4}J_{H\text{-}H}$ = 1.4 Hz, 1H, H_{Ar}], 6.95–6.99 [m, 1H, H_{Ar}], 7.09–7.16 [m, 11H, H_{Ar}], 7.16–7.19 [m, 1H, H_{Ar}], 7.68–7.73 [m, 6H, H_{Ar}], 7.78–7.82 [m, 2H, H_{Ar}]. **^{13}C{^{1}H} NMR** (101 MHz, C_6D_6, 298 K): δ[ppm] = 29.5 [s, C(*C*H$_3$)$_3$], 52.5 [s, *C*(CH$_3$)$_3$], 113.3 [s, *C*H$_{Ar}$], 113.1 [s, *C*H$_{Ar}$], 117.7 [s, *C*H$_{Ar}$], 117.8 [s, *C*H$_{Ar}$], 128.3 [s, *C*H$_{Ar}$], 128.3 [s, *C*H$_{Ar}$], 130.4 [s, *C*H$_{Ar}$], 130.6 [s, *C*H$_{Ar}$], 135.6 [s, *C*H$_{Ar}$], 135.6 [s, *C*H$_{Ar}$], 136.3 [s, *C*$_{Ar}$], 137.1 [s, *C*$_{Ar}$], 138.0 [s, *C*$_{Ar}$]. **^{29}Si{^{1}H} NMR** (79 MHz, C_6D_6, 298 K): δ[ppm] = −40.0 [s, *Si*Ph$_3$], −17.0 [s, *Si*N]. **CHN Analysis** $C_{34}H_{34}N_2OSi_2$: calculated: C 75.23, H 6.31, N 5.16, O 2.95, Si 10.35; found: C 74.58, H 6.11, N 5.85. **HR-MS(FD+)**, calculated m/z for $C_{34}H_{34}N_2OSi_2$ [M+H$^+$]: 542.22042; found: 542.21889.

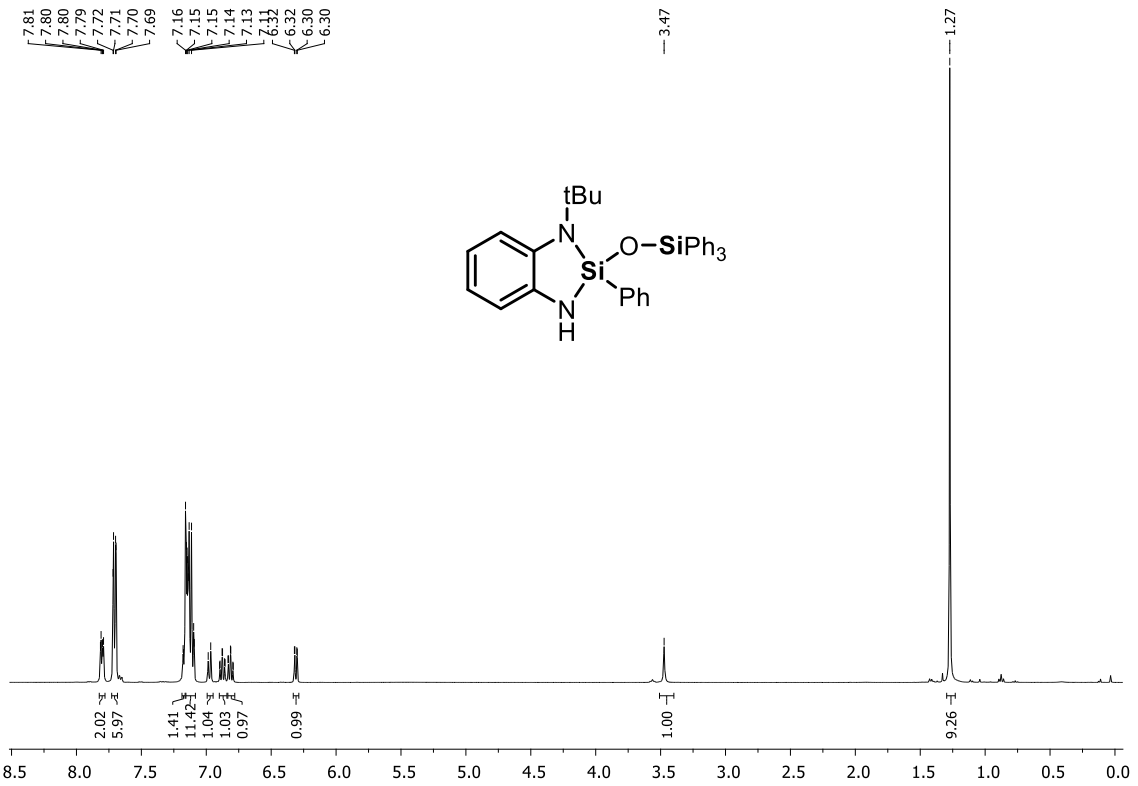

Figure S4.23. ^{1}H NMR spectrum (C_6D_6, 298 K) of **S3**.

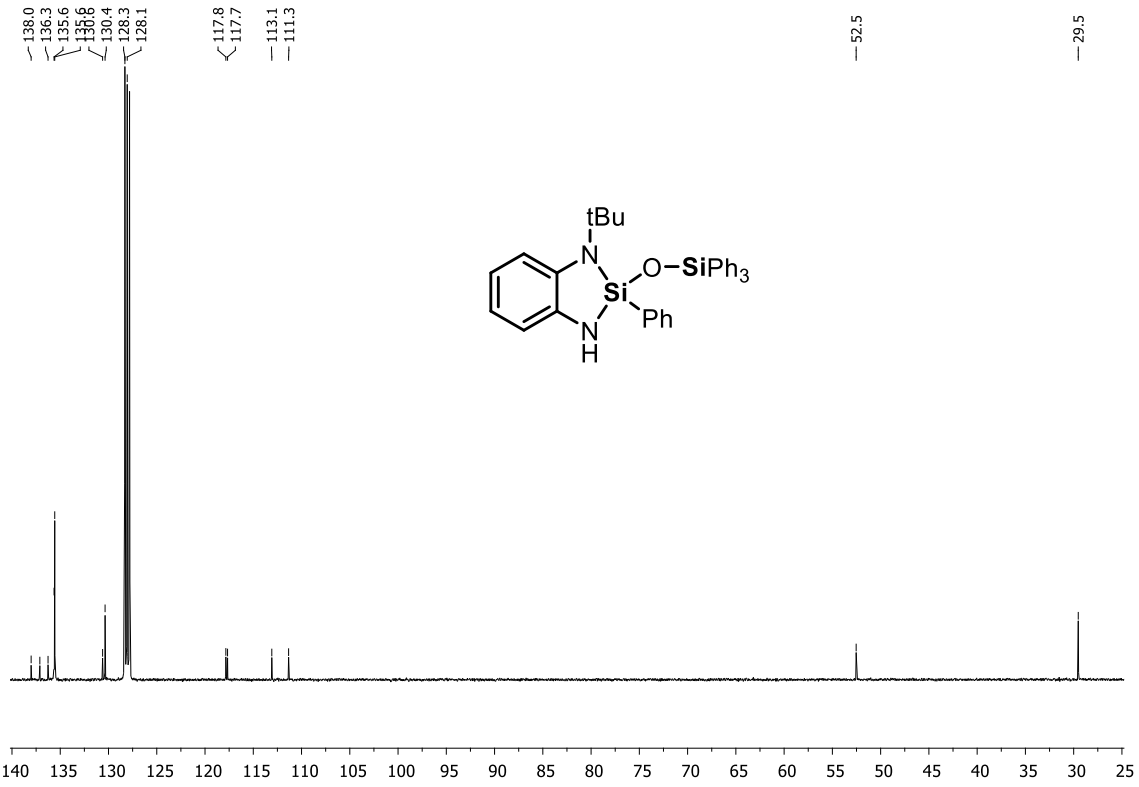

Figure S4.24. $^{13}C\{^{1}H\}$ NMR spectrum (C_6D_6, 298 K) of **S3**.

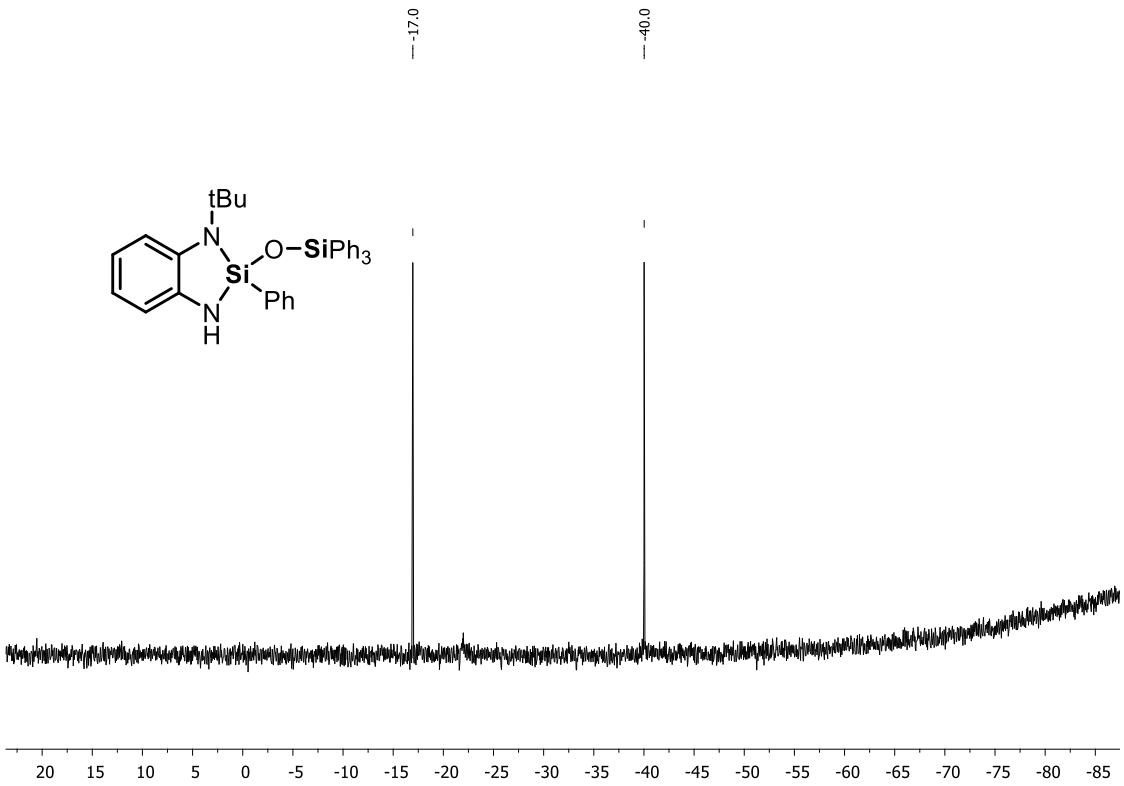

Figure S4.25. $^{29}Si\{^{1}H\}$ NMR spectrum (C_6D_6, 298 K) of **S3**.

4.6.3 Mechanistic investigations

4.6.3.1 General procedure for the reaction of 1 with Ph_3SiOH

Compound **1** (4 mg, 10 µmol, 1.0 equiv.) was weighed into a Young NMR tube and dissolved in 0.6 mL of THF–d8. The tube was cooled down to −80 °C using a isopropanol/N_2 cooling bath and triphenylsilanol (3 mg, 10 µmol, 1.0 equiv.) was added with a funnel. The tube was quickly shaken and within minutes transferred to a 400 MHz Bruker NMR spectrometer.

4.6.3.2 Variable temperture NMR study of reaction of compound 1 with Ph_3SiOH

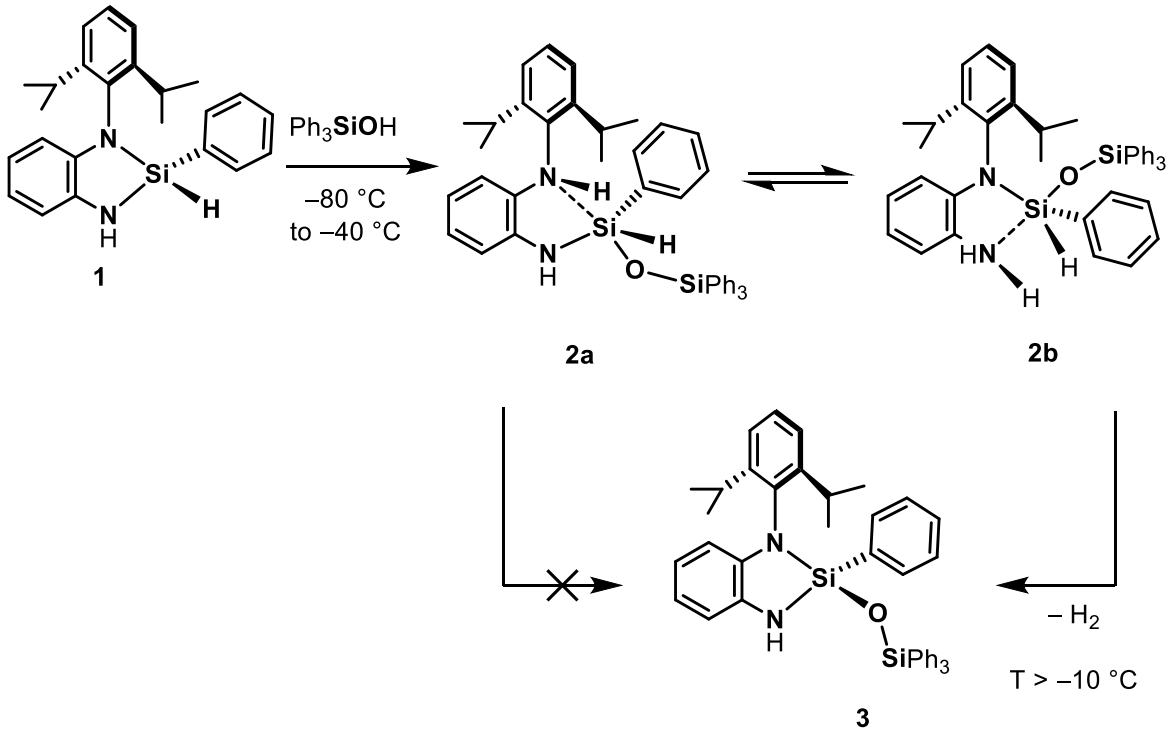

General procedure 3.1 was applied. Variable tempertaure ^{1}H NMR spectra were recorded starting at −80 °C to −10 °C in 10 °C steps. Finally, the tube was stirred at room temperature for another 16 h and a final NMR spectrum was recorded.

Compound **2a/2b**:

^{1}H NMR (600 MHz, THF-d_8, 163 K): δ[ppm] = 0.75 [d, $^{3}J_{H\text{-}H}$ = 6.8 Hz, 3H, CH(CH_3)$_2$], 0.80 [d, $^{3}J_{H\text{-}H}$ = 6.7 Hz, 3H, CH(CH_3)$_2$], 0.90 [d, $^{3}J_{H\text{-}H}$ = 6.8 Hz, 3H, CH(CH_3)$_2$], 1.05 [d, $^{3}J_{H\text{-}H}$ = 6.8 Hz, 3H, CH(CH_3)$_2$], 3.24 [sept, $^{3}J_{H\text{-}H}$ = 6.8 Hz, 1H, CH(CH$_3$)$_2$], 3.64 [sept, $^{3}J_{H\text{-}H}$ = 6.8 Hz, 1H, CH(CH$_3$)$_2$], 5.07 [s, 2H, NH_2], 5.59 [s, 1H, SiH], 5.96 [d, $^{3}J_{H\text{-}H}$ = 8.0 Hz, 1H, H_{Ar}], 6.56–6.61 [m, 1H, H_{Ar}], 6.82–6.86 [m, 1H, H_{Ar}], 6.97 [d, $^{3}J_{H\text{-}H}$ = 7.2 Hz, 1H, H_{Ar}], 7.15–7.19 [m, 12H, H_{Ar}], 7.21–7.23 [m, 3H, H_{Ar}], 3-29–3.33 [m, 3H, H_{Ar}], 7.39–7.43 [m, 1H, H_{Ar}], 7.64–7.66 [m, 3H, H_{Ar}]. **^{29}Si NMR** (119 MHz, THF-d_8, 163 K): δ[ppm] = −81.0 [d, $^{1}J_{Si\text{-}H}$ = 258 Hz, *Si*H], −22.6 [s, *Si*Ph$_3$].

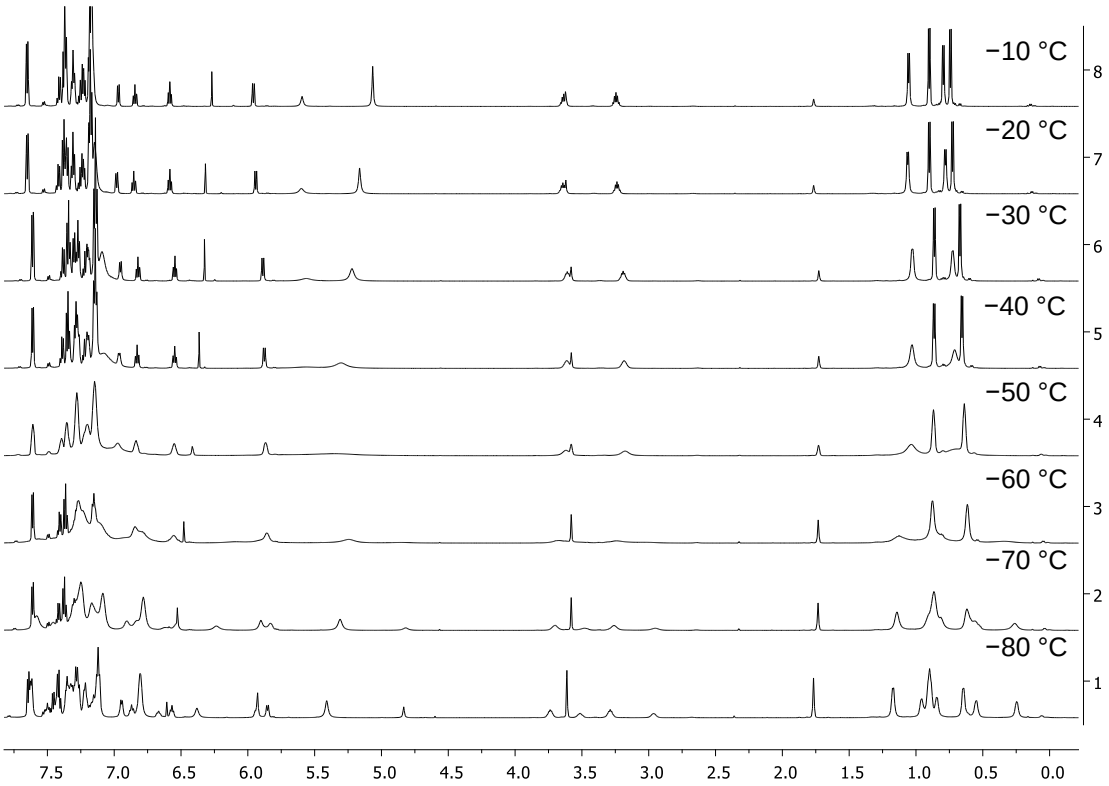

Figure S4.26. VT ^{1}H NMR of the reaction of **1** with Ph_3SiOH from −80 °C to −10 °C.

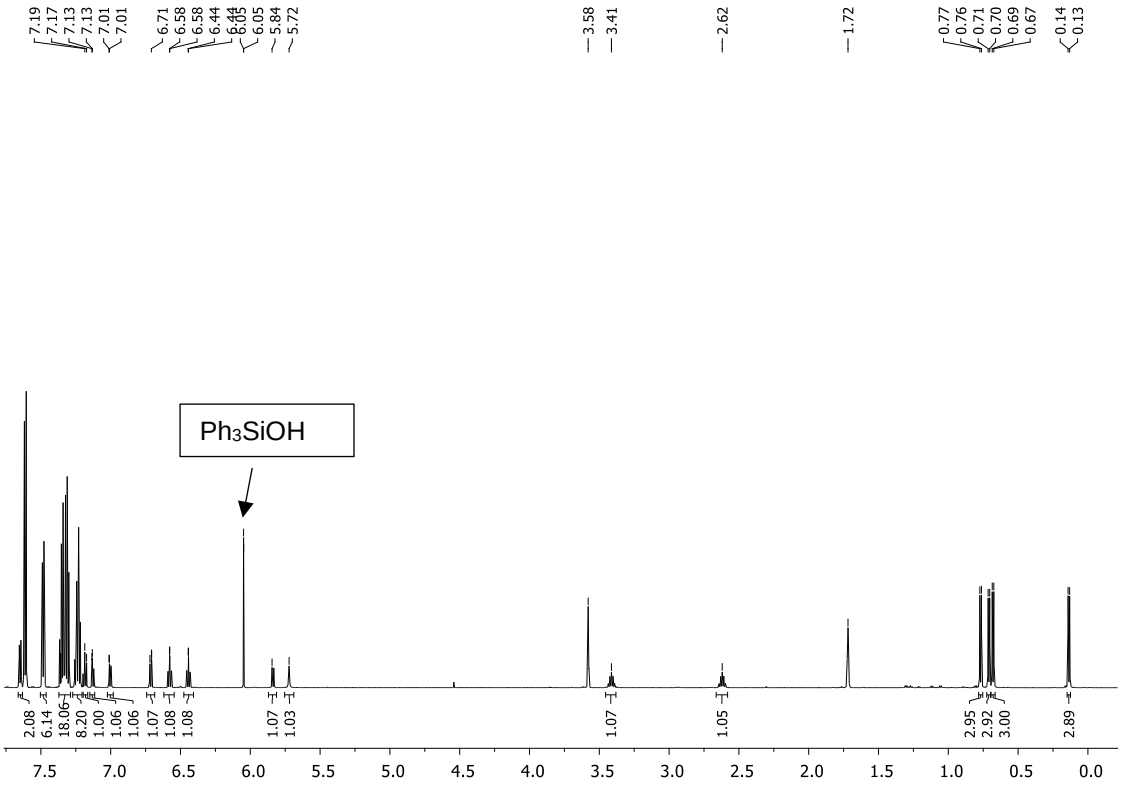

Figure S4.27. ^{1}H NMR of the reaction of **1** with Ph_3SiOH from at RT after 16 h. The spectrum only shows product **3** and excess Ph_3SiOH.

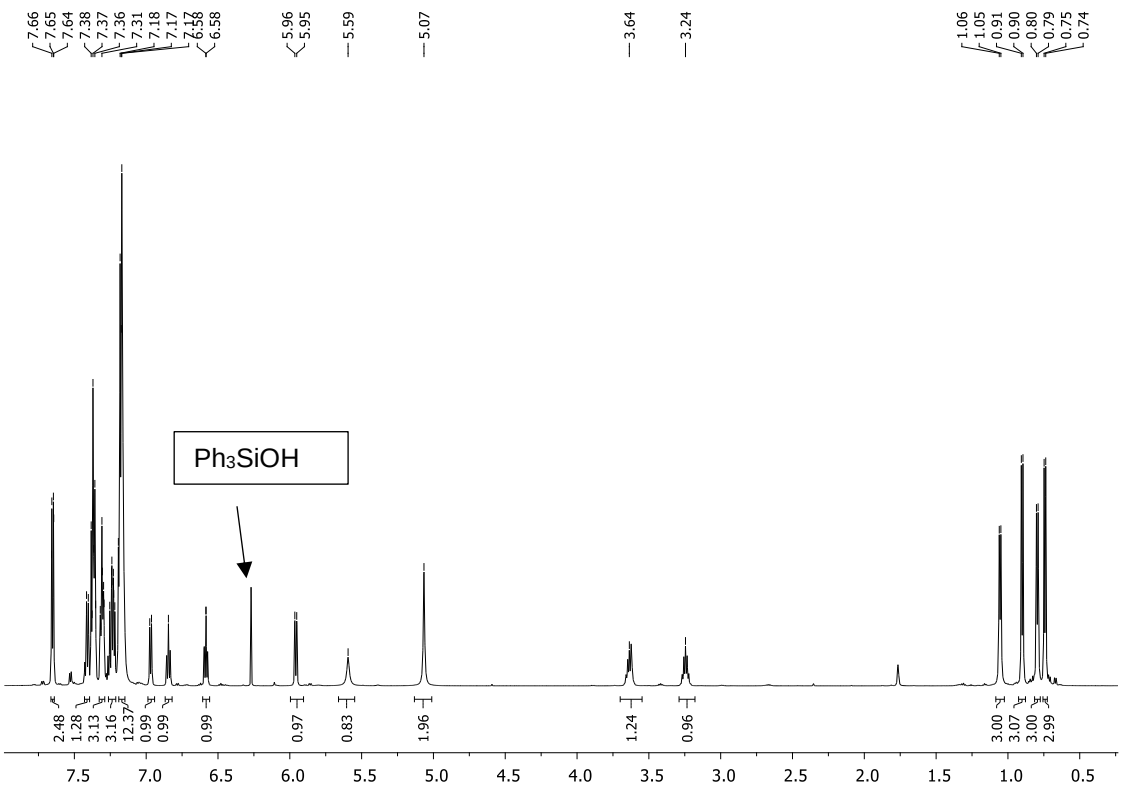

Figure S4.28. ^{1}H NMR of the intermediate **2** at 263 K in THF–d8.

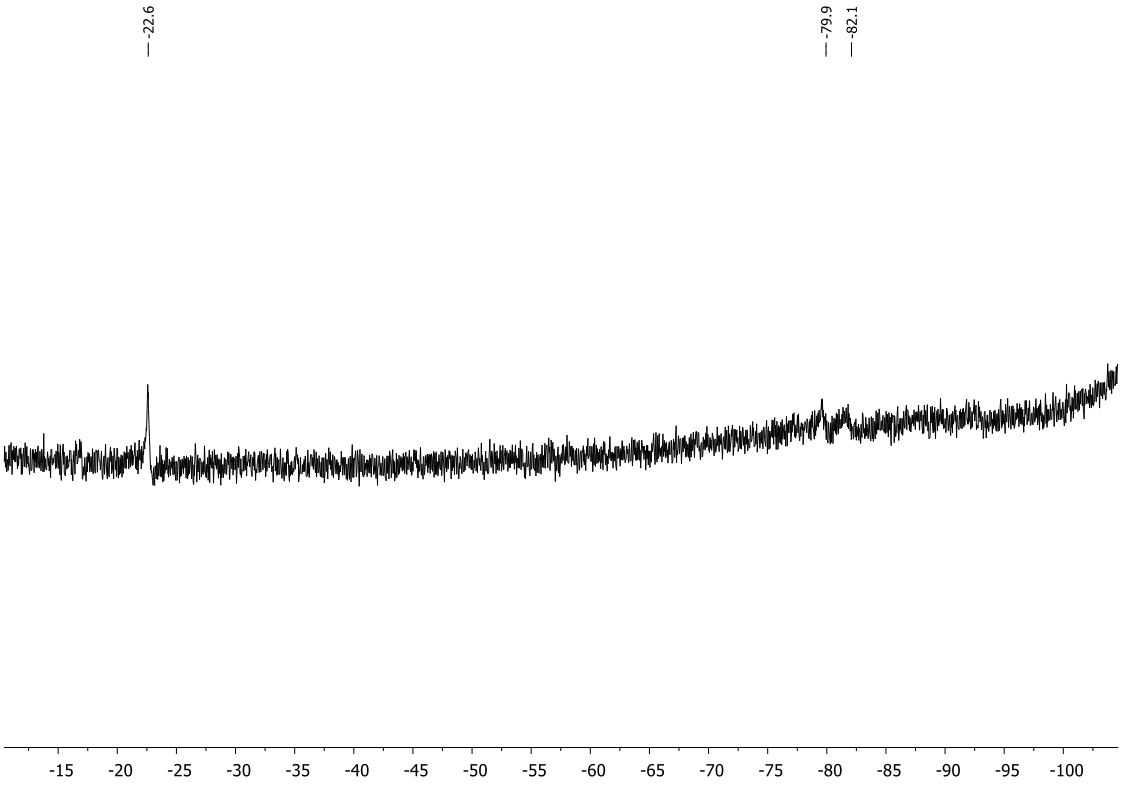

Figure S4.29. ^{29}Si NMR of the intermediate **2** at -10 °C in THF–d8. The spectrum shows very bad resolution for the dublett at −81.0 ppm. Better signals were obtained in a separate reaction when the ^{29}Si NMR was measured at room temperature (s. Figure **S4.32**).

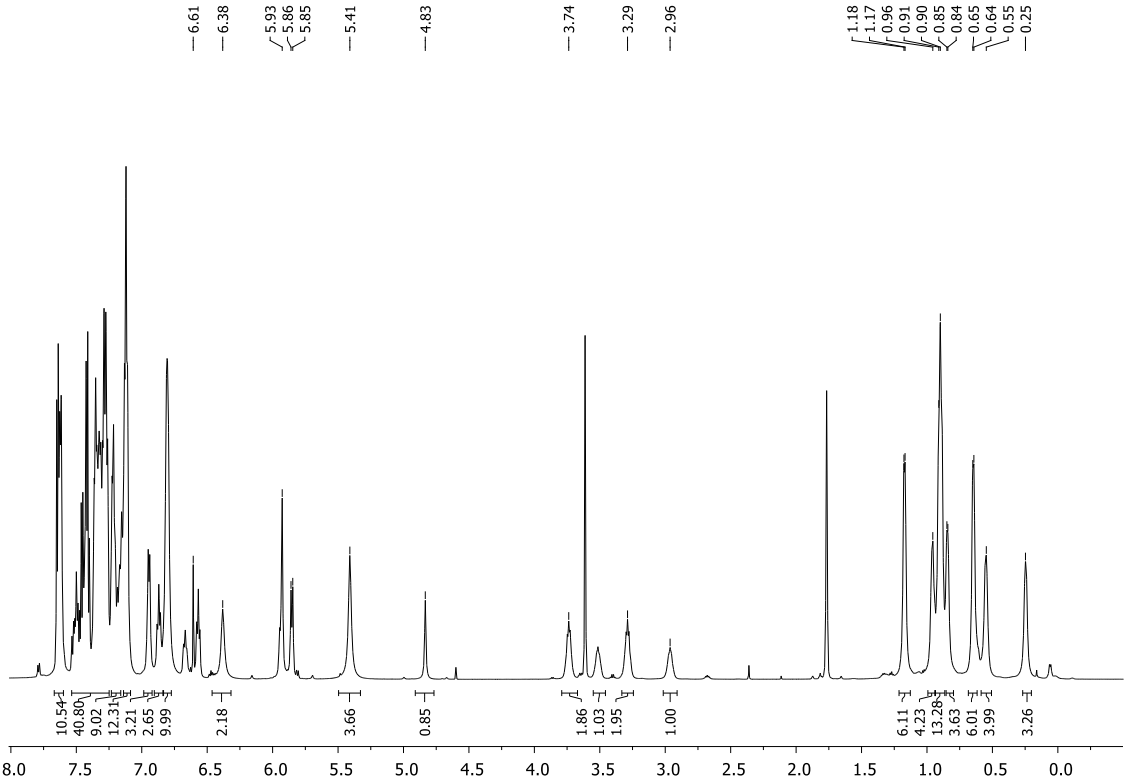

Figure S4.30. ^{1}H NMR of the intermediates **2a/2b** at −80 °C in THF–d8.

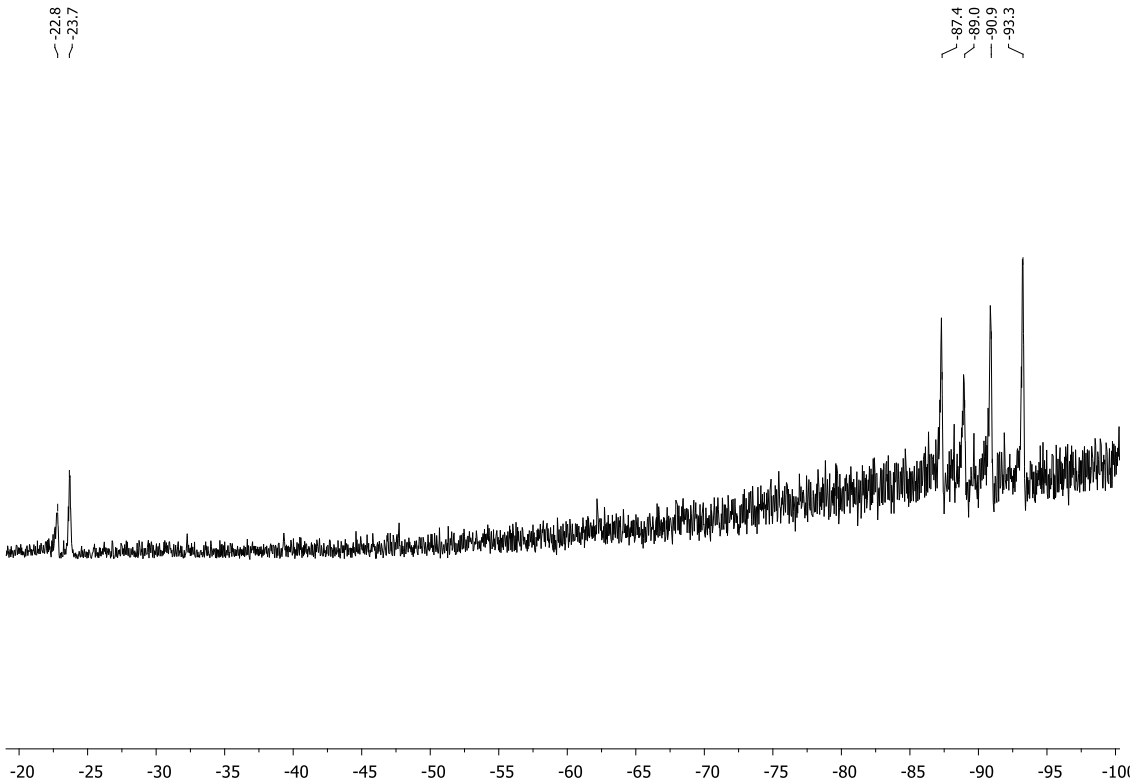

Figure S4.31. ^{29}Si NMR of the intermediates **2a/2b** at −80 °C in THF–d8.

4.6.3.3 ^{29}Si NMR measurement at room temperature after short reaction time

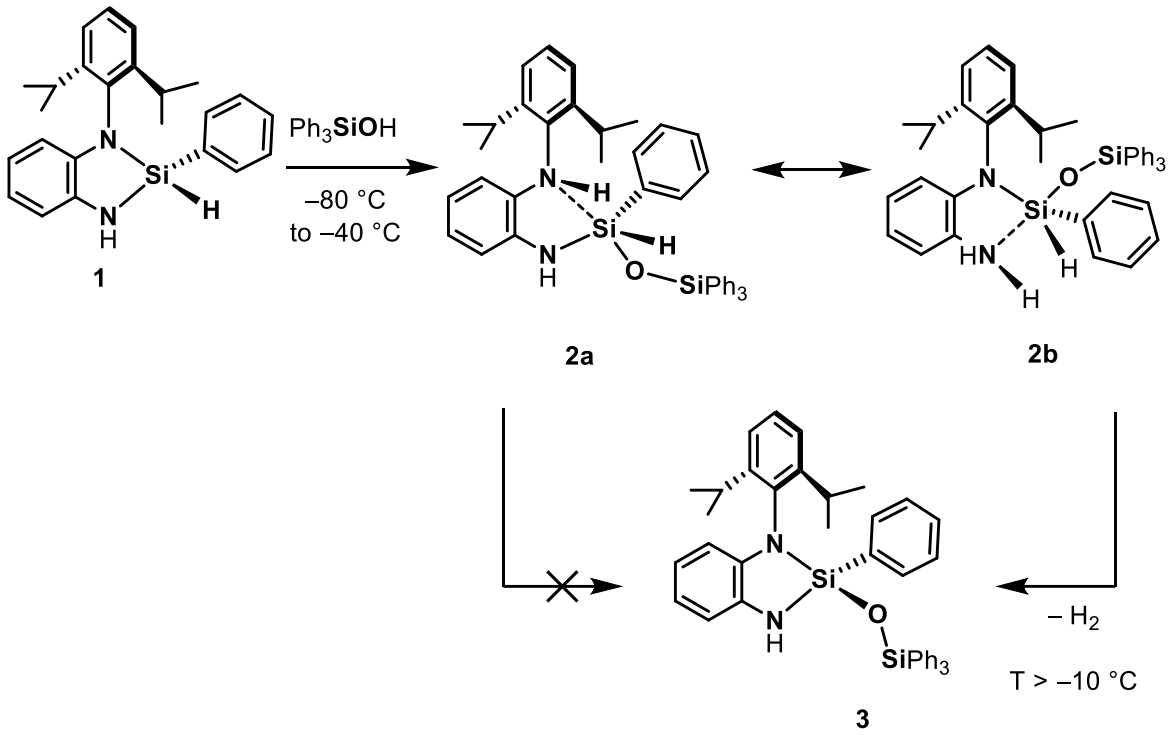

General procedure 3.1 was applied. The tube was then let to warm up to room temperature. After some minutes, ^{29}Si NMR was recorded at room temperature with the purpose to better observe the highfield shifted singlet of the pentacoordinated intermediates **2**. Such short reaction times lead to the parallel presence of educt **1**, intermediate **2** and product **3**. Since neither educt nor product show signals at chemical shifts below δ = −70 ppm, the signals in that region can be unequivovally assigned to intermediate **2**.

Compound **2**:

^{29}Si NMR (119 MHz, THF-d_8, 293 K): *δ*[ppm] = −41.0 [s, *Si*Ph$_3$], −75.4 [d, $^1J_{Si-H}$ = 243.9 Hz, *Si*H].

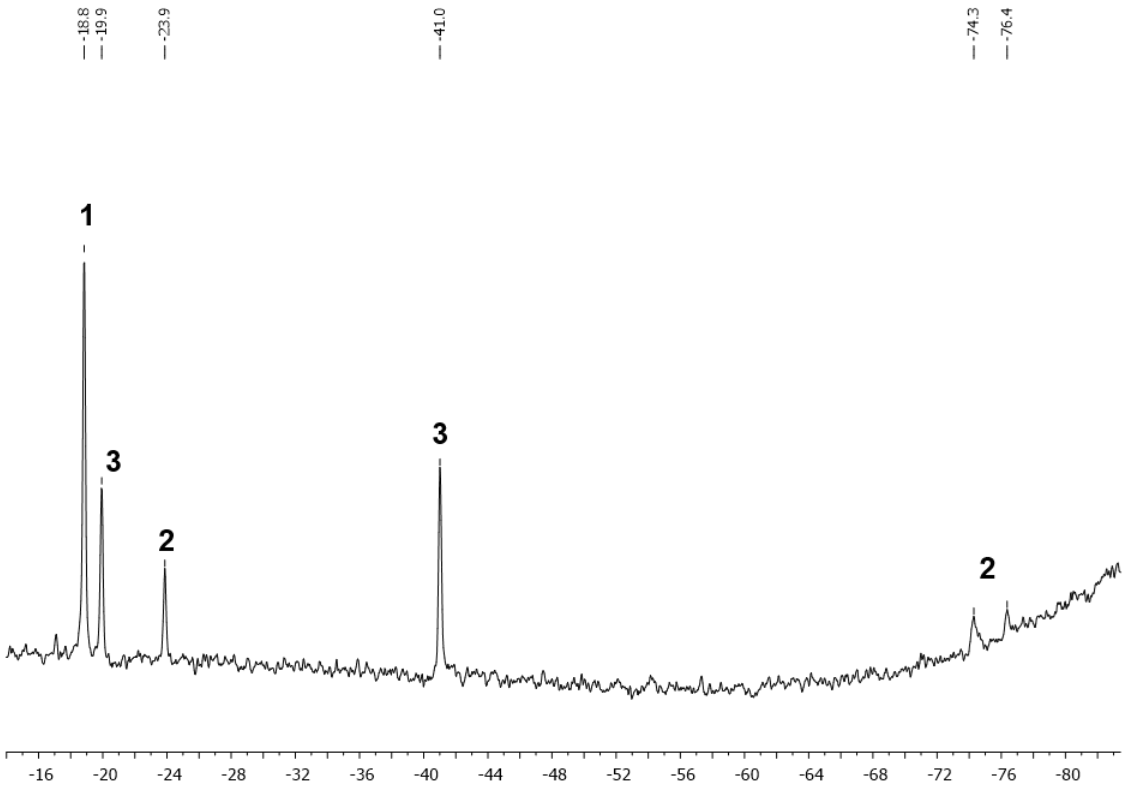

Figure S4.32. ^{29}Si NMR of the reaction of **1** with Ph_3SiOH after some minutes at room temperature.

4.6.3.4 Reaction monitoring when keeping the NMR tube at −20 °C.

General procedure 3.1 was applied. The tube was kept in a freezer at −20 °C and ^{1}H NMR spectra were recorded at 0 °C after 1 day, 2 days, 3 days and 6 days and the ratios of compounds **1**, **2** and **3** were determined based on the integrals of the spectra.

Table S4.1. Approximated relative and absolute amounts of compounds **1**, **2** and **3** in the mixture when the NMR tube is stored at −20 °C. The absolute substrate concentration is $1.7 \cdot 10^{-2}$ mol•L^{-1}.

Storage time [d]	Relative amount of **1** [%]	Absolute amount of **1** [mmol•L^{-1}]	Relative amount of **2** [%]	Absolute amount of **2** [mmol•L^{-1}]	Relative amount of **3** [%]	Absolute amount of **3** [mmol•L^{-1}]
0	100	16,7	0,0	0,0	0,0	0,0
1	55	9,2	39,0	6,5	6,0	1,0
2	27	4,5	60,0	10,0	13,0	2,2
3	13	2,2	67,0	11,2	20,0	3,3
6	0	0,0	64,0	10,7	36,0	6,0

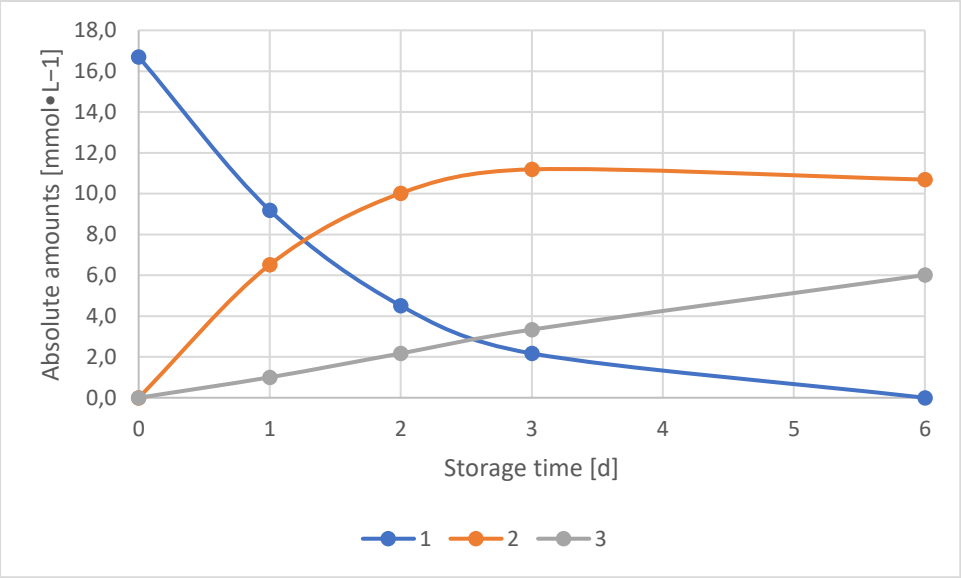

Figure S4.33. Graphical depiction of the estimated absolute amounts of compounds **1**, **2**, and **3** after time when stored at −20 °C.

Table S4.1 and Figure S4.33 show that the decline of educt **1** is decreasing after time, while the formation of product **3** stays more or less constant. The intermediate **2** is formed until a ratio of 67% and then starts do decrease again slowly. The linear functions for the formation of compound **3** and the nearly linear parts in the curves of compounds **1** and **2** beween 0 d and 1 d and also between 3 d and 6 d are given in Figures S4.34 and S4.35.

Table S4.2. Approximated reaction rates of compounds **1**, **2** and **3** for the linear parts between 0 and 1 day and between 3 and 6 days. The reaction rates are based on a sample conentration of $1.7 \cdot 10^{-2}$ mol•L^{-1}.

time span [d]	Reaction rate of **1** [mmol•L^{-1}•d^{-1}]	Reaction rate of **2** [mmol•L^{-1}•d^{-1}]	Reaction rate of **3** [mmol•L^{-1}•d^{-1}]
0-1	-7,515	6,513	1,002
3-6	-0,167	-0,167	0,891

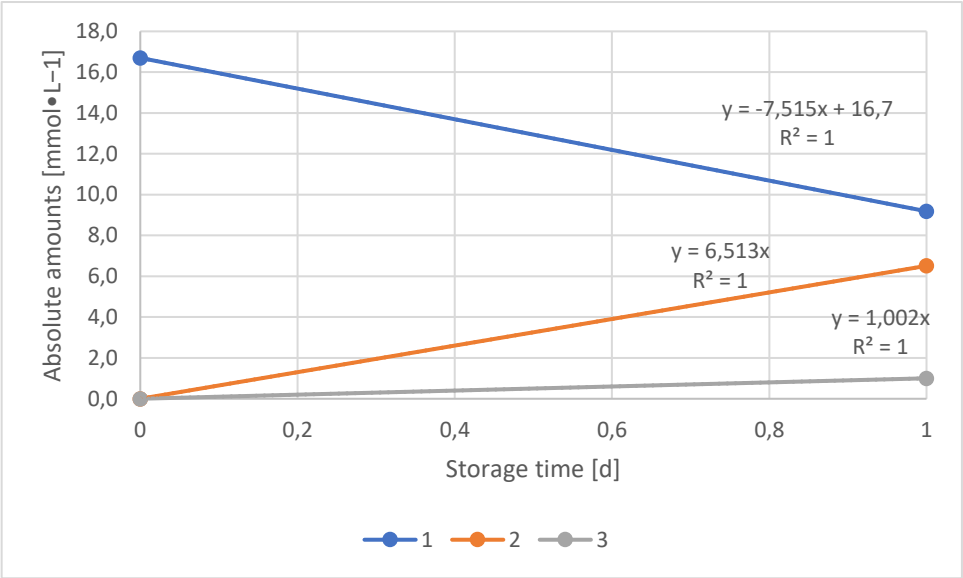

Figure S4.34. Graphical depiction of the estimated absolute amounts of compounds **1**, **2**, and **3** when stored at −20 °C between 0 and 1 day. Linear approximations were done giving the respective functions.

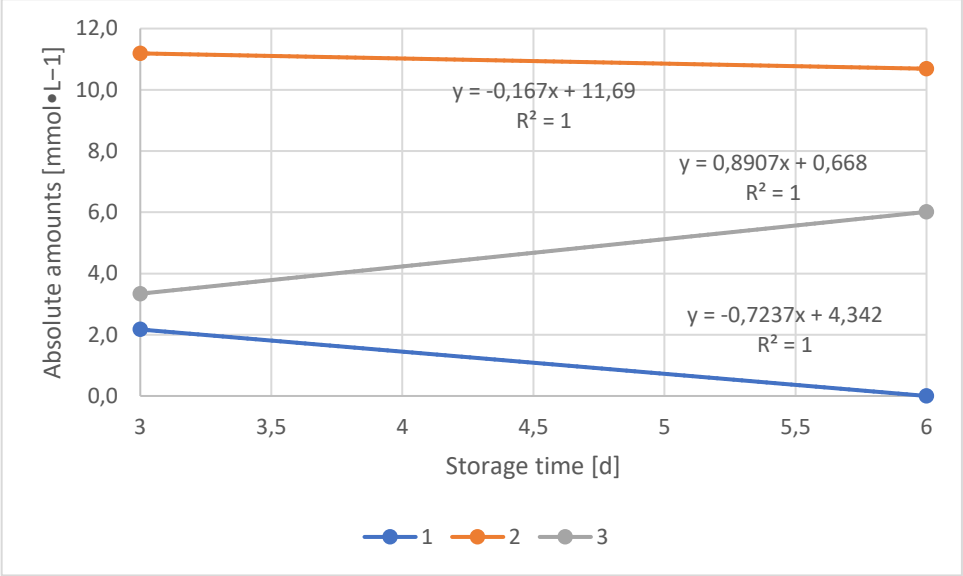

Figure S4.35. Graphical depiction of the estimated absolute amounts of compounds **1**, **2**, and **3** when stored at −20 °C between 3 and 6 days. Linear approximations were done giving the respective functions.

The slopes in these linear parts of the curves can be seen as reaction rates in mmol•L^{-1}•d^{-1} and are summarized in Table S.4.2. During the first day of reaction (Figure S4.34), the decline of educt **1** and build-up of intermediate **2** have rather similar reaction rates of −7.515 mmol•L^{-1}•d^{-1} and 6.513 mmol•L^{-1}•d^{-1}. After 3 d, a point is reached in which the amount of **2** starts to decline again which is accompanied with a negative reaction rate of −0.167 mmol•L^{-1}•d^{-1} in the region between 3 d and 6 d (Figure S4.35). This is the result of the fact that educt **1** is transformed at a much slower rate of only −0.7237 mmol•L^{-1}•d^{-1} compared to the initial −7.515 mmol•L^{-1}•d^{-1}. When product **3** builds up in a rather constant way with a reaction rate of 1.002 mmol•L^{-1}•d^{-1} and 0.8907 mmol•L^{-1}•d^{-1}, it can be concluded that in fact the build-up of **2** must decrease with the

decrease in educt decline until a point is reached where the product formation is faster than the educt conversion. From that point on, compound **2** is decreasing again which allows the conclusion, that compound **2** is in fact a true intermediate in that reaction that builds up from compound **1** and transforms into compound **3**. Unfortunately, the experiment was not carried on for further time. However, after educt **1** is completely consumed after 6 d, the slope of intermediate **2** decline should be exactly opposite to the slope of product **3** formation until reaching a zero point.

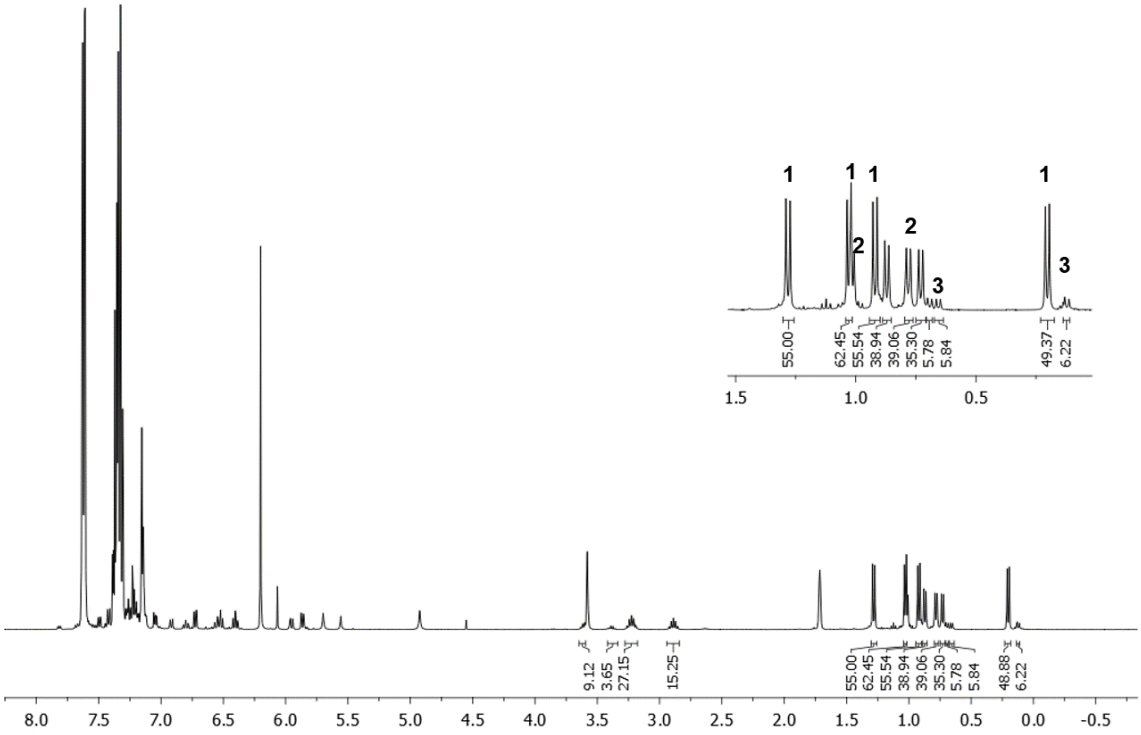

Figure S4.36. ^{1}H NMR (C_6D_6, 273 K) after storing the NMR tube at −20 °C for 1 day.

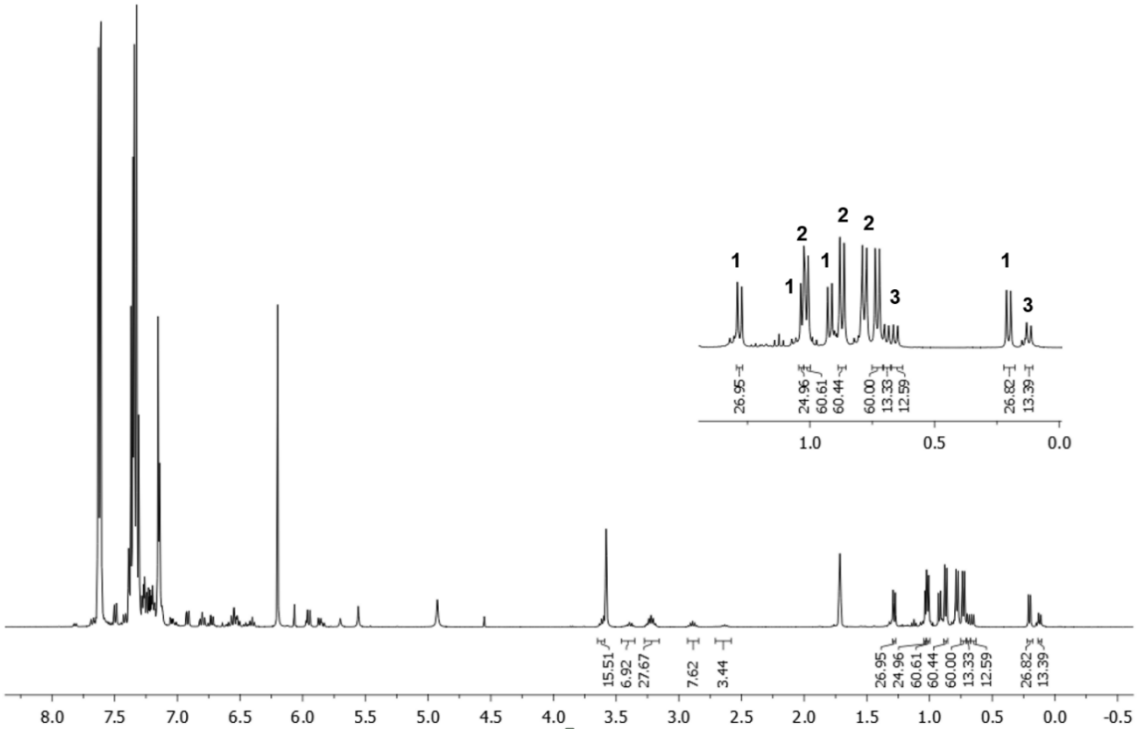

Figure S4.37. ^{1}H NMR (C_6D_6, 273 K) after storing the NMR tube at −20 °C for 2 days.

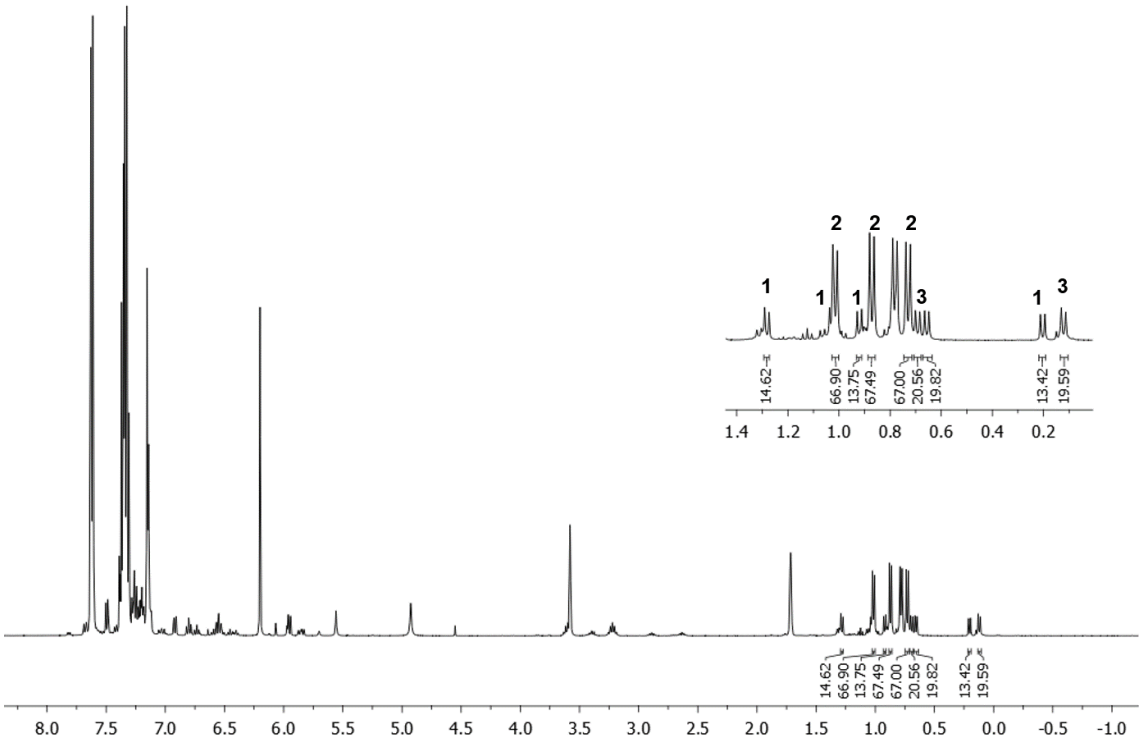

Figure S4.38. ^{1}H NMR (C_6D_6, 273 K) after storing the NMR tube at −20 °C for 3 days.

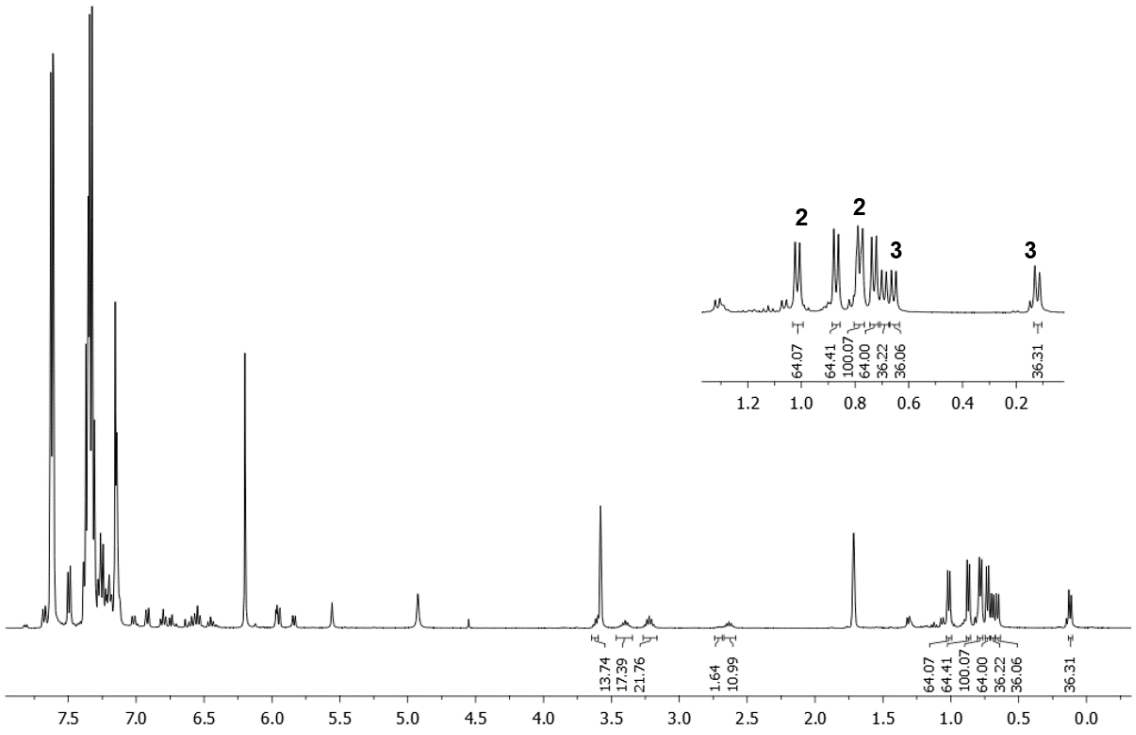

Figure S4.39. ^{1}H NMR (C_6D_6, 273 K) after storing the NMR tube at −20 °C for 6 days.

4.6.3.5 Variable temperature NMR study of reaction of compound 4 with Ph_3SiOH

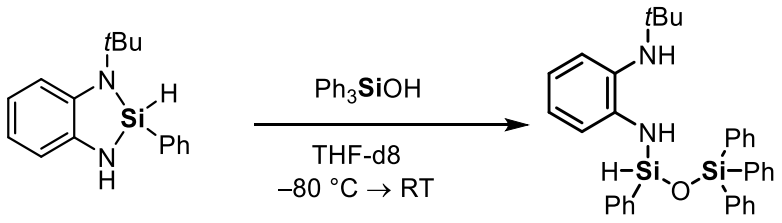

4 **5**

Compound **4** (3 mg, 10 µmol, 1.0 equiv.) was weighed into a Young NMR tube and dissolved in 0.6 mL of THF–d8. The tube was cooled down to −80 °C using a isopropanol/N_2 cooling bath and triphenylsilanol (3 mg, 10 µmol, 1.0 equiv.) was added with a funnel. The tube was quickly shaken and within minutes transferred to a 400 MHz Bruker NMR spectrometer. Variable tempertaure ^{1}H NMR spectra were recorded starting at −80 °C towards room temperature in 20 °C steps. Finally, the tube was stirred for another 16 h and a final NMR spectrum was recorded.

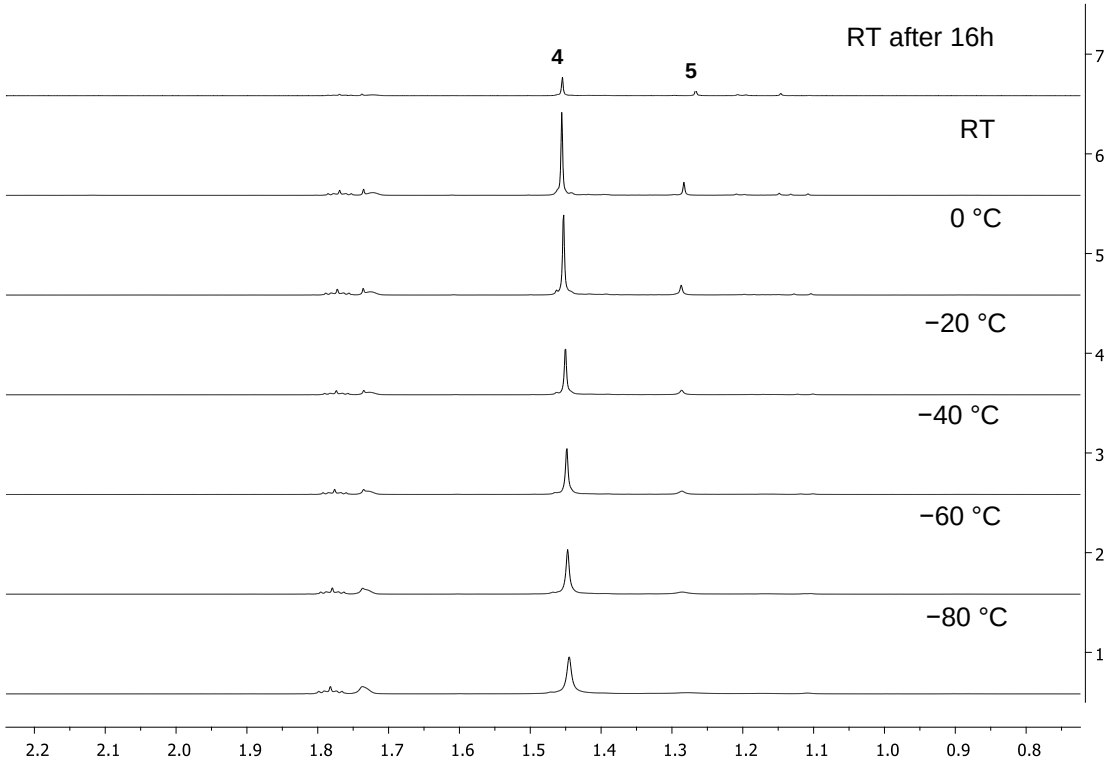

Figure S4.40. VT ^{1}H NMR of the reaction of **4** with Ph_3SiOH. The region of δ = 0.8 ppm to δ = 2.2 ppm showing the *t*Bu singlets predominatnly from starting material **4** and a slow formation of **5**.

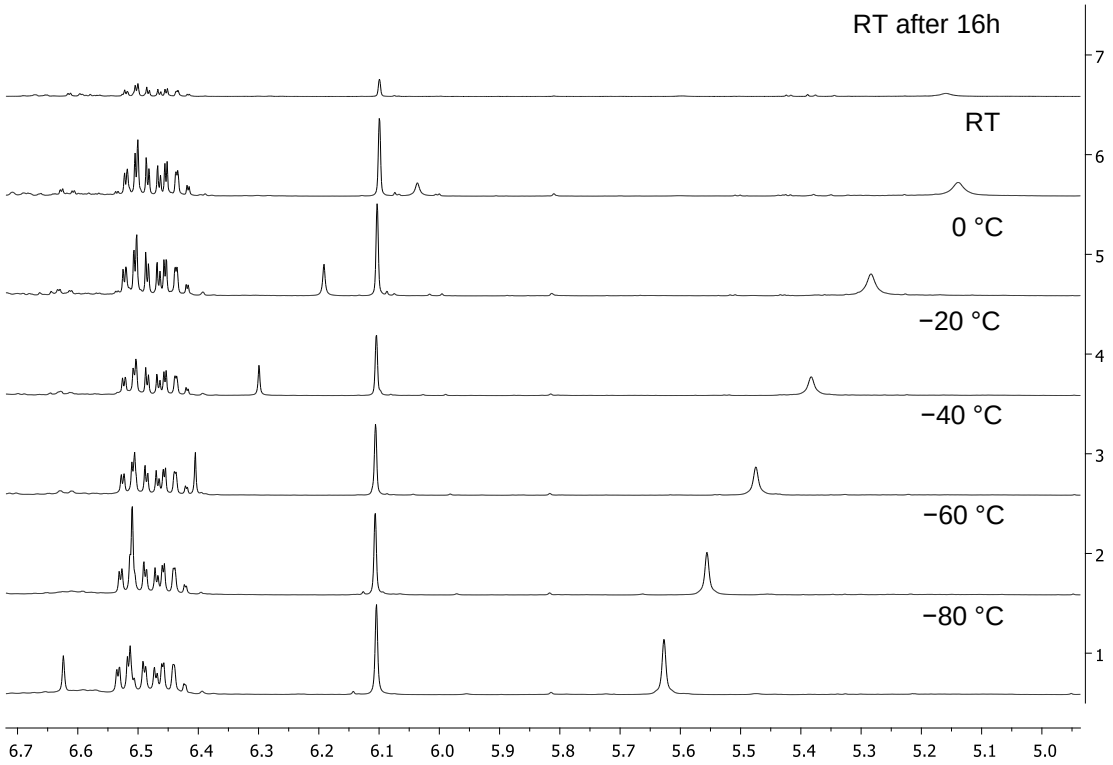

Figure S4.41. VT ^{1}H NMR of the reaction of **S3** with Ph_3SiOH. The region of δ = 5.0 ppm to δ = 6.7 ppm showing all SiH and NH signals, the shifting OH signal of remaining Ph_3SiOH and some aromatic multiplets.

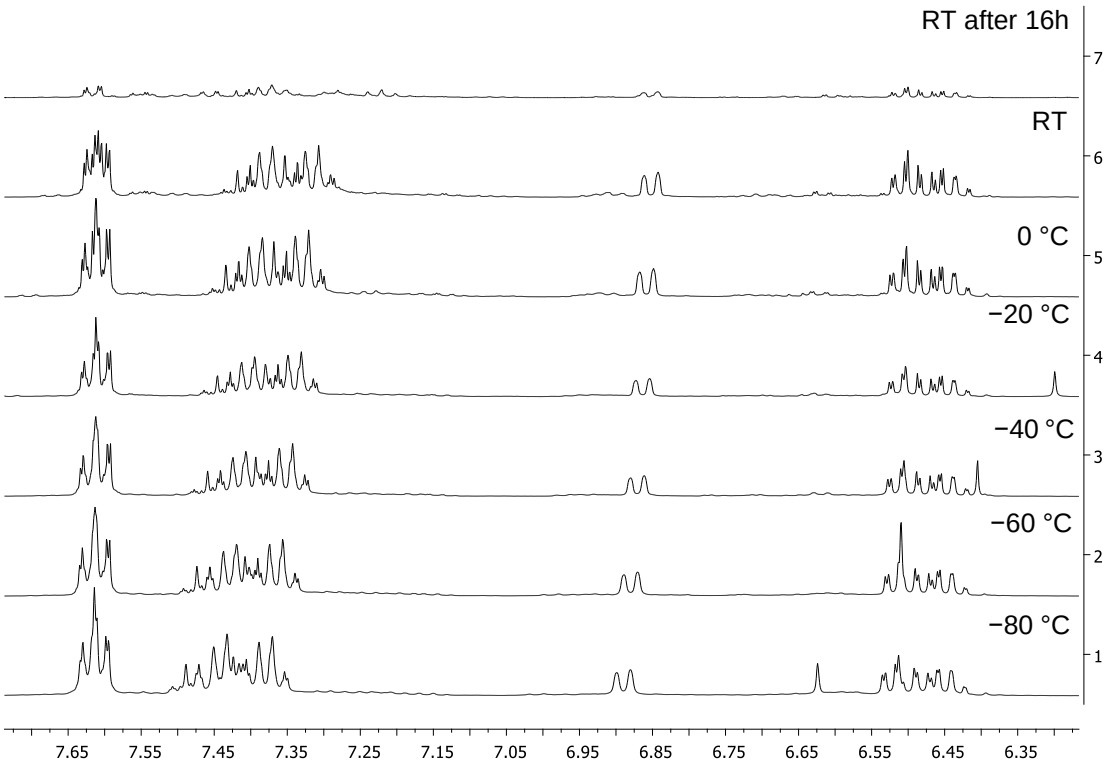

Figure S4.42. VT ^{1}H NMR of the reaction of **4** with Ph_3SiOH. The region of δ = 6.35 ppm to δ = 7.65 ppm showing OH singlets from remaining Ph_3SiOH and 3 aromatic multiplets.

4.6.4 X-ray crystallographic details

The crystals were selected and measured on a Gemini Ultra diffractometer equipped with an Atlas S2 CCD detector (**S4**), XtaLAB Synergy R, DW system diffractometer equipped with a HyPix-Arc 150 detector (**S5**), a GV50 diffractometer equipped with a TitanS2 detector (**S7**) or a Supernova, diffractometer equipped with an Atlas detector (**1, 3**). The crystals were kept at T = 123(1) K during data collection. Data collection and reduction were performed with **CrysAlisPro** [Version 1.171.41.54a or Version 1.17.41.76a.[2] A numerical absorption correction using spherical harmonics as implemented in SCALE3 ABSPACK was applied. Using **Olex2**,[3] the structures were solved with **ShelXT**[4] and a least-square refinement on F^2 was carried out with **ShelXL**[5] for all structures. All non-hydrogen atoms were refined anisotropically. Hydrogen atoms at the carbon atoms were located in idealized positions and refined isotropically according to the riding model. Figures were created with **Olex2**.[3]

Compound **1**: The asymmetric unit contains one molecule of compound **1**.
Compound **3**: The asymmetric unit contains one molecule of compound **3**.
Compound **S4**: The asymmetric unit contains one molecule of compound **S4**.
Compound **S5**: The asymmetric unit contains one molecule of compound **S5**.
Compound **S7**: The asymmetric unit contains one molecule of compound **S7**.

Table S4.3. Crystallographic data for compounds **1**, **3**, and **5**.

Compound	**1**	**3**	**5**
Data set (internal naming)	TG348	TG353	TG251
Formula	$C_{24}H_{28}N_2Si$	$C_{42}H_{42}N_2OSi_2$	$C_{34}H_{36}N_2OSi_2$
$\rho_{calc.}$ / g cm^{-3}	1.160	1.224	1.199
m/mm^{-1}	1.030	1.184	1.282
Formula Weight	372.57	646.95	544.83
Color	Clear colourless	Clear colourless	Clear colourless
Shape	Block	Block	Block
Size/mm^3	0.244×0.195×0.092	0.172×0.089×0.059	0.553×0.347×0.305
T/K	123.00(10)	123.00(10)	293(2)
Crystal System	Monoclinic	Triclinic	Triclinic
Space Group	$P2_1/c$	P-1	P-1
a/Å	10.00150(10)	9.5270(3)	9.9562(2)
b/Å	12.0551(2)	11.1155(4)	11.9185(2)
c/Å	17.7528(3)	16.8771(6)	14.1045(3)
α/°	90	98.976(3)	72.173(2)
β/°	94.7500(10)	94.987(3)	74.637(2)
γ/°	90	93.751(3)	75.329(2)
V/Å^3	2133.09(5)	1755.54(11)	1509.12(6)
Z	4	2	2
Z'	1	1	1
Wavelength/Å	1.54184	1.54184	1.54184
Radiation type	Cu K_α	Cu K_α	Cu K_α
$2\Theta_{min}$/°	8.872	8.078	6.724
$2\Theta_{max}$/°	152.226	145.852	143.984
Measured Refl.	17365	19642	36898
Independent Refl.	4374	6828	5848
R_{int}	0.0195	0.0287	0.0307
Parameters	256	432	363
Restraints	0	0	0
Largest Peak	0.33	0.36	0.35
Deepest Hole	-0.26	-0.30	-0.30
GooF	1.049	1.034	1.033
wR_2 (all data)	0.0951	0.0906	0.0842
wR_2	0.0935	0.0856	0.0827
R_1 (all data)	0.0350	0.0416	0.0333
R_1	0.0333	0.0345	0.0316

Table S4.4. Crystallographic data for compound **6** and **S3**.

Compound	**6**	**S3**
Data set (internal naming)	TG397	TG291
Formula	$C_{42}H_{36}O_2Si_3$	$C_{34}H_{34}N_2OSi_2$
$\rho_{calc.}$ / g cm^{-3}	1.236	1.228
m/mm^{-1}	1.508	0.952
Formula Weight	656.98	542.81
Color	Clear colourless	Clear colourless
Shape	Plate	Block
Size/mm^3	0.26×0.1×0.08	0.22×0.12×0.1
T/K	100.01(10)	124(1)
Crystal System	Triclinic	Triclinic
Space Group	P-1	P-1
a/Å	12.6336(6)	10.8425(4)
b/Å	13.1403(6)	12.0185(5)
c/Å	13.3843(4)	12.4936(4)
α/°	67.363(4)	104.816(3)
β/°	62.497(4)	92.098(3)
γ/°	68.033(4)	109-754(4)
V/Å^3	1765.90(15)	1467.69(10)
Z	2	2
Z'	1	1
Wavelength/Å	1.54184	1.39222
Radiation type	Cu K_α	Cu K_β
$2\Theta_{min}$/°	7.508	6.67
$2\Theta_{max}$/°	147.074	148.432
Measured Refl.	54619	21102
Independent Refl.	6889	7807
R_{int}	0.0399	0.0425
Parameters	428	359
Restraints	0	0
Largest Peak	0.63	0.47
Deepest Hole	-0.38	-0.37
GooF	1.062	1.043
wR_2 (all data)	0.1046	0.1305
wR_2	0.1006	0.1198
R_1 (all data)	0.0444	0.0583
R_1	0.0375	0.0464

Compound 1

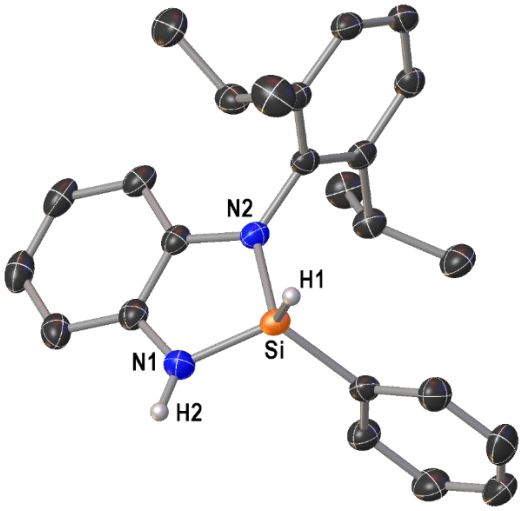

Selected Bond Lengths in Å		Selected Bond Angles in ˚	
Si–N1	1.7238(10)	**N1–Si–N2**	91.19(5)
Si–N2	1.7382(9)		
Si–H1	1.447(15)		

Compound 3

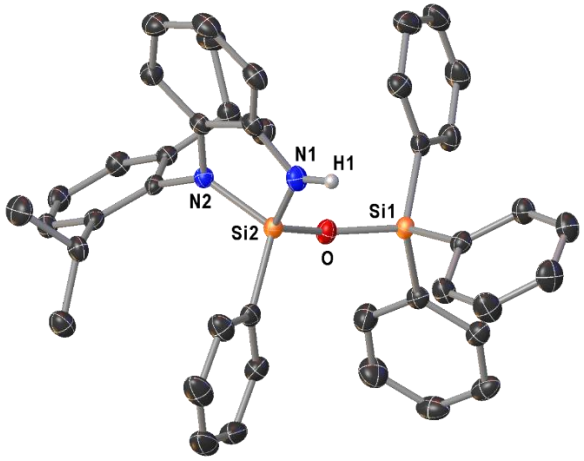

Selected Bond Lengths in Å		Selected Bond Angles in ˚	
Si1–O	1.6419(10)	**Si1–O–Si2**	147.82(7)
Si2–O	1.6182(10)	**N1–Si2–N2**	91.82(6)
Si2–N1	1.7243(12)	**O–Si2–N1**	115.85(6)
Si2–N2	1.7326(11)	**O–Si2–N2**	114.13(5)

Compound 5

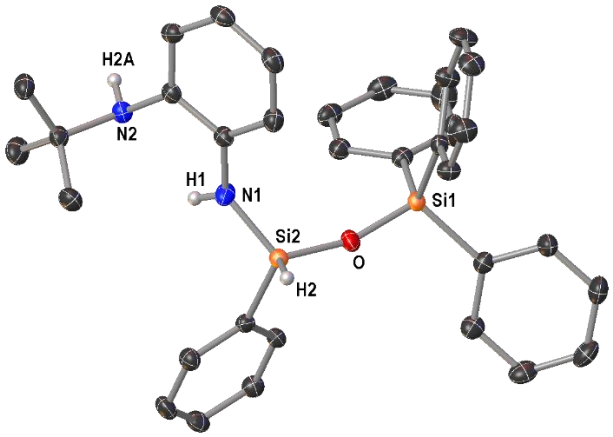

Selected Bond Lengths in Å		Selected Bond Angles in °	
Si1–O	1.6239(8)	**Si1–O–Si2**	162.46(6)
Si2–O	1.6218(8)	**O–Si2–N1**	113.59(5)
Si2–N1	1.7093(11)		
Si2–H2	1.366(16)		

Compound 6

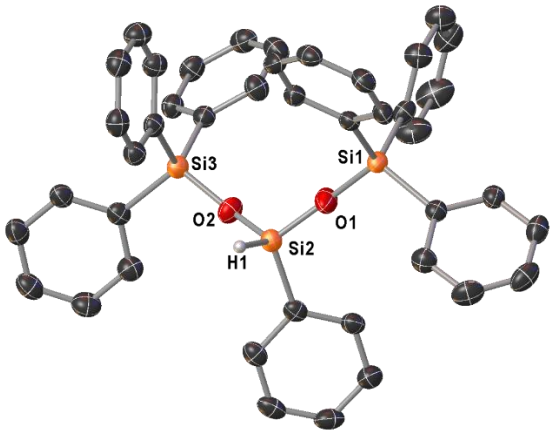

Selected Bond Lengths in Å		Selected Bond Angles in °	
Si1–O1	1.6226(12)	**Si1–O1–Si2**	165.35(11)
Si2–O1	1.5983(13)	**O1–Si2–O2**	108.94(7)
Si2–O2	1.6106(12)	**Si2–O2–Si3**	151.94(8)
Si3–O2	1.6326(12)		
Si2–H1	1.421(19)		

Compound S3

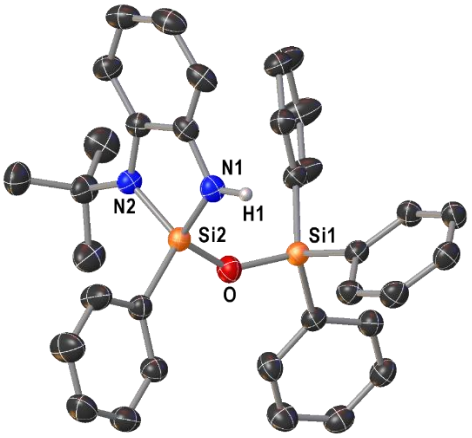

Selected Bond Lengths in Å		Selected Bond Angles in °	
Si1–O	1.6421(12)	**Si1–O–Si2**	140.10(8)
Si2–O	1.6252(12)	**O–Si2–N1**	113.78(7)
Si2–N1	1.7193(15)	**O–Si2–N2**	116.68(7)
Si2–N2	1.7338(13)	**N1–Si2–N2**	92.55(7)

4.6.5 Quantum chemical calculations

Optimization and additional harmonic vibrational frequency analyses were performed with the software package Gaussian 09 (Revision E.01) at the M062X/6-311+G(d,p) level of theory without symmetry restrictions.[6] The GJF input files and the figures of the optimized structures were created with the program GaussView version 5.0.9.[7] For the ground state structures, the vibrational frequency analysis showed no imaginary frequency in the harmonical approximation. Energies (Δ*G*) are given based on the sum of electronic and thermal free energies (Gibbs energies) at 298.15 K in kJ mol^{-1}. The sum of electronic and thermal free energies (Gibbs energies) at 298.15 K are summarized in Table S.4.4, and the Cartesian coordinates of the calculated systems can be found in Tables S4.5–S4.10. The Hartree units were converted as follows:[8] 1 hartree = 2625.4995 kJ mol^{-1}.

Table S4.4. Sum of electronic and thermal free energies (Gibbs energies) at 298.15 K of the optimized structures.

Optimized structure	Method/Basis	Gibbs energies [Hartree]
Int-A	M062X/6-311+G(d,p)	−1814.900836
TS-A	M062X/6-311+G(d,p)	−1814.839771
Prod-A	M062X/6-311+G(d,p)	−1814.920036
Int-B	M062X/6-311+G(d,p)	−1814.903175
TS-B	M062X/6-311+G(d,p)	−1814.831364
Prod-B	M062X/6-311+G(d,p)	−1814.927032

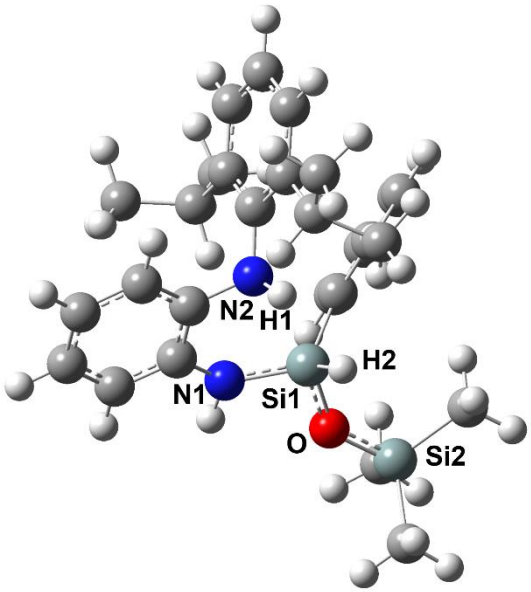

Figure S4.41. Optimized structure of **Int-A** [B3LYP/6-311+G(d,p)].

Table S4.5. Cartesian coordinates of the optimized structure of **Int-A** [B3LYP/6-311+G(d,p)].

Atomic symbol	X	Y	Z
C	2.7754690	2.5159760	0.1887980
C	1.5104610	1.9414940	0.1885970
C	2.9700370	3.8076860	-0.2853390
C	0.3985660	2.6582680	-0.2756770
C	1.8743620	4.5197640	-0.7665600
C	0.6066460	3.9566040	-0.7607800
H	3.6137130	1.9210950	0.5388280
H	3.9594320	4.2466810	-0.2885740
H	2.0059610	5.5241910	-1.1516780
H	-0.2411720	4.5193020	-1.1371600
N	1.2820150	0.5944870	0.6484350
N	-0.8645020	2.0846280	-0.2636850
Si	-1.4920020	0.6374050	0.4802400
O	-3.1079980	1.0014210	0.4156820
Si	-4.5819450	0.3281350	0.7958450
C	-1.3569020	-1.0014130	-0.4167090
C	-2.1836650	-1.2320710	-1.5247450
C	-0.6049310	-2.0716750	0.0759890
C	-2.2715870	-2.4911090	-2.1086570
H	-2.7796910	-0.4176560	-1.9274280
C	-0.6860310	-3.3354350	-0.5041000
H	0.0505390	-1.9270860	0.9283590
C	-1.5273300	-3.5484860	-1.5913990
H	-2.9211600	-2.6503580	-2.9620260
H	-0.0941400	-4.1510760	-0.1050160
H	-1.5991530	-4.5332250	-2.0388260
H	-1.0985700	0.4833310	1.8982570

H	1.1834380	0.5968130	1.6555680
H	-1.5949060	2.6968060	-0.6029400
C	-4.3143470	-1.3665140	1.5505750
H	-3.6430080	-1.3128840	2.4129160
H	-5.2622570	-1.7894730	1.8955760
H	-3.8764170	-2.0596800	0.8265520
C	-5.6007080	0.1962280	-0.7681040
H	-6.6300090	-0.0909450	-0.5353050
H	-5.6319560	1.1539530	-1.2938730
H	-5.1913800	-0.5542330	-1.4487090
C	-5.4230090	1.4673210	2.0167400
H	-4.8295490	1.5656170	2.9292510
H	-5.5502270	2.4656570	1.5907200
H	-6.4107950	1.0912790	2.2961650
C	2.2328060	-0.3923640	0.2399770
C	3.0269470	-1.0379160	1.2095510
C	2.3326020	-0.7239990	-1.1236890
C	3.9020180	-2.0396520	0.7910420
C	3.2455110	-1.7109540	-1.4926760
C	4.0188900	-2.3734400	-0.5511560
H	4.5197270	-2.5527070	1.5177030
H	3.3394970	-1.9772830	-2.5393570
H	4.7132260	-3.1453680	-0.8611830
C	1.4784810	-0.0604090	-2.1924300
H	0.6428600	0.4361010	-1.6963300
C	2.9275250	-0.6579170	2.6814090
H	2.8131360	0.4323220	2.7355560
C	1.7040370	-1.3099860	3.3462860
H	1.6471110	-1.0353080	4.4027880
H	0.7596360	-1.0228350	2.8760700
H	1.7864110	-2.3985460	3.2791050
C	4.1835250	-0.9975820	3.4863870
H	4.2965890	-2.0772440	3.6136470
H	5.0849520	-0.6115550	3.0064230
H	4.1095520	-0.5592010	4.4839500
C	0.8806150	-1.0871490	-3.1614380
H	0.1138600	-0.6094360	-3.7767060
H	1.6405560	-1.4865510	-3.8387360
H	0.4217330	-1.9198610	-2.6273940
C	2.2709970	0.9928920	-2.9804970
H	1.6319190	1.4443570	-3.7442050
H	2.6500050	1.7888910	-2.3384470
H	3.1212970	0.5244050	-3.4857930

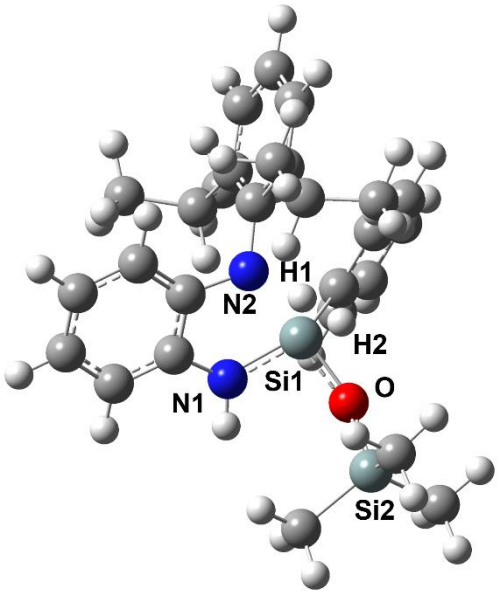

Figure S4.42. Optimized structure of **TS-A** [B3LYP/6-311+G(d,p)].

Table S4.6. Cartesian coordinates of the optimized structure of **TS-A** [B3LYP/6-311+G(d,p)].

Atomic symbol	X	Y	Z
C	1.6747030	-2.8755640	0.6281930
C	0.6598390	-1.9342980	0.6456980
C	1.6087740	-3.9672680	1.4983230
C	-0.4326430	-2.0732720	1.5164700
C	0.5352800	-4.1001970	2.3689420
C	-0.4923980	-3.1531010	2.3856080
H	2.5174400	-2.7433710	-0.0420440
H	2.4014350	-4.7051160	1.4949200
H	0.4901260	-4.9441960	3.0465950
H	-1.3265660	-3.2542380	3.0710880
N	0.5774220	-0.7717830	-0.1561900
N	-1.3743590	-1.0549840	1.3716490
Si	-1.1778170	0.1494740	0.1251870
O	-2.8011800	0.4189480	-0.1527420
Si	-4.2338120	-0.2479590	-0.6487130
C	-0.6230970	1.9234770	0.3204970
C	-1.1492680	2.6537640	1.3936030
C	0.1951950	2.5917470	-0.5959930
C	-0.8567620	4.0031980	1.5565780
H	-1.8016010	2.1652040	2.1116780
C	0.4817710	3.9459040	-0.4425420
H	0.6234820	2.0623400	-1.4412400
C	-0.0410450	4.6528050	0.6347120
H	-1.2685750	4.5481410	2.3981920
H	1.1175710	4.4447440	-1.1647070
H	0.1853050	5.7057940	0.7561910
H	-1.1045950	-0.2766360	-1.5884100
H	-0.3240500	-0.6897500	-1.2184790
H	-2.2726170	-1.1950240	1.8105320

C	-3.9924740	-1.0448940	-2.3273170
H	-3.2849250	-1.8770480	-2.2735960
H	-4.9374850	-1.4377450	-2.7126440
H	-3.6078110	-0.3224570	-3.0519700
C	-5.4946800	1.1247240	-0.7364630
H	-6.4663470	0.7517850	-1.0710870
H	-5.6297040	1.5916490	0.2421860
H	-5.1692620	1.9000300	-1.4340680
C	-4.7704410	-1.5531400	0.5894940
H	-4.0564830	-2.3811330	0.6278510
H	-4.8680430	-1.1322310	1.5947090
H	-5.7431500	-1.9713120	0.3154920
C	1.8226650	-0.1397240	-0.4870410
C	2.3278300	-0.2490300	-1.7941730
C	2.5195250	0.5835600	0.5041750
C	3.4949900	0.4482520	-2.1173440
C	3.6914940	1.2406000	0.1397040
C	4.1691160	1.1944370	-1.1644590
H	3.8857350	0.3939860	-3.1277740
H	4.2359840	1.8086490	0.8855750
H	5.0736440	1.7286650	-1.4311370
C	2.0471720	0.6497770	1.9473160
H	1.0029230	0.3308000	1.9837530
C	1.6655090	-1.1047060	-2.8633190
H	0.8817250	-1.7004390	-2.3885960
C	1.0269370	-0.2387050	-3.9557300
H	0.5243080	-0.8640540	-4.6980530
H	0.2935610	0.4565970	-3.5405390
H	1.7921900	0.3490760	-4.4708960
C	2.6573860	-2.0990850	-3.4800350
H	3.4478970	-1.5847790	-4.0320510
H	3.1280890	-2.7136810	-2.7098900
H	2.1398050	-2.7603530	-4.1791000
C	2.1198370	2.0712390	2.5179080
H	1.5689630	2.1194870	3.4604490
H	3.1536920	2.3577810	2.7301330
H	1.6934820	2.8041710	1.8320640
C	2.8624410	-0.3065210	2.8309610
H	2.5123690	-0.2497500	3.8650950
H	2.7767730	-1.3407660	2.4960370
H	3.9195490	-0.0241030	2.8142290

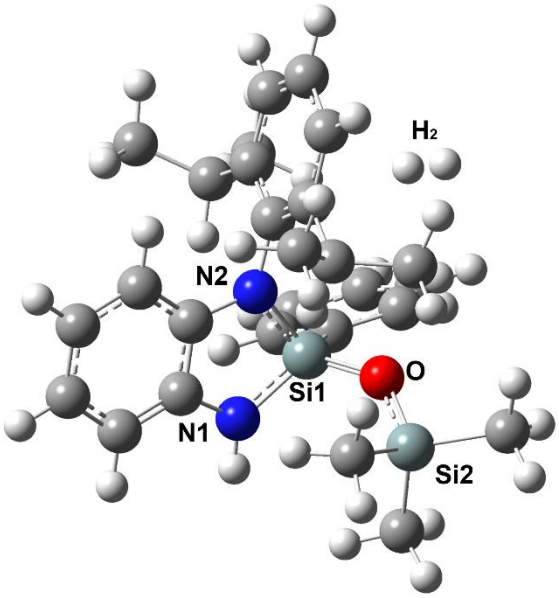

Figure S4.43. Optimized structure of **Prod-A** [B3LYP/6-311+G(d,p)].

Table S4.7. Cartesian coordinates of the optimized structure of **Prod-A** [B3LYP/6-311+G(d,p)].

Atomic symbol	X	Y	Z
C	0.2940750	-2.7259880	1.7319480
C	-0.0086700	-1.3890990	1.5247730
C	-0.0416060	-3.3184350	2.9539090
C	-0.6504370	-0.6374710	2.5351980
C	-0.6727600	-2.5817260	3.9457550
C	-0.9839620	-1.2337240	3.7392860
H	0.7890870	-3.2928780	0.9510960
H	0.1955940	-4.3617600	3.1223650
H	-0.9292350	-3.0487360	4.8886300
H	-1.4790890	-0.6560270	4.5123400
N	0.2526840	-0.6326320	0.3713290
N	-0.8750310	0.6899060	2.1453570
Si	-0.4019240	0.9775440	0.4966250
O	-1.6479920	1.2750420	-0.5258800
Si	-3.3174010	1.3454330	-0.4015080
C	0.8202610	2.3525570	0.2658340
C	1.7478270	2.6384580	1.2756130
C	0.8639770	3.1008490	-0.9160160
C	2.6983600	3.6387730	1.1079770
H	1.7257050	2.0695150	2.2009890
C	1.8247560	4.0921600	-1.0936630
H	0.1411840	2.9007840	-1.6998860
C	2.7417790	4.3600130	-0.0819960
H	3.4091600	3.8507840	1.8983550
H	1.8562510	4.6574410	-2.0178520
H	3.4889800	5.1333430	-0.2192740
H	1.2927050	0.9522060	-3.5439020
H	1.3172980	0.4231980	-3.0227650
H	-1.2681850	1.3263510	2.8195500

C	-3.9705640	-0.3026490	0.2004930
H	-3.3867640	-0.6478980	1.0612460
H	-5.0118010	-0.2062060	0.5211970
H	-3.9276310	-1.0761040	-0.5690110
C	-3.9911760	1.8236720	-2.0745940
H	-5.0753430	1.9579460	-2.0241280
H	-3.5527360	2.7692820	-2.4036880
H	-3.7804310	1.0697620	-2.8348580
C	-3.7381370	2.6751390	0.8511030
H	-3.4297530	2.3818150	1.8581300
H	-3.2429630	3.6177210	0.6032550
H	-4.8155160	2.8597770	0.8792210
C	0.9194790	-1.2382570	-0.7385500
C	0.1633350	-1.9235110	-1.7053960
C	2.3212150	-1.1703240	-0.8267900
C	0.8307160	-2.5186080	-2.7755150
C	2.9470600	-1.7795570	-1.9154300
C	2.2123550	-2.4476660	-2.8842100
H	0.2601260	-3.0443730	-3.5336130
H	4.0272000	-1.7312640	-2.0027620
H	2.7160430	-2.9145580	-3.7227860
C	3.1650860	-0.4697600	0.2207790
H	2.4888080	-0.0550710	0.9701140
C	-1.3474300	-2.0192860	-1.6186610
H	-1.6575970	-1.5374690	-0.6907230
C	-1.9963040	-1.2667360	-2.7853050
H	-3.0872300	-1.3205330	-2.7195010
H	-1.6956900	-0.2162540	-2.7778190
H	-1.6999700	-1.7018200	-3.7439790
C	-1.8206780	-3.4755570	-1.5646960
H	-1.5735840	-4.0099780	-2.4862290
H	-1.3594380	-4.0041540	-0.7276580
H	-2.9058750	-3.5149500	-1.4364040
C	3.9619950	0.6857200	-0.3955160
H	4.5060230	1.2276930	0.3823730
H	4.6922400	0.3150740	-1.1208440
H	3.3026950	1.3934840	-0.9051100
C	4.0919520	-1.4623960	0.9322740
H	4.6589730	-0.9540730	1.7163770
H	3.5191620	-2.2708680	1.3918650
H	4.8074710	-1.9037030	0.2326590

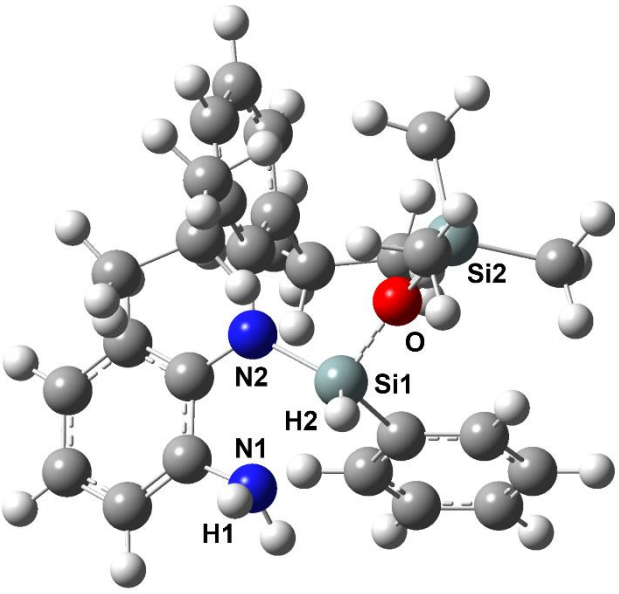

Figure S4.44. Optimized structure of **Int-B** [B3LYP/6-311+G(d,p)].

Table S4.8. Cartesian coordinates of the optimized structure of **Int-B** [B3LYP/6-311+G(d,p)].

Atomic symbol	X	Y	Z
C	0.9724630	3.0910730	0.4210680
C	1.0014330	1.9891680	-0.4465340
C	1.9030030	4.1156950	0.2805540
C	1.9799490	1.9776010	-1.4529790
C	2.8780930	4.0801550	-0.7100760
C	2.9063530	2.9973520	-1.5849970
H	0.2201660	3.1444130	1.1978710
H	1.8618750	4.9559800	0.9640480
H	3.5997150	4.8810210	-0.8062740
H	3.6465310	2.9411790	-2.3766930
N	0.1274630	0.9046130	-0.3866190
N	1.9237790	0.8127470	-2.2954700
Si	0.4401840	-0.6392270	-1.2309150
O	-0.7437540	-1.5630010	-0.5096490
Si	-2.0876760	-2.5137290	-0.5297670
C	1.9832490	-1.5672280	-0.6539750
C	3.1292710	-0.9447700	-0.1416230
C	1.9505630	-2.9666810	-0.6469760
C	4.1957760	-1.6865530	0.3582220
H	3.1906200	0.1397910	-0.0984630
C	3.0210870	-3.7169980	-0.1695940
H	1.0641920	-3.4804400	-1.0049340
C	4.1461700	-3.0768960	0.3390280
H	5.0628820	-1.1795060	0.7661690
H	2.9717500	-4.7999250	-0.1828400
H	4.9771200	-3.6570880	0.7234030
H	2.8384070	0.3965330	-2.4483470
C	-3.1336750	-2.0724420	0.9524070
H	-3.5542800	-1.0693020	0.8545630

H	-3.9544130	-2.7815620	1.0910570
H	-2.5163920	-2.0786100	1.8559410
C	-1.5595430	-4.3115130	-0.4138700
H	-2.4294060	-4.9653130	-0.3034390
H	-1.0195620	-4.6315910	-1.3095750
H	-0.9081880	-4.4707180	0.4503470
C	-3.0102840	-2.2458700	-2.1415950
H	-3.2659450	-1.1927420	-2.2842490
H	-2.3966050	-2.5571600	-2.9916660
H	-3.9385630	-2.8234910	-2.1693830
C	-0.9153460	0.9856840	0.6045610
C	-2.1968550	1.4055170	0.2086850
C	-0.6286980	0.6845230	1.9455860
C	-3.1697360	1.5823890	1.1934260
C	-1.6393960	0.8496520	2.8939250
C	-2.8942410	1.3132960	2.5278060
H	-4.1630710	1.9128060	0.9147570
H	-1.4392850	0.6151750	3.9337400
H	-3.6648490	1.4476210	3.2782650
C	0.7316420	0.1606240	2.3689520
H	1.4306920	0.3455810	1.5528270
C	-2.5170360	1.6505900	-1.2571040
H	-1.9548840	0.9096450	-1.8358250
C	-4.0011380	1.4643330	-1.5838720
H	-4.1424790	1.4535190	-2.6673330
H	-4.3931990	0.5283640	-1.1777500
H	-4.6036460	2.2858740	-1.1868340
C	-2.0585970	3.0451470	-1.7045990
H	-2.5777290	3.8123730	-1.1224140
H	-0.9861850	3.1857420	-1.5652260
H	-2.2942790	3.2029270	-2.7607070
C	0.6718900	-1.3566150	2.5966820
H	1.6724870	-1.7500550	2.7992850
H	0.0291880	-1.5865960	3.4529340
H	0.2737800	-1.8680510	1.7180180
C	1.2816220	0.8770220	3.6058800
H	2.3011170	0.5383790	3.8066890
H	1.3029690	1.9596050	3.4596550
H	0.6843380	0.6626720	4.4959000
H	1.5157320	1.0252070	-3.2018610
H	0.0475000	-0.7739200	-2.6542410

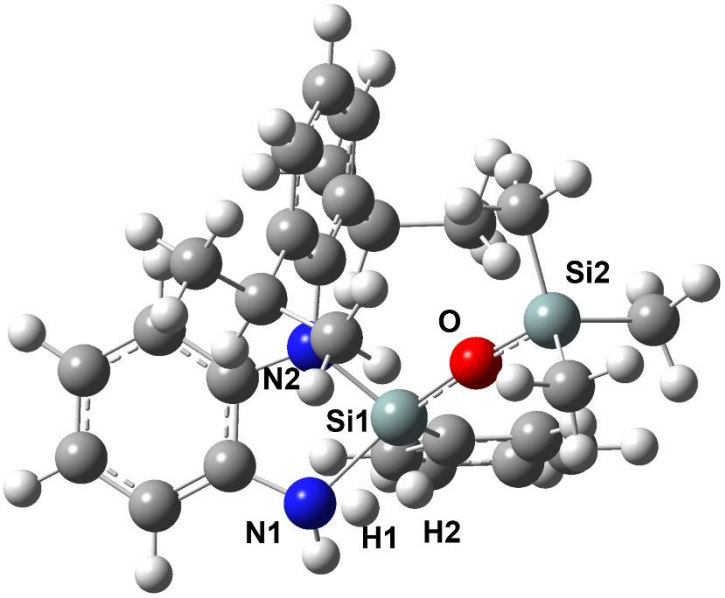

Figure S4.45. Optimized structure of **TS-B** [B3LYP/6-311+G(d,p)].

Table S4.9. Cartesian coordinates of the optimized structure of **TS-B** [B3LYP/6-311+G(d,p)].

Atomic symbol	X	Y	Z
C	-2.2653140	2.4701370	0.4991820
C	-1.2824130	1.9220940	-0.3137670
C	-2.7183810	3.7681640	0.2411710
C	-0.7567360	2.6746120	-1.3796620
C	-2.1956990	4.5092630	-0.8079500
C	-1.2058160	3.9586610	-1.6288410
H	-2.6707250	1.8946020	1.3232220
H	-3.4857210	4.1954090	0.8753670
H	-2.5523270	5.5141420	-0.9969490
H	-0.7906810	4.5243980	-2.4557990
N	-0.7189640	0.6391510	-0.1978360
N	0.2427970	1.9638210	-2.0749760
Si	0.7403480	0.3200230	-1.1316440
O	0.9092690	-1.3053550	-0.8986130
Si	1.0156050	-2.9567230	-0.9268190
C	2.4348600	0.9271870	-0.5859600
C	2.5780700	2.2375730	-0.1097340
C	3.5497850	0.0852710	-0.5385920
C	3.7861120	2.6834020	0.4160330
H	1.7279750	2.9158340	-0.1264140
C	4.7711870	0.5345320	-0.0448550
H	3.4574580	-0.9377780	-0.8824620
C	4.8877590	1.8322400	0.4418200
H	3.8706280	3.6931610	0.8008510
H	5.6269240	-0.1307890	-0.0281370
H	5.8335730	2.1811020	0.8405270
H	0.9786350	2.5429640	-2.4679160
C	-0.1447160	-3.6619020	0.3509860
H	-1.1819660	-3.3858630	0.1499170

H	-0.0759860	-4.7535280	0.3721980
H	0.1065160	-3.2838280	1.3459780
C	2.7721090	-3.4688250	-0.5054420
H	2.8110660	-4.5545600	-0.3755850
H	3.4823360	-3.2087730	-1.2949580
H	3.1123180	-3.0115210	0.4278380
C	0.6125540	-3.5776390	-2.6484320
H	-0.4375030	-3.4287470	-2.9079730
H	1.2227270	-3.0663590	-3.3980210
H	0.8255430	-4.6481850	-2.7214370
C	-1.3076880	-0.2501060	0.7606730
C	-2.5221710	-0.8846390	0.4337490
C	-0.7151860	-0.4182870	2.0211070
C	-3.1043940	-1.7274080	1.3774340
C	-1.3222570	-1.2906180	2.9286460
C	-2.5024410	-1.9430150	2.6126060
H	-4.0376010	-2.2278970	1.1489820
H	-0.8667430	-1.4498910	3.9001440
H	-2.9625240	-2.6126020	3.3301690
C	0.5538530	0.3136500	2.4173690
H	0.7419300	1.0857700	1.6699950
C	-3.1583810	-0.6822800	-0.9325690
H	-2.9211710	0.3307710	-1.2641060
C	-2.5458570	-1.6598130	-1.9430920
H	-2.9513320	-1.4879630	-2.9440380
H	-1.4610160	-1.5476790	-1.9858740
H	-2.7694380	-2.6930980	-1.6572830
C	-4.6824950	-0.8087660	-0.9198780
H	-5.0034880	-1.8382880	-0.7403740
H	-5.1283070	-0.1704030	-0.1536960
H	-5.0837220	-0.5083590	-1.8903740
C	1.7527700	-0.6428350	2.4272800
H	2.6807950	-0.0941280	2.6130800
H	1.6316050	-1.3977560	3.2111370
H	1.8489950	-1.1555870	1.4685390
C	0.4117910	1.0236790	3.7678390
H	1.3084650	1.6135910	3.9735980
H	-0.4501540	1.6945430	3.7698920
H	0.2906220	0.3107340	4.5873560
H	0.1752100	0.8044780	-2.7985140
H	0.4873210	-0.1180690	-2.8245390

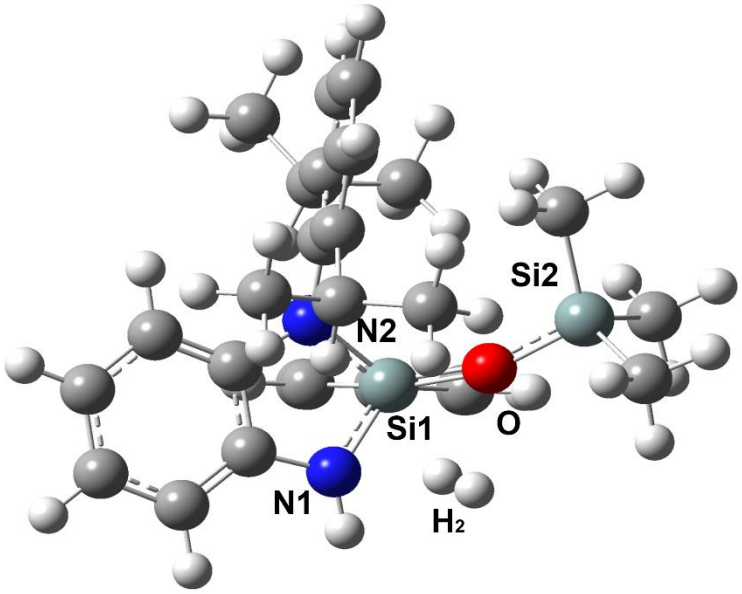

Figure S4.46. Optimized structure of **Prod-B** [B3LYP/6-311+G(d,p)].

Table S4.10. Cartesian coordinates of the optimized structure of **Prod-B** [B3LYP/6-311+G(d,p)].

Atomic symbol	X	Y	Z
C	2.3578310	-2.4609070	0.4330160
C	1.3762270	-1.8141670	-0.2985160
C	3.0346140	-3.5429800	-0.1395860
C	1.0628560	-2.2396870	-1.6087650
C	2.7263040	-3.9636110	-1.4255860
C	1.7367790	-3.3124610	-2.1688350
H	2.5913410	-2.1201420	1.4359370
H	3.8011450	-4.0548900	0.4292890
H	3.2526810	-4.8031710	-1.8630340
H	1.4991850	-3.6346640	-3.1766380
N	0.5971300	-0.7140690	0.1184360
N	0.0534710	-1.4672980	-2.1985190
Si	-0.6812280	-0.4038810	-1.0330590
O	-0.8323630	1.1643560	-1.4155800
Si	-1.0694520	2.8082920	-1.2417240
C	-2.3606740	-1.0609220	-0.5554600
C	-2.4308720	-2.3202260	0.0556460
C	-3.5522660	-0.3687650	-0.7850370
C	-3.6504880	-2.8564780	0.4517800
H	-1.5179340	-2.8843390	0.2338290
C	-4.7781870	-0.9032780	-0.3980890
H	-3.5212310	0.6021940	-1.2657880
C	-4.8264430	-2.1438760	0.2285740
H	-3.6870100	-3.8273000	0.9323800
H	-5.6930750	-0.3517770	-0.5819320
H	-5.7786240	-2.5586850	0.5389310
H	-0.3549790	-1.8137210	-3.0523140
C	-0.2543100	3.4175720	0.3231710
H	0.8159890	3.2061820	0.3551530

H	-0.3900760	4.5007570	0.4043620
H	-0.7016480	2.9587120	1.2093430
C	-2.9071720	3.1606530	-1.1354360
H	-3.0614690	4.2411530	-1.0572350
H	-3.4445440	2.8161270	-2.0230010
H	-3.3605470	2.6992920	-0.2540240
C	-0.3839050	3.6371280	-2.7692600
H	0.6954720	3.5073090	-2.8644280
H	-0.8500520	3.2243290	-3.6676130
H	-0.5939280	4.7101380	-2.7444480
C	1.1147250	0.1891910	1.0987220
C	2.2958710	0.9072110	0.8180390
C	0.4416000	0.3544710	2.3224550
C	2.7893280	1.7738960	1.7925820
C	0.9543390	1.2611880	3.2514060
C	2.1240560	1.9616110	2.9962170
H	3.7008310	2.3283100	1.5955190
H	0.4383600	1.4098910	4.1932570
H	2.5169390	2.6529500	3.7327820
C	-0.8386390	-0.4018340	2.6207690
H	-0.8795940	-1.2487770	1.9347810
C	3.0345540	0.8036900	-0.5088750
H	2.4963120	0.1129430	-1.1591400
C	3.0708460	2.1584140	-1.2251290
H	3.5948760	2.0646420	-2.1796370
H	2.0603910	2.5156880	-1.4300720
H	3.5873940	2.9149850	-0.6280660
C	4.4556380	0.2597880	-0.3187450
H	5.0597550	0.9455350	0.2822370
H	4.4426440	-0.7121560	0.1766360
H	4.9453680	0.1407210	-1.2883580
C	-2.0607000	0.4876910	2.3546110
H	-2.9853910	-0.0948540	2.4080790
H	-2.1088480	1.2960890	3.0917150
H	-2.0164370	0.9444800	1.3628410
C	-0.8880660	-0.9637800	4.0440950
H	-1.7690430	-1.6005490	4.1579260
H	-0.0009210	-1.5609370	4.2652870
H	-0.9604890	-0.1702090	4.7922040
H	1.3428980	0.6616950	-3.3951040
H	1.5854110	1.1578180	-3.8920370

4.6.6 Supplementary references

[1] T. Götz, A. Falk, J. O. Bauer, *Chem. Eur. J.* **2022**, *28*, e202103531.

[2] CrysAlisPro Software System, Rigaku Oxford Diffraction, **2020**.

[3] O. V. Dolomanov, L. J. Bourhis, R. J. Gildea, J. A. K. Howard, H. Puschmann, *J. Appl. Crystallogr.* **2009**, *42*, 339–341.

[4] G. M. Sheldrick, *Acta Crystallogr*. **2015**, *A71*, 3–8.

[5] G. M. Sheldrick, *Acta Crystallogr.* **2015**, *C71*, 3–8.

[6] Frisch, M. J.; Trucks, G. W.; Schlegel, H. B.; Scuseria, G. E.; Robb, M. A.; Cheeseman, J. R.; Scalmani, G.; Barone, V.; Mennucci, B.; Petersson, G. A.; Nakatsuji, H.; Caricato, M.; Li, X.; Hratchian, H. P.; Izmaylov, A. F.; Bloino, J.; Zheng, G.; Sonnenberg, J. L.; Hada, M.; Ehara, M.; Toyota, K.; Fukuda, R.; Hasegawa, J.; Ishida, M.; Nakajima, T.; Honda, Y.; Kitao, O.; Nakai, H.; Vreven, T.; Montgomery, J. A., Jr.; Peralta, J. E.; Ogliaro, F.; Bearpark, M.; Heyd, J. J.; Brothers, E.; Kudin, K. N.; Staroverov, V. N.; Kobayashi, R.; Normand, J.; Raghavachari, K.; Rendell, A.; Burant, J. C.; Iyengar, S. S.; Tomasi, J.; Cossi, M.; Rega, N.; Millam, J. M.; Klene, M.; Knox, J. E.; Cross, J. B.; Bakken, V.; Adamo, C.; Jaramillo, J.; Gomperts, R.; Stratmann, R. E.; Yazyev, O.; Austin, A. J.; Cammi, R.; Pomelli, C.; Ochterski, J. W.; Martin, R. L.; Morokuma, K.; Zakrzewski, V. G.; Voth, G. A.; Salvador, P.; Dannenberg, J. J.; Dapprich, S.; Daniels, A. D.; Farkas, O.; Foresman, J. B.; Ortiz, J. V.; Cioslowski, J.; Fox, D. J. *Gaussian 09*, revision E.01; Gaussian, Inc.: Wallingford, CT, **2009**.

[7] Dennington, R. D.; Keith, T. A.; Millam, J. M., II *GaussView 5.0*; Gaussian, Inc.: Wallingford, CT, **2008**.

[8] Foresman, J. B.; Frisch, A. *Exploring Chemistry with Electronic Structure Methods*, 2nd ed.; Gaussian, Inc.: Pittsburgh, PA, **1996**.

5 Synthesis and characterization of diastereomerically pure *Si*-stereogenic aminosilanes

Preface

The following chapter and supporting information are based on a manuscript in preparation about synthesis and characterization of a *Si*-stereogenic chlorosilane and chiral diaminosilanes.

Authors

T. Götz and J. O. Bauer

Author contribution

All the reported syntheses and characterizations in this work were performed by T. Götz. The manuscript draft was prepared by T. Götz

Acknowledgements

This work was jointly supported by the Elite Network of Bavaria (ENB), the Bavarian State Ministry of Science and the Arts (StMWK), and the University of Regensburg (N-LW-NW-2016-366).

5.1 Abstract

The easy and straightforward synthesis of diastereomerically pure *Si*-stereogenic silanes is presented using commercially available (*S*)-methylbenzylamine as chiral auxiliary. The compounds presented in this work are valuable precursors for further functionalization reactions based on their easy-to-substitute Si–Cl and Si–N moieties. In a special case, we observed a scarce solvent-dependent fractional crystallization behavior in which control over the molecular crystal composition is achieved by the choice of the solvent system. This resulted either in the pure crystalline diastereomer or in a 1:1 mixture of diastereomers.

5.2 Introduction

In his famous experiment, Louis Pasteur was able to separate the enantiomers of sodium ammonium tartrate by hand-picking the respective conglomerate crystals.[1,2] In most cases however, the separation of enantiomers by crystallization is impossible or impractical at best. The selective preparation and separation of optically pure compounds has become more and more important over the last few decades and has led to many industrially and socially important products such as fine chemicals and pharmaceuticals.[3] Formation of diastereomeric compounds under the use of chiral auxiliaries is a frequently used strategy to create compounds with distinguishable physical properties and therefore also crystallization behavior. Diastereomers predominantly crystallize as conglomerates which makes it a reliable separation technique for optically active molecules. In some special situations, however, 1:1 mixtures of diastereomers can be obtained with both molecules in the asymmetric unit of the crystal structure.[2,4–14] These observations have often been referred to as “failures” in fractional crystallization and represent unforeseen obstacles in the preparation of many optically pure compounds.[6] Condition-controlled crystallizations are highly important not only for academic research but also for the quality of fine chemicals and pharmaceutical products.[15] However, examples in which diastereomeric compounds could be crystallized as pure diastereomer *and* as a 1:1 mixture of both diastereomers remain, to the best of our knowledge, limited to a specific ruthenium complex by Brunner *et. al*.[16,17] The fact that the different crystallization results arose from the use of either ethanol or methanol emphasizes a major influence of solvents on this behavior. This observation suggests that a condition-controlled crystallization of either the 1:1 mixture of diastereomers or an optically pure diastereomer is generally feasible. However, such examples for main-group metal-based compounds, like silanes for instance, are not reported in the literature so far. Classical approaches for the preparation of *Si*-chiral compounds typically include the use of chiral auxiliaries like (–)-menthol[18] or other chiral organic reagents[19,20–23] to create diastereomers with distinguishable chemical and physical properties which allows them to be separated. Given the broad application and high importance of chiral silicon compounds, new synthetic techniques were developed in recent years. Many catalytic preparation strategies have emerged using hydrosilanes as prochiral

precursors for asymmetric transition metal catalyzed formation of *Si*-stereogenic silanes.[24,25] Other recent procedures exploit the coordination behavior of organolithium nucleophiles for asymmetrically substituted nucleophilic substitution on prochiral silicon electrophiles.[26,27] However, most of the examples focus on asymmetric silanes bearing only Si–C or Si–H bonds. Surprisingly few examples can be found in which the chiral silicon atom still has more than one functional substituent.[20–24,27,28]

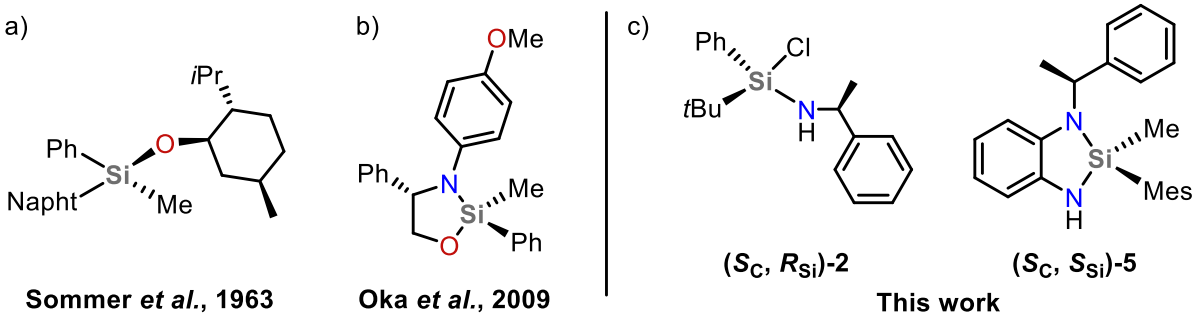

Figure 5.1. Previously reported *Si*-stereogenic silanes with chiral auxiliaries. a) Historical preparation using (–)-menthol.[5] b) Chiral silane with two Si-heteroatom bonds for further functionalization.[22] c) Chiral silane with (*S*)-methylbenzylamine as chiral auxiliary reported herein.

Regarding their synthetic value for further functionalization, it is evident that additional approaches to synthesize versatile chiral silanes are strongly required. The commercially available chiral amine (*S*)-methylbenzylamine **(*S*C)-1** has been highly useful in the preparation of chiral phosphines,[29] but analogous examples in silicon chemistry are widely unexplored.[30] In regard of some promising applications of achiral trimethylsilyl-substituted methylbenzylamine derivatives in the preparation of chiral organic molecules,[31] the transfer towards *Si*-chiral congeners seemed exceedingly desirable. Our group has previously demonstrated the synthetic use of unsymmetrically substituted *ortho*-phenylenediamine substituents in silicon chemistry for the selective siloxane bond formation and as molecular scissors for a defined siloxane bond cleavage.[32] For the purpose of creating chiral non-racemic functionalized siloxanes, the incorporation of (*S*)-methylbenzylamine **(*S*C)-1** into an unsymmetrical *ortho*-phenylenediamine bears high potential in creating the *Si*-chiral diastereomeric silanes. Additionally, the *Si*-stereogenic center can be exploited as stereochemical probe for further detailed mechanistic investigation in these types of reactions.

5.3 Results and discussion

Herein, we describe the synthesis of some diastereomerically pure *Si*-chiral silanes using (*S*)-methylbenzylamine **(*S*C)-1** as commercially available chiral anchor. The amine is demonstrated to be a synthetically powerful tool to produce non-racemic *Si*-stereogenic chlorosilanes and chiral diaminosilanes via transformation of the amine into a chiral aromatic *ortho*-phenylenediamine. In one case of chiral diaminosilane, a 1:1 mixture of diastereomers was crystallized with both isomers present in the asymmetric unit. However, it was possible to separate the diastereomers by change of the solvent system and additionally crystallize only one of the isomers.

5.3.1 Synthesis of diastereomerically pure *Si*-stereogenic chloro-aminosilanes

The synthesis of the chlorosilane was rather straightforward and achieved by simple lithiation of the amine and reaction with dichloro-*tert*-butylphenylsilane (Scheme 5.1).

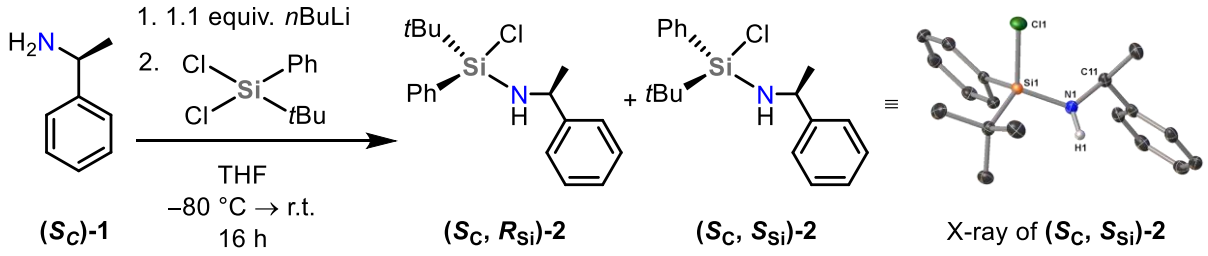

Scheme 5.1. Synthesis of *Si*-chiral chlorosilanes **(*S*C, *R*Si)-2** and **(*S*C, *S*Si)-2**. The crystal structure of compound **(*S*C, *S*Si)-2** is displayed with displacements ellipsoids set at the 50% probability level.

A slight preference for the **(*S*C, *S*Si)-2** conformer was already observed in the crude mixture in which a diastereomeric ratio of approximately 40:60 could be assigned via ^{1}H NMR spectroscopy. After four recrystallization repetitions from pentane solution and storing at −80 °C, it was possible to obtain diastereomerically pure **(*S*C, *S*Si)-2** as a crystalline solid. Diastereomer **(*S*C, *R*Si)-2** was obtained by drying the combined filtrates *in vacuo* and following the same crystallization procedure. However, only amorphous solid with a diastereomeric ratio of >99:1 according to ^{1}H NMR was obtained in that case. These *Si*-chiral compounds have great potential for further modification as they inherit both reactive nucleophilic (NH) and electrophilic (SiCl) functions. Investigations regarding asymmetric siloxane syntheses will be carried out in the future.

5.3.2 Synthesis and crystal structures of chiral cyclic diaminosilanes

For the preparation of non-racemic *Si*-chiral diaminosilanes as stereochemical probes for investigating the mechanistic scenarios at silicon centers, it is necessary to implement the (*S*)-methylbenzylamine auxiliary **(*S*C)-1** into an aromatic diamine. Albeit synthesis and characterization of compound **(*S*C)-3** has been published already by Rivas *et al.*,[33] we found a more straightforward synthesis via nucleophilic aromatic substitution of *ortho*-nitrofluorobenzene and subsequent palladium-catalyzed hydrogenation. The installation of stereogenic or non-stereogenic silicon atoms was achieved by reaction of **(*S*C)-3** with dichlorosilanes and addition of external amine bases like Et_3N or DMAP (Scheme 5.2).

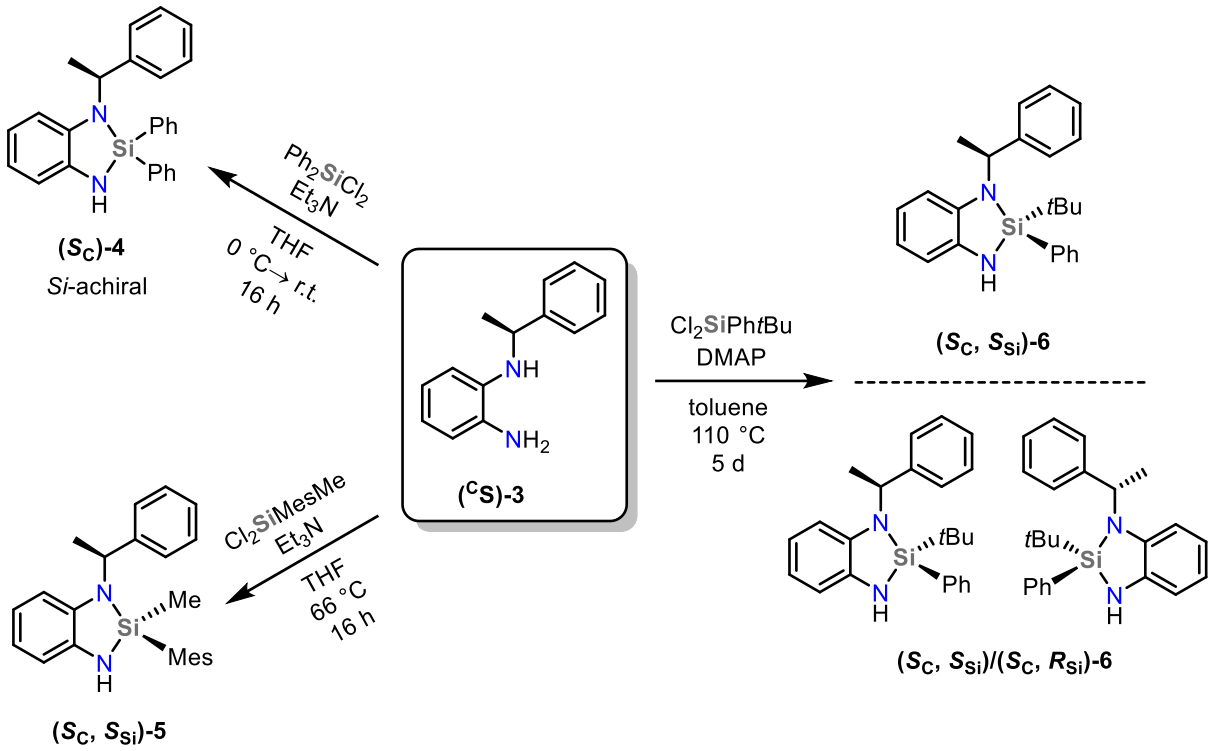

Scheme 5.2. Syntheses of compounds **(*S*C)-4**, **(*S*C, *S*Si)-5**, **(*S*C, *S*Si)-6** and **(*S*C, *S*Si)/ (*S*C, *R*Si)-6**.

Our initial attempt was to synthesize the enantiomeric compound **(*S*C)-4** as a prove of concept for the feasible synthesis of such chiral diaminosilanes. And indeed, we could isolate **(*S*C)-4** after the reaction with dichlorodiphenylsilane in THF at ambient conditions and using triethylamine as acid scavenger. The product could be crystallized from pentane at 8 °C (Figure 5.2, left). The next step was to introduce additional *Si*-centered chirality into the molecule. This was achieved by using the prochiral dichloromesitylmethylsilane and dichloro-*tert*-butyl-phenylsilane. Compound **(*S*C, *S*Si)-5** could be successfully prepared using essentially the same procedure as in the case of **(*S*C)-4**. However, heating at reflux conditions was required for this reaction presumably due to higher steric demand of the mesityl group combined with a significantly less electrophilic silicon center. Since both diastereomers are formed during the reaction it was necessary to separate them. Fortunately, the two isomers of compound **5** exhibit rather strong solubility differences

which allowed for a simple separation already in the workup steps. After completeness of the reaction and removal of the Et_3NHCl salts, the reaction mixture was dried *in vacuo* and the remaining brownish residue was washed with pentane. Due to the low solubility of **(S_C, S_{Si})-5** in pentane compared to a higher solubility of diastereomer **(S_C, R_{Si})-5**, we obtained selectively compound **(S_C, S_{Si})-5** in stereochemically pure form. Crystals suitable for single-crystal X-ray crystallographic analysis were obtained from pentane solution at 8 °C (Figure 5.2, right).

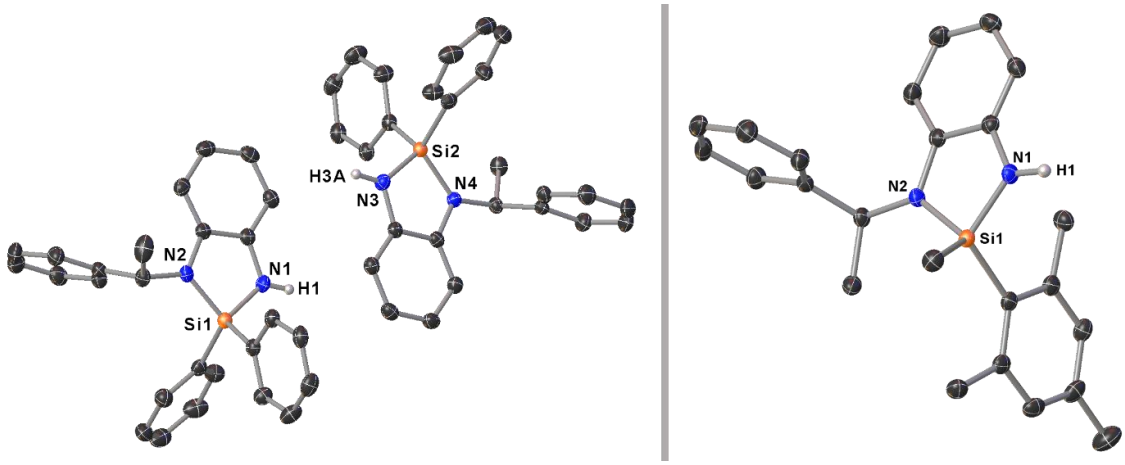

Figure 5.2. Molecular structures of **(S_C)-4** (left) and **(S_C, S_{Si})-5** (right) in the crystalline state (displacement ellipsoids set at the 50% probability level). Hydrogen atoms, except for the N–H, are omitted for clarity. Selected bond lengths [Å] and angles [°]: Compound **(S_C)-4**: Si1–N1 1.713(2), Si1–N2 1.7376(19), Si2–N3 1.720(2), Si2–N4 1.7487(18), N1–Si1–N2 91.67(10), N3–Si2–N4 91.27(10); Compound **(S_C, S_{Si})-5**: Si1–N1 1.743(5), Si1–N2 1.756(4), N1–Si1–N2 90.7(2).

Compound **(S_C)-4** crystallized in the space group $P2_1$ and shows two molecules in the asymmetric unit. The chiral (*S*)-methylbenzyl anchor can adopt two possible rotational conformations related to the N–C bond axis which can both be seen in the crystal structure. Due to the equivalent substituents on the Si atom, there is no preferred rotational arrangement of the methyl and phenyl groups on the stereogenic carbon which is very well reflected by that observation. In contrast to that, compound **(S_C, S_{Si})-5** crystallized in the space group $P2_12_12_1$ as a single rotamer. The small methyl group at the Si atom combined with the sterically demanding mesityl group strongly favors the orientation where the phenyl group on the stereogenic carbon atom points towards the small methyl group. The importance of the nature of the substituents thus seems to play a substantial role in the crystallization behavior of these compounds. In the case of the *Si*-chiral compound **6** with *t*Bu and Ph substituent on the silicon atom in which the steric difference between the substituents is less pronounced compared to **5**, we found an additional crystallization speciation depending on the solvent system. The reaction of **(S_C)-4** and dichloro-*tert*-butyl-phenylsilane was found to be very slow as reaction times of multiple days even at temperatures of 110 °C were required to obtain sufficient conversions. The reaction had to be performed in toluene under addition of higher boiling DMAP instead of Et_3N. The crude mixture was purified by Kugelrohr distillation and a diastereomeric mixture of **(S_C, S_{Si})-6** and **(S_C, R_{Si})-6** (d.r.: 57:53) was obtained which was poorly soluble in pentane. Crystals suitable for single-crystal X-ray crystallographic analysis were obtained from toluene/pentane (4:1) mixture at 8 °C (Figure 5.3, left). To our

surprise, the crystal structure revealed both diastereomers co-crystallizing in a 1:1 ratio in the asymmetric unit which is also reflected in the ^{1}H NMR spectrum by measuring a single crystal. We could reproduce the same crystalline result even after repeating the recrystallization for three times with the same solvent mixture. This behavior of a 1:1 co-crystallization of diastereomeric pairs is a well-known phenomenon that often prevents the successful isolation of pure diastereomers.[2,4–14] Nonetheless we were able to crystallize the diastereomerically pure compound **(*S*$_C$, *S*$_{Si}$)-6** by changing the solvent system to a mixture of THF/pentane (4:1) and storing the solution at −80 °C. Such examples in which a compound could be crystallized in diastereomerically pure form *and* as a mixture of diastereomers are, to the best of our knowledge, limited to only one example so far.[16] This observation suggests that many "failed" diasteromeric resolutions can indeed be successful by the choice of the right solvent system and crystallization conditions. Compound **(*S*$_C$, *S*$_{Si}$)-6** crystallized in the $P2_12_12_1$ space group (Figure 5.3, right).

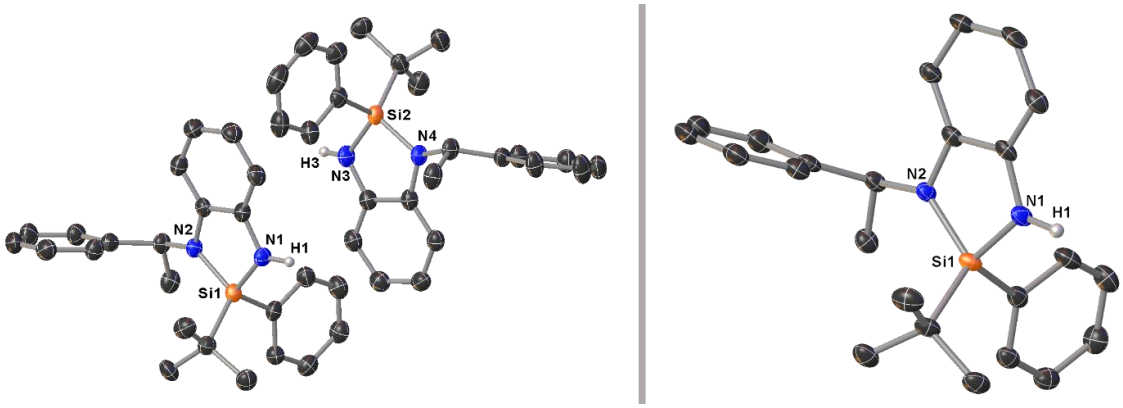

Figure 5.3. Molecular structures of **(*S*$_C$, *S*$_{Si}$)/(*S*$_C$, *R*$_{Si}$)-6** (left) and **(*S*$_C$, *S*$_{Si}$)-6** (right) in the crystalline state (displacement ellipsoids set at the 50% probability level). Hydrogen atoms, except for the N–H, are omitted for clarity. Selected bond lengths [Å] and angles [°]: Compound **(*S*$_C$, *S*$_{Si}$)/(*S*$_C$, *R*$_{Si}$)-6**: Si1–N1 1.726(4), Si1–N2 1.757(3), Si2–N3 1.724(4), Si2–N4 1.742(4), N1–Si1–N2 91.52(17), N3–Si2–N4 91.54(18); Compound **(*S*$_C$, *S*$_{Si}$)-6**: Si1–N1 1.743(5), Si1–N2 1.756(4), N1–Si1–N2 90.7(2).

The stacking in **(*S*$_C$, *S*$_{Si}$)/(*S*$_C$, *R*$_{Si}$)-6** seems to be significantly better since crystals were obtained already at 8 °C while cooling to −80 °C was necessary to obtain the pure diastereomer **(*S*$_C$, *S*$_{Si}$)-6.** The other diastereomer with (*R*)-configuration at the silicon atom could not be crystallized so far indicating that the conformation with the two phenyl groups pointing into different directions and with the hydrogen atom located at the same side as the phenyl group on the silicon atom seems to be favored in the solid-state. The finding that it is possible to influence the crystallization outcome simply by changing the solvent system highlights the importance of solvents, especially electron donating solvents like THF in the behavior of such systems.

5.4 Conclusions

In conclusion, we have applied the commercially available (*S*)-methylbenzylamine **(*S*$_C$)-1** as chiral anchor in the preparation of the *Si*-stereogenic chlorosilanes **(*S*$_C$, *S*$_{Si}$)-2** and **(*S*$_C$, *R*$_{Si}$)-2** and the chiral cyclic diaminosilanes with non-stereogenic [**(*S*$_C$)-3**] and stereogenic [**(*S*$_C$, *S*$_{Si}$)-5** and **(*S*$_C$, *S*$_{Si}$)-6**] silicon atoms. The diastereomers were separated by fractional crystallization and examined by single-crystal X-ray crystallographic analysis. A scarce solvent-dependent crystallization behavior is presented which demonstrates the feasible control over co-crystallizing diastereomers **(*S*$_C$, *S*$_{Si}$)/(*S*$_C$, *R*$_{Si}$)-6** or crystallization of only the **(*S*$_C$, *S*$_{Si}$)-6** isomer. The herein reported chlorosilanes can potentially be of high interest in nucleophilic *and* electrophilic modification reactions while the cyclic diaminosilanes represent promising model compounds for mechanistic investigations regarding Si–N bond substitutions and follow-up reactions. The chiral silicon centers can be used as mechanistical probes in various types of reactions and therefore are of high significance in stereochemistry. Application in siloxane bond formation and cleavage strategies presented by our group can give rise to new methods for the kinetic resolution of chiral silanols and will be investigated in the future.

5.5 References

[1] G. B. Kauffman, I. Bernal, H.-W. Schütt, *Enantiomers* **1999**, *4*, 33–45.

[2] H. Brunner, *Coord. Chem. Rev*. **2003**, *242*, 3–13.

[3] H.-U. Blaser, *Rend. Fis. Acc. Lincei* **2013**, *24*, 213–216.

[4] O. Seiler, C. Burschka, T. Fenske, D. Troegel, R. Tacke, *Inorg. Chem*. **2007**, *46*, 5419–5424.

[5] S. Chaudhury, S. Blaurock, E. Hey-Hawkins, *Eur. J. Inorg. Chem*. **2001**, *2001*, 2587–2596.

[6] S. P. Kelley, L. Fábián, C. P. Brock, *Acta Crystallogr. B Struct. Sci*. **2011***, 67*, 79–93.

[7] H. Brunner, T. Neuhierl, B. Nuber, *Eur. J. Inorg. Chem*. **1998**, *1998*, 1877–1881.

[8] V. A. Alfonsov, A. A. Bredikhin, Z. A. Bredikhina, R. M. Eliseenkova, O. N. Kataeva, I. A. Litvinov, M. A. Pudovik, *Struct. Chem*. **2008**, *19*, 873–878.

[9] H. Brunner, T. Zwack, M. Zabel, W. Beck, A. Böhm, *Organometallics* **2003**, *22*, 1741–1750.

[10] O. A. Lodochnikova, L. T. Hoang, A. R. Zaripova, A. R. Kayumov, I. A. Litvinov, A. R. Kurbangalieva, *Russ. Chem. Bull*. **2016**, *65*, 2672–2677.

[11] E. Vedejs, R. W. Chapman, S. Lin, M. Müller, D. R. Powell, *J. Am. Chem. Soc*. **2000**, *122*, 3047–3052.

[12] T. J. Davis, P. J. Carroll, P. J. Walsh, *J. Organomet. Chem*. **2002**, *663*, 70–77.

[13] H. Brunner, M. Weber, M. Zabel, T. Zwack, *Angew. Chem. Int. Ed*. **2003**, *42*, 1859–1862; *Angew. Chem*. **2003**, *115*, 1903–1907.

[14] J. A. Baus, C. Burschka, R. Bertermann, C. F. Guerra, F. M. Bickelhaupt, R. Tacke, *Inorg. Chem*. **2013**, *52*, 10664–10676.

[15] a) M. K. Choudhary, M. Kumar, J. D. Rimer, *Angew. Chem. Int. Ed*. **2019**, *58*, 15712–15716; *Angew. Chem*. **2019**, *131*, 15859–15863; b) Z. Q. Yu, J. W. Chew, P. S. Chow, R. Tan, *Chem. Eng. Res. Des*. **2007**, *85*, 893–905.

[16] H. Brunner, T. Tsuno, M. Bodensteiner, S. Gärtner, C. Miyahara, S. Ito, T. Kurosawa, K. Koyama, Eur. *J. Inorg. Chem.* **2016**, *2016*, 5405–5410.

[17] H. Brunner, T. Kurosawa, M. Muschiol, T. Tsuno, G. Balázs, M. Bodensteiner, *Organometallics* **2013**, *32*, 4904–4911.

[18] a) M. Oestreich, *Synlett* **2007**, *2007*, 1629–1643; b) L.-W. Xu, L. Li, G.-Q. Lai, J.-X. Jiang, *Chem. Soc. Rev*. **20**11, *40*, 1777–1790; c) L. H. Sommer, C. L. Frye, G. A. Parker, K. W. Michael, *J. Am. Chem. Soc*. **1964**, *86*, 3271–3276.

[19] a) D. Terunuma, K. Murakami, M. Kokubo, K. Senda, H. Nohira, *Bull. Chem. Soc. Jpn*. **1980**, *53*, 789–794; b) R. Tacke, D. Reichel, M. Kropfgans, P. G. Jones, E. Mutschler, J. Gross, X. Hou, M. Waelbroeck, G. Lambrecht, *Organometallics* **1995**, *14*, 251–262; c) R. Tacke, T. Kornek, T. Heinrich, C. Burschka, M. Penka, M. Pülm, C. Keim, E. Mutschler, G. Lambrecht, *J. Organomet. Chem*. **2001**, *640*, 140–165; d) S. Rendler, G. Auer, M. Oestreich, *Angew. Chem. Int. Ed*. **2005**, *44*, 7620–7624; e) P. Jankowski, E. Schaumann,

J. Wicha, A. Zarecki, G. Adiwidjaja, *Tetrahedron: Asymmetry* **1999**, *10*, 519–526; f) P. Jankowski, J. Wicha, A. Zarecki, E. Schaumann, G. Adiwidjaja, M. Asztemborska, *Chem. Commun*. **2000**, 1029–1030; g) A. Nakazaki, J. Usuki, K. Tomooka, *Synlett* **2008**, *2008*, 2064–2068.

[20] J. F. Klebe, H. Finkbeiner, J. *Am. Chem. Soc*. **1968**, *90*, 7255–7261.

[21] K. Tomooka, A. Nakazaki, T. Nakai, *J. Am. Chem. Soc*. **2000**, *122*, 408–409.

[22] N. Oka, M. Nakamura, N. Soeda, T. Wada, *J. Organomet. Chem*. **2009**, *694*, 2171–2178.

[23] J. W. A. Kinnaird, P. Y. Ng, K. Kubota, X. Wang, J. L. Leighton, *J. Am. Chem. Soc*. **2002**, *124*, 7920–7921.

[24] D. R. Schmidt, S. J. O'Malley, J. L. Leighton, *J. Am. Chem. Soc*. **2003**, *125*, 1190–1191.

[25] a) Y. Yasutomi, H. Suematsu, T. Katsuki, *J. Am. Chem. Soc*. **2010**, *132*, 4510–4511; b) A. Holt, A. Jarvie, G. J. Jervis, *J. Organomet. Chem*. **1970**, *21*, 75–77; c) T. Ohta, M. Ito, A. Tsuneto, H. Takaya, J. Chem. Soc., *Chem. Commun*. **1994**, 2525–2526; d) K. Igawa, D. Yoshihiro, N. Ichikawa, N. Kokan, K. Tomooka, *Angew. Chem. Int. Ed*. **2012**, *51*, 12745–12748; *Angew. Chem*. **2012**, *124*, 12917–12920; e) R. Shintani, E. E. Maciver, F. Tamakuni, T. Hayashi, *J. Am. Chem. Soc*. **2012**, *134*, 16955–16958; f) Y. Guo, M.-M. Liu, X. Zhu, L. Zhu, C. He, *Angew. Chem. Int. Ed*. **2021**, *60*, 13887–13891; *Angew. Chem*. **2021**, *133*, 14006–14010; g) R. Shintani, H. Otomo, K. Ota, T. Hayashi, *J. Am. Chem. Soc*. **2012**, *134*, 7305–7308; h) Y. Sato, C. Takagi, R. Shintani, K. Nozaki, *Angew. Chem. Int. Ed.* **2017**, *56*, 9211–9216; *Angew. Chem*. **2017**, *129*, 9339–9334; i) Y. Kuninobu, K. Yamauchi, N. Tamura, T. Seiki, K. Takai, *Angew. Chem. Int. Ed*. **2013**, *52*, 1520–1522; *Angew. Chem*. **2013**, *125*, 1560–1562; j) M. Murai, Y. Takeuchi, K. Yamauchi, Y. Kuninobu, K. Takai, *Chem. Eur. J.* **2016**, *22*, 6048–6058; k) W. Ma, L.-C. Liu, K. An, T. He, W. He, *Angew. Chem. Int. Ed*. **2021**, *60*, 4245–4251; *Angew. Chem.* **2021**, *133*, 4291–4297; l) D. Mu, W. Yuan, S. Chen, N. Wang, B. Yang, L. You, B. Zu, P. Yu, C. He, *J. Am. Chem. Soc*. **2020**, *142*, 13459–13468; m) Q.-W. Zhang, K. An, L.-C. Liu, Q. Zhang, H. Guo, W. He, *Angew. Chem. Int. Ed*. **2017**, *56*, 1125–1129; *Angew. Chem*. **2017**, *129*, 1145–1149 n) W. Yuan, L. You, W. Lin, J. Ke, Y. Li, C. He, *Org. Lett*. **2021**, *23*, 1367–1372; o) S. Chen, D. Mu, P.-L. Mai, J. Ke, Y. Li, C. He, *Nat. Commun*. **2021**, *12*, 1249; p) X. Bi, J. Feng, X. Xue, Z. Gu, *Org. Lett*. **2021**, *23*, 3201–3206; q) Y. Wu, P. Wang, *Angew. Chem. Int. Ed*. **2022**, 61, e202205382; Angew. Chem. **2022**, 134, e202205382.

[26] a) K. Igawa, J. Takada, T. Shimono, K. Tomooka, *J. Am. Chem. Soc*. **2008**, *130*, 16132–16133; b) J. O. Bauer, C. Strohmann, *J. Am. Chem. Soc*. **2015**, *137*, 4304–4307.

[27] J. O. Bauer, C. Strohmann, *Angew. Chem. Int. Ed*. **2014**, 53, 720–724; *Angew. Chem*. **2014**, *126*, 738–742.

[28] a) J. F. Klebe, H. Finkbeiner, *J. Am. Chem. Soc*. **1966**, *88*, 4740–4741; b) R. Corriu, G. F. Lanneau, G. L. Royo, *J. Organomet. Chem*. **1972**, *35*, 35–49; c) R. Corriu, J. Moreau, *J. Organomet. Chem*. **1977**, *127*, 7–17; d) A. Kawachi, H. Maeda, K. Mitsudo, K. Tamao, *Organometallics* **1999**, *18*, 4530–4533; e) J. O. Bauer, C. Strohmann, *Eur. J. Inorg. Chem*. **2016**, *2016*, 2868–2881.

[29] a) T. Huber, N. A. Espinosa-Jalapa, J. O. Bauer, *Chem. Eur. J.* **2022**, e202202608; b) M. Revés, C. Ferrer, T. León, S. Doran, P. Etayo, A. Vidal-Ferran, A. Riera, X. Verdaguer, *Angew. Chem. Int. Ed*. 2010, *49*, 9452–9455; *Angew. Chem*. **2010**, *122*, 9642–9645; c) A. Flores-Gaspar, S. Orgué, A. Grabulosa, A. Riera, X. Verdaguer, *Chem. Commun*. **2015**, 51, 1941–1944; d) E. Salomó, A. Prades, A. Riera, X. Verdaguer, *J. Org. Chem*. **2017**, *82*, 7065–7069; e) O. I. Kolodiazhnyi, E. V. Gryshkun, N. V. Andrushko, M. Freytag, P. G. Jones, R. Schmutzler, *Tetrahedron: Asymmetry* **2003**, *14*, 181–183.

[30] H. Q. Liu, J. F. Harrod, Can. *J. Chem*. **1992**, *70*, 107–110.

[31] a) D. L. Poeira, A. C. R. Negrão, H. Faustino, J. A. S. Coelho, C. S. B. Gomes, P. M. P. Gois, M. M. B. Marques, *Org. Lett*. **2022***, 24*, 776–781; b) I. S. Nizamov, E. M. Mart'yanov, I. D. Nizamov, A. R. Nurmukhametov, R. A. Cherkasov, *Russ. J. Org. Chem*. **2013**, *49*, 526–529; c) R. P. Polniaszek, C. R. Kaufman, *J. Am. Chem. Soc*. **1989**, *111*, 4859–4863; d) M. Xu, A. R. Jupp, M. S. E. Ong, K. I. Burton, S. S. Chitnis, D. W. Stephan, *Angew. Chem. Int. Ed*. **2019**, *58*, 5707–5711; *Angew. Chem*. **2019**, *131*, 5763–5767.

[32] T. Götz, A. Falk, J. O. Bauer, *Chem. Eur. J*. **2022**, *28*, e202103531.

[33] F. M. Rivas, A. J. Giessert, S. T. Diver, *J. Org. Chem*. **2002**, *67*, 1708–1711.

5.6 Syntheses and characterizations

5.6.1 General remarks

All experiments except for the synthesis of ((*S*)-PhMeCH$_2$NH)Ph(NO$_2$) were performed in an inert atmosphere of purified nitrogen by using standard Schlenk techniques or an MBraun Unilab 1200/780 glovebox. Glassware was heated at 600 °C prior to use. Diethyl ether (Et$_2$O), dichloromethane (DCM), hexane, pentane, tetrahydrofuran (THF), and toluene were dried and degassed with an MBraun SP800 solvent purification system. *n*-Butyllithium (2.5 M solution in hexane, Merck KGaA), *tert*-Butyllithium (1.7 M solution in hexane, Merck KGaA), trichlorophenylsilane (97%, Alfa Aesar), dichlorodiphenylsilane (98%, Merck KGaA), trichloromethylsilane (99%, Merck KGaA), bromomesitylene (98%, Merck KGaA), 1-fluoro-2-nitrobenzene (99%, Fluorochem Ltd), (*S*)-1-phenylethan-1-amin **(*S*$_C$)-1** (98%, Merck KGaA), *N*,*N*-dimethylformamide DMF (99.5%, Acros), NaBH$_4$ (98%, Merck KGaA), Pd/C (10% Pd, Merck KGaA) and 4-dimethylaminopyridine (≥98%, Merck KGaA) were used as received without any further purification. Triethylamine (≥99%, Merck KGaA) was heated at reflux over CaH$_2$ and distilled prior to use. C$_6$D$_6$ used for NMR spectroscopy was dried over 3 Å molecular sieves and degassed by a standard freeze-pump-thaw procedure. NMR spectra were either recorded using a Bruker Avance 300 (300.13 MHz), a Bruker Avance 400 (400.13 MHz) or a Bruker Avance III HD 400 (400.13 MHz) at 25 °C. Chemical shifts (δ) are reported in parts per million (ppm). ^{1}H and ^{13}C{^{1}H} NMR spectra are referenced to tetramethylsilane (SiMe$_4$, δ = 0.0 ppm) as external standard, with the deuterium signal of the solvent serving as internal lock and the residual solvent signal as an additional reference. ^{29}Si{^{1}H} NMR spectra are referenced to SiMe$_4$. For the assignment of the multiplicities, the following abbreviations are used: s = singlet, d = doublet, t = triplet, q = quartet, br = broad, m = multiplet. For simplicity, multiplets of order higher than one are described approximating them to the closest first-order type. High-resolution mass spectrometry was carried out on a Jeol AccuTOF GCX and an Agilent Q-TOF 6540 UHD spectrometer. Elemental analyses were performed on a Vario MICRO cube apparatus.

5.6.2 Synthesis of precursors

5.6.2.1 ((*S*)-PhMeCH$_2$NH)Ph(NO$_2$)

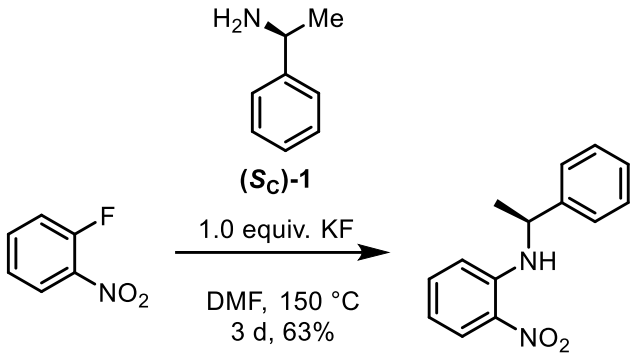

1-fluoro-2-nitrobenzene (21.1 mL, 200.0 mmol, 1.0 equiv.), compound **(*S*$_C$)-1** (25.5 mL, 200.0 mmol, 1.0 equiv.), and potassium fluoride (11.62 g, 200.0 mmol, 1.0 equiv.) were dissolved in 200 mL of DMF and heated to 150 °C while stirring for 3 days. The red mixture was treated with ethyl acetate (ca. 200 mL) and water (ca. 200 mL) and extracted using a separation funnel. The aqueous phase was again extracted with ethyl acetate (3 × 100 mL). The combined organic phases were extracted with brine (ca. 200 mL) and then dried over $MgSO_4$. After removal of the solids via filtration, all volatiles were removed via rotatory evaporation. The remaining DMF was removed by vacuum distillation (70 °C, 1.0×10^{-2} bar) to afford compound ((*S*)-PhMeCH$_2$NH)Ph(NO$_2$) as the remaining orange oil (30.44 g, 126.0 mmol. 63%).

^{1}H NMR (300 MHz, $CDCl_3$, 298 K): δ [ppm] = 1.57 [d, $^3J_{H\text{-}H}$ = 6.8 Hz, 3H, C*H*$_3$], 4.61 [q, $^3J_{H\text{-}H}$ = 6.7 Hz, 1H, C*H*], 6.49–6.58 [m, 2H, *H*$_{Ph}$], 7.15–7.22 [m, 2H, *H*$_{Ph}$], 7.24–7.29 [m, 4H, *H*$_{Ph}$], 8.01–8.12 [m, 1H, *H*$_{Ph}$], 8.35 [br, 1H, N*H*]. **^{13}C{^{1}H} NMR** (75 MH, $CDCl_3$, 298 K): δ [ppm] = 25.2 [s, *C*H$_3$], 53.3 [s, *C*H], 115.3 [s, *C*$_{Ph}$], 115.7 [s, *C*$_{Ph}$], 125.7[s, *C*$_{Ph}$], 126.9 [s, *C*$_{Ph}$], 127.5 [s, *C*$_{Ph}$], 129.1 [s, *C*$_{Ph}$], 132.3 [s, *C*$_{Ph}$], 136.1 [s, *C*$_{Ph}$], 143.7 [s, *C*$_{Ph}$], 144.6 [s, *C*$_{Ph}$]. **CHN Analysis** $C_{14}H_{14}N_2O_2$ calculated: C 69.41, H 5.82, N 11.56, O 13.21; found: C 69.67, H 6.12, N 11.34. **HR-MS (ESI+)**, calculated m/z for $C_{14}H_{14}N_2O_2$ [M+H$^+$]: 243.1128; found: 243.1131.

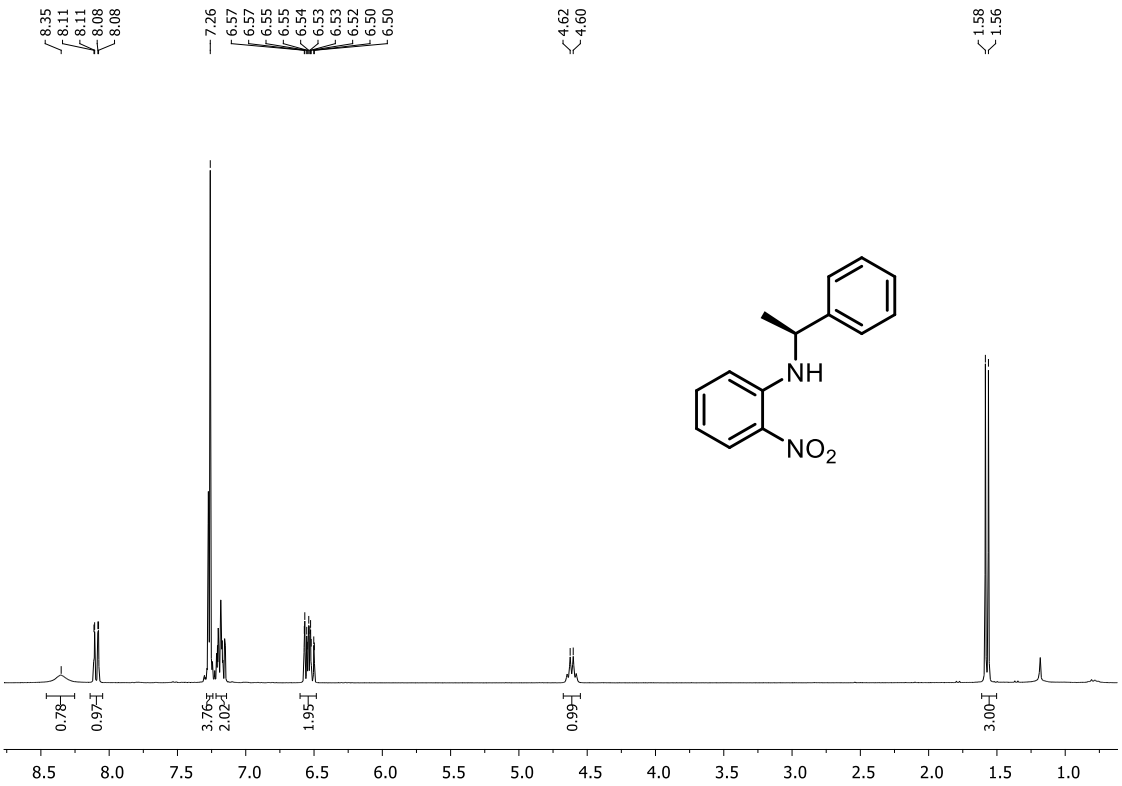

Figure S5.1. ^{1}H NMR spectrum ($CDCl_3$, 298 K) of ((*S*)-$PhMeCH_2NH)Ph(NO_2$).

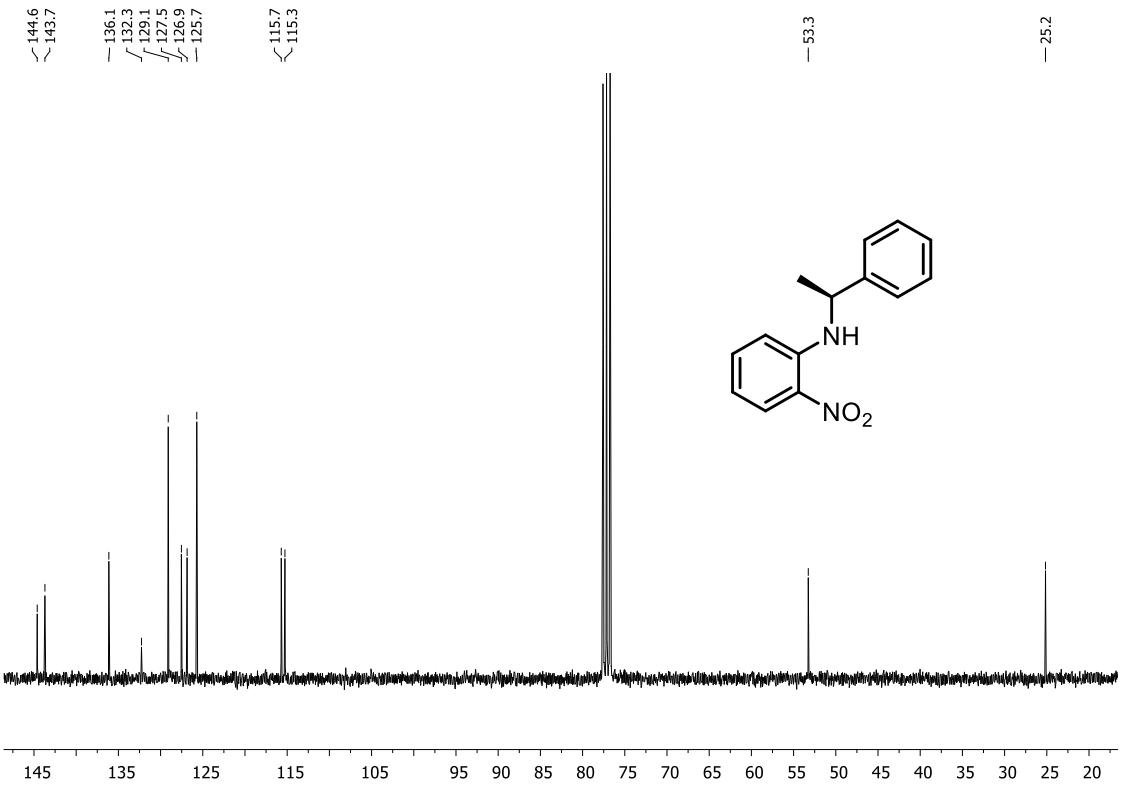

Figure S5.2. $^{13}C\{^{1}H\}$ NMR spectrum ($CDCl_3$, 298 K) of ((*S*)-$PhMeCH_2NH)Ph(NO_2$).

5.6.2.2 Compound (S_C)-3

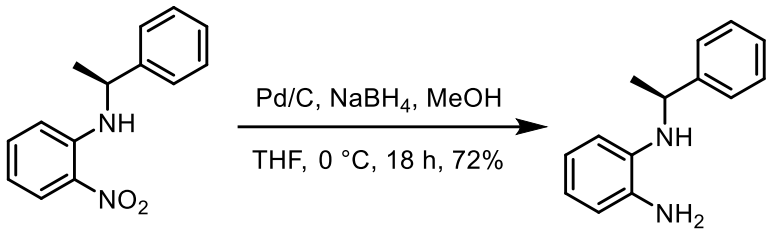

In a modified literature procedure,[1] ((*S*)-PhMeCH$_2$NH)Ph(NO$_2$) (30.44 g, 126.0 mmol, 1.0 equiv.), Pd/C (1.38 g, 1.3 mmol, 1.0 mol%), and sodium borohydride (11.92 g, 315.0 mmol, 2.5 equiv.) were dissolved in 200 mL of THF and cooled down to 0 °C. Methanol (ca. 100 mL) was added dropwise under gas formation. After the addition was completed, the wine-red reaction mixture was stirred for further 18 h. The solids were filtered off and the filtrate was extracted with ethyl acetate (3 × 100 mL) and brine (100 mL) using a separation funnel. The combined organic phases were dried over MgSO$_4$ and the solids removed by filtration. All volatiles were removed via rotatory evaporation to afford compound **(S_C)-3** as a wine-red oil which turned solid after one day (19.19 g, 90.4 mmol 72%).

^{1}H NMR (400 MHz, C$_6$D$_6$, 298 K): δ[ppm] = 1.61 [d, $^3J_{H\text{-}H}$ = 6.7 Hz, 3H, C*H*$_3$], 4.56 [q, $^3J_{H\text{-}H}$ = 6.7 Hz, 1H, C*H*], 6.49–6.53 [m, 1H, *H*$_{Ph}$], 6.61–6.77 [m, 3H, *H*$_{Ph}$], 7.19–7.25 [m, 3H, *H*$_{Ph}$], 7.28–7.40 [m, 4H, *H*$_{Ph}$].

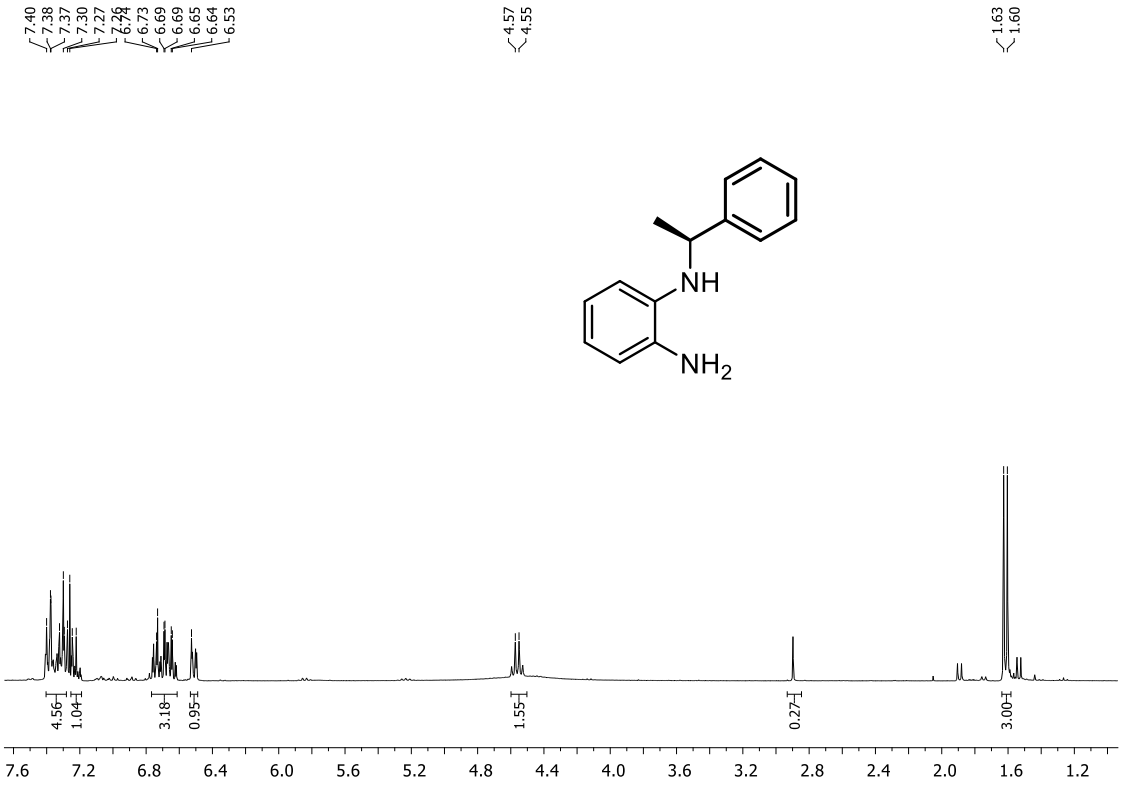

Figure S5.3. ^{1}H NMR spectrum (C$_6$D$_6$, 298 K) of **(S_C)-3**.

5.6.2.3 $Cl_2SiPh(tBu)$

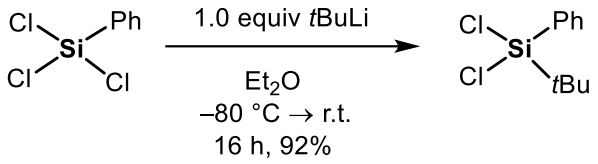

In a modified literature procedure,[2] trichlorophenylsilane (2.40 mL, 15.0 mmol, 1.0 equiv.) was dissolved in 100 mL of diethylether and cooled down to −80 °C. *t*BuLi (8.82 mL, 15.0 mmol, 1.0 equiv. of a 1.7 mol/L solution in hexanes) was added dropwise via syringe and the colorless mixture was stirred for 16 h while slowly warming to room temperature. The formed white solids were removed via cannula filtration and the colorless filtrate was dried *in vacuo* to afford dichloro-*tert*-butyl-phenylsilane as a colorless liquid (3.22 g, 13.8 mmol, 92%).

^{1}H NMR (300 MHz, C_6D_6, 298 K): δ[ppm] = 0.97 [s, 9H, C(CH_3)], 6.49–6.53 [m, 1H, H_{Ph}], 67.04–7.12 [m, 3H, H_{Ph}], 7.66–7.72 [m, 2H, H_{Ph}].

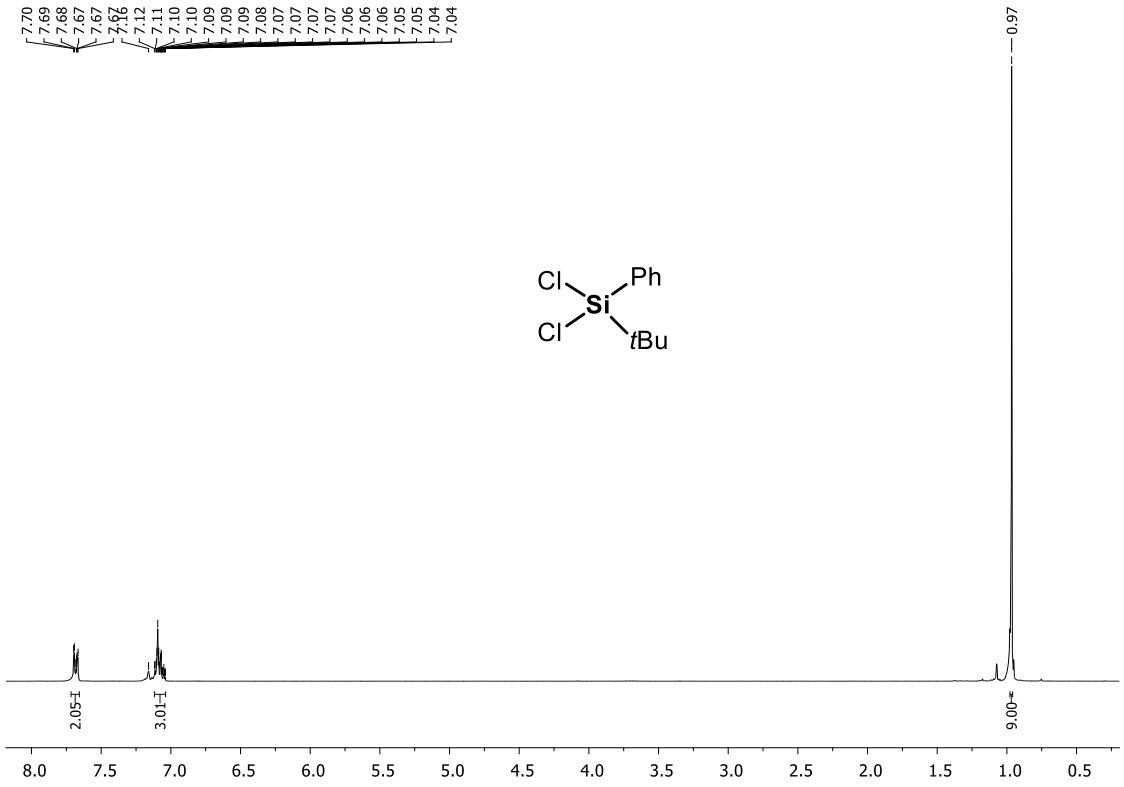

Figure S5.4. ^{1}H NMR spectrum (C_6D_6, 298 K) of $Cl_2SiPh(tBu)$.

5.6.2.4 $Cl_2SiMesMe$

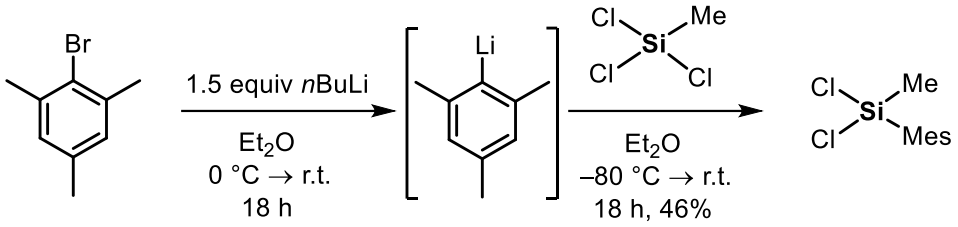

In a modified literature procedure,[3] bromomesitylene (7.54 mL, 50.0 mmol, 1.0 equiv.) was dissolved in 100 mL of diethyl ether and cooled down to 0 °C. *n*BuLi (30.0 mL, 75.0 mmol, 1.5 equiv. of a 2.5 mol/L solution in hexanes) was added via syringe and the colorless solution was stirred for 18 h while slowly warming to room temperature. The formed white solids were isolated via cannula filtration and then suspended in 150 mL of diethyl ether. It was cooled down to −80 °C and trichloromethylsilane (8.33 mL, 50.0 mmol, 1.0 equiv.) was added in one portion. The mixture was stirred for 18 h while slowly warming to room temperature. The remaining solids were filtered off via cannula filtration and the clear colorless filtrate was dried *in vacuo* to afford dichloromethylmesitylsilane as a white solid (6.86 g, 23.2 mmol, 46%).

^{1}H NMR (300 MHz, C_6D_6, 298 K): *δ*[ppm] = 0.89 [s, 3H, C*H*$_3$], 2.00 [s, 3H, *para*-C*H*$_3$], 2.39 [s, 6H, *ortho*-C*H*$_3$], 6.59 [s, 2H, *H*$_{Ph}$].

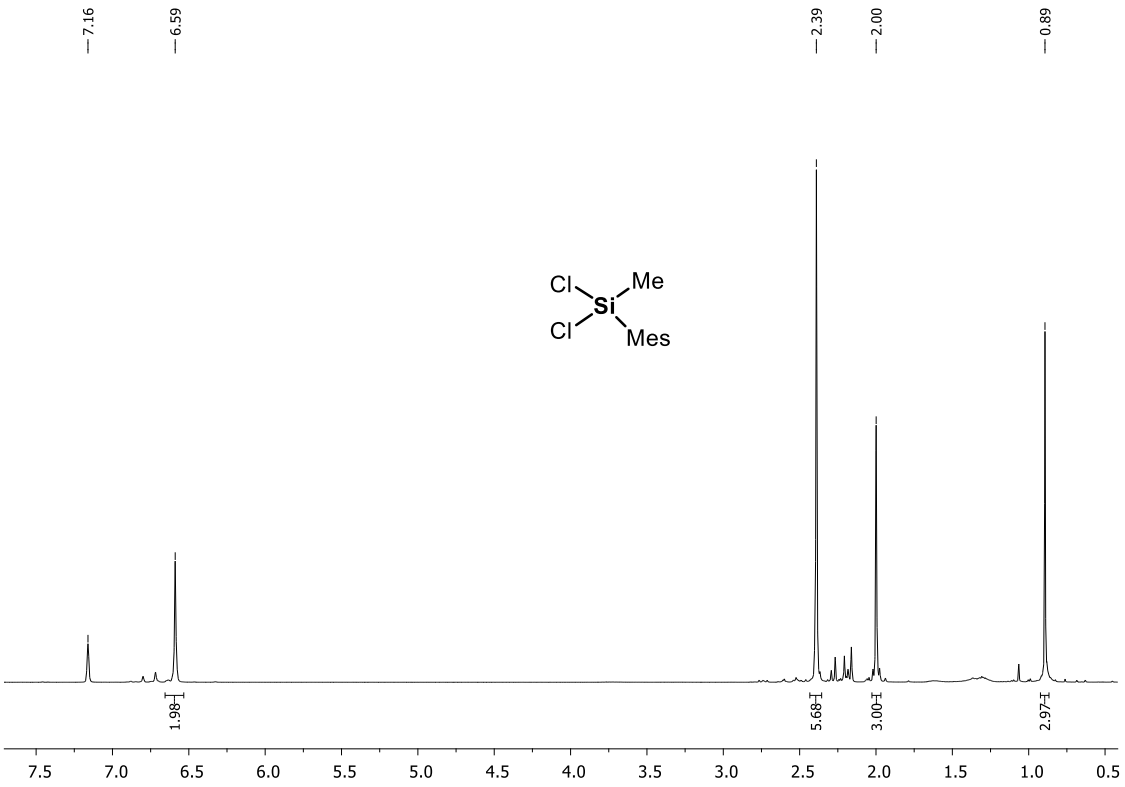

Figure S5.5. ^{1}H NMR spectrum (C_6D_6, 298 K) of $Cl_2SiMesMe$.

5.6.3 Syntheses of chiral compounds

5.6.3.1 Compounds (S_C, S_{Si})-2 and (S_C, R_{Si})-2

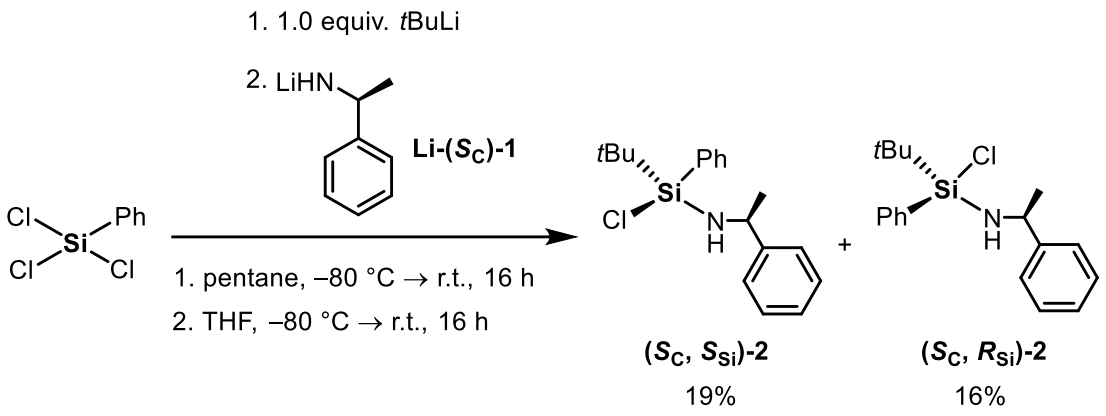

Trichlorophenylsilane (1.60 mL, 10.0 mmol, 1.0 equiv.) was dissolved in 100 mL of pentane and cooled down to −80 °C. *t*BuLi (5.88 mL, 10.0 mmol, 1.0 equiv. of a 1.7 mol/L solution in hexanes) was added dropwise and it was stirred for 16 h while slowly warming to room temperature. The formed white solids were removed via cannula filtration and the colorless filtrate was dried *in vacuo*. In a separate Schlenk flask, **(S_C)-1** (1.28 mL, 10.0 mmol, 1.0 equiv.) was dissolved in 30 mL of THF and *n*BuLi (4.40 mL, 11.0 mmol, 1.1 equiv. of a 2.5 mol/L solution in hexanes) was added dropwise and the mixture was stirred at room temperature for 10 min. Dichloro-*tert*-butyl-phenylsilane was dissolved in 30 mL of THF and cooled down to −80 °C. The solution containing the lithiated amine was then added to the cold silane solution via cannula and the mixture was stirred for 16 h while slowly warming up to room temperature. The formed solids were removed by cannula filtration and the filtrate was dried *in vacuo*. The remaining colorless wax was purified by Kugelrohr distillation (120 °C oven temperature, 1.4×10^{-2} mbar) to obtain a colorless oil containing a diastereomeric mixture (d.r.: 60:40). The oil was dissolved in 50 mL of pentane and stored at −80 °C for one day resulting in the precipitation of a white solid. The solid was isolated by cannula filtration and recrystallized three times from pentane at −80 °C resulting in the isolation of diastereomerically pure **(S_C, S_{Si})-2** as a white crystalline solid suitable for single-crystal X-ray crystallographic analysis (503 mg, 1.6 mmol, 16%). The filtrates were combined, dried *in vacuo* and recrystallized following the same procedure to obtain **(S_C, R_{Si})-2** as a white solid (601 mg, 1.9 mmol, 19%).

(S_C, S_{Si})-2:

^{1}H NMR (400 MHz, C_6D_6, 298 K): δ[ppm] = 1.05 [s, 9H, C(CH_3)$_3$], 1.38 [d, $^3J_{H\text{-}H}$ = 6.6 Hz, 3H, PhCH(CH_3)], 1.62 (d, $^3J_{H\text{-}H}$ = 11.3 Hz, 1H, N*H*], 4.10–4.21 [m, 1H, PhC*H*(C*H*)$_3$], 7.11–7.29 [m, 8H, H_{Ph}], 7.78–7.84 [m, 2H, H_{Ph}]. **^{13}C{^{1}H} NMR** (101 MHz, C_6D_6, 298 K): δ[ppm] = 20.0 [s, *C*(CH$_3$)$_3$], 26.2 [s, C(*C*H$_3$)$_3$], 27.6 [s, PhCH(*C*H$_3$)], 51.5 [s, Ph*C*H(CH$_3$)], 125.8 [s, *C*H$_{Ph}$], 126.8 [s, *C*H$_{Ph}$], 128.1 [s, *C*H$_{Ph}$], 128.6 [s, *C*H$_{Ph}$], 130.7 [s, *C*H$_{Ph}$], 131.9 [s, *C*$_{Ph}$], 136.1 [s, *C*H$_{Ph}$], 148.0 [s, *C*$_{Ph}$].

^{29}Si{^{1}H} NMR (79 MHz, C_6D_6, 298 K): *δ*[ppm] = 4.7 [s]. **CHN Analysis** $C_{18}H_{24}ClNSi$ calculated: C 68.00, H 7.61, Cl 11.15, N 4.41, Si 8.83; found: C 67.98, H 7.14, N 4.23. **HR-MS(EI+)**, calculated m/z for $C_{18}H_{24}ClNSi$ [M+H$^+$]: 317.13611; found: 317.13421.

(S_C, R_{Si})-2:

^{1}H NMR (400 MHz, C_6D_6, 298 K): *δ*[ppm] = 0.95 [s, 9H, C(C*H*$_3$)$_3$], 1.23 [d, $^{3}J_{H\text{-}H}$ = 6.8 Hz, 3H, PhCH(C*H*$_3$)], 1.55 (d, $^{3}J_{H\text{-}H}$ = 10.7 Hz, 1H, N*H*], 4.11–4.21 [m, 1H, PhC*H*(C*H*)$_3$], 7.01–7.09 [m, 1H, *H*$_{Ph}$], 7.11–7.22 [m, 7H, *H*$_{Ph}$], 7.84–7.90 [m, 2H, *H*$_{Ph}$]. **^{13}C{^{1}H} NMR** (101 MHz, C_6D_6, 298 K): *δ*[ppm] = 20.4 [s, *C*(CH$_3$)$_3$], 26.3 [s, C(*C*H$_3$)$_3$], 27.4 [s, PhCH(*C*H$_3$)], 51.6 [s, Ph*C*H(CH$_3$)], 126.1 [s, *C*H$_{Ph}$], 126.9 [s, *C*H$_{Ph}$], 128.2 [s, *C*H$_{Ph}$], 128.6 [s, *C*H$_{Ph}$], 130.7 [s, *C*H$_{Ph}$], 133.0 [s, *C*$_{Ph}$], 135.8 [s, *C*H$_{Ph}$], 147.7 [s, *C*$_{Ph}$]. **^{29}Si{^{1}H}** NMR (79 MHz, C_6D_6, 298 K): *δ*[ppm] = 4.3 [s].

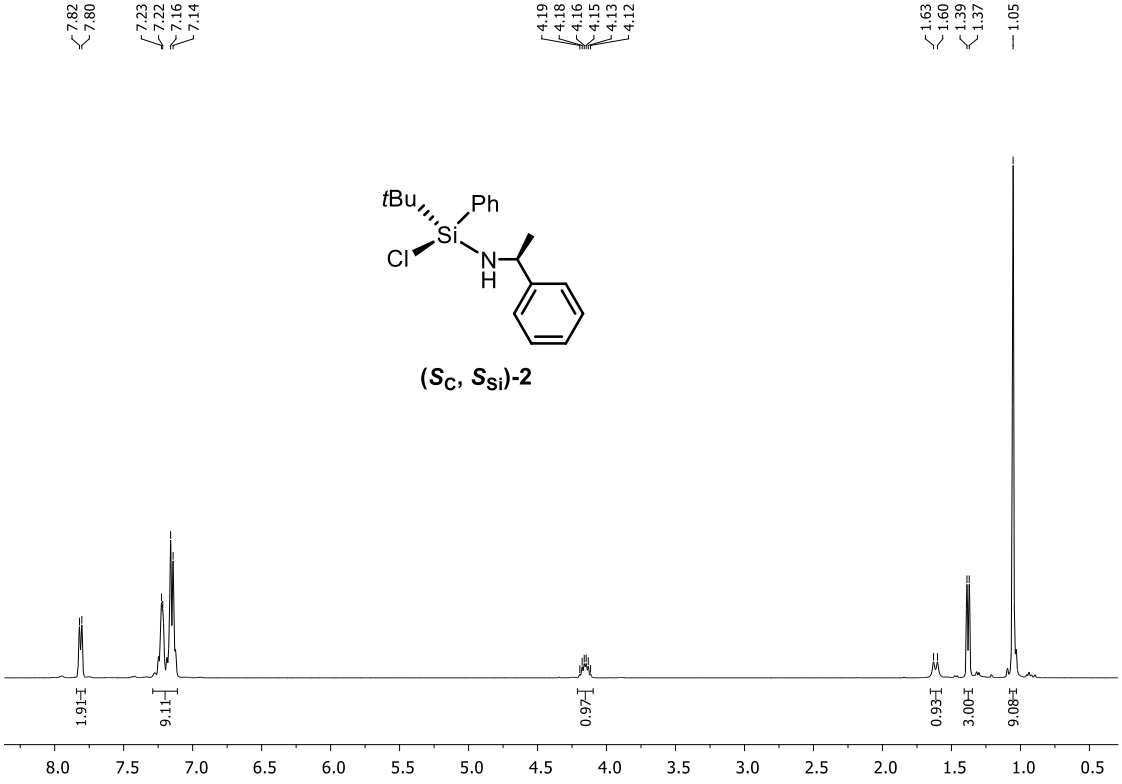

Figure S5.6. ^{1}H NMR spectrum (C_6D_6, 298 K) of **(S_C, S_{Si})-2**.

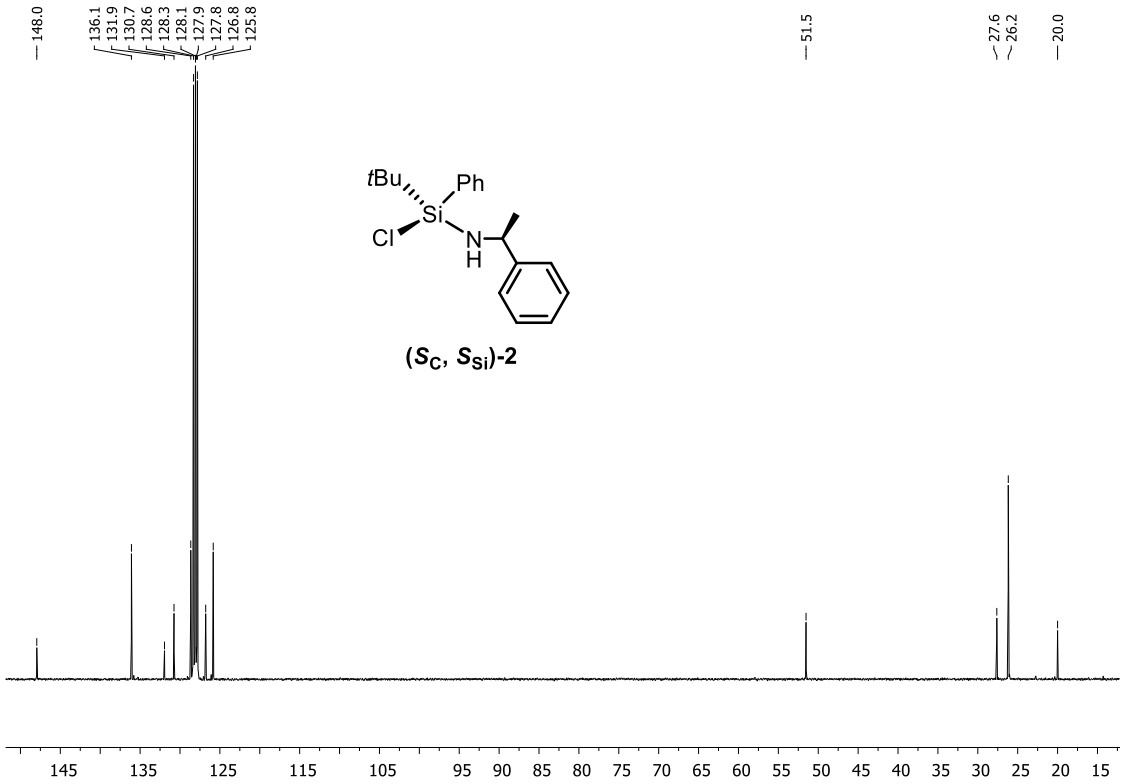

Figure S5.7. $^{13}C\{^{1}H\}$ NMR spectrum (C_6D_6, 298 K) of **(S_C, S_{Si})-2**.

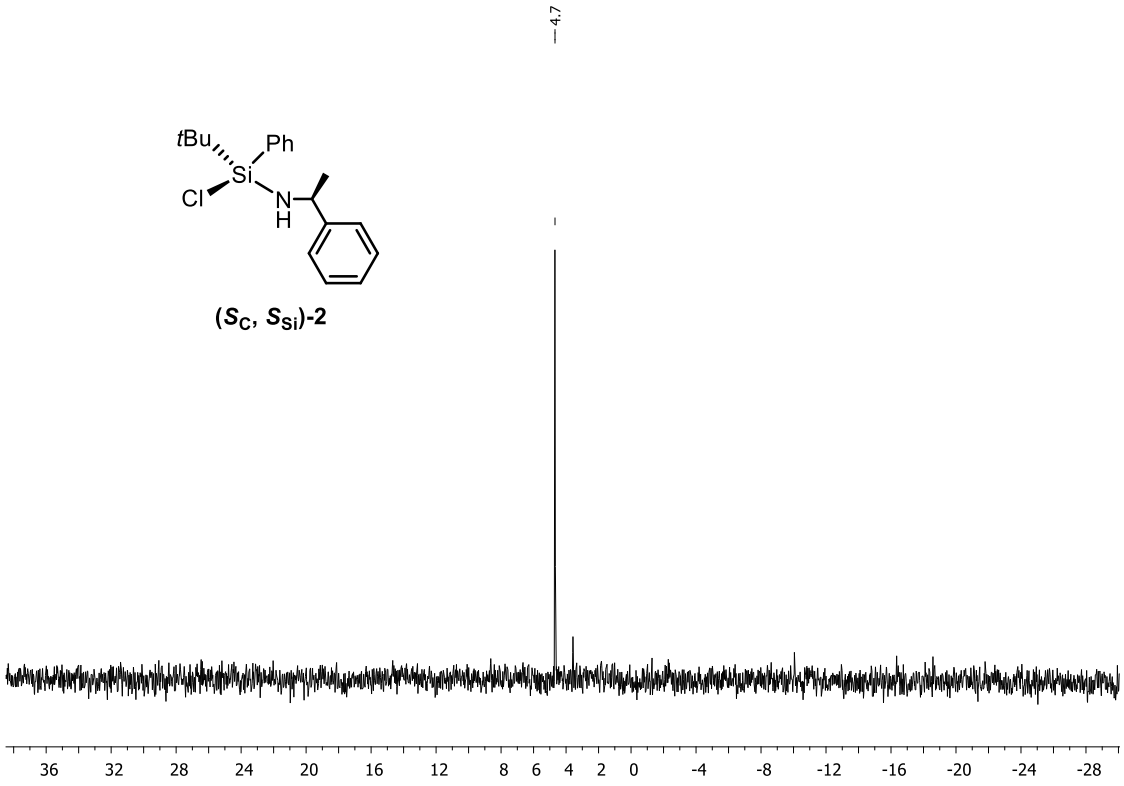

Figure S5.8. $^{29}Si\{^{1}H\}$ NMR spectrum (C_6D_6, 298 K) of **(S_C, S_{Si})-2**.

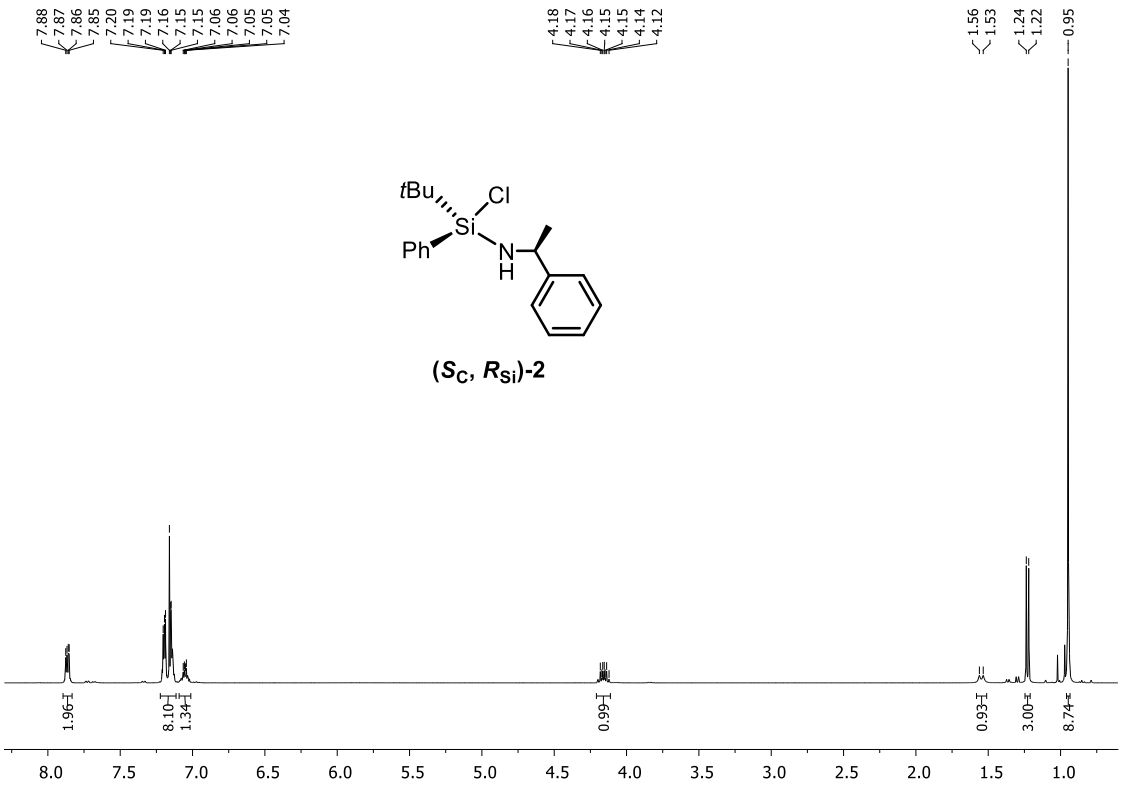

Figure S5.9. ^{1}H NMR spectrum (C_6D_6, 298 K) of **(S_C, R_{Si})-2**.

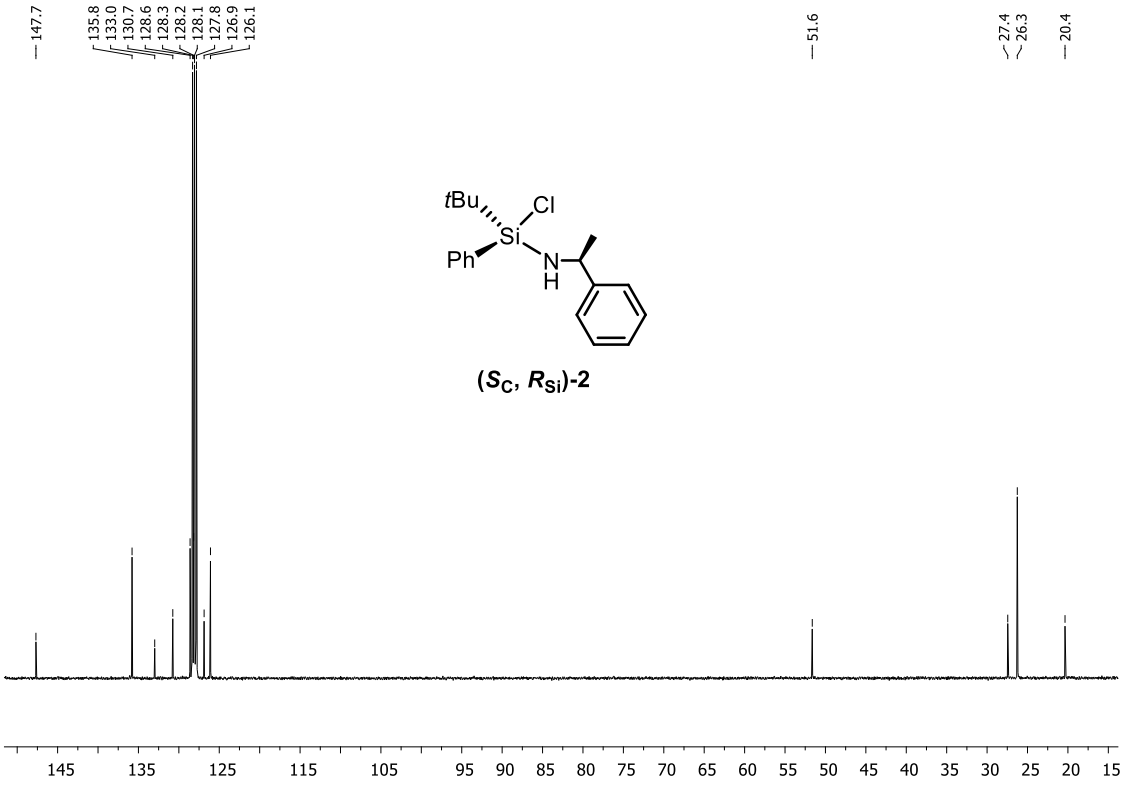

Figure S5.10. $^{13}C\{^{1}H\}$ NMR spectrum (C_6D_6, 298 K) of **(S_C, R_{Si})-2**.

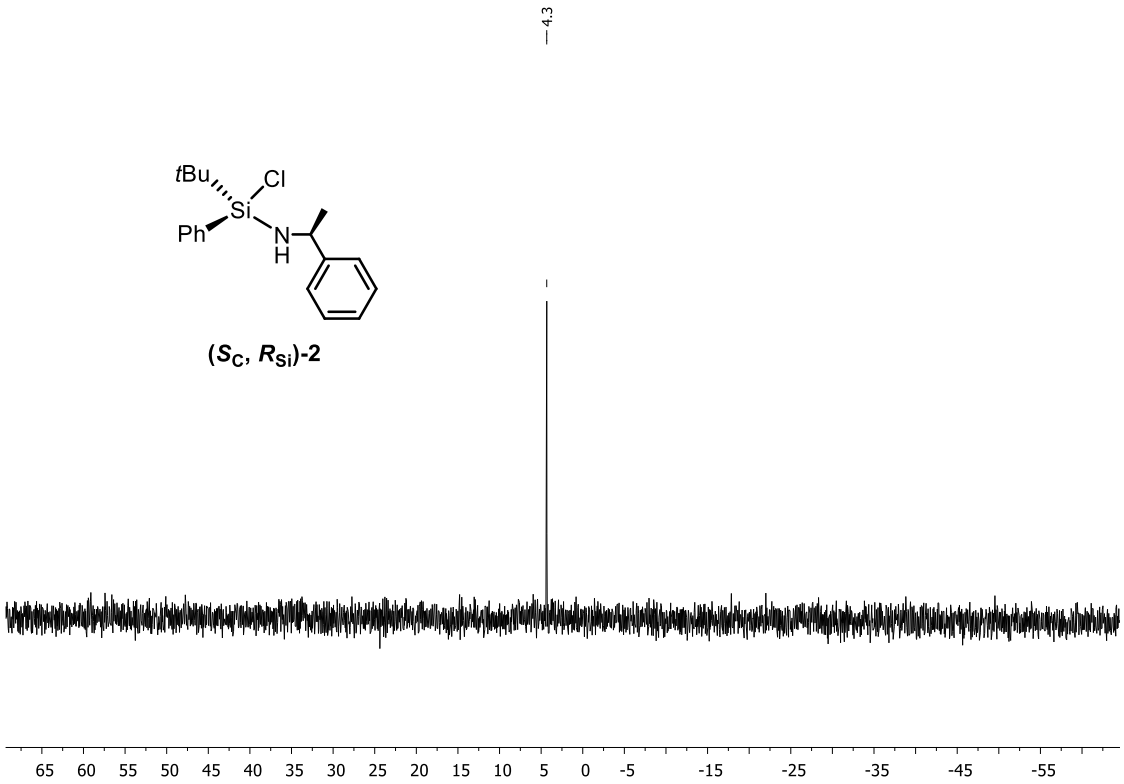

Figure S5.11. $^{29}Si\{^{1}H\}$ NMR spectrum (C_6D_6, 298 K) of **(S_C, R_{Si})-2**.

5.6.3.1 Compound (S_C)-4

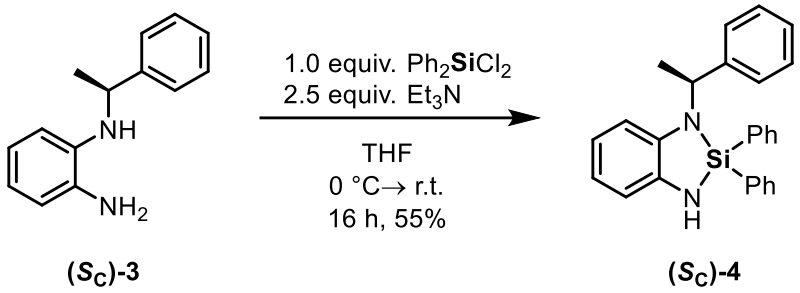

Compound **(S_C)-3** (3.18 g, 15.0 mmol, 1.0 equiv.) was dissolved in 100 mL of THF and triethylamine (5.20 mL, 37.5 mmol, 2.5 equiv.) was added via syringe. The red solution was cooled down to 0 °C in an ice bath and dichlorodiphenylsilane (2.40 mL, 15.0 mmol, 1.0 equiv.) was added via syringe. The brown solution was stirred for 16 h, before all volatiles were removed *in vacuo*. The remaining brown cake was taken up in 30 mL of Et_2O and the white solids were removed via cannula filtration. The brown filtrate was dried *in vacuo* and purified by Kugelrohr distillation (220 °C oven temperature, 2.1×10^{-2} mbar) to obtain compound **(S_C)-4** as a yellow solid (3.24 g, 8.3 mmol, 55%). Crystals suitable for single-crystal X-ray crystallographic analysis were obtained after recrystallization from pentane and storage at 8 °C for one day.

^{1}H NMR (400 MHz, C_6D_6, 298 K): *δ*[ppm] = 1.45 [d, $^{3}J_{H\text{-}H}$ = 7.0 MHz, 3H, C*H*$_3$], 3.28 [s, 1H, N*H*], 4.75 [q, $^{3}J_{H\text{-}H}$ = 7.0 MHz, 1H, C*H*], 6.47–6.50 [m, 1H, *H*$_{Ph}$], 6.53–6.56 [m, 1H, *H*$_{Ph}$], 6.74–6.79 [m, 1H, *H*$_{Ph}$], 6.85–6.96 [m, 3H, *H*$_{Ph}$], 6.98–7.02 [m, 2H, *H*$_{Ph}$], 6.47–6.50 [m, 1H, *H*$_{Ph}$], 7.12–7.16 [m, 3H, *H*$_{Ph}$], 7.16–7.23 [m, 3H, *H*$_{Ph}$], 7.63–7.72 [m, 4H, *H*$_{Ph}$]. **^{13}C{^{1}H} NMR** (101 MHz, C_6D_6, 298 K): *δ*[ppm] = 24.2 [s, *C*H$_3$], 54.7 [s, *C*H], 110.8 [s, *C*$_{Ph}$], 111.3 [s, *C*$_{Ph}$], 126.7 [s, *C*$_{Ph}$], 126.8 [s, *C*$_{Ph}$], 128.2 [s, *C*$_{Ph}$], 128.3 [s, *C*$_{Ph}$], 130.7 [s, *C*$_{Ph}$], 134.0 [s, *C*$_{Ph}$], 135.6 [s, *C*$_{Ph}$], 136.0 [s, *C*$_{Ph}$], 136.4 [s, *C*$_{Ph}$], 139.1 [s, *C*$_{Ph}$], 139.2 [s, *C*$_{Ph}$], 145.1 [s, *C*$_{Ph}$]. **^{29}Si{^{1}H} NMR** (79 MHz, C_6D_6, 298 K): *δ*[ppm] = −11.7 [s]. **CHN Analysis** $C_{26}H_{24}N_2Si$: calculated: C 79.55, H 6.16, N 7.14, Si 7.15; found: C 79.76, H 5.92, N 7.05. **HR-MS (EI+)**, calculated m/z for $C_{26}H_{24}N_2Si$ [M+H$^+$]: 392.16996; found: 392.17033.

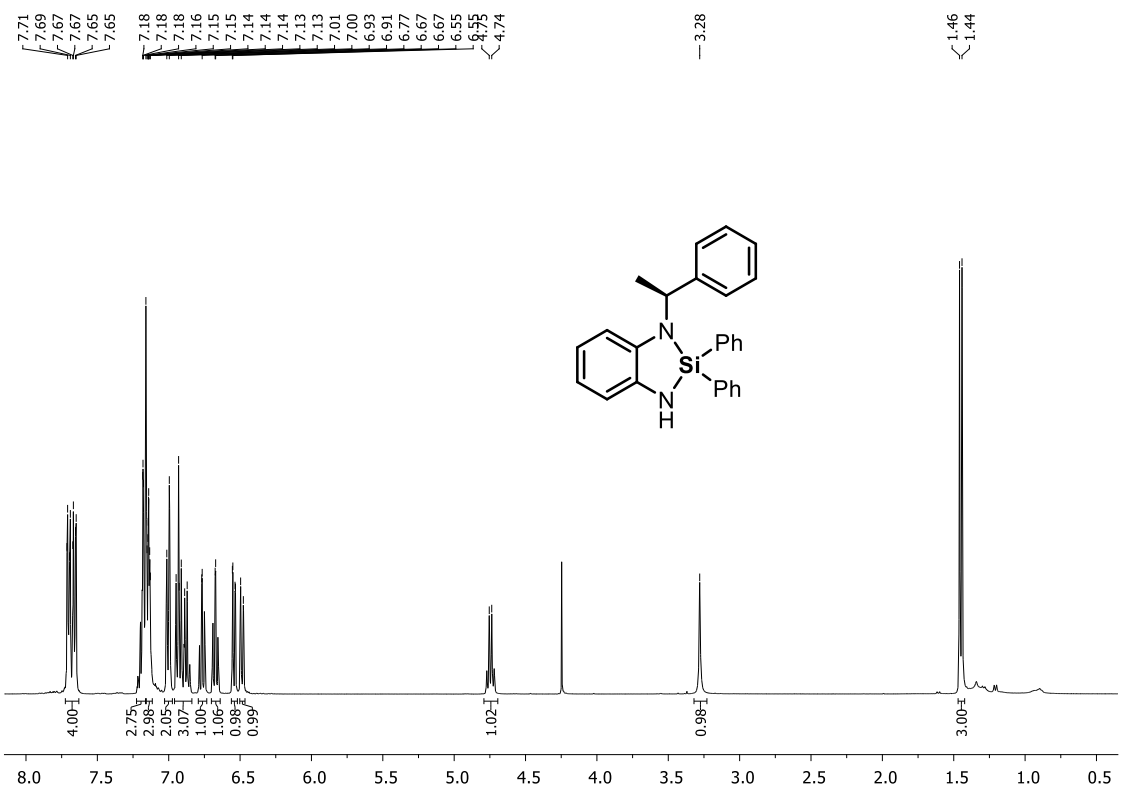

Figure S5.12. ^{1}H NMR spectrum (C_6D_6, 298 K) of **(*S*$_C$)-4**.

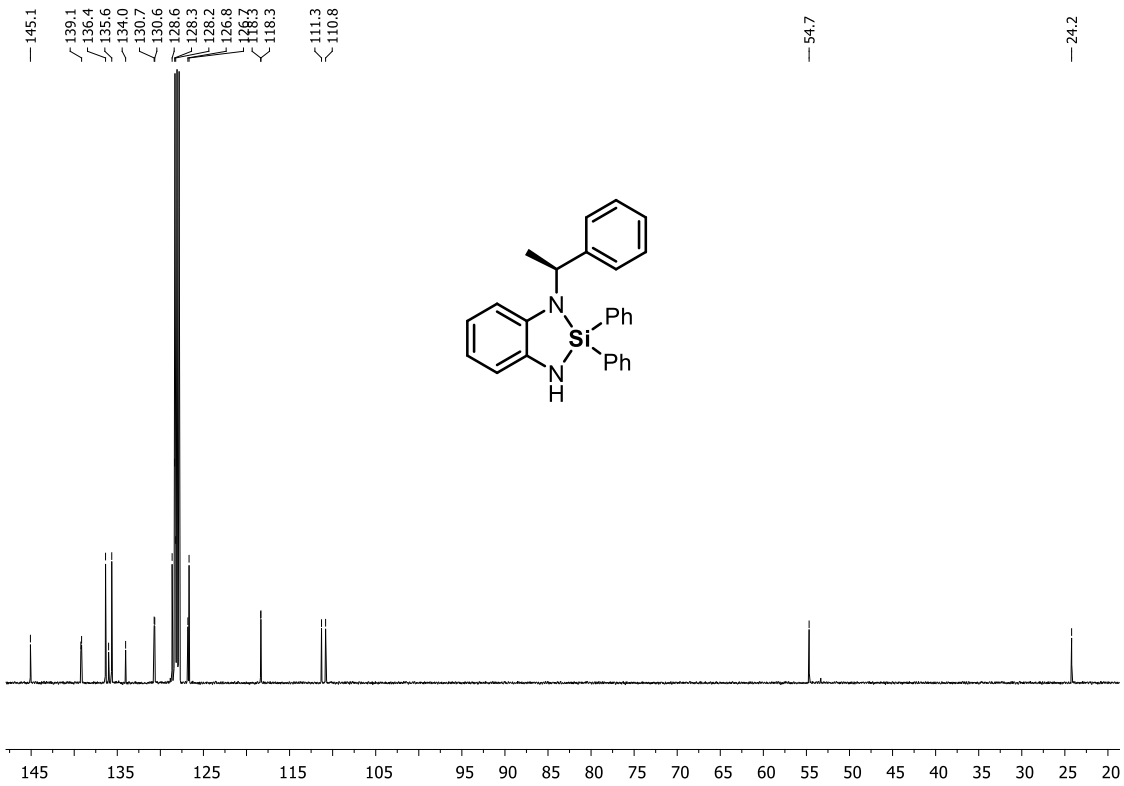

Figure S5.13. $^{13}C\{^{1}H\}$ NMR spectrum (C_6D_6, 298 K) of **(*S*$_C$)-4**.

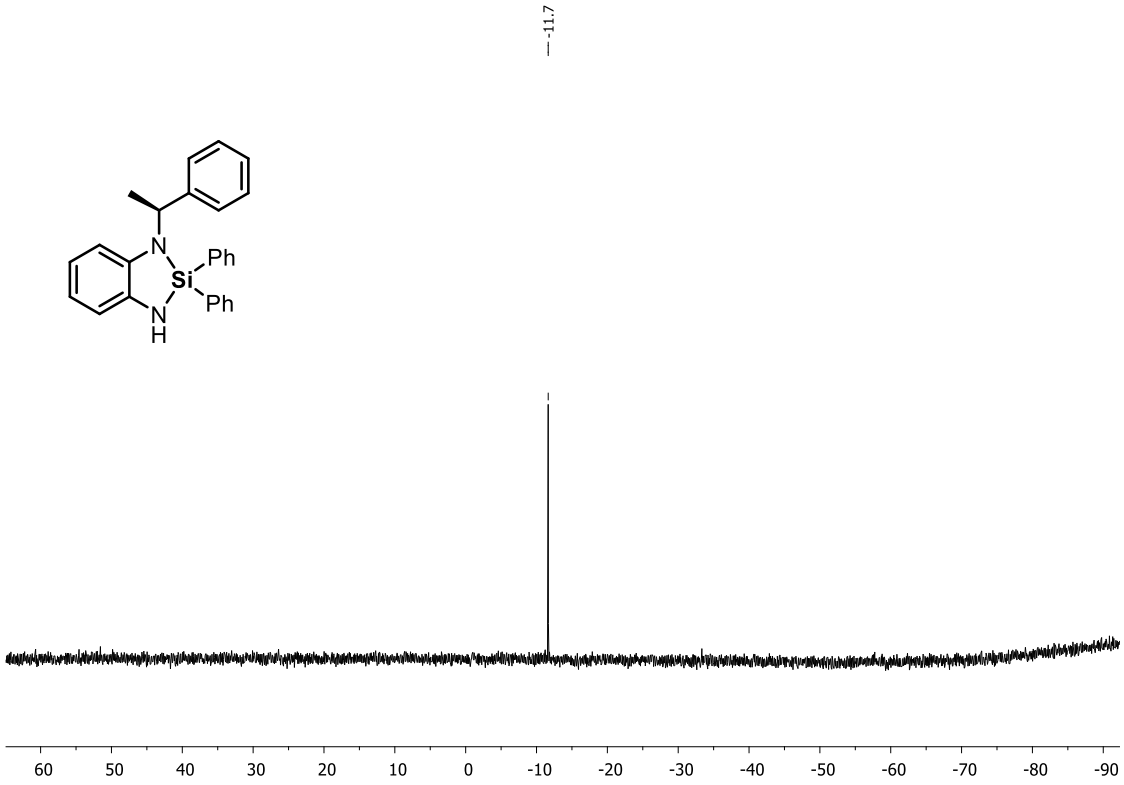

Figure S5.14. $^{29}Si\{^{1}H\}$ NMR spectrum (C_6D_6, 298 K) of **(*S*$_C$)-4**.

5.6.3.2 Compound (S_C, S_{Si})-5

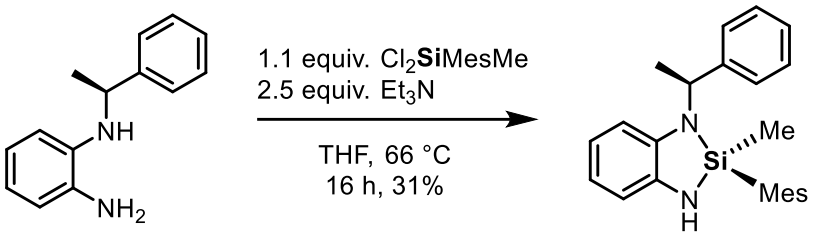

(S_C)-3 **(S_C, S_{Si})-5**

Compound **(S_C)-3** (2.12 g, 10.0 mmol, 1.0 equiv.) was dissolved in 50 mL of THF and triethylamine (3.46 mL, 25.0 mmol, 2.5 equiv.) was added. Dichloromethylmesitylsilane (2.59 g, 11.0 mmol, 1.1 equiv.) was added and the brown solution was heated to reflux at 66 °C for 16 h. All volatiles were removed *in vacuo* and the remaining brown wax was washed with 10 mL of pentane. The residue was taken up in 10 mL of toluene and the formed solids were removed by cannula filtration. The brown filtrate was dried *in vacuo* and recrystallized in a mixture of toluene (5 mL) and pentane (20 mL) to afford **(S_C, S_{Si})-5** as crystalline brown solid suitable for single-crystal X-ray crystallographic analysis (1.16 g, 3.1 mmol, 31%).

^{1}H NMR (400 MHz, C_6D_6, 298 K): δ[ppm] = 0.55 [s, 3H, CH_3], 1.32 [d, $^3J_{H\text{-}H}$ = 6.8 Hz, 3H, PhCH(CH_3)], 2.10 [s, 3H, *para*-CH_3], 2.22 [s, 6H, *ortho*-CH_3], 2.86 [s, 1H, N*H*], 4.55 [q, $^3J_{H\text{-}H}$ = 6.9 Hz, 1H, PhC*H*(CH_3)], 6.40–6.45 [m, 1H, H_{Ph}], 6.49–6.53 [m, 1H, H_{Ph}], 6.69–6.73 [m, 1H, H_{Ph}], 6.74 [s, 2H, H_{Mes}], 6.76–6.82 [m, 1H, H_{Ph}], 7.00–7.06 [m, 1H, H_{Ph}], 7.06–7.12 [m, 1H, H_{Ph}], 7.14 [s, 1H, H_{Ph}]. **^{13}C{^{1}H} NMR** (101 MHz, C_6D_6, 298 K): δ[ppm] = 11.1 [s, *C*H_3], 21.0 [s, *para*-*C*H_3], 22.5 [s, PhCH(*C*H_3)], 24.3 [s, *ortho*-*C*H_3], 54.4 [s, Ph*C*H(CH_3)], 110.2 [s, *C*H_{Ph}], 110.5 [s, *C*H_{Ph}], 118.1 [s, *C*H_{Ph}], 118,2 [s, *C*H_{Ph}], 127.1 [s, *C*H_{Ph}], 127.1 [s, *C*H_{Ph}], 128.8 [s, *C*H_{Ph}], 130.3 [s, *C*H_{Ph}], 131.9 [s, *C*$_{Ph}$], 139.5 [s, *C*$_{Ph}$], 139.7 [s, *C*$_{Ph}$], 140.1 [s, *C*$_{Ph}$], 145.1 [s, *C*$_{Ph}$], 145.7 [s, *C*H_{Ph}]. **^{29}Si{^{1}H}** NMR (79 MHz, C_6D_6, 298 K): δ[ppm] = −2.7 [s]. **CHN Analysis** $C_{24}H_{28}N_2Si$ calculated: C 77.37, H 7.58, N 7.52, Si 7.54; found: C 77.54, H 7.53, N 7.40. **HR-MS(EI+)**, calculated m/z for $C_{24}H_{28}N_2Si$ [M+H$^+$]: 372.20163; found: 372.20188.

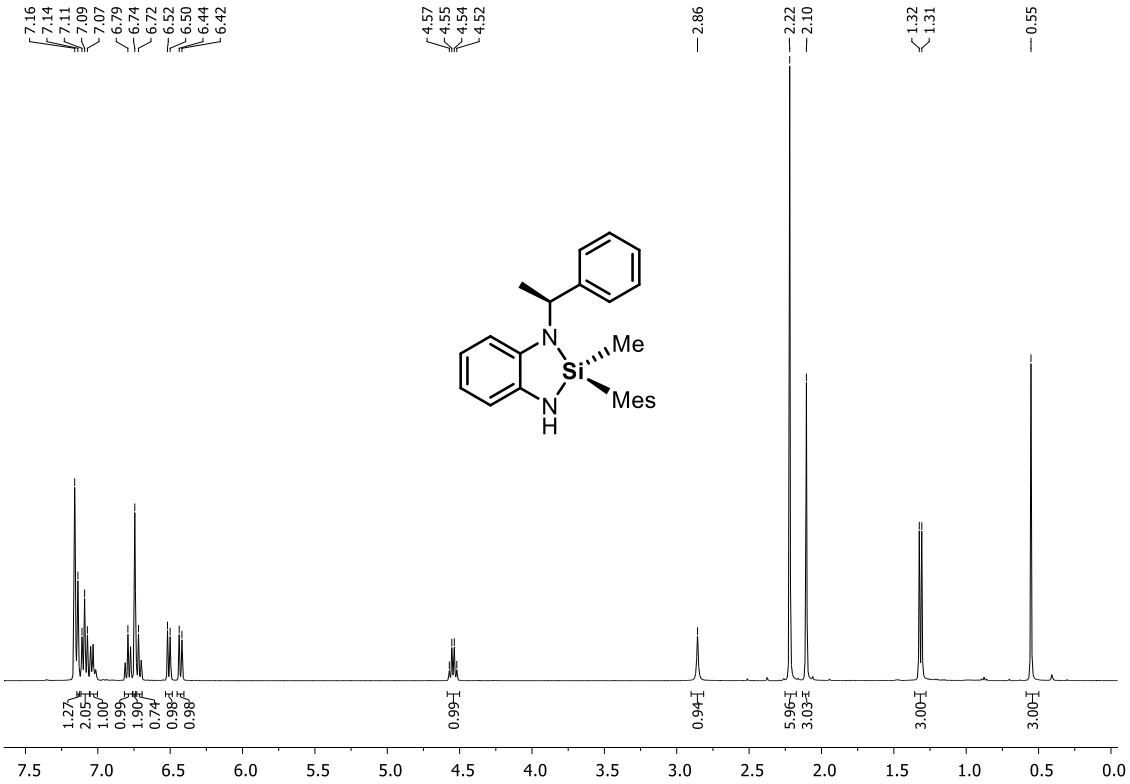

Figure S5.15. ^{1}H NMR spectrum (C_6D_6, 298 K) of **(S_C, S_{Si})-5**.

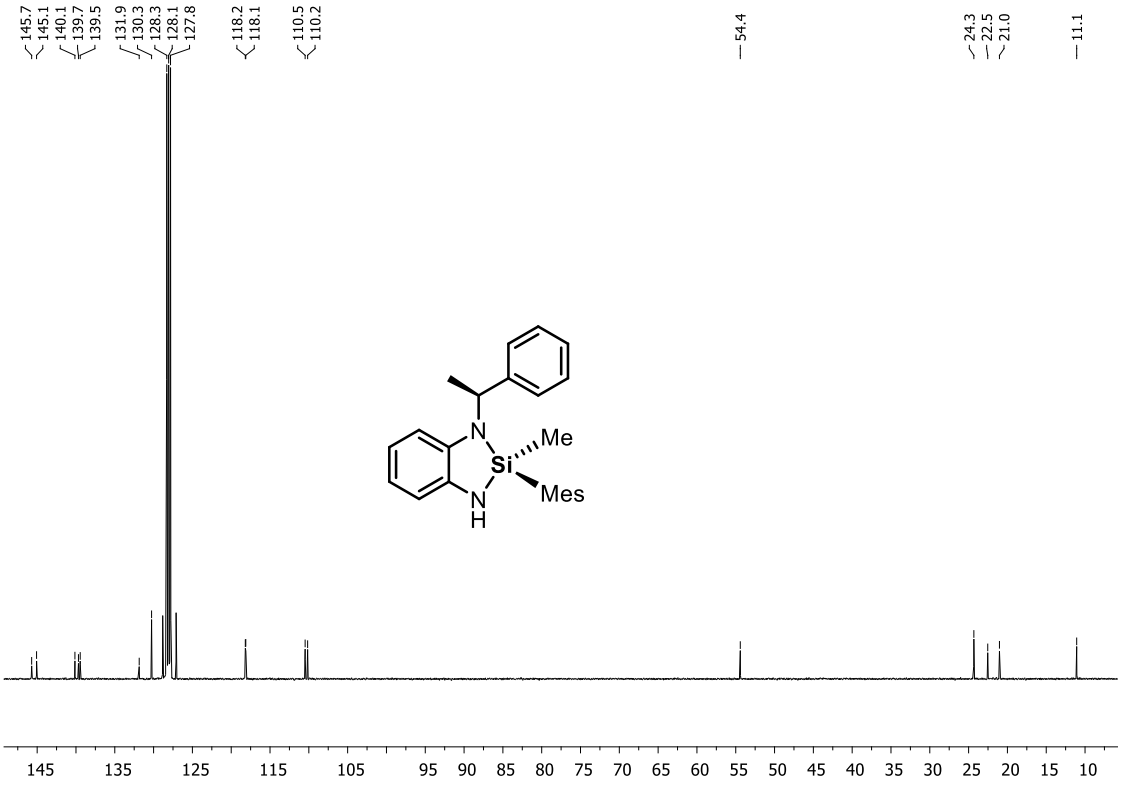

Figure S5.16. $^{13}C\{^{1}H\}$ NMR spectrum (C_6D_6, 298 K) of **(S_C, S_{Si})-5**.

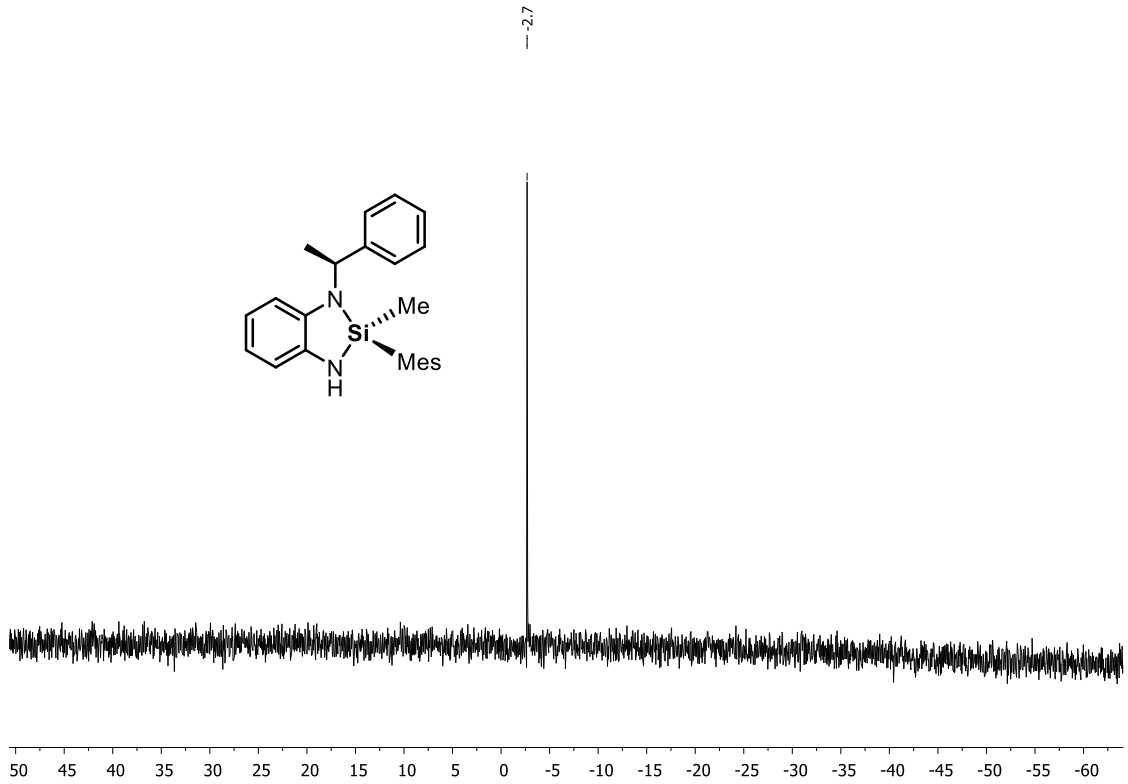

Figure S5.17. $^{29}Si\{^{1}H\}$ NMR spectrum (C_6D_6, 298 K) of **(S_C, S_{Si})-5**.

5.6.3.3 Compounds (S_C, S_{Si})-6 and (S_C, S_{Si})/ (S_C, R_{Si})-6

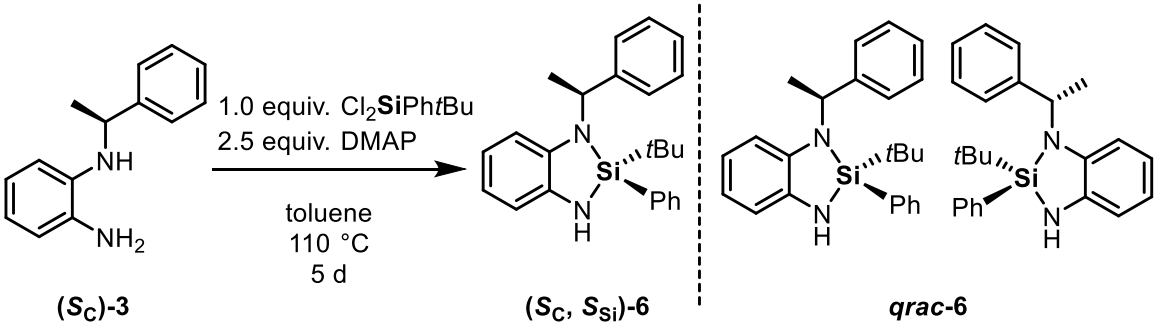

Compound **(S_C)-3** (1.06 g, 5.0 mmol, 1.0 equiv.) and 4-dimethylaminopyridine (1.53 g, 12.5 mmol, 2.5 equiv.) were dissolved in 30 mL of toluene. Dichloro-*tert*-butyl-phenylsilane (1.16 g, 5.0 mmol, 1.0 equiv.) was added. The brown solution was stirred a 110 °C for five days. The formed solids were removed via cannula filtration and the brown filtrate was dried *in vacuo* and then purified by Kugelrohr distillation (200 °C oven temperature, 1.0×10^{-3} mbar) to obtain a diastereomeric mixture of **6** with a ratio of ca. 47:53. Crystallization in a 4:1 mixture of toluene and pentane resulted in a 1:1 mixture of **(S_C, S_{Si})-6** and **(S_C, R_{Si})-6** as crystalline solid. The diastereomeric ratio is reflected in the crystal structure, where we observed both diastereomers within the unit cell.

Recrystallization in a 4:1 mixture of THF and pentane at −80 °C led to the precipitation of diastereomerically highly enriched **(S_C, S_{Si})-6** as observed via single-crystal X-ray analysis.

for **(S_C, S_{Si})-6**:

^{1}H NMR (400 MHz, C_6D_6, 298 K): δ[ppm] = 1.04 [s, 9H, C(CH_3)$_3$], 1.57 [d, $^3J_{H\text{-}H}$ = 7.0 Hz, 3H, PhCH(CH_3)], 3.38 [s, 1H, NH], 4.78 [q, $^3J_{H\text{-}H}$ = 6.9 Hz, PhCH(CH$_3$)], 6.40–6.43 [m, 1H, H_{Ph}], 6.60–6.67 [m, 2H, H_{Ph}], 6.76–6.81 [m, 1H, H_{Ph}], 7.12–7.22 [m, 5H, H_{Ph}], 7.60–7.63 [m, 2H, H_{Ph}]. **^{13}C{^{1}H} NMR** (101 MHz, C_6D_6, 298 K): δ[ppm] = 21.5 [s, C(CH$_3$)$_3$], 21.5 [s, CH(CH$_3$)], 27.1 [s, C(CH$_3$)$_3$], 53.3 [s, CH(CH$_3$)], 110.7 [s, CH$_{Ph}$], 112.0 [s, CH$_{Ph}$], 118.0 [s, CH$_{Ph}$], 118.1[s, CH$_{Ph}$], 126.9 [s, CH$_{Ph}$], 127.2 [s, CH$_{Ph}$], 128.2 [s, CH$_{Ph}$], 128.6 [s, CH$_{Ph}$], 130.2 [s, CH$_{Ph}$], 135.0 [s, CH$_{Ph}$], 136.1 [s, C_{Ph}], 139.3 [s, C_{Ph}], 139.7 [s, C_{Ph}], 144.0 [s, C_{Ph}]. **^{29}Si{^{1}H}** NMR (79 MHz, C_6D_6, 298 K): δ[ppm] = −1.6 [s]. **CHN Analysis** $C_{24}H_{28}N_2Si$ calculated: C 77.37, H 7.58, N 7.52, Si 7.54; found: C 77.25, H 7.50, N 7.52. **HR-MS(EI+)**, calculated m/z for $C_{24}H_{28}N_2Si$ [M+H$^+$]: 372.20163; found: 372.20166.

for **(S_C, S_{Si})/ (S_C, R_{Si})-6:**

^{1}H NMR (400 MHz, C_6D_6, 298 K): δ[ppm] = 1.04 [s, 9H, (S)-C(CH_3)$_3$], 1.06 [s, 9H, (S)-C(CH_3)$_3$], 1.46 [d, $^3J_{H\text{-}H}$ = 7.0 Hz, 3H, (R)-PhCH(CH_3)], 1.57 [d, $^3J_{H\text{-}H}$ = 7.0 Hz, 3H, (S)-PhCH(CH_3)], 3.38 [s, 2H, (S)+(R)-NH], 4.78 [q, $^3J_{H\text{-}H}$ = 6.9 Hz, (S)+(R)-PhCH(CH$_3$)], 6.40–6.43 [m, 1H, (S)-H_{Ph}], 6.43–6.47 [m, 1H, (R)-H_{Ph}], 6.60–6.67 [m, 4H, (S)+(R)-H_{Ph}], 6.76–6.82 [m, 2H, (S)+(R)-H_{Ph}], 7.96–7.22 [m, 14H, (S)+(R)-H_{Ph}], 7.26–7.30 [m, 2H, (S)+(R)-H_{Ph}], 7.60–7.66 [m, 4H, (S)+(R)-H_{Ph}].

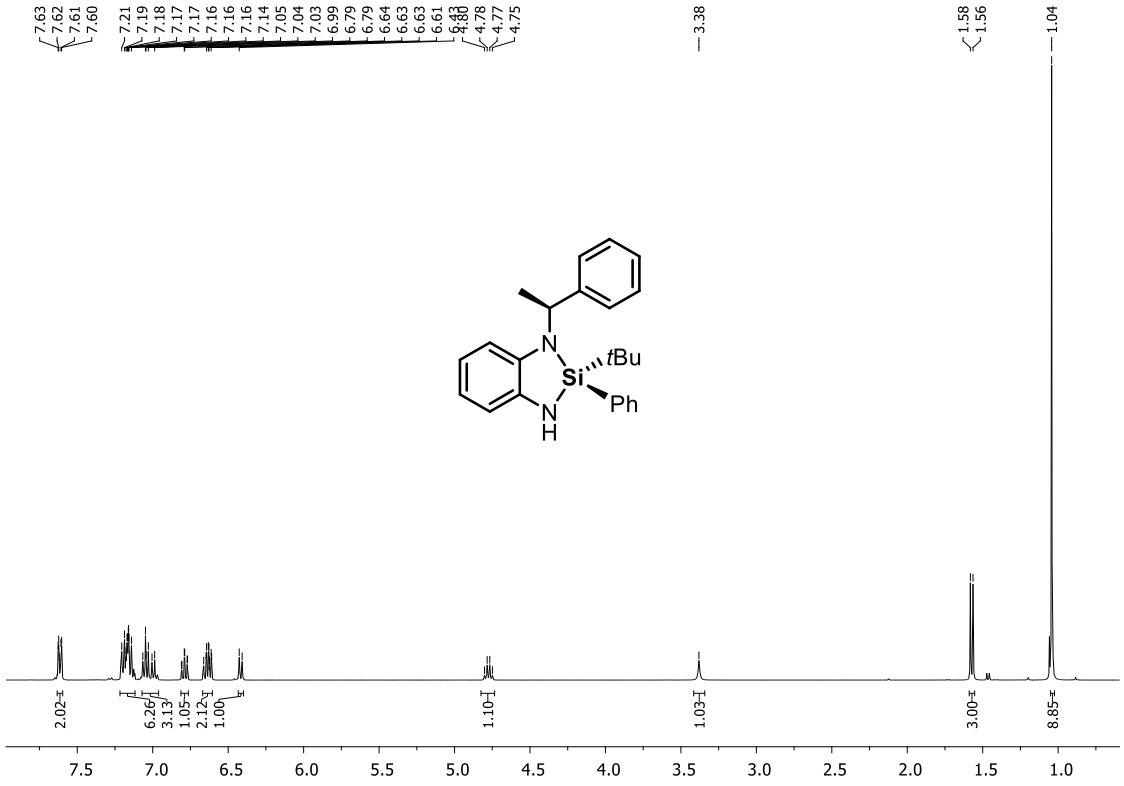

Figure S5.18. ^{1}H NMR spectrum (C_6D_6, 298 K) of **(S_C, R_{Si})-6**.

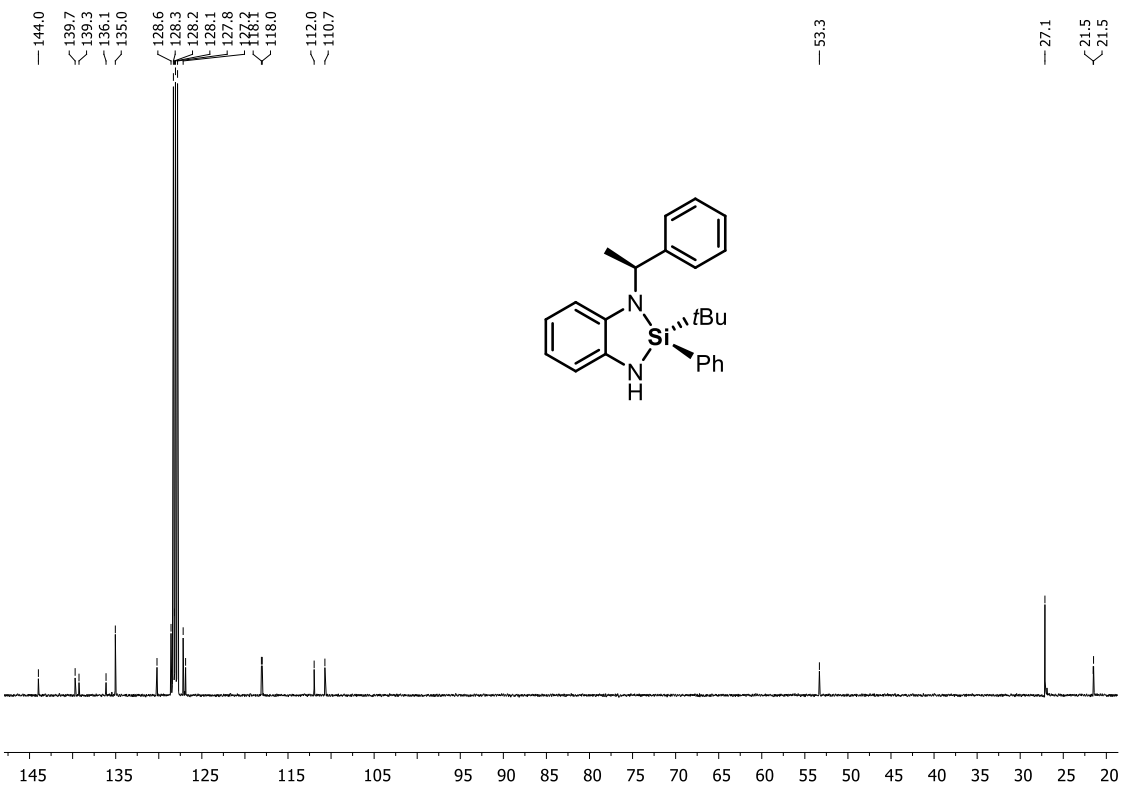

Figure S5.19. $^{13}C\{^{1}H\}$ NMR spectrum (C_6D_6, 298 K) of **(S_C, R_{Si})-6**.

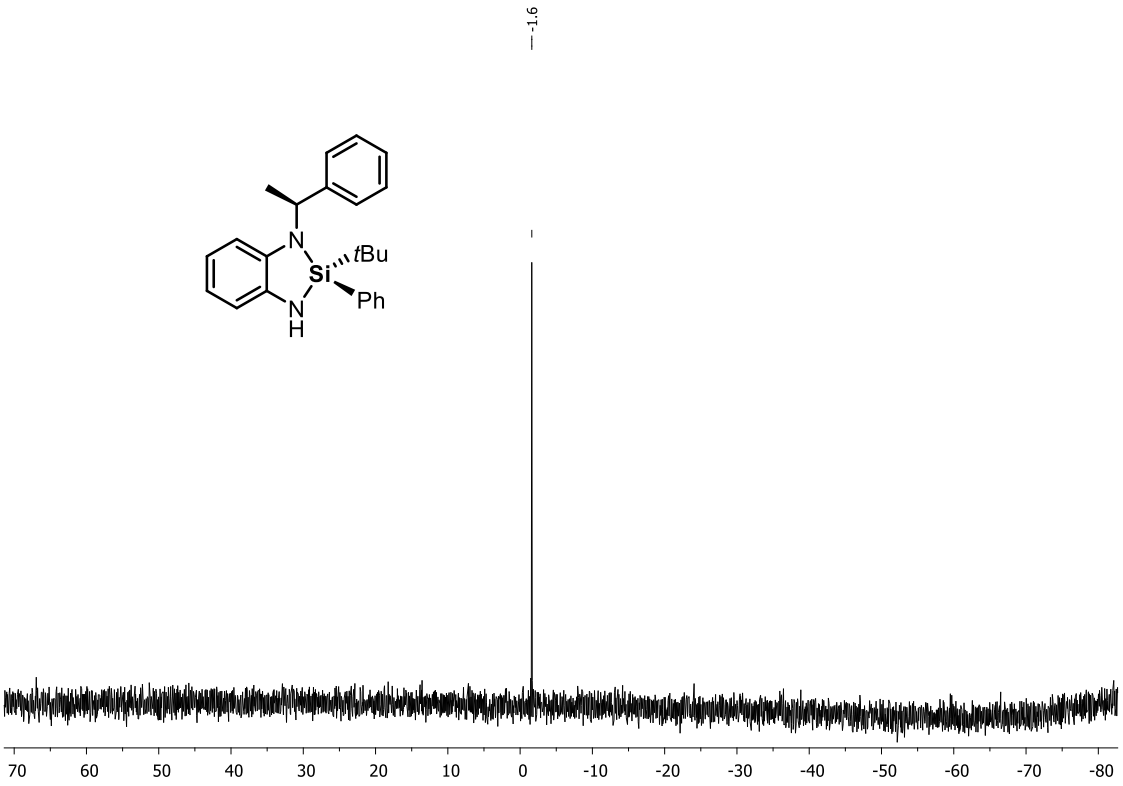

Figure S5.20. $^{29}Si\{^{1}H\}$ NMR spectrum (C_6D_6, 298 K) of **(S_C, R_{Si})-6**.

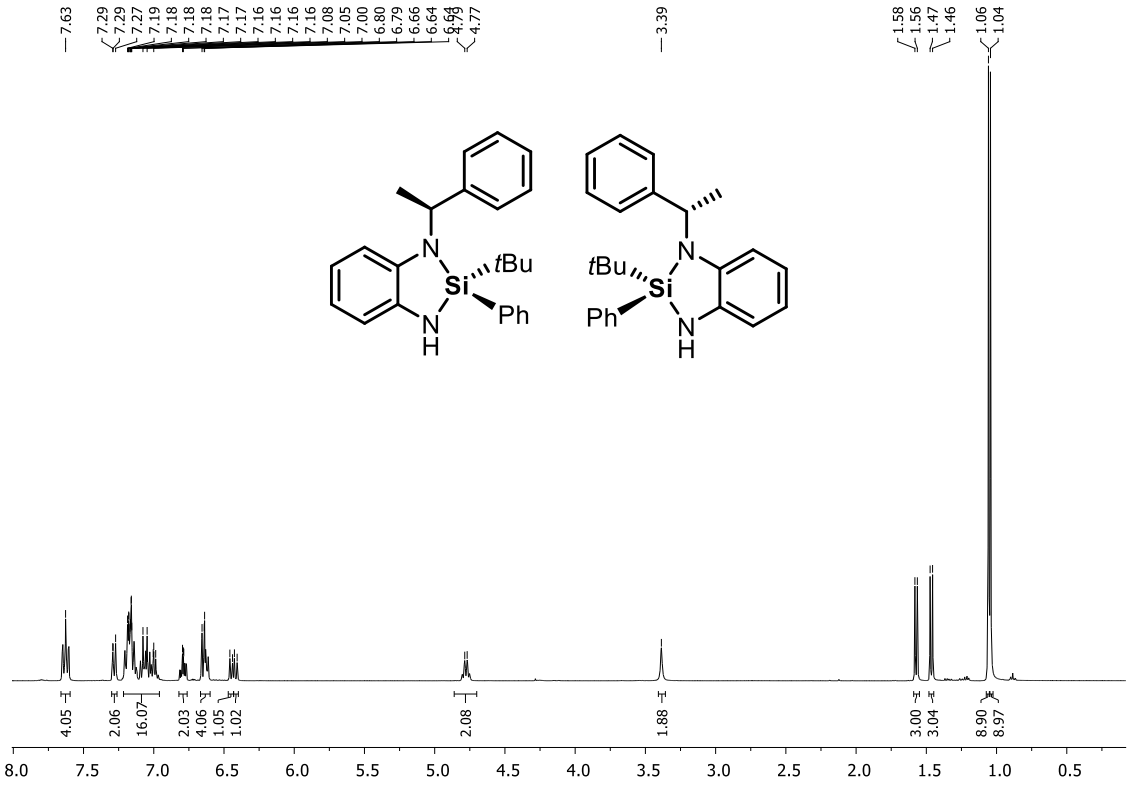

Figure S5.21. ^{1}H NMR spectrum (C_6D_6, 298 K) of **(*S*$_C$, *S*$_{Si}$)/(*S*$_C$, *R*$_{Si}$)-6**.

5.7 X-ray crystallographic details

The crystals were selected and measured either on a SuperNova Dualflex diffractometer equipped with a TitanS2 detector [**(*S*C, *S*Si)-2**, **(*S*C)-4, (*S*C, *S*Si)-5, (*S*C, *S*Si)-6**] or a XtaLAB Synergy R, DW system, equipped with a HyPix-Arc 150 detector (**(*S*C, *S*Si)/ (*S*C, *R*Si)-6**). Data collection and reduction were performed with **CrysAlisPro** [Version 1.171.41.54a or 1.17.41.76a].[4] A numerical absorption correction using spherical harmonics as implemented in SCALE3 ABSPACK was applied. Using **Olex2**,[5] the structures were solved with **ShelXT**[6] and a least-square refinement on F_2 was carried out with **ShelXL**.[7] All non-hydrogen atoms were refined anisotropically. Hydrogen atoms at the carbon atoms were located in idealized positions and refined isotropically according to the riding model. The hydrogen atoms on the nitrogen atoms were located from the difference Fourier map and refined without restraints. Figures were created with **Olex2**.[5]

Compound (*S*C, *S*Si)-2: The asymmetric unit contains one molecule.
Compound (*S*C)-4: The asymmetric unit contains two molecules.
Compound (*S*C, *S*Si)-5: The asymmetric unit contains one molecule.
Compound (*S*C, *S*Si)/ (*S*C, *R*Si)-6: The asymmetric unit contains one molecule of **(*S*C, *S*Si)-6** and one molecule of **(*S*C, *R*Si)-6.**
Compound (*S*C, *S*Si)-6: The asymmetric unit contains one molecule.

Table S5.1. Crystallographic data for compounds **(S_C, S_{Si})-2**, **(S_C)-4**, and **(S_C, S_{Si})-5**.

Compound	**(S_C, S_{Si})-2**	**(S_C)-4**	**(S_C, S_{Si})-5**
Data set (internal naming)	TG685-F-prec	TG692	TG745-(S)
Formula	$C_{18}H_{24}ClNSi$	$C_{26}H_{24}N_2Si$	$C_{24}H_{28}N_2Si$
$\rho_{calc.}$ / g·cm^{-3}	1.233	1.235	1.196
μ/mm^{-1}	2.574	1.074	1.062
Formula Weight	317.92	392.56	372.57
Color	clear colorless	clear colorless	clear colorless
Shape	block	block	block
Size/mm^3	0.24×0.17×0.08	0.19×0.18×0.1	0.24×0.14×0.12
T/K	122.99(10)	122.99(10)	123.00(10)
Crystal System	orthorhombic	monoclinic	orthorhombic
Flack Parameter	−0.002(9)	0.010(14)	−0.014(12)
Space Group	$P2_12_12_1$	$P2_1$	$P2_12_12_1$
a/Å	7.38930(10)	17.8218(3)	6.25260(10)
b/Å	10.31930(10)	6.71930)10)	17.1502(2)
c/Å	22.4563(3)	19.7512(4)	19.2970(2)
α/°	90	90	90
β/°	90	116.768(2)	90
γ/°	90	90	90
V/Å^3	1712.35(4)	2111.74(7)	2069.28(5)
Z	4	4	4
Z'	1	2	1
Wavelength/Å	1.54184	1.54184	1.54184
Radiation type	Cu K_α	Cu K_α	Cu K_α
$2\Theta_{min}$/°	7.874	9.008	6.896
$2\Theta_{max}$/°	133.934	133.944	133.92
Measured Refl.	13668	20129	14614
Independent Refl.	3048	6794	3679
R_{int}	0.0412	0.0422	0.0379
Parameters	194	533	356
Restraints	0	1	0
Largest Peak	0.26	0.23	0.18
Deepest Hole	−0.31	−0.31	−0.22
GooF	1.052	1.033	1.054
wR_2 (all data)	0.0765	0.0943	0.0735
wR_2	0.0763	0.0930	0.0730
R_1 (all data)	0.0287	0.0341	0.0283
R_1	0.0284	0.0350	0.0280

Table S5.2. Crystallographic data for compounds **(S_C, S_{Si})-6** and **(S_C, S_{Si})/ (S_C, R_{Si})-6.**

Compound	(S_C, S_{Si})-6	(S_C, S_{Si})/ (S_C, R_{Si})-6
Data set (internal naming)	TG722-(S)	TG694
Formula	$C_{24}H_{28}N_2Si$	$C_{24}H_{28}N_2Si$
$\rho_{calc.}$ / g·cm^{-3}	1.203	1.208
μ/mm^{-1}	1.068	1.072
Formula Weight	372.57	372.57
Color	clear colorless	clear colorless
Shape	block	block
Size/mm^3	0.19×0.14×0.13	0.24×0.14×0.1
T/K	123.00(10)	122.99(11)
Crystal System	triclinic	triclinic
Flack Parameter	−0.10(6)	0.06(3)
Space Group	P1	P1
a/Å	6.8660(2)	7.1941(2)
b/Å	8.8336(3)	9.0235(3)
c/Å	9.1349(2)	16.5387(5)
α/°	109.908(3)	74.324(3)
β/°	98.045(2)	85.253(2)
γ/°	91.419(3)	82.841(2)
V/Å^3	514.25(3)	1024.28(6)
Z	1	2
Z'	1	2
Wavelength/Å	1.54184	1.54184
Radiation type	Cu K_α	Cu K_α
$2\Theta_{min}$/°	10.43	5.558
$2\Theta_{max}$/°	133.752	147.918
Measured Refl.	9793	23811
Independent Refl.	3540	7300
R_{int}	0.0907	0.0645
Parameters	252	503
Restraints	3	3
Largest Peak	0.71	0.59
Deepest Hole	−0.51	−0.39
GooF	1.031	1.100
wR_2 (all data)	0.2174	0.1643
wR_2	0.2129	0.1590
R_1 (all data)	0.0884	0.0586
R_1	0.0862	0.0554

Compound (S_C, S_{Si})-2

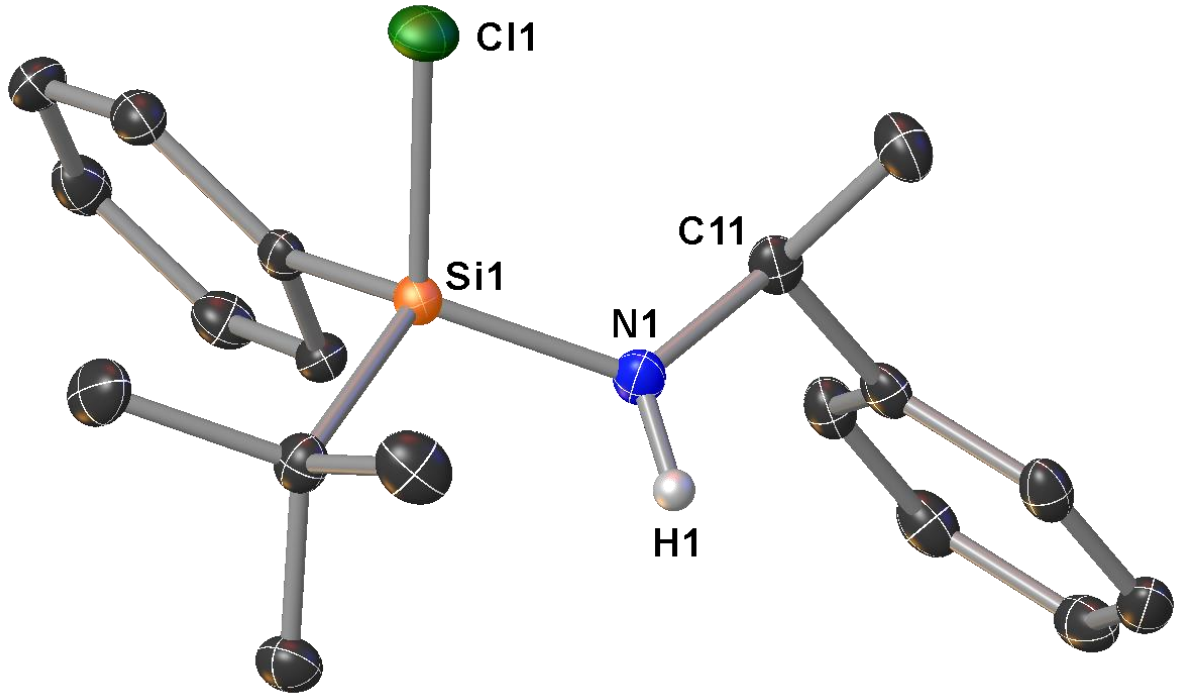

Selected Bond Lengths in Å		Selected Bond Angles in °	
Si1–N1	1.704(2)	**Cl1–Si1–N1**	111.88(8)
Si1–Cl1	2.0993(8)		
N1–C11	1.477(3)		

Compound (S_C)-4

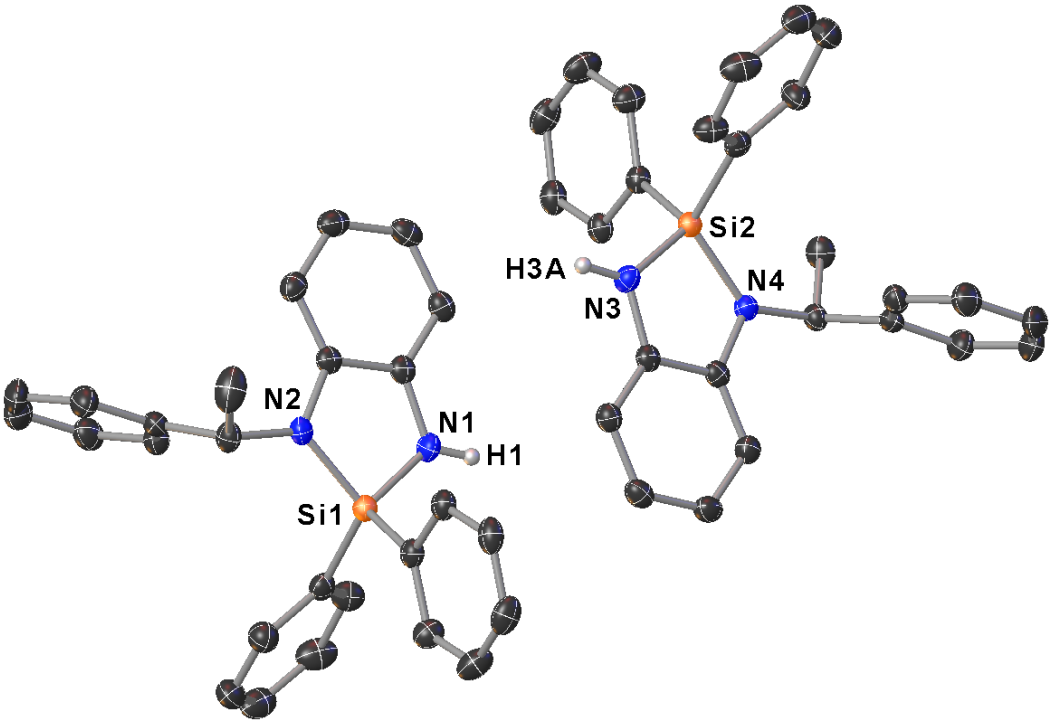

Selected Bond Lengths in Å		Selected Bond Angles in °	
Si1–N1	1.713(2)	**N1–Si1–N2**	91.67(10)
Si1–N2	1.7376(19)	**N3–Si2–N4**	91.27(10)
Si2–N3	1.720(2)		
Si2–N4	1.7487(18)		

Compound (S_C, S_{Si})-5

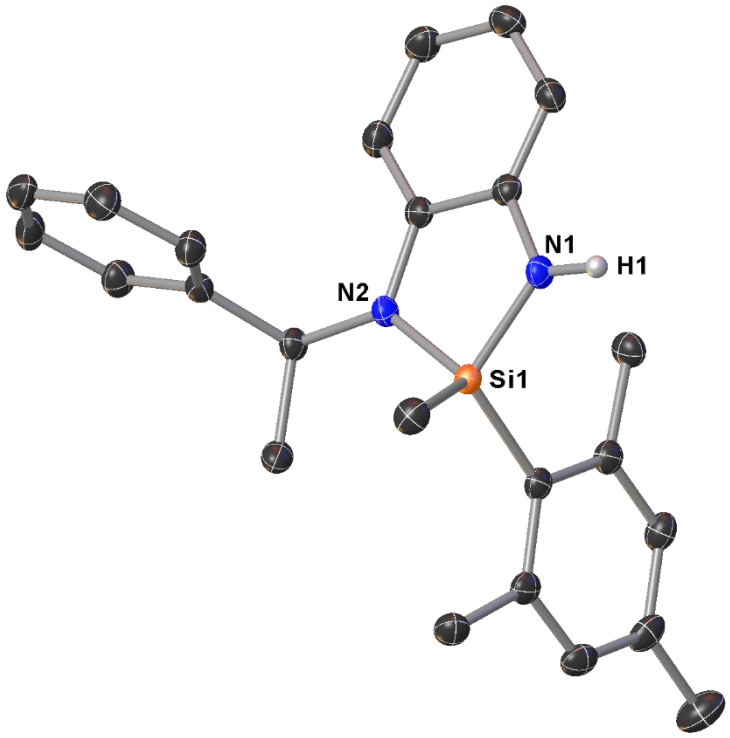

Selected Bond Lengths in Å		Selected Bond Angles in °	
Si1–N1	1.7318(18)	**N1–Si1–N2**	90.79(8)
Si1–N2	1.7546(16)		

Compound (S_C, S_{Si})/ (S_C, R_{Si})-6

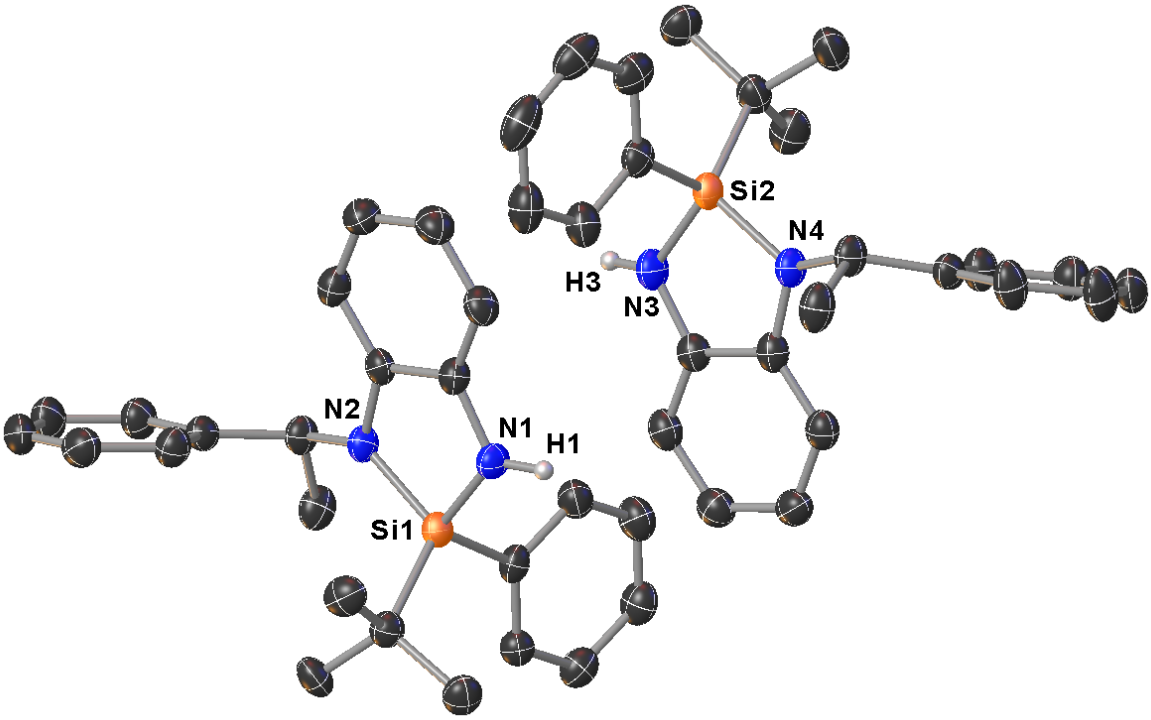

Selected Bond Lengths in Å		Selected Bond Angles in °	
Si1–N1	1.726(4)	**N1–Si1–N2**	91.52(17)
Si1–N2	1.757(3)	**N3–Si2–N4**	91.54(18)
Si2–N3	1.724(4)		
Si2–N4	1.742(4)		

Compound (S_C, S_{Si})-6

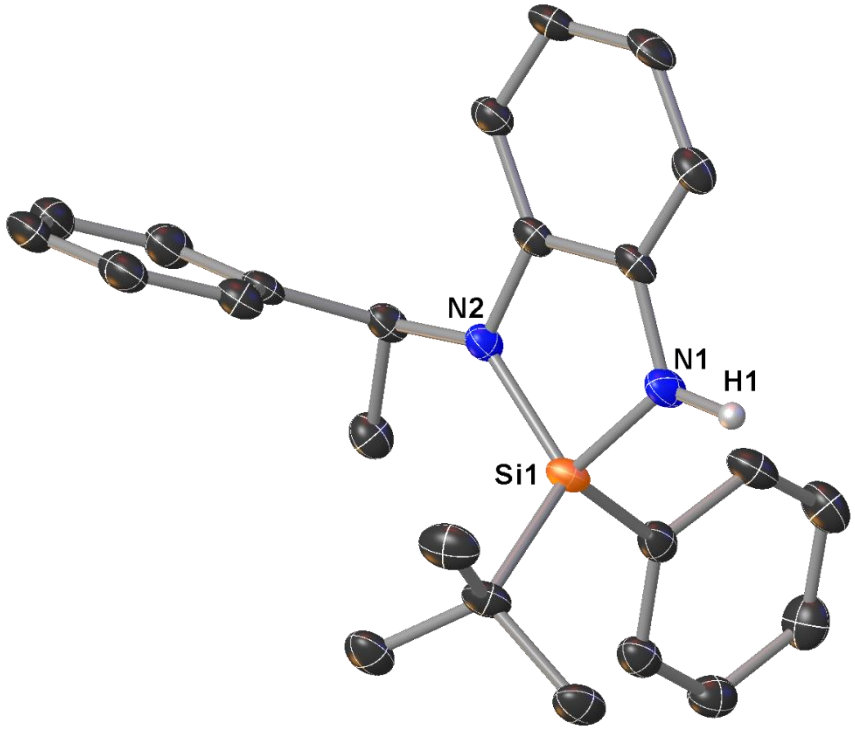

Selected Bond Lengths in Å		Selected Bond Angles in °	
Si1–N1	1.743(5)	**N1–Si1–N2**	90.7(2)
Si1–N2	1.756(4)		

5.8 Supplementary references

[1] F. M. Rivas, A. J. Giessert, S. T. Diver, *J. Org. Chem.* **2002**, *67*, 1708–1711.

[2] S. Scholz, I. Sänger, F. Schödel, M. Bolte, H.-W. Lerner, *Inorg. Chem. Commun.* **2014**, *44*, 50–52.

[3] A. Kunai, T. Sakirai, E. Toyoda, M. Ishikawa, *Organometallics* **1996**, *15*, 2478–2482.

[4] CrysAlisPro Software System, Rigaku Oxford Diffraction, **2020**.

[5] O. V. Dolomanov, L. J. Bourhis, R. J. Gildea, J. A. K. Howard, H. Puschmann, *OLEX2*: a complete structure solution, refinement and analysis program, *J. Appl. Crystallogr.* **2009**, *42*, 339–341.

[6] G. M. Sheldrick, *SHELXT* – Integrated space-group and crystal-structure determination, *Acta Crystallogr*. **2015**, *A71*, 3–8.

[7] G. M. Sheldrick, Crystal structure refinement with *SHELXL*, *Acta Crystallogr.* **2015**, *C71*, 3–8.

6 Additional findings

Preface

The following chapter contains additional findings that were not discussed in the chapters before. It includes fully characterized compounds, but also some compounds where detailed characterization is missing. The collected procedures and data are available for further use by the group of Dr. J. O. Bauer.

Authors

T. Götz and Dr. J. O. Bauer

Author contribution

All the reported syntheses and characterizations in this work were performed by T. Götz.

Acknowledgements

This work was jointly supported by the Elite Network of Bavaria (ENB), the Bavarian State Ministry of Science and the Arts (StMWK), and the University of Regensburg (N-LW-NW-2016-366).

6.1 General remarks

All experiments were performed in an inert atmosphere of purified nitrogen by using standard Schlenk techniques or an MBraun Unilab 1200/780 glovebox. Glassware was heated at 600 °C prior to use. Diethyl ether (Et_2O), dichloromethane (DCM), hexane, pentane, tetrahydrofuran (THF), and toluene were dried and degassed with an MBraun SP800 solvent purification system. *n*-Butyllithium (2.5 M or 1.6 M solution in hexane, Merck KGaA), diphenylchlorosilane (96%, abcr GmbH) and $W(CO)_6$ (97%, Merck KGaA) were used as received without any further purification. Triethylamine (≥99%, Merck KGaA) was heated at reflux over CaH_2 and distilled prior to use. Compounds **8**,[1] **10**,[2] **11**,[3] $Ge(HMDS)_2$[4] and Ph*t*BuSiHCl[3] were synthesized according to previously published procedures. The synthesis of compounds **1**, **2**, **6**, **15** and **17** is already described in chapter 3 in this work. C_6D_6 used for NMR spectroscopy was dried over 3 Å molecular sieves and degassed by a standard freeze-pump-thaw procedure. NMR spectra were either recorded using a Bruker Avance 300 (300.13 MHz), a Bruker Avance 400 (400.13 MHz) or a Bruker Avance III HD 400 (400.13 MHz) at 25 °C. Chemical shifts (δ) are reported in parts per million (ppm). ^{1}H and $^{13}C\{^{1}H\}$ NMR spectra are referenced to tetramethylsilane ($SiMe_4$, δ = 0.0 ppm) as external standard, with the deuterium signal of the solvent serving as internal lock and the residual solvent signal as an additional reference. $^{29}Si\{^{1}H\}$ NMR spectra are referenced to $SiMe_4$, $^{7}Li\{^{1}H\}$ spectra to LiCl (1 M in D_2O). For the assignment of the multiplicities, the following abbreviations are used: s = singlet, d = doublet, t = triplet, sept = septet, m = multiplet. For simplicity, multiplets of order higher than one are described approximating them to the closest first-order type. High-resolution mass spectrometry was carried out on a Jeol AccuTOF GCX and an Agilent Q-TOF 6540 UHD spectrometer. Elemental analyses were performed on a Vario MICRO cube apparatus.

6.2 Substitution of diorganochlorosilanes with nitrogen-based substituents

6.2.1 Results and discussion

In scope of the work presented in the chapters above, some interesting compounds and reactivities have been observed which were not discussed before. For instance, we used the *ortho*-aminoanilines **1** and **2** and reacted them with diorganochlorosilanes hoping to achieve the syntheses of a series of functional silanes featuring N–H protic and Si–H hydridic sites in the same molecule. However, lithiation of the diamines with 1.1 equiv. of *n*BuLi and reaction with *tert*-butylchlorophenylsilane resulted in some surprising observations. Depending on the substituent (Dipp or *t*Bu) on the diamine and the type of solvent, different types of reaction products were observed (Scheme 6.1, top). The conversion of Dipp-substituted compound **1** resulted in the

quantitative formation of the cyclized diaminosilane **3**. Both the protic N–H and the hydridic Si–H functions were removed with formation of H_2. This reactivity is similar to the one observed for the Dipp-substituted hydrosilane in chapter 4 and is suspected to proceed through a similar pentacoordinated intermediate. The formation of dilithiated diamine like described in chapter 3 is not likely as the solvent toluene cannot stabilize this compound. The *t*Bu analogue **2**, however, showed a solvent dependent reactivity. Performing the reaction in toluene resulted in the formation of the desired open aminosilane **4** where both N–H and Si–H functions are still present. Once more, these observations suggest a high importance of the aromatic Dipp group when it comes to the stabilization of the highercoordinated intermediate and the resulting loss of H_2. However, using THF as a solvent in the reaction of **Li-2** with *tert*-butyl-chlorophenylsilane resulted in the lithiated dimer **5** as we have examined via single-crystal X-ray crystallographic analysis. The mechanistic pathway leading to this product has yet to be examined in detail. Gerenally, there are two possibilities for the formation of compound **5**. On the one hand, diamine **2** could be dilithiated like described in chapter 3, followed by the removal of LiCl and LiH after reaction with *tert*-butyl-chlorophenylsilane and deprotonation of the free NH function by the LiH to obtain compound **5**. On the other hand, diamine **1** can be monolithiated and reacts to compound **4** in the first step. With THF as electron donating solvent, a pentacoordination could occur similar to the one described in chapter 4 which leads to the developent of H_2 followed by deprotonation of the NH group by *n*BuLi. However, in chapter 4 we discussed that the *t*Bu substituent seems to significantly disfavor the pentacoordination. It is therefore more likely that compound **5** is formed via the dilithiatated diamine **2**. Similar to compound **5,** a lithiated silylamide **7** could be easily synthesized through the reaction of the cyclic diaminosilane analogue **6** with *n*BuLi (Scheme 6.1, bottom left). A successful formation of a hydrosilane **9** with a N–H and a hydridic Si–H function was achieved with the use of amidine **8** instead of aromatic diamines. Lithiation with *n*Buli and subsequent reaction with diphenylchlorosilane afforded compound **9** (Scheme 6.1, bottom right). The loss of H_2 seems to be disfavored in that case as the formed three-membered heterocycle would be significantly less stable.

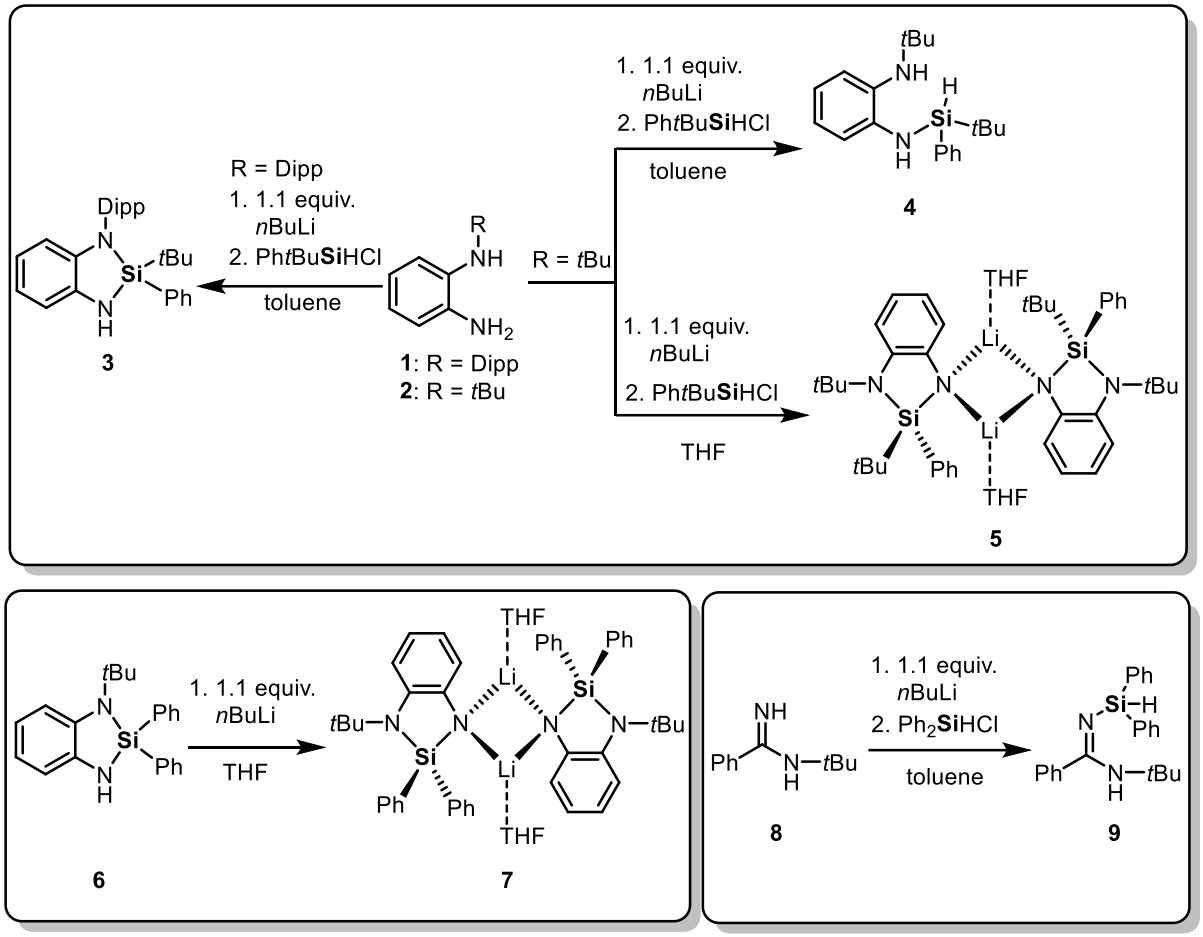

Scheme 6.1. Reactivities observed in the substitution of diorganochlorosilanes.

6.2.2 Syntheses and characterizations

6.2.2.1 Synthesis of Compound 3

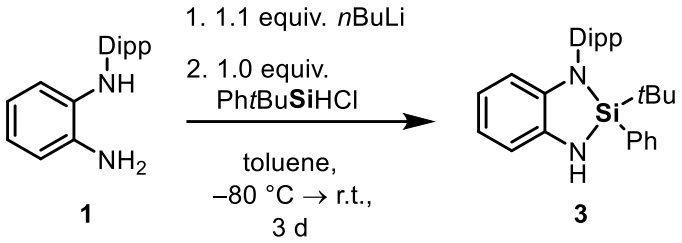

Compound **1** (268 mg, 1.0 mmol, 1.0 equiv.) was dissolved in 10 mL of toluene and cooled down to 0 °C. *n*BuLi (0.44 mL, 1.1 mmol, 1.1 equiv. of a 2.5 mol/L solution in hexane) was added dropwise via syringe. The brown mixture was stirred for 1 h while warming to room temperature. Then, it was cooled down to −80 °C and *tert*-butylchlorophenylsilane was added. The mixture was stirred for three days while slowly warming up to room temperature. All volatiles were removed *in vacuo* and the brown residue was taken up in 20 mL of pentane. The solids were removed by cannula filtration and the brown filtrate was dried *in vacuo* to obtain **3** as a brown solid (428 mg, 0.99 mmol, 99%).

^{1}H NMR (400 MHz, C_6D_6, 298 K): *δ*[ppm] = 0.19 [d, $^{3}J_{H\text{-}H}$ = 6.7 Hz, 3H, CH(CH_3)$_2$], 0.69 [d, $^{3}J_{H\text{-}H}$ = 6.7 Hz, 3H, CH(CH_3)$_2$], 0.99 [s, 9H, C(CH_3)$_3$], 1.26 [d, $^{3}J_{H\text{-}H}$ = 6.7 Hz, 3H, CH(CH_3)$_2$], 1.41 [d, $^{3}J_{H\text{-}H}$ = 6.7 Hz, 3H, CH(CH_3)$_2$], 2.49 [sept, $^{3}J_{H\text{-}H}$ = 6.7 Hz, 1H, CH(CH$_3$)$_2$], 3.69 [s, 1H, NH], 3.90 [sept, $^{3}J_{H\text{-}H}$ = 6.7 Hz, 1H, CH(CH$_3$)$_2$], 6.19–6.22 [m, 1H, H_{Ph}], 6.58–6.64 [m, 1H, H_{Ph}], 6.68–6.72 [m, 1H, H_{Ph}], 6.79–6.85 [m, 1H, H_{Ph}], 6.99–7.10 [m, 4H, H_{Ph}], 7.18–7.25 [m, 2H, H_{Ph}], 7.28–7.33 [m, 2H, H_{Ph}]. **^{13}C{^{1}H} NMR** (101 MHz, C_6D_6, 298 K): *δ*[ppm] = 22.2 [s, C(CH$_3$)$_3$], 22.2 [s, CH(CH$_3$)$_2$], 23.7 [s, CH(CH$_3$)$_2$], 25.8 [s, CH(CH$_3$)$_2$], 26.2 [s, C(CH$_3$)$_3$], 26.8 [s, CH(CH$_3$)$_2$], 28.4 [s, CH(CH$_3$)$_2$], 28.9 [s, CH(CH$_3$)$_2$], 111.1 [s, CH$_{Ph}$], 113.2 [s, CH$_{Ph}$], 118.0 [s, CH$_{Ph}$], 119.1 [s, CH$_{Ph}$], 124.1 [s, CH$_{Ph}$], 125.6 [s, CH$_{Ph}$], 128.0 [s, CH$_{Ph}$], 129.9 [s, CH$_{Ph}$], 133.0 [s, C_{Ph}], 134.5 [s, CH$_{Ph}$], 137.4 [s, C_{Ph}], 139.0 [s, C_{Ph}], 142.5 [s, CH$_{Ph}$], 148.8 [s, CH$_{Ph}$], 149.1 [s, CH$_{Ph}$]. **^{29}Si{^{1}H}** NMR (79 MHz, C_6D_6, 298 K): *δ*[ppm] = −2.3 [s]. **CHN Analysis** $C_{28}H_{36}N_2Si$ calculated: C 78.45, H 8.46, N 6.53, Si 6.55; found: C 78.07, H 8.07, N 5.89. **HR-MS (FD+)**, calculated m/z for $C_{28}H_{36}N_2Si$ [M+H$^+$]: 428.26423; found: 428.26329.

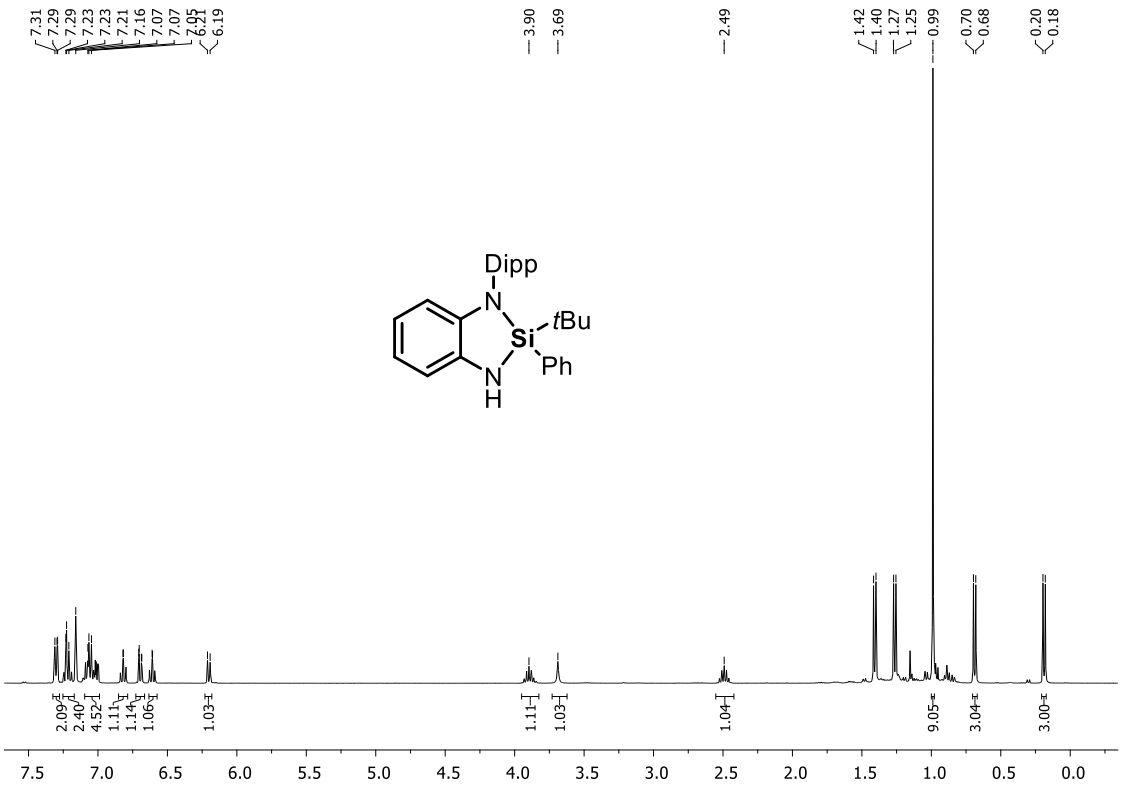

Figure 6.2. ^{1}H NMR spectrum (C_6D_6, 298 K) of **3**.

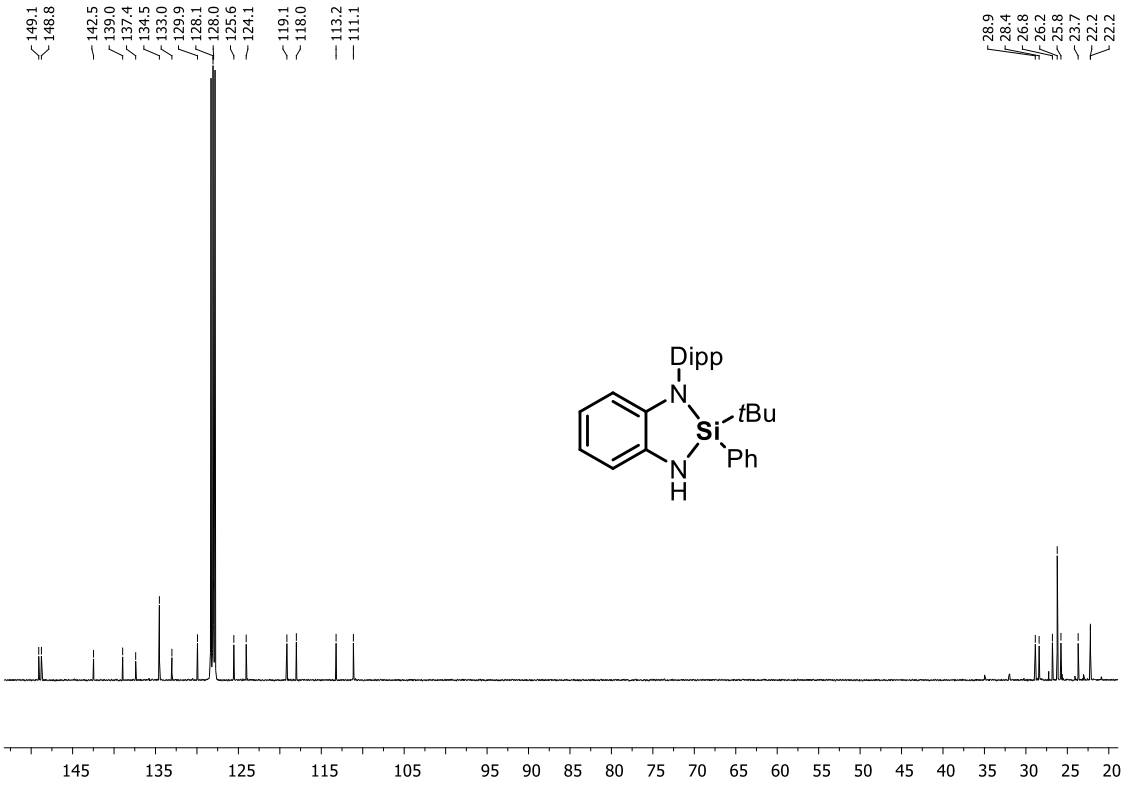

Figure 6.3. $^{13}C\{^{1}H\}$ NMR spectrum (C_6D_6, 298 K) of **3**.

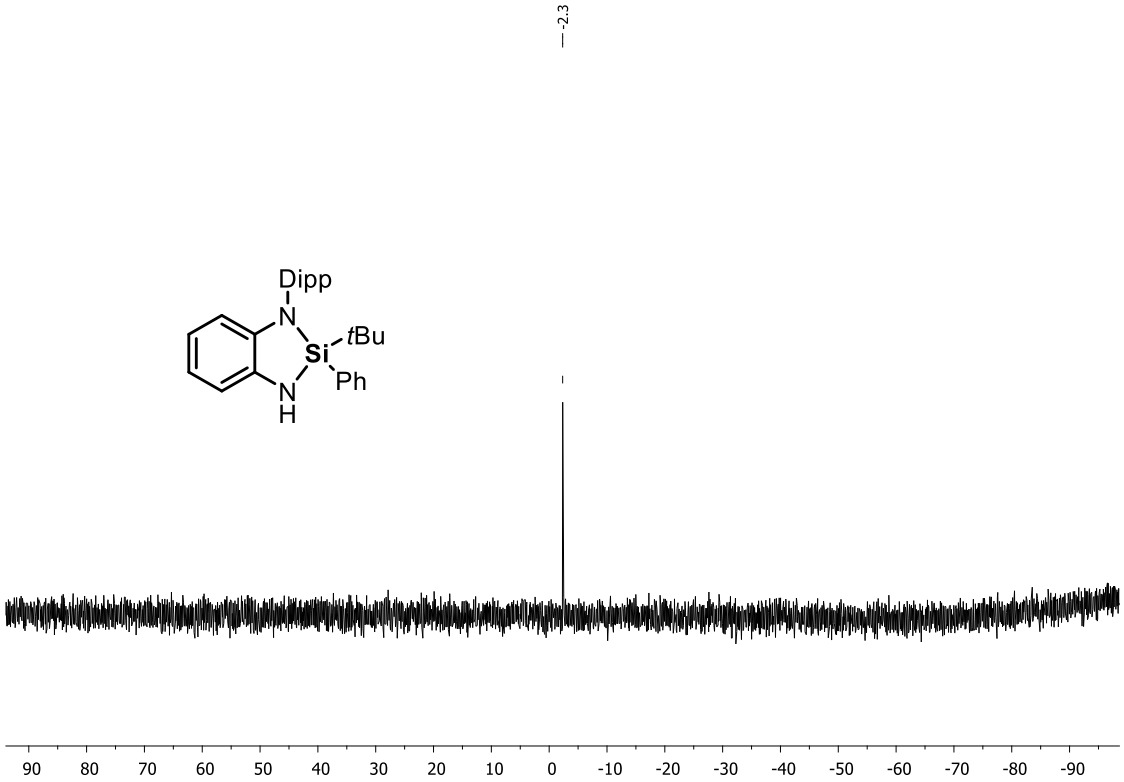

Figure 6.4. $^{13}C\{^{1}H\}$ NMR spectrum (C_6D_6, 298 K) of **3**.

6.2.2.2 Synthesis of compound 4

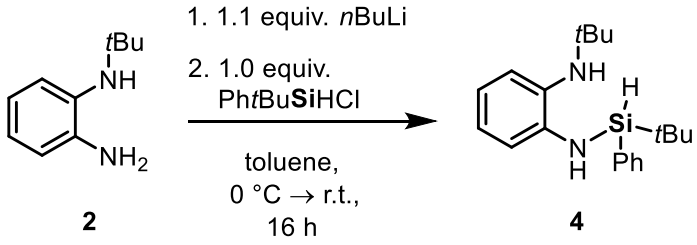

Compound **2** (164 mg, 1.0 mmol, 1.0 equiv.) was dissolved in 10 mL of toluene and cooled down to 0 °C. *n*BuLi (0.44 mL, 1.1 mmol, 1.1 equiv. of a 2.5 mol/L solution in hexane) was added dropwise via syringe and the solution was stirred for 30 min. Then, *tert*-butyl-chlorophenylsilane (198 mg, 1.0 mmol, 1.0 equiv.) was added and the solution was stirred for 16 h while warming to room temperature. All volatiles were removed *in vacuo* and the brown residue was taken up in 10 mL of pentane. The solids were removed by cannula filtration and the brown filtrate was dried *in vacuo* to obtain compound **4** as a brown wax (280 mg, 0.86 mmol, 86%).

^{1}H NMR (400 MHz, C_6D_6, 298 K): δ[ppm] = 1.09 [s, 9H, SiC(CH_3)$_3$], 1.09 [s, 9H, NC(CH_3)$_3$], 2.03 [s, 1H, SiNH], 5.16 [d, $^{3}J_{H\text{-}H}$ = 2.7 Hz, 1H, Si*H*], 5.64 [s, 1H, N*H*], 6.61–6.66 [m, 1H, H_{Ph}], 6.79–6.85 [m, 2H, H_{Ph}], 6.88–6.92 [m, 1H, H_{Ph}], 7.17–7.20 [m, 3H, H_{Ph}], 7.67–7.70 [m, 2H, H_{Ph}]. **^{13}C{^{1}H} NMR** (101 MHz, C_6D_6, 298 K): δ[ppm] = 17.0 [s, Si*C*(CH_3)$_3$], 26.9 [s, SiC(*C*H_3)$_3$], 29.9 [s, NC(*C*H_3)$_3$], 54.5 [s, N*C*(CH_3)$_3$], 115.9 [s, *C*H$_{Ph}$], 117.8 [s, *C*H$_{Ph}$], 126.4 [s, *C*H$_{Ph}$], 128.3 [s, *C*H$_{Ph}$],

128.9 [s, *C*H$_{Ph}$], 130.2 [s, *C*H$_{Ph}$], 132.6 [s, *C*$_{Ph}$], 134.3 [s, *C*$_{Ph}$], 15.0 [s, *C*H$_{Ph}$], 146.3 [s, *C*$_{Ph}$]. **MS (ESI+)**, calculated m/z for $C_{20}H_{30}N_2Si$ [M+H$^+$]: 326.2178; found: 326.2425.

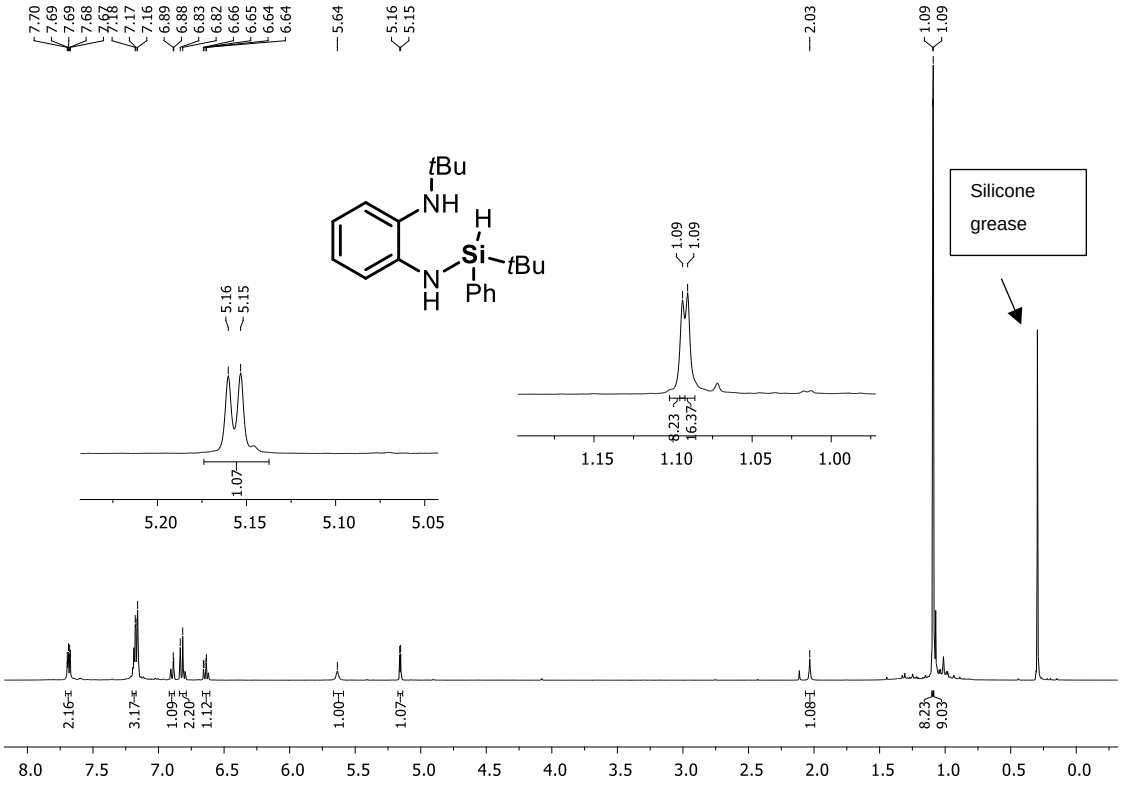

Figure 6.5. ^{1}H NMR spectrum (C_6D_6, 298 K) of **4**.

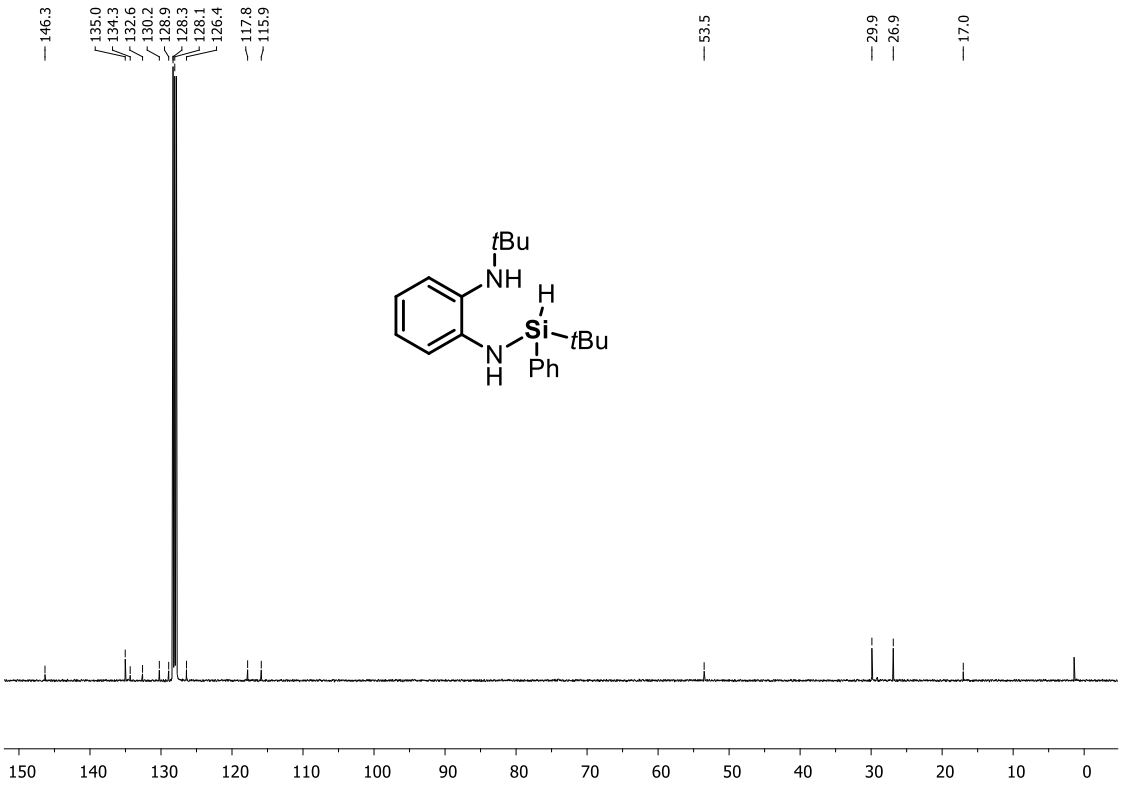

Figure 6.6. $^{13}C\{^1H\}$ NMR spectrum (C_6D_6, 298 K) of **4**.

6.2.2.3 Synthesis of compound 5

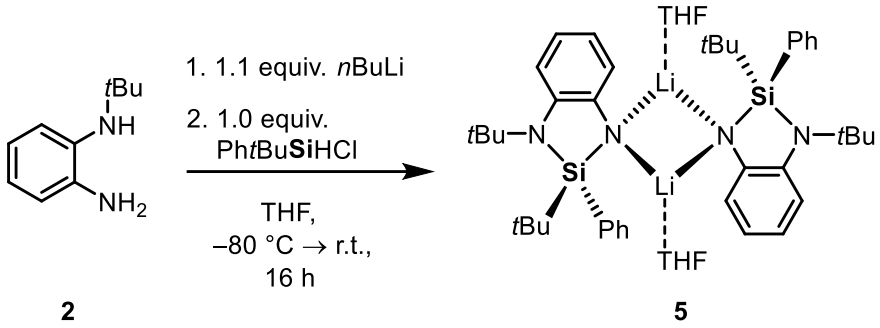

2 **5**

Compound **2** (164 mg, 1.0 mmol, 1.0 equiv.) was dissolved in 10 mL of THF and cooled down to −80 °C. *n*BuLi (0.44 mL, 1.1 mmol, 1.1 equiv. of a 2.5 mol/L solution in hexanes) was added dropwise via syringe and the formed yellow solution was stirred for 10 min. Then, *tert*-butyl-chlorophenylsilane (198 mg, 1.0 mmol, 1.0 equiv.) was added and the mixture was stirred for 16 h while warming to room temperature. The yellow solution was dried *in vacuo* and taken up in 10 mL of hexane. The formed solids were filtered off by cannula filtration and the green solution was left to crystallize at 8 °C. Compound **5** was obtained as clear colorless crystals suitable for single-crystal X-ray crystallographic analysis.

^{1}H NMR (300 MHz, C_6D_6, 298 K): δ[ppm] = 1.08 [s, 9H, SiC(CH_3)$_3$], 1.33 [s, 9H, NC(CH_3)$_3$], 6.53–6.58 [m, 1H, H_{Ph}], 6.82–6.88 [m, 2H, H_{Ph}], 6.94–7.01 [m, 1H, H_{Ph}], 7.09–7.15 [m, 3H, H_{Ph}], 7.66–7.72 [m, 2H, H_{Ph}].

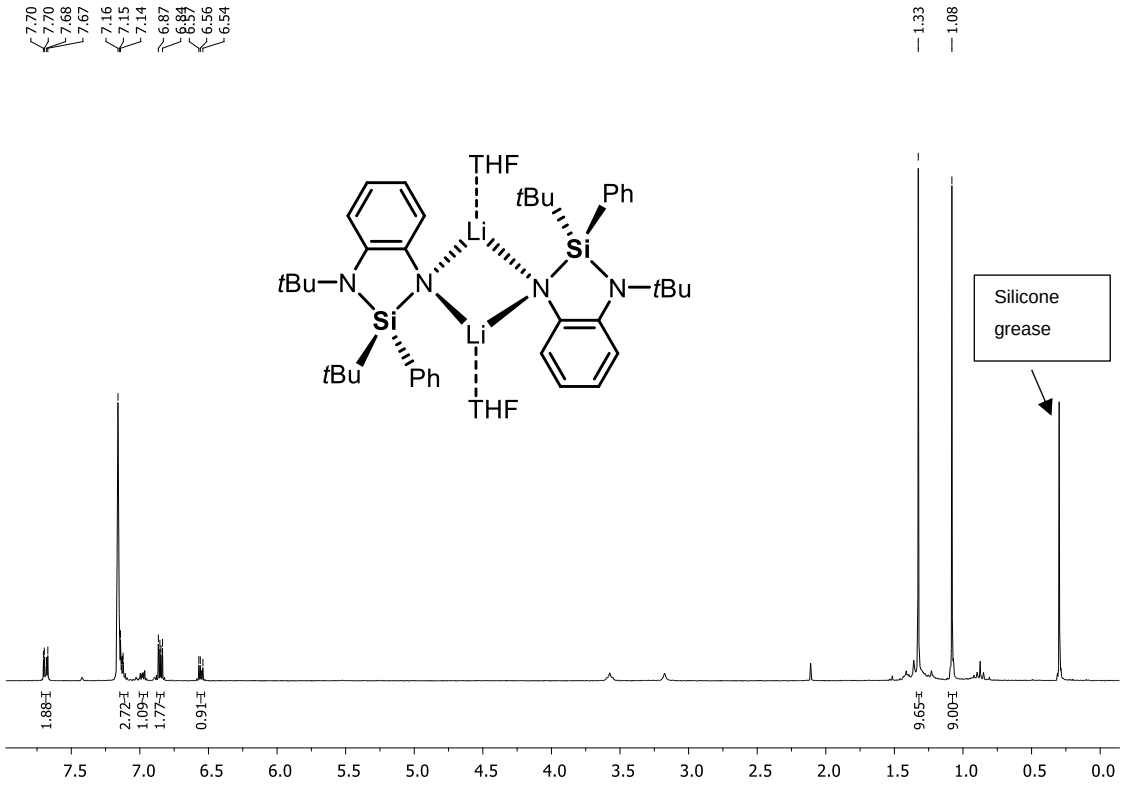

Figure 6.7. ^{1}H NMR spectrum (C_6D_6, 298 K) of **5**.

6.2.2.4 Synthesis of compound 7

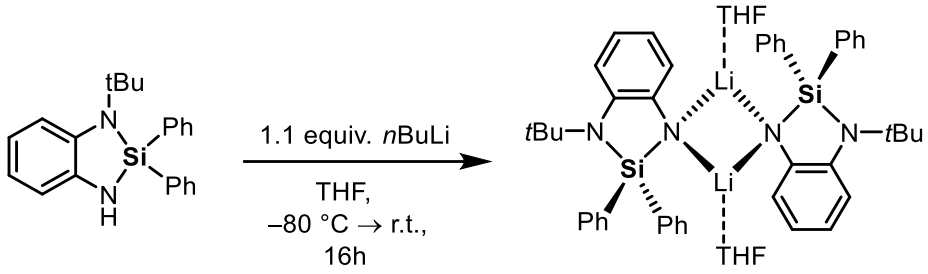

6 **7**

Compound **6** (345 mg, 1.0 mmol, 1.0 equiv.) was dissolved in 10 mL of THF and cooled down to −80 °C. *n*BuLi (0.69 mL, 1.1 mmol, 1.1 equiv.) was added dropwise via syringe. The yellow solution was stirred for 16 h and then layered with 10 mL of pentane. After three days, some colorless crystals formed which were isolated by cannula filtration and washed with pentane to obtain compound **7** as crystalline solid suitable for single-crystal X-ray crystallographic analysis (30 mg, 0.04 mmol, 4%).

^{1}H NMR (400 MHz, C_6D_6, 298 K): *δ*[ppm] = 1.02 [m, 8H, $CH_2CH_2CH_2CH_2O$], 1.48 [s, 18H, $C(CH_3)_3$], 2.82 [m, 8H, $CH_2CH_2CH_2CH_2O$], 6.04 [br, 1H, H_{Ph}], 6.41 [br, 1H, H_{Ph}], 6.68 [br, 2H, H_{Ph}], 6.95–7.01 [m, 2H, H_{Ph}], 7.18–7.32 [m, 10H, H_{Ph}], 7.38–7.80 [br, 2, H_{Ph}], 7.95 [br, 6H, H_{Ph}]. **^{7}Li{^{1}H} NMR** (156 MHz, C_6D_6, 298 K): *δ*[ppm] = 1.23 [s].

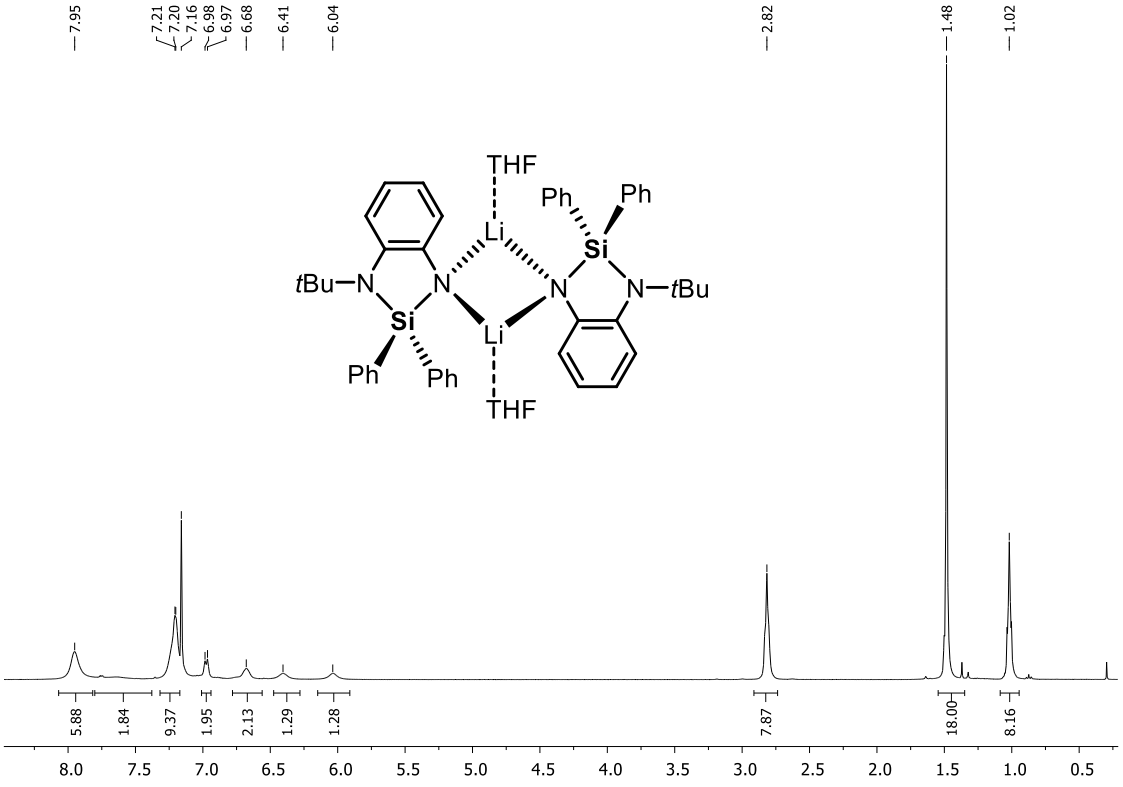

Figure 6.8. ^{1}H NMR spectrum (C_6D_6, 298 K) of **7**.

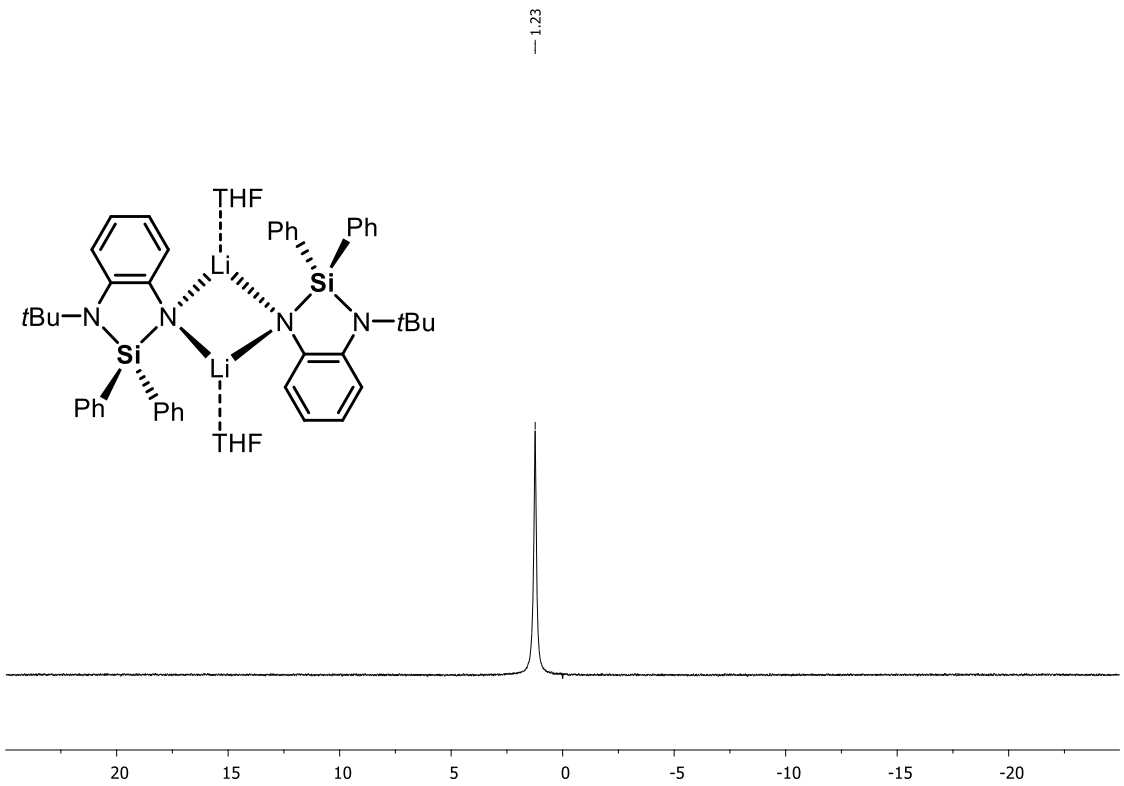

Figure 6.9. ^{7}Li{^{1}H} NMR spectrum (C_6D_6, 298 K) of **7**.

6.2.2.5 Synthesis of compound 9

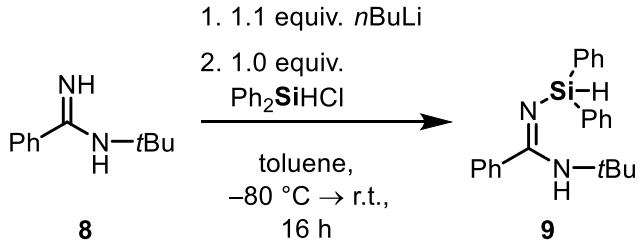

8 **9**

Compound **8** (176 mg, 1.0 mmol, 1.0 equiv.) was dissolved in 10 mL of toluene and cooled down to 0 °C. *n*BuLi (0.44 mL, 1.1 mmol, 1.1 equiv. of a 2.5 mol/L solution in hexane) was added dropwise via syringe. After stirring the solution for 30 min, chlorodiphenylsilane was added at 0 °C and the mixture was stirred for 3 d while slowly warming up to room temperature. All volatiles were removed *in vacuo* and the product was taken up in 20 mL of DCM. The solids were removed by cannula filtration and the filtrate was dried *in vacuo* to obtain a beige precipitate which was recrystallized in 20 mL of pentane. Storing the solution at −20 °C afforded compound **9** as colorless crystalline solid suitable for single-crystal X-ray crystallographic analysis (83 mg, 0.23 mmol, 23%).

^{1}H NMR (400 MHz, C_6D_6, 298 K): δ[ppm] = 1.32 [s, 9H, C(C*H*$_3$)$_3$], 4.25 [s, 1H, N*H*], 5.67 [s, 1H, Si*H*], 6.89–6.96 [m, 3H, *H*$_{Ph}$], 7.07–7.15 [m, 7H, *H*$_{Ph}$], 7.17–7.19 [m, 1H, *H*$_{Ph}$], 7.77–7.82 [m, 4H, *H*$_{Ph}$]. **^{13}C{^{1}H} NMR** (101 MHz, C_6D_6, 298 K): δ[ppm] = 28.8 [s, C(*C*H$_3$)$_3$], 51.9 [s, *C*(CH$_3$)$_3$], 127.0 [s, *C*H$_{Ph}$], 128.1 [s, *C*H$_{Ph}$], 128.5 [s, *C*H$_{Ph}$], 129.1 [s, *C*H$_{Ph}$], 129.4 [s, *C*H$_{Ph}$], 135.1 [s, *C*H$_{Ph}$], 138.8

[s, C_{Ph}], 140.1 [s, C_{Ph}], 162.6 [s, C_{Ph}]. **^{29}Si{^{1}H} NMR** (79 MHz, C_6D_6, 298 K): δ[ppm] = −28.3 [s]. **^{29}Si NMR** (79 MHz, C_6D_6, 298 K): δ[ppm] = −28.3 [dm, $^{1}J_{Si-H}$ = 200 Hz, *Si*H].

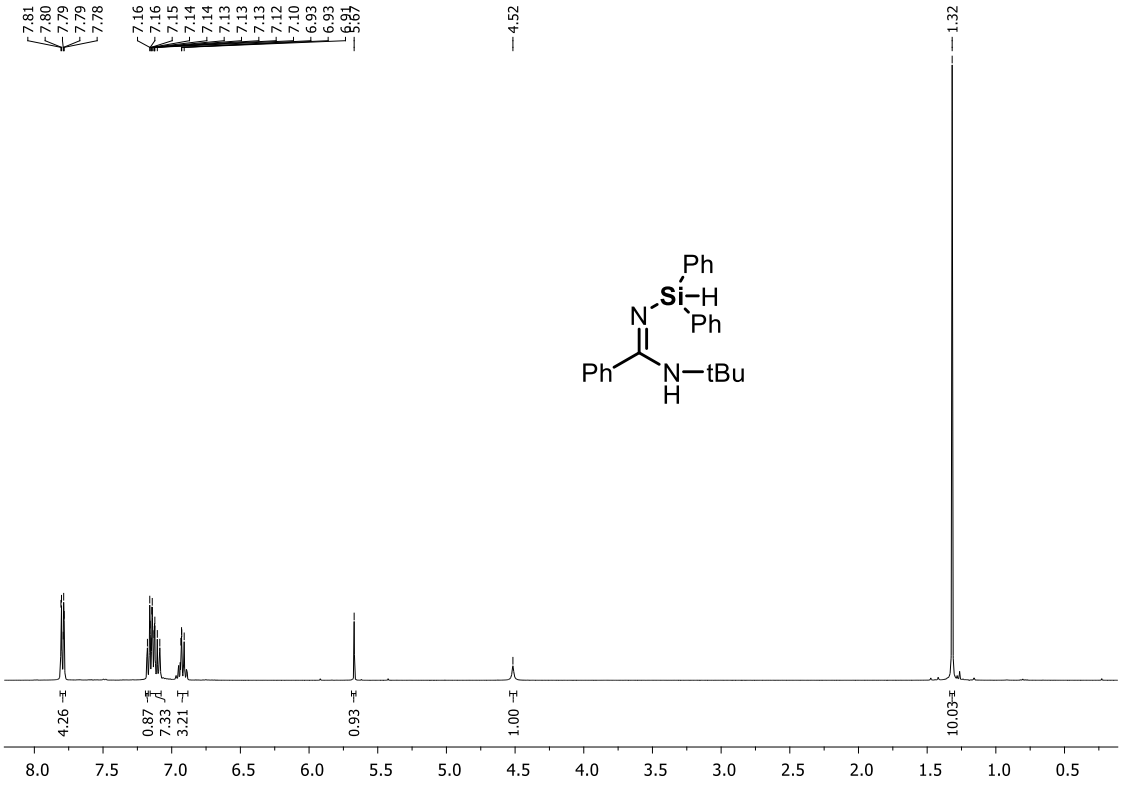

Figure 6.10. ^{1}H NMR spectrum (C_6D_6, 298 K) of **9.**

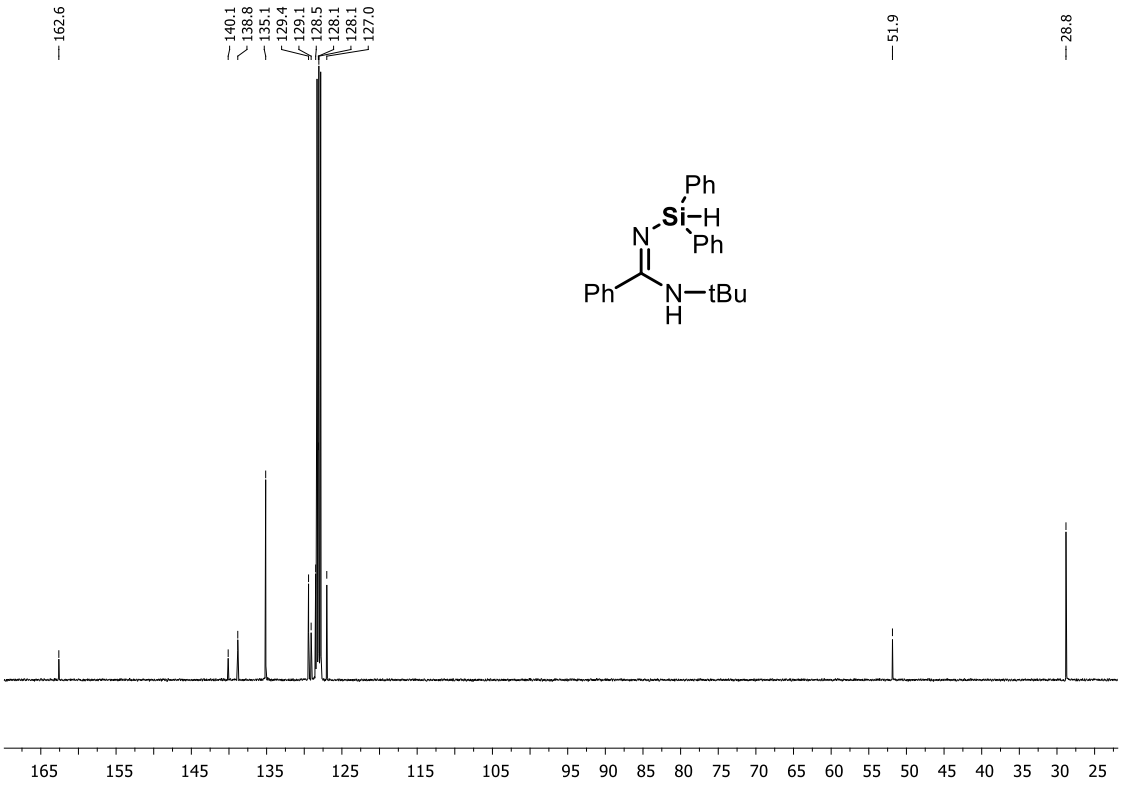

Figure 6.11. ^{13}C{^{1}H} NMR spectrum (C_6D_6, 298 K) of **9.**

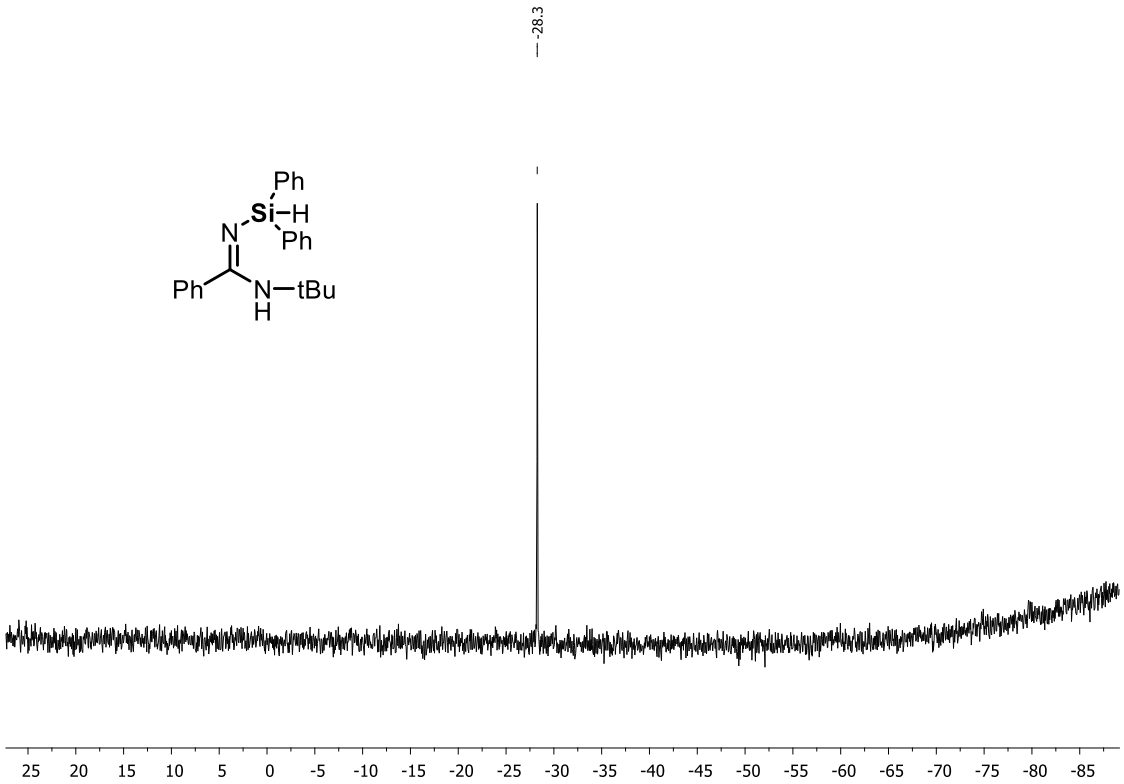

Figure 6.12. $^{29}Si\{^{1}H\}$ NMR spectrum (C_6D_6, 298 K) of **9.**

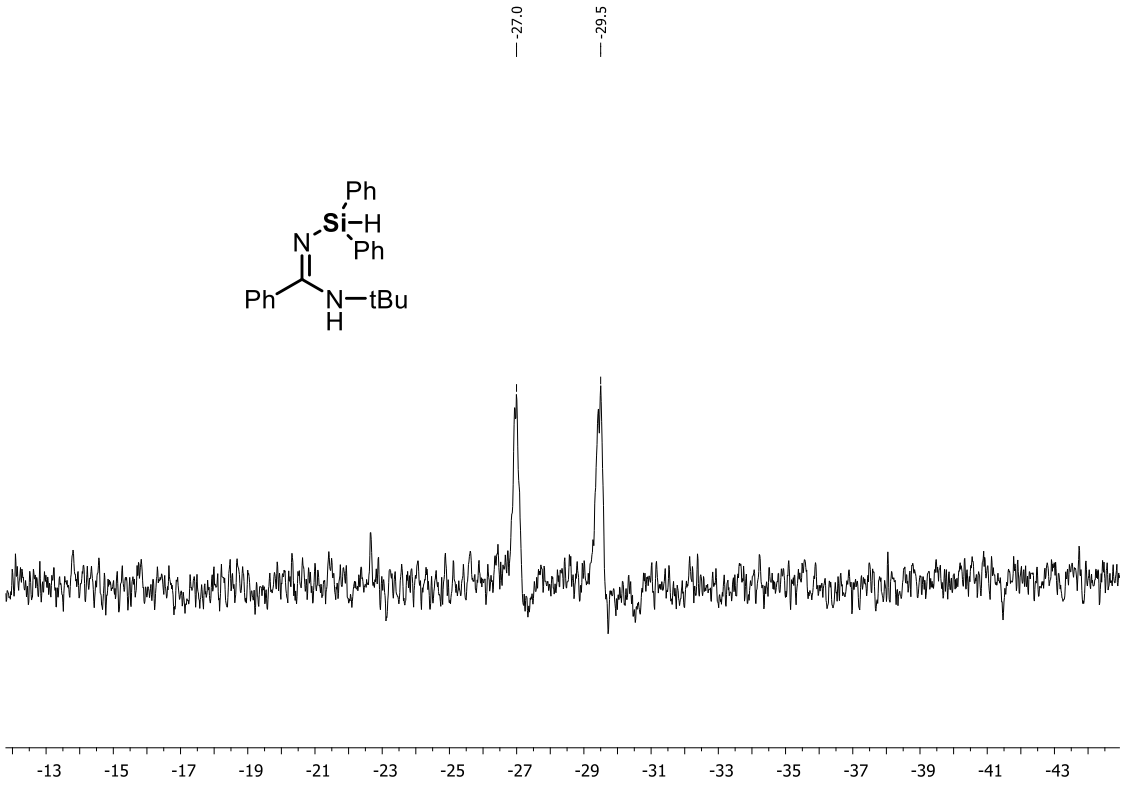

Figure 6.13. ^{29}Si NMR spectrum (C_6D_6, 298 K) of **9.**

6.3 Syntheses of diaminosiloxane-based germylenes

6.3.1 Results and discussion

Silylium ions are promising reactive compounds with extraordinary high Lewis acidity. They have found application in countless transformations including Diels-Alder reactions, C–H arylations or silylation reactions to name a few.[5] Our target was the synthesis of silylium ions incorporated into a siloxane framework which are, to the best of our knowledge, not presented in the literature thus far. The closest to that has been achieved in our group by N. Fontana *et al.* who synthesized a cyclic siloxane-based phosphonium borate ion pair which expresses silylium type reactivity.[3] The herein presented attempt was to create stable silylium ions via intramolecular stabilization by germylene units that is not too strong to quench the silylium ion reactivity. N-heterocyclic Ge(II) compounds have been shown to be promising candidates for such approaches due to their moderate electron donating properties.[6] *En route* to this goal, we synthesized siloxane compounds with diamino substituents bearing two N–H functions which could be transformed into stable Ge(II) containing molecules with a Si–O–Si backbone. Another requirement for the molecular design is a Si–H function for the possibility of hydride abstraction and formation of silylium ions. Following these necessities, we synthesized compound **10** and tried to install a Ge(II) unit. Since lithiation and subsequent reaction with $GeCl_2$ leads to the cleavage of the siloxane bond as demonstrated in chapter 3, the choice for the germanium source fell on $Ge(HMDS)_2$. This reagent is able to deprotonate both N–H functions and bind the Ge atom in a single step. Decomposition of the siloxane fragment is therefore prevented. Using this procedure, we were able to identify the siloxane-based germylene compound **11** based on ^{1}H NMR spectroscopy. Nonetheless, excess $Ge(HMDS)_2$ and byproduct hexamethyldisilazane could not be fully separated from the product, as compound **11** could never be obtained in crystalline or solid form. In an attempt to crystallize the Ge(II) compound, we added an *in situ* produced solution of $W(CO)_5$•THF in THF to form a tungsten complex with the germylene compound as ligand. Crystals suitable for single-crystal X-ray crystallographic analysis were obtained after layering the THF solution with pentane and revealed compound **12** as reaction product. Apparently, the Si–N bond was broken during the reaction resulting in the coordination of the diamine-substituted germylene-tungsten complex without the siloxane backbone. The molecule is forming a dimer which is additionally stabilizing the Ge(II) atom by coordination of another nitrogen atom (Scheme 6.14).

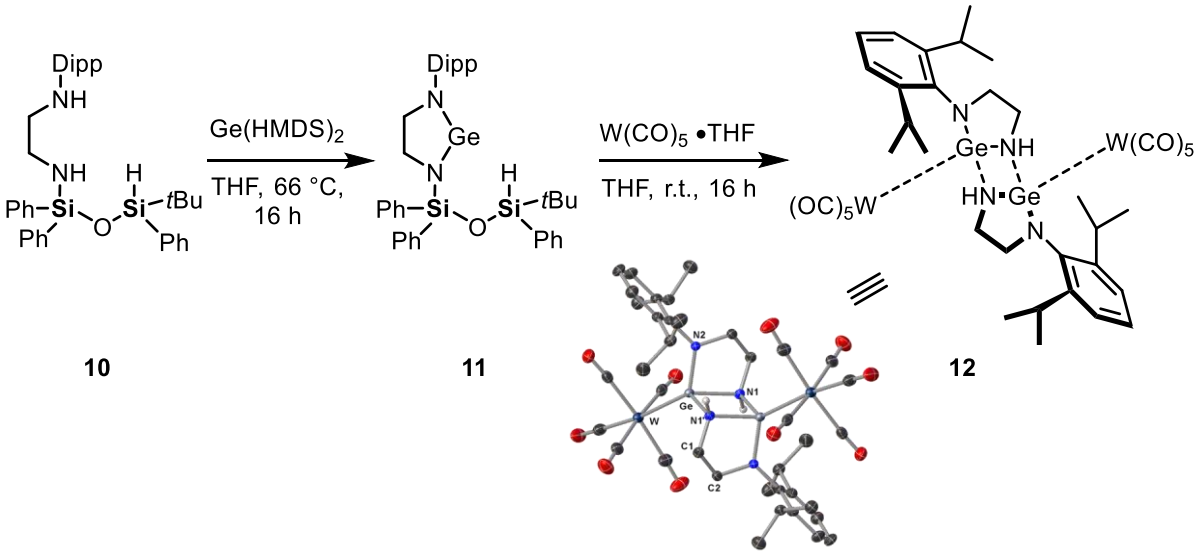

Scheme 6.14. Synthesis of germylene **11** and reaction with $W(CO)_5$•THF to obtain the dimeric complex **12**.

The observed removal of the siloxane moiety and the additional stabilization of the germylene through dimer formation led us to the conclusion that better stabilized germylene compounds need to be prepared which ideally can be crystallized and isolated. We therefore proceeded with aminosiloxanes **13** and **15** having aromatic instead of aliphatic diamine substituents which are additionally stabilizing the Ge(II) unit and improving the crystallization behavior. Both compounds were treated with $Ge(HMDS)_2$ and resulted in the isolation of compounds **14** and **16** (Scheme 6.15, top and bottom left). Compound **14** could be isolated as a brown amorphous solid and characterized by ^{1}H NMR spectroscopy, ^{13}C NMR spectroscopy and mass spectrometry. Attempts to obtain crystals suitable for singe-crystal X-ray crystallographic analysis were not successful so far. The crystals of compound **16** were the result of an oxidation reaction of the desired germylene compound with O_2 which accidently came into the reaction flask. A crystallization attempt after addition of $W(CO)_5$•THF was successfully carried out and revealed the desired germylene complex in the form of adduct **17** as reaction product (Scheme 6.15, bottom right). Unfortunately, the obtained single crystals were not pure enough for further analysis of the compound. Nonetheless, the molecular crystal structure unequivocally demonstrates the possibility to synthesize such germylene compounds with siloxane backbones and to use them as ligands in transition metal chemistry. The next step in this project would be the introduction of a Si–H group similar to compound **11** and to perform hydride abstraction reactions for the preparation of silylium ions. Attempts in that direction were already carried out with compound **11**, but were not successful.

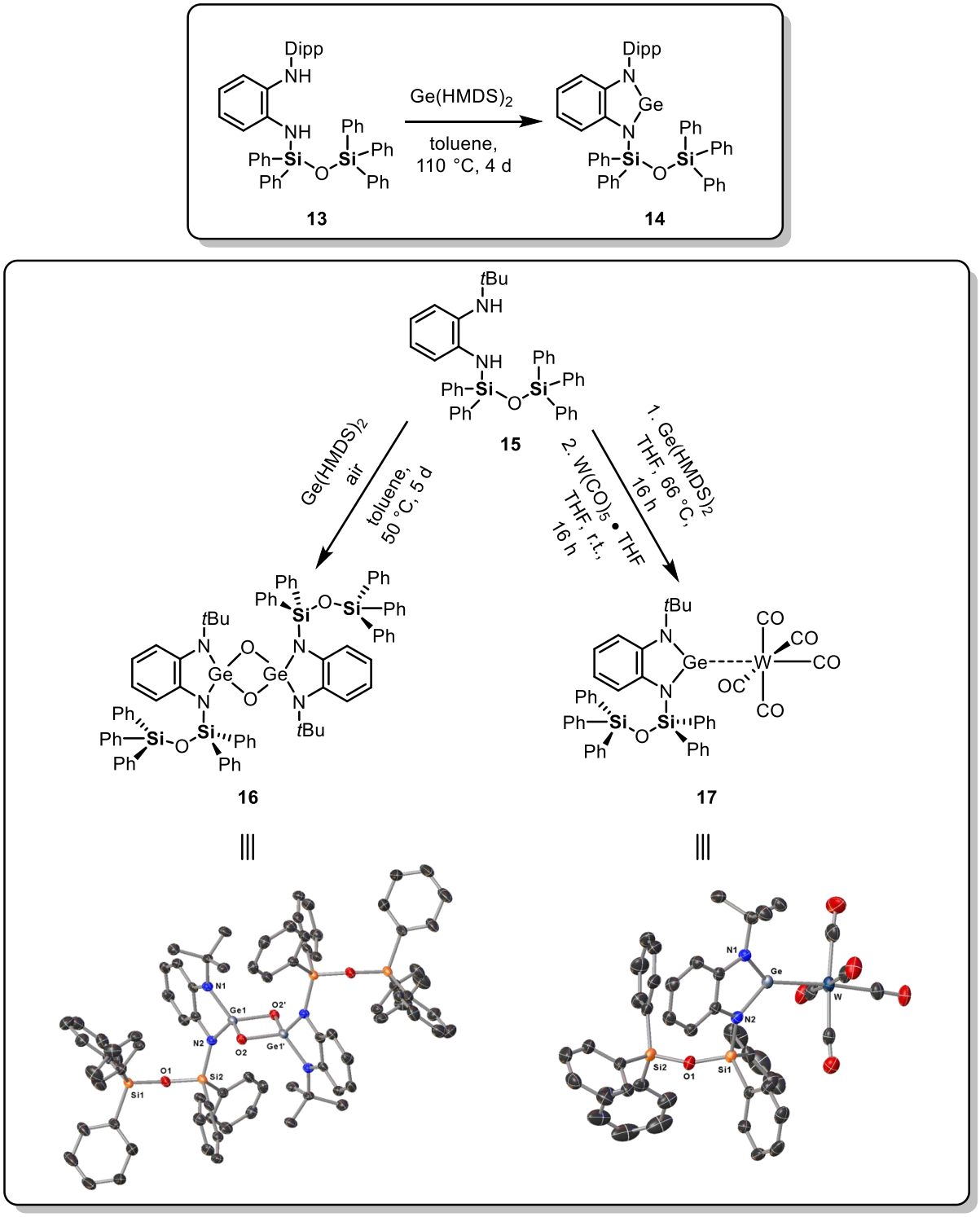

Scheme 6.15. Synthesis of compound **14** (top) and isolations of crystalline compounds **16** (bottom left) and **17** (bottom right).

6.3.2 Syntheses and characterizations

6.3.2.1 Synthesis of compound 10

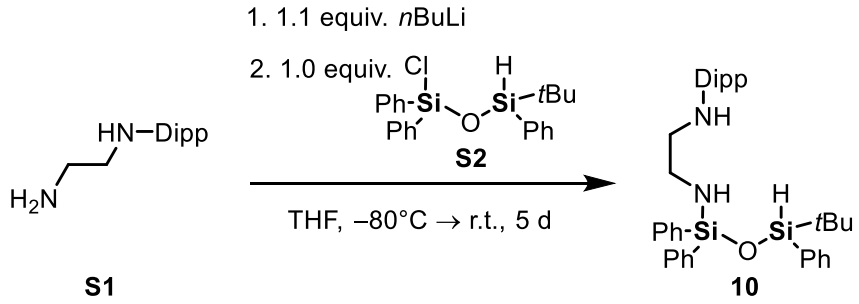

Compound **S1** (375 mg, 1.7 mmol. 1.0 equiv.) was dissolved in 10 mL of THF and cooled down to −80 °C. *n*BuLi (0.76 mL, 1.9 mmol, 1.1 equiv. of a 2.5 mol/L solution in hexane) was added dropwise via syringe and the solution was stirred for 1 h while warming up to room temperature. Then, the mixture was cooled down to −80 °C again and a solution of chlorosiloxane **S2**[3] (670 mg, 1.7 mmol, 1.0 equiv.) in 5 mL of THF was added to the mixture in one portion. The mixture was stirred for 5 d while slowly warming to room temperature. All volatiles were removed *in vacuo* and the crude product was taken up in 10 mL of pentane. The solids were filtered off via cannula filtration and the filtrate was dried *in vacuo* to obtain compound **10** as a colorless wax (990 mg, 1.7 mmol, >99%).

^{1}H NMR (400 MHz, C_6D_6, 298 K): *δ*[ppm] = 1.08 [s, 9H, C(C*H*$_3$)$_3$], 1.22 [d, $^{3}J_{H\text{-}H}$ = 6.8 Hz, 12H, CH(C*H*$_3$)$_2$], 1.72 [t, $^{3}J_{H\text{-}H}$ = 7.7 Hz, 1H, SiNH(CH$_2$)(CH$_2$)N*H*], 2.76–2.81 [m, 2H, SiNH(CH$_2$)(C*H*$_2$)NH], 2.91 [t, $^{3}J_{H\text{-}H}$ = 7.7 Hz, 1H, SiN*H*(CH$_2$)(CH$_2$)NH], 2.93–3.00 [m, 2H, SiNH(C*H*$_2$)(CH$_2$)NH], 3.35 [sept, $^{3}J_{H\text{-}H}$ = 6.8 Hz, C*H*(CH$_3$)$_2$], 5.30 [s, 1H, Si*H*], 7.10–7.12 [m, 4H, *H*$_{Ph}$], 7.17–7.24 [m, 8H, *H*$_{Ph}$], 7.69–7.72 [m, 2H, *H*$_{Ph}$], 8.84–7.88 [m, 4H, *H*$_{Ph}$]. **^{29}Si{^{1}H} NMR** (79 MHz, C_6D_6, 298 K): *δ*[ppm] = −30.6 [s, *Si*N], −5.9 [s, *Si*H]. **^{29}Si NMR** (79 MHz, C_6D_6, 298 K): *δ*[ppm] = −30.6 [s, *Si*N], −5.9 [dm, $^{1}J_{Si\text{-}H}$ = 205.3 MHz, *Si*H]. **CHN Analysis** $C_{36}H_{48}N_2O_2Si$ calculated: C 74.43, H 8.33, N 4.82, O 2.75, Si 9.67; found: C 73.43, H 7.78, N 4.11. **HR-MS (ESI+)**, calculated m/z for $C_{36}H_{48}N_2O_2Si$ [M+H$^+$]: 581.3378; found: 581.3382.

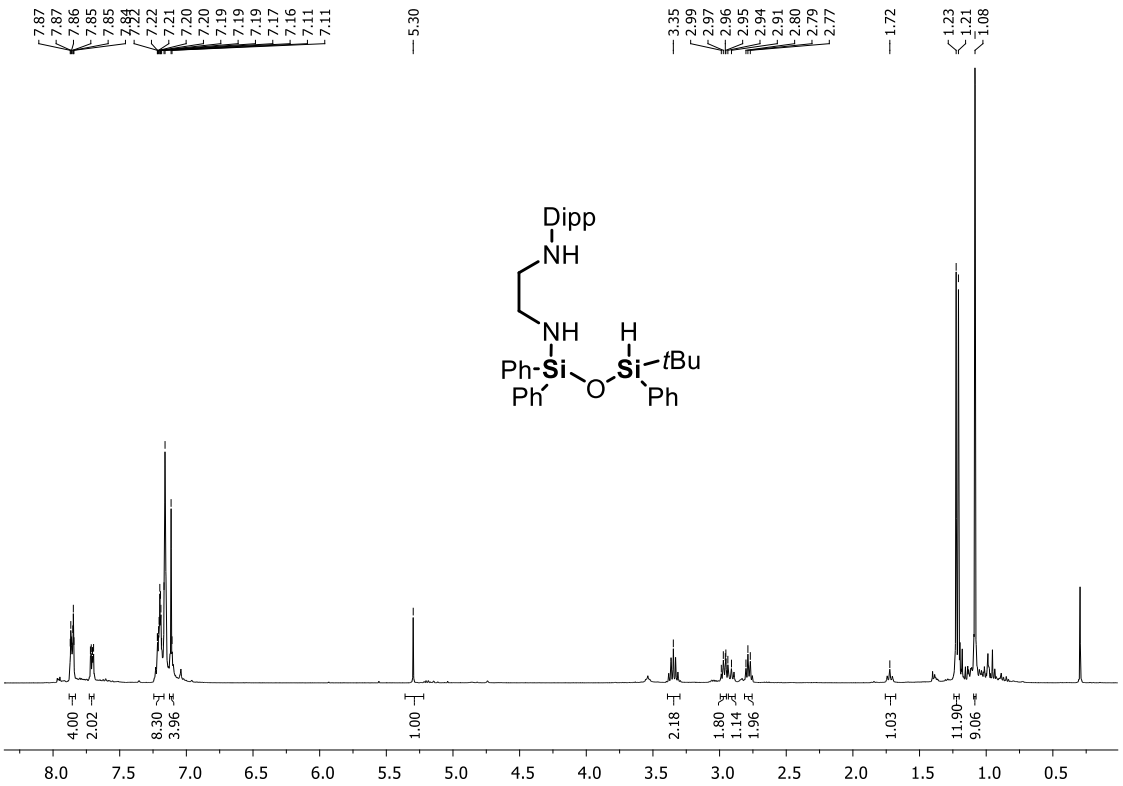

Figure 6.16. ^{1}H NMR spectrum (C_6D_6, 298 K) of **10.**

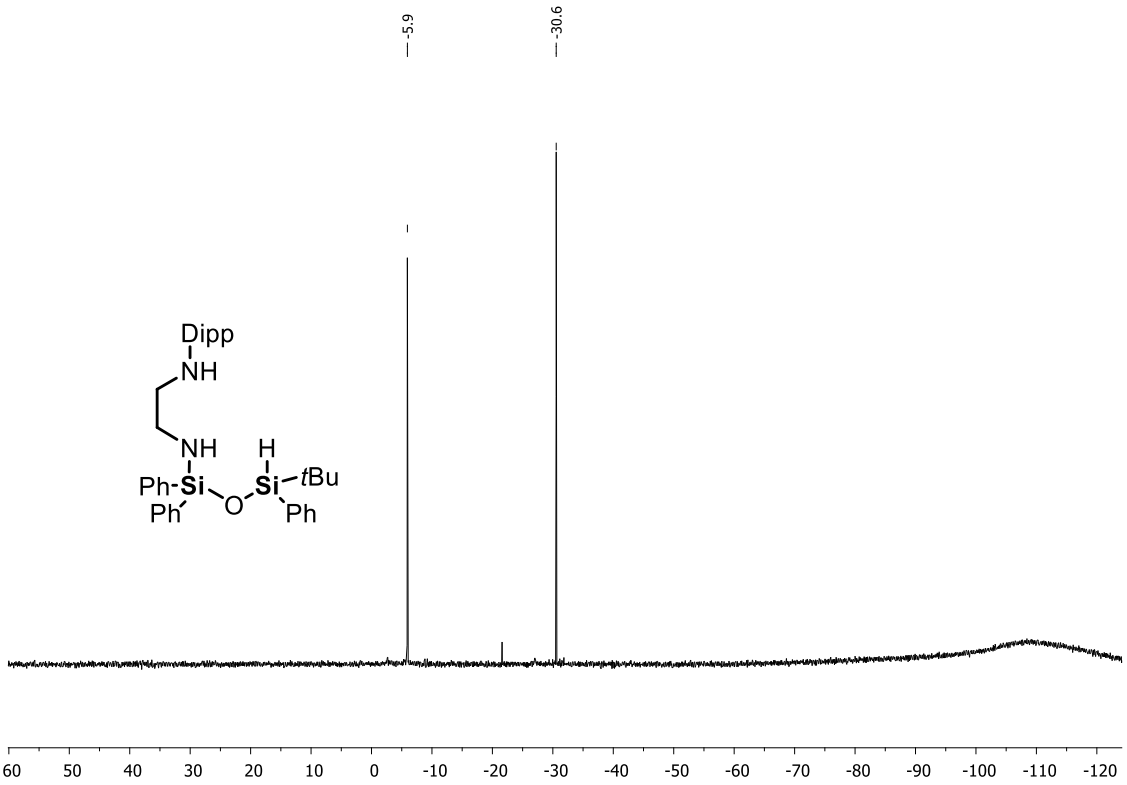

Figure 6.17. $^{29}Si\{^{1}H\}$ NMR spectrum (C_6D_6, 298 K) of **10.**

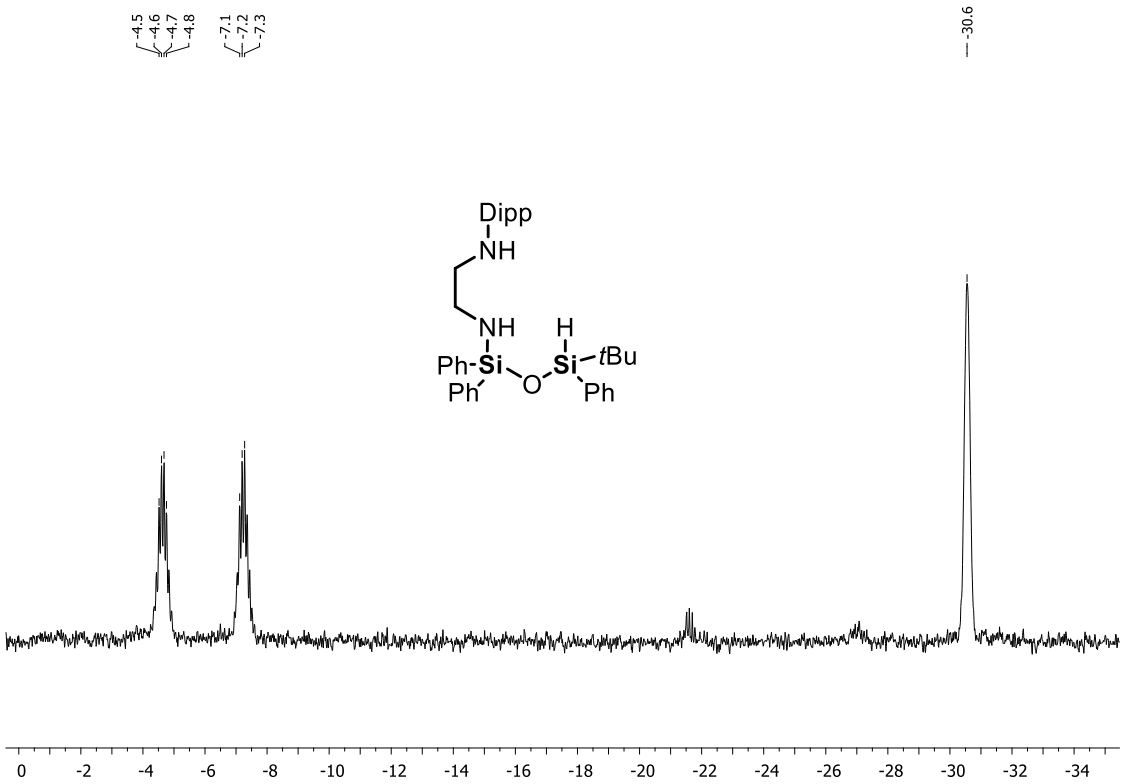

Figure 6.18. ^{29}Si NMR spectrum (C_6D_6, 298 K) of **10.**

6.3.2.2 Targeted synthesis of compound 11

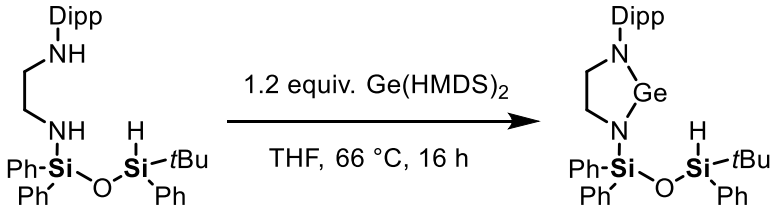

10 **11**

Compound **10** (2.08 g, 4.4 mmol, 1.0 equiv.) and Ge(HMDS)$_2$[4] (2.06 g, 5.2 mmol, 1.2 equiv.) were dissolved in 40 mL of THF and heated to reflux at 66 °C for 16 h. All volatiles were removed *in vacuo* to obtain a brown wax which is proposed to be compound **11** according to the ^{1}H NMR spectrum (Figure 6.16). The spectrum essentially shows one species with similar signal patterns to **10** but both NH signals are gone suggesting the binding of the Ge atom to that moiety. Unreacted Ge(HMDS)$_2$ and byproduct hexamethyldisilazane can be identified in the NMR spectrum as well. Further purification of the compound was not possible.

^{1}H NMR (400 MHz, C_6D_6, 298 K): δ[ppm] = 1.12 [s, 9H, C(C*H*$_3$)$_3$], 1.16–1.26 [m, 12H, CH(C*H*$_3$)$_2$], 3.39–3.45 [m, 4H, SiN(C*H*)$_2$(CH$_2$)N + C*H*(CH$_3$)$_2$], 3.67 [t, $^3J_{H\text{-}H}$ = 7.4 Hz, 2H, SiN(CH)$_2$(C*H*$_2$)N], 5.34 [s, 1H, Si*H*], 7.17–7.22 [m, 10H, *H*$_{Ph}$], 7.72–7.75 [m, 3H, *H*$_{Ph}$], 7.89–7.95 [m, 5H, *H*$_{Ph}$].

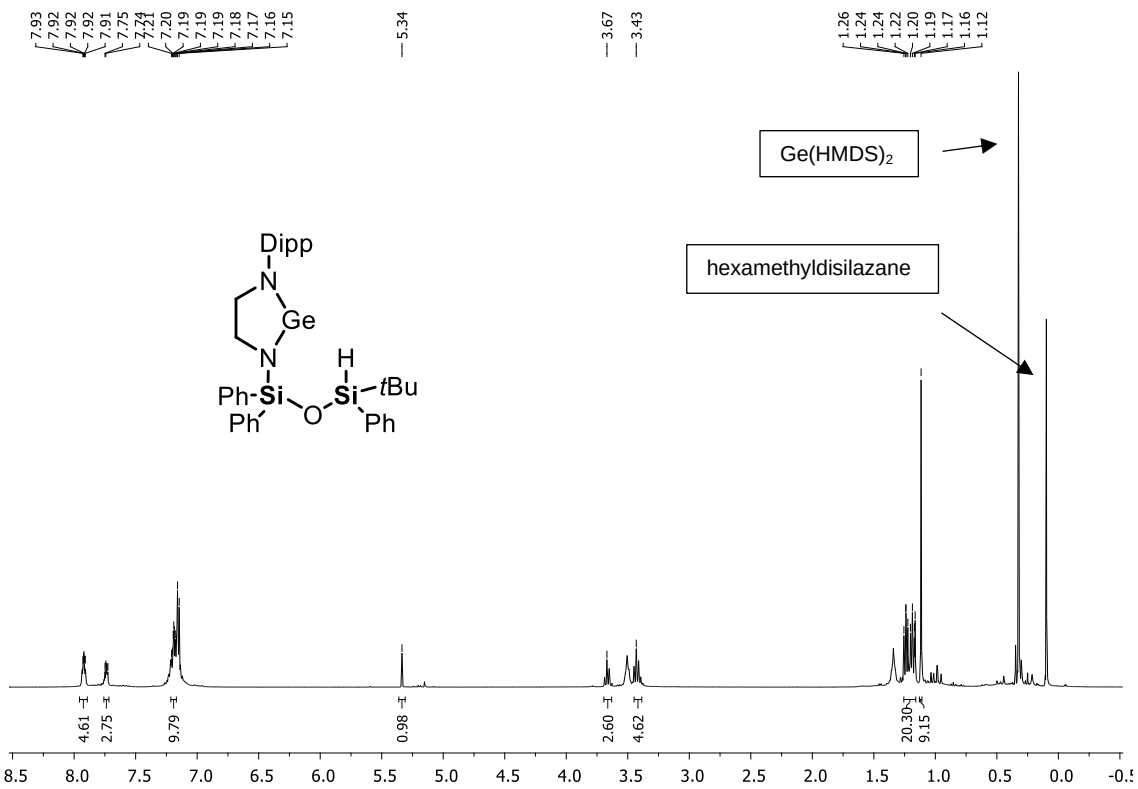

Figure 6.19. Suggested ^{1}H NMR spectrum (C_6D_6, 298 K) of **11.**

6.3.2.3 Synthesis of compound 12

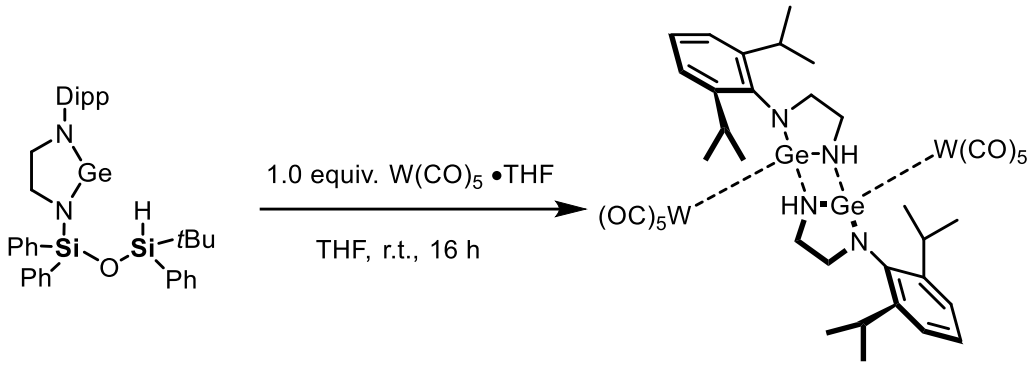

11 **12**

A reaction vessel featuring a cooler and a UV lamp (254 nm) was loaded with $W(CO)_6$ (352 mg, 1.0 mmol, 1.0 equiv.) in THF (10 mL). The solution was irradiated for 4 h during which the color turned intensely yellow. The solution was then transferred to a solution of compound **11** (652 mg, 1.0 mmol, 1.0 equiv.) in 12 mL of THF and the yellow solution was stirred at room temperature for 16 h. The solution was then layered with 10 mL of pentane and stored at 8 °C. Some crystals were obtained after 7 d which were analyzed by X-ray crystallographic analysis and revealed compound **12**.

6.3.2.4 Synthesis of compound 14

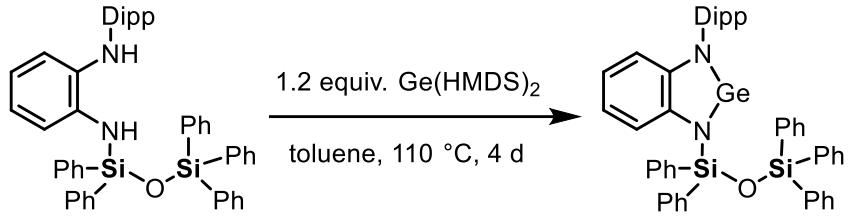

13 **14**

Compound **13** (725 mg, 1.0 mmol, 1.0 equiv.) and $Ge(HMDS)_2$ (472 mg, 1.2 mmol, 1.2 equiv.) were dissolved in 10 mL of toluene and heated to reflux at 110 °C for 4 d. All volatiles were removed *in vacuo* and the remaining brown residue was dissolved in 10 mL of pentane. Storing the solution at 8 °C for 2 d resulted in the precipitation of a brown solid which was isolated by cannula filtration to obtain compound **14** as an amorphous solid (155 mg, 0.19 mmol, 19%).

^{1}H NMR (400 MHz, C_6D_6, 298 K): δ[ppm] = 1.11 [d, $^3J_{H\text{-}H}$ = 6.8 Hz, 6H, $CH(CH_3)_2$], 1.17 [d, $^3J_{H\text{-}H}$ = 6.8 Hz, 6H, $CH(CH_3)_2$], 2.95 [sept, $^3J_{H\text{-}H}$ = 6.8 Hz, 6H, $CH(CH_3)_2$], 6.52–6.61 [m, 2H, H_{Ph}], 6.77–6,82 [m, 2H, H_{Ph}], 7.07–7.15 [m, 6H, H_{Ph}], 7.17–7.25 [m, 9H, H_{Ph}], 7.27–7.36 [m, 3H, H_{Ph}], 7.47–7.51 [m, 1H, H_{Ph}], 7.77–7.82 [m, 6H, H_{Ph}], 7.88–7.92 [m, 4H, H_{Ph}]. **^{13}C{^{1}H} NMR** (101 MHz, C_6D_6, 298 K): δ[ppm] = 24.1 [s, $CH(CH_3)_2$], 26.4 [s, $CH(CH_3)_2$], 28.5 [s, $CH(CH_3)_2$], 112.0 [s, CH_{Ph}], 117.9 [s, CH_{Ph}], 118.9 [s, CH_{Ph}], 120.8 [s, CH_{Ph}], 124.1 [s, CH_{Ph}], 127.9 [s, CH_{Ph}], 128.2 [s, CH_{Ph}], 128.5 [s, CH_{Ph}], 130.3 [s, CH_{Ph}], 130.9 [s, CH_{Ph}], 134.8 [s, C_{Ph}], 130.9 [s, C_{Ph}], 135.7 [s, CH_{Ph}], 135.8 [s, C_{Ph}], 135.8 [s, CH_{Ph}], 137.6 [s, C_{Ph}], 141.6 [s, C_{Ph}], 146.3 [s, C_{Ph}], 146.7 [s, C_{Ph}]. **MS (FD+)**, calculated m/z for $C_{48}H_{46}GeN_2OSi_2$ [$M+H^+$]: 796.2360; found: 796.2168.

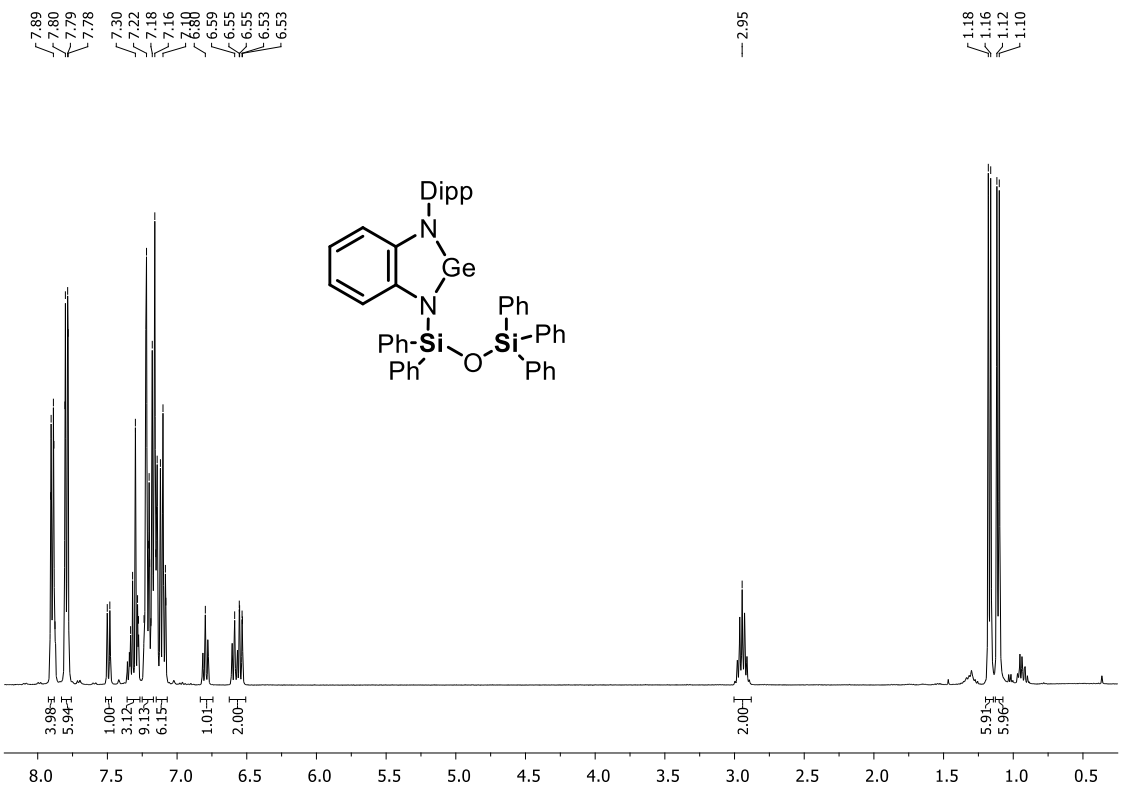

Figure 6.20. ^{1}H NMR spectrum (C_6D_6, 298 K) of **14.**

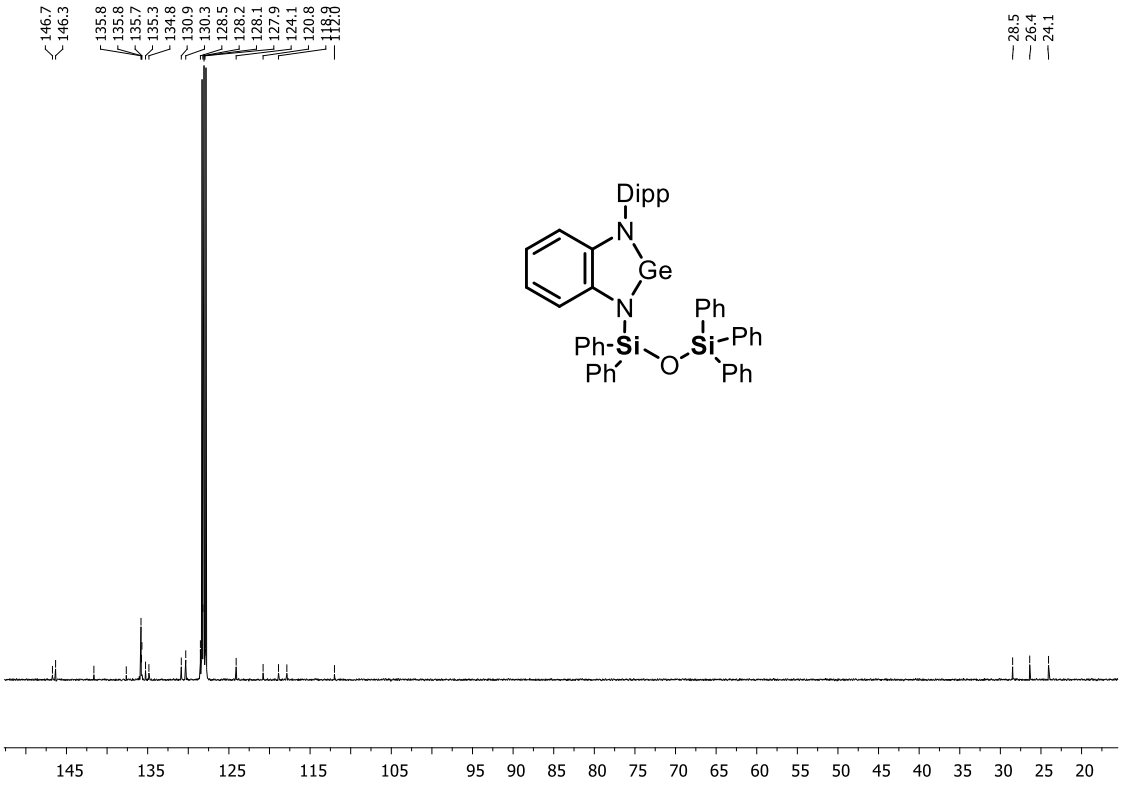

Figure 6.21. $^{13}C\{^{1}H\}$ NMR spectrum (C_6D_6, 298 K) of **14.**

6.3.2.5 Synthesis of compound 16

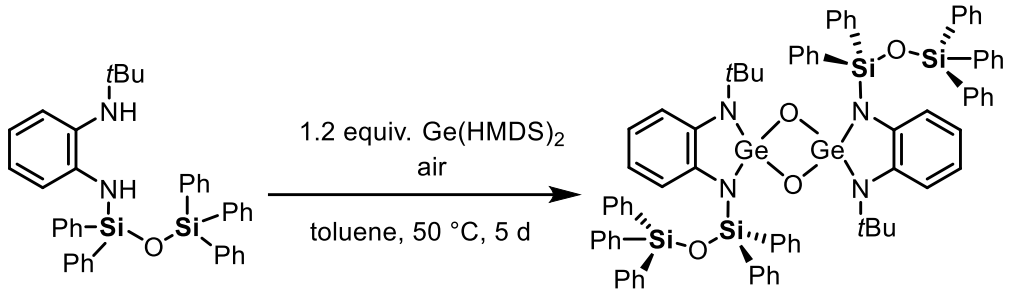

15 **16**

Compound **15** (621 mg, 1.0 mmol, 1.0 equiv.) and $Ge(HMDS)_2$ (472 mg, 1.2 mmol, 1.2 equiv.) were dissolved in 10 mL of toluene and heated to 50 °C for 5 d. All volatiles were removed *in vacuo* to obtain a beige sticky wax. The crude product was taken up in 10 mL of Et_2O and the solids were removed by cannula filtration. Storing the filtrate at room temperature for 5 d afforded some yellow crystals which were further analyzed by X-ray crystallographic analysis to reveal compound **16.** Apparently, O_2 from air accidently came into the reaction vessel at some point and resulted in the formation of an oxygen-bridged Ge(IV) dimer instead of the targeted Ge(II) compound. Further analysis of the compound was not successful.

6.3.2.6 Synthesis of compound 17

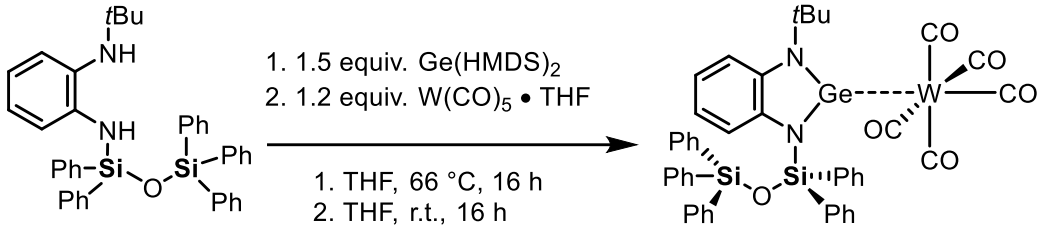

15 **17**

Compound **15** (621 mg, 1.0 mmol, 1.0 equiv.) and $Ge(HMDS)_2$ (590 mg, 1.5 mmol, 1.5 equiv.) were dissolved in 10 mL of THF and heated to reflux at 66 °C for 16 h. All volatiles were removed *in vacuo* resulting in a yellow solid which was dissolved in 10 mL of THF. In a separate vessel featuring a cooler and a UV lamp (254 nm), $W(CO)_6$ (422 mg, 1.2 mmol, 1.2 equiv.) was dissolved in THF (10 mL). The solution was irradiated for 4 h during which the color turned intensely yellow. The *in situ* formed $W(CO)_5$•THF solution was transferred to the mixture containing the germylene compound and the light orange solution was stirred for 16 h at room temperature. All volatiles were removed *in vacuo* and the remaining crude product was recrystalized from 25 mL of pentane. Storing the pentane solution at room temperature for 1 d resulted in the formation of yellow crystals. X-ray crystallographic analysis was performed to identify the desired tungsten complex **17** with the diaminosiloxane germylene ligand.

6.4 Byproducts in the syntheses of diaminosilane 18

6.4.1 Results and discussion

The synthesis and isolation of cyclic diaminohydrosilane **18** (Chapter 4) was carried out multiple times and was found to be rather difficult owing to the high reactivity of the product. Two general methods were applied: One attempt was based on the conversion of diamine **1** and dichlorophenylsilane with the addition of triethylamine as HCl scavenger, while the other attempt proceeds via twofold *in situ* lithiation of **1** and subsequent reaction with dichlorophenylsilane. Both procedures proved problematic as we often isolated byproducts instead of compound **18** (Scheme 6.22). Some of these compounds could be characterized by means of single-crystal X-ray crystallographic analysis.

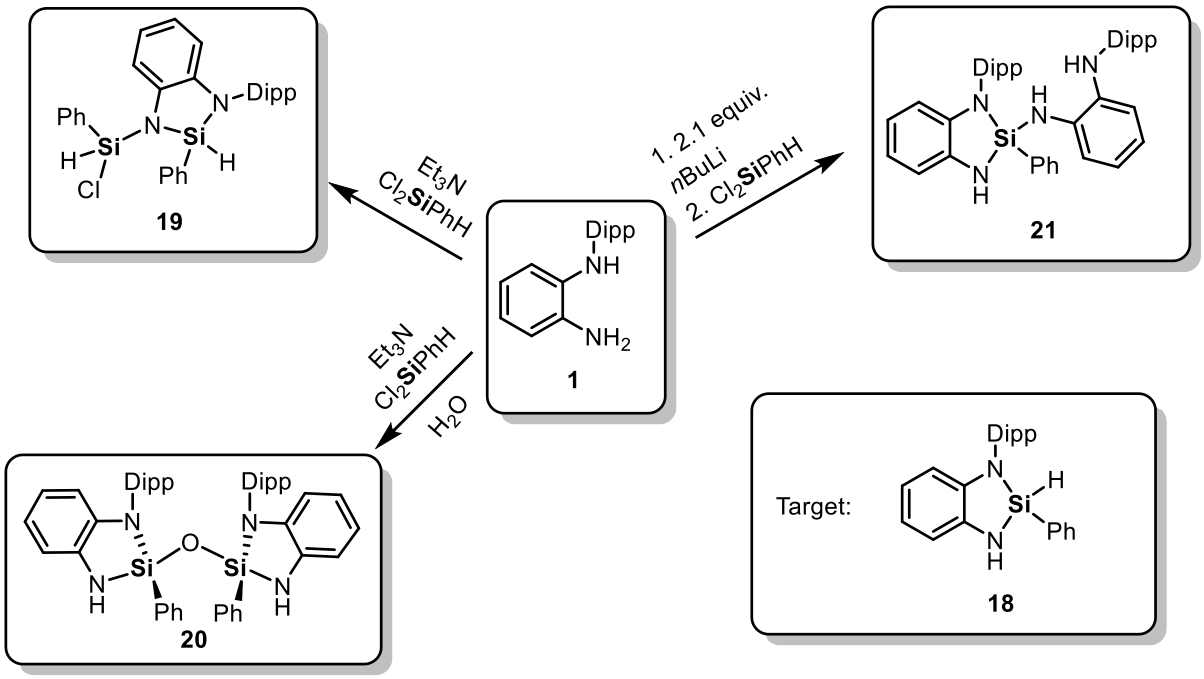

Scheme 6.22. Identified byproducts **19**, **20** and **21** in the targeted synthesis of **18**.

Compound **19** is formed after reaction of product **18** with another molecule of dichlorophenylsilane and shows a typical Si–N–Si silazane motif. This discovery emphasizes that the silane should not be used in excess. The fact that the reaction in which **19** was obtained was performed at room temperature additionally suggests the requirement of cooling to −80 °C in order to prevent the undesired reaction to occur. During the same reaction, also compound **20** could be crystallized out of the mixture which displays an unexpected siloxane Si–O–Si motif. This compound presumably formed due to wet solvents or reagents which led to the hydrolysis of compound **18** and subsequent condensation to the homosiloxane. Both byproducts **19** and **20** have two *Si*-chiral stereocenters and were obtained as a mixture of diastereomers which could not be separated so far. However, especially compound **20** can potentially be used as chelating

ligand with siloxane backbone with its two remaining N–H functions. In the synthesis attempt using *n*BuLi to create dilithiated diamide and react it with dichlorophenylsilane, compound **21** was often obtained. It is the product of the reaction of targeted silane **18** with the diamine **1** or its monolithiated analogue. The reason behind the formation of this compound arguably lies in the concentration of the reactants in the THF solution. In order to selectively obtain the desired silane **18**, it is advisable to use high dilutions in order to prevent such intermolecular side reactions.

6.4.2 Syntheses and characterizations

6.4.2.1 Isolation of crystalline compounds 19 and 20

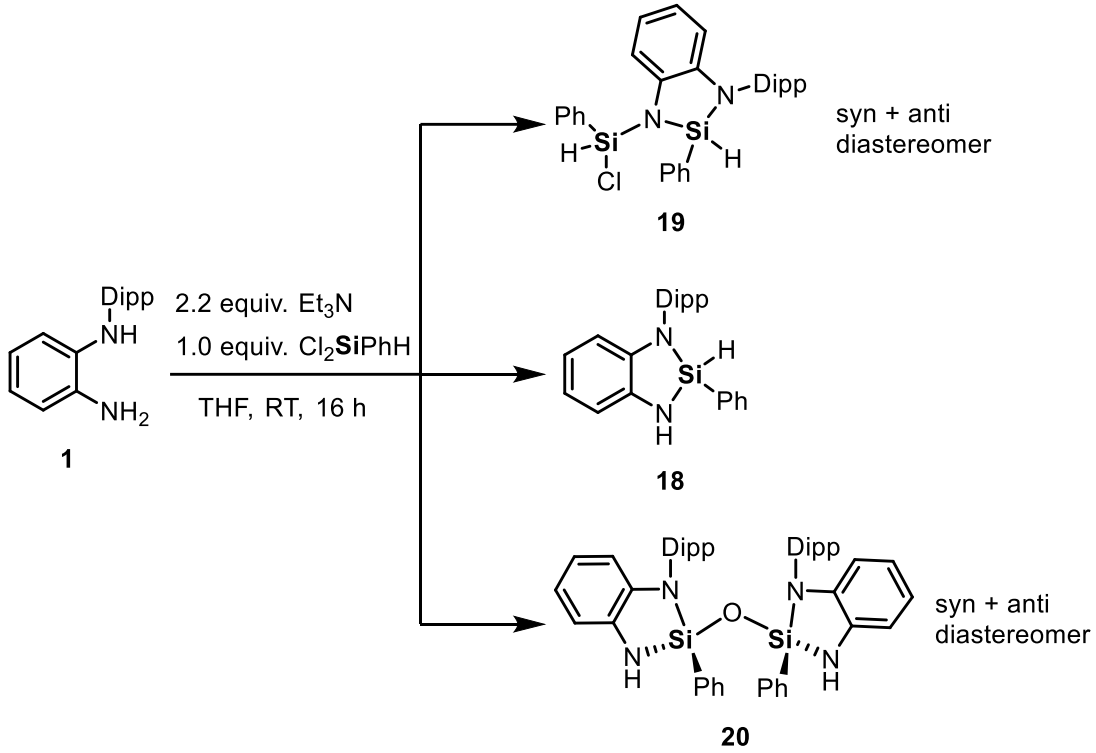

Compound **1** (8.05 g, 30.0 mmol, 1.0 equiv.), triethylamine (9.15 mL, 66.0 mmol, 2.2 equiv.) were dissolved in 200 mL of THF) and dichlorophenylsilane (4.85 mL, 33.0 mmol, 1.1 equiv.) was added dropwise via syringe. The mixture was stirred at room temperature resulting in a green suspension. All volatiles were removed *in vacuo* and the crude mixture was taken up in 250 mL of hexane. The solids were removed via cannula filtration and the green filtrate was dried *in vacuo*. The residue was recrystallized in 20 mL of toluene. Storing the solution at 8 °C resulted in the formation of crystalline compound **19** which was suitable for X-ray crystallographic analysis. ^{1}H NMR analysis of the crystals revealed both diastereomers of compound **19** which could not be separated so far. The Schlenk flask with the initially removed solids was treated with 20 mL of toluene and again filtered by cannula filtration. The filtrate was stored at 8 °C and crystals suitable for X-ray crystallographic analysis of compound **20** were obtained. Again, also for compound **20**, both diastereomers were obtained, which could not be separated so far.

6.4.2.2 Isolation of crystalline compound 21

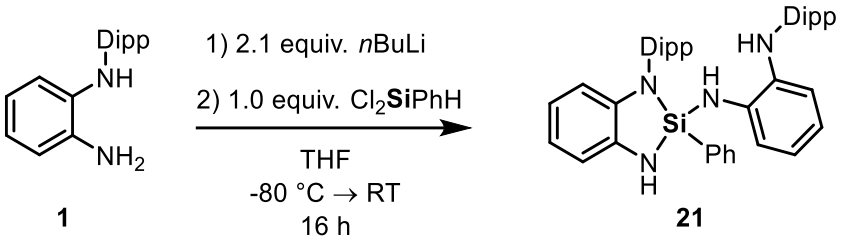

Compound **1** (2.68 g, 10.0 mmol, 1.0 equiv.) was dissolved in 100 mL of THF and cooled down to −80 °C. *n*BuLi (8.40 mL, 21.0 mmol, 2.1 equiv. of a 2.5 mol/L solution in hexane) was added via syringe and it was stirred for 1 h while warming to room temperature. The mixture was cooled to −80 °C again and dichlorophenylsilane (1.47 mL, 10.0 mmol, 1.0 equiv.) was added via syringe. The brown suspension was stirred for 16 h while slowly warming up to room temperature. All volatiles were removed *in vacuo* and the crude mixture was treated with 100 mL of pentane. The solids were removed via cannula filtration and the brown filtrate was stored at 8 °C upon which a white precipitate formed after one day. The precipitate was isolated by cannula filtration and washed with pentane. Recrystallization in 5 mL of hot toluene afforded compound **21** as a crystalline white solid suitable for single-crystal X-ray crystallographic analysis.

^{1}H NMR (400 MHz, C_6D_6, 298 K): δ[ppm] = 0.24 [d, $^3J_{H\text{-}H}$ = 6.8 Hz, 3H, CH(CH_3)$_2$], 0.88 [d, $^3J_{H\text{-}H}$ = 6.8 Hz, 3H, CH(CH_3)$_2$], 0.92–1.01 [m, 6H, CH(CH_3)$_2$], 1.08–1.18 [m, 12H, CH(CH_3)$_2$], 2.68 [sept, $^3J_{H\text{-}H}$ = 6.8 Hz, 1H, CH(CH$_3$)$_2$], 2.95–3.07 [m, 2H, CH(CH$_3$)$_2$], 3.64 [sept, $^3J_{H\text{-}H}$ = 6.8 Hz, 1H, CH(CH$_3$)$_2$], 3.72 [s, 1H, NH], 4.68 [s, 1H, NH], 4.90 [s, 1H, NH], 6.21–6.24 [m, 1H, H_{Ph}], 6.43–6.47 [m, 1H, H_{Ph}], 6.53–6.63 [m, 2H, H_{Ph}], 6.69–6.74 [m, 2H, H_{Ph}], 6.81–6.90 [m, 2H, H_{Ph}], 6.97–7.05 [m, 4H, H_{Ph}], 7.09–7.15 [m, 3H, H_{Ph}], 7.18–7.23 [m, 2H, H_{Ph}], 7.49–7.54 [m, 2H, H_{Ph}].

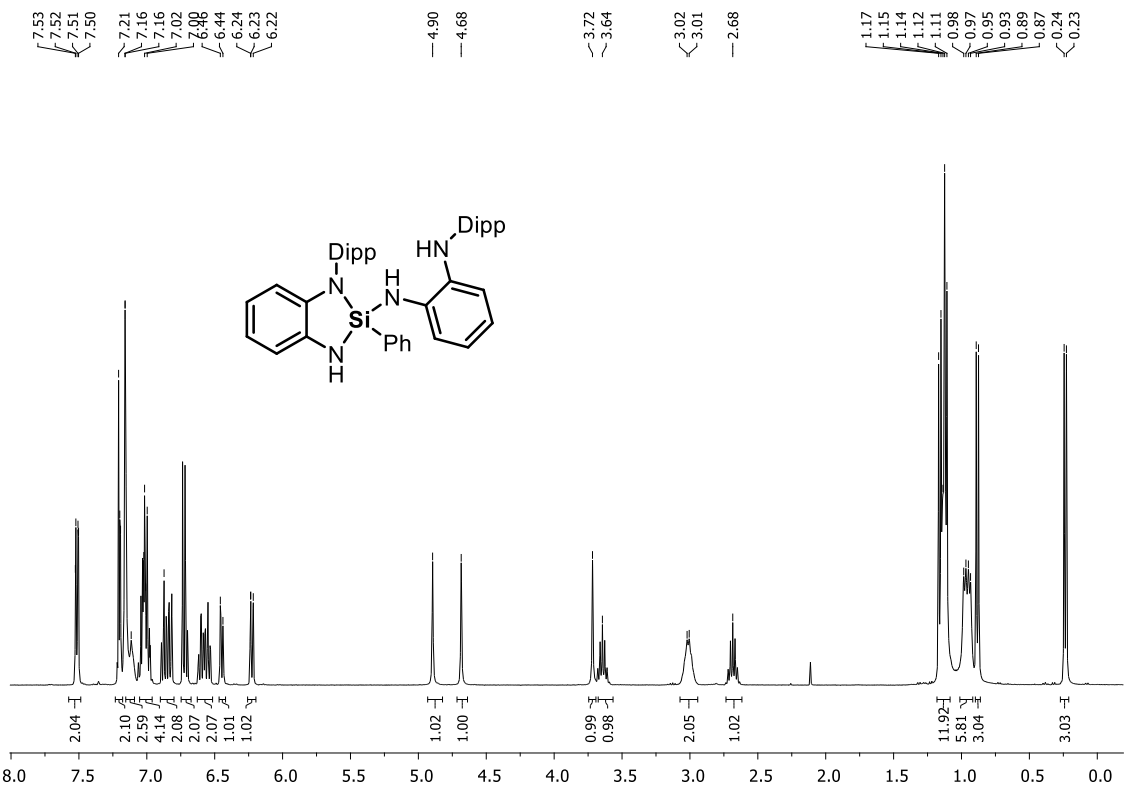

Figure 6.23. ^{1}H NMR spectrum (C_6D_6, 298 K) of **21.**

6.5 X-ray crystallographic details

The crystals were selected and measured either on a GV50 diffractometer equipped with a TitanS2 detector (**20**), a Gemini Ultra diffractometer equipped with an Atlas S2 CCD detector (**5**), a SuperNova Dualflex diffractometer equipped with a TitanS2 detector (**17, 19**), a XtaLAB Synergy R, DW system, equipped with a HyPix-Arc 150 detector (**2, 12, 16, 21**) or on a Superova diffractometer equipped with an Atlas detector (**7, 9**). Data collection and reduction were performed with **CrysAlisPro** [Version 1.171.41.54a or 1.17.41.76a].[7] A numerical absorption correction using spherical harmonics as implemented in SCALE3 ABSPACK was applied. Using **Olex2**,[8] the structures were solved with **ShelXT**[9] and a least-square refinement on F^2 was carried out with **ShelXL**[10]. All non-hydrogen atoms were refined anisotropically. Hydrogen atoms at the carbon atoms were located in idealized positions and refined isotropically according to the riding model. The hydrogen atoms on the nitrogen atoms were located from the difference Fourier map and refined without restraints. Figures were created with **Olex2**[8].

Compound 5: The asymmetric unit contains half of the molecule. The full dimer can be obtained by the command “grow”.

Compound 7: The asymmetric unit contains half of the molecule. The full dimer can be obtained by the command “grow”.

Compound 9: The asymmetric unit contains one molecule.

Compound 12: The asymmetric unit contains half of the molecule. The full dimer can be obtained by the command “grow”.

Compound 16: The asymmetric unit contains two times half of the molecule. The full two dimers can be obtained by the command “grow”. Additionally, three Et_2O moieties are found in the asymmetric unit, which were modeled using SIMU restraints.

Compound 17: The asymmetric unit contains one molecule.

Compound 19: The asymmetric unit contains one molecule of **19** and half a toluene molecule. The Si–H and Si–Cl units are mixed occupied and modeled using EXYZ and dfix restraints.

Compound 20: The asymmetric unit contains one molecule.

Compound 21: The asymmetric unit contains one molecule.

Table 6.1. Crystallographic data for compounds **5**, **7** and **9**.

Compound	**5**	**7**	**9**
Data set (internal naming)	TG165	TG405	TG258
Formula	$C_{24}H_{35}LiN_2OSi$	$C_{26}H_{31}LiN_2OSi$	$C_{23}H_{26}N_2Si$
$\rho_{calc.}$ / g·cm^{-3}	1.156	1.202	1.154
μ/mm^{-1}	1.004	1.025	1.047
Formula Weight	402.57	422.56	358.55
Color	clear colorless	clear colorless	clear colorless
Shape	block	block	block
Size/mm^3	0.29 × 0.244 × 0.106	0.17 × 0.14 × 0.07	0.363 × 0.218 × 0.117
T/K	123.00(10)	100.00(10)	293(2)
Crystal System	monoclinic	monoclinic	monoclinic
Space Group	$P2_1/n$	$P2_1/c$	$P2_1$
a/Å	9.7162(3)	10.88850(10)	9.21280(10)
b/Å	10.3396(3)	11.1361(10)	11.9462(2)
c/Å	23.1571(7)	19.9375(2)	9.45200(10)
α/°	90	90	90
β/°	96.022(3)	104.9720(10)	97.2950(10)
γ/°	90	90	90
V/Å^3	2313.56(12)	2335.46(4)	1031.85(2)
Z	4	4	2
Z'	1	1	1
Wavelength/Å	1.54184	1.54184	1.54184
Radiation type	Cu K_α	Cu K_α	Cu K_α
$2\Theta_{min}$/°	7.678	8.406	9.434
$2\Theta_{max}$/°	147.152	148.234	143.426
Measured Refl.	7852	25598	21950
Independent Refl.	4440	4572	3931
R_{int}	0.0220	0.0337	0.0298
Parameters	268	283	246
Restraints	0	0	1
Largest Peak	0.43	0.30	0.21
Deepest Hole	−0.22	−0.30	−0.15
GooF	1.065	1.034	1.037
wR_2 (all data)	0.1074	0.0918	0.0709
wR_2	0.1002	0.0903	0.0701
R_1 (all data)	0.0456	0.0372	0.0284
R_1	0.0395	0.0346	0.0273
Flack parameter	-	-	−0.010(14)

Table 6.2. Crystallographic data for compounds **12, 16** and **17**.

Compound	**12**	**16**	**17**
Data set (internal naming)	TR17	TG399	TG429
Formula	$C_{19}H_{22}GeN_2O_5W$	$C_{90}H_{100.96}Ge_2N_4O_{6.5}Si_4$	$C_{45}H_{38}GeN_2O_6Si_2W$
$\rho_{calc.}$ / g·cm^{-3}	1.927	1.263	1.481
μ/mm^{-1}	11.909	1.858	6.296
Formula Weight	614.82	1600.24	1015.39
Color	yellow	yellow	yellow
Shape	block	block	block
Size/mm^3	0.12 × 0.1 × 0.06	0.11 × 0.11 × 0.05	0.19 × 0.13 × 0.11
T/K	123.15	100.01(10)	123.15
Crystal System	monoclinic	monoclinic	monoclinic
Space Group	*I*2/*a*	$P2_1/n$	$P2_1/n$
a/Å	18.3275(2)	19.4448(4)	11.73320(10)
b/Å	10.11250(10)	23.7536(3)	12.00480(10)
c/Å	23.0118(2)	20.3324(4)	32.5588(3)
α/°	90	90	90
β/°	96.5100(10)	116.357(2)	96.8460(10)
γ/°	90	90	90
V/Å^3	4237(7)	8414.9(3)	4553.36(7)
Z	8	4	4
Z'	1	1	1
Wavelength/Å	1.54184	1.54184	1.54184
Radiation type	Cu K_α	Cu K_α	Cu K_α
$2\Theta_{min}$/°	7.734	5.236	7.754
$2\Theta_{max}$/°	146.53	151.006	133.98
Measured Refl.	23282	63144	60969
Independent Refl.	4175	16939	8037
R_{int}	0.0294	0.0403	0.0357
Parameters	257	1060	529
Restraints	0	18	0
Largest Peak	0.49	0.91	1.02
Deepest Hole	−0.84	−0.90	−1.09
GooF	1.071	1.053	1.097
wR_2 (all data)	0.0468	0.1189	0.0639
wR_2	0.0464	0.1114	0.0634
R_1 (all data)	0.0199	0.0742	0.0273
R_1	0.0188	0.0549	0.0265

Table 6.3. Crystallographic data for compounds **19, 20** and **21**.

Compound	**19**	**20**	**21**
Data set (internal naming)	TG400 hexane extract	TG308-F4	TG662-byproduct-orthorhombic
Formula	$C_{33.5}H_{36.51}Cl_{0.99}N_2Si_2$	$C_{48}H_{54}N_4OSi_2$	$C_{42}H_{50}N_4Si$
$\rho_{calc.}$ / g·cm^{-3}	1.207	1.216	1.169
μ/mm^{-1}	2.018	1.089	0.823
Formula Weight	558.43	759.13	638.95
Color	clear colorless	clear colorless	clear colorless
Shape	block	block	plate
Size/mm^3	0.21 × 0.14 × 0.11	0.411 × 0.152 × 0.136	0.38 × 0.09 × 0.06
T/K	123.00(10)	293(2)	123.03(10)
Crystal System	triclinic	monoclinic	orthorhombic
Space Group	*P*-1	$P2_1/n$	$Pca2_1$
a/Å	10.39710(10)	13.64280(10)	18.8426(3)
b/Å	12.5758(2)	17.34430(10)	12.2184(2)
c/Å	13.5031(2)	17.87370(10)	15.7655(3)
α/°	109.3110(10)	90	90
β/°	99.4840(10)	101.3550(10)	90
γ/°	106.0330(10)	90	90
V/Å^3	1536.24(4)	4146.58(5)	3629.64(11)
Z	2	4	4
Z'	1	1	1
Wavelength/Å	1.54184	1.54184	1.54184
Radiation type	Cu K_α	Cu K_α	Cu K_α
$2\Theta_{min}$/°	7.232	7.17	7.234
$2\Theta_{max}$/°	133.724	147.862	147.982
Measured Refl.	42234	46336	23784
Independent Refl.	5439	8287	6606
R_{int}	0.0354	0.0401	0.0211
Parameters	389	512	444
Restraints	1	0	1
Largest Peak	0.52	0.43	0.14
Deepest Hole	−0.76	−0.38	−0.20
GooF	1.077	1.029	1.068
wR_2 (all data)	0.0926	0.0926	0.0706
wR_2	0.0915	0.0907	0.0703
R_1 (all data)	0.0402	0.0367	0.0277
R_1	0.0385	0.0347	0.0270
Flack parameter	-	-	0.359(9)

Compound 5

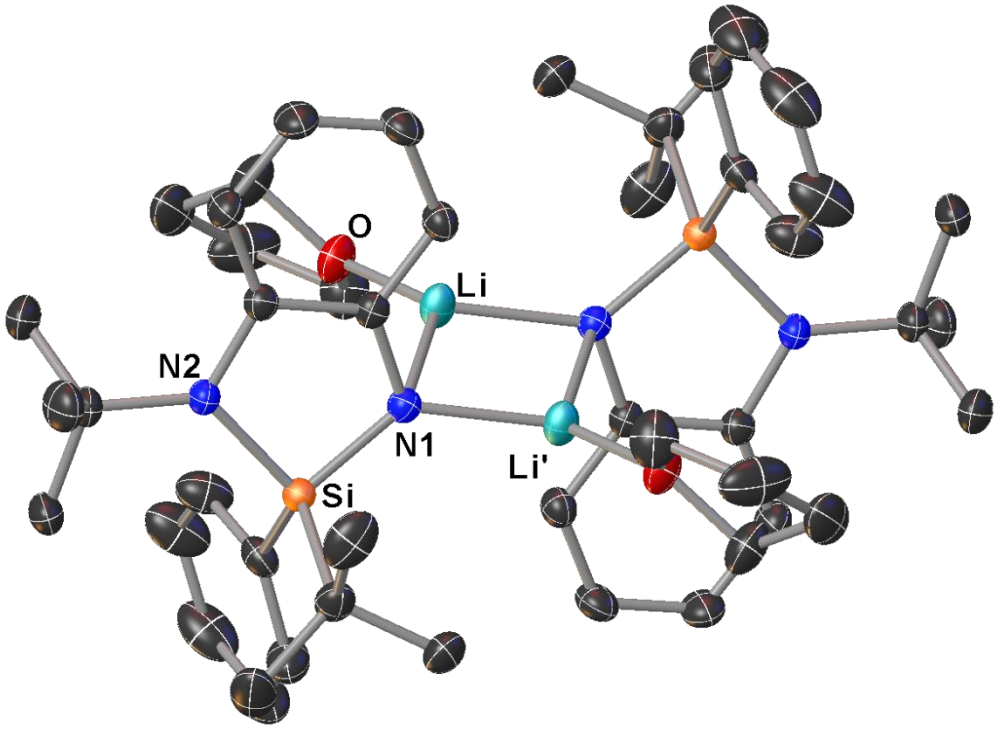

Selected Bond Lengths in Å		Selected Bond Angles in °	
Si–N1	1.7199(11)	**N1–Si–N2**	95.30(5)
Si–N2	1.7774(11)	**Li–N1–Li'**	75.36(11)
N1–Li	2.054(3)		
N1–Li'	1.983(3)		
Li–O	1.889(3)		

Compound 7

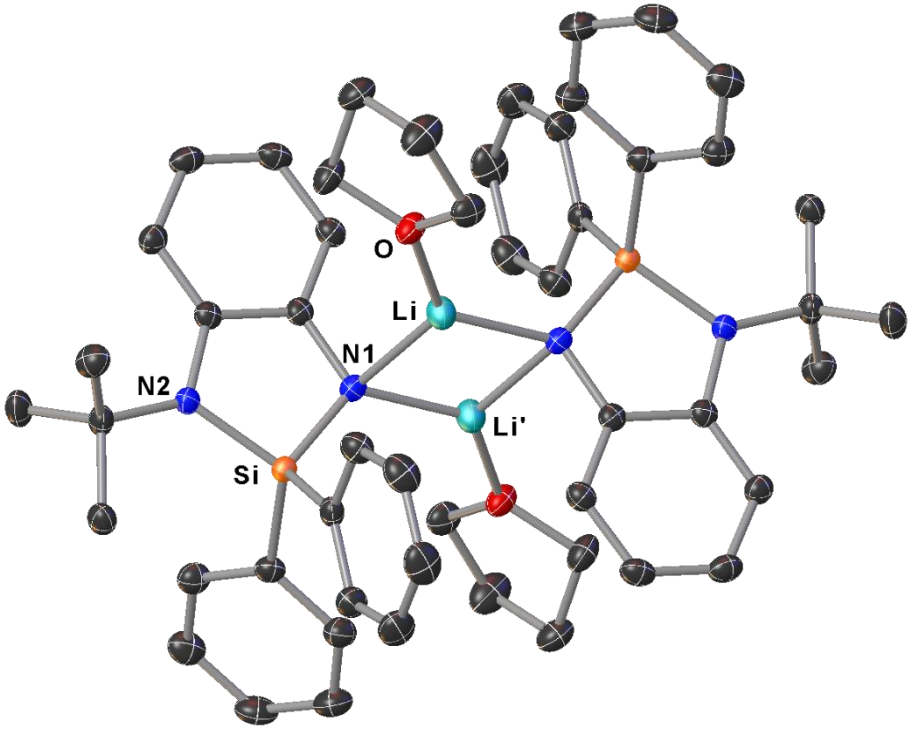

Selected Bond Lengths in Å		Selected Bond Angles in °	
Si–N1	1.7078(11)	**N1–Si–N2**	96.41(5)
Si–N2	1.7559(10)	**Li–N1–Li'**	77.66(10)
N1–Li	1.975(2)		
N1–Li'	2.045(2)		
Li–O	1.929(2)		

Compound 9

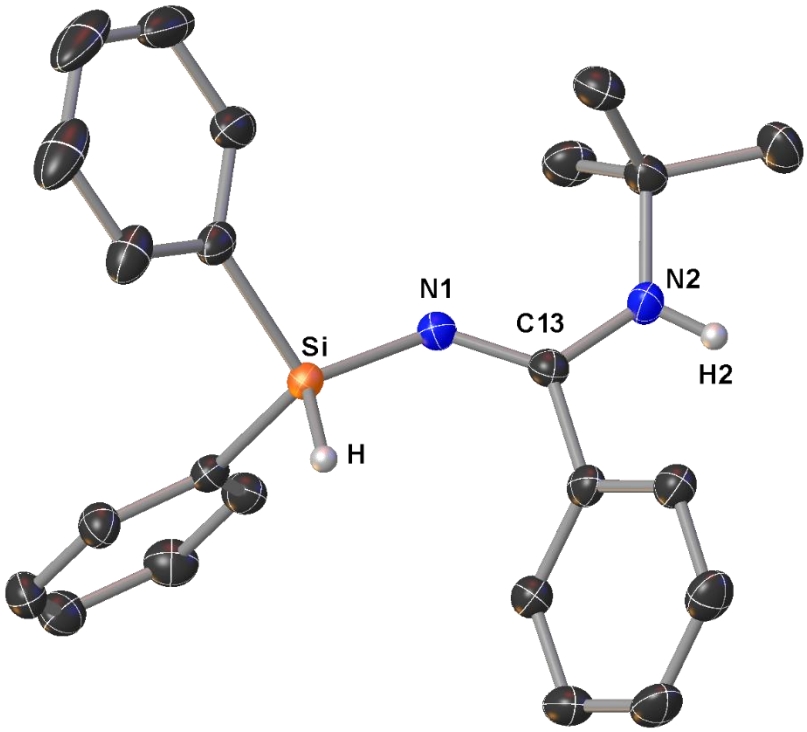

Selected Bond Lengths in Å		Selected Bond Angles in °	
Si–N1	1.7014(17)	**Si–N1–C13**	130.79(15)
Si–H	1.41(3)	**N1–C13–N2**	122.80(18)
N1–C13	1.286(3)		
N2–C13	1.353(3)		

Compound 12

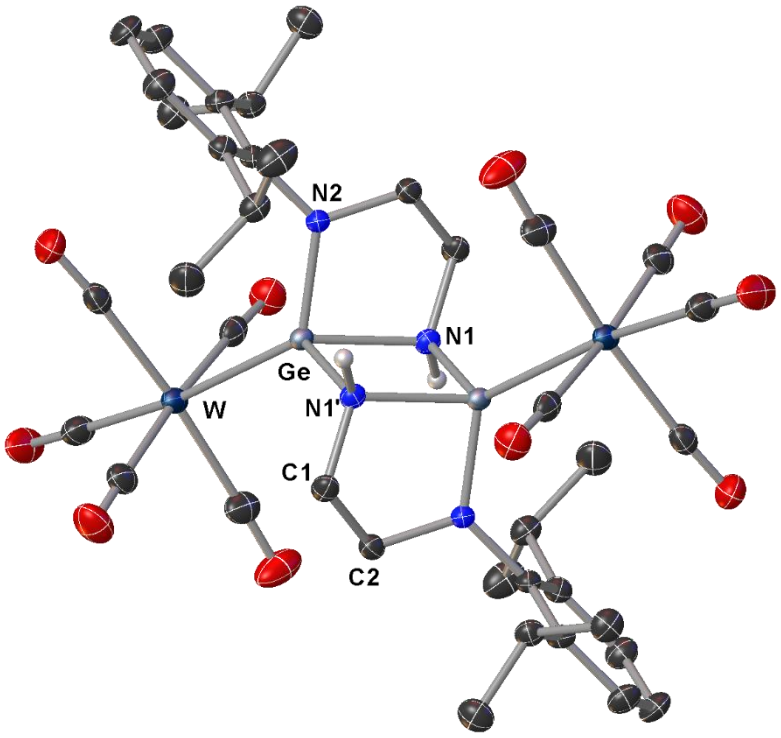

Selected Bond Lengths in Å		Selected Bond Angles in °	
Ge–N1	1.993(29	**N1–Ge–N2**	86.36(9)
Ge–N1'	2.0517(19)	**N1–Ge–N1'**	80.87(9)
Ge–N2	1.8358(19)	**N2–Ge–N1'**	103.30(9)
Ge–W	2.5695(3)		

Compound 16

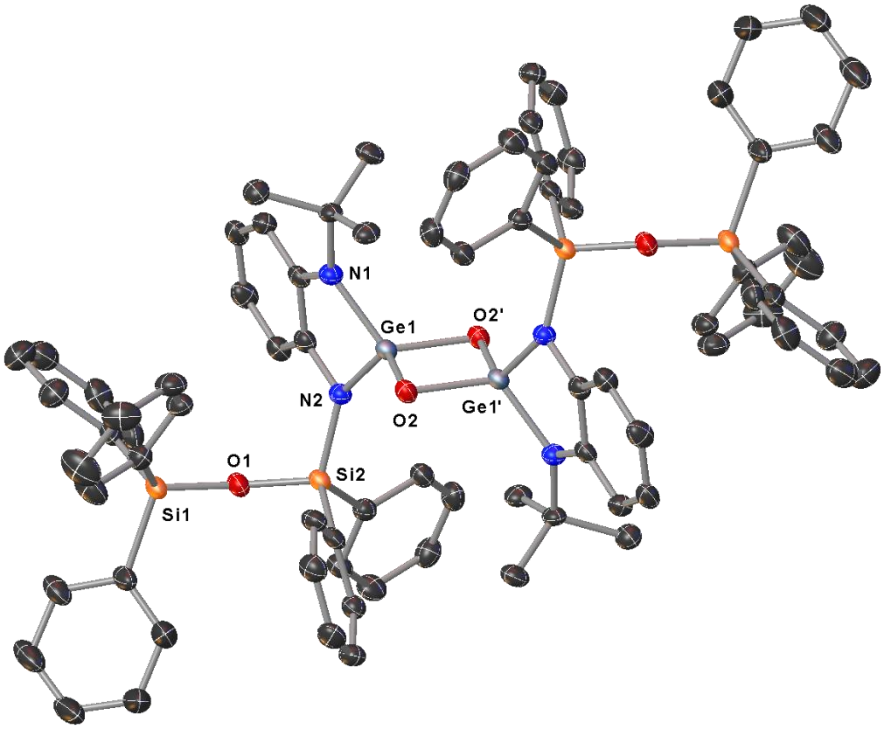

Selected Bond Lengths in Å		Selected Bond Angles in °	
Si1–O1	1.629(2)	**Si1–O1–Si2**	156.11(16)
Si2–O1	1.624(2)	**O1–Si2–N2**	108.59(12)
Si2–N2	1.751(3)	**N1–Ge1–N2**	92.12(11)
Ge1–N1	1.824(3)	**O2–Ge1–O2'**	86.93(9)
Ge1–N2	1.830(2)	**Ge1–O2–Ge1'**	93.07(9)
Ge1–O2	1.823(2)		
Ge1–O2'	1.776(2)		

Compound 17

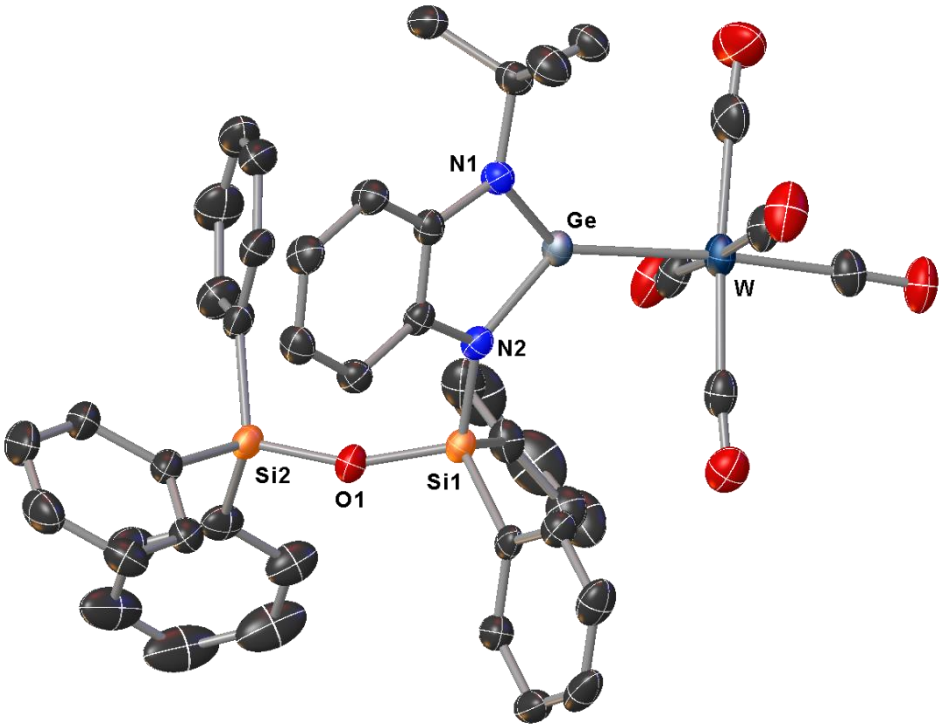

Selected Bond Lengths in Å		Selected Bond Angles in °	
Si1–O1	1.629(2)	**Si1–O1–Si2**	155.95(14)
Si2–O1	1.629(2)	**N1–Ge–N2**	88.76(10)
Si1–N2	1.754(2)	**N1–Ge–W**	136.30(8)
Ge–N1	1.840(2)	**N2–Ge–W**	129.27(7)
Ge–N2	1.847(2)		
Ge–W	2.5766(3)		

Compound 19

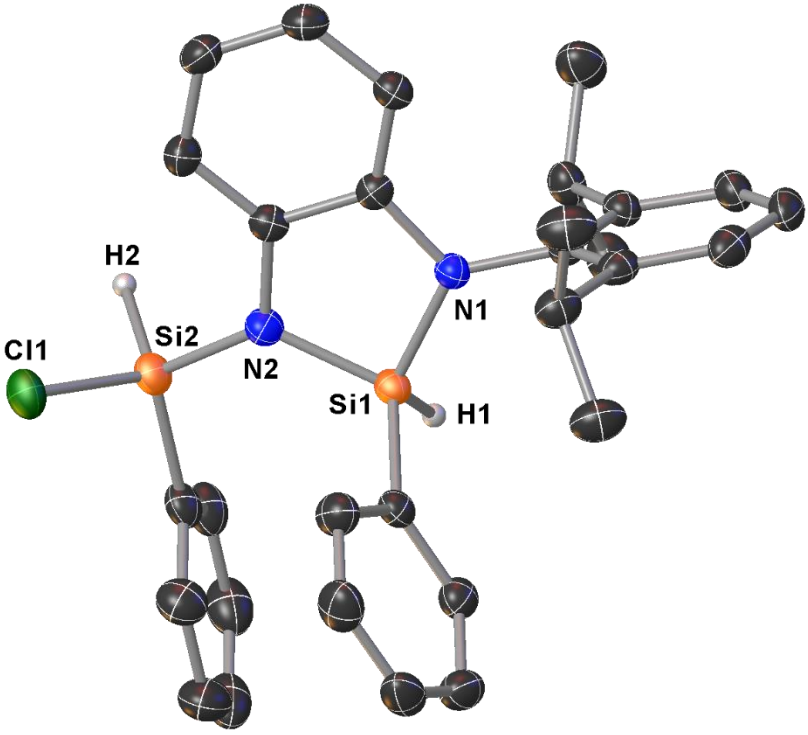

Selected Bond Lengths in Å		Selected Bond Angles in °	
Si1–N1	1.7335(14)	**N1–Si1–N2**	92.63(7)
Si1–N2	1.7493(15)	**Si1–N2–Si2**	126.47(9)
Si1–H1	1.362(19)	**Cl1–Si2–N2**	109.96(6)
Si2–N2	1.7166(15)		
Si2–Cl1	2.0500(7)		
Si2–H2	1.783(4)		

Compound 20

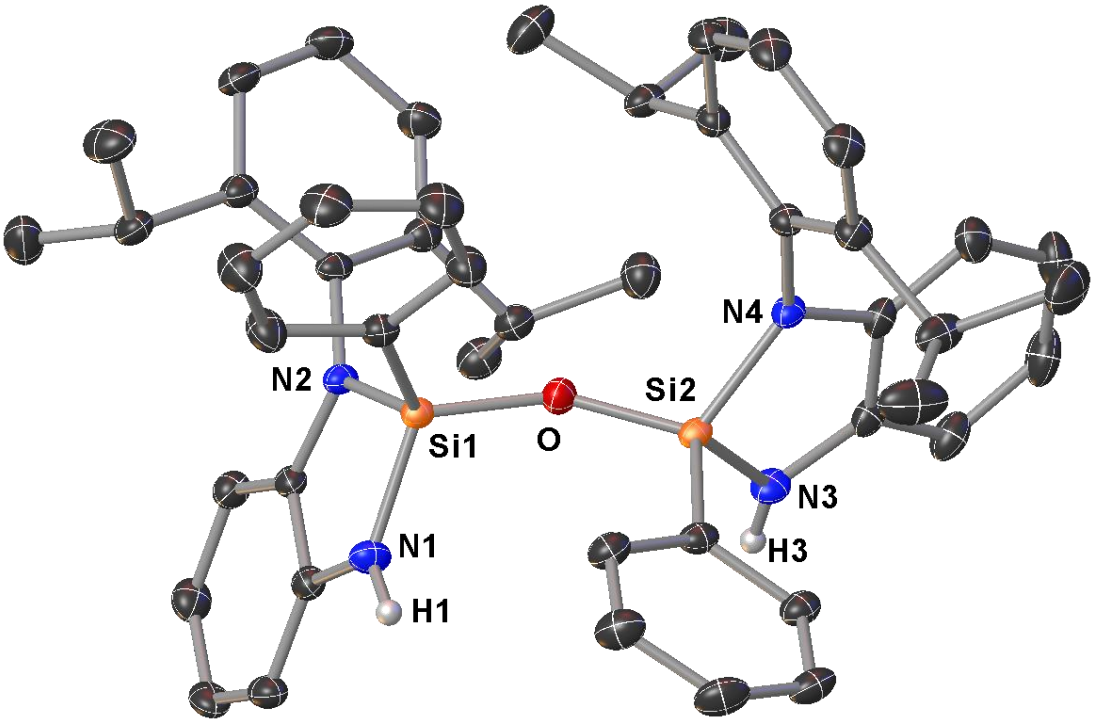

Selected Bond Lengths in Å		Selected Bond Angles in °	
Si1–N1	1.7209(11)	**N1–Si1–N2**	91.89(5)
Si1–N2	1.7318(10)	**N3–Si2–N4**	92.19(5)
Si1–O	1.6282(8)	**Si1–O–Si2**	153.11(6)
Si2–N3	1.7120(11)		
Si2–N4	1.7397(10)		
Si2–O	1.6174(8)		

Compound 21

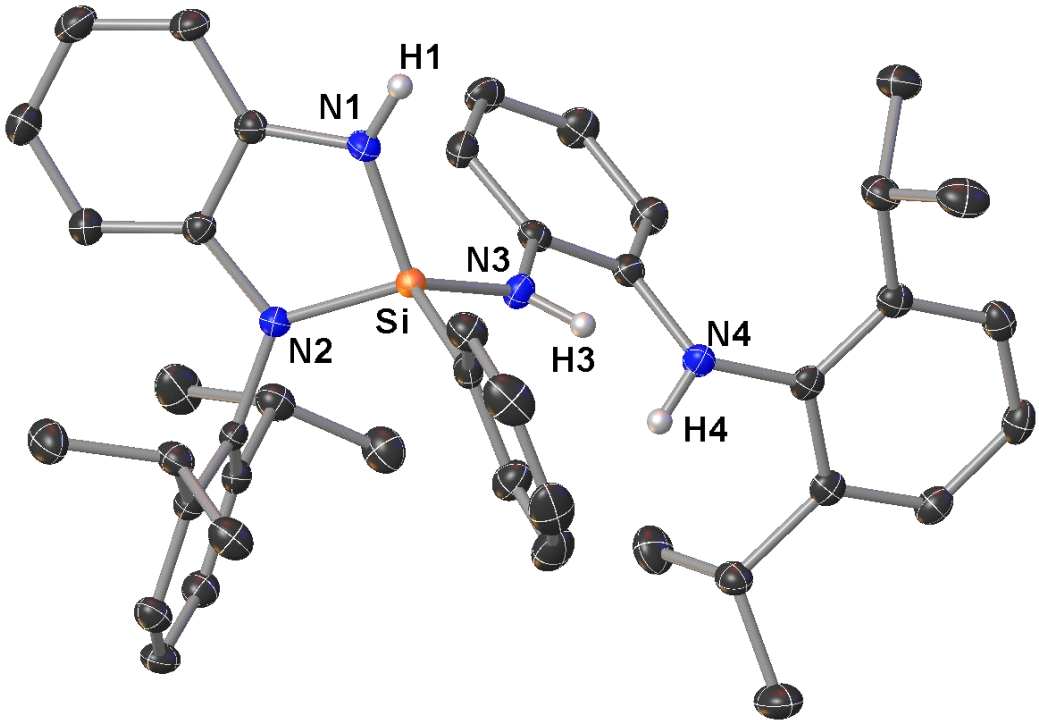

Selected Bond Lengths in Å		Selected Bond Angles in °	
Si–N1	1.7232(17)	**N1–Si–N2**	91.46(8)
Si–N2	1.7417(17)	**N1–Si–N3**	115.67(8)
Si–N3	1.7149(17)	**N2–Si–N3**	115.64(8)

6.6 References

[1] M. Q. Tran, T. B. Nguyen, W. R. Sawadogo, L. Ermolenko, S. Song, P. Retailleau, M. Diederich, A. Al-Mourabit, *Eur. J. Org. Chem.* **2018**, *2018*, 5878–5884.

[2] C. Marshall, M. F. Ward, J. M. Skakle, *Synthesis* **2006**, 1040–1044.

[3] N. Fontana, N. A. Espinosa-Jalapa, M. Seidl, J. O. Bauer, *Chem. Commun.* **2022**, *58*, 2144–2147.

[4] T. Heidemann, S. Mathur, *Chem. Ber.* **2014**, *2014*, 506–510.

[5] a) J. C. L. Walker, H. F. T. Klare, M. Oestreich, *Nat. Rev. Chem.* **2020**, *4*, 54–62; T. Müller in *Structure and Bonding*, *Vol. 155* (Ed.: D. Scheschkewitz), Springer, Cham, **2014**, 107–162.

[6] O. Kühl, *Coord. Chem. Rev.* **2004**, *248*, 411–427.

[7] CrysAlisPro Software System, Rigaku Oxford Diffraction, **2020**.

[8] O. V. Dolomanov, L. J. Bourhis, R. J. Gildea, J. A. K. Howard, H. Puschmann, *OLEX2*: a complete structure solution, refinement and analysis program, *J. Appl. Crystallogr.* **2009**, *42*, 339–341.

[9] G. M. Sheldrick, *SHELXT* – Integrated space-group and crystal-structure determination, *Acta Crystallogr*. **2015**, *A71*, 3–8.

[10] G. M. Sheldrick, Crystal structure refinement with *SHELXL*, *Acta Crystallogr.* **2015**, *C71*, 3–8.

7 Conclusions

Within the scope of this work, the substitution of silicon compounds with amines – especially unsymmetrically substituted *ortho*-phenylenediamines – was investigated. The synthesized aminosilanes and -siloxanes were prepared for the first time and structurally characterized in detail using combinations of NMR spectroscopy, mass spectrometry, elemental analysis, and single-crystal X-ray diffraction. Chapter 3 describes the syntheses of a series of cyclic five-membered diaminosilanes combined with reactivity studies concerning their synthetic use in the formation of functionalized siloxane compounds. The diaminosilanes were successfully converted into a library of amino-substituted di- or trisiloxanes by reaction with various silanols. The transformations were found to proceed with high selectivities and yields of up to 98% which provides a new synthetic method for the controlled preparation of siloxane compounds. Additionally, we were able to demonstrate the selective removal of the attached diamine from the siloxane scaffold through simple hydrolysis, generating siloxanol compounds, which could undergo further substitution. Another exciting use of the diamine compounds was established in its application as “molecular scissors” for the selective cutting of siloxane bonds. A straightforward *in situ* lithiation of the NH function with *n*BuLi resulted in the controlled Si–O–Si bond cleavage and the formation of cyclic five-membered diaminosilanes. Such a precise lithium amide mediated siloxane cleavage was unprecedented in the literature and introduced for the first time in this work. We showed that this method can be transferred to the cleavage of chlorosiloxanes by the addition of *in situ* lithiated diamines to form the cyclic diaminosilanes. In combination of the herein introduced siloxane bond cleavage and -formation, a novel example of silyl group exchange in siloxane compounds could be presented (Scheme 7.1).

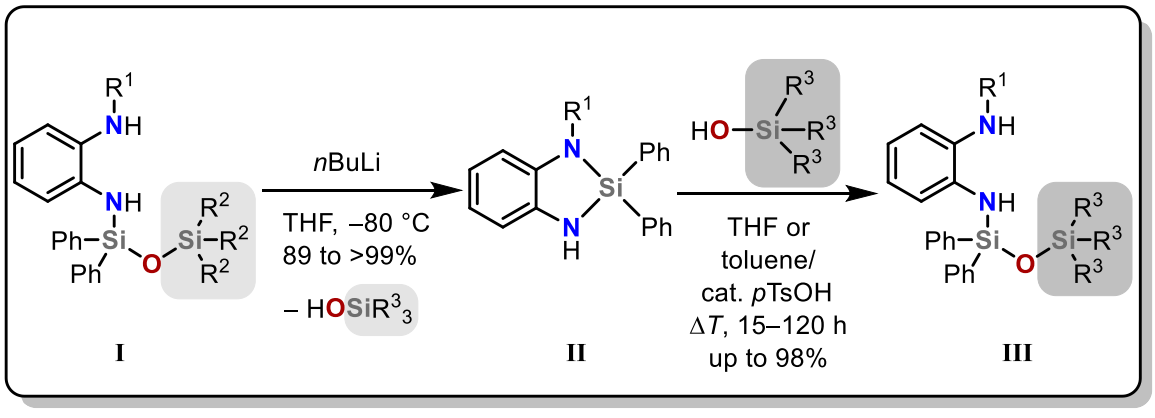

Scheme 7.1. General scheme for the herein introduced exchange of silyl groups on siloxanes.

In attempts to modify the $SiPh_2$ scaffold, we successfully prepared the SiPhH analogues of cyclic diaminosilanes with R^1 = Dipp, *t*Bu (Chapter 4). In the reaction with triphenylsilanol, the compound with R^1 = *t*Bu essentially reacted analogously to the diaminosilanes described in chapter 3 resulting in the substitution of the Si–N bond. Changing the R^1 substituent to a bulky aromatic Dipp group, however, gave rise to a different reaction in which the Si–O–Si bond is formed,

substituting the Si–H bond. Variable temperature ^{1}H and ^{29}Si NMR studies gave detailed insight into the reaction mechanism. We could show that two different siloxane species are presumably formed in the reaction with Ph_3SiOH which are metastable below temperatures of −10 °C. The intermediates were proposed to be pentacoordinated siloxanes after substitution of one of the two Si–N bonds, where the NR_2 amine unit is forming a dative bond to the silicon atom. The two distinct species can be observed by NMR spectroscopy as two sets of signals only at very low temperatures of around −90 °C, and were found to coalesce on the NMR timescale at higher temperatures. This observation was attributed to the dissociative/associative Si–N bond behavior which is faster at higher temperatures. The pentacoordinated species were identified in the ^{29}Si NMR spectra with characteristic signals in the high-field shifted region around δ = −90 ppm. At temperatures above −10 °C, the formation of the final reaction product, along with H_2 as a byproduct, occurred (Scheme 7.2).

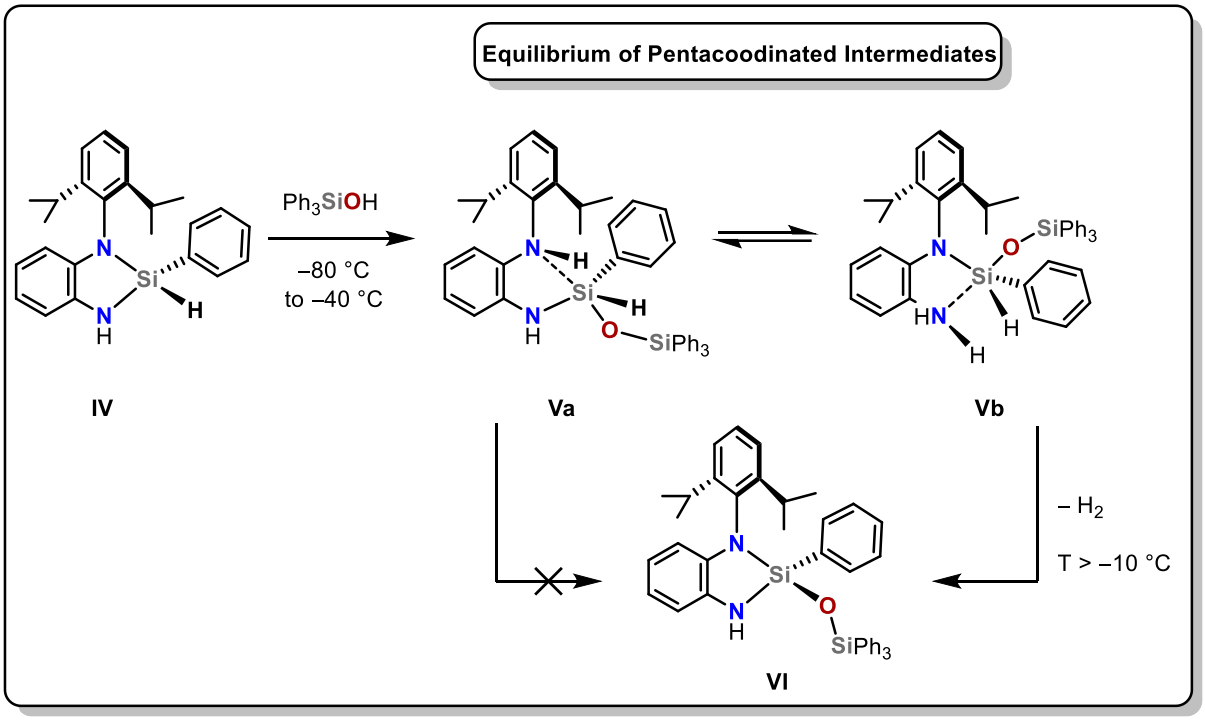

Scheme 7.2. Proposed reaction mechanism in the dehydrogenative siloxane formation.

Quantum chemical calculations on the M062X/6-311+G(d,p) level of theory were performed in which the Gibbs energies (*ΔG*) of the H_2 evolution step from the two intermediates were obtained. The calculations suggested a clear preference in the transition state energies of 39 kJ mol^{-1} for the **Vb** isomer (Scheme 7.2). Based on these calculations, the H_2 formation resulting only from the kinetically preferred intermediate **Vb** was suggested. The detailed mechanistic insights gathered in this chapter add to a better understanding of the chemistry of higher coordination modes in main group element-based compounds. The obtained information helps to explain reactivities in silicon chemistry and can be fundamental for the design of new reactive hydrosilanes. Moreover, the concept can be further exploited and might give rise to new compounds capable of reversible H_2 activation, which are highly interesting for H_2 storage

applications. After introducing unsymmetrical aromatic 1,2 diamines in silicon chemistry and demonstrating their use as “molecular scissors”, our goal was to modify the diamine unit by introducing a stereochemically pure organic substituent and transfer stereochemical information to the silicon atom. Thereby, chiral *Si*-stereogenic molecules were targeted as chiral probes for detailed mechanistic investigations (Chapter 5). The commercially available (*S*)-methylbenzylamine was utilized as the enantiomerically pure chiral anchor. We demonstrated that it can be used directly for the formation and separation of diastereomerically pure *Si*-stereogenic chloro-aminosilanes, which are versatile precursors for further silane functionalization. Incorporation of the (*S*)-methylbenzylamine into 2-bromoaniline yielded a chiral *ortho*-phenylenediamine which could be further reacted with dichloro-diorganosilanes to obtain a series of cyclic diaminosilanes (Scheme 7.3).

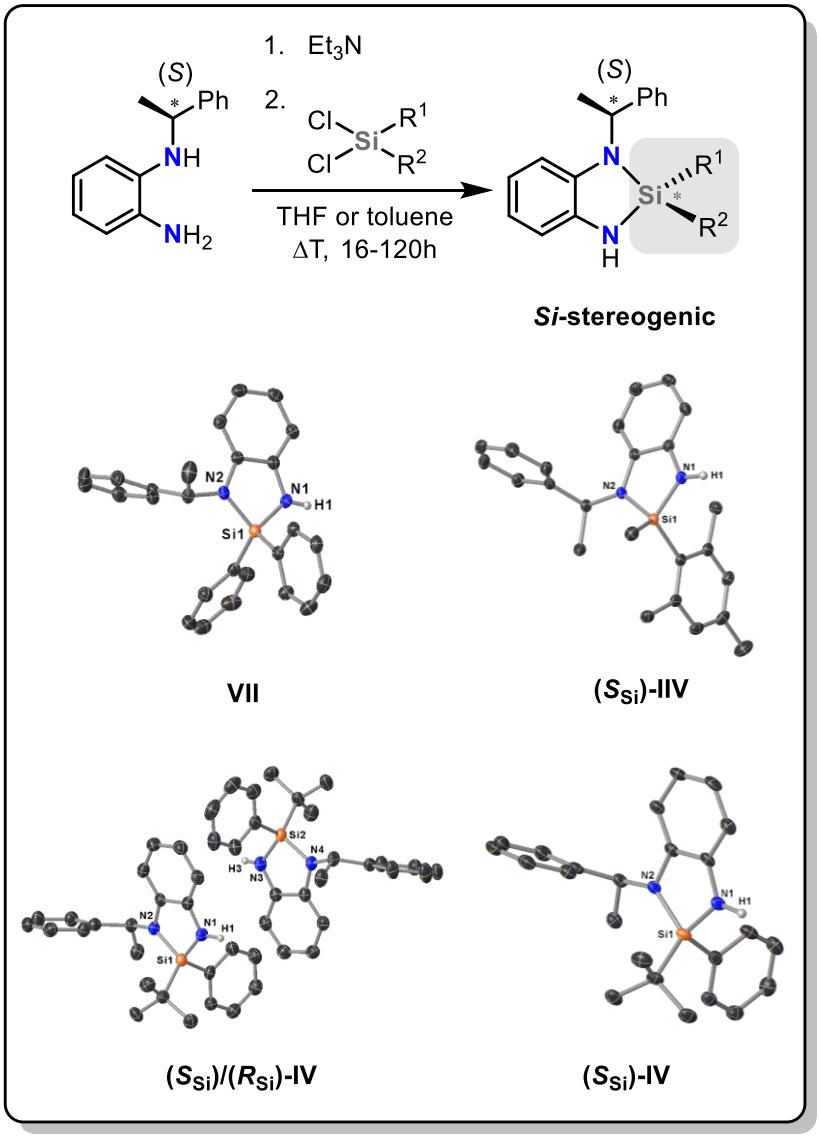

Scheme 7.3. General scheme for the synthesis of *Si*-chiral cyclic diaminosilanes.

The synthesis was achieved for a *C*-stereogenic cyclic diaminosilane with the silicon atom not being a stereogenic center (**VII**) and for two different *C*-stereogenic and *Si*-stereogenic congeners

(**(S_{Si})-IIV and (S_{Si})-IIV**). The diastereomers could additionally be separated and isolated in their optically pure form following fractional crystallization procedures. These compounds were fully characterized, and the absolute configurations of the silicon atoms were determined by single-crystal X-ray diffraction. The resulting *Si*-chiral cyclic diaminosilanes are promising candidates for the chiral resolution of racemic silanols following the sequence of siloxane bond formation (Chapter 3), fractional crystallization of the aminosiloxane, and *n*BuLi induced siloxane bond cleavage (Chapter 3). Additionally, the chiral information on the silicon center serves as a mechanistic probe and may give an even more detailed mechanistic picture of the reactivities of silyl group exchange (Chapter 3) and dehydrogenative siloxane formation via pentacoordinate intermediates (Chapter 4) in ongoing work in the group of Dr. Bauer. Moreover, a rare solvent-dependent crystallization behavior in the case of compound **IV** was observed. Crystallization in toluene/pentane (4:1) resulted in the formation of a crystalline material with a 1:1 mixture of both diastereomers (**(S_{Si})/(R_{Si})-IV**) in the asymmetric unit. Recrystallization in THF/pentane (4:1) yielded the optically pure (S_{Si})-diastereomer which was confirmed by NMR and single crystal X-ray analysis. This solvent control over the success of fractional crystallization is scarcely reported in the literature and could be fundamental for preparative stereochemistry and crystal engineering.

In conclusion, we have established, on the one hand, a powerful new synthetic tool for the controlled modification of siloxane scaffolds by introducing unsymmetrical *ortho*-phenylenediamines as “molecular scissors”. On the other hand, detailed mechanistic investigations gave valuable insight into the presence and importance of highercoordinated species in main group element chemistry. The H_2 evolution from this reaction is irreversible but the gathered mechanistic knowledge is fundamental for the development of similar compounds capable of reversible H_2 activation for use in hydrogen storage systems. Additionally, *Si*-chirality was introduced and a series of optically pure aminosilanes was isolated. The chiral information on the silicon center serves as mechanistic probe and the compounds can lead to the development of applications in chirality transfer reactions in the future. The combined knowledge received from this work provides a valuable addition to preparative methods and mechanistic studies in silicon chemistry and helps to further understand the influences of diamino substituents on the reactivities of silicon-based compounds. This field of silicon chemistry is still rather unexplored and leaves great potential for further improvements and discoveries. We hope that the results summarized in this thesis initiate curiosity and imagination of silicon chemists to continue creating new methodologies and push the boundaries of what is possible in synthetic chemistry and materials science.

8 Acknowledgements

Zum Abschluss möchte ich hiermit noch ein paar Danksagungen aussprechen, an alle die mich in dieser lehrreichen und prägenden Zeit begleitet haben. Allen voran möchte ich Jonathan Bauer danken, der mich 2018 in seiner Arbeitsgruppe aufgenommen hat und mir diese Promotion somit ermöglicht hat. Ich danke ihm auch für die vielen interessanten Gespräche und das Vertrauen, das er mir stets geschenkt hat. Ebenso möchte ich Prof. Scheer für seine stetige Unterstützung unserer Gruppe danken und dafür, dass er sich bereit erklärt hat, das Zweitgutachten für diese Arbeit zu verfassen. Danke auch an Prof. Matysik und Apl. Prof. Müller dafür, dass sie als Drittprüfer bzw. Prüfungsvorsitz bereit stehen. Danke an meine Kollegen Tanja, Nicoló, Noël, Alex, Robin, Simon und Sarah für die zahlreichen fachlichen Diskussionen, das großartige Arbeitsklima und die tollen Unternehmungen abseits des Labors. Danke auch an die gesamte Gruppe des AK Scheer, insbesondere des Stammtisches, Anna, Schotti, Michi und Gabor, für die vielen tollen Gespräche, das gesellige Miteinander und natürlich die fachliche Hilfe. Ich danke den technischen Angestellten Schotti, Petra, Martina, Lukas, Julian, Matthias und Sophie für ihre Unterstützung im Laboralltag. In diesem Zuge möchte ich auch der NMR Abteilung und der zentralen Analytik danken für ihre Hilfe bei jeglichen Messungen und die allgemein gute Zusammenarbeit. Ein weiterer großer Dank geht an Freunde während des Studiums und der Promotion, die bisher noch nicht erwähnt wurden: Andi, Eiser, Marion, Markus, Maxi, Nagi, Philipp, Susi, Tami und Willi. Ohne euch hätte diese Zeit nicht annähernd so schön und erfolgreich sein können. Ich danke auch meiner Familie, insbesondere meinen Eltern Regina und Bernhard und meinem Bruder Philipp für ihre stetige Unterstützung in diesem und jedem anderen Lebensabschnitt. Last but not least, möchte ich meiner Freundin Susi danken, für den unnachgiebigen Rückhalt sowie die nicht nachlassende Inspiration, die sie mir immerzu gegeben hat.